

The Influence of Urban Green Space upon Air Pollutant Concentrations

by

Dewi Komalasari

A thesis submitted to the University of Birmingham for the degree of
DOCTOR OF PHILOSOPHY

Division of Environmental Health and Risk Management
School of Geography, Earth, and Environmental Sciences
College of Life and Environmental Sciences
University of Birmingham

2021

UNIVERSITY OF
BIRMINGHAM

University of Birmingham Research Archive

e-theses repository

This unpublished thesis/dissertation is copyright of the author and/or third parties. The intellectual property rights of the author or third parties in respect of this work are as defined by The Copyright Designs and Patents Act 1988 or as modified by any successor legislation.

Any use made of information contained in this thesis/dissertation must be in accordance with that legislation and must be properly acknowledged. Further distribution or reproduction in any format is prohibited without the permission of the copyright holder.

Abstract

Greenspace has an essential role in influencing the concentration of pollutants in urban areas. The processes for improving air quality are dispersion and deposition, but their relative contributions to reducing air pollution are unclear.

Temporal and spatial variability of pollutant concentrations from a roadside into a park were generated using diffusion tubes measurements. Sampling was carried out in urban park areas in Birmingham and London, UK, specifically in Cannon Hill Park, Tile Cross Park, University of Birmingham (UoB), and Hyde Park. The difference in NO_2 concentrations between the roadside and the park was 32% at Cannon Hill Park, 30% at Hyde Park and 38% at the UoB site, and was statistically significant ($p < 0.01$). For Tile Cross Park, the difference was 14% and was not statistically significant ($p > 0.05$).

Dispersion and dry deposition modelling were performed using the ADMS-Roads model. The set-up and evaluation of dispersion modelling are presented, incorporating the meteorological data, background concentration, emissions set-up, and the ratio of NO_2:NO_x in the emissions. The evaluation of the model was performed using observational data from two different sites (BROS and EROS) measured by automatic analysers, and by comparison with the diffusion tube spatial profiles.

NO_x deposition velocities were estimated by the gradient method in a grassed quadrangle area of the Biosciences building at UoB, using an analogy with carbon particles which were used to estimate the eddy diffusivity. Although the method showed major weaknesses, the average value of NO_x deposition velocity (0.0014 ± 0.0024 m s^{-1}) was in the range of literature values, which is from 0.0010 m s^{-1} to 0.0067 m s^{-1}.

The results of NO_2 measurements and the modelling of the dispersion and dry deposition processes provide an understanding that dispersion plays a dominant role in reducing pollutant concentrations in urban parks. The methods developed in this research have a useful potential role in the urban planning process with respect to the location of urban greenspace and parks. Special consideration needs to be given to the distance from major roads and the location with respect to prevailing wind direction.

"Indeed, in the creation of the heavens and the earth and in the alternation of night and day, and in the ships which sail through the sea with that which benefits people, and in the water which Allah sends down from the sky, giving life thereby to the earth after its lifelessness and dispersing therein every (kind of) moving creature, and [His] directing of the winds and the clouds controlled between the heaven and the earth – are indeed Signs for the people who use reason"

(Al Quran 2:164)

Acknowledgement

First and foremost, praise and thanks to Allah, the Almighty for giving me the opportunity, determination, help, knowledge, and strength to do this research and to complete it.

There are a lot of thanks due to people and associations.

I would like to express my sincere gratitude to my supervisors: Professor Roy M Harrison for his patience and excellent guidance, input, feedback, and support during my PhD and for the intense meetings leading to the submission of this thesis; my sincere thanks also go to Professor Zongbo Shi for the encouragement, support, and excellent guidance he has given.

I would like to thank Birmingham City Council for giving me permission to conduct the research at Cannon Hill Park and Tile Cross Park. Special thanks to Mr Nick Grayson, Climate Change and Sustainability Manager; Mr Mike Hinton, Parks Development Manager; Mr Paul Gallagher, ranger support officer, and his team; and Mr Mark Wolstencroft, Head of Environmental Protection Unit. Thanks also go to Mr Garry Dalton, District Engineer of Edgbaston Road area, and Mr Alan Porter, Senior Service Manager for the Tile Cross area, for their permission to place the diffusion sampling tubes on lamp posts near the roads.

I would like to thank the Royal Parks management team for giving me permission to carry out air quality sampling at Hyde Park, especially to Mr Ian Nightingale, a technical officer from Hyde Park, for his assistance during the sampling period, and to Ms Julia Balfour, Head of Ecology of The Royal Parks.

Thanks to the University of Birmingham for giving permission to undertake the sampling collection at the UoB campus and Biosciences building; to Mr Kevin Mangan and the office team from the Estate Department; to Mr Jared Smith, college buildings and facilities manager; to Mr Dom Hickey, Health & Safety Manager LES. Special thanks to Mr Dean Scranage for his assistance and for providing the letter of permission every time I needed access to the roof.

I am also thankful and indebted to Dr Louisa Kramer, Dr Leigh Crilley, Dr Tara Rasoul, and Dr Roberto Sommariva for their support, knowledge sharing, and for the technical assistance on NO_x and O_3 instruments. They are a team under the supervision of Professor Bill Bloss, who I would like to thank for allowing me to work in and use the facilities at Wolfson Lab. Thanks also to Dr David Beddows for the advice and help given in setting the container for the instruments at Biosciences, and James Brean for assistance with the micro-aethalometer instrument.

I would like to acknowledge and say thanks to Professor Grant Allen from The University of Manchester and Professor Rob MacKenzie for taking the time to examine this thesis and for their feedback which has helped to improve it.

Thanks to the CERC team, specially to James Oneill for all the discussion and to the helpdesk team for their quick response when answering my emails.

Many thanks to Mary Harding for her kind advice and all the support on administrative matters through my PhD years. Thanks also go to Gretchel Coldicott and Rosie for administration support and general help given.

I would also like to thank Jamie Pert, Richard, and Nicholas Davidson “Nick” for their assistance; Andy and Steve from the Biosciences workshop team for giving me the place to do a deployment of my diffusion tubes on their working area; Dr Maria Thompson and Dr Eimear Orgill for help on the laboratory works.

I thank all my colleagues, Tara, Indrani, Clarissa, Jeremy, James, Ed Bannister, Karn, Ying, Jiali, Agung, Nezha, Maryam, Ruixin, Ulku; thanks for the discussions, ideas, and kind help during my study. Thanks also to Chai, Muchtar, Sulaiman, Declan, and all friends at the UoB. I will never forget the joy, discussions and refreshing moments being with you all. Special thanks to Tara and her family for their generosity and making me feel at home.

This study was funded by Riset-Pro, from the Ministry of Research and Technology, The Republic of Indonesia. Thank you for giving me the opportunity to do this research. Thanks to the management of National Standardization Agency of Indonesia, for helping me to pursue my dream!

This thesis was copy edited for conventions of grammar by The PhD Proofreaders Ltd.

My deepest gratitude to mom and dad for the prayers and the unconditional love. Thanks to my sisters Dian and Desi for all the support and the encouragement. I cannot thank you all enough. Special thanks for my husband, Radityo Aribowo, who always supports me. Thank you for all the love, sacrifices, trust, and honour. Thank you for giving me a hand in the fieldwork. The fieldwork is more colourful with you by my side.

Alhamdulillah.

Table of Contents

Abstract i
Acknowledgement iii
Table of Contents v
List of Figures viii
List of Tables xvii
Chapter 1. Introduction 1
1.1. Background 1
1.2. Air pollution sources and pathways in the atmosphere 3
1.2.1. Nitrogen oxides (NO_x = NO + NO_2) 3
1.2.2. Ozone (O_3) 7
1.2.3. Black Carbon (BC) 8
1.3. Dispersion and deposition processes of atmospheric pollutants 8
1.4. Urban Green Space 13
1.5. What is the benefit of parks for air quality? 15
1.6. Measurement of pollutant and modelling 18
1.6.1. Measurement 18
1.6.2. Air quality modelling 19
1.7. Research objectives 23
1.8. Thesis structure 24
Chapter 2. Materials and Methodology 25
2.1. Introduction 25
2.2. Measurement Uncertainty 27
2.2.1. Uncertainty Analysis 27
2.2.2. Uncertainties in measurement using automatic analyser 28
2.2.3. Uncertainties in measurement using diffusion tubes 29
2.3. Oxides of nitrogen and ozone in urban green space 32
2.3.1. Diffusion tubes 33
2.3.2. Automatic analyser 45
2.3.3. Sampling locations 48
2.4. The set up and evaluation of dispersion modelling 54
2.4.1. Setup 55
2.4.2. Source 56
2.4.3. Meteorology 56

2.4.4. Background 56
2.4.5. Grids 57
2.4.6. Output 57
2.4.7. Dry deposition 57
2.5. Deposition velocity of gases from vertical gradient of pollutant concentrations 59
2.5.1. Sampling instrumentation 61
2.5.2. Sampling location 62
Chapter 3. Oxides of Nitrogen and Ozone in Urban Greenspace 64
3.1. Introduction 65
3.2. Methods 66
3.2.1. Monitoring sites using automatic analysers 66
3.2.2. Monitoring sites using passive diffusion tube samples 66
3.2.3. Statistical analysis 67
3.3. Results and discussion 69
3.3.1. Diffusion tube evaluation 69
3.3.2. Measurement of NO_2 concentration in urban green space 82
3.3.3. Statistical analysis 104
3.4. Limitation of the study 111
3.5. Summary 111
Chapter 4. The Set Up and Evaluation of Dispersion Modelling 113
4.1. Introduction 113
4.2. Method 114
4.2.1. Model input and output 117
4.2.2. Statistical evaluation 121
4.3. Results and discussion 122
4.3.1. Observation data from automatic analyser 122
4.3.2. Input variables in the ADMS-Roads model 124
4.3.3. Sensitivity analysis 129
4.3.4. Modelling output 154
4.4. Limitation of the study 177
4.5. Summary 178
Chapter 5 Deposition Velocity of Gases from Vertical Gradient of Pollutant Concentrations 180
5.1. Introduction 180
5.2. Method 182
5.3. Results and discussion 183
5.3.1. Profiles of pollutant concentrations at the roof and the ground 183

5.3.2. Aspect ratio and influence of wakes in the courtyard of the Biosciences building 193
5.3.3. Meteorological observations 197
5.3.4. Literature describing experiments on measuring dry deposition and deposition velocity 200
5.3.5. Deposition velocity of NO_x 207
5.4. Limitation of the study 217
5.5. Summary 217
Chapter 6. Conclusion and Recommendations for Future Research 219
6.1. NO_2 in urban green space 219
6.1.1. Conclusion 219
6.1.2. Recommendations for Future Research 220
6.2. The set up and evaluation of dispersion modelling 220
6.2.1. Conclusion 220
6.2.2. Recommendations for Future Research 222
6.3. Deposition velocity of gases from vertical gradient of pollutant concentrations 222
6.3.1. Conclusion 222
6.3.2. Recommendations for Future Research 222
6.4. Summary 223
Appendix 224
References 295

List of Figures

Figure 1.1. Photochemical air pollution, from emission to deposition (National Research Council, 1992) 2
Figure 1.2. Sources of NO_x emissions in the City of London in year 2011 (Duffield, 2011) 5
Figure 1.3. Air pollution pathways in the atmosphere (Adopted from Mayer, 1999) 9
Figure 1.4. Gaussian plume (Vallero, 2019) 10
Figure 1.5. Resistance model in dry deposition (Seinfeld and Pandis, 2016) 11
Figure 1.6. Leaf section (Vallero, 2019) 11
Figure 1.7. Green space position in an urban area (Swanwick *et al*., 2003) 14
Figure 1.8. Comparison of trendlines calculated using ADMS Roads and CALINE4 (Ellis *et al.*, 2001) 20
Figure 1.9. Input, process, and output of ADMS-Roads (CERC, 2017) 23
Figure 2.1. Fishbone diagram in reviewing variables of the uncertainties from diffusion tubes measurement, (adopted from: Hamilton and Heal, 2004; Targa and Loader, 2008; Cape, 2009; Heal *et al*., 2019) 29
Figure 2.2. Map with markers that shows location of BROS, EROS and city centre in Birmingham, UK (https://www.google.com/maps/place/University+of+Birmingham/@52.4592561,-1.9598751,12z) 32
Figure 2.3. Picture of Spectrometer Jenway 6800 33
Figure 2.4. **(a)** NO_2 diffusion tube with open end; and **(b)** components of diffusion tube with open end consist of an acrylic tube, two stainless steel grids and two caps 34
Figure 2.5. **(a)** NO_2 diffusion tube with membrane; and **(b)** components of diffusion tube with membrane consist of an acrylic tube, two stainless steel grids, two caps and additional stainless steel #60 meshes in the open cap 35
Figure 2.6. The shock-proof dial vernier caliper was used to measure component of diffusion tube 36
Figure 2.7. NO_x diffusion tube components with membrane consist of an acrylic tube, two stainless steel grids, a spacer, a filter, two caps, and a stainless steel #60 meshes in the open cap, ... 41
Figure 2.8. Schematic diagram showing NO_x DT deployment 41
Figure 2.9. Schematic diagram of NO_x analyser (Thermoscientific, 2007) 46
Figure 2.10. Schematic diagram of O_3 analyser (Thermoscientific, 2017) 47
Figure 2.11. Ideal design of placing diffusion tubes at an axis perpendicular from roadside 48
Figure 2.12. Location of diffusion tube at Cannon Hill Park 50
Figure 2.13. Location of Tile Cross Park 50
Figure 2.14. Map of Tile Cross Park which location of diffusion tubes divided into two groups. Group 1 is TL 8, TL 9, TL 10, TL 11, TL 12 and TL 13; Group 2 is TL 2, TL 3, TL 4, TL 5, TL 6, TL, 7, TL 14, TL 15. 51
Figure 2.15. Map showing the location of DT at BROS, EROS and other locations at the University of Birmingham site 52
Figure 2.16. Map of Biosciences building with diffusion tube locations and automatic analyser locations. A, B, C were DT location on the roof, X and Y were DT on the ground. The blue dot was instrument location on the roof and purple dot was instrument location on the ground. 53
Figure 2.17. Map location of DT at Hyde Park, London (map source: https://www.royalparks.org.uk/__data/assets/pdf_file/0005/41639/hydepark_english_map.pdf) 54
Figure 2.18. The interface of ADMS-Roads screen (CERC, 2017) 55
Figure 2.19. The interface of ADMS-Roads with the model options **(a)** chemistry, **(b)** chemistry and dry deposition (CERC, 2017) 58

Figure 2.20. Picture of micro-aethalometer AE51 61
Figure 2.21. Illustration of park / grassland area in the Biosciences building 62
Figure 2.22. Map of Biosciences building showing the location of the open park and the instruments at **(a)** the roof, **(b)** and ground sites 63
Figure 3.1. A schematic of the broader sampling approach and sites. The blue line is the identification of measurements using an automatic analyser to measure air pollutants (NO_2 and O_3), and the orange line is the identification of measurements using diffusion tubes to measure air pollutants at the sampling locations. 64
Figure 3.2. NO_2 concentrations were measured by diffusion tubes with open end (orange line), diffusion tubes with membrane (green line) and automatic analyser (blue dashed line) at EROS and BROS for the period August 2016 – April 2018. Measurements numbered 1 to 28 were conducted at the EROS site, while 29 to 37 were measured at the BROS site due to refurbishment of the EROS site, and 38 to 39 were measured at the EROS site (trailer cabin). A diffusion tube with stainless steel mesh at the end as a membrane was used starting on 15 October 2017 (no. 32). NO_2 concentrations at each point are presented as mean concentration and standard deviation (mean ± SD). The x-axis shows the samples number that represents sampling period of number as data points, and the y-axis, NO_2 concentrations in µg m^{-3} from diffusion tubes with open end (orange), diffusion tubes with membrane (green) and automatic analysers (blue). Error bars for the diffusion tubes show standard deviation from triplicate of diffusion tubes, and error bars for the automatic analysers, uncertainty was estimated as 10% from each measured mean concentration for NO_x instruments (Stevenson *et al.*, 2009). 70
Figure 3.3. Reduced Major Axis (RMA) regression model **(a)** between NO_2 automatic analyser and NO_2 concentration from diffusion tubes with open end for the period August 2016 to April 2018 (N=39 samples); and **(b)** between NO_2 automatic analyser and NO_2 concentration from diffusion tubes with membrane for the period October 2017 to April 2018 (N=8 samples). The green dots are samples, blue dashed line is the RMA regression line and the grey lines indicate the upper and lower limits of the 95% confidence intervals. The inverse of the equation is used to correct the DT measurement. The NO_2 concentration adjustment for DT with open end was True NO_2 = (DT_NO_2 + 1.048) / 0.978, and for DT with membrane was True NO_2 = (DT_NO_2 + 20.64) / 1.402. 74
Figure 3.4. Comparison of exposure time of NO_2 concentration in µg m^{-3} measured by automatic analysers (x-line) and diffusion tubes measurement (y-line) for **(a)** 2-week, **(b)** 3-week, **(c)** 4-week, and **(d)** 6-week periods 76
Figure 3.5. NO_x, NO and NO_2 concentrations from diffusion tubes along with automatic analysers on the roof and the ground of the Biosciences building. **(a)** NO_x concentrations on the roof and the ground from diffusion tubes and automatic analysers. **(b)** NO concentrations on the roof and the ground from diffusion tubes and automatic analysers. **(c)** NO_2 concentrations on the roof and the ground from diffusion tubes and automatic analysers. The blue box with the dashes is concentration of pollutants (NO_x, NO and NO_2) from automatic analysers on the roof; the blue dot with lines is concentration of pollutants (NO_x, NO and NO_2) from diffusion tubes on the roof; the orange box with dashes is concentration of pollutants (NO_x, NO and NO_2) from automatic analysers on the ground; and the orange dot with lines is concentration of pollutants (NO_x, NO and NO_2) from diffusion tubes on the ground. Standard deviation of automatic analyser was estimated as 10% of the mean (Stevenson *et al.*, 2009) and standard deviation of diffusion tubes was generated from triplicate measurement. 77
Figure 3.6. Comparison of O_3 concentration from diffusion tubes and O_3 automatic analysers, in four different locations at BROS, EROS, and the roof and ground of the Biosciences building. 79

Figure 3.7. O_3 concentration at UoB sites from the BROS site (3.6 m from A38 road) to H site (1093.6 m from A38 road), from five sampling times 80
Figure 3.8. O_3 concentrations at Cannon Hill site from CH1 (at 1.5 m from Edgbaston road) into the park (689 m from Edgbaston Road), from five sampling times 80
Figure 3.9. O_3 concentrations on the roof and the ground of Biosciences site, at three sampling times 81
Figure 3.10. Pattern of NO_2 concentration with respect to distance from the road to the inside of Cannon Hill Park (sampling period October 2016 – November 2017) using diffusion tubes with open end with bias adjustment, True NO_2 = (DT_NO_2 + 1.048) / 0.978. The blue dots represent the mean NO_2 concentration at each sampling point in the sampling period and error bars represent standard deviation (N = 24 data points). The line of best fit used in the graph was a logarithmic trendline obtained from mean data. 82
Figure 3.11. Pattern of NO_2 concentration with respect to distance from the road to the inside of Cannon Hill Park (sampling period November 2017 – January 2019) using diffusion tubes with membrane with bias adjustment, True NO_2 = (DT_NO_2 + 20.64) / 1.402. The blue dots represent the mean NO_2 concentration at each sampling point in the sampling period and error bars represent standard deviation (N = 13 data points). The line of best fit used in the graph was a logarithmic trendline obtained from mean data. 83
Figure 3.12. NO_2 concentrations at 13 locations (CH1 to CH12) in the Cannon Hill Park from October 2016 to November 2017. **(a)** The blue line represents a site near the road (CH1), while other lines (CH12, CH11, CH2, CH3, CH10, CH4, CH5, CH6, CH7, CH8 and CH9) represent sampling sites that are spread at various locations in the park. NO_2 concentrations at each point are presented as mean concentration and standard deviation (mean ± SD) from triplicate diffusion tubes. **(b).** NO_2 concentrations inside the park (CH12, CH11, CH2, CH3, CH10, CH4, CH5, CH 6, CH7, CH8 and CH9) are plotted as a single line (green line), and plotted with NO_2 at near road (CH1) (orange line) during sampling period, October 2016 to November 2017. NO_2 concentrations near the road are presented as mean concentrations and error bars represent standard deviation from triplicate diffusion tubes (mean ± SD). NO_2 concentrations inside the park are presented as mean concentrations and error bars represent standard deviations at sampling points inside the park (N== 11 data points). 85
Figure 3.13. NO_2 concentrations at 13 locations (CH1 to CH12) in the Cannon Hill Park from November 2017 to January 2019. **(a)** The blue line represents a site near the road (CH1), while other lines (CHX, CH12, CH11, CH2, CH3, CH10, CH4, CH5, CH7 and CH9) represent sampling sites that are spread at various locations in the park. NO_2 concentrations at each point are presented as mean concentration and standard deviation (mean ± SD) from triplicate diffusion tubes. **(b).** NO_2 concentrations inside the park (CH12, CH11, CH2, CH3, CH10, CH4, CH5, CH 6, CH7 and CH9) are plotted as a single line (green line), and plotted with NO_2 at near road (CH1) (orange line) during sampling period, November 2017 to January 2019. NO_2 concentrations near the road are presented as mean concentrations and error bars represent standard deviation from triplicate diffusion tubes (mean ± SD). NO_2 concentrations inside the park are presented as mean concentrations and error bars represent standard deviations at sampling points inside the park (N== 10 data points). 86
Figure 3.14. NO_2 concentration based on seasonality (during spring, summer, autumn and winter), at Cannon Hill Park, from October 2016 to January 2019. Orange bars represent mean NO_2 concentration near road (sampling site CH1), while green bars show mean NO_2 concentration in the park (sampling site CH 7). Error bars represent standard error of the mean. 87
Figure 3.15. NO_2 ambient concentration at Hyde Park, London, on a transect **(a)** from Victoria Gate Shrubbery (VGS) to Rangers Lodge (RL) and the Dell (TD), and **(b)** from Cumberland Gate Lodge (CGL) to Rangers Lodge (RL) and Bowling Green (BG). The blue dots represent the mean NO_2 concentration at each sampling point during the sampling period

and error bars represent the standard deviation (N = 16 data points). The line of best fit used in the graph is a polynomial order 2 trendline through mean data. Diffusion tube bias adjustment, True NO_2 = (DT_NO_2 + 1.048) / 0.978. 89
Figure 3.16. NO_2 concentrations at 5 locations in the Hyde Park monitoring sites from December 2016 to December 2017. **(a)** The blue dash line represents a location in the park (RL), while other lines are roadsides at four locations (VGS, TD, CGL and BG) around the park. NO_2 concentrations at each point are presented as mean concentration and standard deviation (mean ± SD) from triplicate diffusion tubes. **(b)** NO_2 concentrations near the roadsides are plotted as a single line (orange line) and compared with NO_2 inside the park (green line). NO_2 concentrations in the park are presented as mean concentrations and error bars represent standard deviation from triplicate diffusion tubes (mean ± SD). NO_2 concentrations near the roads are presented as mean concentrations and error bars represent standard deviations at sampling points (N= 4 data points). 90
Figure 3.17. NO_2 concentration based on seasonality (during spring, summer, autumn and winter), at Hyde Park, from December 2016 to December 2017. Orange bars represent mean NO_2 concentration near the road (CGL site), while the green bars show mean NO_2 concentration in the park (RL site). Error bars represent standard error of the mean. 91
Figure 3.18. The pattern of NO_2 concentration to distance from the roadside into Tile Cross Park (sampling period October 2016 – July 2017) using diffusion tubes with open end with bias adjustment, True NO_2 = (DT_NO_2 + 1.048) / 0.978. The blue dots represent the mean NO_2 concentration at each sampling point in the sampling period and error bars represent standard deviation (N = 14 data points). The line of best fit used in the graph was a logarithmic trendline obtained from mean data. 92
Figure 3.19. NO_2 concentrations at 15 locations at Tile Cross Park during October 2016 to July 2017. **(a)** The blue line represents a location near the road (TL1), and others (TL2 to TL15) represent sampling sites in the Tile Cross Park. NO_2 concentrations at each point are presented as mean concentration and standard deviation (mean ± SD) from triplicate diffusion tubes. **(b)** NO_2 concentrations inside the park are plotted as a single line (green line) and compared with NO_2 near the road (orange line). NO_2 concentrations near the road are presented as mean concentrations and error bars represent standard deviation from triplicate diffusion tubes (mean ± SD). NO_2 concentrations in the park are presented as mean concentrations and error bars represent standard deviations at sampling points (N== 14 data points). 93
Figure 3.20. Map shows distance of diffusion tube location at TL 1 near bus station and the kerbside 94
Figure 3.21. NO_2 concentrations near the main road (orange) are compared with NO_2 inside park as group 1, location near road (blue dash) and inside the park as group 2, location near residential area (purple dot). NO_2 concentrations near the road are presented as mean concentrations and error bars represent standard deviation from triplicate diffusion tubes (mean ± SD). NO_2 concentrations in the park are presented as mean concentrations and error bars represent standard deviations at sampling points (N Group 1 = 6 data points; N Group 2 = 8 data points). 95
Figure 3.22. NO_2 concentration based on seasonality (during spring, summer, autumn and winter), at Tile Cross Park, from October 2016 to July 2017. Orange bars represent mean NO_2 concentration near the road (sampling site TL 1), while the green bars show mean NO_2 concentration in the park (sampling site TL 4). Error bars represent standard error of the mean. 95
Figure 3.23. The pattern of NO_2 concentration with respect to distance from the road at BROS moving towards the background site at the EROS location inside the University of Birmingham (sampling period November 2016 to November 2017) using diffusion tubes with open end with bias adjustment, True NO_2 = (DT_NO_2 + 1.048) / 0.978. The blue dots

represent the mean NO_2 concentration at each sampling point in the sampling period and error bars represent standard deviation (N = 20 data points). The line of best fit used in the graph was a logarithmic trendline obtained from mean data. 96
Figure 3.24. The pattern of NO_2 concentration to distance from the road at BROS moving towards the background site at EROS location inside the University of Birmingham (sampling period October 2017 to January 2019) using diffusion tubes with membrane with bias adjustment, True NO_2 = (DT_NO_2 + 20.64) / 1.402. The blue dots represent the mean NO_2 concentration at each sampling point in the sampling period and error bars represent standard deviation (N = 18 data points). The line of best fit used in the graph was a logarithmic trendline obtained from mean data. 97
Figure 3.25. NO_2 concentrations at 12 locations in the University of Birmingham monitoring site from November 2016 to November 2017. **(a)** The blue line represents a site near the road (BROS), while other lines represent sampling sites that are spread at various locations in the park. NO_2 concentrations at each point are presented as mean concentration and standard deviation (mean ± SD) from triplicate diffusion tubes. **(b)**. NO_2 concentrations measurement data in green area (B, C, J, F, EROS, G sites) are plotted as a single line (green line) and compared with NO_2 near the road (orange line), from November 2016 to November 2017. NO_2 concentrations near the road are presented as mean concentrations and error bars represent standard deviation from triplicate diffusion tubes (mean ± SD). NO_2 concentrations inside the park are presented as mean concentrations and error bars represent standard deviations at sampling points inside the park (N== 20 data points). 99
Figure 3.26. **(a)** NO_2 concentrations at 12 locations (CH1 to CH12) in the University of Birmingham monitoring site from October 2017 to January 2019. NO_2 concentrations at each point are presented as mean concentration and standard deviation (mean ± SD) from triplicate diffusion tubes. **(b)** NO_2 concentrations measurement data in green area (B, C, F, EROS, G sites) are plotted as a single line (green line) and compared with NO_2 near the road (orange line), from October 2017 to January 2019. NO_2 concentrations near the road are presented as mean concentrations and error bars represent standard deviation from triplicate diffusion tubes (mean ± SD). NO_2 concentrations inside the park are presented as mean concentrations and error bars represent standard deviations at sampling points inside the park (N== 20 data points). 100
Figure 3.27. NO_2 concentration based on seasonality (during spring, summer, autumn and winter), at the University of Birmingham, from November 2016 to January 2019. Orange bars represent mean NO_2 concentration near the road (BROS), while the green bars show mean NO_2 concentration in the park (EROS). Error bars represent standard error of the mean. .. 101
Figure 3.28. Boxplot of NO_2 concentrations at BROS and EROS site, November 2016 to January 2019 (N = 38). Top of box plot represents the 75^{th} percentile; bottom of box plot represents the 25^{th} percentile; mean is the x sign in each box; median is the solid line in each box; whiskers above and below represent 90^{th} and 10^{th} percentiles. 102
Figure 3.29. NO_2 concentrations at ground (green line) compared with NO_2 at the roof (orange line). Each point represents the mean NO_2 concentration in the sampling period and error bars represent the standard deviation from diffusion tubes. 103
Figure 3.30. Boxplot of NO_2 concentrations at roof and ground floor, Biosciences building, December 2017 to May 2018 (N roof = 17, and N Ground = 12). Top of box plot represents the 75^{th} percentile; bottom of box plot represents the 25^{th} percentile; mean is the x sign in each box; median is the solid line in each box; whiskers above and below represent 90^{th} and 10^{th} percentiles. 103
Figure 4.1. Licensed vehicle composition in **(a)** Birmingham, and **(b)** London, UK, in 2018. The highest percentage of vehicles (licensed) come from cars (Adopted from Table VEH0105: Licensed vehicles at the end of the year by body type and upper and lower tier local

authority, including diesel cars and vans, United Kingdom in 2018, from Department for Transport, (DfT, 2020)) 114
Figure 4.2. Flow chart of ADMS-Roads modelling 118
Figure 4.3. Concentrations of **(a)** NO, **(b)** NO_2, **(c)** NO_x, and **(d)** O_3 at two different sites, BROS (blue line) and EROS (red dash) on 2-11 February 2018 123
Figure 4.4. Demarcating the segments on the map of sampling location, the University of Birmingham 126
Figure 4.5. Vehicle traffic factors on weekdays (blue line), Saturday (orange line) and Sunday (grey line). Traffic factors were generated from the time-varying emission factor (TRA 0307 in 2018) by dividing the number of vehicles on weekdays, Saturday and Sunday for each hour with average daily flow of the week (Monday to Sunday). Refer to Appendix 4.4 (data adopted from Table TRA 0307 in 2018, Motor vehicles traffic distribution by time of day and day of the week on all roads Great Britain, Department for Transport, (DfT, 2019b)) 127
Figure 4.6. Number of vehicles per hour at roads near the University of Birmingham refer to Appendix 4.5, Table A.4.5.8. Resume data of traffic flows in 2018 (adopted from observation data and Traffic count ID data from Department for Transport (DfT, 2019a)) 128
Figure 4.7. Map and location of weather stations near sampling sites (http://maps.google.com/) 132
Figure 4.8. Comparison of modelled and measured NO_2 concentration from different weather stations at receptor locations. The x-axis represents the distance in metres from the road near BROS site (A38 road) and y-axis is NO_2 concentration in µg m^{-3}. 132
Figure 4.9. Comparison of modelled and measured O_3 concentration from different weather stations at receptor locations. The x-axis represents the distance in metres from the road near BROS site (A38 road) and y-axis is O_3 concentration in µg m^{-3}. 134
Figure 4.10. Comparison of wind rose from different weather stations, 2-11 February 2018 135
Figure 4.11. Comparison of wind speed from different weather stations 136
Figure 4.12. Wind rose (wind speed and wind direction) plot of **(a)** Winterbourne No.2 – BUCL, and **(b)** Coundon weather station. Data from January 2016 to June 2018, and **(c)** linear regression of wind speed from Winterbourne No.2 – BUCL and Coundon. 137
Figure 4.13. Windrose plots from **(a)** Winterbourne No.2, **(b)** Coundon after implementing the correction factor of wind speed data for Coundon ($x = (y - 0.5464) / 1.5101$), and **(c)** linear regression from Coundon after implementing the correction factor. 138
Figure 4.14. Comparison of temperature from different weather stations 139
Figure 4.15. Cloud cover from Coleshill weather station 140
Figure 4.16. Comparison of relative humidity from different weather stations 140
Figure 4.17. Location of urban background sites from AURN monitoring station in Birmingham 141
Figure 4.18. **(a)** NO_x concentration at EROS (green line) and Birmingham Acocks Green (light brown line) sites; and **(b)** wind direction (blue circle) and wind speed (orange triangle) from Winterbourne No. 2 UoB at sampling date, 2-11 February 2018 142
Figure 4.19. NO_2 concentration at EROS (green line) and Birmingham Acocks Green (light brown line) sites, 2-11 February 2018 143
Figure 4.20. O_3 concentration at EROS (green line) and Birmingham Acocks Green (light brown line) sites, 2-11 February 2018 143
Figure 4.21. Measured (blue line) and modelled (orange line) NO_2 concentration at EROS sites using background concentration from **(a)** EROS site, and **(b)** Birmingham Acocks Green 144
Figure 4.22. Comparison between measured NO_x concentrations (red line) and modelled NO_x concentrations (blue dash line) at BROS, and their linear regression from different settings for minimum speed at **(a)** 5 km h^{-1}, **(b)** 8 km h^{-1}, and **(c)** 10 km h^{-1} 148
Figure 4.23. Measured NO_2 concentrations (red line) and modelled NO_2 concentrations (blue dash line) at BROS and the linear regression from speed setting at 10 km h^{-1} 149

Figure 4.24. Comparison between measured NO_2 concentrations (red line) and modelled NO_2 concentrations (blue dash line) at BROS, and their linear regression from different settings for the NO_2:NO_x ratio at **(a)** 10% , **(b)** 15% , and **(c)** 20% 151
Figure 4.25. Percent reduction of NO_x (orange dotted line), NO_2 (blue dotted line) and O_3 (grey dotted line) concentrations at various settings of NO_x deposition velocities (0.001 to 0.0067 m s^{-1}) and at the same value of NO_2 and O_3 deposition velocities, 0.002 m s^{-1} and 0.004 m s^{-1}, respectively 152
Figure 4.26. Graph of measured and modelled concentrations of NO_2 and NO_x at BROS and EROS sites 155
Figure 4.27. Wind rose pattern from the sampling period 2-11 February 2018 155
Figure 4.28. Modelled NO_x concentration at perpendicular location from chemistry (blue line) and chemistry with dry deposition model (orange triangle), 2-11 February 2018 156
Figure 4.29. Modelled NO_2 concentration at perpendicular location from chemistry (blue line) and chemistry with deposition model (orange triangle), 2-11 February 2018 157
Figure 4.30. Modelled O_3 concentration at perpendicular location from chemistry (blue line) and chemistry with deposition model (orange triangle), 2-11 February 2018 157
Figure 4.31. Road sources and receptors at University of Birmingham as shown by ADMS Mapper. The blue line identifies the road sources, and green squares identify the receptors, where diffusion tubes were located. 158
Figure 4.32. Modelled and measured NO_2 concentration from diffusion tube data, 18 March – 15 April 2018. This table shows **(a)** information of background concentration from automatic analysers from EROS; **(b)** wind rose from meteorology data; **(c)** information of meteorology data input; **(d)** background concentration input in the model at the first run, and conversion unit of NO_2 concentration from ppb to µg m^{-3}; **(e)** graph of modelled NO_2 concentration from first run of model, measured NO_2 DT and NO_2 from analyser at EROS; **(f)** regression line and equation from measured NO_2 DT and modelled NO_2 concentration from first run; **(g)** adjusted NO_2 background concentration; **(h)** graph of modelled NO_2 concentration from second run of model, measured NO_2 DT and NO_2 from analyser at EROS; **(i)** regression line and equation from measured NO_2 DT and modelled NO_2 concentration from second run. 162
Figure 4.33. Modelled and measured NO_2 concentration from diffusion tube data, 15 April – 13 May 2018. This table shows **(a)** information of background concentration from automatic analysers from EROS; **(b)** wind rose from meteorology data; **(c)** information of meteorology data input; **(d)** background concentration input in the model at the first run, and conversion unit of NO_2 concentration from ppb to µg m^{-3}; **(e)** graph of modelled NO_2 concentration from first run of model, measured NO_2 DT and NO_2 from analyser at EROS; **(f)** regression line and equation from measured NO_2 DT and modelled NO_2 concentration from first run; **(g)** adjusted NO_2 background concentration; **(h)** graph of modelled NO_2 concentration from second run of model, measured NO_2 DT and NO_2 from analyser at EROS; **(i)** regression line and equation from measured NO_2 DT and modelled NO_2 concentration from second run. 165
Figure 4.34. Modelled and measured NO_2 concentration from diffusion tube data, 21 October – 20 November 2018. This table shows **(a)** information of background concentration from automatic analysers from Biosciences site; **(b)** wind rose from meteorology data; **(c)** information of meteorology data input; **(d)** background concentration input in the model at the first run, and conversion unit of NO_2 concentration from ppb to µg m^{-3}; **(e)** graph of modelled NO_2 concentration from first run of model, measured NO_2 DT and NO_2 from analyser at Biosciences site; **(f)** regression line and equation from measured NO_2 DT and modelled NO_2 concentration from first run; **(g)** adjusted NO_2 background concentration; **(h)** graph of modelled NO_2 concentration from second run of model, measured NO_2 DT and NO_2 from analyser at Biosciences site; **(i)** regression line and equation from measured NO_2 DT and modelled NO_2 concentration from second run. 168

Figure 4.35. Modelled and measured NO_2 concentration from diffusion tube data, 20 – 28 November 2018. This table shows **(a)** information of background concentration from automatic analysers from Biosciences site; **(b)** wind rose from meteorology data; **(c)** information of meteorology data input; **(d)** background concentration input in the model at the first run, and conversion unit of NO_2 concentration from ppb to µg m^{-3}; **(e)** graph of modelled NO_2 concentration from first run of model, measured NO_2 DT and NO_2 from analyser at Biosciences site; **(f)** regression line and equation from measured NO_2 DT and modelled NO_2 concentration from first run; **(g)** adjusted NO_2 background concentration; **(h)** graph of modelled NO_2 concentration from second run of model, measured NO_2 DT and NO_2 from analyser at Biosciences site; **(i)** regression line and equation from measured NO_2 DT and modelled NO_2 concentration from second run. 172
Figure 4.36. Modelled and measured NO_2 concentration from diffusion tube data, 28 November 2018 – 6 January 2019. This table shows **(a)** information of background concentration from air monitoring site at Birmingham Acocks Green; **(b)** wind rose from meteorology data; **(c)** information of meteorology data input; **(d)** background concentration input in the model at the first run, and conversion unit of NO_2 concentration from ppb to µg m^{-3}; **(e)** graph of modelled NO_2 concentration from first run of model, measured NO_2 DT and NO_2 from air monitoring data; **(f)** regression line and equation from measured NO_2 DT and modelled NO_2 concentration from first run; **(g)** adjusted NO_2 background concentration; **(h)** graph of modelled NO_2 concentration from second run of model, measured NO_2 DT and NO_2 from air monitoring data; **(i)** regression line and equation from measured NO_2 DT and modelled NO_2 concentration from second run. 175
Figure 5.1. BC concentration in µg m^{-3} at the roof (blue line) and the ground (orange line) of the Biosciences building, sampling period from 1 May to 29 November 2018 183
Figure 5.2. BC concentration in µg m^{-3} at the roof (blue line) and the ground (orange line) of the Biosciences building, sampling period from 23 January to 2 March 2019 184
Figure 5.3. NO, NO_2 and O_3 concentrations in ppb at the roof (solid line) and on the ground (dashed line), 20 – 29 November 2018 185
Figure 5.4. NO, NO_2 and O_3 concentrations in ppb at the roof (solid line) and on the ground (dashed line), 23 January – 2 March 2019 186
Figure 5.5. **(a)** NO_x concentration in ppb at the roof (blue colour) and the ground (orange colour) as an example of the storage phenomenon in the quadrangle site caused by the storage of clean air from the dataset on 30-31 January 2019 at 1 hour mean from 13:00 to 01:00; and **(b)** storage of polluted air from the dataset on 3-4 February 2019 at 1 hour mean from 13:00 to 01:00. Error bar of the automatic analysers, uncertainty was estimated as 10% from each measured mean concentration for NO_x instruments (Stevenson *et al.*, 2009). 189
Figure 5.6. Schematic diagram of the courtyard of the Biosciences building (≈) and locations of surrounding buildings. Symbols H, W, L correspond to the building height, building width and building length, respectively. No scale for this diagram. 193
Figure 5.7. Trees locations in the courtyard of Bioscience building. **(a)** Trees locations at the grassland area; **(b)** Schematic diagram of canopy dimensions (Verma *et al.*, 2016); **(c)** information of each tree with identification number, crown length, trunk height and tree height in meter; **(d)** pictures of trees location, number 1 to 4; **(e)** pictures of trees location, number 5 to 10; and **(f)** picture of tree location, number 11. 195
Figure 5.8. Schematic diagram shows how trees influence air circulation in the courtyard of the Biosciences site. The increased turbulence due to the air flows through the branches of tree that generates turbulence, and the decreased turbulence due to the existence of tree is blocking the flows (Adapted from Oke, 2002; AQEG, 2018). 196
Figure 5.9. Logarithmic wind profiles over stability variation (Koleiny, 2009). 198

Figure 5.10. Wind speed on the roof (blue line) and ground (orange line) at the Biosciences building. The observation was conducted for 1-hour in 9 days (10 observation points), 13 to 29 May 2019 198
Figure 5.11. The temperature on the roof (blue line) and ground (orange line) at the Bioscience building. The observation was conducted for 1-hour in 9 days (10 observation points), 13 to 29 May 2019 199
Figure 5.12. Mass size distribution of BC core (dM/dLogDc), taken from Liu *et al.* (2014). 208
Figure 5.13. Deposition velocity on grass as a function of particle size (Giardina and Buffa, 2018) 209
Figure 5.14. Deposition velocity dependence upon particle diameter for a small range of sizes (0.08 μm to 0.5 μm) refer to the data points from Table. 5.10. The points represent the relationship between BC diameter particle (Dp) in μm as x-axis and deposition velocity (V_d) in cm s^{-1} as y-axis 210
Figure 5.15. Elemental Carbon (EC) concentration and deposition velocity (V_d) from literature (Matsuda *et al.*, 2012), research conducted in Thailand, 2010 211
Figure 5.16. Diurnal plots of BC with bars indicate ± standard error of the mean, 1 May – 29 November 2018, **(a)** Diurnal plot of BC concentration on the roof and ground; **(b)** Diurnal plot of eddy diffusivity (K) of BC 213
Figure 5.17. Diurnal plots of NO_x concentrations with ± standard error of the mean on the roof and the ground and their fluxes with standard error of the mean, on the period of **(a)** 20–29 November 2018; **(b)** 23 January–13 February 2019; and **(c)** 23 January–2 March 2019 214
Figure 5.18. Diurnal deposition velocity of NO_x with ± standard error of the mean during period on **(a)** 20 – 29 November 2018; **(b)** 23 January – 13 February 2019; and **(c)** 23 January – 2 March 2019 216

List of Tables

Table 1.1. Sources and sinks of nitric oxide 4
Table 1.2. Sources and sinks of nitrogen dioxide 4
Table 1.3. Air Quality objectives for NO_2, O_3 and PM in UK 6
Table 1.4. Sources and sinks of ozone 7
Table 1.5. Sources and sinks of black carbon 8
Table 1.6. Model statistics comparison from all test days for the Idaho Falls tracer study (Heist *et al*., 2013) 22
Table 1.7. Performance of models against the Caltrans Highway 99 data set for receptors downwind and upwind of the roadway (Heist *et al*., 2013) 22
Table 2.1. Information about location, instrument, analysis, and date conducted in each study in this thesis 26
Table 2.2. Calculated uncertainty of Automatic Urban and Rural Air Quality Monitoring Network (AURN) data using CEN methodology for NO_x and O_3 analysers (Stevenson *et al.*, 2009) 28
Table 2.3. Sources of errors in deployment of diffusion tubes (DT) 30
Table 2.4. Measurement results of tube length, tube diameter, stainless steel mesh, membrane, filter and spacer for NO_2 and NO_x Diffusion Tube (DT) using dial vernier caliper 36
Table 2.5. Dimension and sampling rate of diffusion tubes 37
Table 2.6. Dimension and sampling rate of NO_x diffusion tubes (two tubes consist of NO_x and NO_2 tubes) 42
Table 2.7. Deposition velocities for short vegetation (grass) 58
Table 2.8. Equations for the uncertainty in deposition velocities of gases from vertical gradient of pollutant concentrations 60
Table 3.1. Results of statistical test with Kolmogorov-Smirnov to check the normality of the data 67
Table 3.2. Validation result of NO_2 diffusion tubes for precision and accuracy, August 2016 – April 2018 71
Table 3.3. Examples of bias and factors influencing bias percentage of NO_2 quantification in ambient air from previous research 72
Table 3.4. Bias adjustment factors of diffusion tubes from August 2016 to April 2018 in the UoB site, Birmingham 73
Table 3.5. Precision and accuracy of NO_x diffusion tubes (NO_x, NO_2 and NO levels) on the roof and the ground of the Biosciences building, 28 January to 11 March 2019 78
Table 3.6. Validation result of O_3 diffusion tubes for precision and bias 79
Table 3.7. NO_2 concentration on the roof and ground, December 2017 – May 2018 103
Table 3.8. T-test result and air pollution change (%) 104
Table 3.9. Pearson correlation matrix of NO_2 concentration inside park, near road and meteorological factors 106
Table 3.10. The model equation and R^2 from multiple linear regression analysis 109
Table 4.1. Information needed, purpose, and data input for the ADMS-Roads model 115
Table 4.2. Mean pollutant concentrations at BROS and EROS sites 124
Table 4.3. Road sources and emission data 125
Table 4.4. ID of the weather station in the CEDA website, Latitude, Longitude and parameter of weather data 130
Table 4.5. Evaluation results from ADMS-Roads modelling using meteorological input from different weather stations 133
Table 4.6. Coefficient of determination (R^2) and linear regression of wind speed from Winterbourne and Coundon weather stations, January 2016 – June 2018 138
Table 4.7. Urban background monitoring sites in Birmingham 141

Table 4.8. Evaluation result from different background concentration. EROS site and Birmingham Acocks Green 145
Table 4.9. Speed configurations and vehicles speed at each road 146
Table 4.10. Model evaluation of different vehicle minimum speeds 148
Table 4.11. Example. emission rate at road 2 (A38 road) from baseline setting and 15% setting for NO_2:NO_x ratio 150
Table 4.12. Model evaluation of different settings for the NO_2:NOx ratio 151
Table 4.13. Statistical evaluation of measured and modelled concentrations 154
Table 4.14. Model evaluation statistics calculated from NO_2 diffusion tubes and model of ADMS-Roads for (a) the dispersion and chemistry, (b) deposition, dispersion and chemistry (b) and % reduction in concentrations due to deposition. 176
Table 5.1. Date and time during sampling period when NO_2 concentrations at the ground site were higher than 40 µg m^{-3} 186
Table 5.2. Number of occurrences of lower NO_x concentrations at the roof and lower concentrations at the ground for the period of sampling on 20-29 November 2018 and 23 January-3 March 2019 190
Table 5.3. Date and time during sampling period when NO_x concentrations at the roof decreasing and NO_x concentrations at the roof were lower than the ground (polluted air storage) and when NO_x concentrations at the roof increasing and NO_x concentrations were higher than at the ground (clean air storage) 191
Table 5.4. Measurement of wind speed, temperature and relative humidity on the roof and ground for 1-hour, for 10 observation data 197
Table 5.5. Data of wind speed, temperature and relative humidity from Coleshill weather station data, 13 – 29 May 2019 199
Table 5.6. Deposition velocity of NO_x from references 200
Table 5.7. Deposition velocity of NO_2 from references 201
Table 5.8. Deposition velocity of NO from references 202
Table 5.9. Deposition velocity of O_3 from references 202
Table 5.10. Data for calculating the deposition velocity of BC 209

Chapter 1. Introduction

This chapter presents an overview of air pollution in urban areas, mainly for nitric oxide (NO), nitrogen dioxide (NO_2), ozone (O_3), and black carbon (BC), as well as the effect of green space on pollutant concentrations. The impact of dispersion and deposition on pollutant concentrations in urban green space are presented, followed by an introduction to air pollution measurement and modelling.

1.1. Background

World population is increasing, reaching 7.6 billion in 2018 (Kaneda *et al*., 2018), whereas in 2015 it was 7.3 billion people (Kaneda and Bietsch, 2015), an increase of 0.3 billion in 5 years. The rise in population will also increase the need for housing, food, and transportation. More and more areas are being converted from open space to housing and other facilities. Research from Fuller and Gaston (2009) shows that green space declines rapidly with increases in the density of human population.

The majority of the world's population is living and working in cities, and it is predicted to increase rapidly in the next decades (Baldasano *et al*., 2003; Britter and Hanna, 2003; Grimm *et al.*, 2008; Rydin *et al.*, 2012). Consequently, the concentrations of air pollutants are typically higher in urban areas because of the transformation, dispersion and accumulation of pollutants that are emitted from human activities (Mayer, 1999; Mazzeo *et al.*, 2005).

In urban areas, reduction of green open spaces has contributed to air pollution. Liu and Shen (2014) analysed the impact on air pollution with the changes of urban green areas by applying spatial analysis and landscape ecology metrics in the 48 districts of the Taipei metropolitan area. The pattern showed a negative relationship between the change in urban green areas and the change of air pollution emissions. Increasing green space is beneficial in reducing air pollution. Efforts to reduce air pollution have been carried out as part of an approach to responding to environmental issues, for example by expanding the greening movement and developing green infrastructure (Pauleit *et al.*, 2017; Magaudda *et al.*, 2020; Monteiro *et al*., 2020).

Urban green space influences the air quality through dispersion and deposition (Janhall, 2015). Dispersion is the distribution of air pollution into the atmosphere, and it is influenced by meteorological factors, such as wind direction, wind speed, turbulence and atmospheric stability (Mayer, 1999; AQEG, 2018). Deposition is the process of removing gases and particles from the atmosphere to the surface. However, little study has been conducted to assess the roles of both dispersion and deposition and to examine which of these two processes has the most influence on reducing atmospheric pollutant concentration. The focus of this thesis is to provide a quantification of the dispersion and the deposition processes which then allows a judgment of whether dispersion or deposition is the dominant process in influencing pollutant concentrations within urban green space.

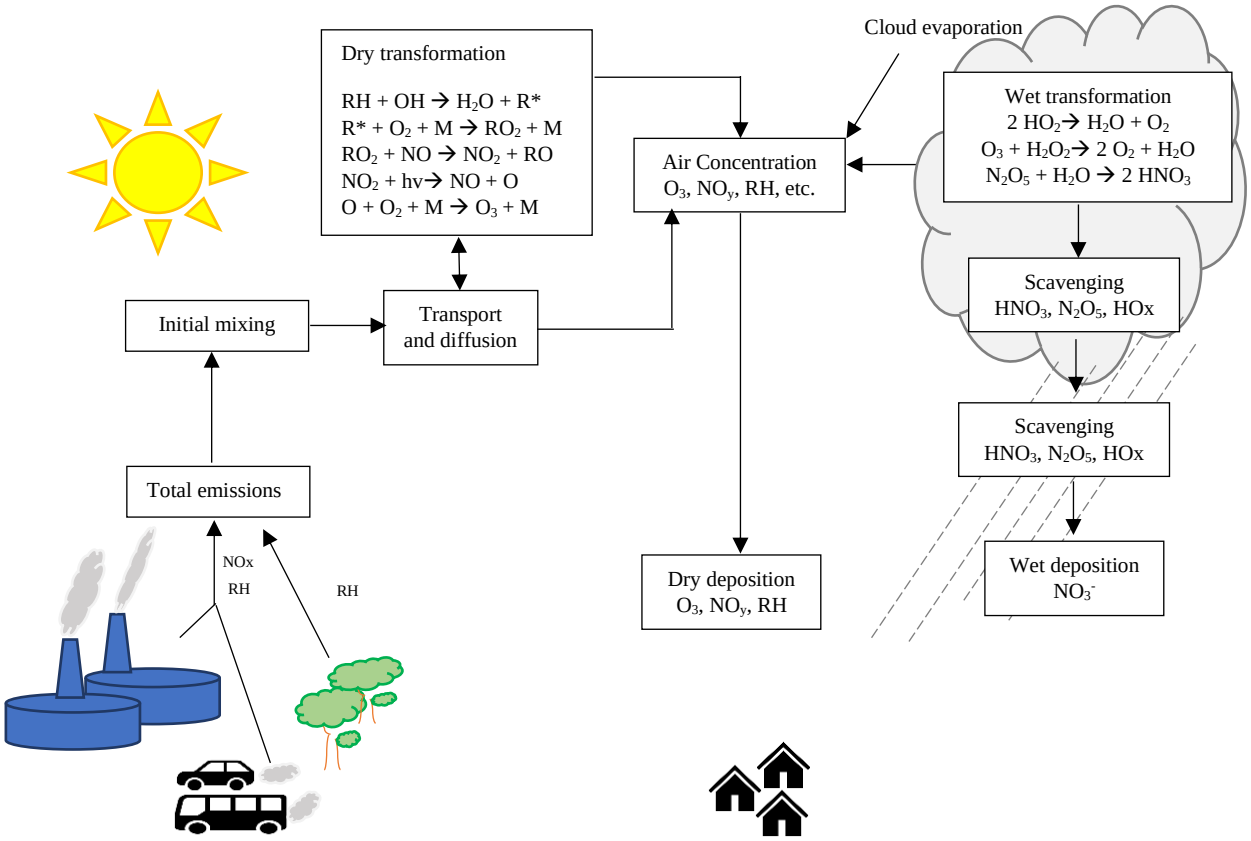


Figure 1.1. Photochemical air pollution, from emission to deposition (National Research Council, 1992)

Figure 1.1. shows a schematic of pollutants in the atmosphere from emission to deposition and their atmospheric chemistry processes. Pollutants are emitted, they mix in the atmosphere, are transported, diluted, or transformed and then removed from the atmosphere by deposition mechanisms.

1.2. Air pollution sources and pathways in the atmosphere

A major environmental problem in cities comes from air pollution (Mayer, 1999; Mazzeo *et al.*, 2005). Air pollution causes serious effects on human health, mainly respiratory and circulatory illnesses, which are linked to nearly 4.2 million deaths annually (WHO, https://www.who.int/health-topics/air-pollution).

Pollutants are substances that in high levels are harmful to humans, animals, or vegetation (Lyons and Scott, 1990; Vallero, 2019). Sources of air pollutants are both natural and anthropogenic. Natural sources include volcanic eruptions which release sulphur dioxide (SO_2), carbon dioxide (CO_2) and dust, salt particles from ocean waves, and biogenic emissions from plants as Biogenic Volatile Organic Compounds (BVOCs). BVOC emissions in the atmosphere can enhance the formation of other pollutants such as O_3 and Particulate Matter (PM) (AQEG, 2018), particularly day-time O_3 production (Kim *et al.*, 2013). For example, BVOCs in the presence of sufficient nitrogen oxides (NO_x) may oxidize NO to NO_2, then NO_2 is photo-dissociated, leading to O_3 production and regeneration of Hydroxide (OH) (Sillman, 1999; Laothawornkitkul *et al.*, 2009). Anthropogenic sources come from human activities, for example, industries (e.g., power plants, coal combustion), and personal activities (e.g., waste disposal, transportation). The main pollutants from road transport are CO_2, NO_x, carbon monoxide (CO), and anthropogenic Volatile Organic Compounds (VOCs) (Eggleston *et al.*, 1998; Colvile *et al.*, 2001; Gilbert *et al.*, 2003).

Pollutants can be primary or secondary. Primary pollutants are released directly from sources into the atmosphere, while secondary pollutants are formed from chemical reaction process in the atmosphere. Examples of primary pollutant are CO, NO and a fraction of NO_2, and PM from vehicles, and examples of secondary pollutant are secondary PM, NO_2 and O_3.

1.2.1. Nitrogen oxides (NO_x = NO + NO_2)

Nitrogen oxides are emitted into the atmosphere as NO and NO_2. NO can be released into the atmosphere either naturally, such as from soils in forests (Horii *et al.*, 2004), or anthropogenically, mainly from transportation, industry and electric power (Jacobson, 2002).

Table 1.1. Sources and sinks of nitric oxide

Sources	Sinks
Denitrification	Atmospheric chemical reaction
Lightning	Dissolution in surface water
Fossil fuel and biofuel combustion high temperature $N_2 + O_2 \rightarrow 2\ NO$	Deposition
Biomass burning	
Photolysis and chemical reaction	

Source: (Jacobson, 2002)

Pure NO_2 gas is brown and has a strong odour. It is primarily produced in the atmosphere from chemical processes involving NO and O_3 (Jacobson, 2002), see R.1.1 to R.1.3 for the chemical reactions. NO_2 can be also directly emitted from transportation, but at lower concentrations than NO. NO_2 is one pollutant regulated as a parameter to improve air quality (DEFRA, 2018). The air quality objectives in the UK for NO_2 are 200 $\mu g\ m^{-3}$ maximum 18 times per year, measured as 1 hour mean, and 40 $\mu g\ m^{-3}$ for annual mean (DEFRA, no date).

At $\lambda < 420$ nm, NO_2 is photolyzed to NO and O (ground state oxygen atom) that quickly reacts with O_2 to becomes O_3. NO is oxidised by O_3 into NO_2. The $NO/NO_2/O_3$ photo-stationary state happens in daytime, and the chemical reactions are as follows:

$$NO_2 + hv\ (\lambda < 420\ nm) \rightarrow NO + O \qquad (R.1.1)$$
$$O + O_2 + M \rightarrow O_3 + M \qquad (R.1.2)$$
$$NO + O_3 \rightarrow NO_2 + O_2 \qquad (R.1.3)$$

Table 1.2. Sources and sinks of nitrogen dioxide

Sources	Sinks
Atmospheric chemical reaction between NO and O_3	Photolysis
Fossil fuel and biofuel combustion	Atmospheric chemical reaction
Biomass burning	Dissolution in surface water
	Deposition

Source: (Jacobson, 2002)

In urban environments, the main source of air pollution is emissions from road traffic and the most significant pollutant is NO_x (AQEG, 2004; Henschel *et al.*, 2015). For example, in

2011, as shown in Figure 1.2., as much as 68% of NO_x emissions in the city of London came from roads (Duffield, 2011).

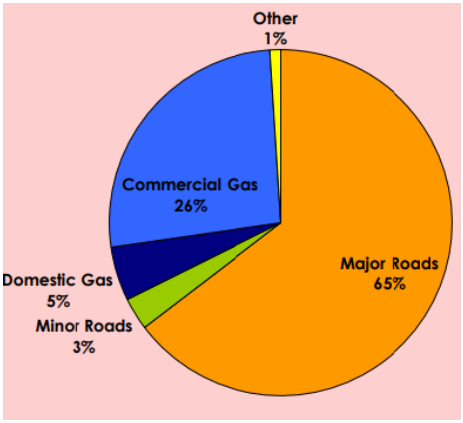


Figure 1.2. Sources of NO_x emissions in the City of London in year 2011 (Duffield, 2011)

NO_2 plays a major role that could contribute to environmental acidification (Varshney and Singh, 2003) and has adverse effects on human health, causing mortality and premature deaths (https://www.who.int/health-topics/air-pollution), respiratory problems (Persinger *et al.*, 2002; Brugge *et al.*, 2007; Pandey *et al.*, 2008) and negative effects on ecosystems (Cox, 2003; Chestnut and Mills, 2005).

NO_2 concentrations are higher near roads and decrease further away from the roadside. This indicates that the source of NO_2 is related to traffic and chemical reactions of air pollutants from road transport. Higher NO_x concentrations near the heavy traffic cause lower O_3 concentrations due to the reaction of NO with O_3 which produces NO_2. NO_2 concentrations decrease to near background levels within 150 to 200 m from a road (Gilbert *et al.*, 2003; Karner *et al.*, 2010; Ducret-Stich *et al.*, 2013).

Air quality in the UK has improved since the 1952 London smog episode. There were major changes in emissions when the coal used as fuel in homes was replaced by electricity and gas, resulting in a significant reduction in SO_2 and particle concentrations. However, the NO_x level did not decline as much as SO_2 in the period of 1970 and 1980 (Williams, 1999). From 1997 to 2003, there was a reduction in NO_x emissions from roadsides in London, but not in NO_2 (Carslaw, 2005). This condition was related to the ratio of NO_2:NO_x emissions from road traffic, which increased from 5-6 vol% in 1997 to 17 vol% in 2003. The change in the NO_2:NO_x emissions ratio from roads was attributed to several potential causes, such

as continual changes of the vehicle fleet, increased use of diesel fuel, changes in traffic management in Central London and the changing technology of using catalysed diesel particulate filters (CDPF). A significant cause of the reduction was associated with the London programme to use CDPF on buses. The CDPF was gradually installed in the bus fleet, as in December 2001, 33% of buses were equipped with CDPF and by 2006 all buses in London were using this technology. CDPF has an oxidation catalyst that oxidises CO and hydrocarbon emissions and was able to change NO to NO_2. NO_2 was used to oxidise trapped particles (Carslaw, 2005). Furthermore, Carslaw (2005) remodelled NO_2 concentrations at Marylebone Road, London using historical data from 1998 to 2002 to estimate the annual NO_2 concentrations with NO_2:NO_x ratio remaining the same at 9.5 vol%. Remodelling NO_2 concentrations showed that without an increase in the NO_2:NO_x ratio, NO_2 concentration decreased statistically. Thus, the NO_2:NO_x emissions ratio affects the trend of NO_2 concentrations.

NO_2 is still a problem in some areas, as concentrations exceed the annual mean concentration limits in ambient air as set by The Air Quality Directive 2008/50/ECs for pollutants in Europe, as shown in Table 1.3 (Anttila *et al*., 2011; Chaloulakou *et al*., 2008; DEFRA, n.d.).

Table 1.3. Air Quality objectives for NO_2, O_3 and PM in UK

No	Pollutants	UK National Air Quality Objective from DEFRA (Department for Environment, Food & Rural Affairs)		
		Objective	Concentration measured	Applies
1.	NO_2	200 µg m^{-3} Not to be exceeded more than 18 times in a year	1 hour mean	UK
		40 µg m^{-3}	Annual mean	UK
2.	O_3	100 µg m^{-3} Not to be exceeded more than 10 times in a year	8-hour mean	UK
		266 µg m^{-3} Not to be exceeded more than 35 times in a year	15 minutes mean	UK
3.	PM_{10}	50 µg m^{-3} Not to be exceeded more than 35 times in a year	24-hour mean	UK
		40 µg m^{-3}	Annual mean	UK
4.	$PM_{2.5}$	25 µg m^{-3}	Annual mean	UK, except Scotland

Pollutant concentrations are very high near roads, so the health effects are most severe there (Venn *et al.*, 2001; Brugge *et al*., 2007). The health risk from air pollutants, include risk of asthma, respiratory symptoms and in the long term exposure to traffic pollutants can cause cancers including leukaemia (Van Vliet *et al.*, 1997; Adar and Kaufman, 2007; Samet and Krewski, 2007; Zhu *et al.*, 2009).

1.2.2. Ozone (O_3)

O_3 is a secondary pollutant that can irritate the respiratory system (Lippmann, 1989) and has a negative effect on plants, such as decreased crop productivity, leaf damage and closure of stomata (Ashmore *et al*., 1988; Sandermann, 1996; Leisner and Ainsworth, 2012; Gao *et al.*, 2017; Vallero, 2019).

In many cities, the O_3 concentration is higher during the weekend than on weekdays (Bronnimann and Neu, 1997; Heuss *et al.*, 2003; Geng *et al.*, 2008). O_3 levels are lower near to busy roads and higher O_3 occurs in rural areas as compared with cities (Geng *et al.*, 2008; Guo *et al*., 2017). This is due to the NO and O_3 reaction being a net sink of O_3 (R.1.3).

Table 1.4. Sources and sinks of ozone

Sources	Sinks
• Chemical reaction of $O_{(g)}$ with $O_{2(g)}$ in the stratosphere $O_2 + hv \rightarrow O + O$ ($\lambda < 242$ nm) $O + O_2 + M \rightarrow O_3 + M$ • Chemical reaction in the troposphere $NO_2 + hv \rightarrow O + NO$ ($\lambda < 400$ nm) $O + O_2 + M \rightarrow O_3 + M$	• Photolysis • Atmospheric reaction • Dissolution in surface water • Deposition

Source: (Jacobson, 2002)

Oxidant (O_x) is the sum of O_3 and NO_2 ($O_x = O_3 + NO_2$). O_x levels in the atmosphere are influenced by local oxidant sources, for example, primary emissions of NO_2 (Mazzeo *et al*., 2005). Mavroidis and Chaloulakou (2011) observed the NO_2:NO_x ratio in Athens from 1987 to 2008, and explained that the composition of O_x at high NO_x level was dominated by NO_2, while O_3 was the main component of O_x at low NO_x concentration.

1.2.3. Black Carbon (BC)

Unlike NO_2 and O_3, which are precise chemical compounds, Black Carbon (BC) is defined based on its chemical, physical and optical characteristics. BC is also known as soot or elemental carbon (EC). However, BC and EC are not entirely the same and are identified by laboratory analysis. EC is thermally stable and can only be oxidized at temperature more than 340 °C. EC can be obtained from measurement with an evolved gas analyser (EGA) measurement, aerosol mass spectroscopy, and Raman spectroscopy measurement (Lack *et al.*, 2014).

BC is the carbonaceous component of particulate matter that is dark in colour. BC comes from incomplete combustion of, for example, fossil fuel, coal and other equipment (Hienola *et al.*, 2013; Yasunari *et al.*, 2013).

A carbonaceous component of particulate matter that is not black led to the name Brown Carbon (BrC) which originates from combustion of organic biomass or humic materials (Andreae and Gelencsér, 2006; Lack *et al.*, 2014). BC and BrC are similar in particle size, but BrC is soluble in some organic compounds (Bond *et al.*, 2013).

BC strongly absorbs all wavelength radiation from sunlight (e.g., 280 – 2500 nm), thus it has a role in climate change (Liu *et al.*, 2002; Novakov and Hansen, 2004; Petzold *et al.*, 2013; Lack *et al.*, 2014; MacDonald *et al.*, 2017). BC contributes to the increase of sea ice and snow melt in the Arctic (Huang *et al.*, 2010) and affects cloud formation and rainfall patterns (Lack *et al.*, 2014).

Table 1.5. Sources and sinks of black carbon

Sources	Sinks
Combustions	Wet and dry deposition
Biomass burning	

Source: (Andreae and Gelencsér, 2006)

1.3. Dispersion and deposition processes of atmospheric pollutants

The pathways of pollutants and their concentrations depend on the transport, chemical reactions, dispersion, and deposition process (Lyons and Scott, 1990; Seinfeld and Pandis, 2016). Figure 1.3. shows the path of air pollution in the atmosphere, starting with the

emission, transmission with the chemistry, dilution, and dispersion processes, then deposition as the final path to remove air pollution from the atmosphere.

Emissions are released from their sources, transported by the wind, then mix in the atmosphere, undergo chemical reactions, and are removed from the atmosphere via deposition processes. During transport, pollutants also transform into degradation product which reduces the pollutant concentration (Mayer, 1999; Vallero, 2019). Turbulence increases the process of mixing and dispersion of pollutants (Lyons and Scott, 1990).

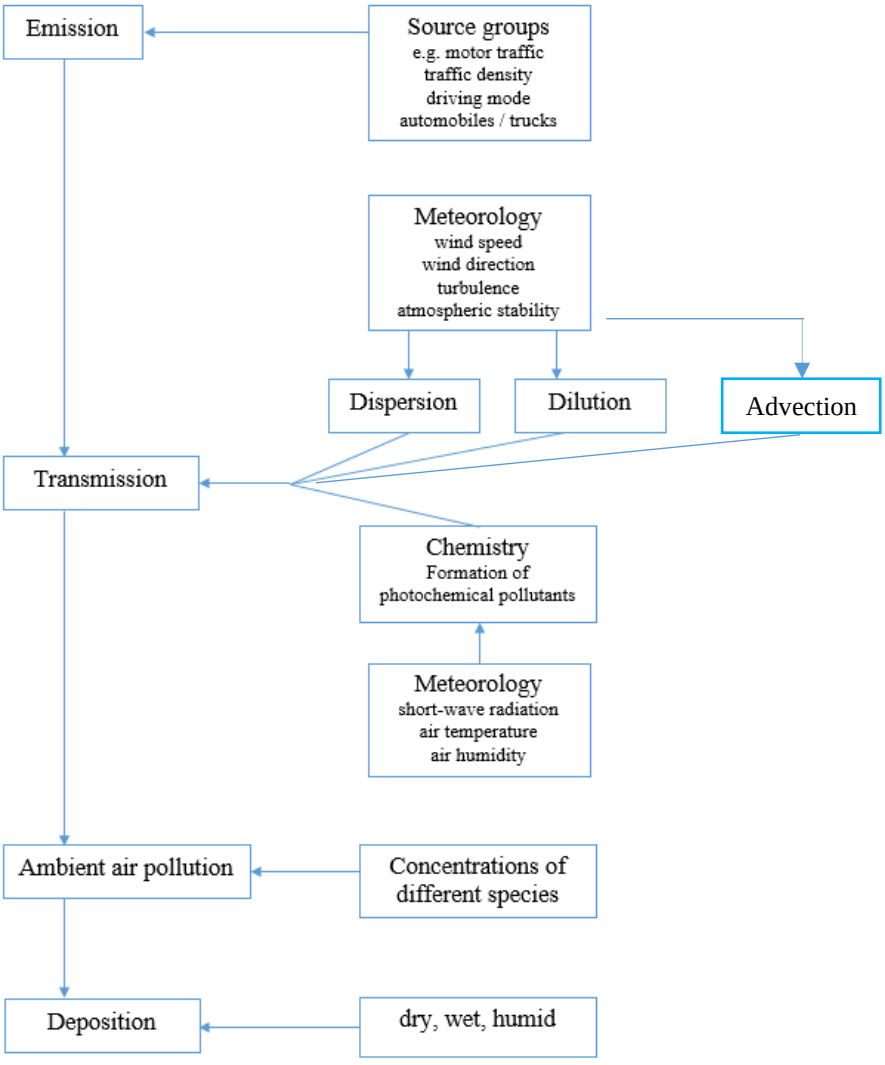


Figure 1.3. Air pollution pathways in the atmosphere (Adopted from Mayer, 1999)

The air pollution disperses following the air flow. The configuration of the vegetation and the air flow create turbulent eddies that affect the dispersion process. The dispersion process

at a local scale has an important role in decreasing or increasing pollutant concentrations in the ambient air (Harrison, 2018). The pollutant concentrations that were emitted from a source of emissions dispersed in the atmosphere can be modelled mathematically considering the direction of the dispersion in longitudinal, horizontal (cross-wind), and vertical planes which are expressed as x, y and z directions, as shown in Figure 1.4 (Seinfeld and Pandis, 2016; Vallero, 2019).

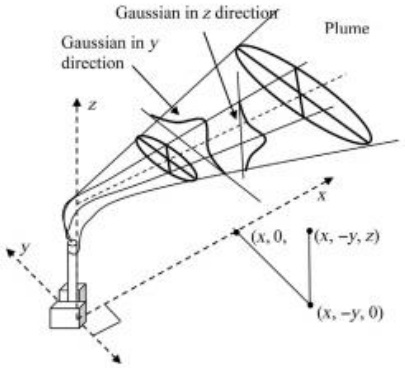


Figure 1.4. Gaussian plume (Vallero, 2019)

In deposition pathways, there are two main processes: dry deposition, and wet deposition (Seinfeld and Pandis, 2016; Vallero, 2019). Dry deposition is the process of removing gases and particles from the atmosphere through contact with surfaces such as buildings, vegetation, or other surface areas under dry condition (Lyons and Scott, 1990; Erisman and Draaijers, 1995; Jacobson, 2002; Seinfeld and Pandis, 2016).

The process of dry deposition consists of three resistances to transport as shown in Figure 1.5. (Seinfeld and Pandis, 2016):

a. The aerodynamic transport (r_a), mechanism carries material from the atmosphere to the surface.
b. In the quasilaminar layer (r_b), the material crosses the surface itself and the resistance to transfer relies on the surface features and molecular properties.
c. Surface (canopy) resistance (r_c). The uptake on the surface is controlled by a variety of factors, such as smoothness and shape of the surface.

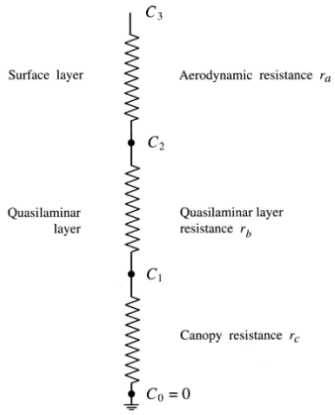


Figure 1.5. Resistance model in dry deposition (Seinfeld and Pandis, 2016)

Eddy diffusivity affects the aerodynamic transport and the efficiency is assigned according to the level of atmospheric turbulence. The quasilaminar layer transports the substance to the surface and it is governed by the physical and chemical properties of the depositing species. The transport mechanism in the quasilaminar layer for gases occurs by molecular diffusion, while the motion of smaller particles is through Brownian diffusion. The canopy resistance relates to the nature of the surface. In vegetation, the surface is leaves, so the particles or gases sticks to the leaf or enter the stomata (Figure 1.6).

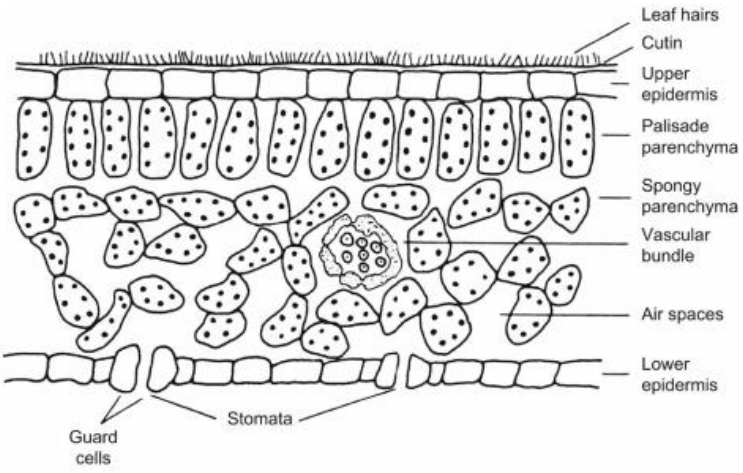


Figure 1.6. Leaf section (Vallero, 2019)

Pollutant concentrations can be reduced via vegetation through the processes of photosynthesis and respiration. The leaves and the branches can trap the particles by impaction or sedimentation and absorb gaseous pollutants through stomata (Fowler, 2002; Jim and Chen, 2008; Fantozzi *et al.*, 2013; Vos *et al.*, 2013; Yli-Pelkonen *et al.*, 2018).

The stomata determine the gas exchange between the atmosphere and the leaves of the vegetation. In response to external stimulants, the guard cells control the process of decreasing or increasing pore surface area (Vallero, 2019). The resistance of stomata is high at night as the stomata are closed, however the resistance during daytime is decreased when stomata are open (Seinfeld and Pandis, 2016).

The eddy diffusivity in the aerodynamic transport is the same for particles and gases but for the quasilaminar layer and canopy layer, the resistance is not the same. That is why different sizes of particles have different deposition velocities, and different gases have different deposition velocities.

The aerodynamic transport is the same for gases and particles except for large particles (diameter particles larger than a few micrometres) where there is additional gravitational settling, so the substances deposit both by gravity and by turbulent diffusion (Wesely and Hicks, 2000; Giardina and Buffa, 2018). Thus, the turbulent diffusion is characterised by the eddy diffusivity. For BC, the diameter particle is very small, so the eddy diffusivity determines the aerodynamic resistance.

Dry deposition depends on the micrometeorological conditions, the physical and chemical properties of the depositing species, and the characteristics of the deposition surface (Wu *et al.*, 2018). Deposition velocity (Vd) can be calculated using the following equation:

$$V_d = \frac{-F}{C} \qquad (E.1.1)$$

Where F is pollutant flux removed per unit area (µg m^{-2} s^{-1}); V_d is deposition velocity (m s^{-1}), and C is concentration at 1 metre above the ground (µg m^{-3}).

The transport of material to the surface is influenced by aerodynamic transport, quasilaminar layer and surface, or canopy resistance as explained in Figure 1.5, and deposition velocity is the inverse of the sum of the three resistances.

$$V_d{}^{-1} = r_t = (r_a + r_b + r_c) \qquad (E.1.2)$$

Where r_a is aerodynamic transport (s cm^{-1}), r_b is quasilaminar layer (s cm^{-1}), and r_c is surface or canopy resistance (s cm^{-1}).

Dry deposition of atmospheric pollutants is estimated from measurement data in the field (Lindberg and Lovett, 1985; Erisman *et al.*, 1993; Schultz, 1993; Horii *et al.*, 2004; Watt *et al.*, 2004; El-Madany *et al.*, 2017), or laboratory (Breuninger *et al.*, 2012; Vohra *et al.*, 2017) or through numerical models (Kramm, 1989; Sorteberg and Hov, 1996).

Pugh *et al*. (2012) outlined a method to reduce pollutant concentrations, by increasing deposition velocity while conducting emission control and increasing dispersion processes. Air pollution concentrations change also because of the dispersion or their chemical reactions and can be quantified through measurements or modelling (Vallero, 2019).

1.4. Urban Green Space

Urban green space has a broader perspective as the term is used across multiple disciplines. Taylor and Hochuli (2017) conducted a review of the definitions used by researchers in their study related to green space and summarised two general interpretations of the term: natural areas and urban vegetation.

Swanwick *et al*. (2003) defined green space as an external environment area, "land that consists predominantly of unsealed, permeable, 'soft' surfaces such as soil, grass, shrubs and trees*".* They describe the research that has been conducted by University of Sheffield on the role and importance of urban green areas. The term "urban green space" was described in their report as shown in Figure 1.7, that green space is not only parks, fields, and gardens.

Swanwick *et al*. (2003) presented the types of green space which are categorised as linear, semi-natural habitats, functional and amenity green spaces. Linear green space describes areas such as cliffs and corridors of transport, e.g., walking routes and semi-natural habitats such as are wetland, woodlands, and other habitats, such as grassland. Amenity green space is recognized as recreational green space (parks, gardens, play areas, sport areas), incidental (housing and other incidental green space), and private green space (domestic parks). Furthermore, examples of functional green space are productive green space (city farms, farmlands), burial grounds (cemeteries) and institutional grounds (school farms, growing

areas, and other institutional grounds). The sampling site of urban green space in this study included parks as amenity green space and University grounds as functional green space.

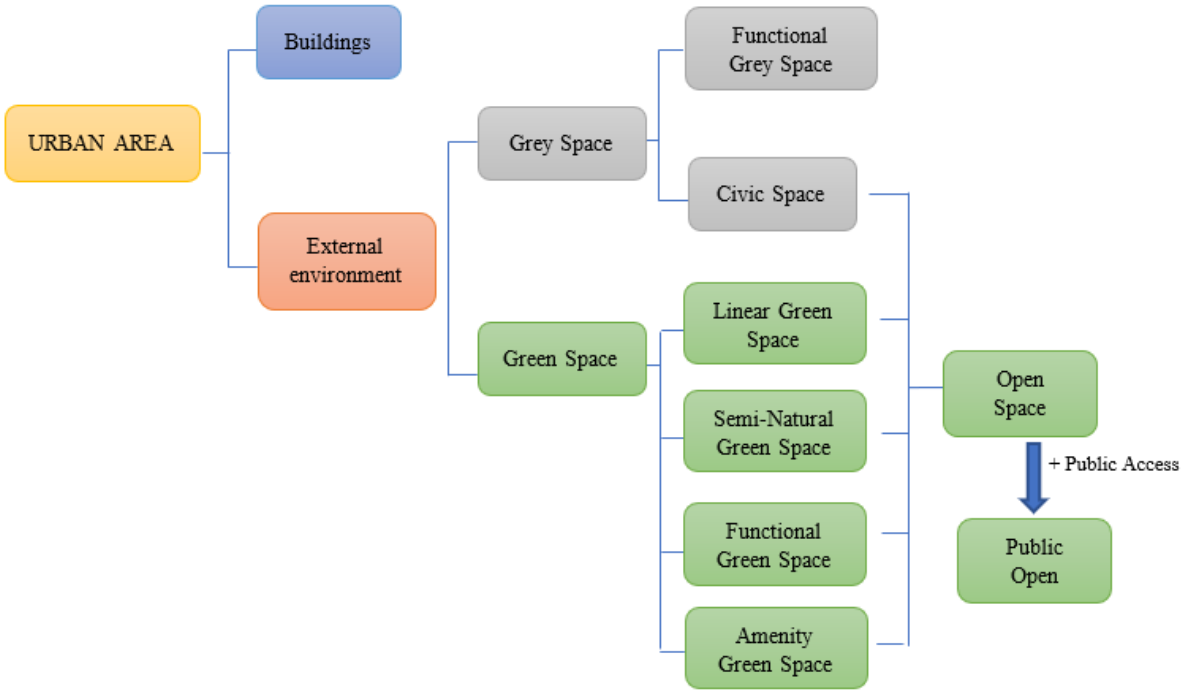


Figure 1.7. Green space position in an urban area (Swanwick *et al*., 2003)

Parks play a significant role in increasing life satisfaction (Bertram and Rehdanz, 2015), improving health, as well as economic and environmental benefits (Swanwick *et al*., 2003; Barbosa *et al.*, 2007). Furthermore, existence of urban trees positively affects quality of life (Heynen *et al*., 2006) and improves air quality (Nowak *et al*., 2006; Yin *et al.*, 2011). Hewitt *et al*. (2020) proposed steps to mitigate air pollution, including emission reduction, extending distance from sources to receptors, and adding more urban green space.

The benefits of urban green space for the environment are well known: to reduce air pollution (Cohen *et al*., 2014; Crompton, 2017), and serve an ecological function for flora and fauna, water and soil conservation. Urban green space provides the citizens with a healthy environment (Orr *et al*., 2014), improves well-being (Bertram and Rehdanz, 2015; Gong *et al*., 2016), and plays a role in tackling climate change via moderating temperature by its shading effect (Gill *et al.*, 2007; Lee and Park, 2008).

1.5. What is the benefit of parks for air quality?

Yin *et al*. (2011) calculated the effect of trees in China in the year 2008 by comparing the pollutant concentration in a park with vegetation and in a park without vegetation. They did not find a different level at the roadside near the park with trees and the park without trees, but there was a difference in pollutant concentration within those two parks, meaning that the vegetation could reduce the pollutant concentration by around 1 to 21% with regards to NO_2 concentration, 2-27% for SO_2 concentrations, and 2-35% for Total Suspended Particles concentration. They concluded that the pollutants were removed from the atmosphere mainly through the influence of distance and crown volume coverage of vegetation. In this regard, tree crown volume was calculated to quantify the improvement of air quality related to the vegetation, and they found pollutant reduction as much as 2.6% of NO_2, 5.3% of SO_2 and 9.1% of TSP.

Vos *et al*. (2013) debated the role of vegetation in improving local air quality near roadsides. The effect of trees on air quality was assessed using three-dimensional Computational Fluid Dynamics model (ENVI-met), and the result showed that vegetation near the roadside could increase pollutant concentrations. They concluded that the aerodynamic effect (dispersion) was more significant in reducing pollutant concentrations than the tree's ability to remove pollutants by deposition.

Yli-Pelkonen *et al*. (2018) compared the pollutant concentrations under the trees and in open areas in Yanji, northeast China using diffusion tubes, and concluded that tree cover affects the O_3 level by lowering the concentration (6.2%) due to the absorption of O_3 by leaves and the effect of lower solar radiation and lower temperature under the trees. However, they found that NO_2 concentrations did not change in open areas and under the trees, which showed that the existence of trees did not affect the NO_2 level.

Trees near a road prevent wind flow and reduce the dilution process. However, the effect of trees in the park, open area and traffic free street could have a different result (Vos *et al.*, 2013). Janhall (2015) reviewed the role of vegetation on air pollution through dispersion and deposition, showing that selection of vegetation and vegetation design were important parameters in improving air quality. However, Janhall concluded that the effects of vegetation on air quality are complex and more studies are needed.

There are monetary values related to pollution removal from trees as calculated by some researchers. Nowak *et al*. (2006) modelled air pollution removal by urban trees and estimated the monetary value of reducing pollutants (O_3, NO_2, CO, SO_2 and PM_{10}) from 55 cities across the US in 1994. The model used tree cover, pollution concentration and meteorological data to estimate the magnitude of air pollution removal. Total pollution removal for each pollutant was calculated by multiplying the total amount of tree cover with the pollution removal rates and average pollutant concentration for every urban area. Totals of pollution removal areas were combined to calculate the total for the nation. Then, the value of pollution removal was estimated using national externality values as a consideration of pollution costs to society that are not accounted for in in the market price. These values are in dollar per metric ton (t), and in 1994 the values were \$6752 t^{-1} for NO_2 and O_3, \$4508 t^{-1} for PM_{10}, \$959 t^{-1} for CO and \$1653 t^{-1} for SO_2. Total annual results showed that 711,000 metric tons of air pollution were removed from 5 pollutants by urban trees, which is equal to \$ 3.8 billion. The air pollution reduction by urban trees is varied according to tree cover, pollution level, meteorological variables, and deposition velocity (Nowak *et al*., 2006).

A study by Jim and Chen (2008) calculated the capability of ecosystem services of urban green space in removing the pollutant concentrations in Guangzhou, China in 2000, by estimating the flux with tree cover. They found that 312.03 Mg of NO_2, SO_2 and Total Suspended Particles had been removed, with benefit at RMB 90.19 thousand (US\$ 1.00 = RMB 8.26). Tallis *et al*. (2011) used the Urban Forest Effects (UFORE) model and pollution flux approach which calculates pollution flux or canopy-covered land multiplied by leaf area index (LAI) to determine the value of deposition of PM_{10} in the urban green area in Greater London. They estimated that urban canopy can eliminate 0.7% to 1.4% (852 to 2121 tonnes) of PM_{10} in a year for Greater London, and predicted that, in the year 2050, if the urban green space in Greater London is increased by 10% from the current 20% of land area in Greater London, then air quality improvement through increasing tree cover can remove PM_{10} in the range of 1.1% to 2.6% (1109 to 2379 tonnes). Air quality improvement was quantified using the Greater London Authority (GLA) plan to increase urban tree cover to 30% of the GLA's land surface by 2050, and compared that to the baseline conditions of green areas in 2006-2008, which had 20% of the total land area in Greater London. There is a plan to increase urban green spaces through tree planting managed by responsible parties, and by encouraging communities to plant trees on their private land, which thereby will increase tree cover in Greater London.

Work has also been carried on in analysing the effect of green areas in street canyons. Pugh *et al*. (2012) emphasized the importance of vegetation for the deposition process as a practical approach in reducing atmospheric pollutant levels. Greater leaf surface area enlarges the deposition surface area. However, researchers found that deposition through a tree canopy has a small impact on air quality (Tiwary *et al.*, 2009; Vos *et al.*, 2013; King *et al.*, 2014).

In dispersion processes, the aerodynamic effect is influencing the air quality (Jeanjean *et al.*, 2016; Tiwari *et al.*, 2019). Xing and Brimblecombe (2018) studied dispersion from traffic emission sources into the parks in Hong Kong in 2017 using gradient transport theory, showing that the atmospheric level of BC and PM_{10} from road decreased along the way into the park. Fantozzi *et al*. (2013) measured NO_2 and O_3 concentrations in Siena, Italy using diffusion tubes placed in an open area and urban park with trees at a distance of 1 m, 5 m, and 10 m from the road. The NO_2 concentration was lower in the park compared to the open area, and the NO_2 level at both sites decreased from the road. However, the O_3 concentration was not significantly different from the road or either location.

There are a few studies about the ways in which parks and vegetation improve air quality through the dispersion and deposition process. Jeanjean *et al*. (2016) used Computational Fluid Dynamic (CFD) modelling to review the influence of trees in Leicester, UK in reducing $PM_{2.5}$. The CFD model reviewed the simulation of tree aerodynamics and deposition on trees and deposition on grass. The result on the aerodynamic effect in open terrain was that trees decrease the pollutant concentration by 9.0%. The deposition on trees (2.8%) has greater impact compared to the grassland (0.6%), and in this regard, the aerodynamic effect has a significant role in reducing the concentration. A recent study from Xing and Brimblecombe (2019) on urban vegetation in the park showed deposition contributing only 2% in air quality improvements, and the dispersion process is the most influential. Those researchers concluded that the dispersion process is significant in influencing the pollutant concentrations compared to the deposition process. In dispersion processes, trees do not remove pollution, they only redistribute pollution (AQEG, 2018).

1.6. Measurement of pollutant and modelling

Monitoring air quality is an important step in identifying air quality problems (Longhurst *et al.*, 1994). Various monitoring techniques are used to measure pollutant concentrations in the urban area.

1.6.1. Measurement

1.6.1.1. Continuous analysers

Air pollutant concentrations are usually measured by continuous analysers. Continuous analysers provide high time resolution data. However, they are expensive, need maintenance, and need power supply and space. Continuous analysers with fast response time are available for NO_x and O_3, and they will be discussed in Chapter 2.

Measurements of air pollutant concentrations using automatic analysers have been used by many studies to carry out air quality projects, for example: INTERCOMP2000, a field campaign for method comparison in measuring aerosol carbon in Europe (ten Brink *et al.*, 2004); O_3 stomatal uptake in Rome, Italy (Manes *et al.*, 2007); the PUMA project (Pollution of the Urban Midlands Atmosphere) in 1999/2000 in West Midlands, UK (Harrison *et al.*, 2006); determining conformity with standards (Bower *et al.*, 1994; Kuttler and Strassburger, 1999; Derwent *et al.*, 2007; Hickman *et al.*, 2018); identifying health effects (Brunekreef and Holgate, 2002); and the results from analysers are used as a reference value to be compared with passive sampler outcomes (Kirby *et al.*, 2000; Hamilton and Heal, 2004; Delgado Saborit and Esteve Cano, 2007; Vardoulakis *et al*., 2009; Heal *et al*., 2019).

1.6.1.2. Passive sampling

Passive samplers are useful for mapping and screening studies in remote areas and have many benefits, such as no need for a power supply, cost effectiveness, suitability for long-term monitoring and suitability for outdoor and indoor deployment (Cape, 2009; Salem *et al.*, 2009). However, passive samplers have limitations, for example, the accuracy is not the same level as a continuous analyser, and the exposure period is usually more than a week, so it cannot be compared with the automatic analyser for hourly mean air quality objectives.

Palmes *et al.* (1976) introduced the method to measure personal exposure to NO_2 using diffusion tubes (Palmes *et al.*, 1976; Cape, 2009). Afterwards, the development of monitoring using passive samplers increased. A type of Palmes tube is still used for measuring pollutant concentration (Boleij *et al.*, 1986; Miller, 1988; Plaisance *et al.*, 2004; Ukpebor *et al*., 2004; Gerboles *et al.*, 2005; Hafkenscheid *et al.*, 2009; Masey *et al.*, 2017). In the UK, diffusion tubes are regularly used for measuring NO_2 to monitor compliance with air quality objectives (Tang *et al*., 2001).

Diffusion tubes consist of small plastic tubes, open at one end, and containing a chemical reagent to absorb the pollutant. Diffusion tubes entrap molecules by molecular diffusion. During molecular diffusion, compounds will move from an area of high concentration to an area of low concentration. The use of diffusion tubes is discussed in chapter 2.

The diffusion tube principle is based on Fick's first law, where the flux is proportional to concentration gradient and diffusion coefficient (Delgado-Saborit and Esteve-Cano, 2007; Targa and Loader, 2008; Vallero, 2019).

$$F = -D\left(\frac{dC}{dZ}\right) \qquad (E.1.3)$$

Where:

F is flux (µg cm^{-2} min^{-1})

D is diffusion coefficient (cm^2 min^{-1}) of gas (1) in gas (2)

C is concentration (µg cm^{-3}) of gas (1) in gas (2)

Z is diffusion path (cm)

1.6.2. Air quality modelling

Local scale dispersion models can be used to evaluate air quality in urban areas (Vardoulakis *et al.*, 2003). In this study, ADMS-Roads was used to investigate the function of deposition velocity in improving the air quality. ADMS-Roads was also used to predict pollutant concentrations through dispersion and deposition processes.

1.6.2.1. ADMS-Roads model

The Atmospheric Dispersion Modelling System (ADMS) is a dispersion model to assess air quality (Carruthers *et al.*, 1997) and it was developed by Cambridge Environmental Research Consultants (CERC). ADMS-Roads is used to model the dispersion of emission from roads and industrial sites (CERC, 2017), and commonly used to study air pollution from road traffic on a local scale (Ellis *et al.*, 2001; Heist *et al.*, 2013; Davidović *et al.*, 2014; Dias *et al.*, 2019). This modelling software is widely accepted within the UK and used throughout the world to estimate pollutant dispersion from road sources. ADMS-Roads is capable of modelling point, line, area and volume source types (Carruthers *et al.*, 1994).

In order to validate predictions, Ellis *et al*. (2001) compared ADMS-Roads with California Line Source Dispersion Model, version 4 (CALINE4), Design Manual for Roads and Bridges (DMRB) and continuous monitoring site data. CALINE4 is a line source dispersion model based on the Gaussian distribution of the plume under steady-state conditions to predict the level of air pollution (Holmes and Morawska, 2006; Heist *et al*., 2013). DMRB is the Design Manual for Roads and Bridges 1999 from UK Department of Transport. For the first set, the California Department of Transportation (Caltrans) Highway 99 data were evaluated by ADMS-Roads and CALINE4, and the results showed ADMS-Roads gave the best fit line close to y=x (see Figure 1.9).

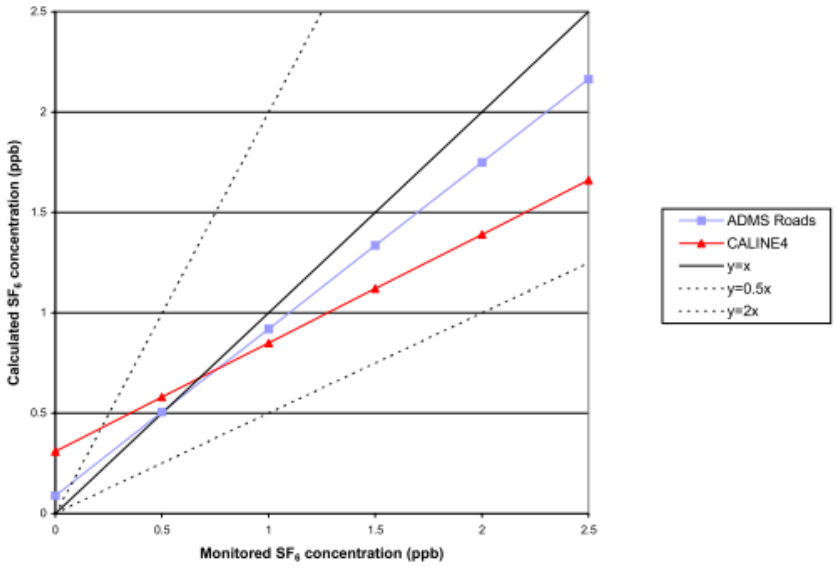


Figure 1.8. Comparison of trendlines calculated using ADMS Roads and CALINE4 (Ellis *et al.*, 2001)

However, both models showed a trend to underestimate high concentrations and overestimate low concentrations. Correlation between observed tracer chemical sulphur hexafluoride (SF_6) data and modelled data from ADMS-Roads and CALINE4 showed that ADMS-Roads results have a higher correlation compared to CALINE4 results: 0.84 and 0.51, respectively.

The second set compared ADMS-Roads with the monitoring result of NO_x, NO_2 and PM_{10} concentrations in 1997 from the M4 road, South-East England. The result from the modelled and measured concentrations showed good agreement with bias: 16.23% for NO_x, 2.74% for NO_2 and -1.11% for PM_{10}. The third set compared ADMS-Roads with DMRB at a typical road, and it found that the concentration from DMRB was higher near the road and declined fast within 150 m from the road, as DMRB did not take into account the meteorological factors and road width. Meanwhile, ADMS-Roads showed the modelled concentrations vary across roads based on four different road orientations and showed that prevailing wind directions affect the dispersion of pollutions from the road. Overall, ADMS-Roads showed good agreement with monitored concentration than the CALINE4 and DMRB.

Heist *et al*. (2013) evaluated four dispersion models, AERMOD, CALINE, ADMS and RLINE to measure the performance of the model in estimating pollutant concentration near the roadside. Field studies were carried out at Idaho Falls and Caltrans Highway 99, and using SF_6 as a tracer gas. Results of these models were compared with field study measurements and their performance was evaluated by statistical comparison using fractional bias (FB), the normalised mean square error (NMSE), the correlation (R) and the fraction of estimates within a factor of two of the measured value (FAC2). FB is systematic bias and ideally equal to 0, with positive values indicating a model underestimation and negative values indicating a model overestimation. NMSE is the mean relative scatter and ideally a better performance is 0; R is the linear relationship between model and observation data and in range between -1 to +1, ideally is +1, and FAC2 is ideally 1.

AERMOD is a dispersion model recommended by the US Environmental Protection Agency (EPA) and is able to model multiple point, area, and volume sources. AERMOD-A is simpler to set up, but this approach does not allow simulation of low-speed plume meander, while AERMOD-V does allow for plume meander. ADMS is a UK model for dispersion, and ADMS-Roads version 3.1 was used in this study for modelling dispersion from road sources. RLINE model is a research tool developed by the US EPA. CALINE version 3 and

4 were compared for dispersion modelling and the main difference was related to the presence of vehicle-induced turbulence in CALINE4. All models are based on a steady-state Gaussian dispersion model formulation (Holmes and Morawska, 2006; Heist *et al.*, 2013; Stocker *et al.*, 2013). For the Idaho Falls study, Heist *et al.* (2013) compared CALINE4, AERMOD-V, AERMOD-A, ADMS, RLINE and their statistical results are presented in Table 1.6.

Table 1.6. Model statistics comparison from all test days for the Idaho Falls tracer study (Heist *et al*., 2013)

Model	FB	NMSE	R	FAC2
CALINE4	0.42	1.94	0.76	0.59
AERMOD-V	0.38	1.26	0.84	0.59
AERMOD-A	0.32	1.25	0.82	0.59
ADMS	0.36	1.14	0.88	0.70
RLINE	0.23	0.96	0.85	0.73

Table 1.6. presents a statistical comparison of results, and FB values from all models were positive and indicated that models under-predict the observation data. The value of correlation coefficient (R) for all models indicated a strong positive linear relationship (> 0.70).

For the Caltrans Highway 99 study on the evaluation of pollutant concentrations, Heist *et al.* (2013) set up the instruments on both sides of the road, so that it was possible to evaluate model performance for downwind and upwind. Table 1.7. showed that the models that reviewed the receptors downwind and gave a strong positive linear relationship (R > 0.70) were AERMOD-V, RLINE and ADMS. All models can estimate downwind concentration; however, a statistical evaluation gave a positive FB, meaning that the models underestimated the observations.

Table 1.7. Performance of models against the Caltrans Highway 99 data set for receptors downwind and upwind of the roadway (Heist *et al*., 2013)

Model	Downwind				Upwind	
	FB	NMSE	R	FAC2	FB	FAC2
CALINE3	0.25	2.26	0.29	0.45		
CALINE4	0.19	0.86	0.47	0.68		
AERMOD-V	0.15	0.28	0.77	0.78	0.01	0.25
AERMOD-A	0.13	0.31	0.72	0.76		
ADMS	0.09	0.20	0.78	0.85	-0.15	0.12
RLINE	0.05	0.34	0.75	0.78	-0.10	0.30

In estimating the upwind level, only ADMS, AERMOD-V and RLINE can estimate upwind concentration from the roadside. The evaluation of pollutant dispersion for receptors upwind of the road used statistics from FB and FAC2. FB values from ADMS and RLINE were negative, means that the models over-predicted the observation data, and for AERMOD-V, the model under-predicted the observation data.

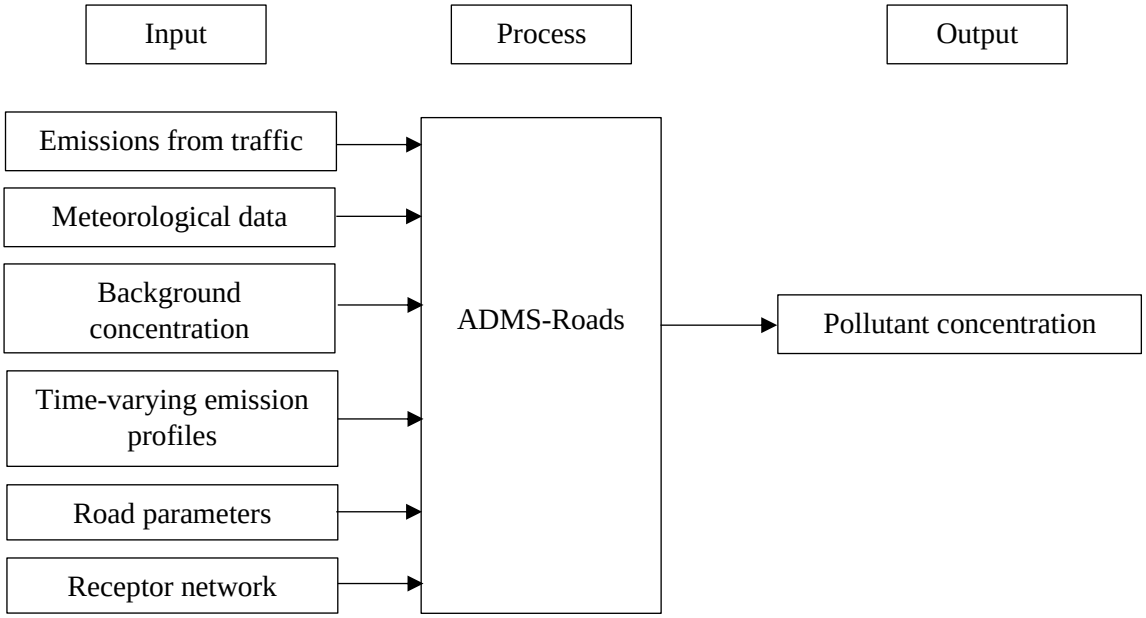


Figure 1.9. Input, process, and output of ADMS-Roads (CERC, 2017)

ADMS-Roads requires as input, for example, the emission sources, meteorological data, background concentration and receptors. It will then process the input data using the ADMS-Roads model to predict the pollutant concentration. Input, process, and output are explained in more details in chapter 4, Section 4.2.

1.7. Research objectives

The ultimate objective of this research is to understand the role of parkland and other grass surfaces in removing pollutants and enhancing air quality by the processes of dispersion and deposition.

The objectives of this study are:

a. To know temporal and spatial variability of pollutant concentrations near the road and across an urban green area using diffusion tube measurements.
b. To develop useful tools (diffusion tubes) that can measure the pollutants in urban green areas.
c. To understand which process (dispersion or deposition) has a larger influence on the reduction of pollutant concentrations in parks using the ADMS-Roads modelling approach.
d. To calculate gases deposition velocities to grassland.

1.8. Thesis structure

Chapter 1 has described the background and information about air pollution sources and pathways in the atmosphere, dispersion and deposition processes of atmospheric pollutants, the measurement and modelling of air quality for urban green spaces.

Chapter 2 describes the materials and methodologies used during sampling process, including the measurement, analysis and modelling approach using ADMS- Roads.

Chapter 3 investigates the air quality measurements in urban green areas.

Chapter 4 explores the set up and evaluation of dispersion modelling.

Chapter 5 evaluates the calculation of gases deposition velocity values.

Chapter 6 summarises conclusions and recommendations for future research.

Chapter 2. Materials and Methodology

2.1. Introduction

The first study of this thesis is to produce a detailed surface-level temporal and spatial variability of the pollutant concentrations in both the roadside and green areas of Birmingham and London. Nitrogen dioxide (NO_2) and ozone (O_3) concentrations were measured using diffusion tubes. The evaluation of the diffusion tube performance was conducted by comparing the diffusion tube (DT) results with those from the automatic analysers (AA) located at the same sampling location, and then calculating their precision in terms of relative standard deviation (%) and accuracy in relative bias (%). The measurement of the NO_2 levels was carried out at Cannon Hill Park for the time period from October 2016 to January 2019 (number of times the samples were taken, N=37); at Tile Cross Park from October 2016 to July 2017 (N=14); at the University of Birmingham site from November 2016 to January 2019 (N=38); at the Biosciences building courtyard (UoB) on the roof and the ground sites from December 2017 to May 2018 (N=6); and at Hyde Park, London from December 2016 to December 2017 (N=16). The O_3 measurements were carried out at Cannon Hill Park, the University of Birmingham site and at the Biosciences building courtyard for the period from March to May 2018 and from October 2018 to January 2019 (N=5).

The second study of this thesis is to investigate the effect of the dispersion and deposition process on removing pollutants at the roadside and in the green areas. A modelling study using ADMS was carried out to predict the pollutant concentrations by dispersion and dry deposition. The set-up and evaluation of ADMS-Roads modelling was established via a series of steps. The sampling location considered in this model was the University of Birmingham. Evaluation of the model set-up was carried out before comparing the observation data from diffusion tubes with the model output.

The third study in this thesis is to calculate deposition velocity at the grassland location. Deposition velocity is one of the factors that influence the deposition process. In the vertical study carried out at the Biosciences building (UoB), deposition velocities for NO_x were estimated using the gradient method. The courtyard inside the building was set as the ground sampling site. At this site, the inlet of the instruments was placed at 1 metre above the

ground. The roof site was 14 metres above the ground sampling location. Measurements of black carbon (BC), NO_x and O_3 were conducted from May 2018 to March 2019. Black carbon data from May to November 2018 were used to estimate the eddy diffusivity values, and NO_x and O_3 data from 20-29 November 2018 and from January to March 2019 were used for calculating the deposition velocity.

Table 2.1. provides a summary with the details of each study and the corresponding chapter in this thesis.

Table 2.1. Information about location, instrument, analysis, and date conducted in each study in this thesis

Study	Location	Instrument	Analysis	Date
1st study Oxides of nitrogen and ozone in urban green space (Chapter 3)	a. Cannon Hill Park, Birmingham b. Tile Cross Park, Birmingham c. Hyde Park, London d. University of Birmingham (UoB) e. Biosciences building, UoB	• Diffusion Tubes • NO_x and O_3 automatic analysers	Spectrophotometry Statistical analysis (SPSS version 23)	October 2016 – February 2019
2nd study The setup and evaluation of dispersion modelling (Chapter 4)	a. University of Birmingham b. BROS and EROS, UoB	Data from study 1 (University of Birmingham site)	ADMS-Roads modelling (version 4.1)	2-11 February 2018 Sampling time of diffusion tubes
3rd study Deposition velocity of gases from vertical gradient of pollutant concentrations (Chapter 5)	Biosciences building, UoB	• Micro-aethalometer • NO_x and O_3 automatic analysers	Gradient concentration method	May 2018 to March 2019 20-29 November 2018 23 January – 2 March 2019

2.2. Measurement Uncertainty

Measurement uncertainty was used to determine the accuracy of the instruments. Accuracy is a measure of how close the instruments' output reading is to the correct value (Moris and Langari, 2012).

2.2.1. Uncertainty Analysis

The calculation of the uncertainty is based on estimation of the uncertainty on each measurement parameter (Erisman *et al.*, 1993; Sorimachi *et al.*, 2003). The uncertainty analysis is useful in showing where the main uncertainties lie.

The uncertainty of a specific measurement, for example, the individual uncertainty of concentration was calculated as standard deviation (SD) or standard error of the mean (SEM). Standard deviation is the amount of variation seen in a set of values.

$$\sigma = \sqrt{\frac{\sum[x - \mu]^2}{N}} \qquad (E.2.1)$$

Where σ is standard deviation, Σ is sum of, x is a value in the data set, μ is the mean of the data set, and N is the number of data points in the population.

Standard error of the mean is a product of the SD divided by the square root of the number of observations of the sample.

$$\sigma_{\bar{x}} = \frac{\sigma}{\sqrt{n}} \qquad (E.2.2)$$

Where $\sigma_{\bar{x}}$ is the SEM, σ is the SD and n is number of observations. The percentage of the individual uncertainty is the uncertainty divided by the mean then multiplied by 100%.

Further, the percentage of the combined uncertainty as the derived parameters is the square root of sum of (n parameter uncertainty squared), as seen in equation E.2.3.

$$\% \text{ Combined uncertainty} = \sqrt{(\% \text{ uncertainty A})^2 + (\% \text{ uncertainty B})^2} \qquad (E.2.3)$$
$$= \sqrt{(\% \text{ SEM A})^2 + (\% \text{ SEM B})^2}$$

2.2.2. Uncertainties in measurement using automatic analyser

The uncertainties of all the elements that are used to determine the final measurement are needed to calculate the overall uncertainty in measurement. For example, an error on the calibration of the O_3 instrument, takes into account the drift in the analyser from zero measurements on the O_3 analyser and the uncertainty of the transfer standard depending on the repeatability, background concentration and span coefficient (Klausen *et al.*, 2003; Galbally *et al.*, 2013). Then, these errors are propagated to get the final uncertainty. The evaluation of the measurement requires an inter-comparison of the ozone analyser with the standard instrument.

For uncertainty of NO_x analyser (Gerboles *et al.*, 2003; Minarro and Ferradaz, 2012), uncertainties arise in the calibration, precision, drift of the analyser and the converter efficiency. Calibration uncertainty will arise from error in the NO standard, error in the sample and standard mass flow controllers and reproducibility of the calculation of the sensitivity. The precision of the measurements is typically determined from multiple measurements at a constant concentration or at zero. Uncertainty is estimated using inter-comparisons or using the response to reference materials.

Stevenson *et al.* (2009) calculated the percentages of uncertainty for an individual measurement of automatic analysers as shown in Table 2.2. Uncertainties of the measurement are described in terms of evaluating the performance of the analyser in fulfilling the Data Quality Objectives of the EU Directive on Ambient Air Quality. The uncertainty is determined using the methodology specified in the European standard by the European Committee for Standardization (CEN).

Table 2.2. Calculated uncertainty of Automatic Urban and Rural Air Quality Monitoring Network (AURN) data using CEN methodology for NO_x and O_3 analysers (Stevenson *et al.*, 2009)

Analysers	NO_x	O_3
Thermo I series Analysers (as Limit Value)	10%	11%
EU Directive Data Quality Objective (at Limit Value)	15%	15%
Horiba 370 series Analysers (as Limit Value)	12%	9%
ME 9800 (UK) series Analysers (at Limit Value)	11%	12%
API A + E series Analysers (at Limit Value)	14%	12%

The uncertainties refer to Thermo I series Analysers are ±10% for NO_x instruments and ±11% for O_3 instruments of each measured mean concentration from the automatic analyser (Stevenson *et al.*, 2009).

2.2.3. Uncertainties in measurement using diffusion tubes

Sources of error in measurement are systematic errors and random errors. In measurement using diffusion tubes, systematic errors come from comparing measurements of diffusion tubes with an automatic analyser. Meanwhile, random errors come from uncertainties of the analysis method, tube dimension, calibration graph and other general random errors.

The variable uncertainties in measurement using diffusion tubes can be described as seen below.

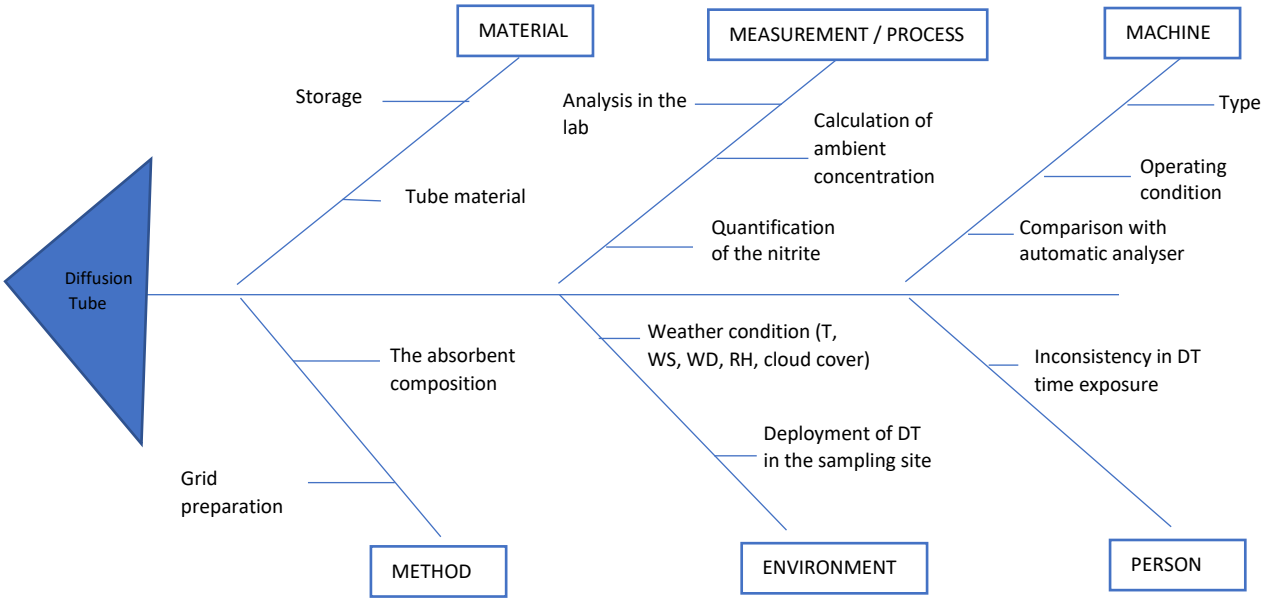


Figure 2.1. Fishbone diagram in reviewing variables of the uncertainties from diffusion tubes measurement, (adopted from: Hamilton and Heal, 2004; Targa and Loader, 2008; Cape, 2009; Heal *et al*., 2019).

Every stage of diffusion tube preparation, deployment in the sites, analysis, quantification of the nitrite, calculation of ambient concentration and comparison with automatic analysers have potential biases and errors (Heal *et al*., 2019). Figure 2.1 shows a fishbone diagram

that reviews possible causes of errors in deployment of diffusion tube, also described in Table 2.3. below.

Table 2.3. Sources of errors in deployment of diffusion tubes (DT)

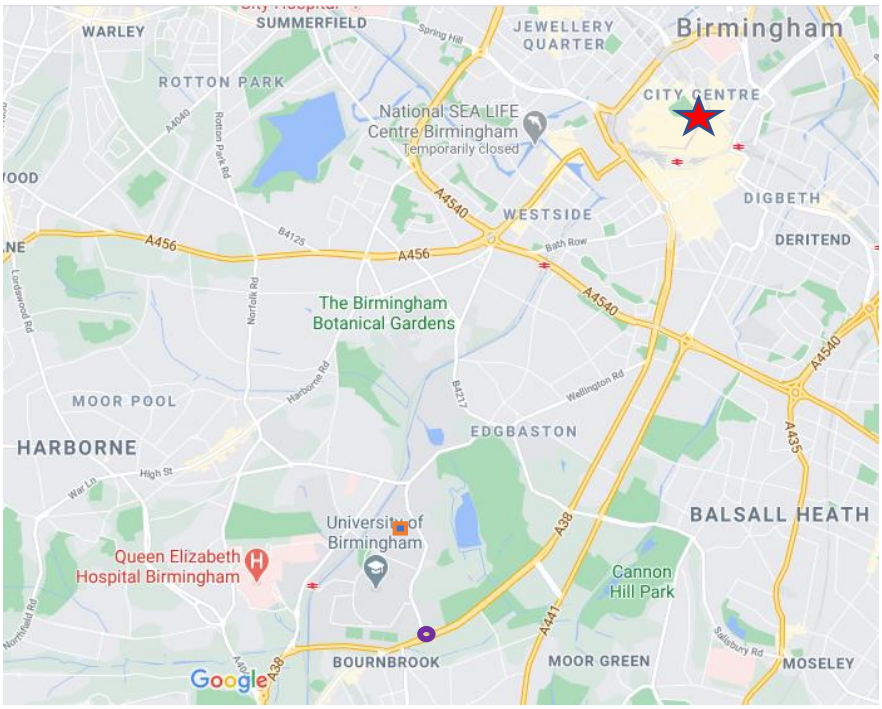
No	Sources of errors	Possible causes	Descriptions	References
1.	Material	Tube material	The length and diameter of DT influence the uptake rate of DT and could influence the extraction efficiency of nitrite.	Vardoulakis *et al.*, 2009; Heal *et al.*, 2019
			Using acrylic or polypropylene to fully transmit UV light. The blocking of UV light could reduce NO_2 photolysis in the tube. Possible bias + 25%	Targa and Loader, 2008; Heal *et al.*, 2019
		Storage	Store the DT in the cool and dark place. High temperatures during storage lead to an apparent reduction of the sampling rate for NO_2.	Cape, 2009; Heal *et al*., 2019
2.	Measurement / process	Analysis in the lab	Inefficient extraction. Use a single laboratory for chemical analysis. Possible bias from -11 to +13%.	Cape, 2009
		Quantification of the nitrite	Conduct high standard of analytical QC/QA. Using a vortex mixer for a minimum of 15 seconds or a vibrating tray for 10-30 minutes to extract nitrite. Colour absorption should be measured within 2 hours. 98% extraction efficiency of nitrite.	Vardoulakis *et al*., 2009; Heal *et al*., 2019
		Calculation of ambient concentration	Variables of temperature, time of exposure, uptake rate, calibration graph and regression / bias correction, can influence the ambient concentration	Vardoulakis *et al*., 2009; Heal *et al*., 2019

No	Sources of errors	Possible causes	Descriptions	References
3.	Machine	Type	Using spectrometer or Ion Chromatography will influence the procedure of DT analysis	Targa and Loader, 2008; Heal *et al.*, 2019
		Operating conditions	Using the optimum wavelength in the range of 540-550 nm if using the spectrophotometer for analysing NO_2 DT	Targa and Loader, 2008
		Comparison with automatic analyser	Overall measurement uncertainty of ± 25% for the EU Directive, and ± 15% for air quality permits	EU Directive, 2008; Heal *et al.*, 2019
4.	Method	The absorbent composition	Consistently use a coating of grids with TEA as absorbent material either pipette or dipping, 20% TEA in water or 50% TEA in water or in acetone	Targa and Loader, 2008; Heal *et al.*, 2019
		Grid preparation	Use 20% of TEA in water, and pipette on the grid The preparation using 10% TEA in water or acetone yielded the uncertainty within 25%	Targa and Loader, 2008; Tarvydaitė and Kazlauskienė, 2014; Heal *et al.*, 2019
5.	Environment	Weather conditions	Overestimated the reference value when temperature, RH and wind speed were at the highest levels The effect of temperature between 15 and 30 °C on uptake rate was ±5%	Gerboles *et al.*, , 2005; Heal *et al.*, 2019
		Deployment in the sampling site	Choose the location that has open circulation, DTs were placed at 2-4 m height Concentration would decrease with height above the source DT should be installed at similar height	Targa and Loader, 2008; Heal *et al.*, 2019
6.	Person	Inconsistency in DT time exposure	Exposure of DT in range of 1-weeks, 2-weeks, 3-weeks, 4-weeks and 6-weeks. Study at urban background for 1-week exposure gives bias + 26% in Edinburgh and +28% in Glasgow	Hamilton and Heal, 2004; Targa and Loader, 2008; Jiménez *et al.*, 2011

Precision and accuracy of diffusion tubes are discussed in Section 2.3.1.4. Standard deviation of diffusion tubes is derived from deployment of triplicate diffusion tubes at each site.

2.3. Oxides of nitrogen and ozone in urban green space

In this study, three passive diffusion tubes were set up along with the automatic analysers at an air quality monitoring site for the evaluation of diffusion tubes. The first location was at Elms Road Observatory Site (EROS) at the University of Birmingham, which represents an urban background site not affected by road emissions and local human activities. EROS is located 3.5 km southwest of the Birmingham city centre and 1 km from BROS (Bristol Road Observatory Site), as the second site. BROS is located 3.6 m away from the heavy traffic of the A38 road, as shown in Figure 2.2.



Note of markers: = BROS; = EROS; = city centre

Figure 2.2. Map with markers that shows location of BROS, EROS and city centre in Birmingham, UK (https://www.google.com/maps/place/University+of+Birmingham/@52.4592561,-1.9598751,12z)

During August 2016 to September 2017, EROS was equipped with a chemiluminescence analyser recording hourly NO_x and NO_2 concentrations. Due to refurbishment at the EROS location, the analyser was set at the BROS site from September 2017 to February 2018. Starting from the 2 February 2018 to 15 April 2018, two instruments (model 42i chemiluminescence analyser and model 49i ozone analyser) were set at the two locations, BROS and EROS (in a trailer). Subsequently, the instruments were moved to the Biosciences building for the vertical sampling campaign, which took place from April 2018 to March 2019.

2.3.1. Diffusion tubes

Diffusion tubes are passive samplers for the measurement of certain pollutants using a process called molecular diffusion. The NO_2 and NO_x diffusion tubes that were used in this study were made according to the Palmes type of diffusion tubes (Figures 2.4 and 2.5 show NO_2 DT images, Figure 2.7 shows NO_x DT images). This type of diffusion tube consists of a plastic tube, two stainless steel grids (#100 mesh) with absorbent reagent and two caps. The diffusion tubes were analysed using a Spectrometer, Jenway 6800 (Figure 2.3). The evaluation of diffusion tube performance is described in Section 2.3.1.4.

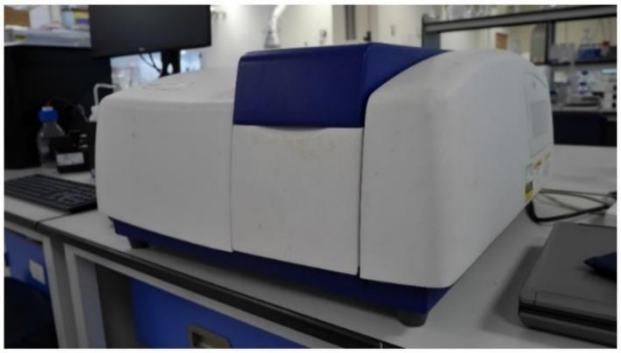


Figure 2.3. Picture of Spectrometer Jenway 6800

2.3.1.1. NO_2 diffusion tubes

NO_2 in the ambient air is captured the absorbent triethanolamine (TEA) in the tube. The NO_2 concentration is higher in the air than in the tube, thus NO_2 diffuses into the tube and is collected by the absorbent at the end of the tube. After exposure, nitrite (NO_2^-) which is

collected on the grids is extracted and reacts with reagents (sulfanilamide and *N*-(1-naphthyl)-ethylenediamine dihydrochloride (NEDD)) to form a purple solution. The intensity of the colour of the purple solution is measured by the spectrophotometer. The concentration of nitrite in the sample is obtained using a calibration graph of standard nitrite solutions. The concentration of nitrite is used to calculate the mass of nitrite collected by the tube during the exposure interval. Then, the average ambient concentration of NO_2 can be calculated (Bryan and Grisham, 2007; Targa and Loader, 2008; Patton and Kryskalla, 2011).

Preparation and analysis of diffusion tubes were conducted in a laboratory at the University of Birmingham (UK). The method used for the preparation of the sample solutions and the standard nitrite solutions for the UV-Vis analysis was from Targa and Loader (2008). NO_2 measurements were performed by UV-Vis analysis, using a Spectrometer Jenway 6800, scanning the wavelength from 530 to 550 nm, and taking the optimum absorbance at 540 nm.

For the NO_2 diffusion tube, the main body consists of an acrylic tube with dimensions (mean ± SEM) of length 71.03 ± 0.06 mm and an internal diameter of 11.05 ± 0.04 mm, two flexible plastic (polyethylene) caps, and two grids (coated with the absorbent). The two grids are made of stainless steel of #100 mesh. These have a thickness of 0.16 ± 0.004 mm and are coated with TEA 20% in water (the absorbent). The two grids are placed at the closed end of the tube. The caps have different colours at the top and at the bottom. We used a specific colour to identify the cap containing the absorbent during sampling. Appendix 2.1 shows a list of materials and reagents needed to manufacture and analyse the NO_2 diffusion tubes.

(a) (b)

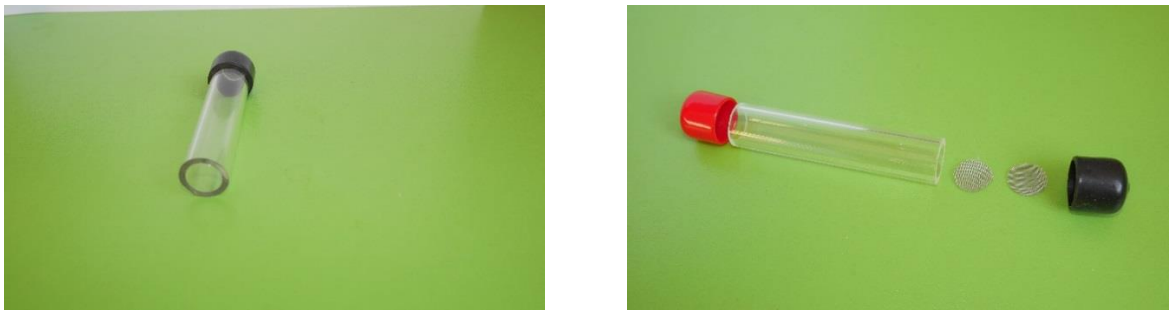


Figure 2.4. **(a)** NO_2 diffusion tube with open end; and **(b)** components of diffusion tube with open end consist of an acrylic tube, two stainless steel grids and two caps

(a) (b)

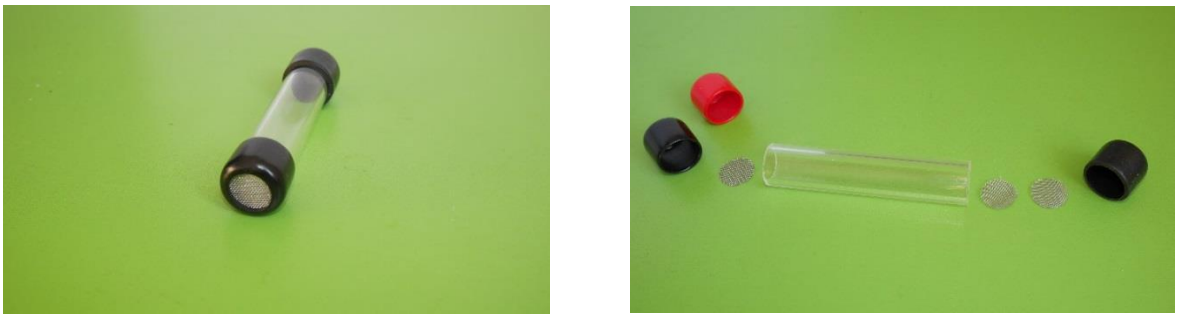


Figure 2.5. **(a)** NO_2 diffusion tube with membrane; and **(b)** components of diffusion tube with membrane consist of an acrylic tube, two stainless steel grids, two caps and additional stainless steel #60 meshes in the open cap

Diffusion tubes with open ends (Figure 2.4) were used from August 2016 to April 2018, and diffusion tubes with membranes (Figure 2.5.) were used from October 2017 to January 2019. The diffusion tube "open end" is a standard tube that is open at one end, while the diffusion tube "with membrane" has an additional stainless steel #60 meshes with 0.31 ± 0.01 mm (mean ± SEM) thickness and is located at the inlet end as a protection to reduce the wind influence. The influence of wind turbulence could be to overestimate the reading due to eddy diffusion which may cause shortening of the effective length of the tube (Bush *et al.*, 2001). Masey *et al.* (2017) confirmed that wind-speed could increase the uptake rates of a diffusion tube, as they found a linear relationship between wind speed and uptake rate. The use of protection with a membrane or mesh at the open end of the tube could be beneficial in reducing the turbulence effect (Masey *et al.*, 2017). However, (Kirby *et al.*, 2000) showed results from their two studies in the UK and they confirmed that overreading of the diffusion tube is more related to chemistry changes in the tube rather than the turbulence effect.

The tube's physical dimensions, mesh, filter and membrane were measured with a shock-proof dial vernier caliper (measuring scale 0 – 150 mm/0.02 mm) as shown in Figure 2.6 and the measurement results appear in Table 2.4.



Figure 2.6. The shock-proof dial vernier caliper was used to measure component of diffusion tube

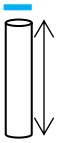
Table 2.4. Measurement results of tube length, tube diameter, stainless steel mesh, membrane, filter and spacer for NO_2 and NO_x Diffusion Tube (DT) using dial vernier caliper

No	Tube in length, mm (for NO_2 and NO_x DT)	Tube diameter, in mm (for NO_2 and NO_x DT)	Stainless steel mesh, in mm (for NO_2 and NO_x DT)	Membrane, in mm (for NO_2 and NO_x DT)	Filter, in mm (for NO_x DT)	Spacer, in mm (for NO_x DT)
1.	70.96	11.03	0.16	0.32	0.12	3.02
2.	70.90	11.01	0.15	0.29	0.09	3.06
3.	70.92	11.02	0.16	0.34	0.10	3.00
4.	71.24	11.16	0.17	0.31	0.13	3.02
5.	71.20	11.18	0.14	0.32	0.14	3.06
6.	70.94	10.91	0.16	0.30	0.10	3.04
Mean	71.03	11.05	0.16	0.31	0.11	3.03
Standard Deviation (SD)	0.15	0.10	0.01	0.02	0.02	0.02
	Tube in length	Tube diameter	Stainless steel mesh	Membrane	Filter	Spacer
Standard Error of the Mean (SEM)	0.06	0.04	0.004	0.01	0.01	0.01
% SEM	0.09%	0.37 %	2.69%	2.28	7.08	0.33
Mean ± SEM	71.03 ± 0.06 mm	11.05 ± 0.04 mm	0.16 ± 0.004 mm	0.31 ± 0.01 mm	0.11 ± 0.01 mm	3.03 ± 0.01 mm
Mean ± % SEM	71.03 mm ± 0.09 %	11.05 mm ± 0.37 %	0.16 mm ± 2.69 %	0.31 mm ± 2.28 %	0.11 mm ± 7.08 %	3.03 mm ± 0.33 %

Uncertainty is calculated using SEM as individual uncertainty and combined uncertainties are calculated using the square root of the sum of squares of the individual uncertainty as percentage; refer to the equations E.2.2 and E.2.3 respectively, in Section 2.2.1. The estimation of combined uncertainties was based on the error of each contributing variable (Adon *et al.*, 2013).

Table 2.5. shows dimension of the tube (mean ± SEM) and calculation of sampling rate from NO_2 diffusion tubes with open end and NO_2 diffusion tubes with membrane.

Table 2.5. Dimension and sampling rate of diffusion tubes

NO_2 tube with open end	**NO_2 tube with membrane**
 Stainless steel mesh absorbent • Diameter of the tube is 11.05 mm ± 0.37 % (mean ± % SEM) • Length of the tube consist of tube and two stainless steel 100 mesh Length of the tube = 71.03 mm ± 0.09 % (mean ± % SEM) Stainless steel 100 mesh = 0.16 mm ± 2.69 % (mean ± % SEM) Two stainless steel 100 mesh = 0.32 mm Percentage uncertainty of stainless steel mesh in total = $\sqrt{(2.69\%)^2 + (2.69\%)^2} = 3.81\%$ 0.32 mm + 3.81% (mean ± % SEM) Total uncertainty = $\sqrt{(0.09\%)^2 + (2.69\%)^2 + (2.69\%)^2} = 3.82\%$ Length of the tube in total = 71.35 mm ± 3.82 % = 71.35 ± 2.73 mm	 Stainless steel mesh absorbent membrane • Diameter of the tube is 11.05 mm ± 0.37 % (mean ± % SEM) • Length of the tube consist of tube, two stainless steel 100 mesh and membrane Length of the tube = 71.03 mm ± 0.09 % (mean ± % SEM) Stainless steel 100 mesh = 0.16 mm ± 2.69 % (mean ± % SEM) Two stainless steel 100 mesh = 0.32 mm Percentage uncertainty of stainless steel mesh in total = $\sqrt{(2.69\%)^2 + (2.69\%)^2} = 3.81\%$ 0.32 mm + 3.81% (mean ± % SEM) Membrane = 0.31 mm ± 2.28 % (mean ± % SEM) Total uncertainty = $\sqrt{(0.09\%)^2 + (2.69\%)^2 + (2.69\%)^2 + (2.28\%)^2} = 4.44\%$ Length of the tube in total = 71.66 mm ± 4.44 % = 71.66 ± 3.18 mm

NO_2 tube with open end	NO_2 tube with membrane
• The cross-sectional area of the tube (A) Tube diameter (d) = 11.05 ± 0.04 mm Tube radius (r) = 5.525 ± 0.02 mm $A = \pi r^2 = \pi (5.525)^2 = 30.53\ \pi$ $= 95.9\ mm^2$ $\Delta A \approx dA = (dA/dr)\ dr$ $= 30.53\ \pi\ dr = 30.53\ \pi\ (0.02)\ mm$ $= 1.92\ mm^2$ $A = 95.9 \pm 1.9\ mm^2$ $= 95.9\ mm^2 \pm 2\ \%$	• The cross-sectional area of the tube (A) Tube diameter (d) = 11.05 ± 0.04 mm Tube radius (r) = 5.525 ± 0.02 mm $A = \pi r^2 = \pi (5.525)^2 = 30.53\ \pi$ $= 95.9\ mm^2$ $\Delta A \approx dA = (dA/dr)\ dr$ $= 30.53\ \pi\ dr = 30.53\ \pi\ (0.02)\ mm$ $= 1.92\ mm^2$ $A = 95.9 \pm 1.9\ mm^2$ $= 95.9\ mm^2 \pm 2\ \%$
• Diffusion Coefficient of NO_2 as STP = 0.136 $cm^2\ s^{-1}$ with uncertainty 10% (Cape, 2009) Diffusion coefficient of NO_2 at 11 °C (284 K) = 0.146 $cm^2\ s^{-1}$	• Diffusion Coefficient of NO_2 as STP = 0.136 $cm^2\ s^{-1}$ with uncertainty 10% (Cape, 2009) Diffusion coefficient of NO_2 at 11 °C (284 K) = 0.146 $cm^2\ s^{-1}$
• Sampling rate = $\frac{D_{12}\ A}{Z}$ $= 7.06 \times 10^{-5}\ m^3\ h^{-1}$ Uncertainty = $\sqrt{(\Delta D)^2 + (\Delta A)^2 + (\Delta Z)^2}$ $= \sqrt{(10\%)^2+(2\%)^2+(3.82)^2}$ $= 11\%$ $= 7.06 \times 10^{-5}\ m^3\ h^{-1} \pm 11\%$ $= 7.06 \times 10^{-5} \pm 0.78 \times 10^{-5}\ m^3\ h^{-1}$	• Sampling rate = $\frac{D_{12}\ A}{Z}$ $= 7.03 \times 10^{-5}\ m^3\ h^{-1}$ Uncertainty = $\sqrt{(\Delta D)^2 + (\Delta A)^2 + (\Delta Z)^2}$ $= \sqrt{(10\%)^2+(2\%)^2+(4.44)^2}$ $= 11\%$ $= 7.03 \times 10^{-5}\ m^3\ h^{-1} \pm 11\%$ $= 7.03 \times 10^{-5} \pm 0.77 \times 10^{-5}\ m^3\ h^{-1}$

The diffusion tubes were deployed in triplicate at each site and at a height of 2.6 – 3.2 m. Temperature may affect DT measurements through the diffusion coefficient, normalisation to 293 K and the gas law changes on mass concentration. Temperature-dependent diffusion coefficients were calculated according to Targa and Loader (2008) and used to change nitrite concentrations to NO_2 in air, using also the dimension of the tube and time of exposure DT in air.

Sampling rate

The rate at which the compound moves into the tube is called the uptake rate or sampling rate.

$$Sampling\ rate\ = \left(\frac{D_{12}\ A}{Z}\right) \qquad (E.2.4)$$

Where, sampling rate = sampling rate of NO_2 ($cm^3\ s^{-1}$) or ($m^3\ h^{-1}$); A = the cross-sectional area of the tube (cm^2); Z = the length of the tube (cm); D_{12} = diffusion coefficient of NO_2 gas through the air, at STP, 0 Celcius (273 K) at 1 atmosphere (101.3 kPa).

Based on (Massman, 1998), the diffusion coefficient for NO_2, NO and O_3 are 0.1361 $cm^2\ s^{-1}$, 0.1988 $cm^2\ s^{-1}$ and 0.1444 $cm^2\ s^{-1}$ respectively at STP. The diffusion coefficient is temperature-dependent and should be corrected to UK ambient temperatures. A typical mean of the UK ambient temperature is based on data from Met Office for the past 10 years is in range of 10 to 12 °C or 284 to 285 K (Targa and Loader, 2008).

The diffusion coefficient is proportional to the temperature to the power of 1.81 (Targa and Loader, 2008). For example, the average temperature in the UK is assumed to be 11 °C or 284 K, so for DT exposed in the UK, the sampling rate (D) should be 0.146 $cm^2\ s^{-1}$, as calculated below.

$$D_{284\,K} = D_{273\,K}\,x\left\{\frac{284}{273}\right\}^{1.81} = 0.136\ cm^2 s^{-1}\ x\left\{\frac{284}{273}\right\}^{1.81} = 0.146\ cm^2 s^{-1} \quad (E.2.5)$$

Calculation of NO_2 concentration

The atmospheric concentration of NO_2 was estimated from the measured total mass of nitrite and using the sampling rate and time of exposure.

1) Calculate the total mass of nitrite in the tube (Targa and Loader, 2008)
2) Calculate the sampling rate ($m^3\ h^{-1}$) (see Equation 2.4, or Table 2.5)
3) Calculate NO_2 concentration (μg m^{-3}) in the ambient air with equation

$$NO_2\ in\ the\ ambient\ air = \frac{T}{293}\ x\ \frac{mass\ of\ nitrite\ in\ the\ tube}{sampling\ rate\ x\ time\ of\ exposure} \qquad (E.2.6)$$

Where, T (in Kelvin) is the average temperature of air over the sampling period. The temperature data was taken from the nearest weather station from the Centre for Environmental Data Analysis (CEDA), http://archive.ceda.ac.uk/midas_stations/. For the Birmingham site, data were taken from Winterbourne No. 2 weather station (ID 56424), and for the London site, data were taken from London City Airport weather station (ID 18929).

The ambient temperature should be normalised to 20 °C or 293 K for the purpose of reviewing and assessing the measured concentrations, and for comparing the measured concentrations with the EU Limit values or AQS Objectives, that the concentrations must be reported in mass unit (µg m^{-3}) at 293 K and 101.3 kPa (Targa and Loader, 2008).

The measured concentration can be reported in µg m^{-3} and ppb. However, the conversion on mass concentration needs the gas law changes. For example, in changing the concentration from µg m^{-3} to ppb is using the equation as seen below.

$$P.V = n.R.T \qquad (E.2.7)$$

Where: P is pressure (Pascals), V is volume (m^3), n is Avogadro constant, R is the ideal gas constant, 8.314 J/(K.mol), and T is temperature of the gas (K).

Example, 10 µg m^{-3} of NO_2 concentration at 13 °C and pressure at 1018 hPa, then the concentration is 5.08 ppb, as calculated below.

n/V = P (R T)

= 101800 / (8.314 x 286)

= 101800 / 2377.8

= 42.81 mol m^{-3}

NO_2 = 14 + 32 = 46 g mol^{-1}

1.10^{-9} x 42.81 mol m^{-3} x 46 g mol^{-1} = 1,969.26 x 10^{-9} g m^{-3} = 1.97 µg m^{-3}

$$10\ \mu g\ m^{-3} \times \frac{1\ ppb}{1.97\ \mu g\ m^{-3}} = 5.08\ ppb$$

2.3.1.2. NO_x diffusion tubes

The NO_x diffusion tubes have a similar configuration as the NO_2 tubes, but we used a filter containing 5% of CrO_3 solution (De Santis *et al.*, 2001, 2002) to oxidise NO from the air. The NO gas trapped in the tube reacts with the oxidant solution to form NO_2 which is then collected by the TEA absorbent. A fiberglass filter was dipped into the solution containing the oxidant for approximately 15 minutes and located at the closed cap. A spacer with a thickness of 3.03 ± 0.01 mm (mean ± SEM) was mounted to separate the oxidant from the #100 mesh containing the TEA absorbent.



Figure 2.7. NO_x diffusion tube components with membrane consist of an acrylic tube, two stainless steel grids, a spacer, a filter, two caps, and a stainless steel #60 meshes in the open cap,

Figure 2.7. shows the component of the NO_x diffusion tubes and Figure 2.8. presented the schematic diagram of NO_x deployment.

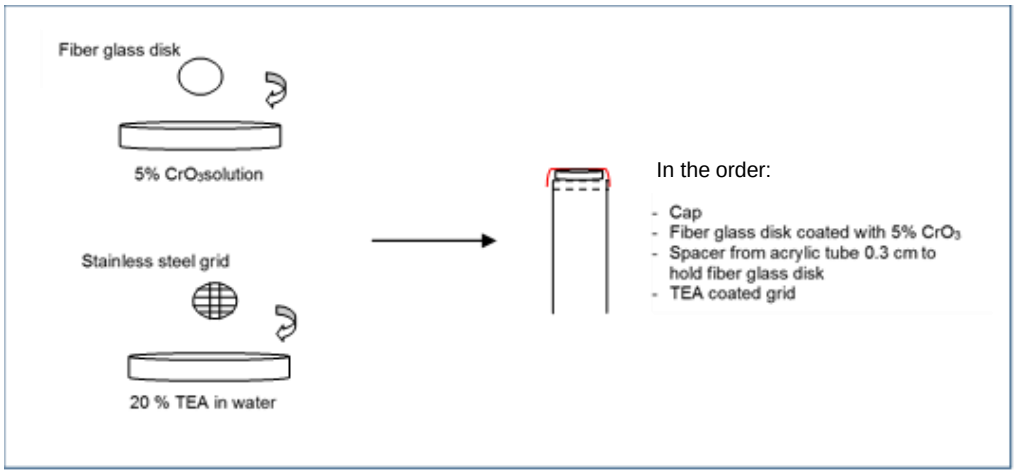
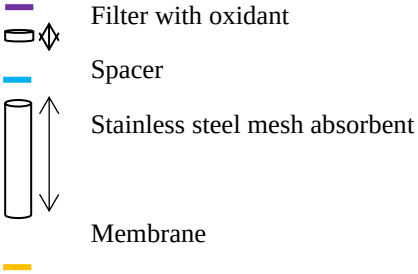
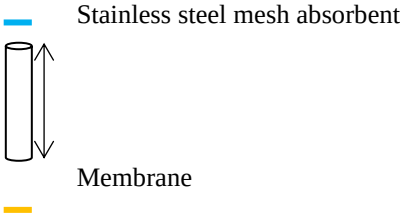


Figure 2.8. Schematic diagram showing NO_x DT deployment

Dimension of the tube, calculation of sampling rate and the uncertainties from NO_x diffusion tubes with membrane and NO_2 diffusion tubes with membrane are described in Table 2.6.

Table 2.6. Dimension and sampling rate of NO_x diffusion tubes (two tubes consist of NO_x and NO_2 tubes)

NO_x tube with membrane	**NO_2 tube with membrane**
	
• Diameter of the tube is 11.05 mm ± 0.37 % (mean ± % SEM)	• Diameter of the tube is 11.05 mm ± 0.37 % (mean ± % SEM)
• Length of the tube in total = 74.8 mm ± 8.37 % = 74.8 ± 6.26 mm	• Length of the tube in total = 71.66 mm ± 4.44 % = 71.66 ± 3.18 mm
• The cross-sectional area of the tube (A) Tube diameter (d) = 11.05 ± 0.04 mm Tube radius (r) = 5.525 ± 0.02 mm $A = \pi r^2 = \pi (5.525)^2 = 30.53\ \pi$ $= 95.9\ mm^2$ $\Delta A \approx dA = (dA/dr)\ dr$ $= 30.53\ \pi\ dr = 30.53\ \pi\ (0.02)\ mm$ $= 1.92\ mm^2$ $A = 95.9 \pm 1.9\ mm^2$ $= 95.9\ mm^2 \pm 2\ \%$	• The cross-sectional area of the tube (A) Tube diameter (d) = 11.05 ± 0.04 mm Tube radius (r) = 5.525 ± 0.02 mm $A = \pi r^2 = \pi (5.525)^2 = 30.53\ \pi$ $= 95.9\ mm^2$ $\Delta A \approx dA = (dA/dr)\ dr$ $= 30.53\ \pi\ dr = 30.53\ \pi\ (0.02)\ mm$ $= 1.92\ mm^2$ $A = 95.9 \pm 1.9\ mm^2$ $= 95.9\ mm^2 \pm 2\ \%$
• Diffusion Coefficient of NO as STP = 0.1988 $cm^2\ s^{-1}$ assuming an uncertainty of 10% Diffusion coefficient of NO at 11 °C (284 K) = 0.214 $cm^2\ s^{-1}$	• Diffusion Coefficient of NO_2 as STP = 0.136 $cm^2\ s^{-1}$ with uncertainty 10% (Cape, 2009) Diffusion coefficient of NO_2 at 11 °C (284 K) = 0.146 $cm^2\ s^{-1}$
• Sampling rate = $\frac{D_{12}\ A}{Z}$ $= 9.85 \times 10^{-5}\ m^3\ h^{-1}$ Uncertainty = $\sqrt{(\Delta D)^2 + (\Delta A)^2 + (\Delta Z)^2}$	• Sampling rate = $\frac{D_{12}\ A}{Z}$ $= 7.03 \times 10^{-5}\ m^3\ h^{-1}$ Uncertainty = $\sqrt{(\Delta D)^2 + (\Delta A)^2 + (\Delta Z)^2}$

NO_x tube with membrane	NO_2 tube with membrane
$= \sqrt{(10\%)^2+(2\%)^2+(8.37)^2}$	$= \sqrt{(10\%)^2+(2\%)^2+(4.44)^2}$
$= 13\%$	$= 11\%$
$= 9.85 \times 10^{-5}\ m^3\ h^{-1} \pm 13\%$	$= 7.03 \times 10^{-5}\ m^3\ h^{-1} \pm 11\%$
$= 9.85 \times 10^{-5} \pm 1.28 \times 10^{-5}\ m^3\ h^{-1}$	$= 7.03 \times 10^{-5} \pm 0.77 \times 10^{-5}\ m^3\ h^{-1}$

Calculation of NO_x concentration

The sampling rates of NO_2 and NO_x samples were $7.03 \times 10^{-5} \pm 0.77 \times 10^{-5}\ m^3\ h^{-1}$ and $9.85 \times 10^{-5} \pm 1.28 \times 10^{-5}\ m^3\ h^{-1}$, respectively.

1) Calculate NO_2 concentrations using equation E.2.4 or Table 2.6)
2) Calculate NO_x as NO_2 concentration

$$NO_x\ concentration\ as\ NO_2 = \frac{T}{293}\ x\ \frac{mass\ of\ nitrite\ in\ NO_x\ tube}{sampling\ rate\ \ x\ \ time\ of\ exposure} \qquad (E.2.8)$$

3) Calculate NO concentration

   NO_x concentration as NO_2 ($\mu g\ m^{-3}$) = NO_2 + NO as NO_2

   NO concentration = (30/46) x NO as NO_2

2.3.1.3. O_3 diffusion tubes

Diffusion tubes for O_3 were supplied from Gradko International Ltd. The O_3 diffusion tube consists of a fluorinated ethylene polymer tube and thermoplastic rubber cap at both ends. The grid containing absorbent was at the black cap and one-micron porosity filter was at the white cap. The tube was 71.0 mm length and had an internal diameter of 11.0 mm and the recommendation of exposure period was 2 - 4 weeks.

The concentrations of nitrate ions were determined by ion chromatography with reference to the calibration curve obtained from the analysis of standard nitrate solutions (https://www.gradko.com/environmental/environmental-products/ozone-diffusion-tubes.shtml). Analysis and result were carried out by Gradko International Ltd. O_3 concentration was reported in $\mu g\ m^{-3}$ and ppb.

2.3.1.4. Performance evaluation of diffusion tubes (precision and accuracy)

Precision and accuracy using relative bias are used to evaluate the performance of diffusion tube. Triplicate tubes were deployed in each of the sampling sites to review the precision. Triplicate tubes of blank samples were also prepared to correct the measurement result from the influence of preparation and laboratory procedures. Blank samples were analysed with the same procedures as for samples.

Relative Standard Deviation (RSD) was used to determine the ability of samplers to produce similar results consistently (Helaleh *et al.*, 2002; Delgado Saborit and Esteve Cano, 2007; Targa and Loader, 2008; DEFRA, 2009). The measurement value is accepted if the RSD ≤ 15%.

$$RSD = \frac{SD}{mean} x100 \qquad (E.2.9)$$

Where SD is standard deviation and mean is the average concentration value at the sampling point (µg m^{-3}).

Here, accuracy of the diffusion tube measurement is defined as the ability to produce the same result as the automatic analyser, used here as reference instruments. The percent difference in the results obtained by the passive diffusion tubes and the automatic analyser were evaluated as bias (Delgado Saborit and Esteve Cano, 2007; Targa and Loader, 2008; DEFRA, 2009), using the formula below:

$$Bias(B) = \frac{(DT - AA)}{AA} x100\% \qquad (E.2.10)$$

The bias adjustment factor was calculated using the equation (DEFRA, 2009, 2018):

$$Bias\ adjustment\ factor(A) = \frac{AA}{DT} \qquad (E.2.11)$$

Where, DT is the mean of triplicate tubes (µg m^{-3}), AA is the mean of concentration given by the automatic analyser (µg m^{-3}) in the same period of time with DT.

Correction for the bias adjustment factor was performed using the linear regression value. Linear regression was established with the automatic analyser as the independent variable and with passive samplers as the dependent variable.

Limit of detection (LoD) is the minimum concentration that is determined by the analytical method (De Santis *et al.*, 1997; Delgado-Saborit and Esteve-Cano, 2007).

$$Limit\ of\ detection\ (LoD) = 3\ x\ SD \qquad (E.2.12)$$

LoD unit is in μg m^{-3}. The SD refers to standard deviation of the blank samples of N data. Where SD is the square root of variance and is done by determining each data point's deviation to the mean, and N is the population data number.

2.3.2. Automatic analyser

2.3.2.1. NO_x analyser

NO, NO_2, and NO_x were measured using chemiluminescence analyser, 42i type from Thermo Scientific, Thermo Scientific and 42C type from Thermo Environmental Instruments.

The air sample enters a filter and passes a flow control capillary, then it splits into NO and NO_x channels. In the NO channel (NO mode, see Figure 2.9), the sample reaches the reaction chamber where it is mixed with O_3. The chemical reaction of NO and O_3 produces light with intensity proportional to the NO concentration. The emitted light is filtered by a selective optical filter and converted to electric signal by a photomultiplier tube.

$$NO + O_3 \rightarrow NO_2 + O_2 + hv \qquad (R.2.1)$$

In the NO_x channel, NO_2 is reduced to NO by a molybdenum NO_2-to-NO converter (NO_x mode, see Figure 2.9), then the sample enters the reaction chamber where it is analysed with the same procedure as for NO. In this case, the electrical signal is proportional to the sum of NO and NO_2 concentrations.

$$3\ NO_2 + Mo \rightarrow 3\ NO + MoO_3 \qquad (R.2.2)$$

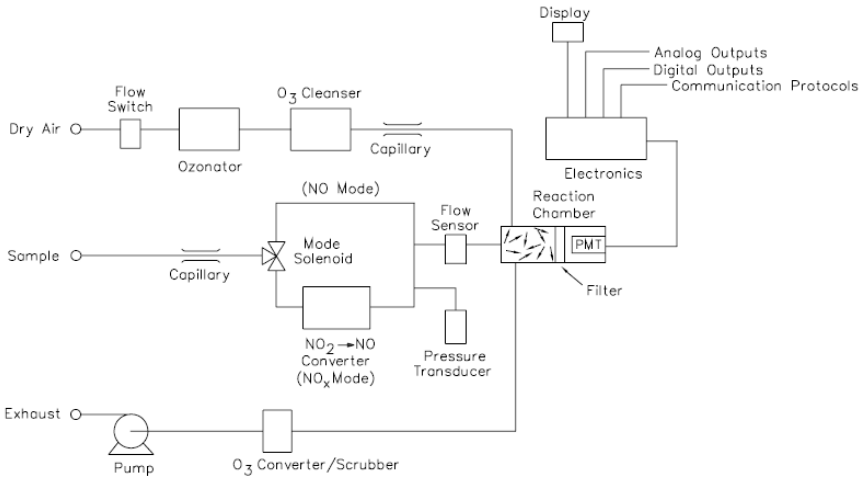


Figure 2.9. Schematic diagram of NO_x analyser (Thermoscientific, 2007)

The NO_2 concentration is calculated from the difference in concentration of NO from the NO_x channel and the NO channel. The Chemiluminescence analyser was calibrated according to European standard and national protocols EN 14211:2012 (BSI, 2012). Calibration and sensitivity adjustment using the equation from BS EN 14211:2012 are as follows:

$$\text{True concentration} = (\text{instrument reading} - \text{Measured ZERO}) \times \frac{\text{True SPAN}}{(\text{Measured SPAN} - \text{Measured ZERO})} \quad \text{(E.2.13)}$$

NO adjustment (BS EN 14211:2012)

$$C_{NO} = (Y_{NO} - C_{NO,ZERO}) \times \frac{C_{CAL\ GAS}}{(C_{NO,CAL} - C_{NO,ZERO})} \quad \text{(E.2.14)}$$

Where:

C_{NO} = the corrected NO reading
$C_{CAL\ GAS}$ = the concentration of NO gas
$C_{NO,CAL}$ = the reading of NO during calibration
$C_{NO,ZERO}$ = the reading of NO during zero check
Y_{NO} = the reading of NO during measurement

NO_x adjustment (BS EN 14211:2012)

$$C_{NOx} = (Y_{NOx} - C_{NOx,\,ZERO}) \times \frac{C_{CAL\,GAS}}{(C_{NOx,\,CAL} - C_{NOx,\,ZERO})} \quad \text{(E.2.15)}$$

Where:
C_{NOx} = the corrected NO_x reading
$C_{CAL\,GAS}$ = the concentration of NO_x gas
$C_{NOx,\,CAL}$ = the reading of NO_x during calibration
$C_{NOx,\,ZERO}$ = the reading of NO_x during zero check
Y_{NOx} = the reading of NO_x during measurement

NO_2 adjustment (BS EN 14211:2012)

$$C_{NO_2} = \frac{C_{NOx} - C_{NO}}{Ec} \times 100 \quad \text{(E.2.16)}$$

Where:
C_{NOx} = the corrected NO_x reading
C_{NO} = the corrected NO reading
E_C = converter efficiency in %

2.3.2.2. O_3 analyser

O_3 was measured using a UV absorption analyser, 49i Thermo Scientific. O_3 absorbs light in the UV spectrum, and the intensity of absorption is proportional to the O_3 level according to the Beer-Lambert Law.

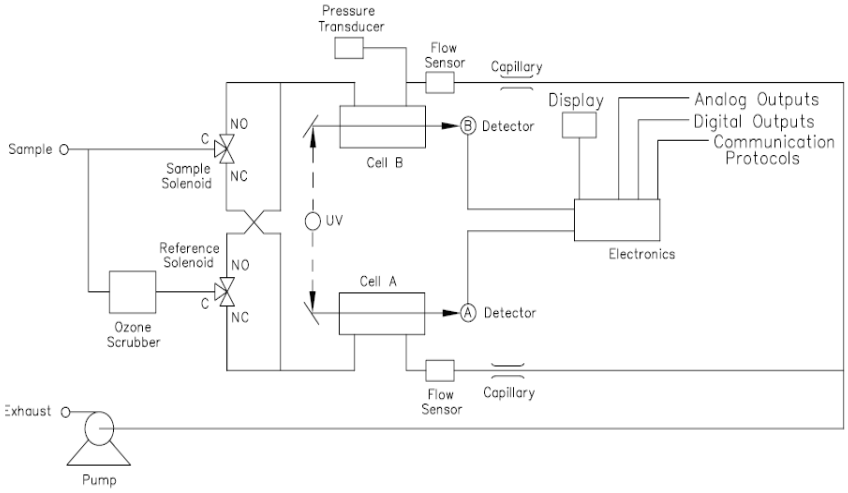


Figure 2.10. Schematic diagram of O_3 analyser (Thermoscientific, 2017)

Air is divided to flow directly to the sample solenoid as sample gas (I), and the other flow to the reference solenoid. In the reference solenoid, air passes through the ozone scrubber, which removes the ozone from the air and becomes reference gas (I_o). The solenoid valve switches the sample gas and the reference gas flow between cell A and cell B, and vice versa (see Figure 2.10). The ozone concentration is the average output from cell detector A and cell detector B. The O_3 analyser was calibrated using the absorption cross-section of O_3.

2.3.3. Sampling locations

Sampling campaign was conducted in Birmingham and London (UK). In this study, parks and grassland areas are referred to as urban green spaces. Diffusion tubes were mounted unsheltered on a pole or lamppost at a height of 2.5 to 3.5 m above the ground and set perpendicularly from the roadside, through the park. The distance of the diffusion tubes from the road was estimated using a measured distance function from a Google map.

Three samples were collected at each point (triplicate). The time exposure for the diffusion tubes was 2-4 weeks. The diffusion tubes were then taken and capped securely, and analysed in the laboratory.

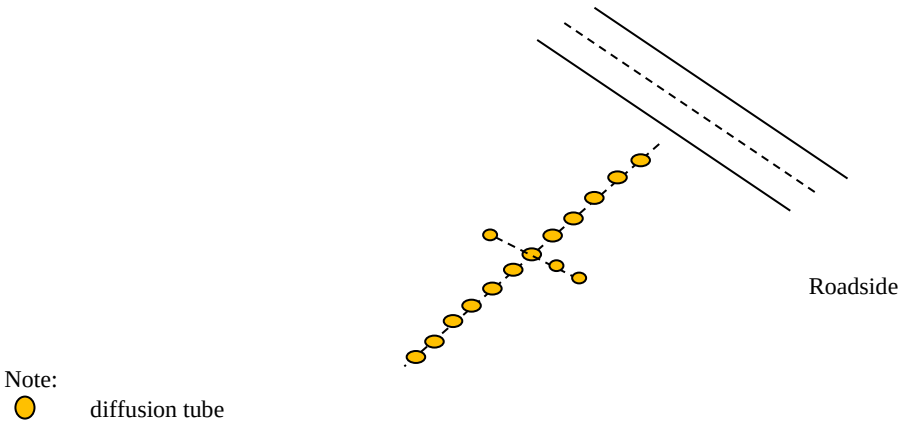


Figure 2.11. Ideal design of placing diffusion tubes at an axis perpendicular from roadside

2.3.3.1. Birmingham, UK

Birmingham is the second largest city and metropolitan area in the UK, after London, with an area of 268 km^2 and a population of 1.14 million in 2019 (BCC, 2020; http://www.emta.com/spip.php?article26). There are 571 parks and gardens in Birmingham, including Cannon Hill Park and Tile Cross Park (https://www.theguardian.com/cities/2014/apr/03/birmingham-san-francisco-oslo-global-green-biophilic-cities-club).

2.3.3.1.1. Cannon Hill Park

Cannon Hill Park opened in 1873 and it is currently managed by the Birmingham City Council. It has an area of 925 m (length) x 314 m (width). The park facilities include areas for recreation, refreshments, walks, events, and education. On the northside, the park is located near Edgbaston Road and opposite the Edgbaston stadium, the Warwickshire Cricket Ground. On the east side, there is Russell Road and at the south, there is a residential area, Moor Green. On the west side, there are other apartments, buildings, and the Birmingham Wildlife Conservation Park bordering the main roads, the A441 and Pershore Road.

Sampling points were set in 13 locations in Cannon Hill Park. The first location, CH 1 was near the road, while CH X and CH 2 - CH 12 were set inside the park (Figure 2.12.). The passive diffusion sampler, CH 1, was fixed onto a lamppost outside of Cannon Hill Park, which is 1.5 meters from the edge of the main road. CHX was inside of Cannon Hill Park, near the main entrance on the Edgbaston Road, and was about 30 meters from the edge of the road. Diffusion tubes at CH X were fixed behind the map board placed at the entrance of the park. CH 12 was 200 meters from the nearest road and the diffusion tube was fixed on the street signpost. The pictures of the location and distance of the diffusion tubes from the road at Cannon Hill Park are provided in Appendix 2.2.



Figure 2.12. Location of diffusion tube at Cannon Hill Park

2.3.3.1.2. Tile Cross Park

Tile Cross Park is located near the Birmingham airport (Figure 2.13). Diffusion tubes were placed at 14 sites inside of the park, and at one site outside of the park (south-east side) near a bus stop (Figure 2.14). The NO_2 diffusion tubes were located 3 meters above ground. To investigate the difference in NO_2 concentrations at the roadside and inside the park, the passive samplers were arranged to form two distinct segments on the left and the right side of the park. The first segment, referred to as Group 1, was located along St Giles Road on the east side of the park. The second segment, referred to as Group 2, was located on the west side and was nearby a residential area.

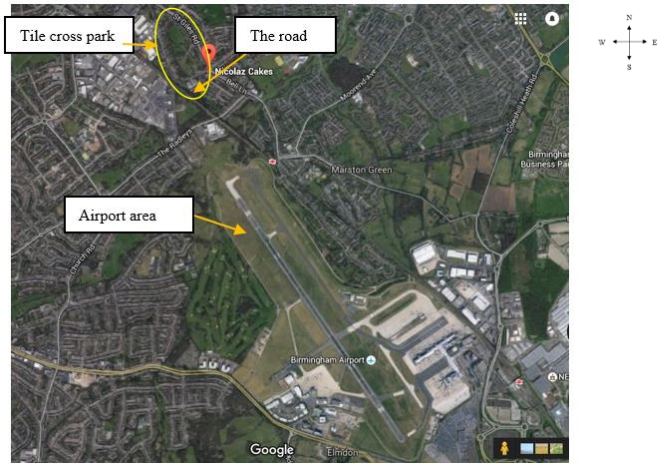


Figure 2.13. Location of Tile Cross Park



Figure 2.14. Map of Tile Cross Park which location of diffusion tubes divided into two groups. Group 1 is TL 8, TL 9, TL 10, TL 11, TL 12 and TL 13; Group 2 is TL 2, TL 3, TL 4, TL 5, TL 6, TL, 7, TL 14, TL 15.

2.3.3.1.3. University of Birmingham

The University of Birmingham (UoB) is located in Edgbaston, 4.8 km south-west of the Birmingham city centre. The sampling campaign at UoB was carried out along a 1 km transect which includes the monitoring sites at BROS (Bristol Road Observation Site) and EROS (Elms Road Observation Site). We also investigated the vertical variation of pollutant concentrations at the courtyard of the Biosciences building.

Sampling sites along the transect

Fourteen sampling locations were placed at UoB, starting from the BROS site along the perpendicular transect of 1 km passing through the EROS site. The BROS site is a traffic site within the UoB campus, 3.6 m from the A38 motorway. The EROS site is an urban background site, located in the open and green area within the UoB campus. The total distance from BROS to EROS is 935 meters. Figure 2.15. shows the map of the sampling sites for the UoB campus.

Five sampling locations near the road, sites X1-X4 and A, were located along the south gate road inside UoB, near the BROS site. The sampling sites E and I were located close to the minor road Pritchatts Road and near the conjunction of Edgbaston Park Road and Somerset Road.



https://www.google.co.uk/maps/place/University+of+Birmingham/

Figure 2.15. Map showing the location of DT at BROS, EROS and other locations at the University of Birmingham site

Courtyard of the Biosciences building, University of Birmingham

The Biosciences building is in the centre of the UoB campus. A small courtyard (48.2 m x 45.5 m) is located inside of the building. To investigate the vertical variation of pollutant concentrations at the top and at the bottom of this enclosed green area, sampling points were located on the roof of the building and at the ground floor inside the park (Figure 2.16). The difference in height between the roof and the ground floor of the Biosciences building is 14 m. Points A, B, C in Figure 2.16 represent the locations of the passive samplers on the roof, while points X and Y represent the passive samplers placed at the ground site. One set of automatic analysers was also placed at both locations.

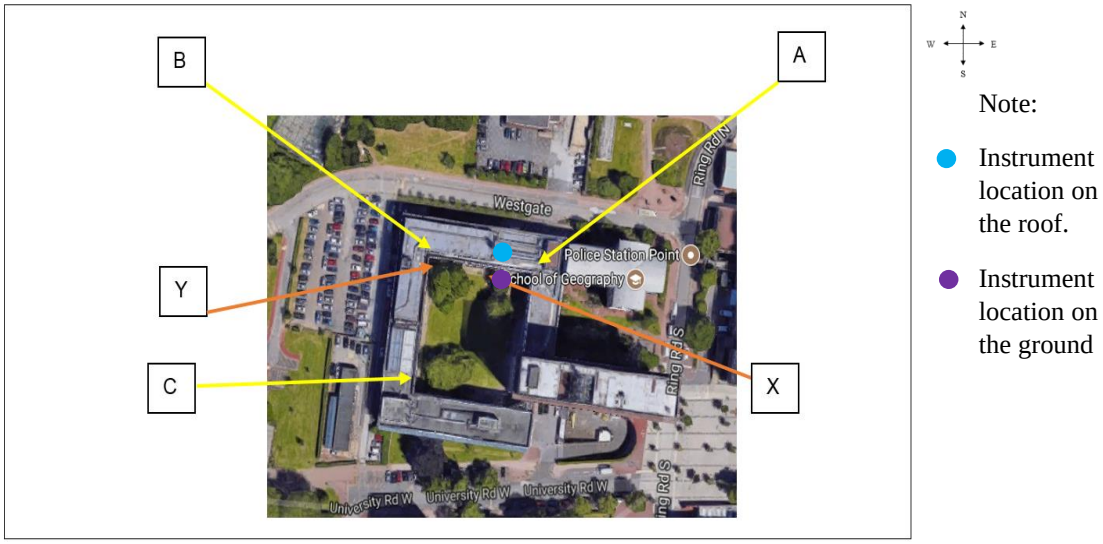


Figure 2.16. Map of Biosciences building with diffusion tube locations and automatic analyser locations. A, B, C were DT location on the roof, X and Y were DT on the ground. The blue dot was instrument location on the roof and purple dot was instrument location on the ground.

2.3.3.2. London, England

London is the capital and largest city of England and the UK. The London area covers 1,572 km^2 and had a population of 8.9 million in 2018 (https://www.trustforlondon.org.uk/data/population-over-time/). London counted 3,000 parks in 2019 and has been declared the first national park city (https://www.london.gov.uk/what-we-do/environment/parks-green-spaces-and-biodiversity/parks-and-green-spaces#).

2.3.3.2.1. Hyde Park

Hyde Park is one of the major parks in London with a total area of 1.4 km^2. Four sampling locations were set at the four corners of the park: Cumberland Gate Lodge (CGL), The Dell (TD), Bowling Green (BG), Victoria Gate Shrubbery (VGS) and another sampling location was placed in the middle of the park, Rangers Lodge (RL).

The sampling sites are shown in Figure 2.17. The CGL sampling site is located at the north-east corner of Hyde Park, the nearby roads include the Cumberland Gate road (11 m) and N Carriage Dr road (32.7 m). The site is also 674.5 m from Rangers Lodge. The TD site is at the south-east corner of the park, near S Carriage Dr road (148.2 m) and 568 m from Rangers

Lodge. The BG site is at the south-west corner, inside the Will to Win Hyde Park Sport Centre, near W Carriage Dr road (55 m) and S Carriage Dr road (95 m), and 675.5 m from Rangers Lodge. The VGS site is located at the north-west corner, near Bayswater Rd (6 m) and N Carriage Dr road (33 m), and 652 m from Rangers Lodge.

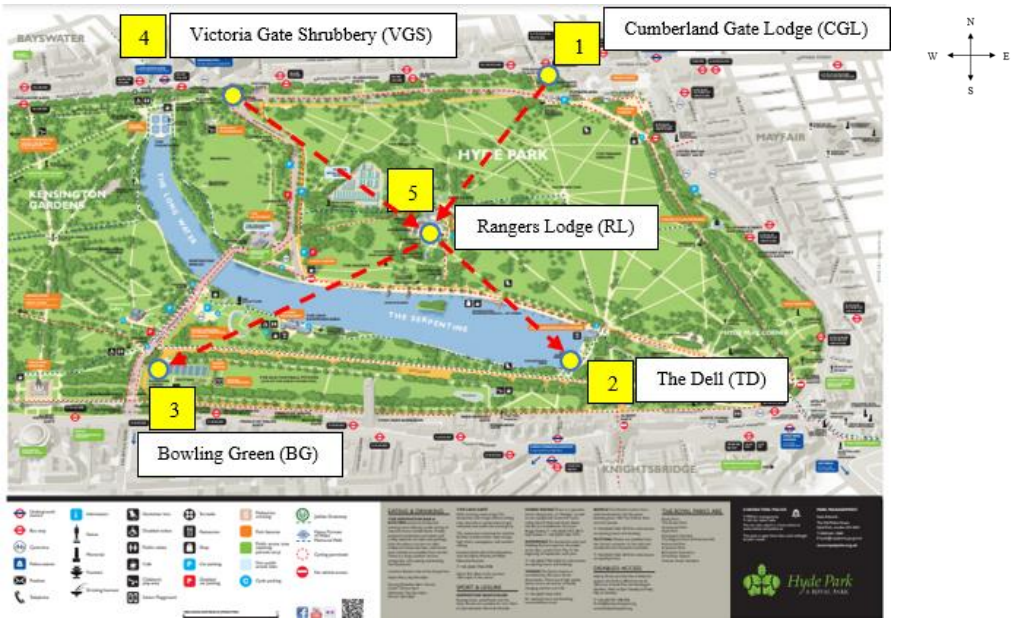


Figure 2.17. Map location of DT at Hyde Park, London (map source: https://www.royalparks.org.uk/__data/assets/pdf_file/0005/41639/hydepark_english_map.pdf)

2.4. The set up and evaluation of dispersion modelling

A modelling study of the dispersion process was carried out using ADMS-Roads (version 4.1) to understand the process of dispersion and deposition of pollutants in selected green areas (Chapter 4). The meteorological data used as input in the model were obtained from the nearest weather station. The model validation was performed using the observation data collected from the NO_x and O_3 automatic analysers during the period from 2-11 February 2018. The NO_2 concentrations from the diffusion tubes measured at 14 points in the UoB site were compared with the modelling results. Details of the model input and model evaluation are given in Chapter 4.

In this section, the general steps of ADMS-Roads modelling are explained. Figure 2.18. shows the interface of ADMS-Roads which includes six different tabs: setup, source, meteorology, background, grid, and output. The details for each tab will be discussed in the sub-sections that follow.

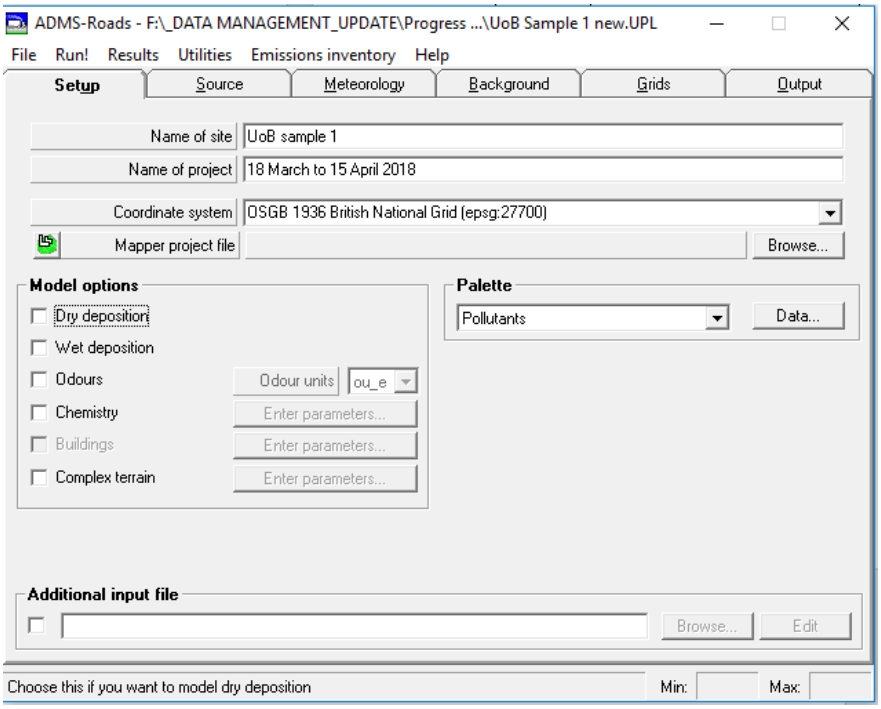


Figure 2.18. The interface of ADMS-Roads screen (CERC, 2017)

2.4.1. Setup

In the setup page, the coordinate system is chosen based on the location. For the UK sites, the coordinate system is OSGB 1936 British National Grid (epsg:27700). For the model options, in this study, chemistry and dry deposition were selected to estimate the contribution of the dry deposition processes in reducing the pollutant concentrations. Wet deposition was not included in the ADMS model runs because the gases NO, NO_2 and O_3 are of low solubility in water, so the error of excluding wet deposition is expected to be small.

2.4.2. Source

In ADMS-Roads, the pollutant sources are divided into road sources and industrial sources. For the road sources, the road elevation, width, and canyon height should be provided. The pollutant emissions can be set manually or can be estimated by the software based on the input for the traffic flows, which includes average speed in km $hour^{-1}$ and the vehicle count $hour^{-1}$ in each vehicle category. The emission factor (g km^{-1}) and emission rate (g km^{-1} s^{-1}) are automatically calculated by the model based on the input data. The EFT, Emission Factors Toolkit (https://laqm.defra.gov.uk/air-quality/air-quality-assessment/emissions-factors-toolkit/) can be used to calculate the emission rates at different locations (e.g., London, England, or Scotland) for a specific year, vehicle speed, road type (e.g., urban, rural or motorway) in each vehicle category (e.g., light duty, LDV, and heavy-duty vehicles, HDV).

2.4.3. Meteorology

The meteorological (Met) data can be generated from the nearest weather station. Met hourly data includes the year, day, hour, wind direction (PHI, in ° clockwise), wind speed (U, in m s^{-1}), temperature (T, in °C), relative humidity (RHUM, in %) and cloud cover (CL, in oktas). For the surface roughness, we selected a value of 0.5 m which corresponds to parkland and suburban areas (at meteorology interface in the dispersion site, Figure 2.18).

2.4.4. Background

Background concentrations of pollutants were obtained from the nearest air quality monitoring station, which is the EROS site, Biosciences building site or Birmingham Acocks Green.

It is important to include background data in the model to predict pollutant concentrations, particularly if the chemistry model option is set in the run (CERC, 2017). The chemistry model option uses background concentrations of NO_x as NO_2, NO_2 and O_3, and the data are from rural background sites. During the day, the background data are assumed to be in equilibrium.

When the ADMS-Roads model is running with NO_x chemistry, the model will calculate concentrations due to emissions of NO_x and NO_2 assuming no chemical reactions, and adds the background concentrations to each pollutant, then performs the chemistry using the chemical reaction scheme in the model (CERC, 2017). If there are no emissions and no chemistry reactions, then the output concentration in the model is equal to background concentration. Therefore, appropriate background concentrations are needed in modelling pollutant concentrations.

2.4.5. Grids

The diffusion tubes sampling sites correspond to the receptor locations. Specified points are selected in the select output and the coordinates of the receptor locations should be inputted as X (latitude), Y (longitude) and Z (height) in meters.

2.4.6. Output

Pollutant output can be specified by selecting the pollutant name, the short or long-term calculations and the output unit.

The output model calculation is selected as long-term to get a single set of concentration data, as an average concentration. Short-term output can be selected for more detailed data, the output consists of concentrations for every line of meteorological data (CERC, 2017).

2.4.7. Dry deposition

To estimate the effect of the dry deposition process, we run the chemistry model first and then the model that includes both chemistry and dry deposition.

Running the model with both dry deposition and chemistry, the model calculates the emissions of NO_x and NO_2 and considers the depletion due to deposition which is related to the deposition velocity. In the model, the NO concentration is set as NO_x minus NO_2 and the background concentration is added to each pollutant before applying the reaction schemes which will affect the output for the O_3 concentrations (CERC, 2017).

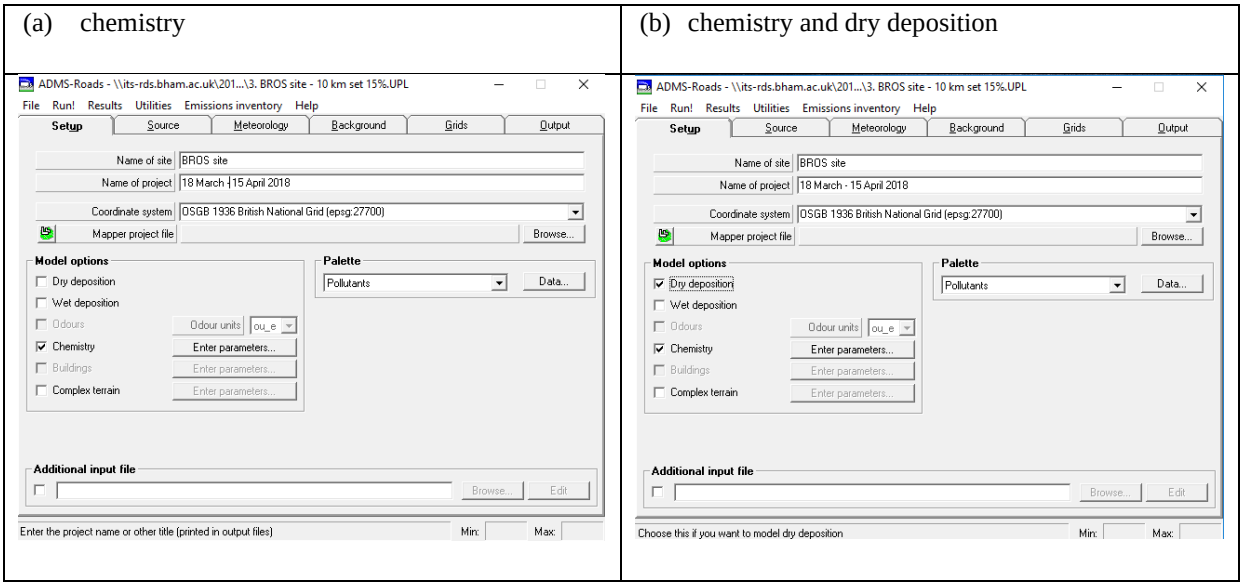


Figure 2.19. The interface of ADMS-Roads with the model options **(a)** chemistry, **(b)** chemistry and dry deposition (CERC, 2017)

The input value of deposition velocity for O_3 was obtained from the literature (Chapter 5), and was set at 0.002 m s^{-1}. For the deposition velocity of NO and NO_2, the dry deposition parameters for short vegetation were used (Table 2.7 as suggested in the ADMS-Roads manual (CERC, 2017). However, surface exchange of NO is two-way, because vegetated surfaces can emit NO.

Table 2.7. Deposition velocities for short vegetation (grass)

Parameter	NO_2	NO	SO_2	NH_3
Deposition velocity (m s^{-1})	0.0015	0.00015	0.012	0.02

Source: (CERC, 2017)

The reduction in pollutant concentration by dry deposition is calculated as follows:

$$\% \text{ reduction concentration} = \frac{(C_{chemistry} - C_{chemistry+dry\ deposition})}{C_{chemistry}} \times 100\ \% \qquad \text{(E.2.17)}$$

where $C_{chemistry}$ is the concentration generated from model with chemistry only, and $C_{chemistry+dry\ deposition}$ is the concentration generated from model with chemistry and dry deposition.

2.5. Deposition velocity of gases from vertical gradient of pollutant concentrations

In this study, NO_x deposition velocities were calculated from the gradient of concentrations of pollutants measured at the courtyard in the Biosciences building at UoB. The gradient method was used to calculate BC and NO_x fluxes based in the equation:

$$F = -V_d C = -K \frac{\Delta C}{\Delta Z} \qquad (E.2.18)$$

Where F is pollutant flux removed per unit area (μg m^{-2} s^{-1}), v_d (m s^{-1}) is deposition velocity, C is the concentration of pollutants measured at 1 metre above the ground (μg m^{-3}), K is eddy diffusivity for the mass transfer of species (m^2 s^{-1}), ΔC/ΔZ is the concentration gradient, ΔC is the difference in the measured concentration (μg m^{-3}) and ΔZ is the difference in height (m). In the vertical study, the pollutant concentrations were measured at the roof and at the ground floor in the courtyard of the Biosciences building (see Section 2.3.3.1.3). The difference in height (ΔZ) of measurement levels in this study is 13 m. The difference in concentration (ΔC) is determined by subtracting the concentration on the roof from the concentration on the ground.

Small particles, such as BC particles range in size from 0.1 μm to 1.0 μm, behave like gases (Vardoulakis *et al.*, 2003) and are transported by diffusion processes. The value of K, eddy diffusivity or turbulent diffusion does not change much at the surface (Garland, 1977; Moene and van Dam, 2014; Seinfeld and Pandis, 2016), therefore it can be used to predict the fluxes and deposition velocity for other pollutants. To define K in the grassland area, BC was set as a tracer. The K is a measure of the atmospheric turbulence called the eddy diffusivity which determines local atmospheric mixing processes. The K is dependent on the surface roughness and atmospheric stability at the lower level, and it is independent of gases or particles that are involved in the process (Seinfeld and Pandis, 2016).

The BC fluxes were determined by multiplying the deposition velocity by the BC concentrations measured at the ground site. The BC deposition velocity (0.0014 m s^{-1}) was estimated using size distribution (Liu *et al.*, 2014), and size-resolved deposition velocity on grassy areas (Pellerin *et al.*, 2017 in Giardina and Buffa, 2018). The NO_x fluxes were calculated by multiplying the eddy diffusivity by the corresponding concentration gradient.

The deposition velocity of NO_x was determined by dividing the flux by their pollutant concentrations at the ground site.

The uncertainties of pollutant concentrations, eddy diffusivity values, fluxes and deposition velocities were calculated with the equations in table 2.8. below:

Table 2.8. Equations for the uncertainty in deposition velocities of gases from vertical gradient of pollutant concentrations

No	Uncertainty	Parameter	Equation for uncertainty
	Individual uncertainty		
a.	Concentration on the ground	C-ground	Uncertainty: $\sigma_{\bar{x}} = \frac{\sigma}{\sqrt{n}}$ Where $\sigma_{\bar{x}}$ is standard error of the mean, σ is standard deviation and n is number of observations. % uncertainty = $\% \sigma_{\bar{x}} = \frac{\sigma_{\bar{x}}}{mean}$ x 100%
b.	Concentration on the roof	C-roof	
	Combined uncertainty		
c.	ΔZ	ΔZ = Z roof – Z ground	Assumption error distance is 30 cm (0.3 m) and ΔZ is 13 m. % uncertainty is (0.3/13) x 100% = 2.3 %
d.	ΔC	ΔC = C roof – C ground	Uncertainty of ΔC = √ sum of (% error C roof)^2 + (% error C ground)^2
e.	Vd carbon	Estimation, Vd = 0.0014 m s^{-1}	Assumption that the error in carbon deposition velocity (V_d) is 100%.
f.	Eddy diffusivity (K)	$K = \frac{-F}{\Delta C/\Delta Z}$	Combined error in K = √ sum of (% error ΔC)^2 + (% error ΔZ)^2 + (% error V_d carbon)^2 + (% error C-ground)^2
g.	Flux (F)	$F = -K \frac{\Delta C}{\Delta Z}$	Combined uncertainty of Flux = √ sum of (% error ΔC)^2 + (% error ΔZ)^2 + (% error K)^2

No	Uncertainty	Parameter	Equation for uncertainty
h.	V_d NO_x	$V_d = \frac{-F}{C\ ground}$. Where, $F = -K \frac{\Delta C}{\Delta Z}$	Combined uncertainty of NO_x = √ sum of (% error ΔC)^2 + (% error $\Delta Z)^2$ + (% error K)^2 + (% error C ground)^2

2.5.1. Sampling instrumentation

2.5.1.1. Automatic analyser

The NO, NO_2 and NO_x concentrations were measured using a chemiluminescence NO_x analyser 42i on the roof, and NO_x analyser 42C on the ground floor of the Biosciences building, UoB. The O_3 concentrations on the roof and the ground floor of the Biosciences building were measured using a 49i ozone analyser with UV absorption at 254 nm. For the measurement of the black carbon (BC) concentrations, we used a micro-aethalometer AE51.

2.5.1.2. Micro-aethalometer AE51



Figure 2.20. Picture of micro-aethalometer AE51

A micro-aethalometer was used to measure the BC concentration. The inter-comparison of the instruments was conducted every month. On the X axis was the micro-aethalometer number 4 (set on the roof), and on the Y axis was the micro-aethalometer number 3 (on the ground).

The mathematical equation to estimate the BC concentration is derived from (Apte *et al.*, 2011) for ATN < 80

$$BC = BC_0\,(0.88Tr + 0.12)^{-1} \qquad (E.2.19)$$

$$Tr = \exp\left(-\frac{ATN}{100}\right) \qquad (E.2.20)$$

Where:
BC = corrected BC concentration
BC_0 = BC uncorrected (BC reading samples)
ATN = attenuation coefficient
Tr = Aethalometer filter transmission

2.5.2. Sampling location

The Biosciences site is located in the middle of the UoB campus. The courtyard between the buildings is mostly grassland area.

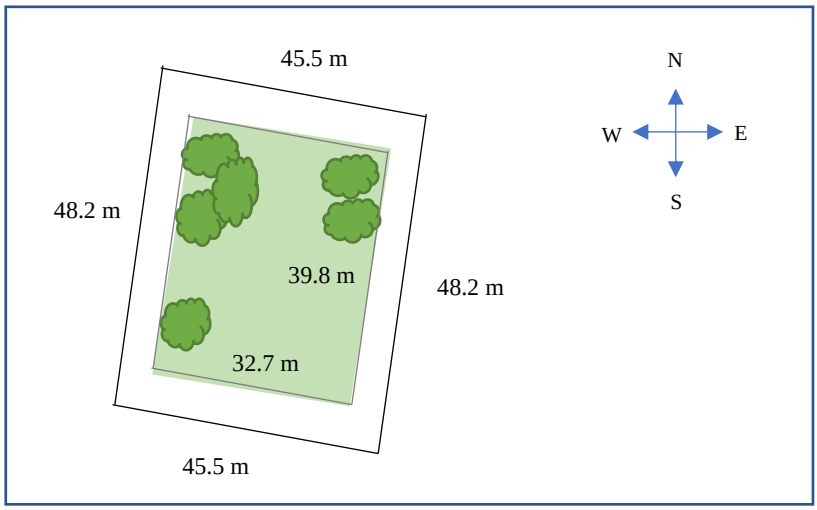


Figure 2.21. Illustration of park / grassland area in the Biosciences building

The grassland area (45.5 m x 48.2 m) is surrounded by concrete floors. The grass height was about 10 to 30 cm before cutting, and the height after cutting was about 2 to 5 cm. There are trees in three corners of the Biosciences quadrangle. The height of the trees at the south-west corner was approximately 13 metres, the height of the trees at the north-west corner was 15 metres, and trees at the north-east corner were 14 metres height.

One sampling container was located in the open park inside the Biosciences building at the northern end of the building, a second sampling container was placed on the roof, vertically above the ground site. The height of the building is 14 metres, and we put the lower instrument at 1 metre above the ground, so the difference in height between the two sites is 13 metres. Aspect ratio (AR) is the relationship between quad's height (H) and width (W), so AR = H/W. In this quad location, the aspect ratio is 14 / 45.5 = 0.3. The heights of the buildings are important in establishing circulations within the quad. The heights of trees also may influence mixing by compartmentalising the quad airspace.

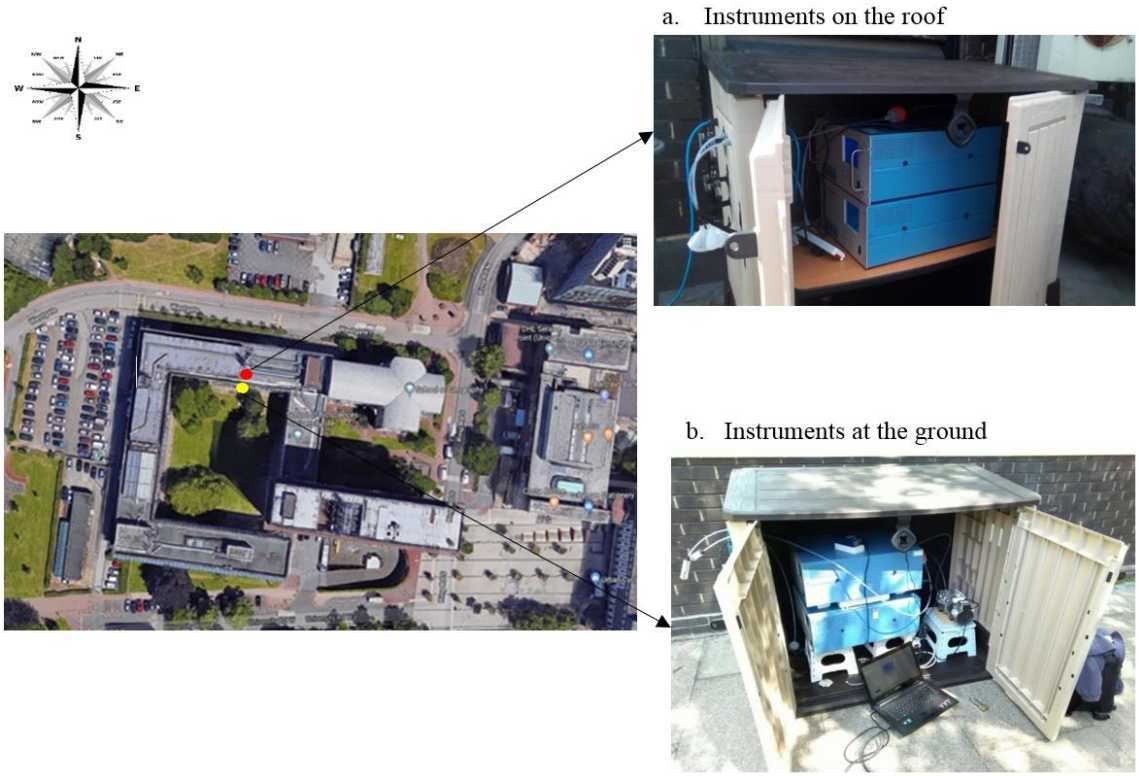


Figure 2.22. Map of Biosciences building showing the location of the open park and the instruments at **(a)** the roof, **(b)** and ground sites

Chapter 3. Oxides of Nitrogen and Ozone in Urban Greenspace

This chapter presents temporal and spatial variability of air pollutant concentrations near roads and along urban green areas as measured by diffusion tubes (DT) at several sites in Birmingham and London, UK. Data measured from diffusion tubes at EROS, BROS and the Biosciences sites were compared with automatic analysers (AA). The work aims to measure the concentrations of nitrogen dioxide (NO_2) and ozone (O_3) using diffusion tubes and to obtain temporal and spatial variability of air pollutant concentrations at the roadside and in green spaces located in urban areas.

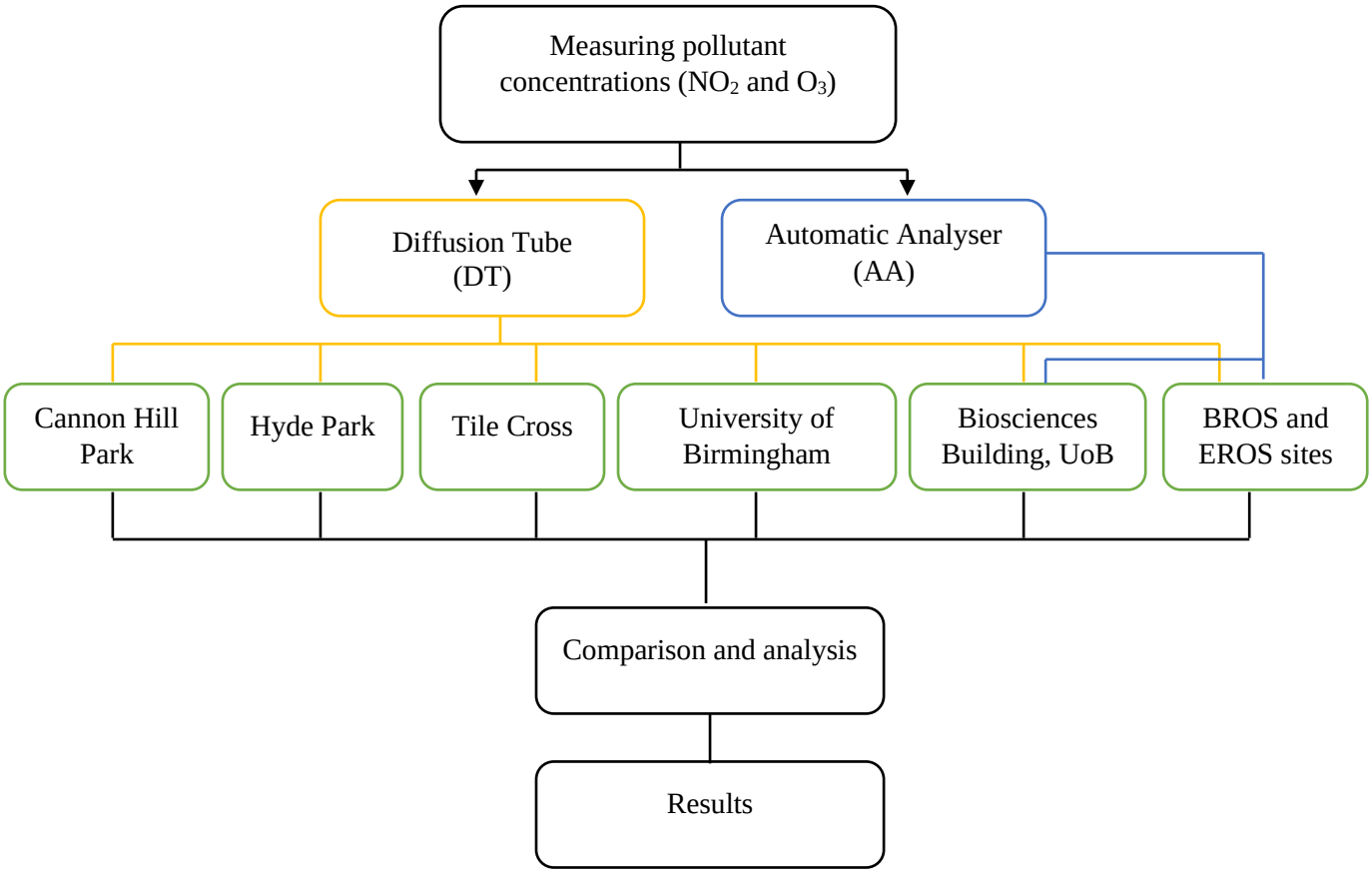


Figure 3.1. A schematic of the broader sampling approach and sites. The blue line is the identification of measurements using an automatic analyser to measure air pollutants (NO_2 and O_3), and the orange line is the identification of measurements using diffusion tubes to measure air pollutants at the sampling locations.

3.1. Introduction

Road transport is considered the main source of air pollution in urban areas in developed countries (Williams, 1999; Colvile *et al.*, 2001) and megacities (Mayer, 1999). Pollutants such as NO_2 and PM are found in higher concentrations at roadside locations compared to urban background areas due to emissions from traffic (Longley *et al*., 2015). In inner London, direct NO_2 emissions from traffic were estimated to be around 15% of total NO_x emissions in 2014 (Carslaw *et al.*, 2016).

Pollutant concentrations related to spatial variations are influenced by characteristics of the pollutants, meteorological conditions, traffic, distance to roads etc. (Pasquier and Andre, 2017). Ducret-Stich *et al*. (2013) found that primary pollutant emissions from vehicles such as NO_2 and elemental carbon (EC) decreased in concentration in proportion to increasing distance from the roadside.

The importance of creating green spaces such as parks in towns and cities to reduce air pollution arising from anthropogenic emissions has been emphasized (Swanwick *et al*., 2003). Urban parks are considered as regional and national sinks for atmospheric pollutants (Xing and Brimblecombe, 2019). In this study, the effect of a green area (park) on air pollutant concentrations has been established by deploying a dense fixed network of diffusion tubes for measuring NO_2 near a road and within an area of urban green space. This deployment will establish a gradient of concentration between the roadside and inside the park.

Diffusion tubes have several limitations in terms of precision and accuracy (Heal *et al*., 2019; Vardoulakis *et al*., 2009). It has been reported that diffusion tubes can overestimate or underestimate the measurement of pollutants such as NO_2 when compared with automatic analysers (Ayers *et al.*, 1998; Heal *et al*., 1999; Kirby *et al*., 2000; Ozden and Dogeroglu, 2008). Bush *et al.* (2001) and Campbell *et al*. (1994) found that diffusion tubes overestimated the concentration levels of NO_2 by up to 30%, while Vardoulakis *et al*. (2009) reported that Palmes-type passive samplers underestimated NO_2 concentration levels by 6.4%.

Many factors affect the concentration of atmospheric pollutants — for example, variations in anthropogenic activities, atmospheric conditions of wind speed and direction, temperature, humidity and atmospheric stability (Tang *et al*., 2001; Chaloulakou *et al.*, 2003; Levy *et al.*, 2003; Aldrin and Haff, 2005; Cape, 2009b; Mavroidis and Chaloulakou, 2011; Šereviciene and Paliulis, 2011; Ševičienė and Paliulis, 2012; Hernandez *et al.*, 2017). Some pollutants such as NO_x and particulate matter (PM) may be considerably higher in the urban atmosphere mainly due to traffic volume (Aldrin and Haff, 2005; Kurtenbach *et al.*, 2012; Al-Rashidi *et al.*, 2018), while O_3 may be more concentrated in rural areas (Melkonyan and Kuttler, 2012).

Traffic volume and meteorological factors, such as wind, may highly influence the concentration of pollutants (Chaloulakou *et al.*, 2003; Levy *et al.*, 2003; Aldrin and Haff, 2005). Pearce *et al*. (2011) analysed the influence of local meteorology — such as temperature, wind and solar radiation — on air quality in Melbourne, Australia, and concluded that, at the local scale, meteorology is a substantial driver for air quality.

3.2. Methods

3.2.1. Monitoring sites using automatic analysers

Automatic chemiluminescence analysers were set up to evaluate the diffusion tubes' performance for the period August 2016 – April 2018. The sampling campaign was carried out from 24th August 2016 to 9th September 2017 at EROS, and then from 9th September 2017 until 2nd February 2018 at BROS. From 2nd February to 15th April 2018, automatic analysers were set up at BROS and in the trailer cabin at the EROS site before being moved to the sampling location at the Biosciences building, the University of Birmingham (UoB), UK.

3.2.2. Monitoring sites using passive diffusion tube samples

The diffusion tube sampling campaign was conducted at the same time and same location alongside the automatic analyser. However, sets of passive diffusion tubes were also set up at different locations — at Cannon Hill Park, various locations within the UoB, Tile Cross Park, Hyde Park and the Biosciences building at the UoB. The locations were described in Chapter 2. Section 2.3.3. Sampling locations.

Palmes diffusion tubes were used to measure NO_2 and O_3 near highly congested roads and in the parks. Palmes tubes with open ends were used at the beginning of the sampling campaign, from 24th August 2016 to 15th April 2018, and diffusion tubes with a membrane using a stainless-steel grid were used from October 2017 at the UoB site and November 2017 at Cannon Hill Park site.

3.2.3. Statistical analysis

Statistical analysis was performed using SPSS version 23. Before performing the data analysis, a statistical evaluation was conducted with the Kolmogorov-Smirnov test to check the normality of the data. Kolmogorov-Smirnov test results for parameters — namely, NO_2 in the park, NO_2 near the road, temperature and RH at each sampling site — showed parametric data (sig > 0.05). Only wind speed data in Cannon Hill Park and the UoB campus were non-parametric (sig < 0.05). The majority of data is normally distributed.

Table 3.1. Results of statistical test with Kolmogorov-Smirnov to check the normality of the data

Data	**Normality test using Kolmogorov-Smirnov**	
	Normal Distribution (Parametric data), sig > 0.05	**Non-Normal Distribution (Non- Parametric), sig < 0.05**
UoB campus	NO_2 in park (sig. 0.200); NO_2 near road (sig. 0.200); RH (sig. 0.200); Temperature (sig. 0.115)	Wind speed (sig 0.000)
Cannon Hill Park	NO_2 in park (sig. 0.200); NO_2 near road (sig. 0.200); RH (sig. 0.162); Temperature (sig. 0.200)	Wind speed (sig. 0.000)
Hyde Park	NO_2 in park (sig. 0.200); NO_2 near road (sig. 0.200); RH (sig. 0.200); Temperature (sig. 0.200); Wind speed (sig. 0.200)	-
Tile Cross	NO_2 in park (Sig 0.200); NO_2 near road (Sig 0.175); RH (Sig 0.200); Temperature (sig. 0.200); Wind speed (Sig 0.081)	-
Biosciences	NO_2 in park (sig. 0.200); NO_2 near road (sig. 0.200); RH (sig. 0.200); Temperature (sig. 0.200); Wind speed (sig. 0.200)	-

The t-test was used to identify significant differences in mean concentrations between the selected sub-groups of observations, which were concentrations at the roadside and inside the park. A Pearson correlation analysis was conducted to evaluate the correlation of NO_2 concentration in the park with NO_2 level near the roads and the meteorological variables (temperature, wind speed, RH).

Multiple linear regression was carried out with the following pattern: the average of NO_2 from each sampling site within the park as the dependent variable, and independent variables being:

a. concentration at the roadside
b. concentration at the roadside and temperature
c. concentration at the roadside, temperature, wind speed and RH.

The result from the multiple linear regression equation can be used to predict the NO_2 concentration inside the park if the NO_2 concentration near the road is known. Furthermore, if meteorological data are available, these parameters can be added as an independent variable to better predict the concentration of NO_2 inside the park.

Air pollution change as a metric for determining air quality improvement was calculated as below:

$$C_{change} = \frac{(C_{roadside} - C_{park})}{C_{roadside}} \; x \; 100\% \qquad (E.3.1)$$

Where C_{change} is change or difference in pollutant concentrations (%). $C_{roadside}$ is pollutant concentrations at roadside, and C_{park} is pollutant concentrations inside the park.

The meteorological parameters of wind speed, ambient temperature, and relative humidity were presented with the NO_2 concentration in the parks. Concentrations in the seasonal periods were also associated with seasonal descriptions: spring (March/April/May); summer (June/July/August); autumn (September/October/November); and winter (December/January/February) in the sampling period.

3.3. Results and discussion

3.3.1. Diffusion tube evaluation

Although there are uncertainties about the accuracy and precision of diffusion tubes, the results are presented as below.

3.3.1.1. NO_2 diffusion tube evaluation

NO_2 diffusion tubes were deployed alongside automatic analysers from 24 August 2016 to 15 April 2018. During this period, 30 data points were obtained from measurements at EROS and 9 at BROS. From the total of 39 samples, the numbers of measured NO_2 from DT with an open end were 39 samples, and measured NO_2 DT with a membrane were 8 samples (see Appendix 3.1). The data are plotted in Figures 3.2. and 3.3.

The use of a membrane at the open end of the tube, or mounting the tube in a sheltered site, can help to reduce the turbulence effect (Campbell *et al*., 1994; Masey *et al.*, 2017). The effect of wind turbulence may lead to an overestimation of the readings due to eddy diffusion which can lead to a shortening of the effective length of the tube (Bush *et al.*, 2001). Masey *et al*. (2017) confirmed that higher wind speed could increase the uptake rates of diffusion tubes and they found a linear relationship between wind speed and uptake rate. However, Kirby *et al*. (2000), sharing results from two studies in the UK, confirmed that over-reading of the diffusion tube is related more to the changes of chemistry in the tube than to the turbulence effect. In our study, the use of a membrane with a stainless-steel mesh #60 decreased the accuracy but increased the precision of the tubes.

Figure 3.2. shows a good agreement between NO_2 measurements with diffusion tubes and with automatic analysers. However, there are some discrepancies where the diffusion tube underestimated or overestimated NO_2. Many factors affect the measured NO_2 concentration, such as wind turbulence, time exposure (Bush *et al.*, 2001), and reduction in the amount of photolysis of NO_2 caused by the material of the tube (Kirby *et al.*, 2000).

The precision of DTs was assessed by calculating % relative standard deviation (RSD) from triplicate DT measurements (see equation E.2.9). The accuracy was expressed as % bias of DT value with respect to automatic analyser data (equation E.2.10).

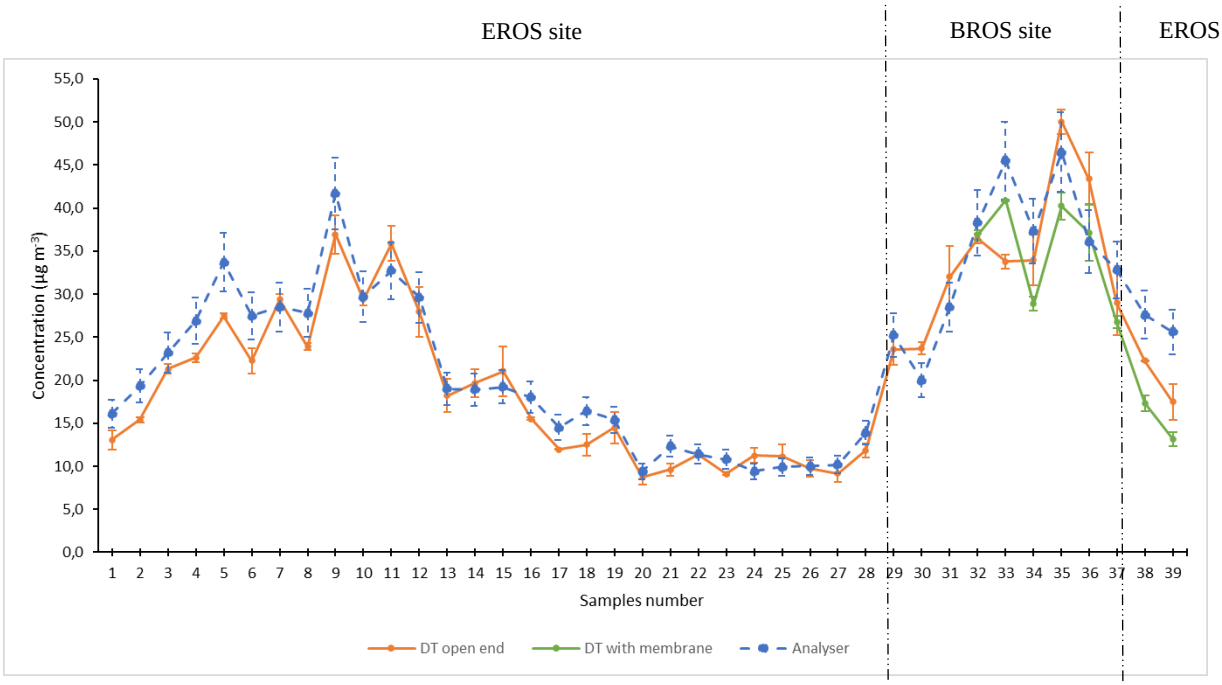


Figure 3.2. NO_2 concentrations were measured by diffusion tubes with open end (orange line), diffusion tubes with membrane (green line) and automatic analyser (blue dashed line) at EROS and BROS for the period August 2016 – April 2018. Measurements numbered 1 to 28 were conducted at the EROS site, while 29 to 37 were measured at the BROS site due to refurbishment of the EROS site, and 38 to 39 were measured at the EROS site (trailer cabin). A diffusion tube with stainless steel mesh at the end as a membrane was used starting on 15 October 2017 (no. 32). NO_2 concentrations at each point are presented as mean concentration and standard deviation (mean ± SD). The x-axis shows the samples number that represents sampling period of number as data points, and the y-axis, NO_2 concentrations in µg m^{-3} from diffusion tubes with open end (orange), diffusion tubes with membrane (green) and automatic analysers (blue). Error bars for the diffusion tubes show standard deviation from triplicate of diffusion tubes, and error bars for the automatic analysers, uncertainty was estimated as 10% from each measured mean concentration for NO_x instruments (Stevenson *et al.*, 2009).

The standard deviation of the diffusion tube was calculated from triplicate of diffusion tubes from each sampling point. The standard deviation of the automatic analysers was estimated to be ±10% of each measured mean concentration from the automatic analyser. The estimated 10% value for the uncertainty of the NO_x automatic analyser refers to the uncertainty calculated from the AURN data using CEN methodology that has been conducted to evaluate the performance of the analysers (Stevenson *et al.*, 2009).

The mean NO_2 concentration with standard deviation (mean ± SD) from 39 samples of diffusion tubes with open end was 22 ± 10 µg m^{-3}, and NO_2 concentrations from automatic analysers was 24 ± 15 µg m^{-3}. NO_2 concentrations (mean ± SD) from 8 samples of diffusion tubes with membrane was 30 ± 4 µg m^{-3}, and NO_2 concentrations from automatic analysers was 36 ± 10 µg m^{-3}.

The limit of detection of NO_2 diffusion tubes with open end for a 2-week exposure period based on the equation E.2.12 was 3 ± 1 µg m^{-3}. This detection limit value was lower than the minimum measured NO_2 concentration.

Overall, there was underestimate and overestimate bias in the range of -32% to 20% for the diffusion tubes with open end, and a range of -49% to 3% for the diffusion tubes with membrane. The relative standard deviation of diffusion tubes with open end was in the range of 0.3% to 14%, with an average of 6%; while that for the diffusion tubes with membrane was within the range of 0.2% to 9%, with an average of 4%. DT with an open end showed a lower bias compared to the DT with the membrane at the end cap. The use of the membrane gives better precision than for open-ended tubes based upon the relative standard deviation value. However, this conclusion is based on results from a small sample size — 8 diffusion tubes with membrane compared to 39 diffusion tubes with open end.

Table 3.2. Validation result of NO_2 diffusion tubes for precision and accuracy, August 2016 – April 2018

Parameter	Indicator	DT with open end		DT with membrane	
		NO_2		NO_2	
		Average (%)	Range (%)	Average (%)	Range (%)
Precision	RSD < 15%	6	0.3 to 14	4	0.2 to 9
Accuracy	% Bias	-7	-32 to 20	-19	-49 to 3

The uncertainty for NO_2 concentrations measured by DT from previous studies was within ± 20% (AQEG, 2004; Cape, 2009). The difference in tube preparation method is one of the factors affecting the diffusion tube performance (AQEG, 2004). Table 3.3 lists examples of potential factors that influence the accuracy of calculations of ambient NO_2 concentrations when diffusion tubes are used as the sampling device.

Table 3.3. Examples of bias and factors influencing bias percentage of NO_2 quantification in ambient air from previous research

Accuracy (% Bias)	Influencing factors	Reference
± 30 %	• Wind shortening effect • Reaction NO with O_3 within sampler (NO reacts with ozone and makes additional NO_2) • Period of exposure time • Method of tube preparation and analysis	Campbell *et al*., 1994; Laxen and Marner, 2006; Tang *et al*., 2001
+ 27%	• Material of diffusion tube • Exposure time • The chemical reactions inside the tube	Heal *et al*., 1999
± 15%	• Modification of the diffusion tube (used carbon-coated filter paper and sodium carbonate + glycerine solution) • Period of exposure time	De Santis *et al*., 2001
+ 7.5 to 27.6%	• The material of the diffusion tube (acrylic, foil-wrapped, UV-transmitting quartz glass) • Period of exposure time	Heal and Cape, 1997
-3.2 to -6.4%	• Meteorology: seasonal variation: underestimate result is different in warm and cold season	Vardoulakis *et al*., 2009
+10%	• Diffusion tube protection • Method of tube preparation and analysis	Glasius *et al*., 1999
10% ± 24-38%	• Period of exposure time • Exposure procedure (sheltered tube)	Bush *et al*., 2001
Using R^2 value: • Palmes type, 0.59 • Ogawa type, 0.87 • Ogawa with absorbent from Palmes type, 0.93	• Type of diffusion tube • Period of exposure time • Method of tube preparation and analysis • Diffusion tube protection	Masey *et al*., 2017

Heal *et al*. (2019) reviewed the biases in NO_2 measurement by Palmes diffusion tubes and presented the potential biases for every stage — preparation of the tube, quantification of the nitrite, deployment in the sampling locations, calculation of the ambient concentration and the potential uncertainty from a comparison of diffusion tubes with the analysers. All of these steps can potentially give a positive or negative bias and influence the accuracy of diffusion tubes.

3.3.1.1.1. Bias adjustment

DEFRA (Department for Environment Food & Rural Affairs) publish the national diffusion tube bias spreadsheet (https://laqm.defra.gov.uk/bias-adjustment-factors/national-bias.html). In 2019, there were 86 local authorities participating in the programme for 178 sampling locations. The measurements are conducted every year with the length of study in a range of 9 to 13 months and using different preparation methods (e.g. 20% TEA in water, 50% TEA in acetone) and at different site types (e.g. kerbside, urban background). The results for bias adjustment factor in 2019 varied, in the range of 0.6 (overestimate 68%, using 50% TEA in acetone) to 1.33 (underestimate -24.8%, using 50% TEA in acetone). The median of bias adjustment factor in 2019 was 0.85 (overestimate 18.2%).

Birmingham City Council joined the database of national diffusion tube bias factors in the years 2000 and 2001 using the method of 50% TEA in water, analysed by Gradko. The results of the bias adjustment factor were 1.14 (underestimate -12.6%) and 1.25 (underestimate -19.9%) in 2000 and 2001 respectively. In our study, as shown in Table 3.4., the bias adjustment factor with a preparation method of 20% TEA in water was 1.09 (underestimate -7%) when using DT with open end, and 1.20 (underestimate -19%) when using DT with membrane.

Table 3.4. Bias adjustment factors of diffusion tubes from August 2016 to April 2018 in the UoB site, Birmingham

Type of Diffusion Tubes	N, samples number	Diffusion Tube Mean Conc. (DT) (µg m^{-3})	Automatic Analyser Mean Conc. (AA) (µg m^{-3})	Bias (B)	Tube Precision	Bias Adjustment Factor (A) (AA/DT)
DT open end	39	22	24	-7%	6%	**1.09**
DT with membrane	8	30	36	-19%	4%	**1.20**

* see Appendix 3.1

Overall, the bias adjustment factors from both diffusion tubes are well (1.09 and 1.2) within the range observed (0.55 - 1.29) from the DEFRA compilation for the bias adjustment factor in 2018 (https://laqm.defra.gov.uk/air-quality/air-quality-assessment/national-bias/).

In this study, a linear regression value was used to adjust the concentration generated from the DT method. Figure 3.3. shows the linear regression between automatic analyser and diffusion tube measurements that was used as a value to adjust the DT bias.

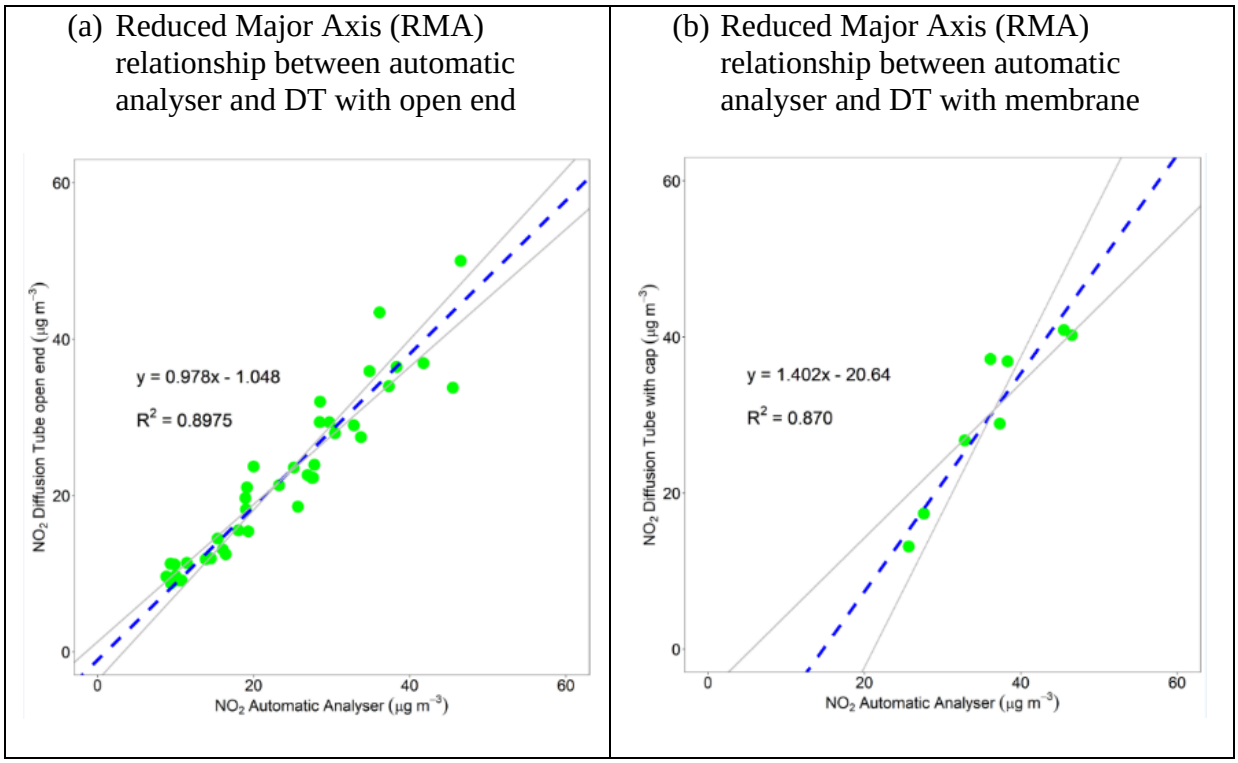


Figure 3.3. Reduced Major Axis (RMA) regression model **(a)** between NO_2 automatic analyser and NO_2 concentration from diffusion tubes with open end for the period August 2016 to April 2018 (N=39 samples); and **(b)** between NO_2 automatic analyser and NO_2 concentration from diffusion tubes with membrane for the period October 2017 to April 2018 (N=8 samples). The green dots are samples, blue dashed line is the RMA regression line and the grey lines indicate the upper and lower limits of the 95% confidence intervals. The inverse of the equation is used to correct the DT measurement. The NO_2 concentration adjustment for DT with open end was True NO_2 = (DT_NO_2 + 1.048) / 0.978, and for DT with membrane was True NO_2 = (DT_NO_2 + 20.64) / 1.402.

Reduced Major Axis (RMA) is a regression method based on the formula that the level of uncertainty to the x (independent) variable is the same with the level of uncertainty to the y (dependent) variable, so that with RMA equation, the resulting regression due to the interchanges of x and y variables is the equivalent of x = (y-a)/b (Harper, 2014), where "b" is gradient and "a" is intercept. The equation from the regression between analyser and diffusion tubes was used as an adjustment as it shows a satisfactory relationship, and using the equation is the best way to do the correction. The strong offset in Figure 3.3. (b). means that for diffusion tube results below about 10, the final result will be dominated by the

constant. The adjustment correction suggests there is systematic loss of NO_2 in the tube with the membrane.

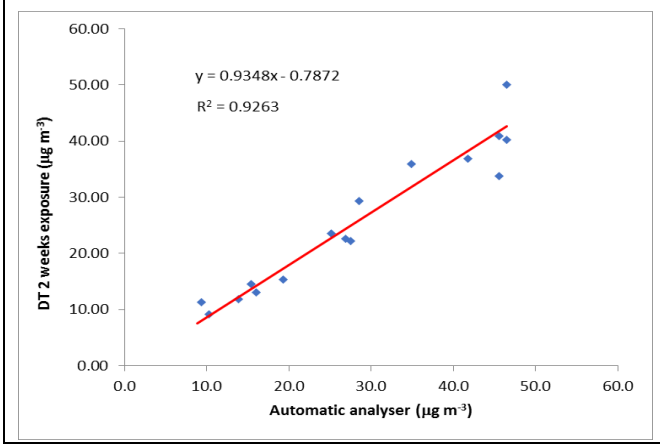
The inverse of the equations is used to correct the DT measurements. The NO_2 concentration adjustment for diffusion tubes with open end was True NO_2 = (DT_NO_2 + 1.048) / 0.978, and for diffusion tubes with membrane True NO_2 = (DT_NO_2 + 20.64) / 1.402.

3.3.1.1.2. The length of exposure period

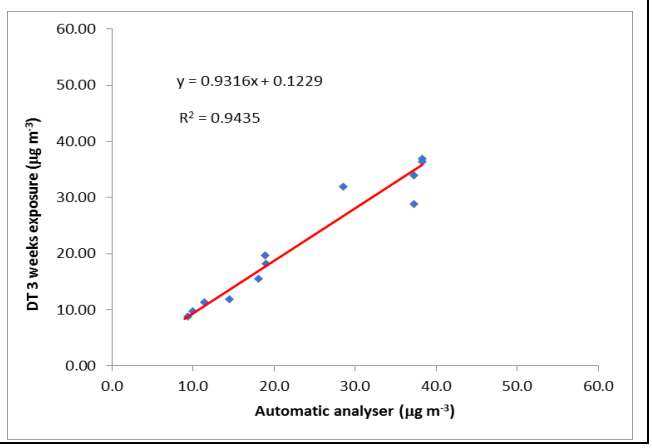
The norm for diffusion tube exposure period in the UK is a month. DEFRA has published monitoring guidelines and tools for NO_2 diffusion tubes (Targa and Loader, 2008), including the monitoring calendars for exposure dates in a monthly recommendation period. In some studies, time exposure can influence the level of NO_2 — a 4-week duration could reduce the concentration compared to 1 or 2-weeks exposure time (Bush *et al*., 2001; Cape, 2009; Heal *et al*., 1999; Masey *et al*., 2017). NO_2 trapped in the tube can be photolyzed into NO and O_3 during daytime (Cape, 2009). However, a study from Vardoulakis *et al*. (2009) found that the NO_2 concentration during a 4-week exposure was underestimated compared to a 5-week exposure.

In our study from August 2016 to April 2018, we varied the time exposure period from 2 to 6 weeks of sampling time. The duration of the exposure period influenced the NO_2 concentration results, as shown in Figure 3.4. There were overestimated and underestimated results from all the exposure times.

(a) 2-week exposure, N = 16.



(b) 3-week exposure, N = 12.



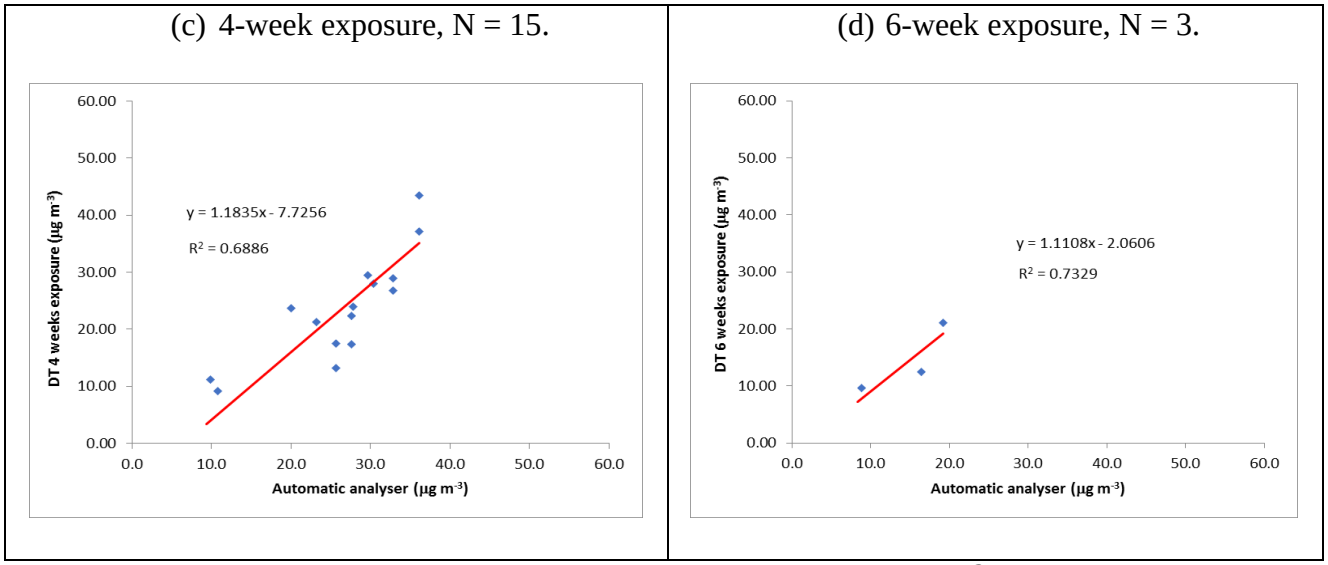


Figure 3.4. Comparison of exposure time of NO_2 concentration in µg m^{-3} measured by automatic analysers (x-line) and diffusion tubes measurement (y-line) for **(a)** 2-week, **(b)** 3-week, **(c)** 4-week, and **(d)** 6-week periods.

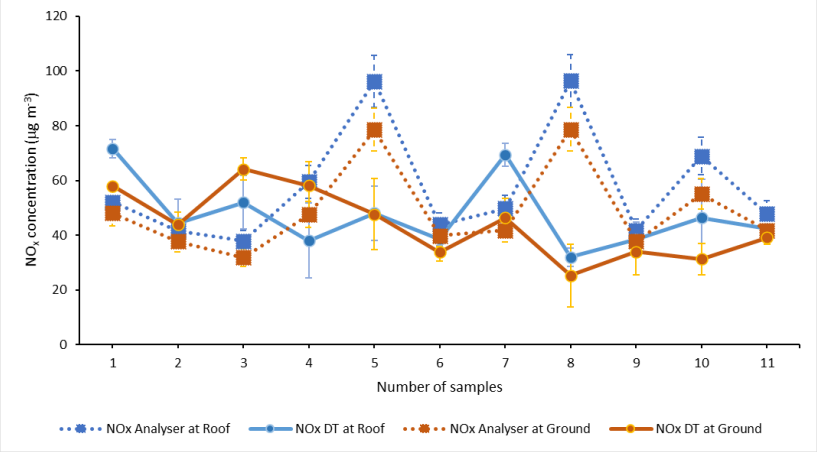
The length of the exposure period also affected the measured NO_2 concentrations, as NO_2 diffusion tubes with 2-weeks and 3-weeks of exposure time show a better comparison with the automatic analyser compared to 4-and 6-weeks exposure periods, but the reasons for this are not clear. A larger number of samples collected over a longer period would be needed to give a clearer view.

3.3.1.2. NO_x diffusion tube evaluation

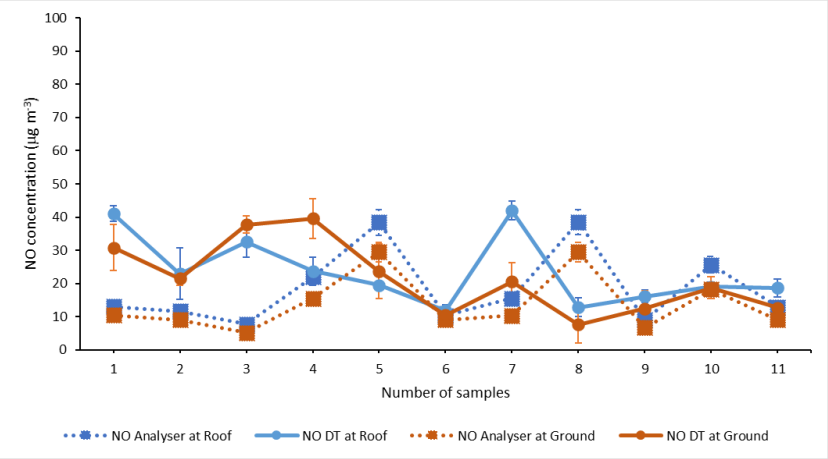
In our study, the bias from NO_x diffusion tubes was highly variable and did not show consistent results, therefore data from the NO_x diffusion tubes were discarded. However, the experimental set-up and results are as follows.

The NO_x diffusion tubes were set up on the roof and at ground level at the UoB Biosciences building. The vertical distance between the two sampling sites was 13 metres. NO_x instrument 42C was set on the roof and NO_x instrument 42i was set at 1-metre height above the ground. NO_x diffusion tube compositions are explained in Chapter 2, Section 2.3.1.2. The samplers were exposed for 1, 2, 3 and 4-week periods over the course of just over 1 month, from 28 January to 11 March 2019. The limit of detection of NO_x for a period of exposure of 2-weeks was 8 ± 2 µg m^{-3}.

(a) NO_x concentrations on the roof and at the ground level from DT and automatic analysers



(b) NO concentrations on the roof and at the ground level from DT and automatic analysers



(c) NO_2 concentrations on the roof and at the ground level from DT and automatic analysers

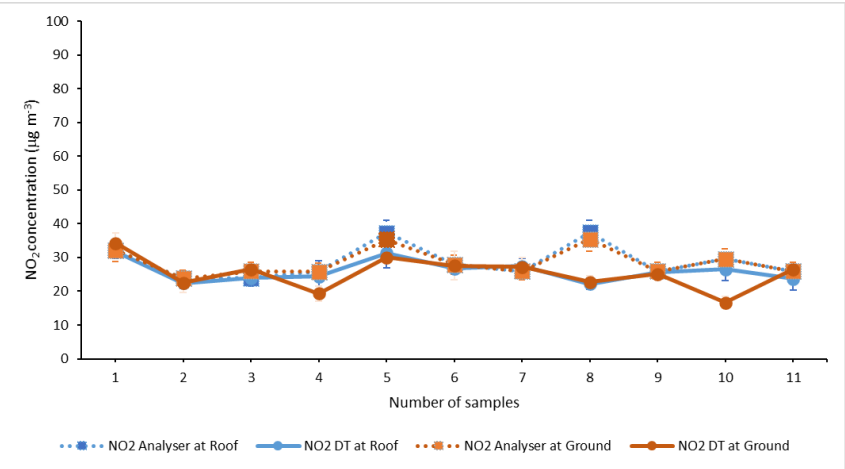


Figure 3.5. NO_x, NO and NO_2 concentrations from diffusion tubes along with automatic analysers on the roof and the ground of the Biosciences building. **(a)** NO_x concentrations on the roof and the ground from diffusion tubes and automatic analysers. **(b)** NO concentrations on the roof and the ground from diffusion tubes and automatic analysers. **(c)** NO_2 concentrations on the roof and the ground from diffusion tubes and automatic

analysers. The blue box with the dashes is concentration of pollutants (NO_x, NO and NO_2) from automatic analysers on the roof; the blue dot with lines is concentration of pollutants (NO_x, NO and NO_2) from diffusion tubes on the roof; the orange box with dashes is concentration of pollutants (NO_x, NO and NO_2) from automatic analysers on the ground; and the orange dot with lines is concentration of pollutants (NO_x, NO and NO_2) from diffusion tubes on the ground. Standard deviation of automatic analyser was estimated as 10% of the mean (Stevenson *et al.*, 2009) and standard deviation of diffusion tubes was generated from triplicate measurement.

Table 3.5. Precision and accuracy of NO_x diffusion tubes (NO_x, NO_2 and NO levels) on the roof and the ground of the Biosciences building, 28 January to 11 March 2019

Pollutant	Parameter	Indicator	Roof		Ground	
			Average (%)	Range (%)	Average (%)	Range (%)
NO_x	Precision	RSD	16	1.5 to 36	16	0.4 to 45
	Accuracy	% bias	-9	-67 to 40	-1	-68 to 101
NO	Precision	RSD	15	6 to 34	25	7 to 72
	Accuracy	% bias	73	-67 to 318	114	-74 to 625
NO_2	Precision	RSD	9	3 to 19	9	4 to 15
	Accuracy	% bias	-8	-41 to 6	-10	-44 to 7

The accuracy of NO_x diffusion tubes fluctuates significantly in the overestimates and underestimates and is in the range of -68% to 101%. The precision of NO_x levels ranged from 0.4% to 45% and averaged 16% on the roof and on the ground site.

Vardoulakis *et al*. (2009) measured NO_x and O_3 at three sampling sites in Birmingham from August 2005 to July 2006. They found a bias of NO_x of -40% and the underestimates of NO_x concentration happened at high levels and increased during wintertime.

3.3.1.3. O_3 diffusion tube evaluation

O_3 diffusion tubes were positioned along with the O_3 instrument at BROS and EROS sites from 18 March to 15 April 2018, and at roof and ground level at the Biosciences building from 22-28 November 2018.

Table 3.6. Validation result of O_3 diffusion tubes for precision and bias

Parameter	Indicator	18/03/2018 – 15/04/2018		22/11/2018 – 28/11/2018	
		O_3 (%)		O_3 (%)	
		BROS (1)	EROS (2)	Roof (3)	Ground (4)
Precision	RSD < 15	8	3	5	14
Bias	%	-8	29	-31	-9

Table 3.6. and Figure 3.6. show that the range of bias for O_3 samples was -31% to +29% and the relative standard deviation between tubes was in the range 3% to 14%. However, the number of samplers (N=4) was not sufficient to draw clear conclusions about precision and bias.

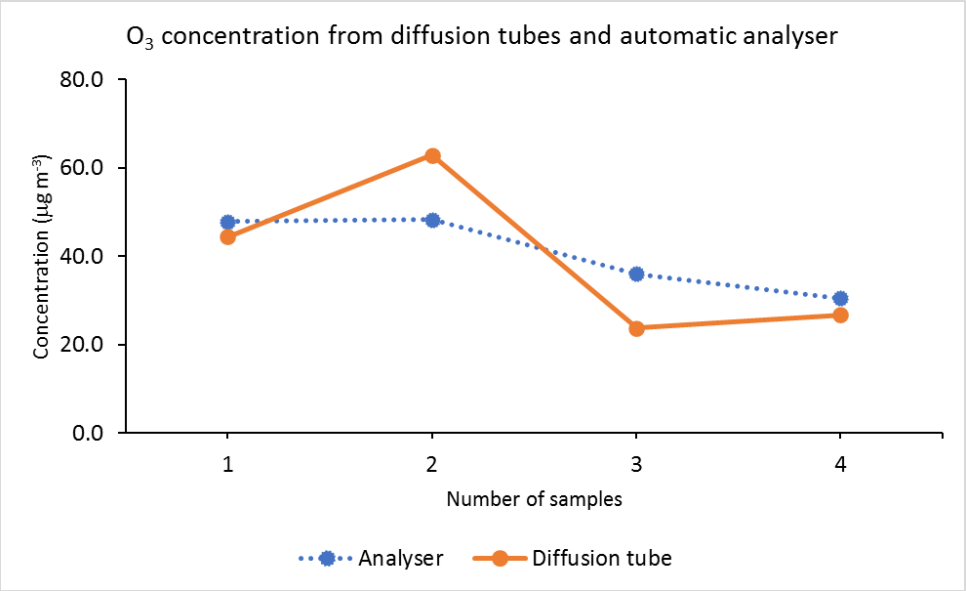


Figure 3.6. Comparison of O_3 concentration from diffusion tubes and O_3 automatic analysers, in four different locations at BROS, EROS, and the roof and ground of the Biosciences building.

In the parks, O_3 diffusion tubes were exposed at the University of Birmingham, Cannon Hill Park and the Biosciences sites for the duration of 4 weeks (N=3), 6 weeks (N=1) and also a 1-week (N=1) exposure period. In the various locations where the diffusion tubes were placed within the campus of UoB for the 1-week exposure (20/11/2018 – 28/11/2018), there were 6 samples below the detection limit. This could be due to the exposure period being shorter than the recommended period of 2 – 4 weeks.

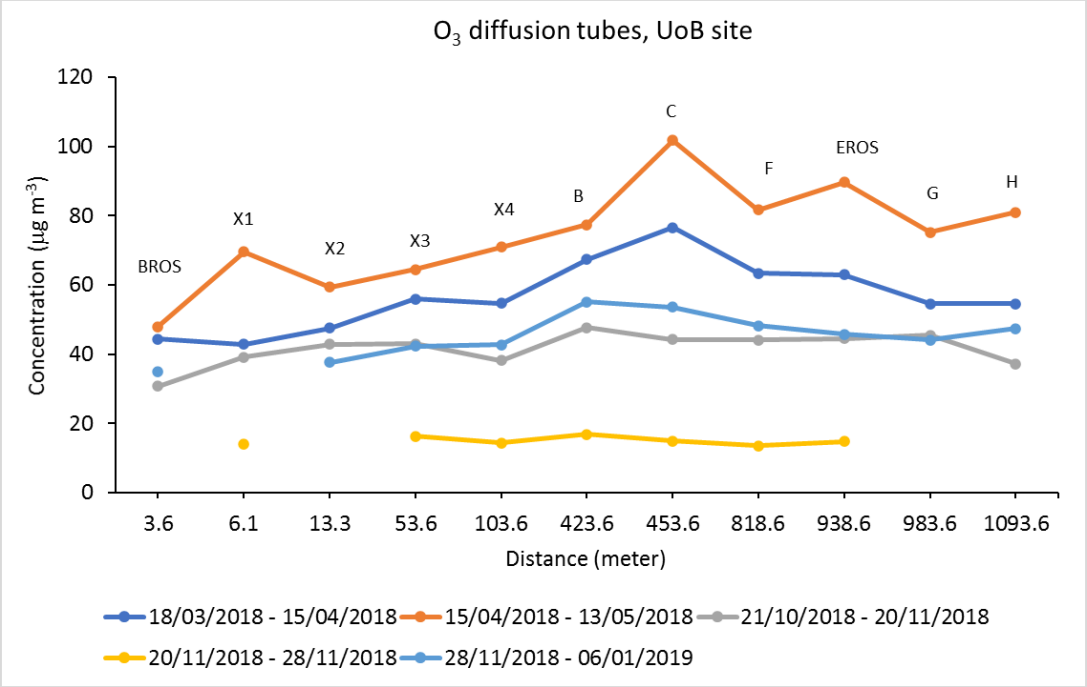


Figure 3.7. O_3 concentration at UoB sites from the BROS site (3.6 m from A38 road) to H site (1093.6 m from A38 road), from five sampling times

As shown in Figure 3.7, the trend of O_3 concentrations was to increase along the distance from near to the road out to the urban background area. The average and standard deviation of O_3 level at BROS (roadside) was 40 ± 8 µg m^{-3} and at EROS (background site) was 52 ± 27 µg m^{-3}, with a difference in concentration of 12 µg m^{-3}.

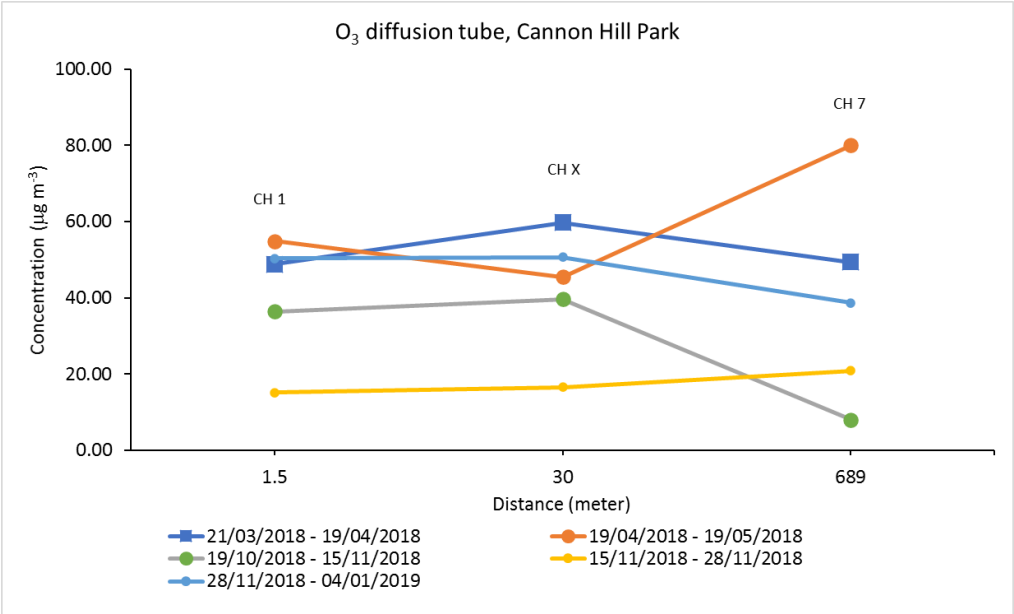


Figure 3.8. O_3 concentrations at Cannon Hill site from CH1 (at 1.5 m from Edgbaston road) into the park (689 m from Edgbaston Road), from five sampling times

In Cannon Hill Park, O_3 diffusion tube samplers were located 1.5 metres from the road (CH1 site), 30 metres from the road (CHX site) and one sampler was inside the park (CH7 site). O_3 concentrations varied from 8 μg m^{-3} to 80 μg m^{-3} during the sampling period. The average and standard deviation of O_3 concentration at the roadside was 41 ± 16 μg m^{-3}, and O_3 concentration inside the park (CH7) was 39 ± 28 μg m^{-3}.

O_3 concentrations near the road are expected to be lower due to the reaction with traffic emissions — for example, NO which is oxidized by O_3 to NO_2 — and increased along the distance. NO_x concentrations are associated with pollutants from traffic that have the highest concentration near the road with levels decreasing at background sites. More O_3 reacts with NO near the road than at the background site, meaning that O_3 concentrations near the road should be lower due to reaction between NO and O_3 being a net sink of O_3. However, at the Cannon Hill Park site, 3 out of 5 samples showed a decrease in O_3 levels in the park.

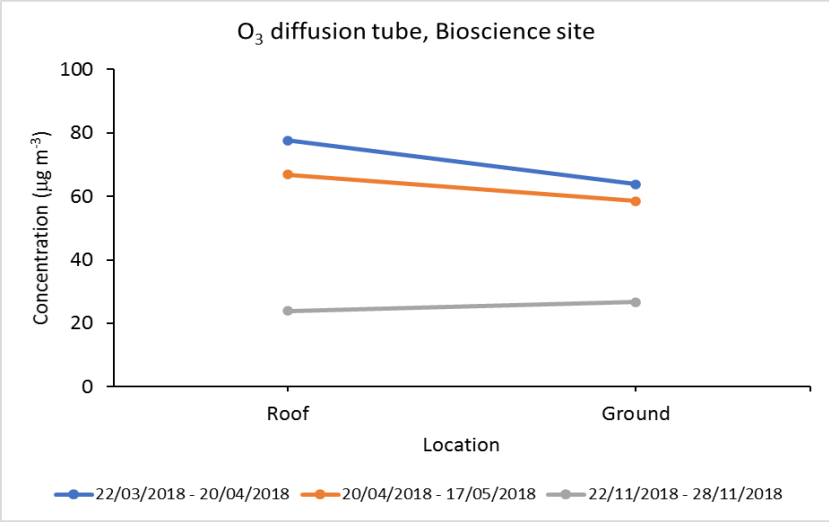


Figure 3.9. O_3 concentrations on the roof and the ground of Biosciences site, at three sampling times

At the Biosciences building, O_3 diffusion tubes were deployed on the roof and on the ground with the average concentration and standard deviation on the roof of 56 ± 29 μg m^{-3}, and on the ground of 50 ± 20 μg m^{-3}, as shown in Figure 3.9.

3.3.2. Measurement of NO_2 concentration in urban green space

Diffusion tubes were set up at locations near heavy traffic roads and within green areas, in order to review the temporal and spatial variability of pollutant concentration near the roads and across the urban green areas.

3.3.2.1. Cannon Hill Park

Locations of diffusion tube placement at Cannon Hill Park (CH) — shown in Figure 2.12. in Chapter 2 and in Appendix 2.2 — were set at 13 locations. NO_2 diffusion tube measurements were conducted from October 2016 to January 2019 (N = 37) with sampling intervals between 2 and 4 weeks. However, CH X was set at Cannon Hill Park for the period 25 December 2017 to 28 November 2018 (N = 11).

Figures 3.10. and 3.11. show the observed average NO_2 concentration between the sampling location at Edgbaston Road to the inside of Cannon Hill Park. The NO_2 concentration decreased from the road into the park with some fluctuations inside the park.

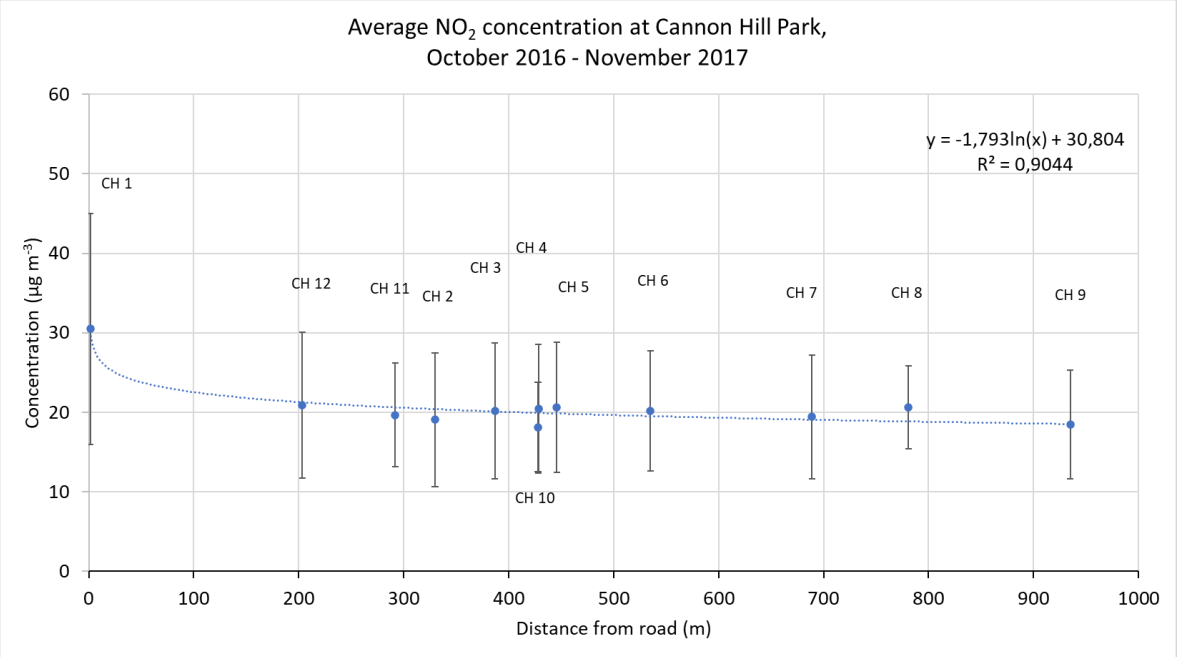


Figure 3.10. Pattern of NO_2 concentration with respect to distance from the road to the inside of Cannon Hill Park (sampling period October 2016 – November 2017) using diffusion tubes with open end with bias adjustment, True NO_2 = (DT_NO_2 + 1.048) / 0.978. The blue dots represent the mean NO_2 concentration at each sampling point in the sampling period and error bars represent standard deviation (N = 24 data points). The line of best fit used in the graph was a logarithmic trendline obtained from mean data.

Appendix 3.3 presents NO_2 concentrations from the raw data of monthly diffusion tube measurements, while Figure 3.10 and Figure 3.11 are graphs of the average NO_2 concentrations that have been adjusted using the RMA regression line from Figure 3.3 to get an estimated value of the true NO_2 concentrations. The data in Figures 3.10 and 3.11 have been adjusted at each sampling location in Cannon Hill Park, and for all sampling periods from October 2016 to November 2017 (Figure 3.10) and from November 2017 to January 2019 (Figure 3.11).

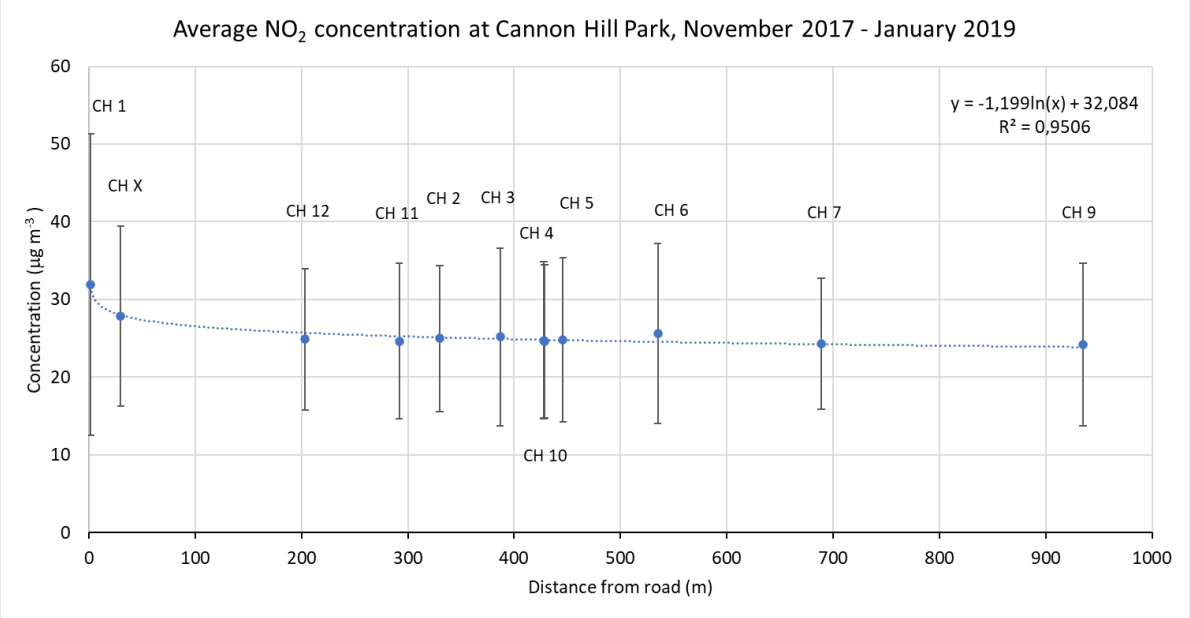


Figure 3.11. Pattern of NO_2 concentration with respect to distance from the road to the inside of Cannon Hill Park (sampling period November 2017 – January 2019) using diffusion tubes with membrane with bias adjustment, True NO_2 = (DT_NO_2 + 20.64) / 1.402. The blue dots represent the mean NO_2 concentration at each sampling point in the sampling period and error bars represent standard deviation (N = 13 data points). The line of best fit used in the graph was a logarithmic trendline obtained from mean data.

The fit of the average data in Figure 3.10 and Figure 3.11 uses logarithmic regression. The regression line appears as a curve that shows higher NO_2 concentrations near the road, decreasing along with the distance from the road. This trend is similar to the graph of monthly data as shown in Appendix 3.3 that also uses logarithmic regression and shows a decrease in NO_2 concentrations as the distance from the road increases. The pattern is for the NO_2 concentration to drop rapidly around 200 m, then the NO_2 levels fluctuate but well below NO_2 concentration at the roadside.

However, the raw data of monthly mean NO_2 concentration at the sampling points more than 200 m showed more fluctuation patterns in several locations, and the NO_2 concentrations were above or below the logarithmic regression line. The monthly mean concentrations show the typical seasonality of NO_2 concentrations level. During winter, the NO_2 concentrations were higher than in the summertime. Local traffic emissions also influence the level of monthly NO_2 concentrations.

NO_2 concentrations were higher near the road and declined towards the park, as distance from the roadside increased. Although there were a few increases at several points, concentration levels were lower than the average NO_2 ambient concentration levels near the road. This result was in line with other studies, such as Gilbert *et al*. (2007, 2003) and Beckerman *et al*. (2008). Wind direction and speed affect the comparison of NO_2 concentrations near the road and in the park. Increases in wind speed would increase dispersion of pollutants (AQEG, 2018). The higher wind speed enhances the dispersion and mixing of pollutant concentrations (Jones *et al*., 2010; Agudelo–Castaneda *et al*., 2014). Furthermore, Gilbert *et al.* (2003) found that NO_2 concentrations decreased as distance from road increased, and concentrations were higher downwind than upwind relative to the road.

Figures 3.12 to 3.13 show the trend of NO_2 concentration near to the road and inside the park. The fluctuation trend of NO_2 concentrations inside the park was relatively similar to the trend outside the park.

Figures 3.12.a. and Figure 3.13.a show the various NO_2 concentrations between the roadside (CH1) and all the locations inside the park. NO_2 levels near the road were higher compared to the NO_2 concentrations in the park, which varied little. For clarity, NO_2 concentrations at all sampling sites in the park (CH12, CH11, CH2, CH3, CH10, CH4, CH5, CH6, CH7, CH8 and CH9) were combined and calculated to generate a mean and standard deviation of NO_2 concentrations in the park and are presented as a single line, then compared to NO_2 at the main road as shown in Figure 3.12.b., for the sampling period October 2016 to November 2017, and Figure 3.13.b. for the sampling period November 2017 to January 2019. The error bars (orange line and green line) represent standard deviation of NO_2 level at the measurement sites near road and in the park.

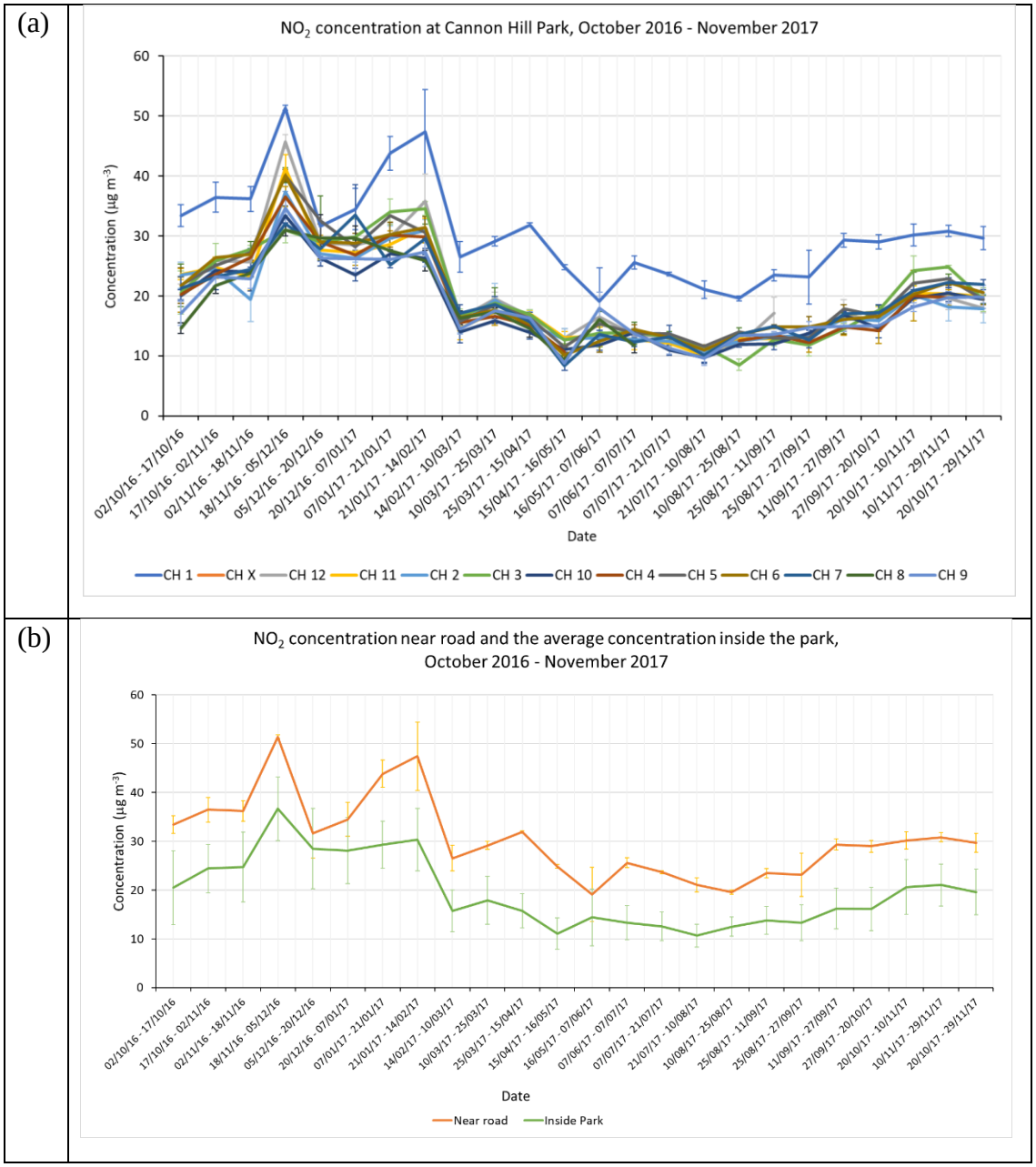


Figure 3.12. NO_2 concentrations at 13 locations (CH1 to CH12) in the Cannon Hill Park from October 2016 to November 2017. **(a)** The blue line represents a site near the road (CH1), while other lines (CH12, CH11, CH2, CH3, CH10, CH4, CH5, CH6, CH7, CH8 and CH9) represent sampling sites that are spread at various locations in the park. NO_2 concentrations at each point are presented as mean concentration and standard deviation (mean ± SD) from triplicate diffusion tubes. **(b).** NO_2 concentrations inside the park (CH12, CH11, CH2, CH3, CH10, CH4, CH5, CH 6, CH7, CH8 and CH9) are plotted as a single line (green line), and plotted with NO_2 at near road (CH1) (orange line) during sampling period, October 2016 to November 2017. NO_2 concentrations near the road are presented as mean concentrations and error bars represent standard deviation from triplicate diffusion tubes (mean ± SD). NO_2 concentrations inside the park are presented as mean concentrations and error bars represent standard deviations at sampling points inside the park (N== 11 data points).

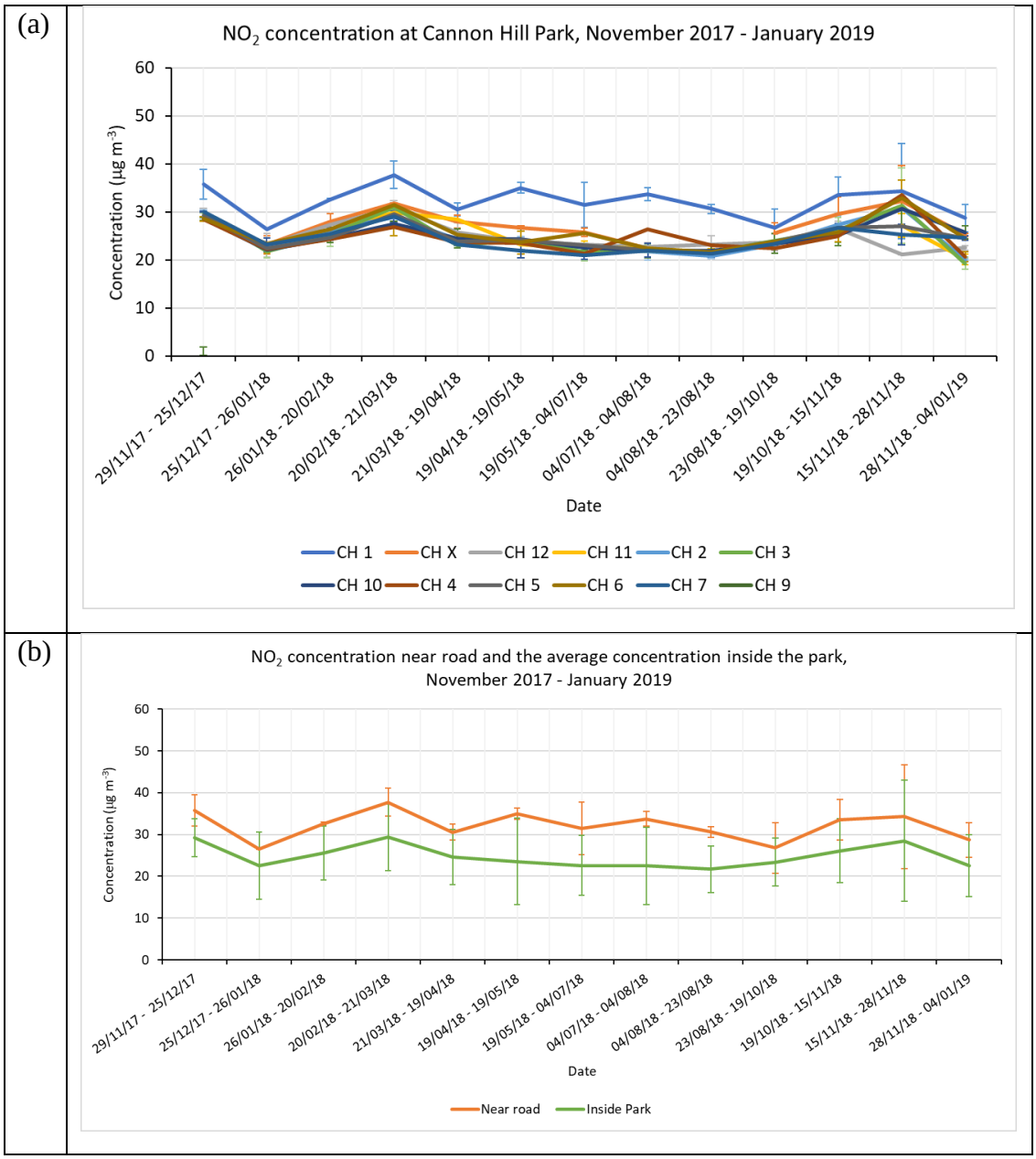


Figure 3.13. NO_2 concentrations at 13 locations (CH1 to CH12) in the Cannon Hill Park from November 2017 to January 2019. **(a)** The blue line represents a site near the road (CH1), while other lines (CHX, CH12, CH11, CH2, CH3, CH10, CH4, CH5, CH7 and CH9) represent sampling sites that are spread at various locations in the park. NO_2 concentrations at each point are presented as mean concentration and standard deviation (mean ± SD) from triplicate diffusion tubes. **(b).** NO_2 concentrations inside the park (CH12, CH11, CH2, CH3, CH10, CH4, CH5, CH 6, CH7 and CH9) are plotted as a single line (green line), and plotted with NO_2 at near road (CH1) (orange line) during sampling period, November 2017 to January 2019. NO_2 concentrations near the road are presented as mean concentrations and error bars represent standard deviation from triplicate diffusion tubes (mean ± SD). NO_2 concentrations inside the park are presented as mean concentrations and error bars represent standard deviations at sampling points inside the park (N== 10 data points).

For the sampling period October 2016 to November 2017, average NO_2 concentration near the road was 30 ± 14 μg m^{-3}, while the concentration at the CH7 sampling location in the middle of the park was 19 ± 8 μg m^{-3}. The difference between concentrations was 11 ± 7 μg m^{-3}. Inside the park, NO_2 concentrations decreased by 37% compared to NO_2 concentration near the road. For the sampling period November 2017 to January 2019, average NO_2 concentration near the road was 32 ± 19 μg m^{-3}, while the concentration at the CH7 sampling location in the middle of the park was 24 ± 8 μg m^{-3}. Inside the park, NO_2 concentrations decreased by 25% compared to NO_2 concentration near the road.

NO_2 concentrations were measured at the roadside and in the park during different seasons. An elevated level of NO_2 in all seasons was found at the roadside (Figure 3.14). The lowest NO_2 concentration was detected in summer for both locations. In summer, NO_2 concentration near the road is 2 times higher than inside the park, due to the greater amount of daylight that results in photolysis of NO_2 causing its concentration to decline in the atmosphere (R 3.1), and also due to enhanced vertical mixing. In winter months, the NO_2 concentration was higher due to lower wind speed and a shallower boundary layer in the cold season (Ducret-Stich *et al.*, 2013).

$$NO_2 + \mathrm{hv} \rightarrow \mathrm{NO} + \mathrm{O} \qquad \text{(R. 3.1)}$$

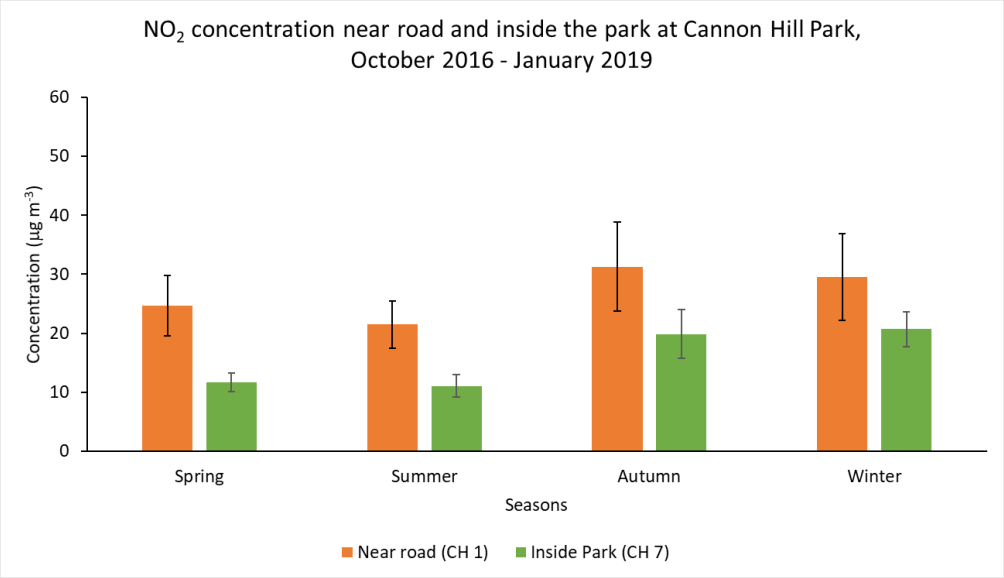


Figure 3.14. NO_2 concentration based on seasonality (during spring, summer, autumn and winter), at Cannon Hill Park, from October 2016 to January 2019. Orange bars represent mean NO_2 concentration near road (sampling site CH1), while green bars show mean NO_2 concentration in the park (sampling site CH 7). Error bars represent standard error of the mean.

The seasonal trend of NO_2 concentrations at Cannon Hill Park during the sampling period (Figure 3.14) shows higher NO_2 levels in autumn and higher NO_2 concentrations at the roadside. This is aligned with Campbell (1988) who measured NO_2 concentrations in Northern Ireland and East Anglia using Palmes diffusion tubes and found that NO_2 concentrations were higher in the winter due to the increase of emission sources and other factors (e.g. meteorological). Factors that influenced the difference between roadside and in-park concentrations other than meteorological factors might be traffic density and anthropogenic activities. NO_2 concentration is reported to be positively correlated with traffic density near the road and negatively correlated with distance from the road (Roorda-Knape *et al.*, 1998; Gilbert *et al.*, 2003). Activities near the road are affected by road traffic which emits pollutants such as NO_2 and PM_{10}, while in the park people are more likely to be walking and cycling which are not a source of NO_x emissions.

3.3.2.2. Hyde Park

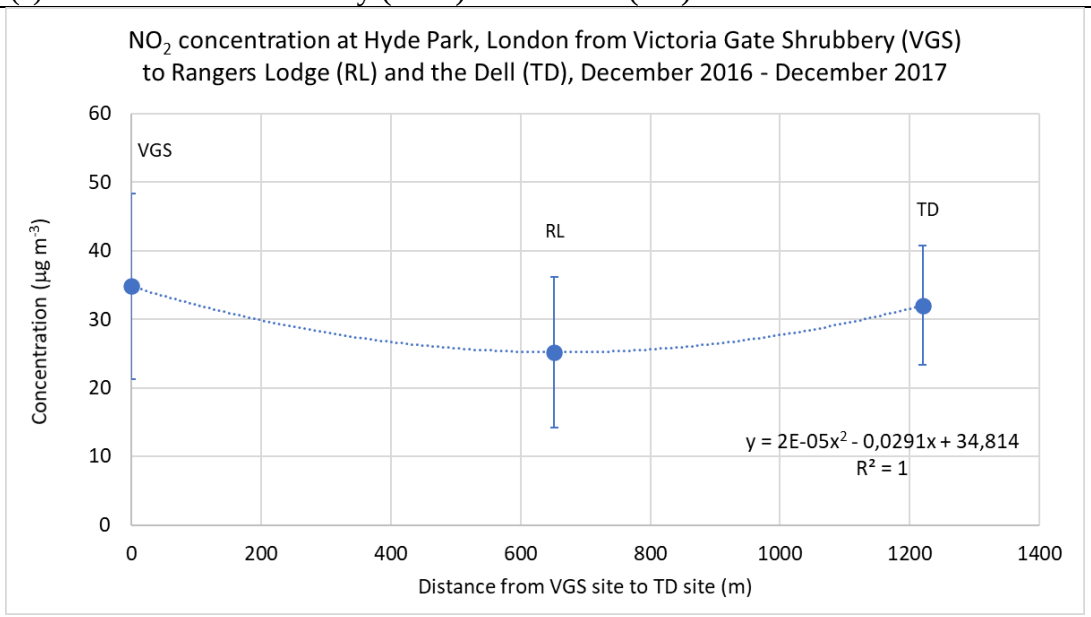
The locations of diffusion tubes at Hyde Park, London, are shown in Chapter 2, Section 2.3.3.2.1. and Appendix 2.3. There were four locations near the roadside and one location in the middle of the park. Cumberland Gate Lodge (CGL), Victoria Gate Shrubbery (VGS), The Dell (TD) and Bowling Green (BG) locations are near roads, while Rangers Lodge (RL) is inside the park. Figure 3.15 shows the transect from VGS to TD that goes through the park, showing the RL location in the middle. The transect from CGL to BG also passes through the RL. NO_2 concentrations near the roads were high and decreased away from the roads into the park. Appendix 3.4 presents NO_2 concentrations from the raw data of diffusion tube measurements at Hyde Park. The line of best fit used in the graph is a polynomial order 2 trendline through mean data.

NO_2 concentrations (mean ± SD) near roads at VGS and the Dell were 35 ± 14 μg m^{-3} and 32 ± 9 μg m^{-3} respectively. The concentration inside the park at Rangers Lodge was 25 ± 11 μg m^{-3}. The difference in concentration is less than 10 μg m^{-3}. The NO_2 level at CGL was 39 ± 15 μg m^{-3} and at BG was 35 ± 9 μg m^{-3}.

The average NO_2 concentrations in the park-centre were lower than roadside measurements in the range of 22% to 36%. The reduction of NO_2 concentrations at a further distance from the road indicates a link with traffic-related air pollutants and the dispersion of pollutants

from roadside into green areas or distance from roads. These result patterns have also been seen in other studies conducted in Canada (Gilbert *et al.*, 2003), the Netherlands (Roorda-Knape *et al.*, 1998), and Hong Kong (Xing and Brimblecombe, 2018).

(a) Victoria Gate Shrubbery (VGS) to The Dell (TD)



(b) Cumberland Gate Lodge (CGL) to Bowling Green (BG)

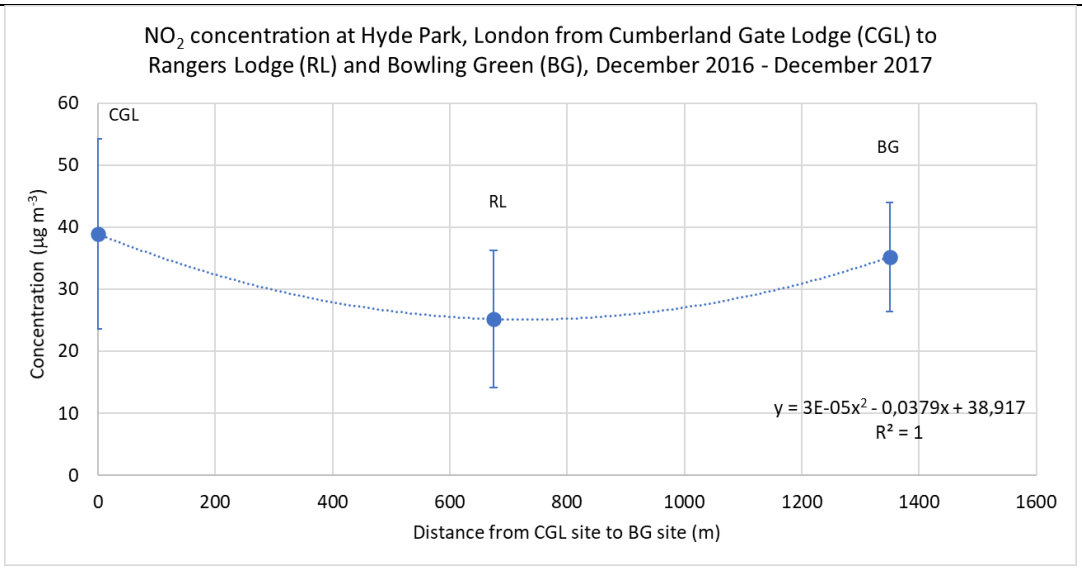


Figure 3.15. NO_2 ambient concentration at Hyde Park, London, on a transect **(a)** from Victoria Gate Shrubbery (VGS) to Rangers Lodge (RL) and the Dell (TD), and **(b)** from Cumberland Gate Lodge (CGL) to Rangers Lodge (RL) and Bowling Green (BG). The blue dots represent the mean NO_2 concentration at each sampling point during the sampling period and error bars represent the standard deviation (N = 16 data points). The line of best fit used in the graph is a polynomial order 2 trendline through mean data. Diffusion tube bias adjustment, True NO_2 = (DT_NO_2 + 1.048) / 0.978.

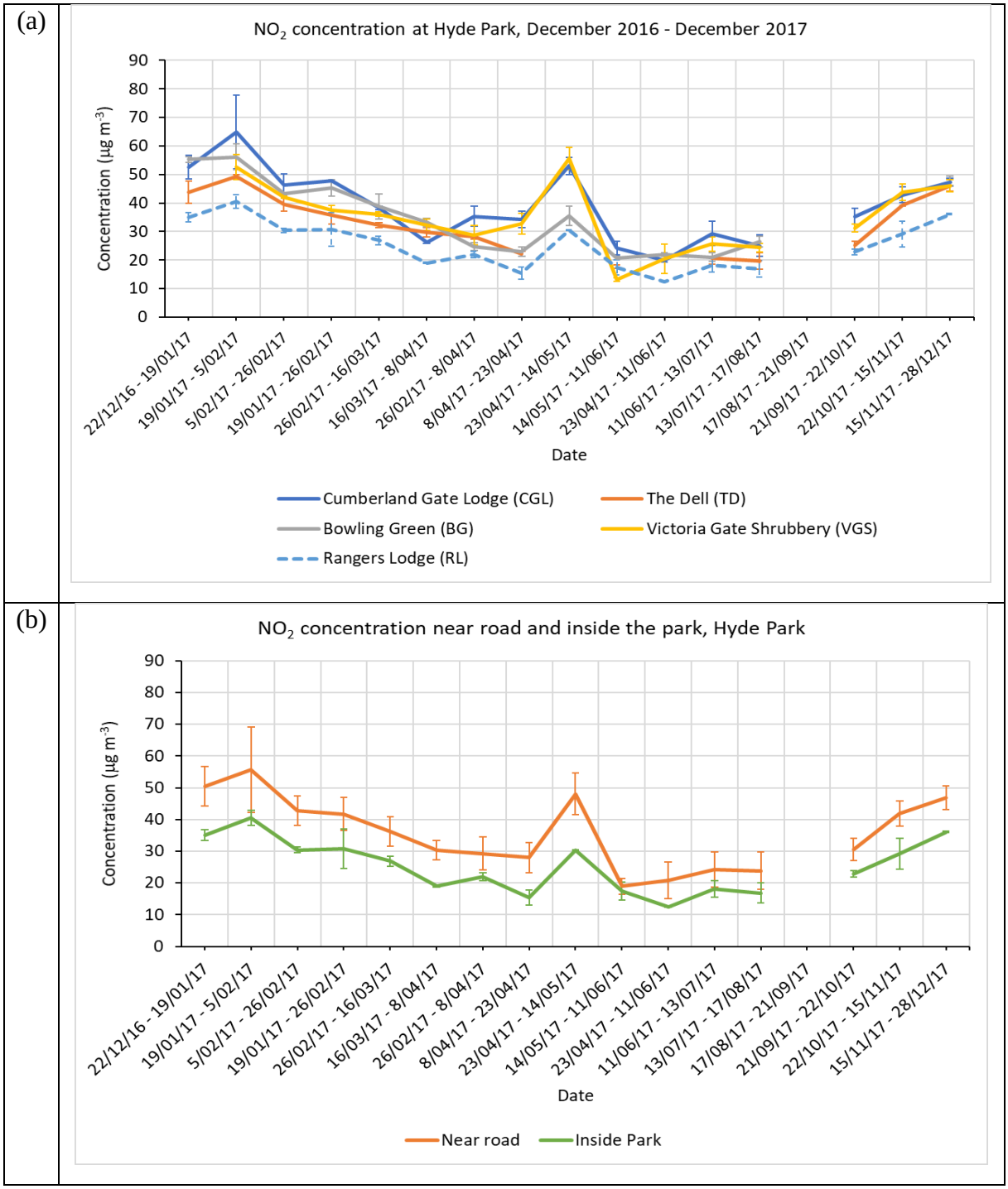


Figure 3.16. NO_2 concentrations at 5 locations in the Hyde Park monitoring sites from December 2016 to December 2017. **(a)** The blue dash line represents a location in the park (RL), while other lines are roadsides at four locations (VGS, TD, CGL and BG) around the park. NO_2 concentrations at each point are presented as mean concentration and standard deviation (mean ± SD) from triplicate diffusion tubes. **(b)** NO_2 concentrations near the roadsides are plotted as a single line (orange line) and compared with NO_2 inside the park (green line). NO_2 concentrations in the park are presented as mean concentrations and error bars represent standard deviation from triplicate diffusion tubes (mean ± SD). NO_2 concentrations near the roads are presented as mean concentrations and error bars represent standard deviations at sampling points (N= 4 data points).

NO_2 concentrations near roads (VGS, TD, CGL, BG) were higher relative to the level in the park (RL), and this was associated with the pollutant emissions from traffic. However, during sampling from 14 May to 11 June 2017, the concentration at Victoria Gate Shrubbery was lower compared to the other roads as shown in Figure 3.16., and this resulted in a non-significant difference between the roadside and park interior sites. The reason for this because the road was closed between Lancaster Terrace and Clarendon Place, including Victoria Gate due to gate and ducting repairs at Victoria Gate starting on May 15th, 2017. Bayswater Road closed for 13 days between the 15th of May to 27th of May 2017 for works on phase 1 and 2 of the cycle superhighway construction programme that impact roads and pedestrians at Victoria Gate (https://www.friendshpkg.org.uk/news/single-news.php).

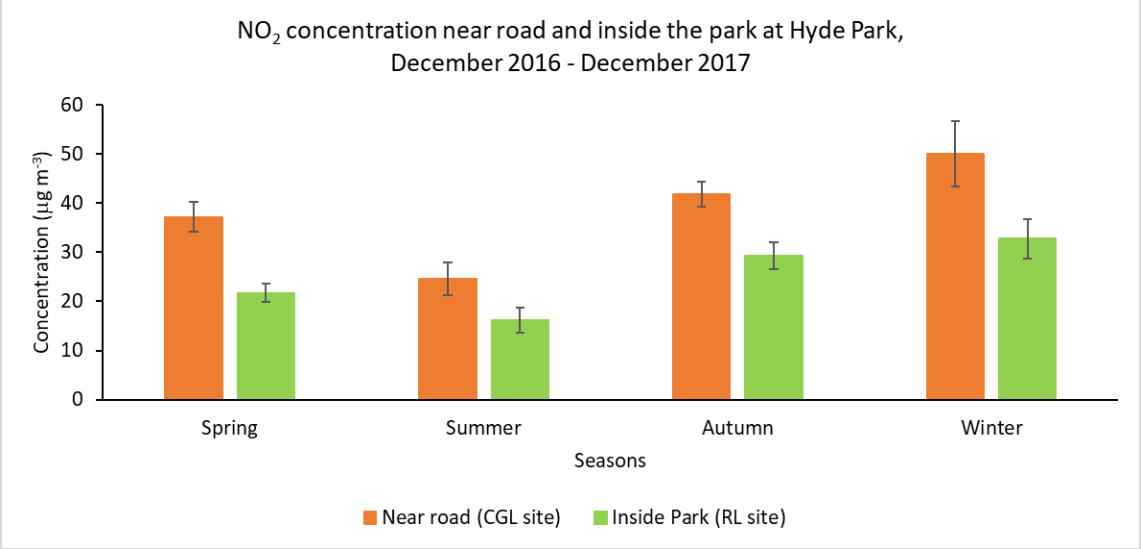


Figure 3.17. NO_2 concentration based on seasonality (during spring, summer, autumn and winter), at Hyde Park, from December 2016 to December 2017. Orange bars represent mean NO_2 concentration near the road (CGL site), while the green bars show mean NO_2 concentration in the park (RL site). Error bars represent standard error of the mean.

Figure 3.17 shows the mean concentration of NO_2 in spring, summer, autumn, and winter in Hyde Park, London. In general, NO_2 levels at the roadside were higher than NO_2 concentrations in the park in all seasons. The highest NO_2 concentrations occurred in winter and the lowest happened in summer. Pollutants in winter are less dispersed due to the combination of the shallower mixing layer, low wind speeds, and low temperatures that usually occur in cold seasons and at night-time (Ducret-Stich *et al.*, 2013).

3.3.2.3. Tile Cross Park

Locations of diffusion tubes at Tile Cross Park are shown in Chapter 2 Section 2.3.3.1.2. and Appendix 2.4. Fifteen diffusion tubes were placed at Tile Cross Park — one was near a bus stop, and fourteen others were inside the park. NO_2 samplers were exposed for 2 – 4 weeks in the period October 2016 to July 2017 (N = 14). The diffusion tubes were placed 3 metres above the ground. Diffusion tubes were lost due to vandalism on 5 occasions at 3 locations (TL 3, TL 11, and TL 15). Appendix 3.5 presents NO_2 concentrations from the raw data of diffusion tube measurements at Tile Cross Park. The trend of the logarithmic regression line from the raw data was similar to the pattern of average NO_2 concentrations from bias adjustment data in Figure 3.18.

Figure 3.18 shows NO_2 concentration generally lower at locations inside the park than at TL 1 — however, as can be seen, NO_2 levels in the park did fluctuate. The NO_2 concentration near the roadside was 29 ± 9 μg m^{-3}, while the concentration inside the park at TL4 was 25 ± 9 μg m^{-3}, and the difference in concentration less than 5 μg m^{-3}.

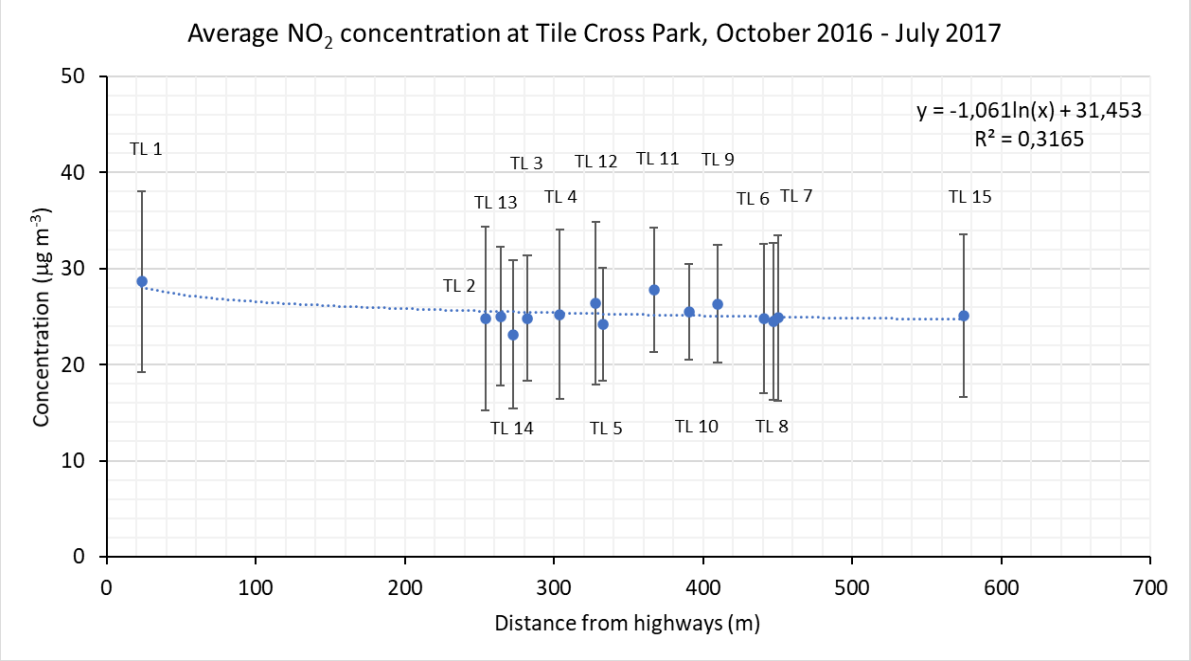


Figure 3.18. The pattern of NO_2 concentration to distance from the roadside into Tile Cross Park (sampling period October 2016 – July 2017) using diffusion tubes with open end with bias adjustment, True NO_2 = (DT_NO_2 + 1.048) / 0.978. The blue dots represent the mean NO_2 concentration at each sampling point in the sampling period and error bars represent standard deviation (N = 14 data points). The line of best fit used in the graph was a logarithmic trendline obtained from mean data.

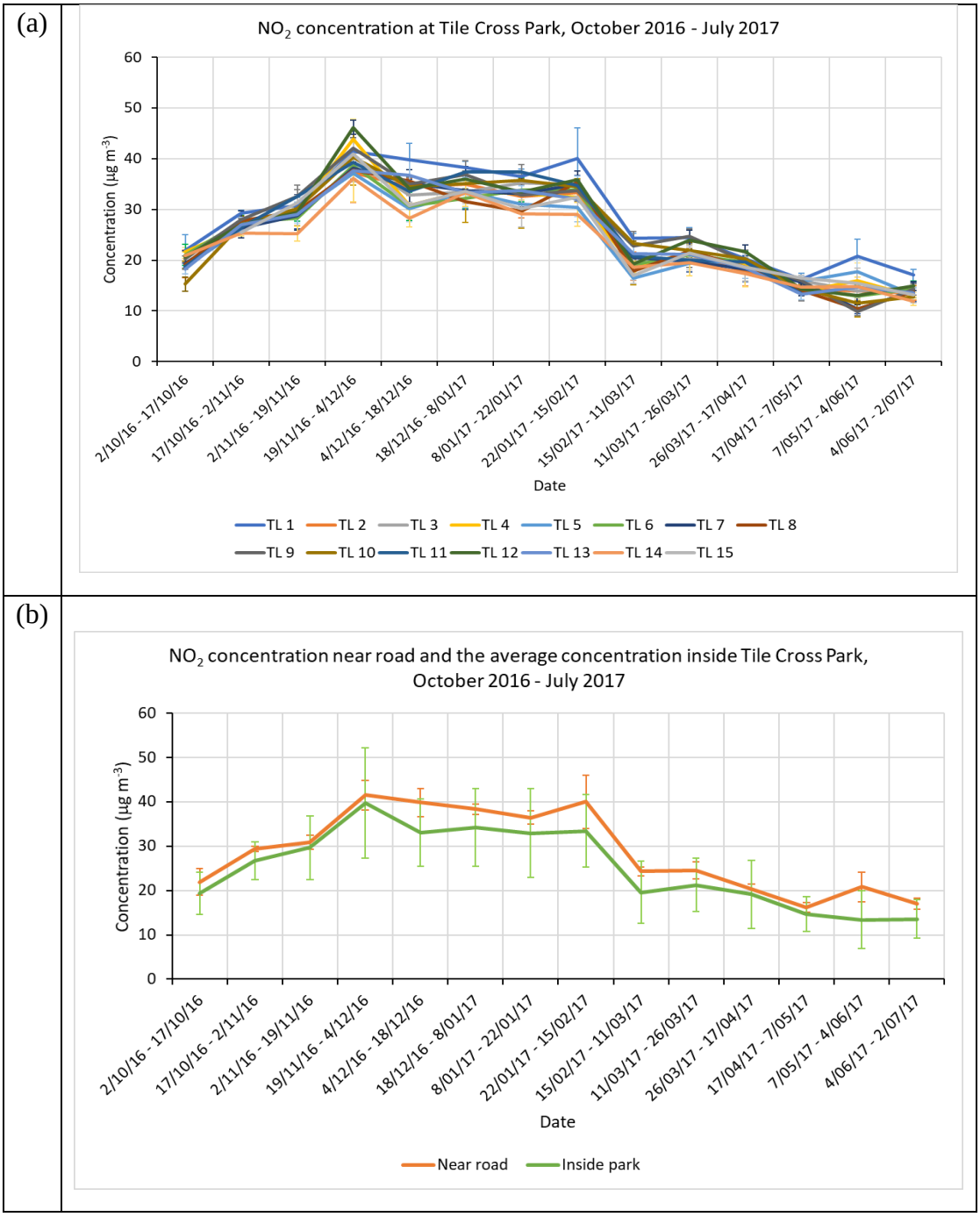


Figure 3.19. NO_2 concentrations at 15 locations at Tile Cross Park during October 2016 to July 2017. **(a)** The blue line represents a location near the road (TL1), and others (TL2 to TL15) represent sampling sites in the Tile Cross Park. NO_2 concentrations at each point are presented as mean concentration and standard deviation (mean ± SD) from triplicate diffusion tubes. **(b)** NO_2 concentrations inside the park are plotted as a single line (green line) and compared with NO_2 near the road (orange line). NO_2 concentrations near the road are presented as mean concentrations and error bars represent standard deviation from triplicate diffusion tubes (mean ± SD). NO_2 concentrations in the park are presented as mean concentrations and error bars represent standard deviations at sampling points (N== 14 data points).

Figure 3.19.a shows the NO_2 concentration near the road, the bus stop (TL 1) and all locations inside the park. The differences in NO_2 levels near road and inside the park were very low, and all the trends of NO_2 concentrations were relatively similar. TL 1 was treated as the 'near road' NO_2 concentration, and all others (TL 2 to TL 15) as NO_2 concentrations 'in the park'. Figure 3.19.b shows NO_2 concentrations in the park (TL2 to TL15) combined and calculated as an average NO_2 concentration (green line) with error bars representing standard deviations (N=14 data points).

There was little difference in concentration between the roadside and inside the park. This could be related to the placement of the diffusion tubes as they were put up on a lamp post near the bus stop and not at the edge of the main road. The distance from the edge of the main road to the lamp post is 23.5 meters (Figure 3.20).



Figure 3.20. Map shows distance of diffusion tube location at TL 1 near bus station and the kerbside

The samplers in Tile Cross Park were placed in such a manner that they formed two distinct segments, one segment near St Giles Road and the other segment near the residential area. The passive samplers placed near St. Giles Road on the left side of the park were named as Group 1 and the passive samplers placed in the segment of the park facing the houses were named Group 2. This was done in order to assess whether there was a significant difference between the NO_2 concentrations near roads and inside the park. The average of the groups was used to calculate average NO_2 concentrations in the park.

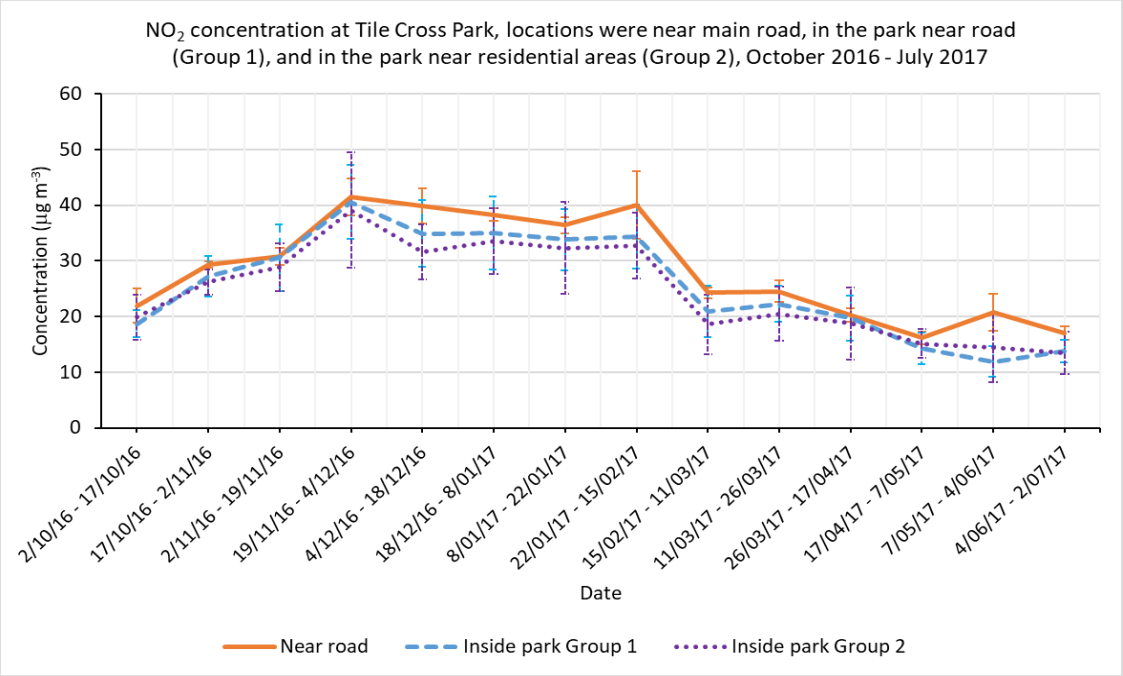


Figure 3.21. NO_2 concentrations near the main road (orange) are compared with NO_2 inside park as group 1, location near road (blue dash) and inside the park as group 2, location near residential area (purple dot). NO_2 concentrations near the road are presented as mean concentrations and error bars represent standard deviation from triplicate diffusion tubes (mean ± SD). NO_2 concentrations in the park are presented as mean concentrations and error bars represent standard deviations at sampling points (N Group 1 = 6 data points; N Group 2 = 8 data points).

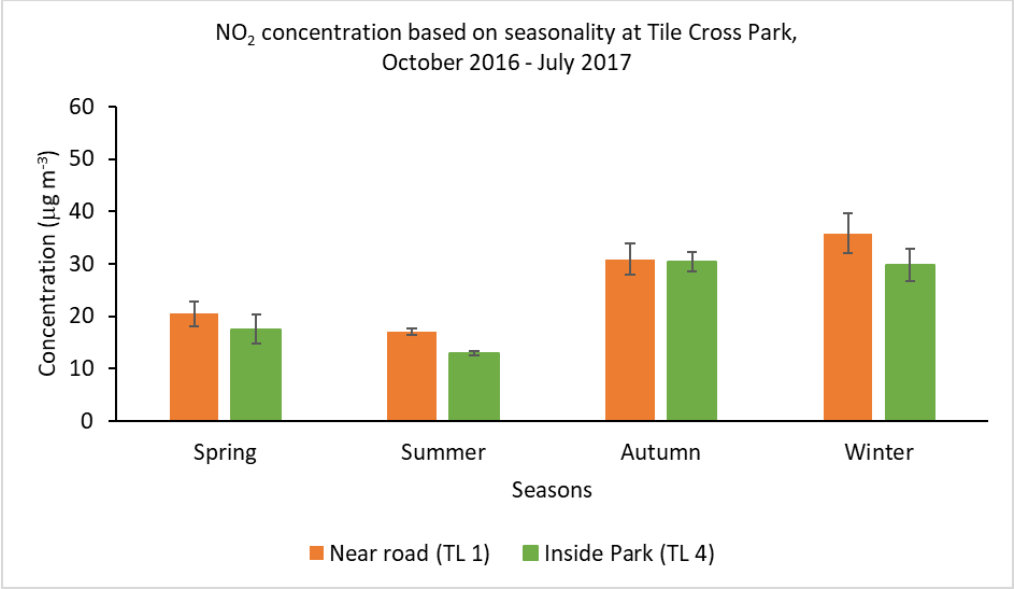


Figure 3.22. NO_2 concentration based on seasonality (during spring, summer, autumn and winter), at Tile Cross Park, from October 2016 to July 2017. Orange bars represent mean NO_2 concentration near the road (sampling site TL 1), while the green bars show mean NO_2 concentration in the park (sampling site TL 4). Error bars represent standard error of the mean.

Figure 3.22 shows that the NO_2 level near the road was slightly higher compared to the concentrations in the park during all four seasons. In wintertime, the NO_2 concentrations were higher. The trend of seasonal NO_2 concentrations was similar to the previous sampling locations. The highest NO_2 level occurred in winter when solar radiation intensities and mixing layer height are at their lowest (Agudelo–Castaneda *et al*., 2014).

3.3.2.4. University of Birmingham

The NO_2 concentration near the roadside was high and decreased rapidly from BROS to site A, then continued to decline slightly (B to J) below the line of best fit, and rise at site E, the location near Pritchatts Road, then fluctuated along the way to EROS in the background area and site I located near Somerset Road. The NO_2 level was slightly elevated at the H and I sites, where the locations are near Edgbaston Park Road and Somerset Road. NO_2 concentrations at the E, H, and I sites were higher than the line of best fit, and these sampling locations are close to roadsides.

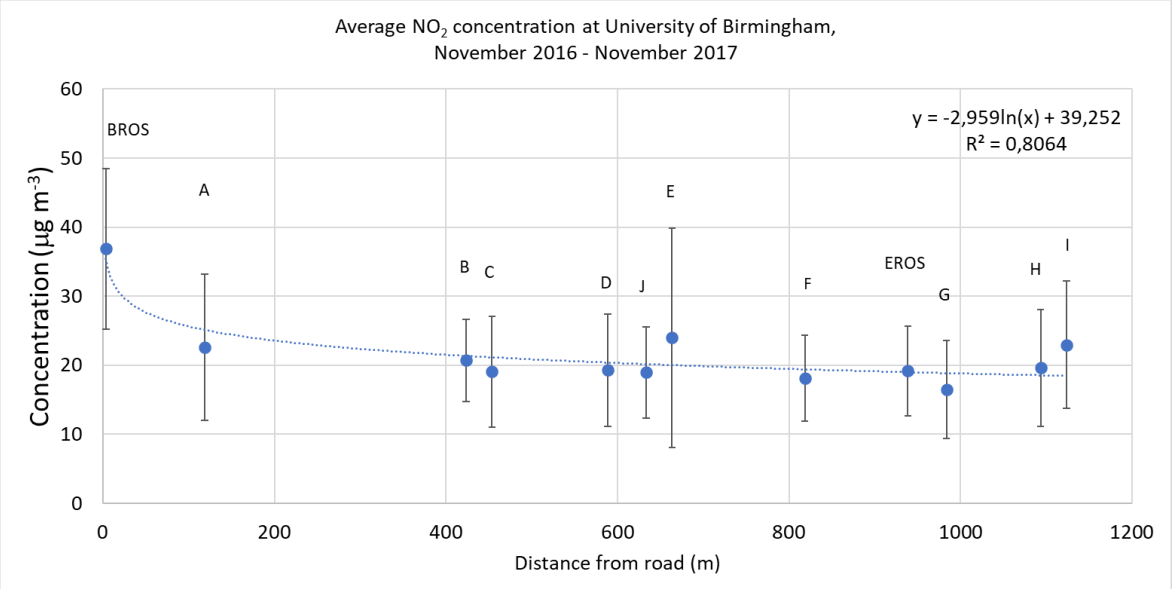


Figure 3.23. The pattern of NO_2 concentration with respect to distance from the road at BROS moving towards the background site at the EROS location inside the University of Birmingham (sampling period November 2016 to November 2017) using diffusion tubes with open end with bias adjustment, True NO_2 = (DT_NO_2 + 1.048) / 0.978. The blue dots represent the mean NO_2 concentration at each sampling point in the sampling period and error bars represent standard deviation (N = 20 data points). The line of best fit used in the graph was a logarithmic trendline obtained from mean data.

Locations of diffusion tubes at the University of Birmingham are shown in Section 2.3.3.1.3. and Appendix 2.5. Appendix 3.6 presents NO_2 concentrations from the raw data of DT measurements at the UoB site. In the period October 2017 to January 2019, we added four sampling locations between BROS and site A to see if there was a trend of lowering NO_2 concentrations in the temporal and spatial variability of air pollutants at distances less than 150 metres. As shown in Figure 3.24 there was a sharper gradient with a rapid decrease from BROS (3.6 m) to X2 (13.3 m) and X3 (53.6 m), and the NO_2 concentration at X4 (103.6 m) was similar to site A (118.6 m). The NO_2 concentration reduces at a distance of tens of metres from the road. This finding is in line with the findings of Xing and Brimblecombe (2018), who used a dispersion model simulation and suggested 17 m as a buffer zone for urban parks in Hong Kong to prevent the impact of traffic emission.

NO_2 concentrations declined from the road to background sites within a distance of around 100 – 150 metres. This result is similar to the findings of other researchers who have found that NO_2 concentrations decreased rapidly to near background within 150 m to 200 m from the roadside (Gilbert *et al.*, 2003, 2007; Beckerman *et al.*, 2008; Karner *et al.*, 2010; Ducret-Stich *et al.*, 2013; Zhang and Batterman, 2013).

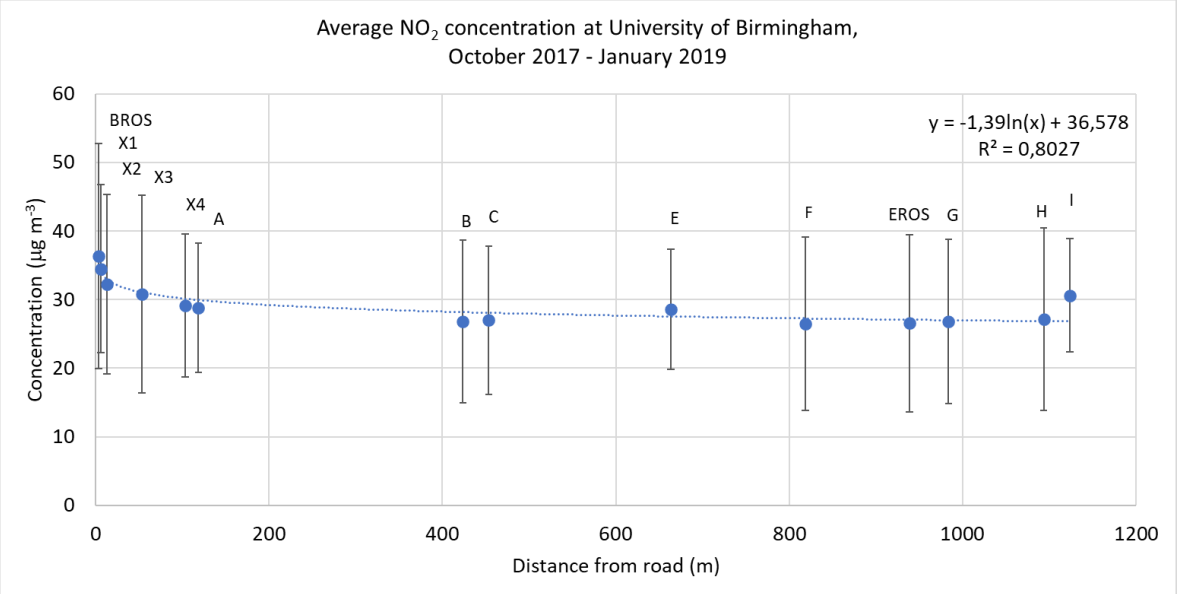


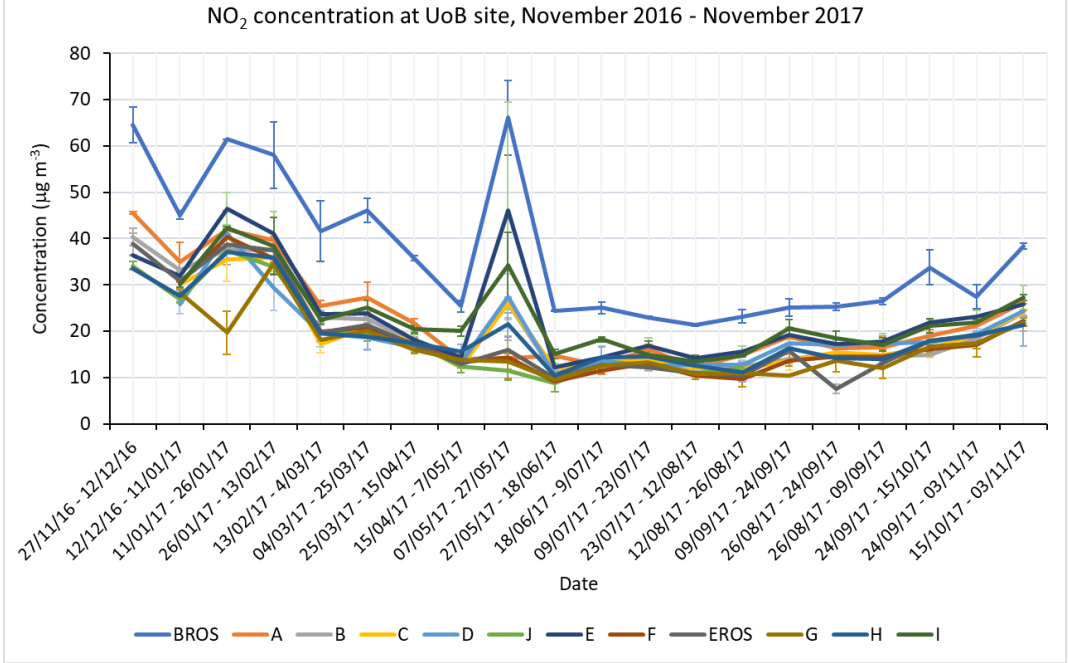
Figure 3.24. The pattern of NO_2 concentration to distance from the road at BROS moving towards the background site at EROS location inside the University of Birmingham (sampling period October 2017 to January 2019) using diffusion tubes with membrane with bias adjustment, True NO_2 = (DT_NO_2 + 20.64) / 1.402. The blue dots represent the mean NO_2 concentration at each sampling point in the sampling period and error bars represent standard deviation (N = 18 data points). The line of best fit used in the graph was a logarithmic trendline obtained from mean data.

The average concentration during sampling dates in the period October 2017 to January 2019 at BROS was 36 ± 16 μg m^{-3} (mean ± SD), below the threshold of the annual mean NO_2 from the UK National Air Quality Objective (40 μg m^{-3}). The concentration decreased from BROS to X2 (difference in distance, 9.7 m) by 4 μg m^{-3} or 11% and from BROS to X3 (difference in distance, 50 m) by 6 μg m^{-3} or 16%. From BROS to X4, the difference in distance was 100 m and the NO_2 concentration was reduced by 7 μg m^{-3} or 20%.

The NO_2 concentration at X4 and site A was relatively the same with a concentration difference between the two sites of 0.3 μg m^{-3}. The reduction from BROS to site A was 20%. The average NO_2 level at locations far from the road (B, C, F, G) and EROS was 27 ± 12 μg m^{-3}. The reduction of NO_2 concentration between BROS and EROS was 27%.

Ducret-Stich *et al*. (2013) observed that the pollutant (NO_2, EC, PM) concentrations decayed by approximately 30-40% when comparing a busy road to a background area 150 m to 200 m distant in a Swiss Alpine valley during measurement with continuous measurement analysers and diffusion tubes between November 2007 and June 2009.

(a)



(b)

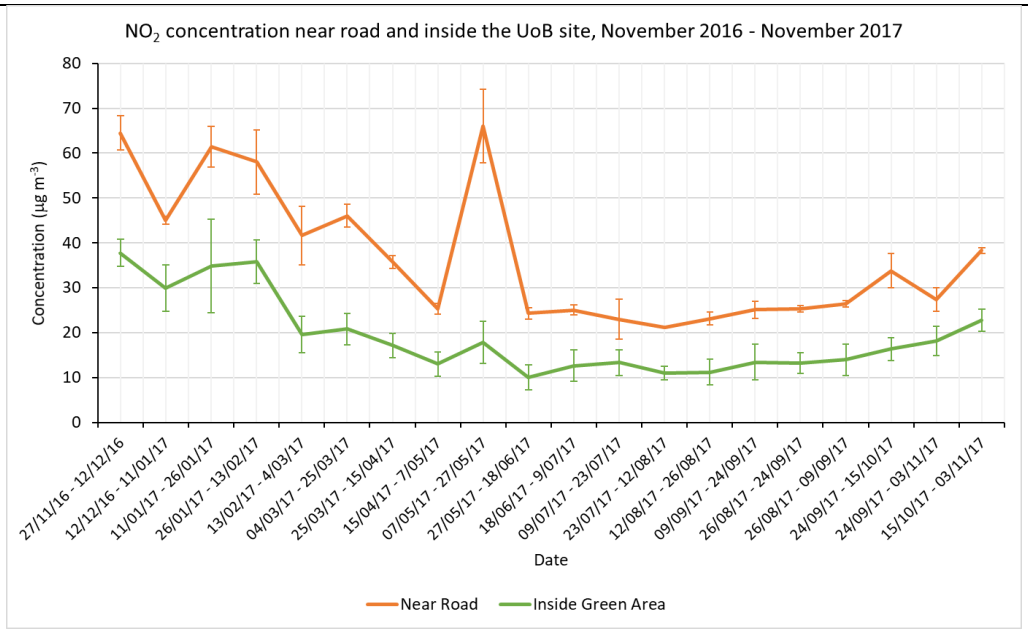


Figure 3.25. NO_2 concentrations at 12 locations in the University of Birmingham monitoring site from November 2016 to November 2017. **(a)** The blue line represents a site near the road (BROS), while other lines represent sampling sites that are spread at various locations in the park. NO_2 concentrations at each point are presented as mean concentration and standard deviation (mean ± SD) from triplicate diffusion tubes. **(b)**. NO_2 concentrations measurement data in green area (B, C, J, F, EROS, G sites) are plotted as a single line (green line) and compared with NO_2 near the road (orange line), from November 2016 to November 2017. NO_2 concentrations near the road are presented as mean concentrations and error bars represent standard deviation from triplicate diffusion tubes (mean ± SD). NO_2 concentrations inside the park are presented as mean concentrations and error bars represent standard deviations at sampling points inside the park (N== 20 data points).

At the UoB site, the location closest to the road is BROS. The other locations on the transect from BROS to EROS which is not influenced by heavy traffic are locations at B, C, F, EROS, and G. Therefore, an average of data from these 5 locations was taken to represent a green urban space. In the period November 2016 to November 2017, the green areas were B, C, J, F, EROS, G, and from October 2017 to January 2019, the green areas were B, C, F, EROS, G.

The trend of NO_2 levels near the road and in the green area from November 2016 to January 2019 shows a pattern of NO_2 concentrations in the green area being consistently lower compared to the roadside with a varying magnitude of concentration due to local emissions from the road. A spike in the period 7-27 May 2017 was probably due to the opening of a new Sport & Fitness building located at the junction of Edgbaston Park Road and Bristol Road, as the main gate is near the BROS.

Figure 3.26.a. presents the NO_2 levels between BROS and the locations inside the green area. Figure 3.26.b. shows the combined concentrations in the green area as a single line (green line) and NO_2 concentration near the roadside (orange line).

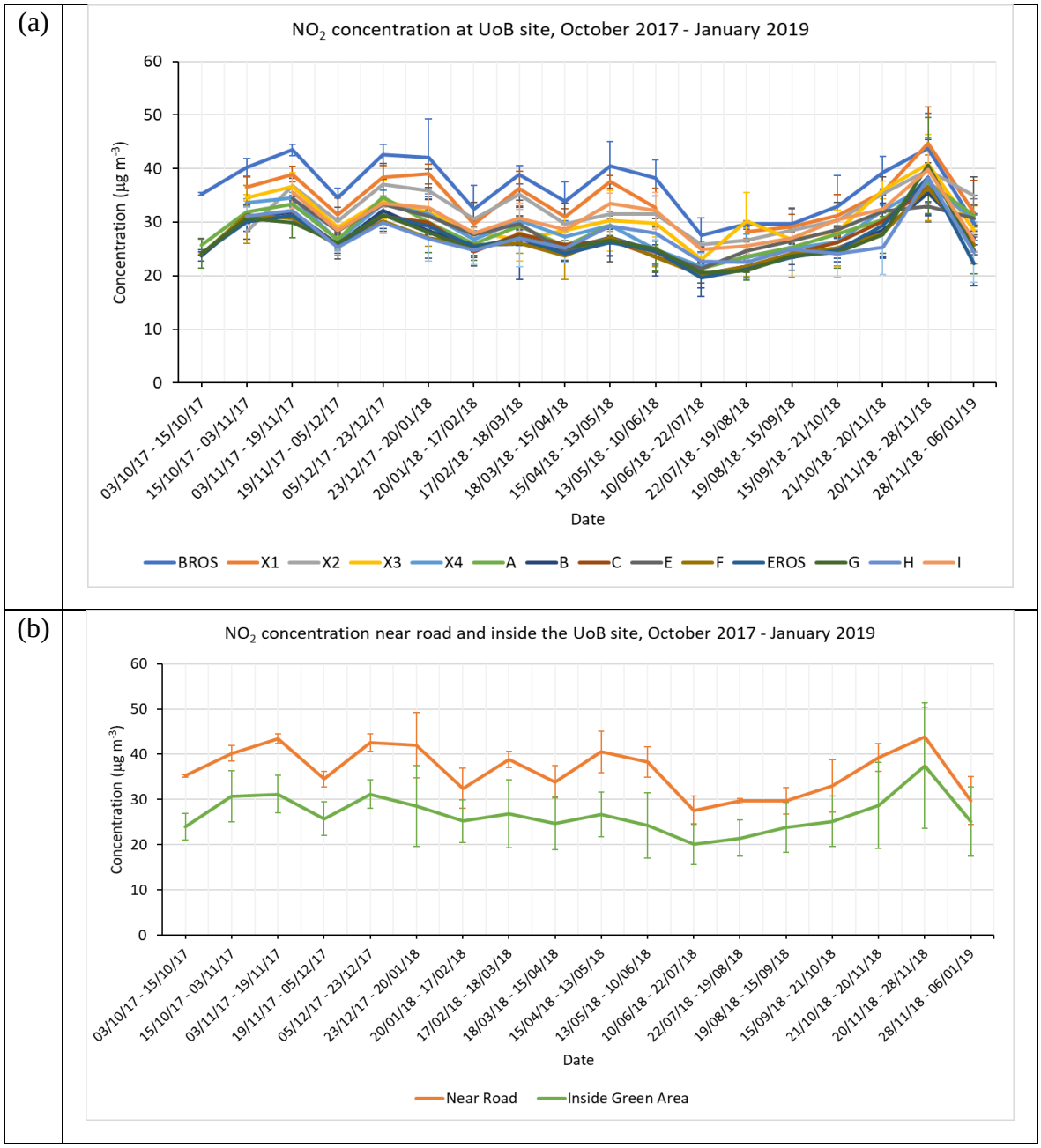


Figure 3.26. **(a)** NO_2 concentrations at 12 locations (CH1 to CH12) in the University of Birmingham monitoring site from October 2017 to January 2019. NO_2 concentrations at each point are presented as mean concentration and standard deviation (mean ± SD) from triplicate diffusion tubes. **(b)** NO_2 concentrations measurement data in green area (B, C, F, EROS, G sites) are plotted as a single line (green line) and compared with NO_2 near the road (orange line), from October 2017 to January 2019. NO_2 concentrations near the road are presented as mean concentrations and error bars represent standard deviation from triplicate diffusion tubes (mean ± SD). NO_2 concentrations inside the park are presented as mean concentrations and error bars represent standard deviations at sampling points inside the park (N== 20 data points).

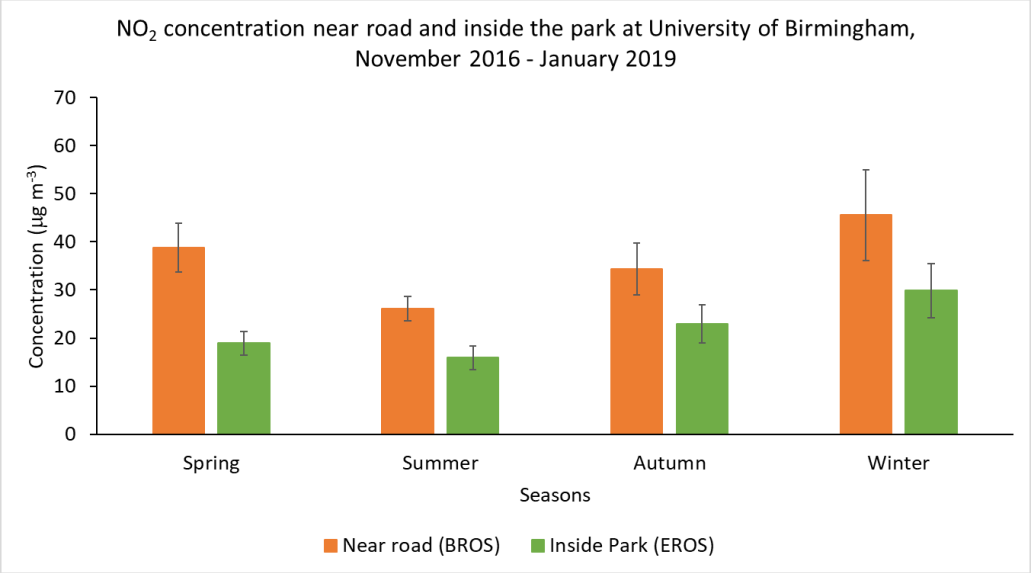


Figure 3.27. NO_2 concentration based on seasonality (during spring, summer, autumn and winter), at the University of Birmingham, from November 2016 to January 2019. Orange bars represent mean NO_2 concentration near the road (BROS), while the green bars show mean NO_2 concentration in the park (EROS). Error bars represent standard error of the mean.

NO_2 concentrations near the road and inside the green area in different seasons are shown in Figure 3.27. The seasonal trend of NO_2 levels shows the lowest concentrations in summer. In warm seasons, the mixing layer increases, and these conditions would increase the dispersion process, thus decreasing the pollutant concentrations (Agudelo–Castaneda *et al*., 2014).

There was similarity in concentrations near the road during spring, autumn, and winter. The increased NO_2 concentration in wintertime was also found in previous studies (Vardoulakis *et al*., 2011). High NO_2 concentrations in cold periods could be associated with low wind speeds and a low mixing layer height (Jayamurugan *et al.*, 2013).

A boxplot of the distribution of NO_2 concentrations at BROS and EROS sites from 27 November 2016 to 6 January 2019 is shown in Figure 3.28. The x sign within the box is the mean concentration. The solid line in the middle of the box indicates the median (50^{th} percentile). The line and point at the highest and the lowest value show the maximum and minimum concentrations of NO_2. The individual point is presented as an outlier in the data. The boxplot in Figure 3.28. indicated the NO_2 levels near traffic roads (BROS) were much greater than the concentration at the urban background site (EROS). This boxplot shows that the data are quite close to a normal distribution, but with a longer tail of high values at BROS.

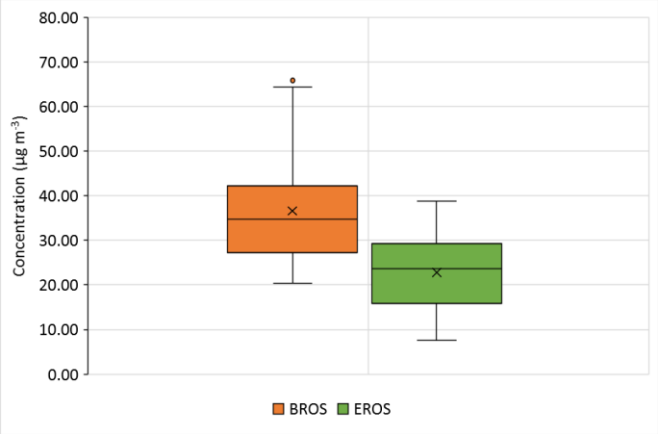


Figure 3.28. Boxplot of NO_2 concentrations at BROS and EROS site, November 2016 to January 2019 (N = 38). Top of box plot represents the 75th percentile; bottom of box plot represents the 25th percentile; mean is the x sign in each box; median is the solid line in each box; whiskers above and below represent 90th and 10th percentiles.

NO_2 concentrations as mean ± standard deviation were 37 ± 12 µg m^{-3} at BROS and 23 ± 8 µg m^{-3} at EROS. NO_2 concentrations at BROS varied between 20 µg m^{-3} and 66 µg m^{-3}, but there were outlier data on NO_2 concentration at 66 µg m^{-3}. The minimum value observed for NO_2 concentration at EROS was 8 µg m^{-3}, and the maximum value was 39 µg m^{-3}.

3.3.2.5. Biosciences building

Locations of diffusion tubes at the Biosciences building are shown in Figure 2.16. in Chapter 2 Section 2.3.3.1.3. and Appendix 2.6. Diffusion tubes were set on the roof and the ground floor of the courtyard of the Biosciences building from December 2017 to May 2018. There were 3 locations on the roof and 2 locations on the ground floor. The NO_2 sampling period was from December 2017 to May 2018 (N = 6) with a time sampling interval of 3-4 weeks. In total, there were 17 samples for the roof and 12 samples for the ground. Appendix 3.7 presents NO_2 concentrations from the raw data of DT measurements at the Biosciences site.

For calculating the average NO_2 concentration, NO_2 levels at the roof and the ground were adjusted by a bias adjustment factor, True NO_2 = (DT_NO_2 + 1.048) / 0.978. Diffusion tubes data were combined and presented as shown in Table 3.7 and Figure 3.29.

Table 3.7. NO_2 concentration on the roof and ground, December 2017 – May 2018

No sampling	Date	NO_2 concentration (µg m^{-3})	
		Roof	Ground
1.	21 December 2017 – 16 January 2018	13 ± 1	14 ± 0.3
2.	16 January 2018 – 5 February 2018	20 ± 1	20 ± 0.2
3.	5 – 28 February 2018	18 ± 2	18 ± 0.3
4.	28 February 2018 – 22 March 2018	21 ± 2	19 ± 2
5.	22 March 2018 – 20 April 2018	15 ± 2	16 ± 0.4
6.	20 April 2018 – 17 May 2018	16 ± 1	15 ± 1

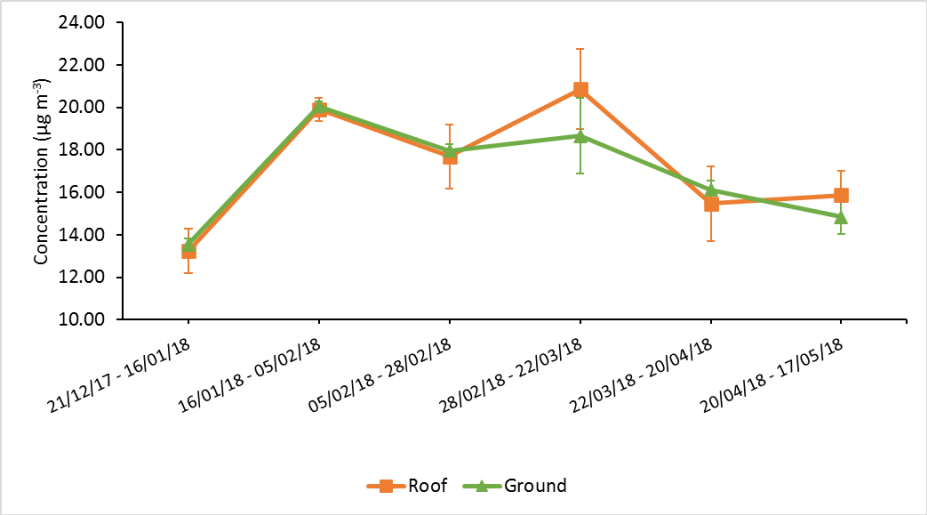


Figure 3.29. NO_2 concentrations at ground (green line) compared with NO_2 at the roof (orange line). Each point represents the mean NO_2 concentration in the sampling period and error bars represent the standard deviation from diffusion tubes.

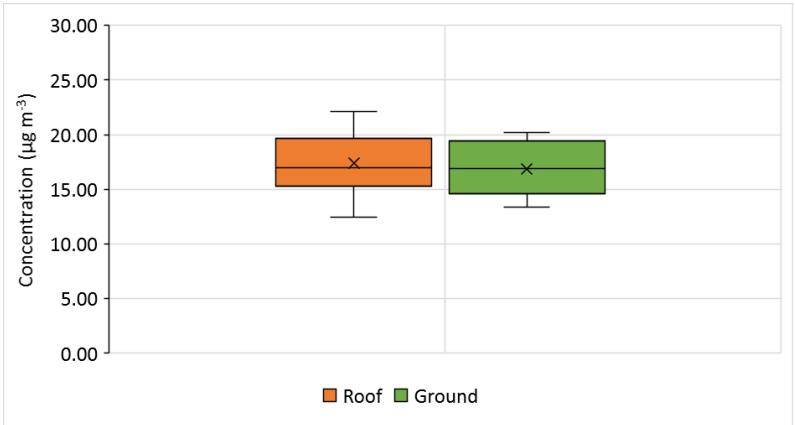


Figure 3.30. Boxplot of NO_2 concentrations at roof and ground floor, Biosciences building, December 2017 to May 2018 (N roof = 17, and N Ground = 12). Top of box plot represents the 75th percentile; bottom of box plot represents the 25th percentile; mean is the x sign in each box; median is the solid line in each box; whiskers above and below represent 90th and 10th percentiles.

The boxplot in Figure 3.30 shows that the NO_2 concentration was slightly higher on the roof site. The mean ± standard deviation of NO_2 concentration on the roof was 17 ± 3 µg m^{-3}. NO_2 concentrations on the roof site varied with a minimum of 12 µg m^{-3} and a maximum of 22 µg m^{-3}. At the ground, the mean ± standard deviation was 17 ± 2 µg m^{-3}. NO_2 concentrations ranged between 13 µg m^{-3} and 20 µg m^{-3}. Further discussion about the vertical concentration gradient will be explored in Chapter 5.

3.3.3. Statistical analysis

An independent t-test was carried out as a statistical test to determine if there is a significant difference of mean value between NO_2 concentrations near the road and inside the park. Pearson correlation analysis was used to investigate the relationships between NO_2 concentrations inside the park, NO_2 concentrations at the roadside, and meteorological factors (temperature, wind speed, RH). A multiple linear regression (MLR) analysis was also used to predict NO_2 concentration inside the park as a dependent variable, based on other independent variables (NO_2 concentration at roadside, temperature, wind speed, and relative humidity).

3.3.3.1. T-Test and air pollution removal

The significance of differences in the NO_2 concentrations near roads and NO_2 levels inside the park was determined using a t-test. The change in pollutant concentrations from the road to the park is calculated using equation E.3.1. Table 3.8. shows the result of the t-test and percentage of air pollution change from sampling locations.

Table 3.8. T-test result and air pollution change (%)

Location		N	Mean (µg m^{-3})	SD (µg m^{-3})	p value	Air Pollution Change or difference (%)
Cannon Hill Park	NO_2 roadside	37	31	7	0.000**	32 %
	NO_2 park	37	21	6		
Hyde Park	NO_2 roadside	16	36	11	0.007**	30 %
	NO_2 park	16	25	8		

Location		N	Mean (μg m^{-3})	SD (μg m^{-3})	p value	Air Pollution Change or difference (%)
Tile Cross Park	NO_2 roadside	14	29	9	0.272	14 %
	NO_2 park	14	25	9		
University of Birmingham (UoB)	NO_2 roadside	38	37	12	0.000**	38 %
	NO_2 park	38	23	8		
Biosciences site	NO_2 Roof	17	17.4	3	0.588	3 %
	NO_2 Ground	12	16.9	2		

Note: **: statistically significant at $p<0.01$
* : statistically significant at $p<0.05$

The t-test for Cannon Hill Park showed a significant difference between NO_2 concentration near the road (31 ± 7 μg m^{-3}) and NO_2 concentration inside the park (21 ± 6 μg m^{-3}). The mean difference of NO_2 concentration measured between the roadside and inside the park was 10 μg m^{-3}. NO_2 near the road was higher (1.5 times) than the NO_2 inside the park ($p<0.01$). T-test for sampling at Tile Cross Park showed there was no significant difference between the NO_2 concentration near the roadside and inside the park. NO_2 concentration near the road (29 ± 9 μg m^{-3}) was only 1.1 times higher than NO_2 concentration inside the park (25 ± 9 μg m^{-3}).

The t-test result from the Hyde Park sampling site showed a significant difference ($p<0.01$) between the locations near roads (36 ± 11 μg m^{-3}) and locations in the park (25 ± 8 μg m^{-3}), with a difference in concentrations of NO_2 of 11 μg m^{-3}. NO_2 near the road was higher by 1.4 times than the NO_2 inside the park ($p<0.01$).

T-test for sampling at the UoB campus showed there was a statistically significant difference ($p<0.01$) between the NO_2 level near the road (37 ± 12 μg m^{-3}) compared with the NO_2 concentration inside the green area (23 ± 8 μg m^{-3}), being higher by 1.6 times. The t-test for Biosciences showed there was no significant difference ($p>0.05$) between the NO_2 concentration on the roof (17 ± 3 μg m^{-3}) and the NO_2 level at the ground (17 ± 2 μg m^{-3}).

Overall, mean concentrations of NO_2 at all sampling locations near the road and inside the park were below the annual limit value of 40 µg m^{-3} (UK National Air Quality Objective for the Annual mean of NO_2). The NO_2 levels near the road were higher compared to the concentrations inside the park with a significance value ($p<0.01$) at Cannon Hill Park, Hyde Park, and the University of Birmingham sites. The differences in NO_2 concentrations between near the road and locations in the park were more than 29 %. However, at Tile Cross Park and the courtyard at the Biosciences building (vertical level), the differences in NO_2 concentrations were not significant ($p >0.05$), and the percentage of air pollution removed from near road to the park at Tile Cross Park and from the roof to the ground at the courtyard in the Biosciences building was 14 % and 3 % respectively (Table 3.8).

3.3.3.2. Pearson Correlation

Pearson correlation analyses were performed using NO_2 concentrations inside the park and NO_2 concentrations near the road, with temperature, wind speed, and relative humidity as meteorological conditions. The correlation matrix is shown in Table 3.9.

Table 3.9. Pearson correlation matrix of NO_2 concentration inside park, near road and meteorological factors

	Location	Parameter	NO_2 inside park	NO_2 near road	Temperature	WS	RH
(a)	**Cannon Hill Park**	**NO_2 inside park**	1				
		NO_2 roadside	0.85**	1			
		Temperature	-0.65**	-0.60**	1		
		WS	0.25	0.03	0.04	1	
		RH	0.09	-0.11	-0.44**	0.10	1
(b)	**Hyde Park**	**NO_2 inside park**	1				
		NO_2 roadside	0.96**	1			
		Temperature	-0.74**	-0.76**	1		
		WS	-0.62**	-0.62*	0.47	1	
		RH	0.81**	0.73**	-0.74**	-0.41	1
(c)		**NO_2 inside park**	1				

	Location	Parameter	NO_2 inside park	NO_2 near road	Temperature	WS	RH
	Tile Cross Park	**NO_2 roadside**	0.97**	1			
		Temperature	-0.83**	-0.79**	1		
		WS	-0.46	-0.47	0.16	1	
		RH	-0.002	-0.05	0.07	0.12	1
(d)	**University of Birmingham**	**NO_2 inside park**	1				
		NO_2 roadside	0.73**	1			
		Temperature	-0.73**	-0.59**	1		
		WS	0.25	-0.08	-0.02	1	
		RH	0.11	-0.11	-0.35*	0.21	1
			NO_2 Ground	**NO_2 Roof**	**Temperature**	**WS**	**RH**
(e)	**Biosciences**	**NO_2 Ground**	1				
		NO_2 Roof	0.93**	1			
		Temperature	-0.53	-0.46	1		
		WS	0.54	0.54	-0.82	1	
		RH	0.05	-0.099	-0.599	0.74	1

Note: **: statistically significant at $p<0.01$
* : statistically significant at $p<0.05$

NO_2 concentration can be affected by meteorological factors, such as wind speed, temperature, and relative humidity (Plaisance *et al.*, 2004). Meteorological data were obtained to match the diffusion tube sampling times. Meteorological data from 2016 to March 2018 were taken from the weather station Winterbourne No.2, which is located in the University of Birmingham.

In Cannon Hill Park, the temperature has a significantly negative correlation (-0.65) with NO_2 concentration in the park as shown in Table 3.9. (a). Less sunlight has been associated with a low photolysis rate of NO_2 which may result in its persistence in the atmosphere and increase the NO_2 level in the area. The correlation between NO_2 level at the roadside and

NO_2 concentration inside the park was positively and significantly high (0.85). There is no significant correlation between wind speed with NO_2 concentration inside the park and relative humidity with NO_2 concentration in the green area. Low wind speeds can increase NO_2 concentrations.

For the Hyde Park site (Table 3.9. (b)), meteorological data was taken from the London City Airport weather station (EGLC, id 18929). There was a significant correlation between NO_2 concentration inside the park and NO_2 near the road (0.96), wind speed (-0.62), temperature (-0.74), and relative humidity (0.81). The correlation between wind speed and NO_2 level inside the park showed a significant negative correlation (the increase of wind speed would reduce the NO_2 concentration). The correlation of RH with NO_2 level in Hyde Park was high (0.81) and showed a positive correlation with NO_2 concentrations. High values of RH could be related to the existence of cloud cover that can slow down the process of photochemical reaction (Agudelo–Castaneda *et al*., 2014) and to winter conditions when dispersion is less effective.

In Tile Cross Park (Table 3.9. (c)), wind speed showed an inverse correlation (-0.46) with NO_2 concentration in the park, although it was not a significant correlation. The higher wind speed increases the mixing process and dispersion of pollutants, thus decreasing NO_2 concentrations. The trend of temperature and NO_2 level in Tile Cross Park is the same as the trend in all parks, in that it demonstrated a significant negative correlation (-0.83) with temperature. An increase in temperature has been associated with an increase of the photolysis rate of NO_2 and would decrease NO_2 level, and vice versa. These results are similar to other studies e.g. (Hewitt, 1991; Agudelo–Castaneda *et al*., 2014; Predrag *et al*., 2019).

In the UoB site, the NO_2 concentration near the road had a significant positive correlation (0.73) with NO_2 concentration inside the green area. A significant negative correlation (-0.73) was found between NO_2 concentration in the park and temperature. An increase in temperature would result in decreasing concentrations of NO_2. Wind speed and RH were found to have no significant correlation with NO_2 levels in the park (Table 3.9. (d)).

In the courtyard of the Biosciences building (Table 3.9. (e)), there was a significant positive correlation (0.93) only between NO_2 at the roof and NO_2 on the ground.

3.3.3.3. Multiple linear regression

Multiple linear regression was calculated to produce a mathematical model for the relationship between two or more variables. The equations from multiple linear regression between NO_2 concentration inside the park and (1) NO_2 concentration at roadside; (2) NO_2 level at the roadside and temperature; and (3) NO_2 level at the roadside and meteorological factors (temperature, wind speed, and relative humidity) are shown in Table 3.10.

Table 3.10. The model equation and R^2 from multiple linear regression analysis

Location	Parameter	Equation	df		F	R^2
			regression	residual		
Cannon Hill Park	NO_2 roadside **	NO_2 park = -2.739 + (0.776 NO_2 roadside) **	1	35	91.87	0.724
	NO_2 roadside and meteorological factor (T) **	NO_2 park = 4.115 + (0.655 NO_2 roadside) ** + (-0.309 T) *	2	34	52.32	0.755
	NO_2 roadside and meteorological factors (T, WS, RH) **	NO_2 park = -5.512 + (0.666 NO_2 roadside) ** + (– 0.279 T) + (1.999 WS) ** + (0.064 RH)	4	32	35.19	0.815
Hyde Park	NO_2 roadside **	NO_2 park = 0.017 + (0.714 NO_2 roadside) **	1	14	164.2	0.921
	NO_2 roadside and meteorological factor (T) **	NO_2 park = 0.522 + (0.707 NO_2 roadside) ** + (-0.022 T)	2	13	76.3	0.921
	NO_2 roadside and meteorological factors (T, WS, RH) **	NO_2 park = -17.694 + (0.592 NO_2 roadside) ** + (0.221 T) + (-1.278 WS) + (0.343 RH) *	4	11	59.21	0.95
Tile Cross	NO_2 roadside **	NO_2 park = -1.719 + (0.931 NO_2 roadside) **	1	12	213.3	0.947

Location	Parameter	Equation	df		F	R^2
			regression	residual		
	NO_2 roadside and meteorological factor (T) **	NO_2 park = 5.113 + (0.807 NO_2 roadside) ** + (-0.387 T)	2	11	122.9	0.957
	NO_2 roadside and meteorological factors (T, WS, RH) **	NO_2 park = 1.327 + (0.754 NO_2 roadside) ** + (-0.475 T) + (-1.799 WS) + (0.113 RH)	4	9	57.44	0.962
UoB	NO_2 roadside **	NO_2 park = 4.701 + (0.494 NO_2 roadside) **	1	36	40.65	0.530
	NO_2 roadside and meteorological factor (T) **	NO_2 park = 19.556 ** + (0.309 NO_2 roadside) ** + (-0.775 T) **	2	35	34.57	0.664
	NO_2 roadside and meteorological factors (T, WS, RH) ** .p=0.000	NO_2 park = 20.990 + (0.315 NO_2 roadside) ** + (-0.796 T) ** + (2.918 WS) * + (-0.092 RH)	4	33	23.84	0.743

Note: **:p<0.01: *:p<0.05

** and * indicate that the variable is significant at p<0.01, and at p< 0.05 respectively.

The significant predictors of NO_2 level in the park were the concentrations of NO_2 at the roadside and temperature. The R^2 value of multiple linear regression for all the models was higher than 0.5, meaning that more than 50% of the variance is explained by linear regression.

For example, from Table 3.10. at the UoB site, a multiple linear regression was carried out to investigate whether NO_2 concentration at the roadside, taken with temperature, wind speed, and relative humidity could significantly predict NO_2 concentration inside the park.

The results of the regression indicated that the model explained 74.3% of the variance and that it was, therefore, a significant predictor of NO_2 concentration inside the park, F (4, 33) = 23.84, p < 0.000). The predictive model was:

NO_2 in the park = 20.99 + (0.315 x NO_2 roadside) + (-0.796 x T) + (2.918 x WS) + (-0.092 x RH),

NO_2 near road is measured in µg m^{-3}, temperature is measured in °C, wind speed is measured in m s^{-1}, and relative humidity is measured in %. NO_2 concentration near the road and temperature were significant (**, p <0.01) predictors of NO_2 level in the park.

3.4. Limitation of the study

While the NO_2 diffusion tubes appear to work well, the NO_x and O_3 diffusion tubes were not satisfactory. Therefore, it was not possible to measure the chemical interaction within the NO-NO_2-O_3 system.

3.5. Summary

Diffusion tubes were used to assess concentration near roads and in the parks to establish temporal and spatial variability of pollutant concentrations in two different areas. They were used because of their simplicity, low cost and low maintenance requirements and can be used in locations or areas where there is a lack of electricity.

In this study, NO_2, NO_x and O_3 concentrations were measured by Palmes-type diffusion tubes and automatic analysers. However, only the NO_2 diffusion tubes provided good and reliable data.

NO_2 diffusion tubes (Targa and Loader, 2008) were used to measure NO_2 concentrations. Triplicate diffusion tubes and inlets of automatic analysers were placed in the same location and close to each other (maximum 20 cm) to understand the precision and accuracy of the diffusion tubes. The reduction of pollutant concentrations in the park compared with the

location near the roads indicated that distance from the road in any setting could have a role in lowering pollutant concentrations.

The NO_2 concentration near the road has a significant positive correlation with NO_2 level in the park, indicating the pollutant has the same source, which is traffic from the road.

The seasonal trend of NO_2 concentrations at four monitoring sites (Cannon Hill Park, Hyde Park, Tile Cross Park and the University of Birmingham) showed a trend of higher NO_2 levels in winter and autumn, and lower NO_2 concentrations during summer. NO_2 concentrations at the roadside were higher compared to the level in the park during all seasons. High concentrations of NO_2 at roadside at all sampling locations indicate local emissions from vehicles on the roads.

Meteorological conditions influence the NO_2 concentrations. There was significant negative correlation (> 0.5) between NO_2 level and temperature. Low temperature would increase the NO_2 concentration, and this trend was shown in all the sampling sites. However, the correlation between NO_2 concentration with wind speed and RH were found to be different at each of the sampling sites. Hyde Park and Tile Cross Park showed negative correlation (<0.5) between NO_2 concentration and wind speed, but this was not found at Cannon Hill Park and the UoB site. A significant positive correlation (> 0.5) between NO_2 concentration and RH was found only at Hyde Park.

The results of this study imply that parks in urban areas can decrease NO_2 concentrations due to their open spaces that help pollutants to disperse and dilute in the atmosphere, thus reducing the concentrations.

Chapter 4. The Set Up and Evaluation of Dispersion Modelling

In this chapter, the set up and evaluation of a dispersion model using ADMS-Roads are explained. Input variables in the model are detailed in terms of meteorological data, background concentration, emissions set up, and the NO_2:NO_x ratio. The concentrations of NO_x, NO_2 and O_3 measured by the automatic analysers at BROS and EROS on 2-11 February 2018 were used in the evaluation of the model, with sensitivity tests to generate the best-fit inputs in the ADMS-Roads model to the measured data. Input settings for emissions rates, time-varying emission factor, NO_2:NO_x ratio, surface roughness, road sources and receptor coordinates were used in the model. Only input settings of meteorological data and background concentrations were changed and adjusted within the same time period as measurement data when the modelled concentrations were compared with the automatic analyser's measurements or diffusion tubes measurements. Furthermore, ADMS-Roads was used to predict pollutant concentrations (NO_x, NO_2 and O_3) by dispersion and dry deposition. Finally, NO_2 concentrations from diffusion tube (DT) measurements were utilized to compare the predicted concentrations from the model with observed data.

4.1. Introduction

Modelling the dispersion of air pollutants is important to assess air quality and to manage and control air pollution in the area (Arciszewska and McClatchey, 2001; Šereviciene and Paliulis, 2011). Dispersion modelling is a mathematical simulation that can provide complete spatial coverage of air quality, even in areas without extensive air pollution monitoring networks. The modelling can be used to predict the impact of pollutants on air quality (Turner, 1979; Venkatram *et al.*, 2007), and health (Beevers *et al.*, 2013).

Road traffic is considered as the main source of NO_x (NO + NO_2) and primary particulate matter (PM) in an urban area (Gilbert *et al.*, 2007; Williams *et al.*, 2014; Dias *et al.*, 2019). The main source of NO_2 emissions is from vehicles in urban areas and it can adversely affect human health. There is evidence that exposure to high concentrations (hourly ~ 153 µg m^{-3}) of NO_2 is related to sore throats, respiratory diseases and responses (such as inflammation of the airway in healthy people), as well as an increase in respiratory symptoms in people with asthma (Gillespie-Bennett *et al.*, 2011).

Vehicle density is an important factor in determining NO_2 concentration (Campbell *et al.*, 1994). Furthermore, emissions from traffic were found to be positively correlated with the number of vehicles on roads (Fenger, 1999). According to the DfT (Department for Transport, UK), in 2018, there were 796,100 vehicles (licensed) in Birmingham and 3,070,000 vehicles in London with composition as shown in Figure 4.1 (veh0105 from DfT, https://www.gov.uk/government/statistical-data-sets/all-vehicles-veh01).

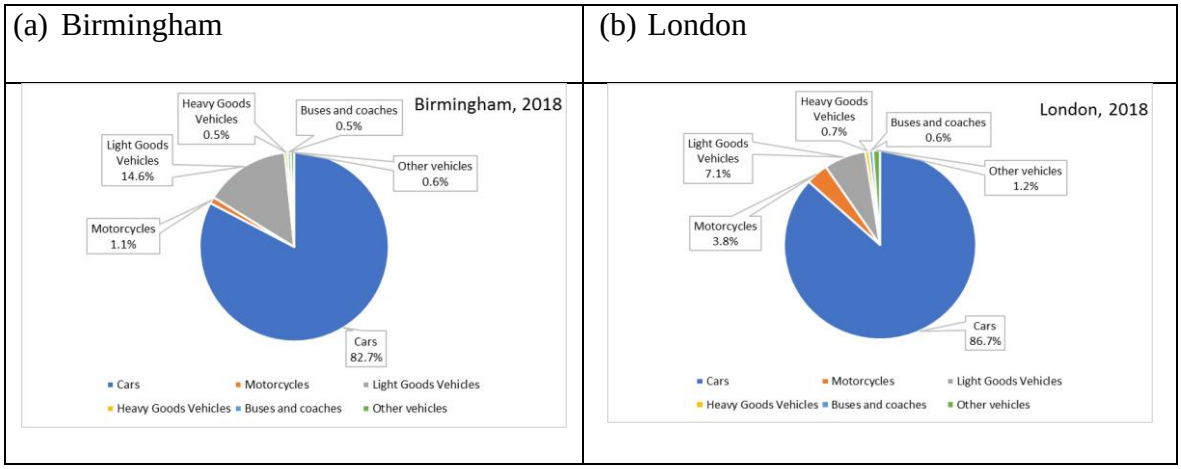


Figure 4.1. Licensed vehicle composition in **(a)** Birmingham, and **(b)** London, UK, in 2018. The highest percentage of vehicles (licensed) come from cars (Adopted from Table VEH0105: Licensed vehicles at the end of the year by body type and upper and lower tier local authority, including diesel cars and vans, United Kingdom in 2018, from Department for Transport, (DfT, 2020))

In this study, ADMS-Roads was used to predict the NO_2 concentrations and the results from the model were compared with the measured data (pollutants monitored in green spaces and nearby roads).

4.2. Method

The University of Birmingham was one of the sites selected for the study. The road links around the sampling site were included as emission sources to consider all vehicle emissions at the site. The evaluation of the ADMS-Roads model (version 4.1) was carried out by comparing the modelled data with measured data from roadside locations and in green areas. NO_x, NO_2 and O_3 were measured using automatic analysers at the BROS and EROS locations. The diffusion tubes were placed 2.6 – 3.2 metres above ground at specific points.

The required input variables for the ADMS-Roads model are details of pollutant sources (e.g. road traffic emissions, road geometry), receptors, meteorological data, and background concentrations. The model uses this information to predict pollutant concentration by modelling the dispersion process of traffic-related pollutants.

Table 4.1. shows the information needed for the ADMS-Roads model, the purpose for such information, and the input data sources or details.

Table 4.1. Information needed, purpose, and data input for the ADMS-Roads model

	Information	**Purpose**	**Data input**
1.	Road geometry - Elevation of road (m) - Road width (m) - Canyon height (m)	To get profile of source dimension and location	Coordinates of the location and the road sources surrounding the site; Google map observation; Observation data; Set up using ADMS mapper
2.	Road traffic emission:		
a.	Vehicle category: - Vehicle count - Average speed (km h^{-1})	To generate emission data dependent on vehicle types To calculate emission factors (g km^{-1}) and emission rate (g km^{-1} s^{-1})	AADF (Annual Average Daily Flow) from Department for Transport, UK to get the data of vehicle count (number of vehicles in an average hour) Or, Observation of traffic flow
b.	Dataset: UK EFT v8.0 (7 VC)	Emission calculation based on type of vehicles for better estimation	Fleet composition from AADF and observation data
c.	Emission year:	To get a more accurate estimation of the emission source	Based on sampling time. In this study: 2018
d.	Road type: - London - England - Scotland - Northern Ireland (Urban, rural, motorway)	Road type description and environmental condition	Based on sampling location. In this study: England

	Information	Purpose	Data input
e.	Option: Time-varying emission factors	Use emission profile for better estimation of output concentration	TRA 0307 (Department for Transport)
3.	Model option: - Dry deposition - Wet deposition - Chemistry - Complex terrain Option: Palette, input for deposition velocity ($m\ s^{-1}$) of pollutants	To obtain pollutant concentration If chemistry model option is selected, then the model calculates the concentration with chemistry only and no deposition.	Data available in ADMS-Roads Chose the model option of: - Chemistry - Chemistry and Dry deposition (insert deposition velocity values of pollutants in the model)
4.	Meteorology data (Wind speed, wind direction, temperature, cloud cover, relative humidity)	To include the influence of meteorological factors during the measurement / sampling period to calculate the emissions	Data from the nearest weather station: • Winterbourne No.2 BUCL • Coundon • Coleshill • Elmdon
5.	Background data	To reduce errors in pollutant estimation	Data from the nearest air pollution monitoring station • EROS • Biosciences location • Birmingham Acocks Green
6.	Receptors: specified points X (m), Y (m) and Z (m)	To set locations where pollutant concentrations will be predicted/modelled	Coordinate locations using manual input x, y, z (m) coordinates in ADMS (grids interface), or set up locations using ADMS mapper.
7.	Output: Pollutants name Type of average time: Short-Term (ST) or Long-Term (LT)	To obtain concentration of a specific pollutant ST type to generate pollutant concentrations for every line of meteorological data. LT type to generate pollutant concentration as averaged overall lines of meteorological data.	Pollutant name: NO_x, NO_2, O_3 Choose the option of ST or LT in the pollutant output

4.2.1. Model input and output

4.2.1.1. Setting the best input in the model using automatic analysers data on 2-11 February 2018

Emissions and meteorological data are required as input data in dispersion modelling (Turner, 1979). Meteorological data, background concentration (where the pollutant levels are not influenced significantly by any single source) and emissions from traffic were used for the same period in which monitoring or sampling was carried out. The study used the year 2018 as the modelling period and so meteorological data, background concentrations and emissions were covered for the same year. Sensitivity analyses were conducted for meteorological data, background concentration, emissions, NO_2:NO_x ratio and deposition velocity to get the best input setting in the model.

Input variables were set in the model by adjusting the emission rates, setting time-varying emission factors, identifying road sources and receptors, adjusting the NO_2:NO_x ratio, input the meteorological data, surface roughness, and background concentrations as explained in Section 4.3.2.

The meteorological data (wind direction, wind speed, temperature, relative humidity, and solar radiation) were obtained from the nearest weather station. Sensitivity analysis was conducted for considering four candidate sites (see Section 4.3.3.1).

Background concentrations were obtained from the nearest air pollution monitoring station for the required sampling period. Sensitivity analysis was conducted for background concentration (see Section 4.3.3.2).

Traffic flow data were obtained from the Department for Transport's database and calculation of traffic count (vehicle number) in one hour of observation (see Appendix 4.5). The modelled NO_x concentration was compared with the measurement data to review the results of the modelled NO_x concentrations. Select the model setting that gives the highest regression value (R^2) of the measured NO_x concentrations with modelled NO_x concentrations. The differences in the magnitude of NO_x concentrations were obtained by adjusting the input of vehicle speeds (see Section 4.3.3.3., sensitivity to emission).

The flow chart of the modelling steps in ADMS-Roads is shown in Figure 4.2. The data used in the model are described below:

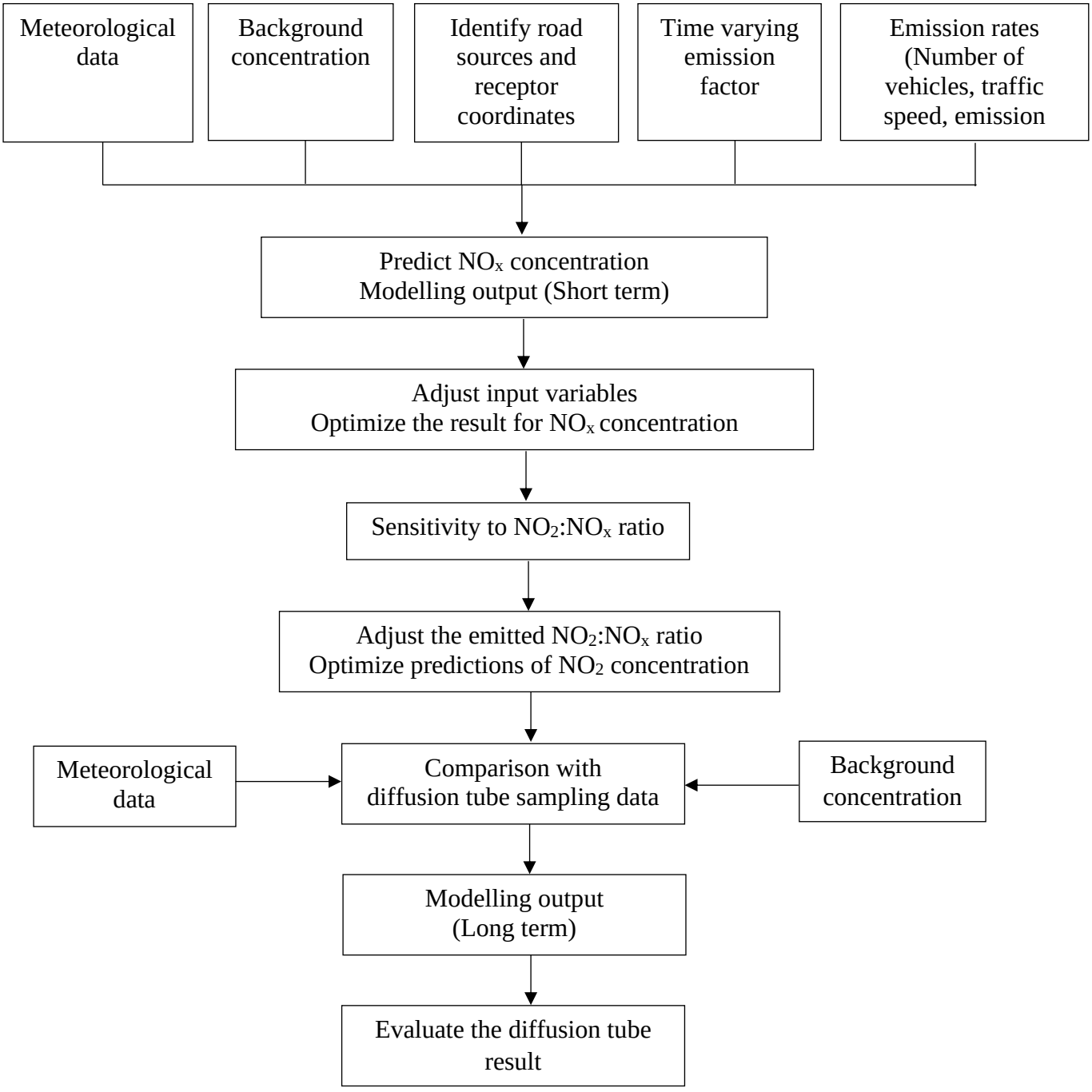


Figure 4.2. Flow chart of ADMS-Roads modelling

The next step is to find the optimum result (good agreement) of modelled NO_2 concentration with measured NO_2 concentration by adjusting the NO_2:NO_x ratio in emissions. The default value of the NO_2:NO_x ratio in the model is 23.8% (CERC, 2017) and it can be adjusted by

changing the value of primary NO_2 (%) in the source setting model or changing the emission rates of NO_2 on each road (see Section 4.3.3.4., sensitivity to NO_2:NO_x ratio).

After this optimisation step, the model is used to calculate the pollutant concentrations and then compared with the measured data. Modelling the dispersion and chemical reaction processes were set up by enabling the model option of chemistry. For modelling the deposition process was set up by enabling the model option of chemistry and dry deposition and inputting the values of deposition velocity of pollutants (NO, NO_2, NO_x and O_3) in ADMS-Roads. The procedure was explained in Chapter 2, Section 2.4.7. The effect of the dry deposition velocity on the reduction of pollutant concentrations were discussed in Section 4.3.3.5., sensitivity to the deposition velocity.

In the model option of wet deposition, wet deposition is estimated using washout coefficient which is independent of the precipitation rate, or it will be calculated using wet deposition parameter and the precipitation (CERC, 2017). The washout coefficient is the amount of material incorporated into precipitation (Price *et al.*, 2010). Washout effect on pollutants is more effective to aerosols (PM_{10}) than on gases (NO_2, O_3, CO) (Yoo *et al.*, 2014).

In this study, wet deposition is not included in the ADMS model runs. The impact of wet deposition on the concentration of NO, NO_2 and O_3 is assumed to be negligible. NO gas is very insoluble and the wet deposition of NO is close to zero (CERC, 2017). NO_2 and O_3 are poorly soluble in water (Alberts, 1994; Egorova *et al.*, 2015). For NO_2, wet deposition rate is also relatively low, 10^{-4} (CERC, 2017). So, the error of excluding wet deposition of NO, NO_2 and O_3 is expected to be small.

The output model for the type of averaging time must be specified and selected in the short-term (ST) to get output in terms of hourly concentration or the long-term (LT) to get the output as mean annual concentration. If the ST output model is selected, the output contains a set of concentrations for every line of meteorological data. However, if the LT output model is selected, the concentration output contains a single set of concentration data, which is averaged over all lines of meteorological data (CERC, 2017).

The Short-Term (ST) output was set in the model to derive hourly time series of modelled concentration. Hourly modelled concentrations were compared with the hourly measured concentrations from automatic analysers.

The average modelled concentration from the LT output model within the period of DT's exposure time is compared with diffusion tube concentration. The adjustment of LT parameter data to obtain the same period of time as the DT's is done by setting the input data of meteorological and background concentration as the same period of DT exposure.

4.2.1.2. Using the input setting to evaluate modelled concentration with diffusion tube measurement data

After evaluating the performance of ADMS-Roads and obtaining the best input settings for the model, the data from diffusion tube samplers were compared with the model results. The model was running with variations in the input of meteorological data and background concentrations based on the exposure time of diffusion tubes at the sampling site (Section 4.3.4.2). The Long-Term (LT) output was set in the model to get the average modelled concentration in each receptor location and compared with measured NO_2 concentrations from the diffusion tubes at the sampling sites.

The single adjustment method (corrections of background concentration using intercept value from linear regression equation) could be used to reduce erroneous results when comparing modelled concentrations with the measured concentrations from diffusion tube data.

Steps for calculating the single adjustment method based on a linear regression line are below:

a) NO_x, NO_2 and O_3 data from automatic analysers in the park or background site (at EROS or on the roof of the Biosciences building or air quality data from Birmingham Acocks Green) were used as background concentration data (depends on the data availability);
b) Run the model;
c) Perform linear regression from NO_2 diffusion tubes (DT) measured and NO_2 modelled concentrations

   $Y = mx + b$

   Where: Y is dependent variable (modelled NO_2); x is independent variable (measured NO_2 DT); m is slope of the line; and, b is intercept;

d) Use the value of the intercept from linear regression to correct the background concentration:
   Adjusted NO_2 background concentration = NO_2 DT – Intercept
e) Run the model with adjusted NO_2 background concentration as background concentration input.

The model options for chemistry only and chemistry with dry deposition were set in the model to generate the modelled pollutant concentrations. These two outputs were used to generate NO_x, NO_2 and O_3 concentrations using two approaches – dispersion only and dispersion with dry deposition.

Modelled concentrations were compared with the measured concentrations, and evaluated using statistical methods of FB (fractional bias), NSME (normalised mean square error), R and R^2.

4.2.2. Statistical evaluation

Pollutant concentrations from on-site measurements were compared to concentrations from the modelling results during the specific sampling time. Fractional bias (FB), normalised mean square error (NMSE), and correlation (R) are some statistics used to evaluate the model's performance (Owen *et al.*, 1999; Chang and Hanna, 2004; Hirtl and Baumann-Stanzer, 2007; Briant *et al.*, 2013; Dėdelė and Miškinytė, 2013; Heist *et al.*, 2013; Stocker *et al.*, 2013; Hood *et al.*, 2018).

Fractional bias, $FB = \frac{(\overline{C_o} - \overline{C_m})}{0.5\,(\overline{C_o} + \overline{C_m})}$ (E. 4.1)

Normalised mean square error, $NMSE = \frac{\overline{(C_o - C_m)^2}}{\overline{C_o}\,\overline{C_m}}$ (E. 4.2)

Correlation, $R = \frac{1}{n-1}\sum_{i=1}^{n}\left(\frac{C_o - \overline{C_o}}{\sigma C_o}\right)\left(\frac{C_m - \overline{C_m}}{\sigma C_m}\right)$ (E. 4.3)

Where C_o is the observed value of pollutant concentration; C_m is the modelled value of pollutant concentration; overbar $\overline{C_o}$ is the average of observed values of pollutant concentration; overbar $\overline{C_m}$ is the average of modelled values of pollutant concentration; σC_o

is the standard deviation of observed concentrations and σC_m is the standard deviation of modelled concentrations.

4.2.2.1. Fractional Bias (FB)

FB is mean systematic bias, reviewing the mean difference between the observed and modelled. The ideal value of FB is zero (Chang and Hanna, 2004; Heist *et al*., 2013; Hood *et al.*, 2018). A negative FB means the model over-estimates the measured data, and a positive FB means the measured data is under-estimated (Hirtl and Baumann-Stanzer, 2007).

4.2.2.2. Normalised Mean Square Error (NMSE)

NMSE measures the overall deviations, reviewing the systematic and random errors. The ideal value of NMSE is zero (Chang and Hanna, 2004; Heist *et al*., 2013; Hood *et al.*, 2018).

4.2.2.3. Coefficient of Correlation (R)

The coefficient of correlation demonstrates the strength of correlation and linear relationship between the observed and predicted data (Chang and Hanna, 2004; Heist *et al*., 2013; Hood *et al.*, 2018). The range of R is between -1 and 1. The value near -1 or 1 indicates there is a strong relationship between the modelled and the observed data.

4.2.2.4. Coefficient of Determination (R^2)

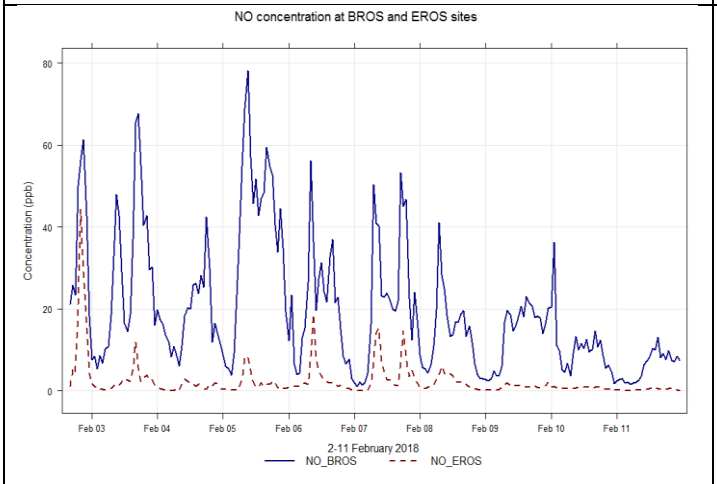
Coefficient of determination represents the total variation of data that one variable can predict in the other variable's data, in range value 0 to 1.

4.3. Results and discussion

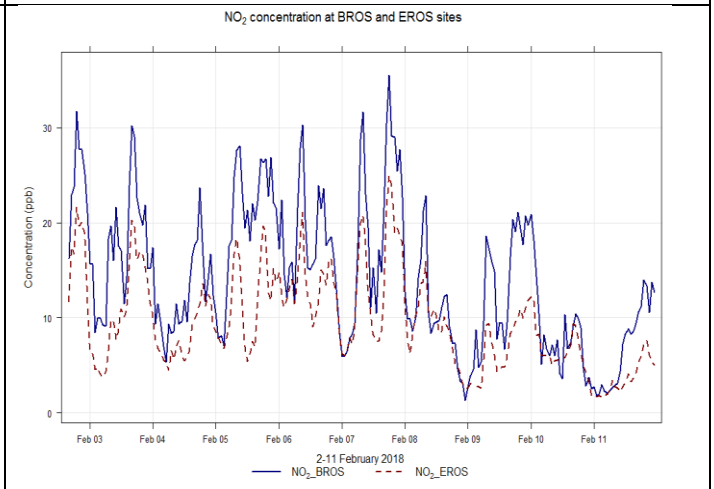
4.3.1. Observation data from automatic analyser

NO, NO_2, NO_x and O_3 concentrations were measured simultaneously using automatic analysers at two different locations close to the road (BROS) and in a green open area away from roads (EROS) at the University of Birmingham for the period 2-11 February 2018.

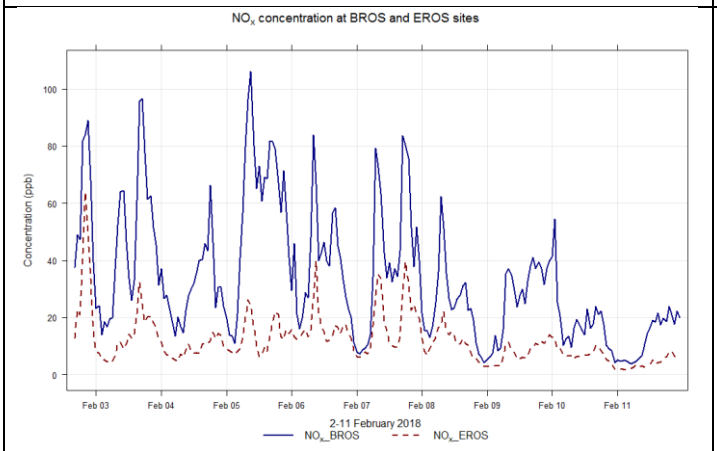
a. NO concentrations at BROS and EROS



b. NO_2 concentrations at BROS and EROS



c. NO_x concentrations at BROS and EROS



d. O_3 concentrations at BROS and EROS

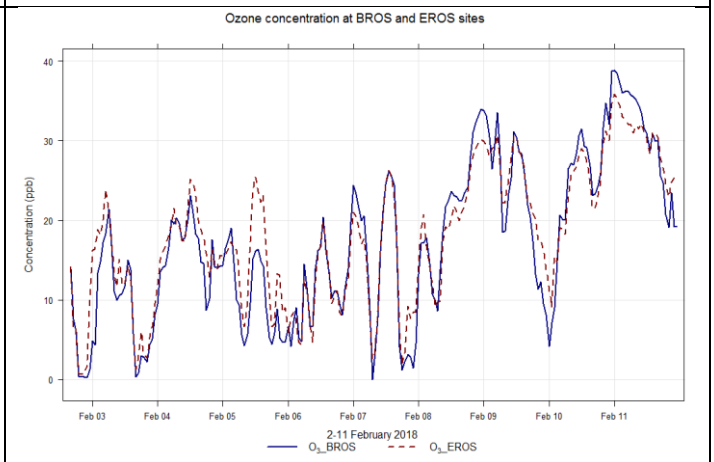


Figure 4.3. Concentrations of **(a)** NO, **(b)** NO_2, **(c)** NO_x, and **(d)** O_3 at two different sites, BROS (blue line) and EROS (red dash) on 2-11 February 2018

Pollutant concentrations are less in the urban park compared to the roadside, as shown in Figure 4.3. Specifically, mean values ± uncertainty in the standard error of the mean, 34 ± 2 ppb NO_x and 14 ± 1 ppb NO_2 were observed near the road and 12 ± 1 ppb NO_x, and 10 ± 0.3 ppb NO_2 were measured in the park. The uncertainty calculation is described in Appendix 4.6.

The NO_2:NO_x ratio can be estimated by calculating the relative concentration of oxidant per unit NO_x, (NO_2 + O_3)/ NO_x , at nearby road and background sites (Jenkin, 2004; Carslaw *et al.*, 2016).

Table 4.2. Mean pollutant concentrations at BROS and EROS sites

Pollutant	Mean concentration ± uncertainty* (ppb)		Δ (ppb) [BROS] – [EROS]
	BROS	EROS	
NO	20 ± 1	2 ± 0.3	18 ± 3
NO_2	14 ± 1	10 ± 0.3	4 ± 0.3
NO_x	34 ± 2	12 ± 1	22 ± 2
O_3	17 ± 1	18 ± 1	-1 ± 0.1
O_x (NO_2+O_3)	31 ± 3	28 ± 2	3 ± 0.3
NO_2:NO_x	0.4 ± 0.1	0.8 ± 0.1	

* = uncertainty as SEM (see Appendix 4.6)

Δ O_x is due to the primary emission of NO_2.
Δ O_x = 3 ppb
Δ NO_x = 22 ppb

$$Primary\ NO_2 = \frac{\Delta\ O_x}{\Delta\ NO_x}\ x\ 100\% \qquad (E.4.4)$$

Primary NO_2 = (3 / 22) x 100% = 13.6 % = 14 %

The result suggests that the primary NO_2 level is approximately 14%.

The ratio of NO_2:NO_x varies at different locations; it is related to the primary emission of NO_2 from vehicles in the area and the use of diesel cars (Mavroidis and Chaloulakou, 2011).

4.3.2. Input variables in the ADMS-Roads model

The dispersion of air pollution is based on several factors, such as turbulence, wind speed, wind direction and atmospheric stability (Mayer, 1999).

Meteorological data

Meteorological data of wind direction, wind speed, temperature, and relative humidity (RH) were taken from the nearest weather station, which was Winterbourne No.2, Coundon, Coleshill or Elmdon over the period of sampling time. Cloud cover data were derived from the Coleshill weather station.

Surface roughness

A surface roughness of 0.5 m was used in this dispersion modelling study. This value is considered appropriate for the sampling area and is suggested within ADMS Roads for parkland and open suburbia.

Background concentration

Automatic analysers data at the EROS or Biosciences site, diffusion tubes data at the EROS, or air quality monitoring data from the Birmingham Acocks Green station were potential data for use in this dispersion modelling assessment to represent background concentrations (NO_2, NO_x and O_3).

Identify road sources and receptor coordinates

In the model, roads are designated as line sources. Line sources near the receptors are included in the model and line sources far from the receptors are ignored (Heist *et al*., 2013). The road was divided into segments in terms of road widths (m) and speed in km hour^{-1} (km h^{-1}). The speed of vehicles near traffic lights was set in the model at the lowest speed, 5 km h^{-1}, and sensitivity analysis of the vehicle speeds was conducted on each link of the roads. The road width was estimated based on Google map measurements.

Table 4.3. Road sources and emission data

Road ID	Information	Emission data
Road 1	Road 1 is A38 Aston Webb Boulevard to the junction B384	calculated from count point of ID number 81576 subtract with the number of vehicles on the road 7 (New Fosse Way / Vincent Dr Road)
Road 2	Road 2 is A38 Bristol Road from the junction to A4029	calculated from count point 81577
Road 3	Road 3 is the Edgbaston Park Road	calculated from traffic observation at Edgbaston Park Road *)
Road 4	Road 4 is the Edgbaston Park Road	calculated from traffic observation at Edgbaston Park Road *)
Road 5	Road 5 is Pritchatts Rd	calculated from traffic observation at Pritchatts Rd. *)
Road 6	Road 6 road at UoB west gate near BROS site	calculated from traffic observation at UoB west gate near BROS site *)
Road 7	Road 7 is New Fosse Way road, Vincent Dr and Farquhar Rd.	calculated from traffic observation at from and to New Fosse Way *)
Road 8	Road 8 is the Somerset Rd	calculated from traffic observation at Somerset Rd *)

*) see Table A.4.5.2. Observation of vehicle number on specific road and explanation in Appendix 4.5



Figure 4.4. Demarcating the segments on the map of sampling location, the University of Birmingham

The coordinate systems of road segments and receptors were identified on the Google map (WGS 84 (4326)) and latitude and longitude were recorded. Conversion of the coordinate system from latitude and longitude to British National Grid (27700) was made using the website http://www.realitygeo.com/coordinates.aspx, which converts the location to X and Y coordinates in metres (see Appendix 4.1. Road Geometry, and Appendix 4.2. Receptor Geometry). Receptor locations were entered in the model as specified points with x, y and z coordinates in metres.

The coordinates for each road were inputted to the ADMS-Roads model in the source settings of the geometry interface. In the ADMS-Roads utilities, ADMS mapper was selected and set into the coordinate system in the same setting as ADMS-Roads, i.e. OSGB 1936 British National Grid (epsg: 27700).

Time-varying emission factor

Time-varying emission factors are emission factors for each hour that show variation in traffic from the hourly average flow (CERC, 2017). These factors are needed to represent the variation of concentrations in a short-term period (Hood *et al.*, 2018). The ADMS-roads model will multiply these factors to give emission rate. Time-varying emission factor data can be obtained from road traffic statistics issued by the local authority. However, if there is no data, then TRA0307 (vehicle traffic distribution data from the Department for Transport, UK, (DfT, 2019b)) can be used, which has been done in this study.

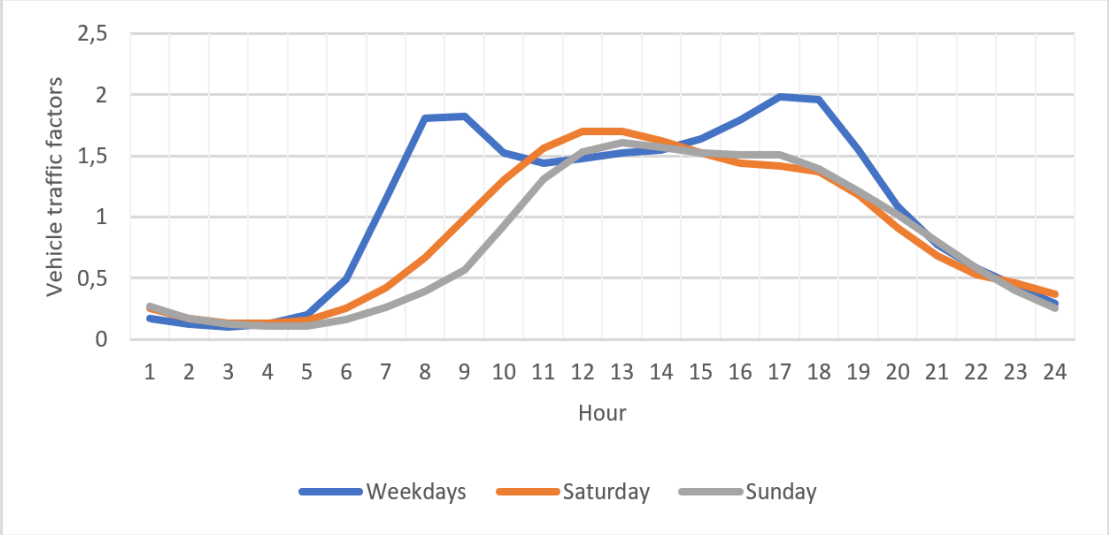


Figure 4.5. Vehicle traffic factors on weekdays (blue line), Saturday (orange line) and Sunday (grey line). Traffic factors were generated from the time-varying emission factor (TRA 0307 in 2018) by dividing the number of vehicles on weekdays, Saturday and Sunday for each hour with average daily flow of the week (Monday to Sunday). Refer to Appendix 4.4 (data adopted from Table TRA 0307 in 2018, Motor vehicles traffic distribution by time of day and day of the week on all roads Great Britain, Department for Transport, (DfT, 2019b))

Figure 4.5 shows vehicle traffic factors adopted from TRA 0307 in 2018 (DfT, 2019b), data on the motor vehicles traffic distribution by time of day and day of the week on all roads in Great Britain. The time-varying emission factors are calculated by averaging the number of

vehicles in each hour from Monday to Friday as weekdays from data in table TRA 0307 (https://www.gov.uk/government/statistical-data-sets/road-traffic-statistics-tra#annual-daily-traffic-flow-and-distribution-tra03). The factor is then derived for each hour by dividing the number of vehicles by the average daily flow for the week. The calculation is the same for Saturday and Sunday, i.e., averaging the number of vehicles each hour and dividing this by the average daily flow for the week (see Appendix 4.4. Time-varying emission rate).

Emission rates

Emissions rates describe the amount of pollutants emitted by vehicles and are derived using data on vehicle speed, vehicle type, number of vehicles, etc. Traffic flow data was generated from the Department for Transport's road traffic statistics (https://roadtraffic.dft.gov.uk/local-authorities/141) vehicle count (Average Annual Daily Flow - AADF) for the sampling area.

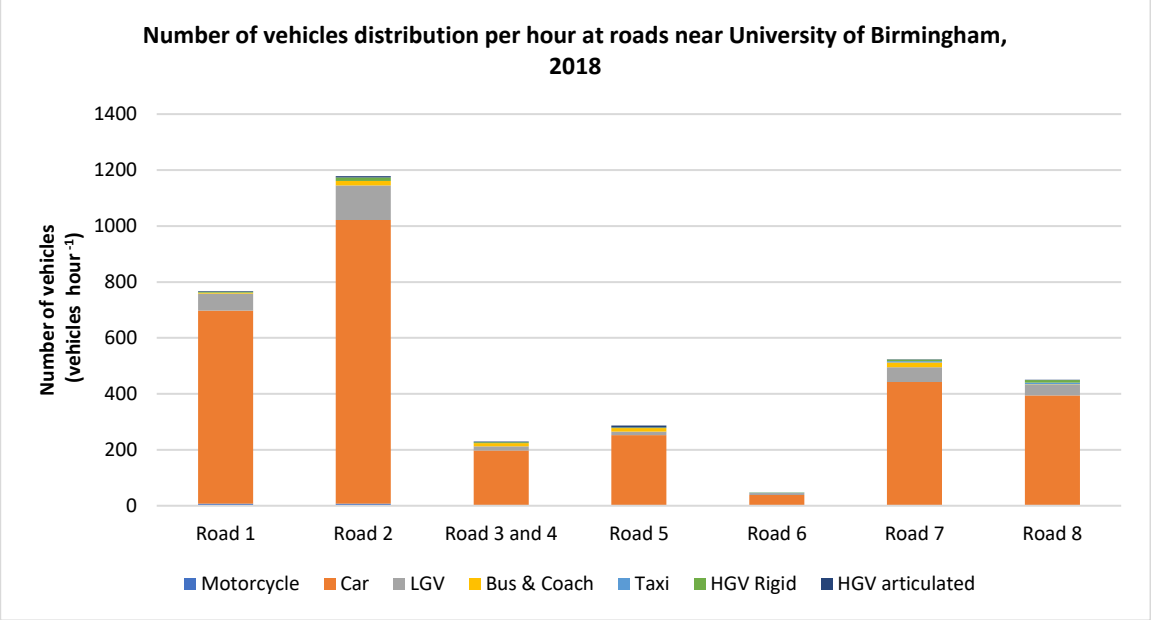


Figure 4.6. Number of vehicles per hour at roads near the University of Birmingham refer to Appendix 4.5, Table A.4.5.8. Resume data of traffic flows in 2018 (adopted from observation data and Traffic count ID data from Department for Transport (DfT, 2019a))

Figure 4.6 shows number of vehicles per hour at roads near the University of Birmingham site. There are eight roads identified, as shown in Figure 4.4 and Table 4.3, and only two locations have current AADF data, ID numbers 81576 and 81577. For roads with no AADF data, the result from the manual one-hour observation data on vehicles count was used. The

TRA0307 vehicle number count for Great Britain is used to find the ratio of vehicle number data on the road in order to generate the vehicle average flow from one-hour observations (see Appendix 4.5).

An increase of traffic emissions would raise the pollution level in the area (Vardoulakis *et al.*, 2003). Measured emission data is needed to derive accurate modelled concentrations (Hood *et al.*, 2018). Therefore, AADF data and observations on vehicle count were used to estimate the distribution of the vehicles per hour on roads near the sampling site, as shown in Figure 4.6. The steps to combine AADF and observation data to produce the number of vehicles is described in Appendix 4.5.

Adjusted NO_2:NO_x ratio

NO_2:NO_x is the ratio of primary NO_2 in the total NO_x concentration (Mavroidis and Ilia, 2012), and the ratio increases with increasing distance from the source (Richmond-Bryant *et al.*, 2017).

4.3.3. Sensitivity analysis

Several sensitivity tests were carried out as presented in the following sections to find the best input data set in the model, to identify errors that arise from the dispersion modelling and reduce the model uncertainties.

4.3.3.1. Sensitivity to meteorological data

Wind direction, wind speed, cloud cover, temperature and relative humidity were used in the modelling. These weather data were downloaded from the Centre for Environmental Data Analysis (CEDA) website. There are 130 weather stations in the UK West Midlands, registered in the CEDA list, but only eight weather stations were working at the time when the model was run (http://archive.ceda.ac.uk/midas_stations/). Furthermore, only three of those eight provided weather data. The stations are Coundon, Elmdon and Winterbourne No.2. In total, four weather stations were reviewed to conduct sensitivity analysis with respect to meteorological data (Table 4.4). The distance between Coleshill weather station and the University of Birmingham is around 16.5 km, and this location is included as input to provide weather data (cloud cover).

Winterbourne No. 2 CEDA was the first weather station recommended for use in this study due to its proximity to the sampling site, and data can be downloaded from the CEDA website; however, the data only includes temperature and relative humidity, and there was no data for wind direction and wind speed. Winterbourne No.2 Birmingham Urban Climate Laboratory (BUCL) records data from the same weather station as Winterbourne No. 2 CEDA, but provides more data, for example wind direction, wind speed, temperature and relative humidity. Weather data from Winterbourne No.2 BUCL were downloaded via an internal connection on the 1st floor at the School of Geography, Earth and Environmental Sciences (GEES), UoB.

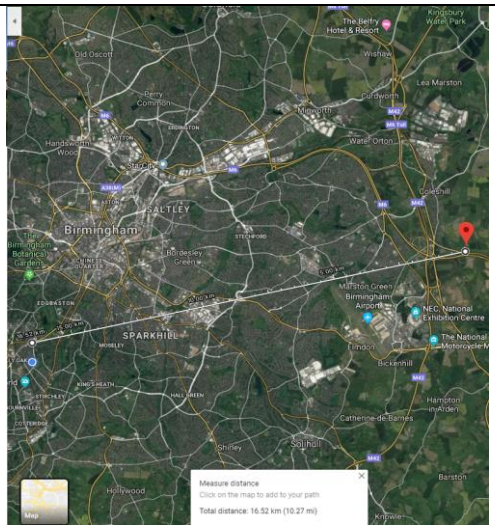
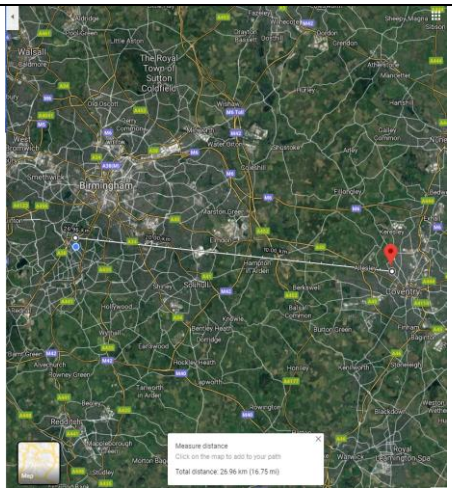
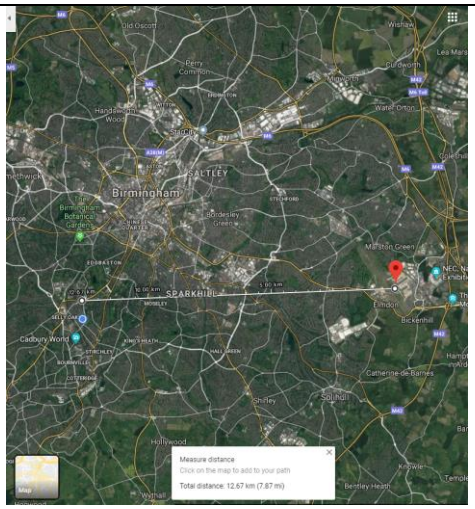
Cloud cover data was not available on the Winterbourne No.2, Elmdon and Coundon weather stations. Therefore, cloud cover data was taken from the Coleshill weather station.

Table 4.4. ID of the weather station in the CEDA website, Latitude, Longitude and parameter of weather data

No	Name of weather station	ID	Latitude	Longitude	Geographic area	Station start	Station end	Parameter				
								WD	WS	CL	T	RH
1.	Winterbourne No2 - CEDA	56424	52.456	-1.92619	West Midlands	03/02/2011	Current				√	√
	Winterbourne No2 – BUCL	56424	52.456	-1.92619	West Midlands	03/02/2010		√	√		√	√
2.	Coleshill	19187	52.4798	-1.68925	Warwickshire	01/09/1997	Current	√	√	√	√	√
3.	Elmdon	593	52.4524	-1.74099	West Midlands	01/01/1949	Current	√	√		√	√
4.	Coundon	24102	52.4241	-1.53498	Coventry, West Midlands	01/10/1998	Current	√	√		√	√

Note: WD = wind direction; WS = wind speed; CL = cloud cover; T = Temperature; RH = Relative Humidity

ADMS modelling assumes a Gaussian dispersion process and depends on the meteorological conditions near the sampling site, and this gives reasonable results within an area ± 50 km from the source (Carruthers *et al.*, 1994). Maps and locations of weather stations near the sampling site are shown in Figure 4.7. The weather station closest to the sampling site is Winterbourne No. 2 because of its location at the University of Birmingham, with a distance of 1.02 km from BROS. However, as previously mentioned, not all weather-parameters were available in this weather station and hence the four closest weather stations were selected for the model.

Distance from weather station to the sampling site	Map
Coleshill – BROS, UoB = 16.52 km	
Coundon – BROS, UoB = 26.96 km	
Elmdon – BROS, UoB = 12.67 km	

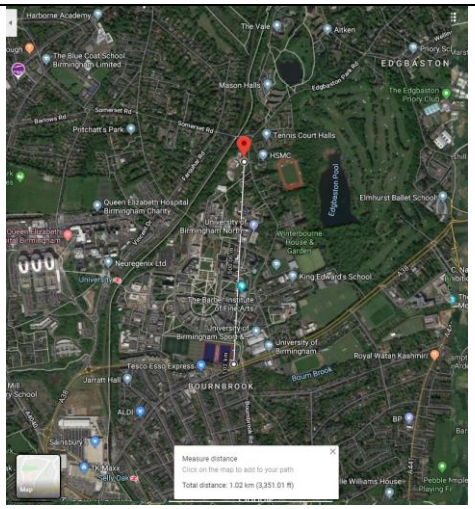
Distance from weather station to the sampling site	Map
Winterbourne No. 2 – BROS, UoB = 1.02 km	

Figure 4.7. Map and location of weather stations near sampling sites (http://maps.google.com/)

The ADMS-Roads model gives different results for the same emissions scenario but with different meteorological inputs. The different data for wind direction and wind speed at different weather stations affects the predicted concentrations.

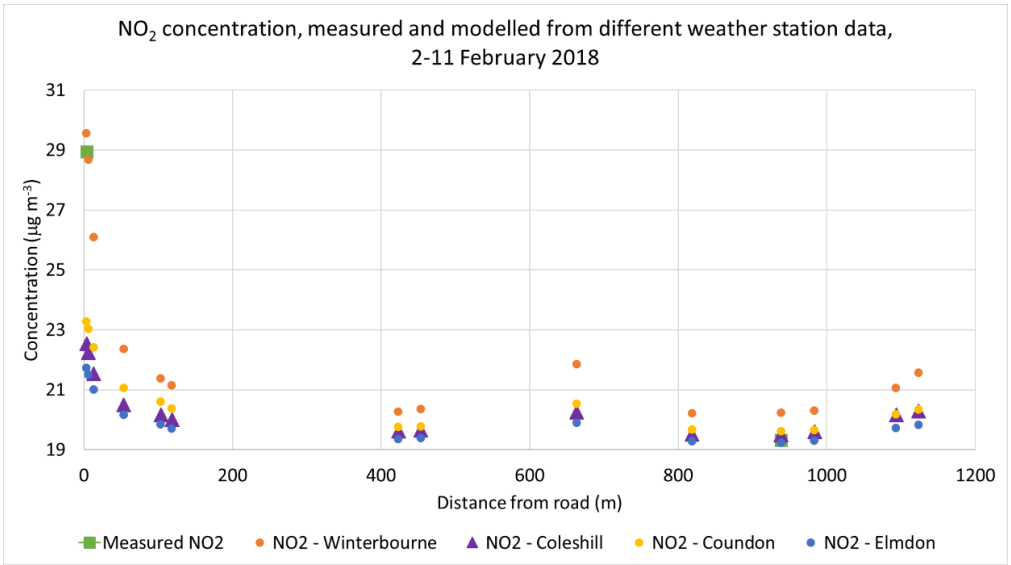


Figure 4.8. Comparison of modelled and measured NO_2 concentration from different weather stations at receptor locations. The x-axis represents the distance in metres from the road near BROS site (A38 road) and y-axis is NO_2 concentration in µg m^{-3}.

As shown in Figure 4.8, the modelled NO_2 concentration from Winterbourne No. 2 weather station gives a slightly higher concentration compared with observed measurement at the

BROS site. While the modelled NO_2 concentrations from other weather stations (Coleshill, Coundon and Elmdon) were significantly lower than the observed data at BROS. The wind speed data from Coleshill, Coundon and Elmdon were higher compared to wind speed from Winterbourne No. 2 data, and give the lowest concentration results.

In this sensitivity analysis, ADMS-Roads was set for the same data input scenario — the only change was the input meteorological data from different weather stations. The modelled concentration results from different weather stations were compared with the measured data and evaluated with FB, NMSE, R and R^2 for pairwise comparisons of inputs from various weather station.

The evaluation of results from ADMS-Roads modelling using meteorological input from different weather stations is shown in Table 4.5. Based on fractional bias, NMSE and coefficient of correlation, the ideal weather station data was Winterbourne No. 2, the second option was Coundon weather station, the third Coleshill, and the last Elmdon.

Table 4.5. Evaluation results from ADMS-Roads modelling using meteorological input from different weather stations

Meteorology station	Pollutant	Measured mean ($\mu g\ m^{-3}$)	Modelled mean ($\mu g\ m^{-3}$)	SD Measured	SD Modelled	FB (Fractional Bias)	NMSE	R	R^2
Winterbourne No. 2	NO_2 BROS	28.95	29.55	15.61	15.55	-0.02	0.000	0.88	0.77
	NO_x BROS	69.01	64.09	46.62	44.31	0.07	0.005	0.82	0.67
	NO_2 EROS	19.33	20.22	10.46	10.58	-0.05	0.002	0.99	0.98
	NO_x EROS	24.10	25.08	17.62	17.65	-0.04	0.002	0.99	0.98
Coundon	NO_2 BROS	28.95	23.28	15.61	12.91	0.22	0.048	0.86	0.74
	NO_x BROS	69.01	42.92	46.62	34.12	0.47	0.230	0.71	0.50
	NO_2 EROS	19.33	19.61	10.46	10.43	-0.01	0.000	0.99	0.98
	NO_x EROS	24.10	24.41	17.62	17.54	-0.01	0.000	0.99	0.98
Coleshill	NO_2 BROS	28.95	22.55	15.61	13.39	0.25	0.063	0.87	0.76
	NO_x BROS	69.01	40.84	46.62	37.12	0.51	0.282	0.74	0.55

Meteorology station	Pollutant	Measured mean (µg m^{-3})	Modelled mean (µg m^{-3})	SD Measured	SD Modelled	FB (Fractional Bias)	NMSE	R	R^2
	NO_2 EROS	19.33	19.50	10.46	10.54	-0.01	0.000	0.99	0.98
	NO_x EROS	24.10	24.31	17.62	17.63	-0.01	0.000	0.99	0.98
Elmdon	NO_2 BROS	28.95	21.73	15.61	12.21	0.28	0.097	0.82	0.67
	NO_x BROS	69.01	37.04	46.62	30.91	0.60	0.425	0.67	0.45
	NO_2 EROS	19.33	19.23	10.46	10.32	0.01	0.001	0.94	0.88
	NO_x EROS	24.10	23.86	17.62	17.30	0.01	0.001	0.95	0.90

The different meteorological data input could create a bias in the model output by either underestimating or overestimating the modelled concentration. However, Arciszewska and McClatchey (2001) stated that the use of meteorological data from different sites in the UK at a distance within a few tens of km from the site could be used in the model with the output of long-term averages. Thus, the meteorological data from the nearest weather station is needed to achieve the most reliable modelling output. Modelled concentration using Winterbourne No.2 showed consistently higher concentration of NO_2 compared to other weather stations, due to lower wind speeds (see Figure 4.11).

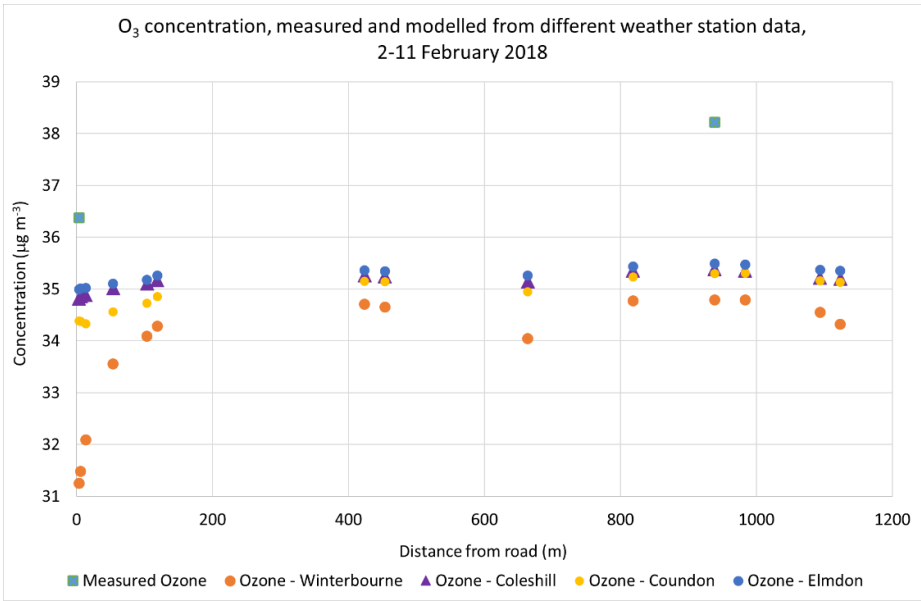


Figure 4.9. Comparison of modelled and measured O_3 concentration from different weather stations at receptor locations. The x-axis represents the distance in metres from the road near BROS site (A38 road) and y-axis is O_3 concentration in µg m^{-3}.

Figure 4.9 shows that the trend of O_3 concentrations is opposite to the trend of NO_2 concentration (Figure 4.8). O_3 concentrations were lower near the roadside and slightly increased along the distance to the urban background. The lowest to the highest values for modelled concentrations were presented by Winterbourne No.2, Coundon, Coleshill, then Elmdon. However, the measured concentrations were all slightly higher than all the modelled concentrations. The difference between measured concentration and modelled concentration using Winterbourne No.2 data was 5 µg m^{-3}.

Wind direction

Wind direction played a significant role in determining the transport of pollutants. The prevailing wind directions were W (west), NW (northwest), NE (northeast), SW (southwest), and from the S (south). There were no major differences between weather stations in terms of wind direction trends. The major difference between weather stations is the wind speed. The wind rose in Figure 4.10 shows the wind speeds and wind directions.

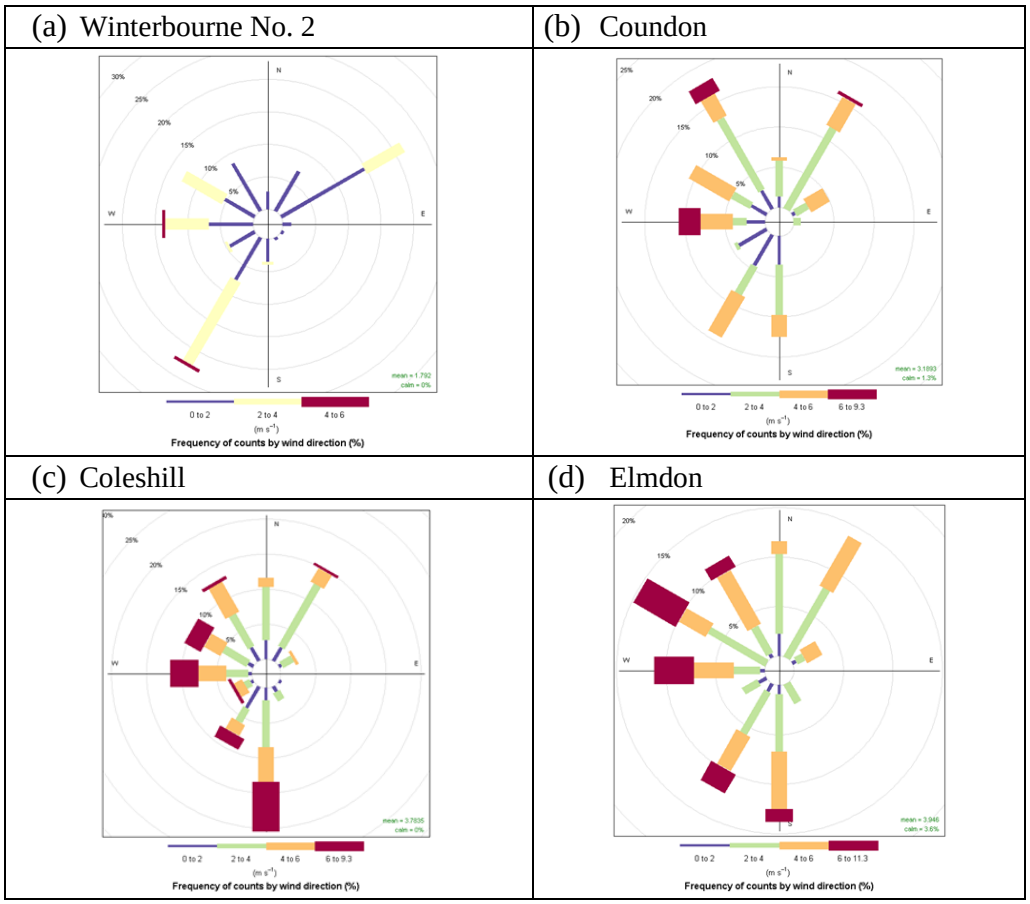


Figure 4.10. Comparison of wind rose from different weather stations, 2-11 February 2018

Wind speed

Wind speeds of less than 0.5 m s^{-1} are considered representative of calm conditions (Carruthers *et al.*, 1994). An increase in wind speed could increase dilution and reduce pollutant concentration (Turner, 1979; Righi *et al.*, 2009). The biggest factors affecting wind measurement are the height of the measurement and the fetch, and these are discussed in Chapter 5, Section 5.3.4.2.

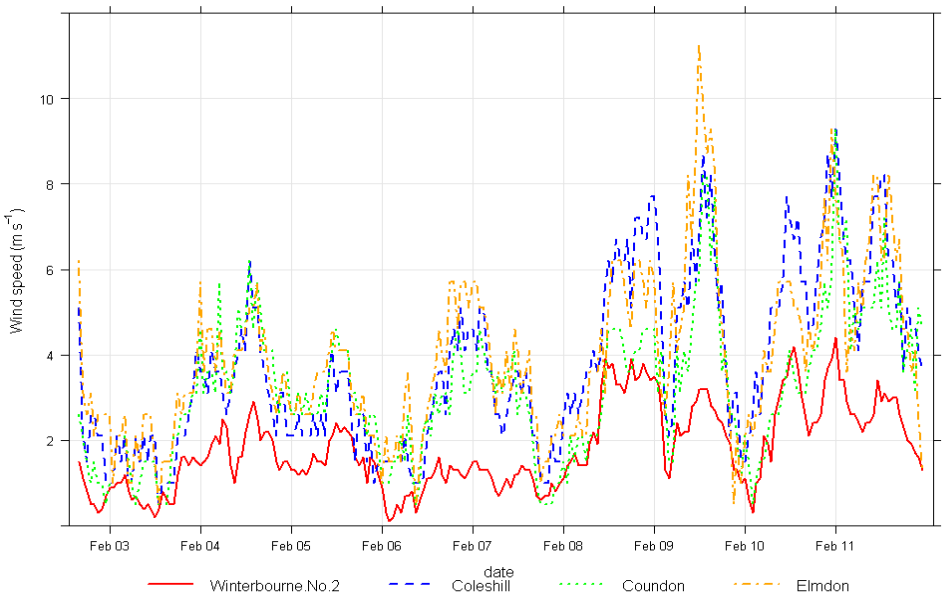


Figure 4.11. Comparison of wind speed from different weather stations

Wind speed data from Winterbourne No.2 was lower compared to the other weather stations. This could be related to the different local conditions at each weather station (Hang *et al.*, 2009). The importance of wind aspect in the dispersion process is also discussed by Karner *et al.* (2010), in a study confirming that the concentration of pollutant near the road is strongly affected by wind speed and wind direction.

Adjusted wind speed

The nearest weather station that shows a good comparison result between the modelled concentration with the measured concentration is Winterbourne No 2. Weather data from Winterbourne No. 2 can be obtained in two ways: online from the CEDA website, and offline from BUCL data. The data available online from CEDA for Winterbourne No.2 are only for temperature (T) and relative humidity (RH). Complete data including wind speed

(WS), wind direction (WD), T, RH and other parameters were generated from Winterbourne No.2 BUCL data. Weather data were downloaded from the BUCL from 2011 to March 2018. However, after April 2018, there were connection issues and no data were available. Data became available again in August 2019.

Data from Winterbourne No. 2 BUCL were used. Data gaps make it impossible to use all data from one meteorology measuring site. Meteorological data from the Coundon weather station was an alternative substitute. In filling the data gaps only wind speed was corrected. Wind direction was not corrected, as differences were small and not consistent between the sites. Wind speed and wind direction are strongly interconnected. However, adjusted wind speed is needed to reduce errors when using different weather data. The interpretation of the data used where alternative meteorological data have been used should be strongly caveated, as replacement of wind data may reflect a poor substitute.

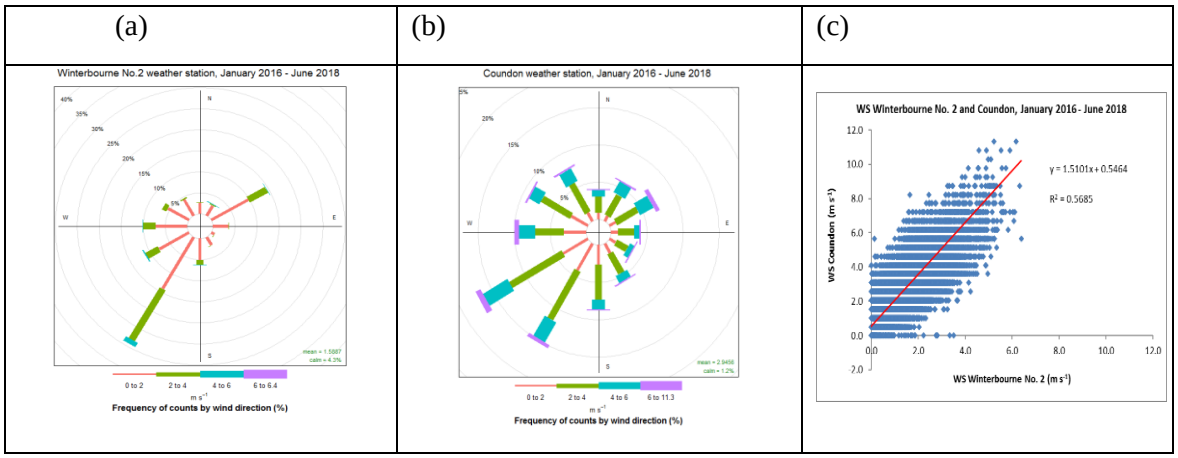


Figure 4.12. Wind rose (wind speed and wind direction) plot of **(a)** Winterbourne No.2 – BUCL, and **(b)** Coundon weather station. Data from January 2016 to June 2018, and **(c)** linear regression of wind speed from Winterbourne No.2 – BUCL and Coundon.

Figures 4.12 (a) and (b) show the wind roses (wind speed and wind direction) from the two weather stations from January 2016 to June 2018. The wind rose from Winterbourne No.2 (a) shows a smaller dash (red line) to reflect the lower wind speed. Winterbourne No.2 recorded wind speed in the range 0 m s^{-1} to 5.6 m s^{-1} and the wind direction was dominated by south-southwest (SSW) and east-northeast (ENE). The wind rose from the Coundon weather station shows a higher wind speed, in the range 0 m s^{-1} to 12 m s^{-1}, and a broader range of wind direction. Wind direction at the Coundon weather station data is generally from west-southwest (WSW), south-southwest (SSW), west (W), and east-northeast (ENE).

The most common wind directions at Winterbourne No.2 were from SSW (28%) and ENE (14%), while at Coundon the WSW direction dominated (17%) followed by SSW (15%). Winterbourne No. 2 also shows lower wind speed values compared to Coundon. Therefore, to achieve a more accurate value for wind speed, a correction factor was needed to reflect the wind speed value from Winterbourne No.2.

Table 4.6. Coefficient of determination (R^2) and linear regression of wind speed from Winterbourne and Coundon weather stations, January 2016 – June 2018

Weather station	R^2	Linear regression	Equation
Winterbourne No. 2 and Coundon	0.57	Y = 1.5101x + 0.5464	$x = \frac{(Y - 0.5464)}{1.5101}$

The coefficient of determination from Coundon weather station (Table 4.6) shows that R^2 was 0.57 and the slope value from linear regression presents the rate of change of wind speed as much as 1.51 m s^{-1} for every 1 m s^{-1} increase in wind speed at Winterbourne No.2.

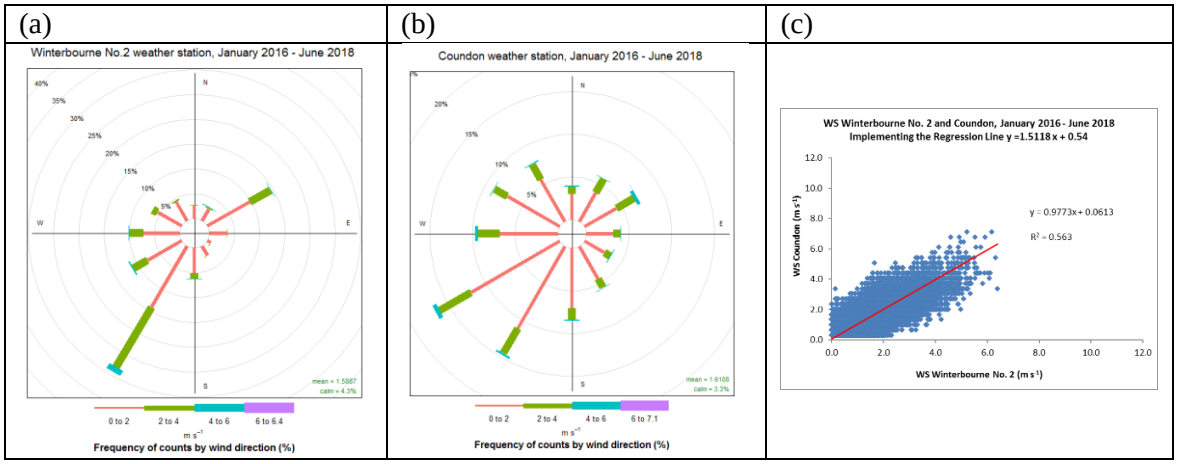


Figure 4.13. Windrose plots from **(a)** Winterbourne No.2, **(b)** Coundon after implementing the correction factor of wind speed data for Coundon (x = (y – 0.5464) / 1.5101), and **(c)** linear regression from Coundon after implementing the correction factor.

Figure 4.13 shows the wind rose plot for Coundon after using the correction factor, alongside the wind rose plot from Winterbourne No.2 as a comparison. The pattern is clearer, as the range of wind speed is smaller and approaching similar wind speed patterns from Winterbourne No.2. The corrected regression value for Coundon was y = 0.9773x + 0.0613 (R^2= 0.56). The implementation of a wind speed correction factor to remove the bias was

performed correctly because the slope of the corrected regression value was very nearly equal to unity.

Overall, the wind speed from Coundon shows a higher magnitude compared to Winterbourne No.2 data. Therefore, a correction to the wind speed data from the inverse equation of regression line was implemented.

Temperature

Temperature trends appear to be more consistent between weather stations, as shown in Figure 4.14. During the measurement on 2-11 February 2018, the temperature fluctuated in the range of -1 °C to 9 °C.

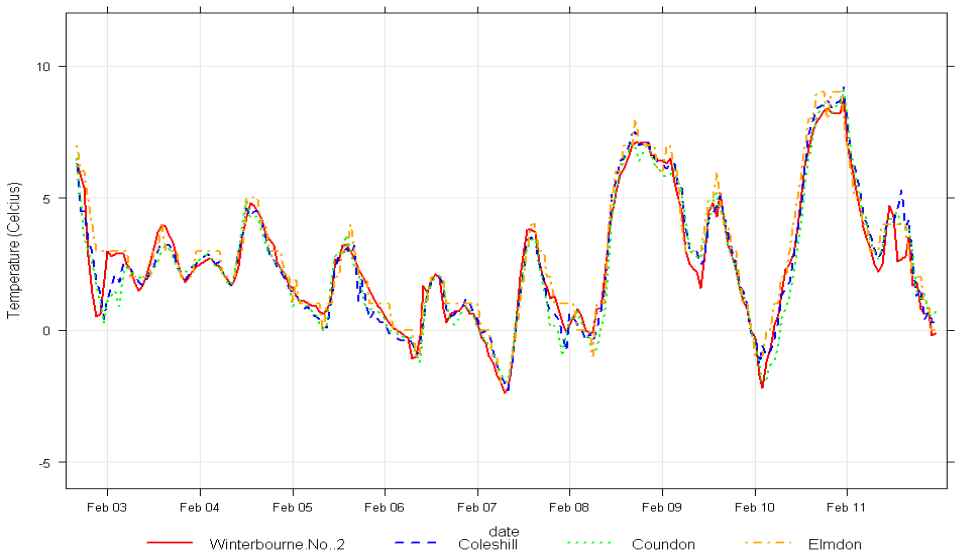


Figure 4.14. Comparison of temperature from different weather stations

Cloud cover

Cloud cover data was taken from the Coleshill weather station. The model used total cloud cover in the range of 1 to 8 oktas. The cloud cover was mainly overcast during the sampling period.

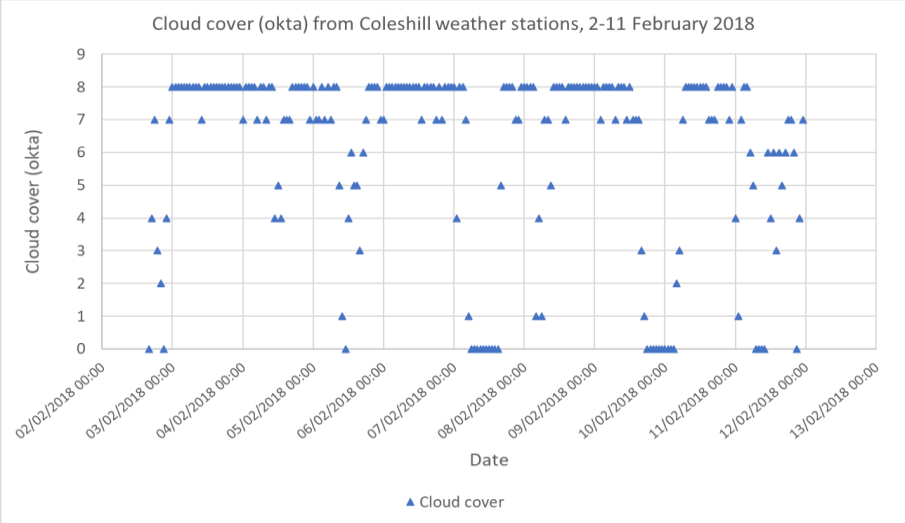


Figure 4.15. Cloud cover from Coleshill weather station

Relative Humidity (RH)

Figure 4.16 shows RH fluctuating in the range 42% to 100% during the sampling period. There was no major difference in trend of RH between weather stations, as shown in Figure 4.16.

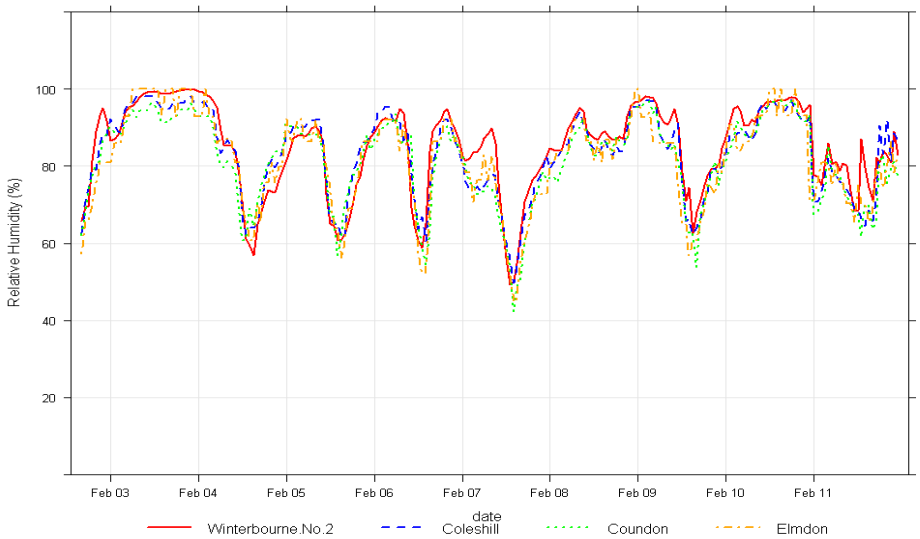


Figure 4.16. Comparison of relative humidity from different weather stations

Overall, meteorological data for temperature, relative humidity and the available data for wind speed, wind direction were obtained from Winterbourne No.2 at the University of Birmingham. The alternative data for wind speed in the area was obtained from Coundon weather station (26.96 km ESE from BROS site).

4.3.3.2. Sensitivity to background concentration

In this study, there are three potential input data sources for conducting sensitivity analysis background concentration — first, secondary data from AURN (Automatic Urban and Rural Network) monitoring stations; second, primary data from automatic analyser monitored at EROS or Biosciences site as a background site in the University of Birmingham; third, the diffusion tub e result at the EROS site.

There are two air quality monitoring stations: 1) Birmingham Acocks Green, and 2) Birmingham Ladywood, located near the University of Birmingham and classified as urban background (Table 4.7 and Figure 4.17) as part of the AURN data, a national network in the UK and the data available at the Defra website (https://uk-air.defra.gov.uk/networks/network-info?view=aurn). The nearest monitoring location to the sampling campaign is Birmingham Ladywood on the north side; however, the data for this monitoring station only became available from June 2019. For this reason, the Birmingham Acocks Green monitoring station was selected as the sole source of background concentrations data from AURN monitoring station.

Table 4.7. Urban background monitoring sites in Birmingham

Site ID	Site type	Latitude / Longitude
Birmingham Acocks Green	Urban background	52.437165, -1.829999
Birmingham Ladywood	Urban background	52.481346, -1.918235

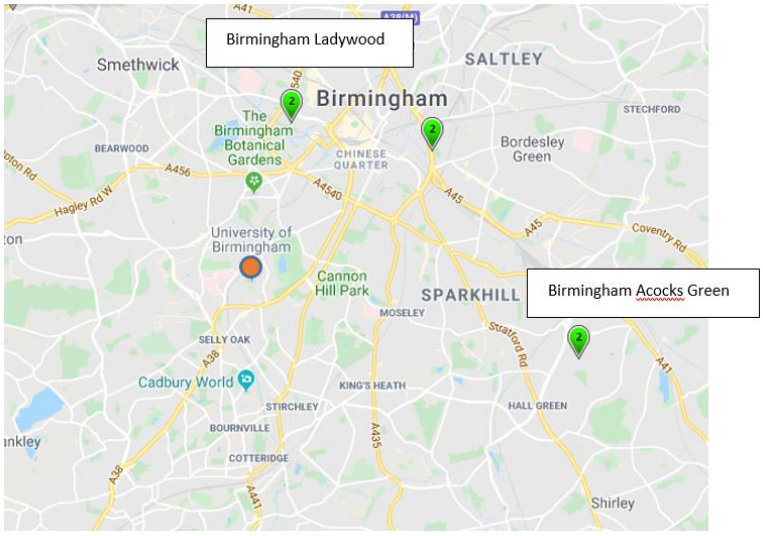


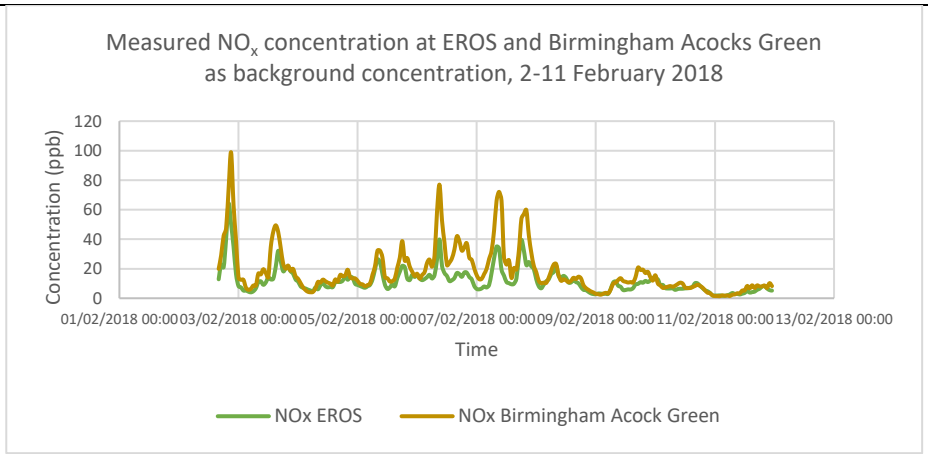
Figure 4.17. Location of urban background sites from AURN monitoring station in Birmingham

The hourly data of NO_x and O_3 from the automatic analysers in the two locations, Birmingham Acocks Green and EROS, were compared to select the best fit of background concentrations for the model.

The location coordinates of Birmingham Acocks Green are 52.437165, -1.829999 (https://uk-air.defra.gov.uk/networks/site-info?site_id=AGRN, 2019). The distance from this monitoring station to the nearest road, Shirley Road, is ± 70 metres. The distance from the A38 to EROS (south to the north) is 940 metres from A38 Bristol Road; 302 metres from Pritchatts Road; and 135 metres from Edgbaston Park Road at the Eastside; 225.5 metres from Somerset Road at the Northside, and 210.5 metres from Farquhar Road at the Westside.

NO_x and NO_2 concentrations at the Birmingham Acocks Green monitoring site were relatively higher than at EROS, as shown in Figures 4.18 and 4.19. EROS was slightly less polluted compared to Birmingham Acocks Green, and this might be related to the distance of the site from the road, a main traffic source of emission.

(a) NO_x concentration



(b) Wind speed and wind direction from Winterbourne No.2

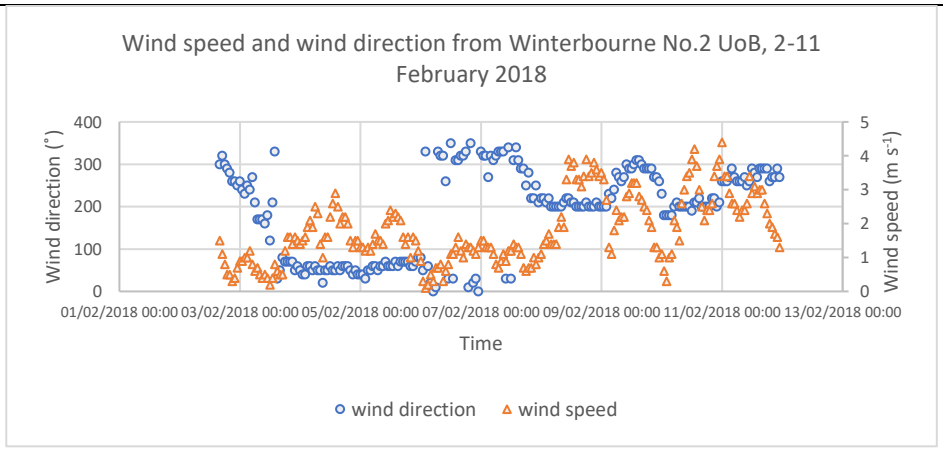


Figure 4.18. **(a)** NO_x concentration at EROS (green line) and Birmingham Acocks Green (light brown line) sites; and **(b)** wind direction (blue circle) and wind speed (orange triangle) from Winterbourne No. 2 UoB at sampling date, 2-11 February 2018

It was found that the difference in concentrations between Birmingham Acocks Green and EROS site mainly occurred when the wind direction was coming from north and northeast, and when wind speeds were below 1.5 m s^{-1}.

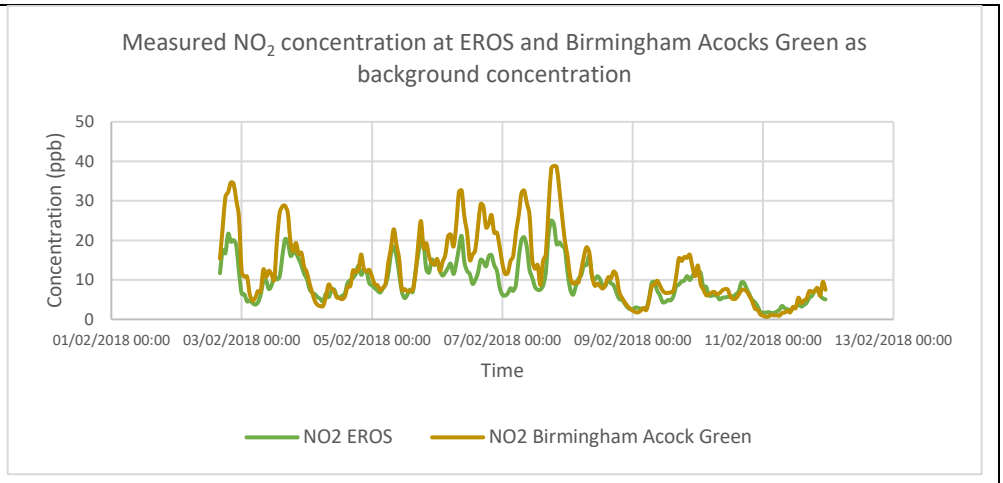
NO_2 concentration	

Figure 4.19. NO_2 concentration at EROS (green line) and Birmingham Acocks Green (light brown line) sites, 2-11 February 2018

NO_2 concentration was higher at Birmingham Acocks Green when the wind direction was coming from north, northeast and east (Figure 4.19). O_3 level was slightly higher at the Birmingham Acocks Green site, and there was no major difference in the trend of concentrations between the Birmingham Acocks Green site and EROS (Figure 4.20).

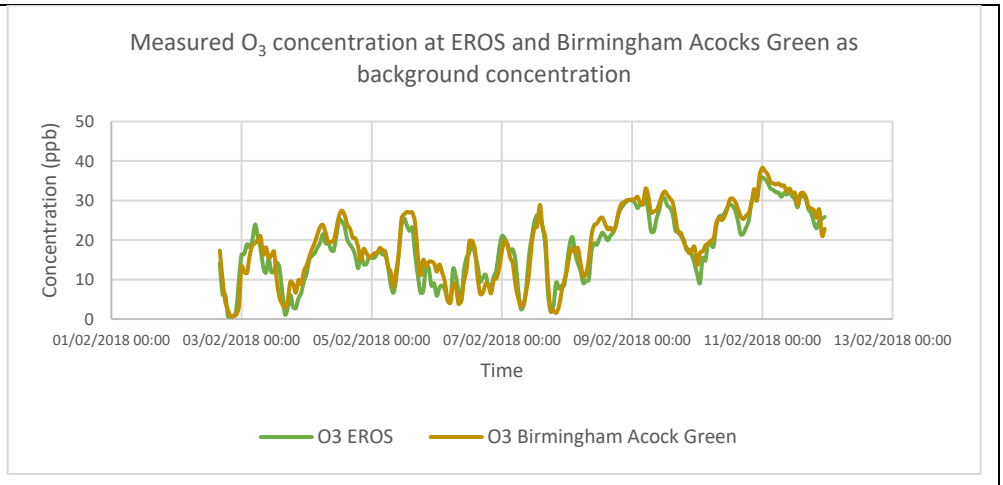
O_3 concentration	

Figure 4.20. O_3 concentration at EROS (green line) and Birmingham Acocks Green (light brown line) sites, 2-11 February 2018

Data from the automatic analysers of NO_x and NO_2 at BROS and EROS on 2-11 February 2018 were compared against the modelled concentrations. Figure 4.21(a) shows the comparison of hourly observed concentrations and hourly modelled concentrations of NO_2 at the EROS location using EROS concentrations as background concentrations data. Figure 4.21(b) presents the observed NO_2 concentration compared to modelled NO_2 concentrations at EROS location using Birmingham Acocks Green concentrations as background concentrations data.

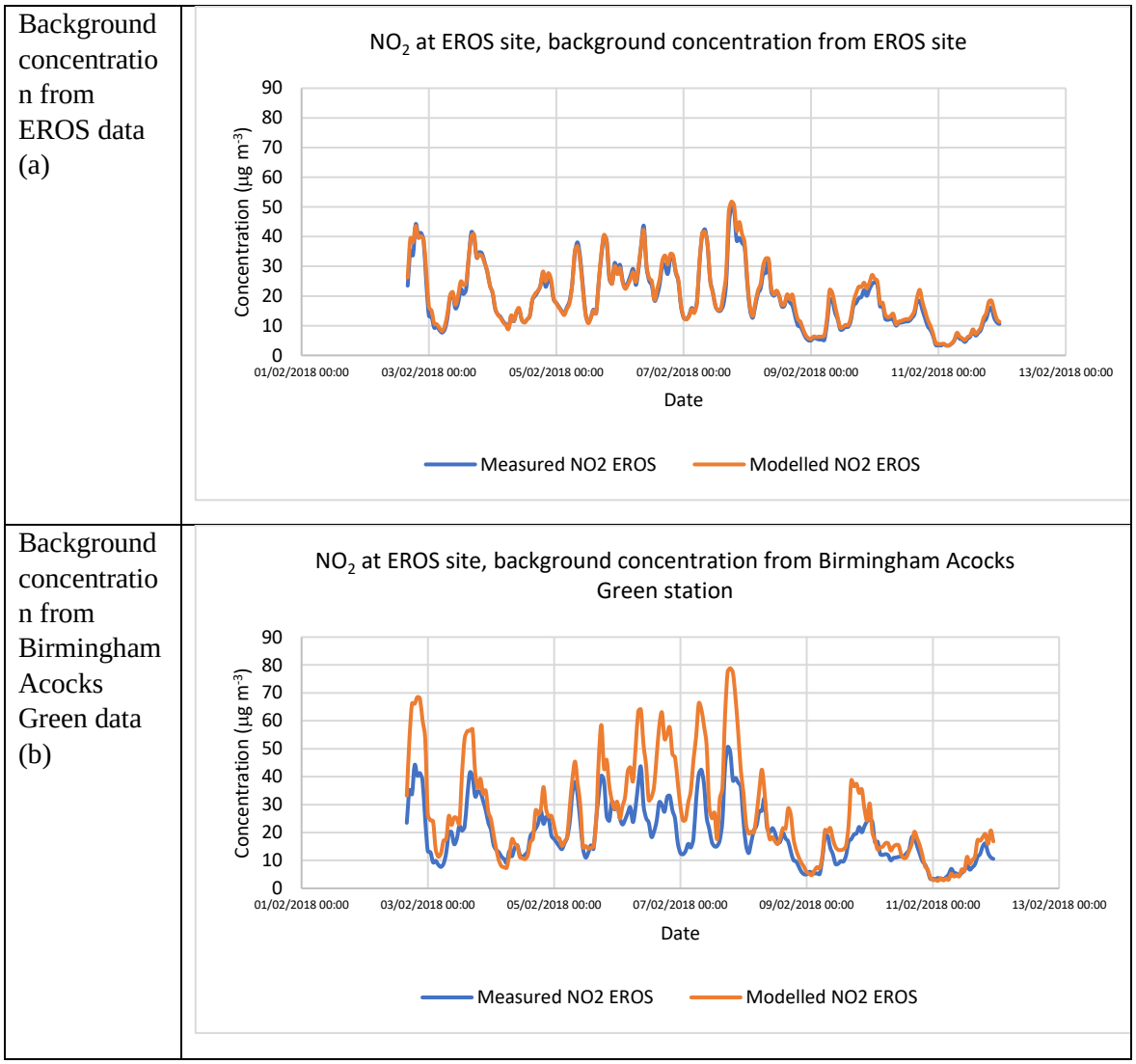


Figure 4.21. Measured (blue line) and modelled (orange line) NO_2 concentration at EROS sites using background concentration from **(a)** EROS site, and **(b)** Birmingham Acocks Green

Measured and modelled NO_2 concentrations give a good agreement when using the data from the EROS as background concentration. However, the modelled NO_2 was higher than the measured NO_2 when data from the Birmingham Acocks Green monitoring site was used as the input of background concentrations in the model.

Evaluation of the ADMS-Roads model was completed using the performance measures: FB, NMSE, R and R^2 with NO_x and NO_2 hourly data at BROS and EROS for the period 2-11 February 2018. The results are presented in Table 4.8.

Table 4.8. Evaluation result from different background concentration. EROS site and Birmingham Acocks Green

Background concentrations	Pollutant	Measured mean ($\mu g\ m^{-3}$)	Modelled mean ($\mu g\ m^{-3}$)	SD Measured	SD Modelled	FB (Fractional Bias)	NMSE	R	R^2
EROS data	NO_2 at BROS	28.95	29.55	15.61	15.55	-0.02	0.000	0.88	0.77
	NO_x at BROS	69.01	64.09	46.62	44.31	0.07	0.005	0.82	0.67
	NO_2 at EROS	19.33	20.22	10.46	10.58	-0.05	0.002	0.99	0.98
	NO_x at EROS	24.10	25.08	17.62	17.65	-0.04	0.002	0.99	0.98
Birmingham Acocks Green data	NO_2 at BROS	28.95	36.53	15.61	21.64	-0.23	0.054	0.87	0.76
	NO_x at BROS	69.01	76.07	46.62	54.19	-0.10	0.009	0.81	0.66
	NO_2 at EROS	19.33	27.13	10.46	17.66	-0.34	0.116	0.91	0.83
	NO_x at EROS	24.10	37.06	17.62	31.29	-0.42	0.188	0.89	0.79

The ADMS-roads model is sensitive to background concentrations. Statistical review of the ADMS-Roads model showed that the lowest mean bias (FB) and the lowest normalised mean square error (NMSE), the highest correlation (R) and coefficient of determination (R^2) occurred when data from EROS were inputted as background concentration. 99% of the variance in modelled NO_2 and NO_x concentrations can be explained by measured NO_2 and NO_x concentrations. Therefore, EROS data was chosen as the first option for background concentration input.

4.3.3.3. Sensitivity to emission

Accurate emissions data is needed to get reliable estimates of concentration (Hood *et al.*, 2018). Birmingham City Council road safety strategy plans for a safer and greener city set the speed limit to 20 mph (32.19 km h^{-1}) for local centres and residential roads (https://www.birmingham.gov.uk/info/50214/20mph_slower_is_safer/324/20mph_speed_limits_in_birmingham_slower_is_safer/2).

Regarding emissions at road junctions, the essential factors are the engine idling during the red-light period and the acceleration at the start of the green light period, both giving different emissions than driving at a constant speed. Speed near the junction is set to the lowest speed of 5 km h^{-1} as the averaging speed for the output concentration in one hour ((DEFRA, 2018). For idling vehicles at a bus stop, 5 km h^{-1} may be assumed as the speed of stationary traffic (DEFRA, 2018). For the data set of EFT v8.0 (7VC), the input setting in the model for the minimum speed is 5 km h^{-1}, and the maximum speed is 140 km h^{-1} (CERC, 2017). The assumptions regarding vehicle speed vary for different traffic conditions near junctions: 20 km h^{-1} is assumed for traffic congestion at busy junctions; an average speed of 40 to 45 km h^{-1} on a motorway close to the junction; and, for other junctions on main roads and at roundabouts, the assumption is 10 km h^{-1} slower than the average free-flowing speed (DEFRA, 2018).

Vehicle speeds are set on each road assuming that the road has light traffic, and speed at the junction is set at 5 km h^{-1}. The minimum vehicle speed configuration setting has been varied at 5 km h^{-1}, 8 km h^{-1} and 10 km h^{-1}. Next, the modelled NO_x concentration results from each configuration setting are compared and evaluated (see Figure 4.22 and Table 4.10).

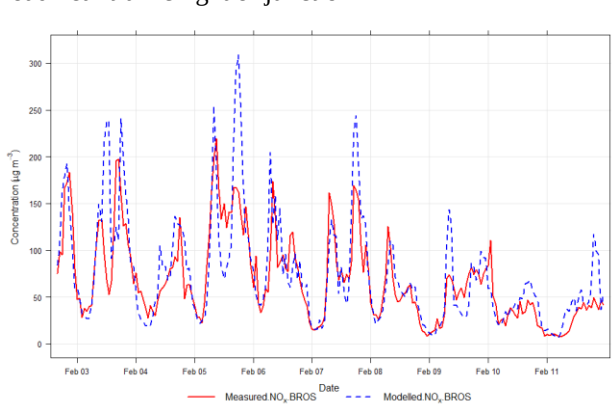
Table 4.9. Speed configurations and vehicles speed at each road

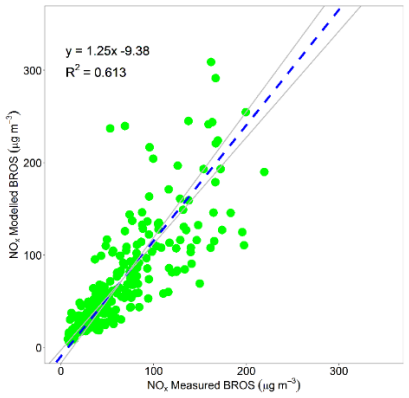
Road ID	**Road Segment**	**Road width (m)**	**Speed configuration setting**			**Information**
			Min 5 km h^{-1}	**Min 8 km h^{-1} (+3)**	**Min 10 km h^{-1} (+5)**	
			Vehicles speed (km h^{-1})	**Vehicles speed (km h^{-1})**	**Vehicles speed (km h^{-1})**	**Details of the road**
Road 1	Road 1a	15	15	18	20	
	Road 1b	10	15	18	20	
	Road 1c	9	10	13	15	Traffic light
	Road 1d	10	5	8	10	Near junction and traffic light
Road 2	Road 2a	12	5	8	10	Traffic light and junction
	Road 2b	15	5	8	10	
	Road 2c	19	5	8	10	Traffic light and junction
	Road 2d	19	5	8	10	
Road 3	Road 3a	12	5	8	10	Traffic light and junction
	Road 3b	9	10	13	15	
	Road 3c	7	10	13	15	
	Road 3d	6	10	13	15	
	Road 3e	6	5	8	10	Traffic light
	Road 3f	6	10	13	15	
	Road 3g	6	10	13	15	T junction

Road ID	Road Segment	Road width (m)	Speed configuration setting			Information
			Min 5 km h^{-1}	Min 8 km h^{-1} (+3)	Min 10 km h^{-1} (+5)	Details of the road
			Vehicles speed (km h^{-1})	Vehicles speed (km h^{-1})	Vehicles speed (km h^{-1})	
Road 4	Road 4a	6	20	23	25	
	Road 4b	6	10	13	15	T junction
Road 5	Road 5a	7	10	13	15	T junction
	Road 5b	6	15	18	20	
	Road 5c	6	10	13	15	Traffic light
	Road 5d	6	10	13	15	T junction
	Road 5e	5	15	18	20	
	Road 5f	6	15	18	20	
	Road 5g	6	10	13	15	T junction
Road 6	Road 6a	5	5	8	10	T junction
	Road 6b	10	10	13	15	
Road 7	Road 7a	12	10	13	15	
	Road 7b	10	10	13	15	
	Road 7c	9	8	11	13	Traffic light and junction
	Road 7d	8	10	13	15	
	Road 7e	8	8	11	13	Traffic light
	Road 7f	7	15	18	20	Junction
Road 8	Road 8a	7	15	18	20	Junction
	Road 8b	5	10	13	15	
	Road 8c	6	15	18	20	
	Road 8d	6	10	13	15	Junction

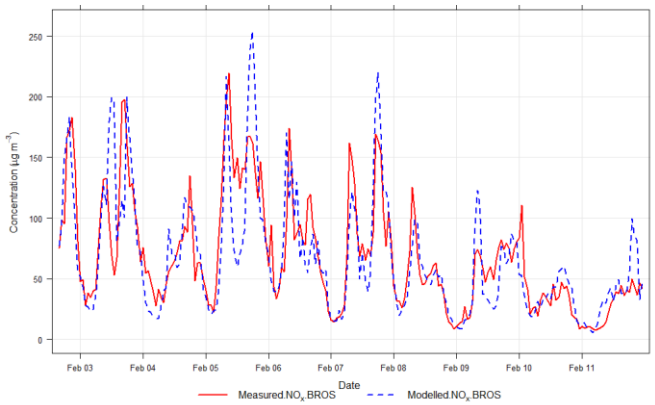
The speed at a traffic light or junction was set variously at 5km h^{-1}, 8 h^{-1}, and 10 $h^{-1,}$ as shown in Figure 4.22, to find the optimum result of NO_x concentrations at BROS by comparing the measured concentrations with the modelled concentrations.

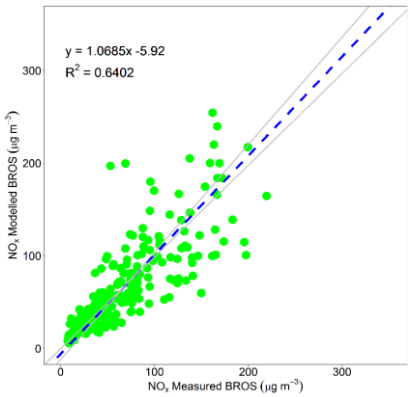
(a) NO_x concentration at BROS, set minimum 5 km h^{-1} at dense road near traffic light or junction



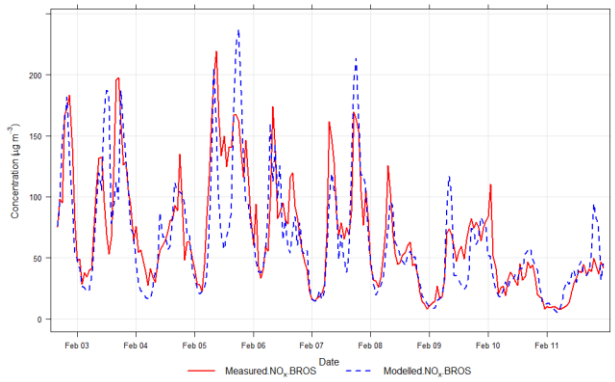


(b) NO_x concentration at BROS, set minimum 8 km h^{-1} at dense road near traffic light or junction





(c) NO_x concentration at BROS, set minimum 10 km h^{-1} at dense road near traffic light or junction



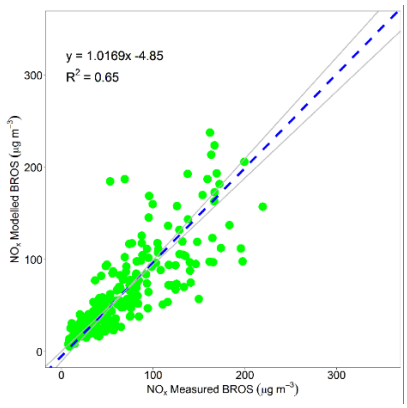


Figure 4.22. Comparison between measured NO_x concentrations (red line) and modelled NO_x concentrations (blue dash line) at BROS, and their linear regression from different settings for minimum speed at **(a)** 5 km h^{-1}, **(b)** 8 km h^{-1}, and **(c)** 10 km h^{-1}

Increasing the speed of vehicles in the modelling would decrease the emission of the pollutant. A setting of 10 km h^{-1} was chosen as minimum vehicle speed for the emissions input in the model.

Table 4.10. Model evaluation of different vehicle minimum speeds

Setting minimum vehicle speed	Pollutant	Measured mean (µg m^{-3})	Modelled mean (µg m^{-3})	SD Measured	SD Modelled	FB (Fractional Bias)	NMSE	R	R^2
5 km h^{-1}	NO_x BROS	69.01	76.88	46.62	58.28	-0.11	0.012	0.78	0.61
8 km h^{-1}	NO_x BROS	69.01	67.81	46.62	49.82	0.02	0.000	0.80	0.64
10 km h^{-1}	NO_x BROS	69.01	65.32	46.62	47.41	0.05	0.003	0.80	0.64

The next step is to review the outcome of modelled NO_2 concentrations at BROS with observed NO_2 concentrations. Figure 4.23 shows NO_2 measured and NO_2 modelled concentrations at BROS site when speed of vehicles was set with a minimum at 10 km h^{-1}.

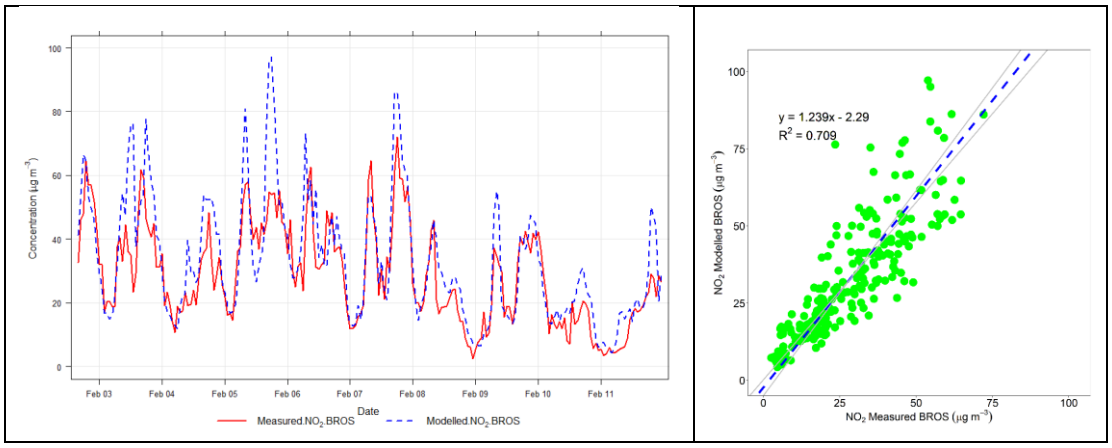


Figure 4.23. Measured NO_2 concentrations (red line) and modelled NO_2 concentrations (blue dash line) at BROS and the linear regression from speed setting at 10 km h^{-1}

The model only calculates NO_x level from traffic data and using NO_2-NO_x correlation to calculate NO_2 level (Šereviciene and Paliulis, 2011). The default setting of the NO_2:NO_x ratio in the model was 23.8% (CERC. 2017); however, as shown by Figure 4.23, modelled NO_2 concentration at BROS was higher than the measured concentrations. Therefore, sensitivity analysis using different NO_2:NO_x ratios - 10%. 15% and 20% - were carried out to determine the best setting of NO_2:NO_x ratios for a good comparison between modelled and observed NO_2 concentrations.

4.3.3.4. Sensitivity to NO_2:NO_x ratio

Cyrys *et al*. (2012) reviewed the NO_2:NO_x ratio in Europe and found that the ratio increases near urban traffic areas in accordance with the increasing primary emissions of NO_2. They found high correlation between NO_2 to NO_x in 36 European countries (R^2 in between 0.81 – 0.97). The increasing NO_2:NO_x varies between cities due to the difference in primary NO_2 in the area (Mavroidis and Ilia, 2012). The primary NO_2:NO_x ratio in Hong Kong was found to be in the range of 10-30% (Yao *et al.*, 2005). Yao *et al*. (2005) investigated the primary NO_2:NO_x ratio in Hong Kong using road tunnels and found that, where O_3 levels were high, the NO_2:NO_x ratio reached 19% and up to 28%. In London, Carslaw *et al*. (2016) found that there has been a decrease in NO_2:NO_x ratio in inner London from 25% (in year 2010) to 15% in 2014, due to the reduction of NO_2 emitted directly from heavy-duty vehicles, buses

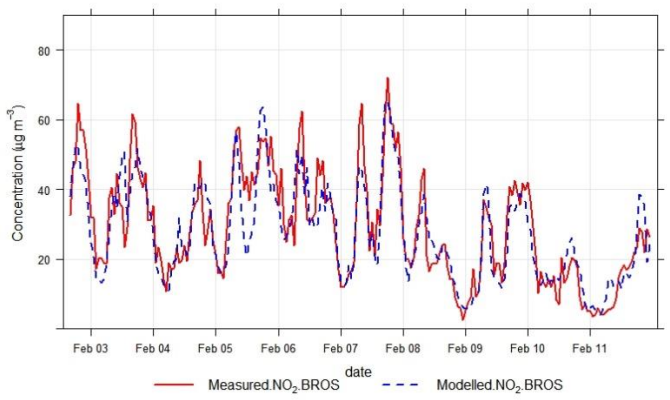
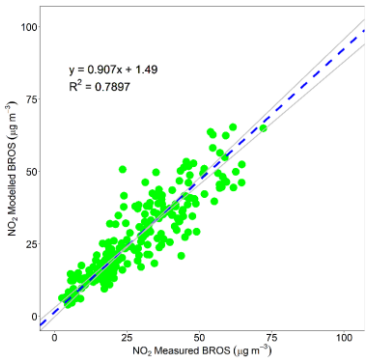
and diesel passenger cars. Matthaios *et al*. (2019) recently evaluated the primary NO_2:NO_x ratio from monitoring sites in the UK during the period 2009-2016 and showed that the NO_2:NO_x ratio in London reduced from 15% to 10% (taken from four monitoring sites near the road and two background sites). In Birmingham, NO_2:NO_x ratio declined from 20% to 10% (taken from Birmingham Tyburn roadside and Birmingham Tyburn site).

Monitoring data of automatic analysers from BROS and EROS, as shown in Table 4.2, were used to quantify the NO_2:NO_x ratio. The primary NO_2 at the University of Birmingham site was 14%. In the ADMS-Roads model, we reviewed the NO_2:NO_x setting to get the best output of modelled NO_2 concentration. The default NO_2:NOx ratio in the model can be changed by changing the emission rates of NO_2 in each road as shown in Table 4.11. Emission rate is expressed in g km^{-1} s^{-1} and obtained from traffic data or from emission inventories.

Table 4.11. Example. emission rate at road 2 (A38 road) from baseline setting and 15% setting for NO_2:NO_x ratio

Pollutant	Emission rate (g km^{-1} s^{-1}), baseline					Emission rate (g km^{-1} s^{-1}), setting 15% for NO_2:NOx ratio			
	Road 1a	Road 1b	Road 1c	Road 1d		Road 1a	Road 1b	Road 1c	Road 1d
NO_x	0.0963	0.0963	0.1074	0.1243		0.0963	0.0963	0.1074	0.1243
PM_{10}	0.0074	0.0074	0.0075	0.0077		0.0074	0.0074	0.0075	0.0077
$PM_{2.5}$	0.0044	0.0044	0.0045	0.0046		0.0044	0.0044	0.0045	0.0046
VOC	0.0076	0.0076	0.0088	0.0104		0.0076	0.0076	0.0088	0.0104
NO_2	0.0275	0.0275	0.0304	0.0346		0.0144	0.0144	0.0161	0.0186
NO_2:NOx ratio	*28.60*	*28.60*	*28.32*	*27.86*		*15.00*	*15.00*	*15.00*	*15.00*

In this study, to find the optimum modelled NO_2 concentration, the NO_2:NO_x ratio was set at 10%, 15%, and 20%.

NO_2:NO_x Ratio	**Graph of NO_2 observation and NO_2 modelled at BROS**	
10%		

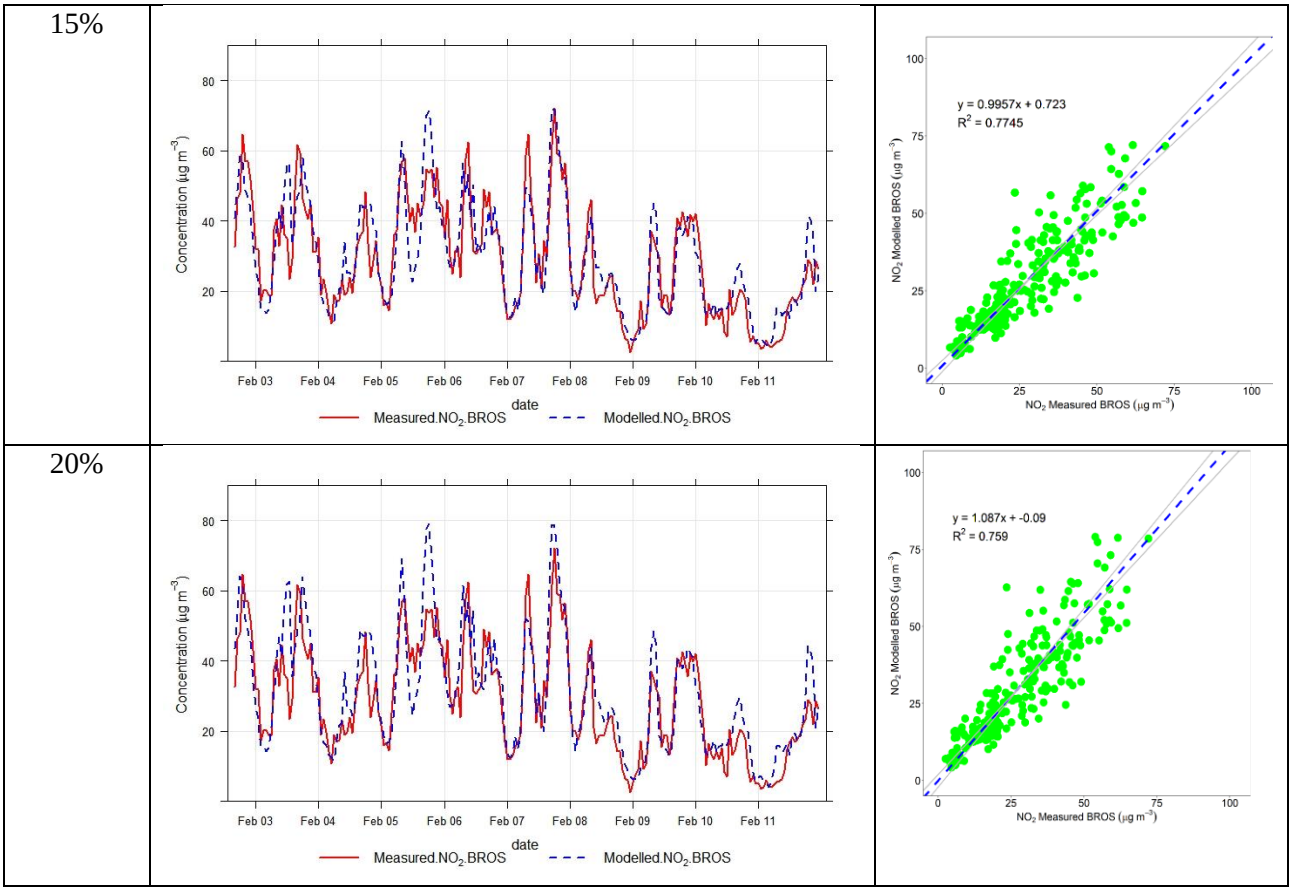


Figure 4.24. Comparison between measured NO_2 concentrations (red line) and modelled NO_2 concentrations (blue dash line) at BROS, and their linear regression from different settings for the NO_2:NO_x ratio at **(a)** 10% , **(b)** 15% , and **(c)** 20%

Table 4.12. Model evaluation of different settings for the NO_2:NOx ratio

Setting NO_2:NOx ratio	Pollutant	Measured mean (µg m^{-3})	Modelled mean (µg m^{-3})	SD Measured	SD Modelled	FB (Fractional Bias)	NMSE	R	R^2
10 %	NO_2 BROS	28.95	27.74	15.61	14.16	0.04	0.002	0.89	0.79
15 %	NO_2 BROS	28.95	29.55	15.61	15.55	-0.02	0.000	0.88	0.77
20 %	NO_2 BROS	28.95	31.37	15.61	16.97	-0.08	0.006	0.87	0.76

From Table 4.12, NO_2 concentration results at the BROS site show changes due to adjustment of NO_2:NO_x ratio. The adjustment of the NO_2:NO_x ratio improves FB and NMSE, especially for setting a 15% adjustment. The impact of the adjusted NO_2:NO_x ratio leads to a higher average NO_2 concentration and reduces the FB from 0.04 (10% NO_2:NO_x) and -0.08 (20% NO_2:NO_x) to -0.02 (15% NO_2:NO_x). and NMSE from 0.002 (10% NO_2:NO_x) and 0.006 (20% NO_2:NO_x) to 0.000 (15% NO_2:NO_x).

The NO_2:NO_x ratio selected in the model is 15% based on the evaluation results of FB and NMSE. This value of the ratio from the sensitivity analysis result is slightly similar to the result of the calculation of primary NO_2 from measurement data at approximately 14%.

4.3.3.5. Sensitivity to the deposition velocity

Sensitivity tests were conducted to assess the effect of dry deposition velocity on the reduction of NO_x, NO_2 and O_3 concentrations. NO_x deposition velocities in the range of 0.001 to 0.0067 m s^{-1} were set in the ADMS-Roads model and deposition velocities for NO_2 and O_3 were set in the same values, 0.002 m $s^{-1}$and 0.004 m s^{-1}, respectively.

It can be seen in Figure 4.25 that with increasing NO_x deposition velocity from 0.001 to 0.0067 m s^{-1}, the percent reduction concentration of NO_x will increase from 0.5% to 2.7%, and the percent reduction concentration of NO_2 will increase from 0.4% to 1.5%. In contrast, for O_3, the percent reduction concentration of O_3 will decrease from 0.1% to 0.9%. In other words, increasing the NO_x deposition velocities will decrease the NO_x and NO_2 concentrations, but will also slightly increase the O_3 concentration.

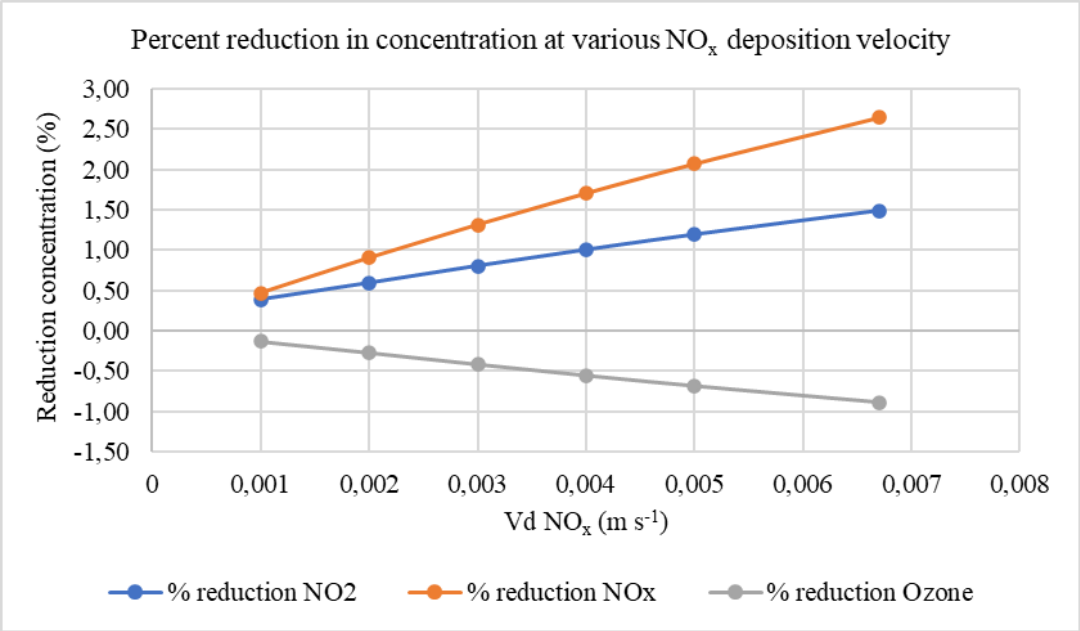


Figure 4.25. Percent reduction of NO_x (orange dotted line), NO_2 (blue dotted line) and O_3 (grey dotted line) concentrations at various settings of NO_x deposition velocities (0.001 to 0.0067 m s^{-1}) and at the same value of NO_2 and O_3 deposition velocities, 0.002 m s^{-1} and 0.004 m s^{-1}, respectively

The modelling results showed that increasing the NO_x deposition velocity from 0.001 to 0.0067 m s^{-1} would increase the percent reduction concentrations of NO_x and NO_2 in a range of 0.5% to 2.7%, and 0.4% to 1.5%, respectively. This result is in line with research from Xing and Brimblecombe (2019) which found that the concentration of pollutants removed from the air through the deposition process was less than 2%. However, Tiwari and Kumar (2020) studied the dispersion and deposition processes in green infrastructure using ADMS-Urban software and concluded that the deposition process was the most influential process on an urban scale.

Tiwari and Kumar (2020) evaluated the effects of deposition and dispersion in reducing pollutant concentrations on an urban scale in Guildford, UK. They simulated eight green infrastructure scenarios using three different types of vegetation — coniferous trees, deciduous trees, and grassland — over available land and traffic line areas. They used ADMS-Urban and set different values of surface roughness based on type of land cover (trees, grassland, etc.) when simulating the scenarios. Pollutant concentrations were decreased by increasing the surface roughness due to increasing the atmospheric turbulence (Barnes et al., 2014). Tiwari and Kumar (2020) found the effect due to dispersion and deposition processes was to reduce the annual pollutant concentrations by up to 35% in NO_x, 21% in PM_{10} and 8% in $PM_{2.5}$, while for the dispersion processes, the percentage reduction of annual pollutant concentrations reached 10% in NO_x, 1% in PM_{10} and 0.8% in $PM_{2.5}$. This shows that the deposition process was more effective than dispersion process in reducing pollutant concentrations on an urban scale.

Overall, our result and the finding from Tiwari and Kumar (2020) are not contradictory, because we investigated the dispersion and deposition processes at the micro scale, whereas Tiwari and Kumar (2020) examined these effects at the urban scale over different scenarios of green infrastructure.

4.3.4. Modelling output

4.3.4.1. Automatic analyser at BROS and EROS, 2-11 February 2018

Figure 4.26 provides a summary of model performance for hourly data gathered using the automatic analyser for the period 2-11 February 2018. The modelled concentration of NO_x and NO_2 was in good agreement with measured data at BROS and EROS, indicating that ADMS-Roads was reliable in predicting NO_x and NO_2 concentrations.

The model was using weather data from Winterbourne No.2 and pollutant (NO_x, NO_2, O_3) concentrations data from EROS monitoring site as background concentration. In emission data, the NO_2:NO_x emission ratio was set at 15%, and speed of vehicles at the major roadside was set to a minimum 10 km h^{-1}.

Agreement between model output and observations is identified by statistical evaluation results as shown in Table 4.13. For the perfect model, the value of FB and NMSE should be close to 0, and the value of R and R^2 should be close to 1.

Table 4.13. Statistical evaluation of measured and modelled concentrations

Pollutant	Measured mean (μg m^{-3})	Modelled mean (μg m^{-3})	SD Measured	SD Modelled	FB (Fractional Bias)	NMSE	R	R^2
NO_2 BROS	28.95	29.55	15.61	15.55	-0.02	0.000	0.88	0.77
NO_x BROS	69.01	67.81	46.62	49.82	0.02	0.000	0.82	0.67
NO_2 EROS	19.33	20.22	10.46	10.58	-0.05	0.002	0.99	0.98
NO_x EROS	24.1	25.08	17.62	17.65	-0.04	0.002	0.99	0.98

The statistical analysis that was conducted for the modelled NO_2 and NO_x at BROS and EROS revealed that the modelled NO_2 and NO_x at EROS was more accurate than for the BROS. ADMS-Roads provided a good prediction of modelled concentration with 67% of the variance in the data explained by the model for NO_x concentrations near road (BROS) and over 98% of the variance in the data explained by the model for NO_x concentrations at the urban background site (EROS). The difference of NO_x and NO_2 concentrations between measured and modelled was up to 1.2 μg m^{-3}, and 0.9 μg m^{-3} respectively.

A summary graph of the regression between the measured and modelled concentrations at BROS and EROS on 2-11 February 2018 is shown in Figure 4.26.

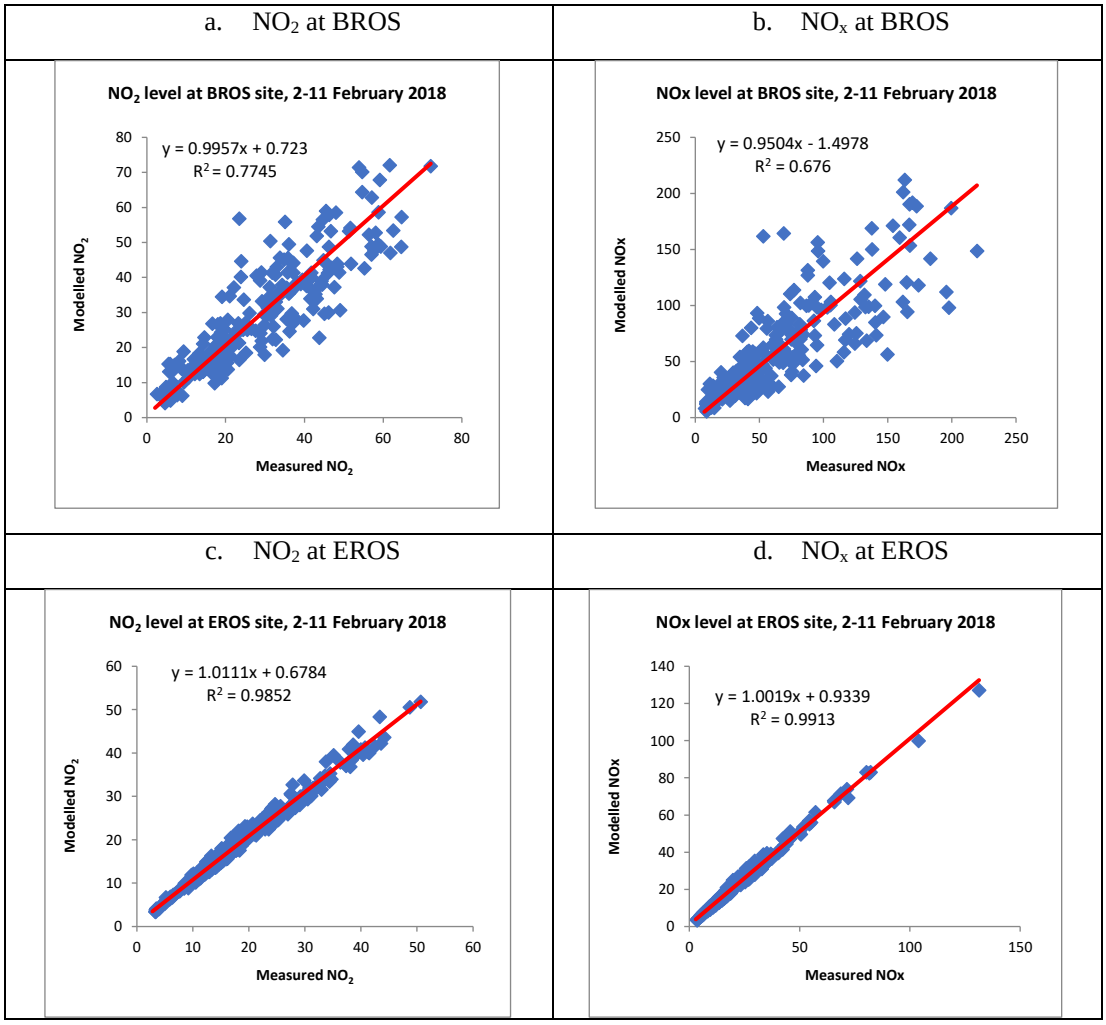


Figure 4.26. Graph of measured and modelled concentrations of NO_2 and NO_x at BROS and EROS sites

Figure 4.27 shows a wind rose plot from the sampling period. Wind directions were coming from SSW (south-southwest), W (west), NW (northwest) and NE (northeast). Wind speed was in the range 0.1 m s^{-1} to 4.4 m s^{-1}, and the average speed was 1.8 m s^{-1}.

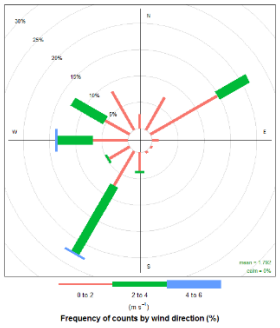


Figure 4.27. Wind rose pattern from the sampling period 2-11 February 2018

Dry Deposition

Sampling data for the period 2-11 February 2018 using automatic analyser was also used to review the implementation of dry deposition velocity in improving the air quality. The results are presented in Figures 4.28 to 4.30.

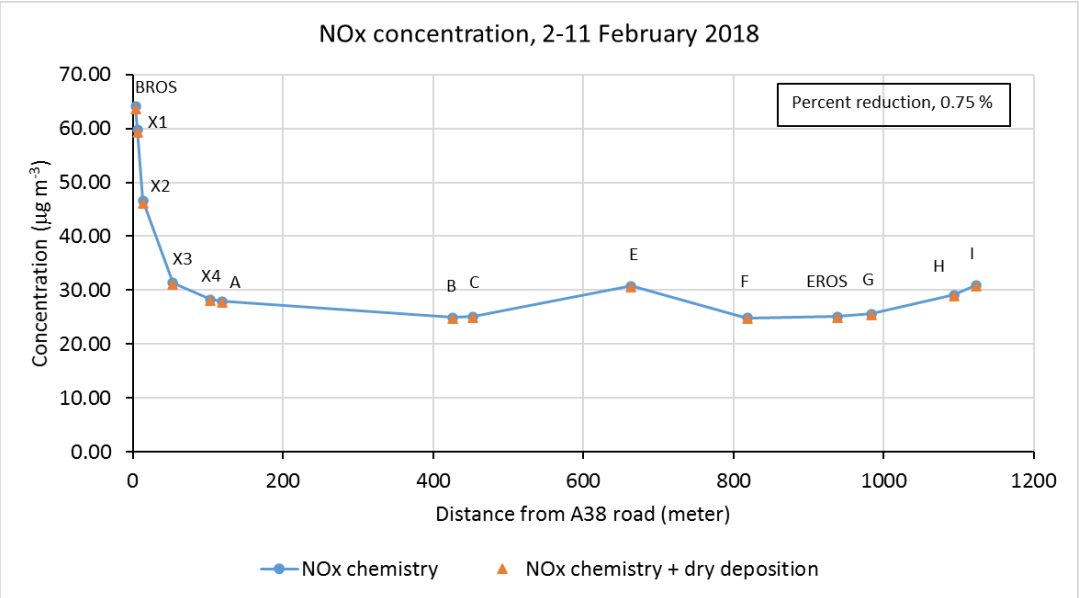


Figure 4.28. Modelled NO_x concentration at perpendicular location from chemistry (blue line) and chemistry with dry deposition model (orange triangle), 2-11 February 2018

NO_x concentration was higher near the traffic road compared to urban background levels. The highest concentration of modelled NO_x was at the BROS site, location of the heavy traffic, the A38 road. The ADMS-Roads model showed NO_x concentration reduced significantly at the distance of ± 50 metres and continued to decline to background level, as shown in Figure 4.28.

The wind was predominantly blowing from southwest, dispersing pollutants from the A38 major road (BROS) to the northeast. It is expected that NO_x and NO_2 concentrations reduce from BROS to EROS. Moreover, there was wind coming from the northeast, which would disperse pollutant concentrations from I site (near Edgbaston Park Road and Somerset Road) further to the background site (EROS).

In terms of the deposition process, there was a reduction in the concentration by 0.8% according to the model of dry deposition.

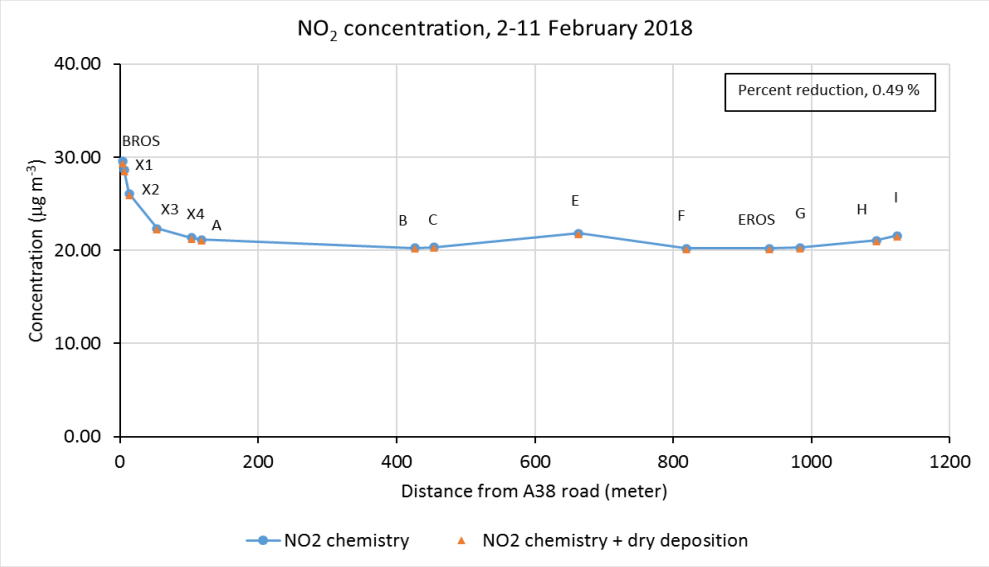


Figure 4.29. Modelled NO_2 concentration at perpendicular location from chemistry (blue line) and chemistry with deposition model (orange triangle), 2-11 February 2018

In Figure 4.29, higher concentrations of NO_2 can be seen near traffic road A38 (BROS). NO_2 concentration at the BROS site was around 30 µg m^{-3} and the lowest concentration at the urban background site was 20 µg m^{-3}. NO_2 decreased sharply to background level at a distance of 100 metres from the road. According to the model of dry deposition, the NO_2 concentration at the UoB site was reduced by up to 0.5%.

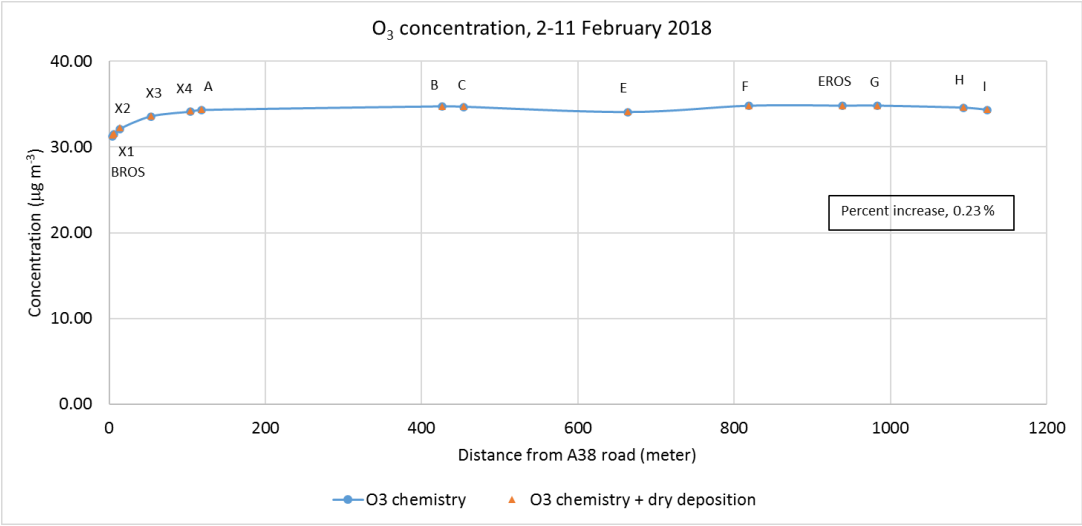


Figure 4.30. Modelled O_3 concentration at perpendicular location from chemistry (blue line) and chemistry with deposition model (orange triangle), 2-11 February 2018

O_3 concentrations increased with distance from the roadside and in inverse relation to the NO_x level. NOx emissions scavenge O_3 at the roadside. The O_3 gradient concentration shows the evidence of reaction between NO and O_3 that produce NO_2, thus reducing the O_3 level near the road. With the lowering NO_x concentration by the process of dry deposition, O_3 concentration was slightly increased by up to 0.2%.

Overall, the modelled output from the ADMS-Roads model was in good agreement with the measurements. The model results revealed greatest NO_x and NO_2 concentrations near the heavy traffic road, and the trend was the opposite with O_3 concentrations which were found to be lower near the roadside. Including or excluding the dry deposition process in the model does not affect the prediction of NO_x and NO_2 levels — the contribution of the deposition process is less than 1% in improving the air quality in the green area.

4.3.4.2. Diffusion tubes modelling results

Figure 4.31 shows the road sources (blue line) and receptors (green square) at the University of Birmingham from ADMS-mapper.

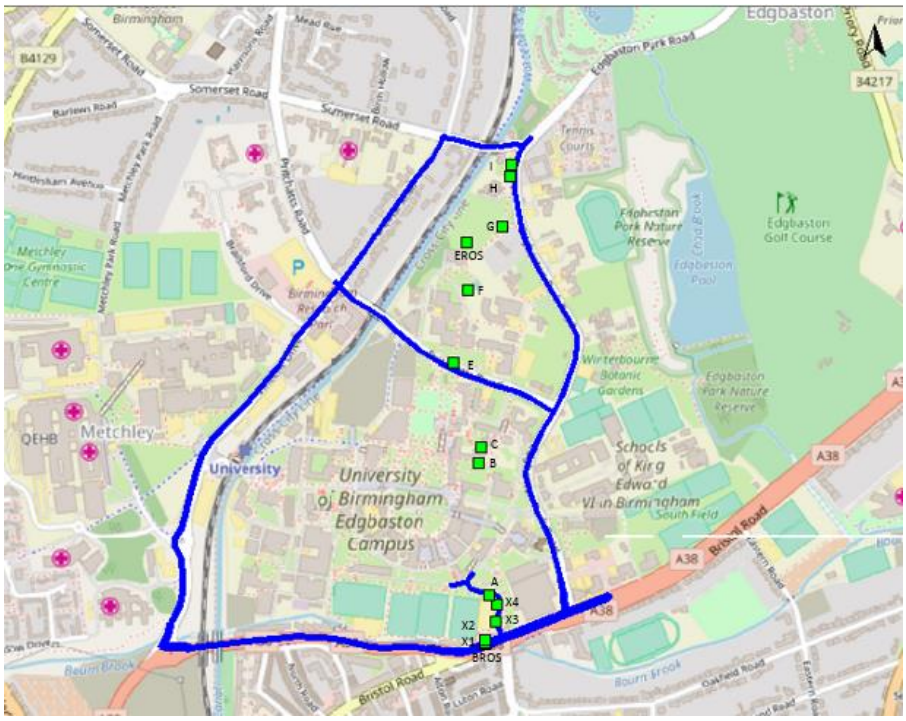


Figure 4.31. Road sources and receptors at University of Birmingham as shown by ADMS Mapper. The blue line identifies the road sources, and green squares identify the receptors, where diffusion tubes were located.

The BROS location is in the southwest area, and the closest emission source comes from the A38 road, while EROS is a background site, and the pollutants come from many roads in the surrounding area. The receptor near Pritchatts Road is E site, and H and I are the receptors near the Edgbaston Park Road and Somerset Road. Overall, the receptor points near the roads were BROS, X1 to X4, A, E, H, and I.

Diffusion tube NO_2 samples deployed at UoB sites for the following dates were reviewed:

1) 18 March – 15 April 2018
2) 15 April – 13 May 2018
3) 21 October – 20 November 2018
4) 20 – 28 November 2018
5) 28 November 2018 – 6 January 2019

Meteorological data and background ambient concentrations were entered into the model as input data based on the DT exposure time, and the model was run with the LT output to obtain the average modelled concentration; then the results were compared with the measured DT concentration.

The meteorological inputs used in this model were parameters WD, WS, T, RH and cloud cover parameters from three weather stations — Winterbourne No.2, Coundon, and Coleshill. Temperature and relative humidity were acquired from Winterbourne No.2. Some data for wind speed and wind direction were derived from Winterbourne No.2 and the missing data was filled from the Coundon weather station. Cloud cover data was taken from Coleshill weather station. A wind speed correction factor was needed when inserting the data for wind speed from Coundon weather station using the equation, $x = (y - 0.5464) / 1.5101$. For background concentrations, NO_2, NO_x and O_3 concentrations from the nearest air monitoring station (EROS and Birmingham Acocks Green) were used as background ambient inputs.

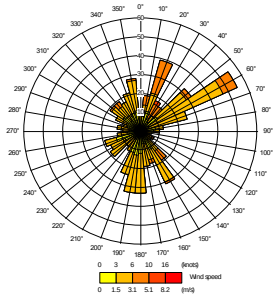
To compare the DT results with the modelling results, a single adjustment method based on linear regression (see Section 4.2.1.2) was used as an approach to improve the accuracy of modelled concentrations. The adjustment of NO_2 was conducted and this value of NO_2 along with NO_x and O_3 concentration were inserted in the model as input of background concentrations.

When using linear regression between measured NO_2 DT (µg m^{-3}) and modelled NO_2 (µg m^{-3}) to compare data — for example, as shown in Figure 4.32 — the first regression equation is identified as Y1 (f). A slope with a value of 1 is indicative of a perfect model. The intercept is related to background concentration, and this intercept indicates the difference between the emissions near the road and the background site.

Intercept value in Y1 (f) equation is used to adjust the background concentration when running the model for a second time. Modelled NO_2 concentrations from the output result were compared with measured DT, as shown in the second graph (h) and a new regression line equation established as Y2 (i).

Figures 4.32 to Figure 4.36 present the modelled NO_2 concentrations compared with the measurement from passive diffusion tubes.

1) 18 March – 15 April 2018

(a) Background concentration from automatic analysers (in ppb)	(b) Wind rose
NO_x = 20.92 ppb NO_2 = 12.86 ppb O_3 = 24.24 ppb Automatic analyser data from EROS site, UoB	

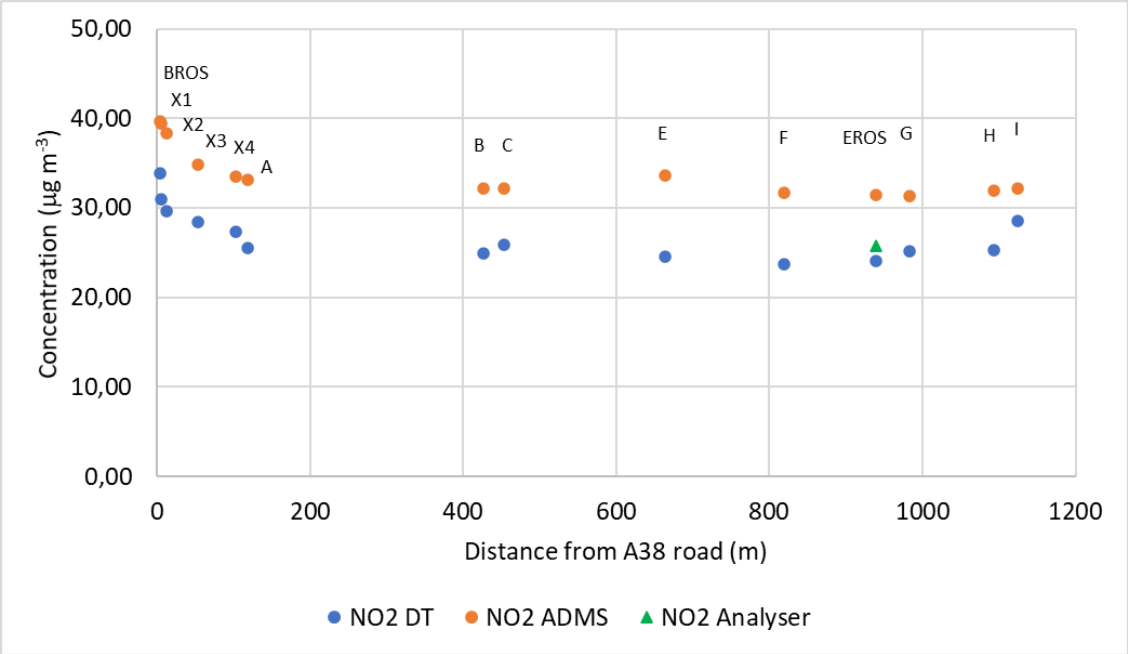
(c) Meteorological data

Parameter	N	% data from Winterbourne No. 2	% data from Coundon	% data from Coleshill
Wind direction	960	27.9 %	72.1 %	
Wind speed	960	27.9 %	72.1 %	
Temperature	960	72.6 %	27.4 %	
Relative Humidity	960	72.6 %	27.4 %	
Cloud cover	960			100 %

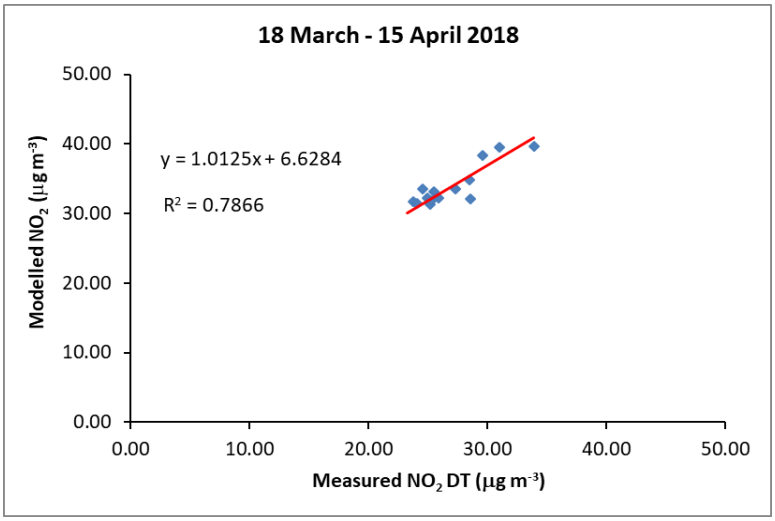
(d) Background concentration input in the model at the first run (in ppb)

NO_x = 20.92 ppb
O_3 = 24.24 ppb
NO_2 background data = 12.86 ppb = 25.75 µg m^{-3}

(e) Graph of modelled NO_2 concentration (from first run of model), measured NO_2 from DT and NO_2 concentration from analysers with distance from A38 roadside at receptor locations



(f) Regression line and the equation from measured NO_2 DT and modelled NO_2 concentration



Y1 = 1.01x + 6.63

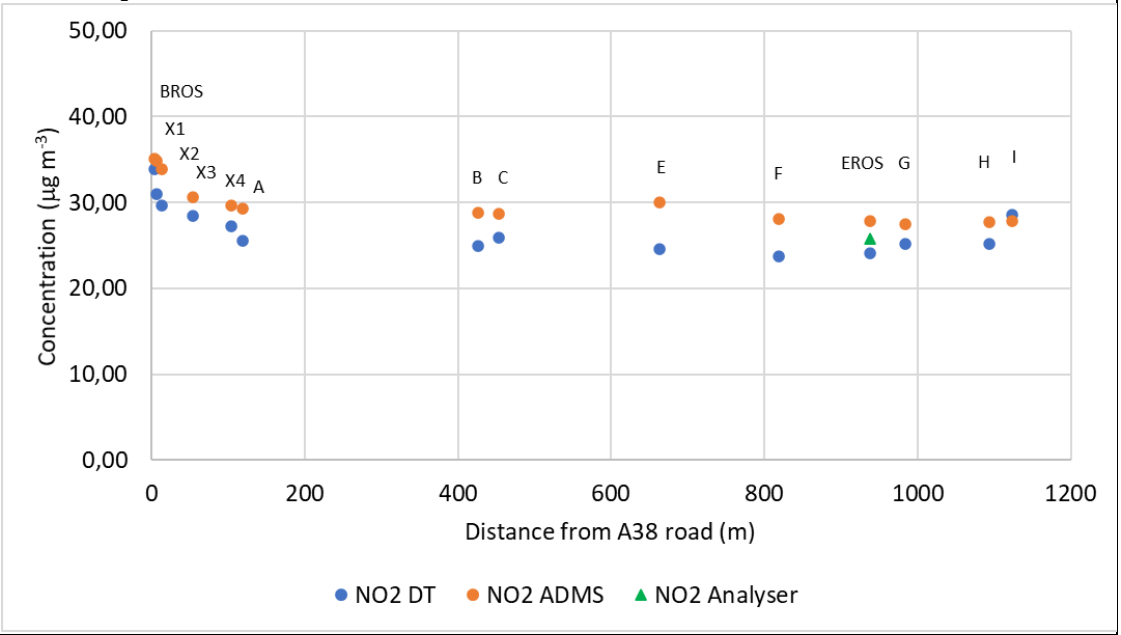
R^2 = 0.78

(g) Adjusted NO_2 background concentration

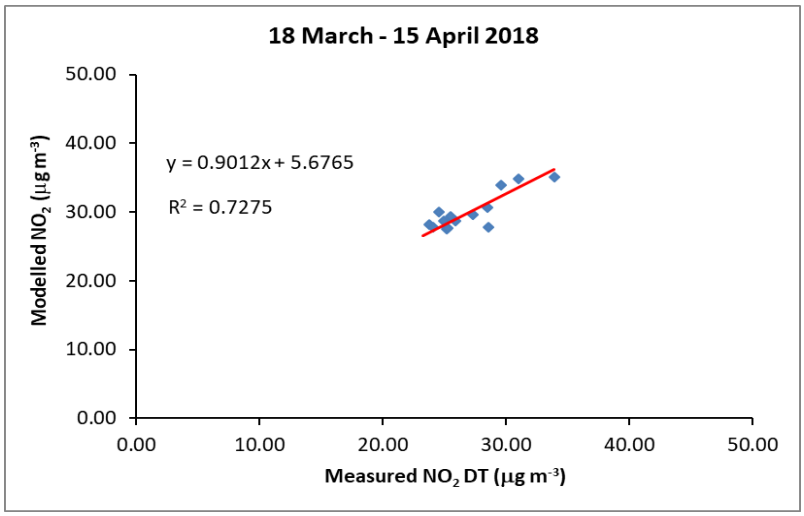
NO_2 background data in the model = 25.75 – 6.63 = 19.12 µg m^{-3}

= 9.56 ppb

(h) Graph of modelled NO_2 concentration (from second run of model), measured NO_2 from DT and NO_2 concentration from analysers with distance from A38 roadside at receptor locations



(i) Regression line and the equation from measured NO_2 DT and modelled NO_2 concentration



Y2 = 0.90x + 5.68

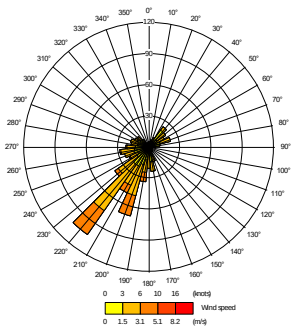
R^2 = 0.73

Figure 4.32. Modelled and measured NO_2 concentration from diffusion tube data, 18 March – 15 April 2018. This table shows **(a)** information of background concentration from automatic analysers from EROS; **(b)** wind rose from meteorology data; **(c)** information of meteorology data input; **(d)** background concentration input in the model at the first run, and conversion unit of NO_2 concentration from ppb to µg m^{-3}; **(e)** graph of modelled NO_2 concentration from first run of model, measured NO_2 DT and NO_2 from analyser at EROS; **(f)** regression line and equation from measured NO_2 DT and modelled NO_2 concentration from first run; **(g)** adjusted NO_2 background concentration; **(h)** graph of modelled NO_2 concentration from second run of model, measured NO_2 DT and NO_2 from analyser at EROS; **(i)** regression line and equation from measured NO_2 DT and modelled NO_2 concentration from second run.

In this sampling period (Figure 4.32), the wind rose data was obtained from Winterbourne No.2 (27.9%) and Coundon weather station (72.1%). The wind predominantly was from the south and southeast directions but it was not as strong as the north-easterly direction. The winds blew mostly from the northeast direction (ENE, NNE), from Edgbaston Park Road and Somerset Road, and dispersed the pollutant in the southwest direction. Therefore, high pollutant concentrations were expected at BROS situated in the southwest direction due to pollutant dispersion from ENE and the low wind from SW. However, 35% of wind was coming from the south at speeds between 2.1 and 5.1 m s^{-1} which dispersed pollutants into the northerly direction thereby decreasing pollutant concentration at BROS and in areas further away from BROS.

The model overestimates NO_2 concentrations. Application of the single adjustment method could change the magnitude of the concentration but does not change the trend of the level. The modelled NO_2 concentrations decrease when using the single adjustment method and demonstrate a good agreement with DT measured data due to the reduction of NO_2 background concentration.

2) 15 April – 13 May 2018

(a) Background concentration from automatic analysers (in ppb)	(b) Wind rose
NO_x = 18.11 ppb NO_2 = 10.28 ppb O_3 = 32.08 ppb Automatic analyser data from EROS site, UoB	

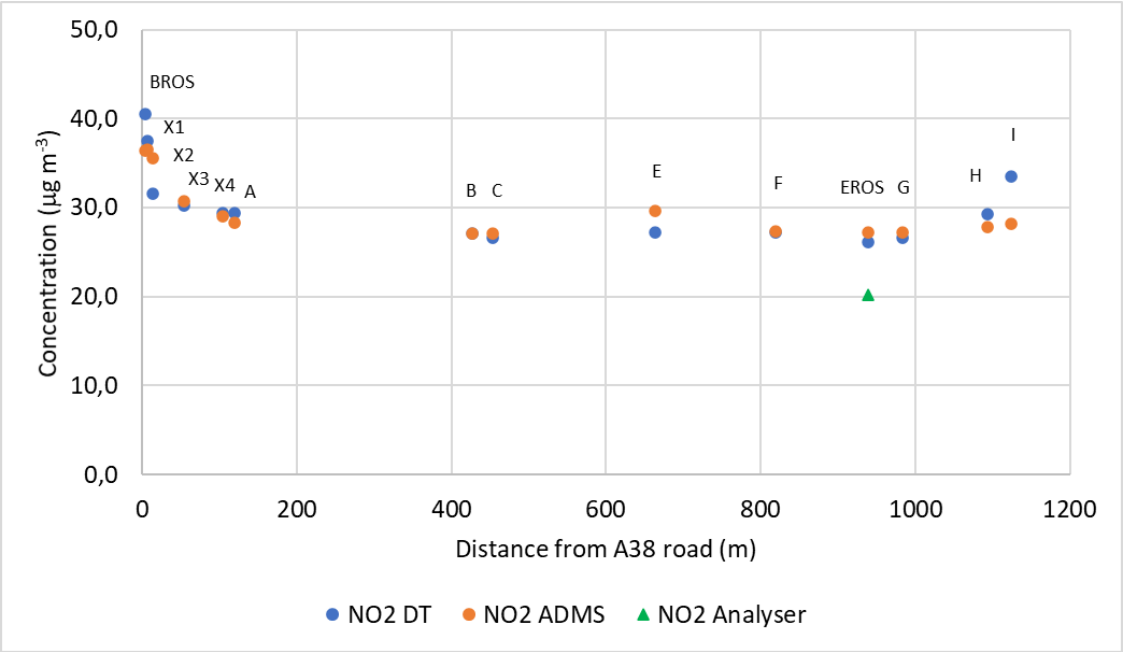
(c) Meteorological data

Parameter	N	% data from Winterbourne No. 2	% data from Coleshill
Wind direction	696	100 %	
Wind speed	696	100 %	
Temperature	696	100 %	
Relative Humidity	696	100 %	
Cloud cover	696		100 %

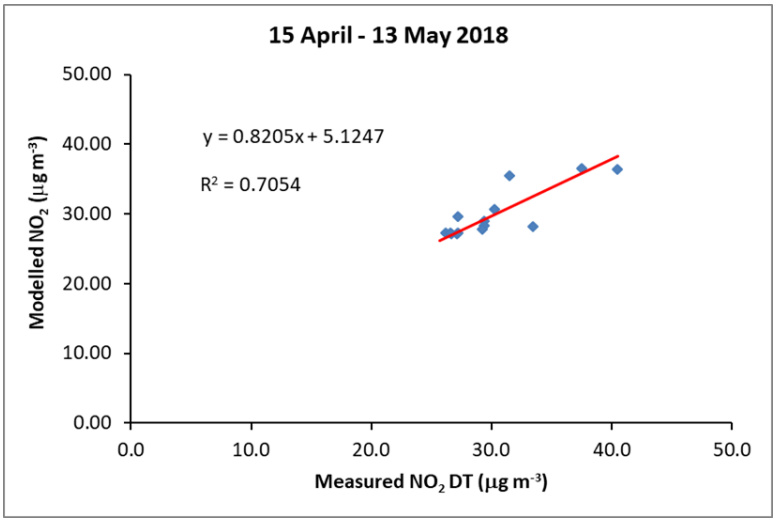
(d) Background concentration input in the model at the first run (in ppb)

NO_x = 18.11 ppb
O_3 = 32.08 ppb
NO_2 background data = 20.26 µg m^{-3}
= 10.28 ppb

(e) Graph of modelled NO_2 concentration (from first run of model), measured NO_2 from DT and NO_2 concentration from analysers with distance from A38 roadside at receptor locations



(f) Regression line and the equation from measured NO_2 DT and modelled NO_2 concentration



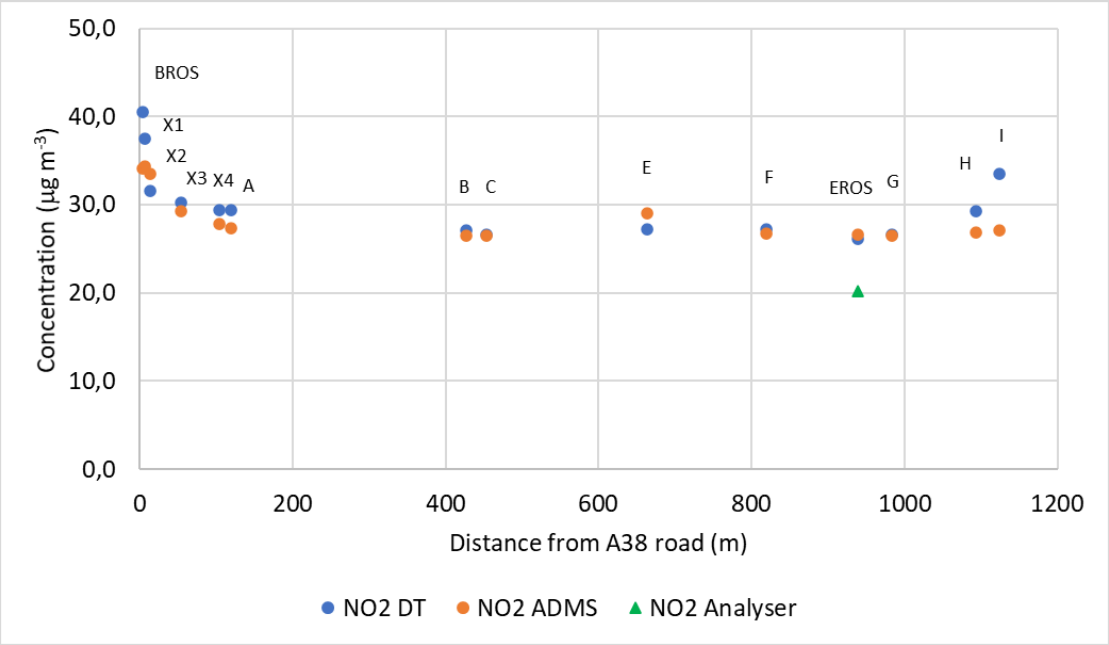
Y1 = 0.82x + 5.12

R^2 = 0.71

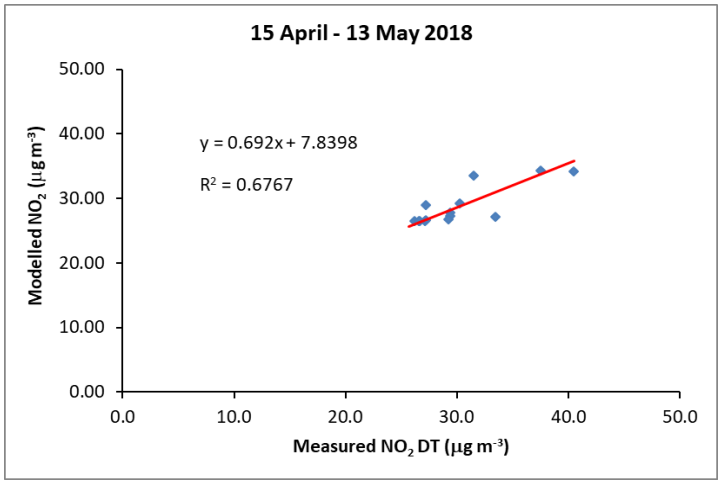
(g) Adjusted NO_2 background concentration

NO_2 background data in the model = 20.26 – 5.12 = 15.14 µg m^{-3}
= 7.68 ppb

(h) Graph of modelled NO_2 concentration (from second run of model), measured NO_2 from DT and NO_2 concentration from analysers with distance from A38 roadside at receptor locations



(i) Regression line and the equation from measured NO_2 DT and modelled NO_2 concentration



Y2= 0.69x + 7.84

R^2 = 0.68

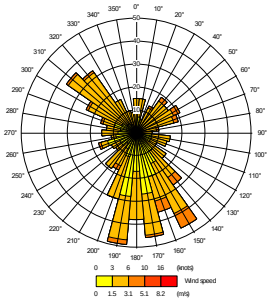
Figure 4.33. Modelled and measured NO_2 concentration from diffusion tube data, 15 April – 13 May 2018. This table shows **(a)** information of background concentration from automatic analysers from EROS; **(b)** wind rose from meteorology data; **(c)** information of meteorology data input; **(d)** background concentration input in the model at the first run, and conversion unit of NO_2 concentration from ppb to µg m^{-3}; **(e)** graph of modelled NO_2 concentration from first run of model, measured NO_2 DT and NO_2 from analyser at EROS; **(f)** regression line and equation from measured NO_2 DT and modelled NO_2 concentration from first run; **(g)** adjusted NO_2 background concentration; **(h)** graph of modelled NO_2 concentration from second run of model, measured NO_2 DT and NO_2 from analyser at EROS; **(i)** regression line and equation from measured NO_2 DT and modelled NO_2 concentration from second run.

In this period, the wind was blowing from southwest to northeast. Pollutants disperse from BROS to the background sites (Figure 4.33). NO_2 concentrations decrease sharply from BROS near the road to further distances up to 100 metres and become somewhat stable at the background sites then slightly increase near the Pritchatts Road (E site) and near Edgbaston Park Road and Somerset Road (I site). There were different results between modelled and measured data at the I site. The NO_2 concentration from DT measurements at site I near Somerset Road was elevated, but the modelled concentration was flat. This could be related to the effect of local emissions during the sampling period which were not accounted for well by the model.

NO_2 concentrations fell more than 10% from BROS, located near the road, at a distance of 100 metres. This could, therefore, be a distance criterion for a park boundary — to be at least 100 metres from a busy road.

NO_2 modelled concentrations mostly present good agreement with measured DT data. This could be related with the best input when using 100% of wind speed and wind direction from Winterbourne No.2 and background concentration from the EROS site.

3) 21 October – 20 November 2018

(a) Background concentration from automatic analysers (in ppb)	(b) Wind rose
NO_x = 12.82 ppb NO_2 = 10.35 ppb O_3 = 20.64 ppb Automatic analyser data from Bioscience site, UoB	

(c) Meteorological data

Parameter	N	% data from Winterbourne No. 2	% data from Coundon	% data from Coleshill
Wind direction	744		100 %	
Wind speed	744		100 %	
Temperature	744	100 %		
Relative Humidity	744	100 %		
Cloud cover	744			100

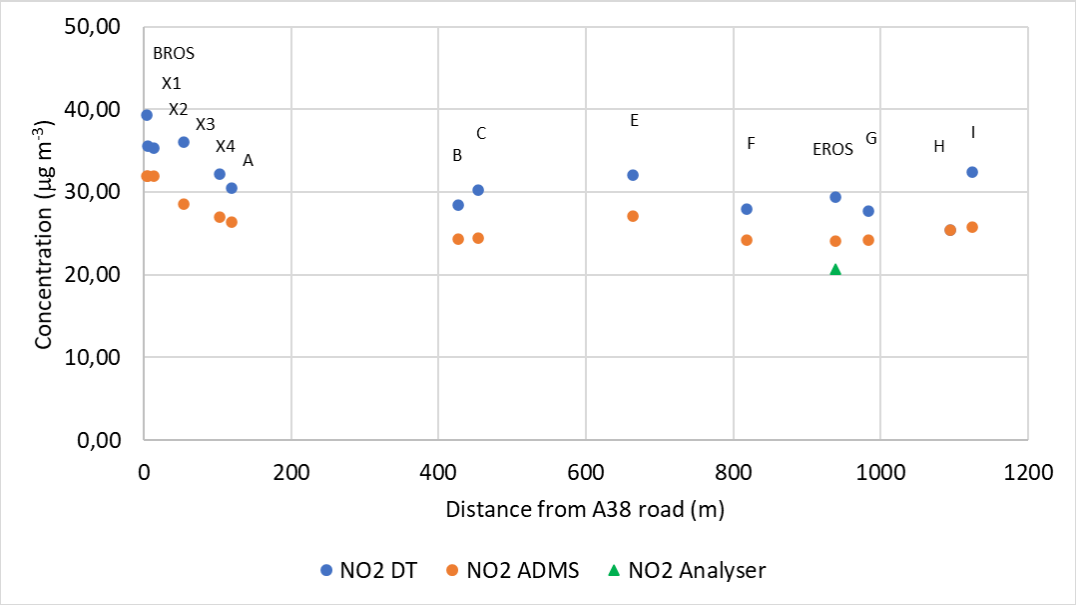
(d) Background concentration input in the model at the first run (in ppb)

NO_x = 12.82 ppb

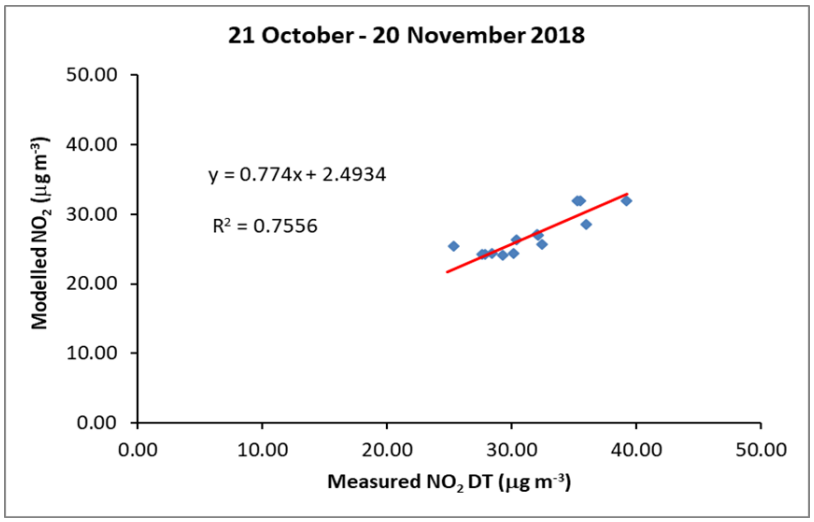
O_3 = 20.64 ppb

NO_2 background data = 10.35 ppb = 20.65 µg m^{-3}

(e) Graph of modelled NO_2 concentration (from first run of model), measured NO_2 from DT and NO_2 concentration from analysers with distance from A38 roadside at receptor locations



(f) Regression line and the equation from measured NO_2 DT and modelled NO_2 concentration



Y1 = 0.77x + 2.49

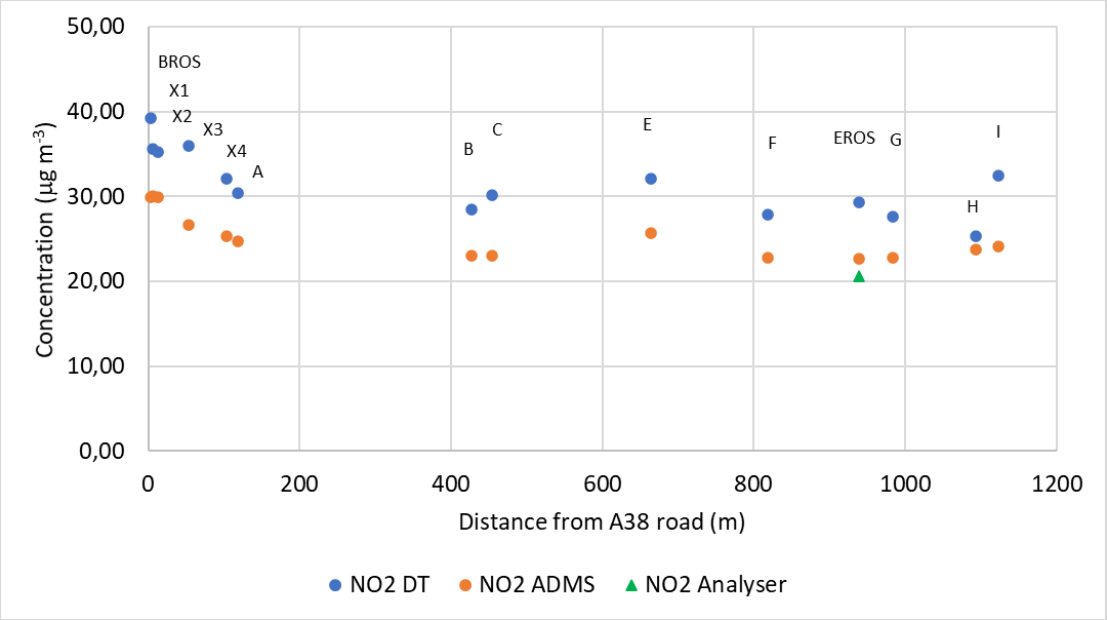
R^2 = 0.76

(g) Adjusted NO_2 background concentration

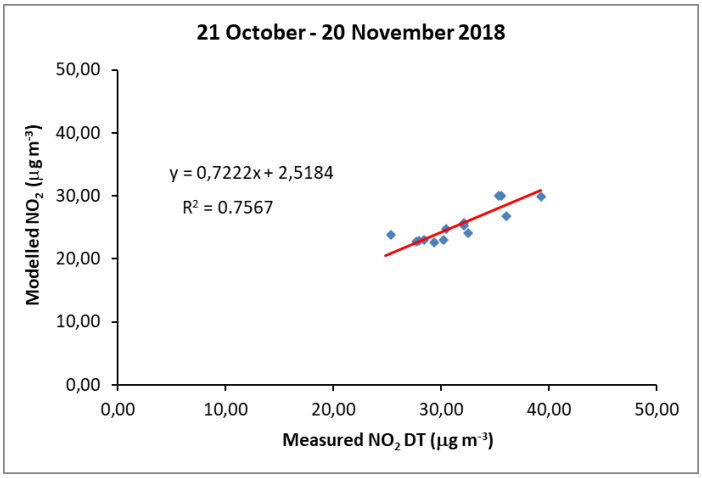
NO_2 background data in the model = 20.65 – 2.49 = 18.16 µg m^{-3}

= 9.05 ppb

(h) Graph of modelled NO_2 concentration (from second run of model), measured NO_2 from DT and NO_2 concentration from analysers with distance from A38 roadside at receptor locations



(i) Regression line and the equation from measured NO_2 DT and modelled NO_2 concentration



Y2= 0.72x + 2.52

R^2 = 0.76

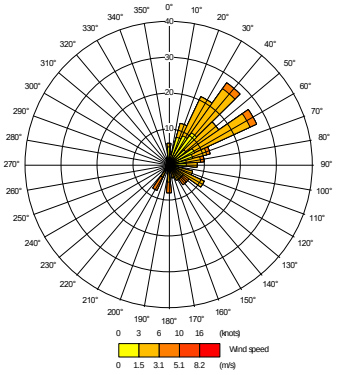
Figure 4.34. Modelled and measured NO_2 concentration from diffusion tube data, 21 October – 20 November 2018. This table shows **(a)** information of background concentration from automatic analysers from Biosciences site; **(b)** wind rose from meteorology data; **(c)** information of meteorology data input; **(d)** background concentration input in the model at the first run, and conversion unit of NO_2 concentration from ppb to µg m^{-3}; **(e)** graph of modelled NO_2 concentration from first run of model, measured NO_2 DT and NO_2 from analyser at Biosciences site; **(f)** regression line and equation from measured NO_2 DT and modelled NO_2 concentration from first run; **(g)** adjusted NO_2 background concentration; **(h)** graph of modelled NO_2 concentration from second run of model, measured NO_2 DT and NO_2 from analyser at Biosciences site; **(i)** regression line and equation from measured NO_2 DT and modelled NO_2 concentration from second run.

The model underestimated the NO_2 concentrations compared with the measured concentration. NO_2 concentrations disperse mostly from the south and southeast, and from the northwest. The predominant direction was southerly. The NO_2 levels were expected to decrease from the A38 road to BROS and present low discrepancies for the background site.

Greater concentrations of NO_2 from both site measurements and the model were observed near the A38 road (BROS). A spike of NO_2 concentration is also observed in the sample points near UoB Westgate (X3), Pritchatts Road (site E) and the junction of Edgbaston Park Road and Somerset Road (site I).

The measured NO_2 concentration at BROS (near road) was 39.3 μg m^{-3} and at EROS (background) 29.3 μg m^{-3}. The concentration reduction was 25 %, or the concentration was lowered by 1.3 times at the background site. In this sampling period, the model underestimated the concentration compared to the measured data. The modelled NO_2 concentration at BROS was 30.3 μg m^{-3} and at EROS was 22.8 μg m^{-3}. From the modelling result, the NO_2 concentration reduced from BROS to EROS by 25 % — 1.3-times lower concentration, therefore, at the background site further from the road. So, although there are differences in the results for concentration between the model and the measurement, the relative reductions in concentration were remarkably similar. The model can predict the trend of pollutant concentrations well.

4) 20-28 November 2018

(a) Background concentration from automatic analysers (in ppb)	(b) Wind rose
NO_x = 23.19 ppb NO_2 = 14.09 ppb O_3 = 11.56 ppb Automatic analyser data from Bioscience site, UoB	

(c) Meteorological data

Parameter	N	% data from Winterbourne No. 2	% data from Coundon	% data from Coleshill
Wind direction	216		100 %	
Wind speed	216		100 %	
Temperature	216	100 %		
Relative Humidity	216	100 %		
Cloud cover	216			100

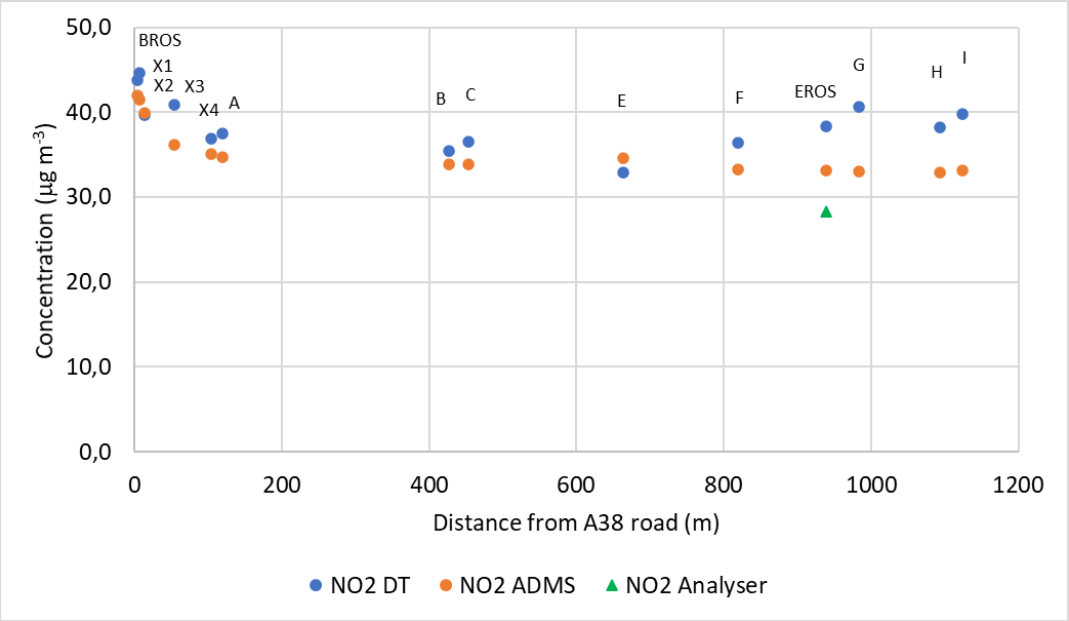
(d) Background concentration input in the model at the first run (in ppb)

NO_x = 23.19 ppb

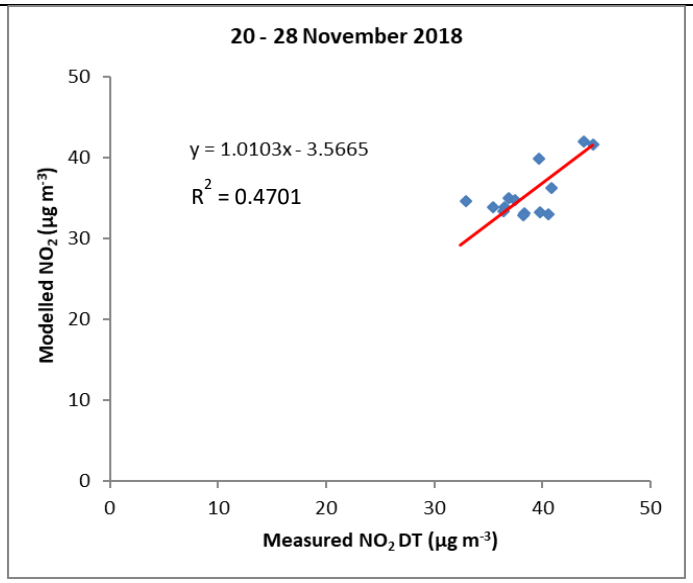
O_3 = 11.56 ppb

NO_2 background data = 14.09 ppb = 28.25 μg m^{-3}

(e) Graph of modelled NO_2 concentration (from first run of model), measured NO_2 from DT and NO_2 concentration from analysers with distance from A38 roadside at receptor locations



(f) Regression line and the equation from measured NO_2 DT and modelled NO_2 concentration



$Y1 = 1.01x - 3.57$

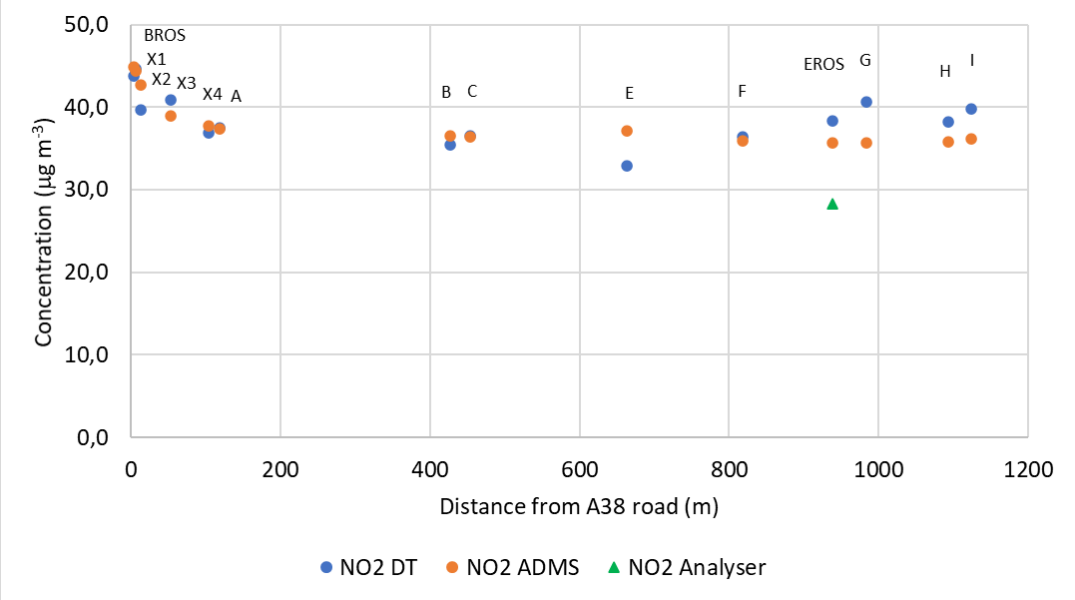
$R^2 = 0.47$

(g) Adjusted NO_2 background concentration

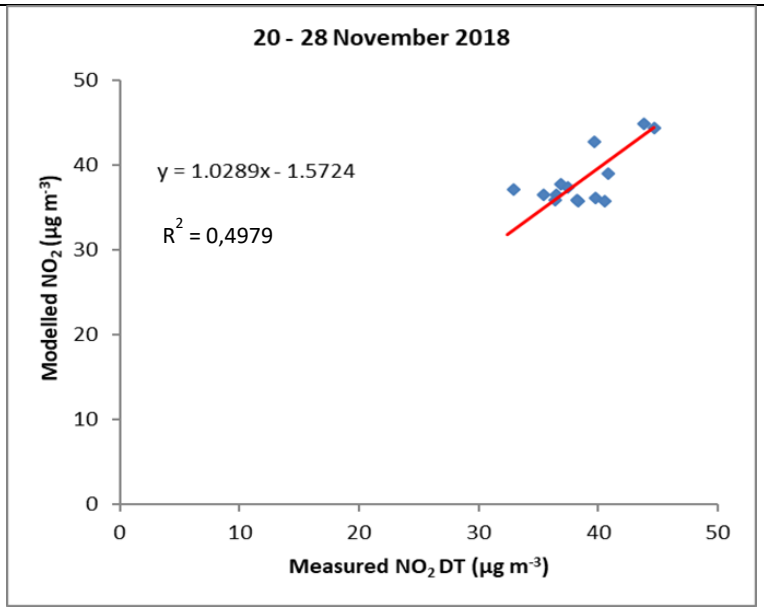
NO_2 background data in the model = 28.25 – (-3.57) = 31.82 µg m^{-3}

= 15.86 ppb

(h) Graph of modelled NO_2 concentration (from second run of model), measured NO_2 from DT and NO_2 concentration from analysers with distance from A38 roadside at receptor locations



(i) Regression line and the equation from measured NO_2 DT and modelled NO_2 concentration



Y2= 1.03x – 1.58

R^2 = 0.50

Figure 4.35. Modelled and measured NO_2 concentration from diffusion tube data, 20 – 28 November 2018. This table shows **(a)** information of background concentration from automatic analysers from Biosciences site; **(b)** wind rose from meteorology data; **(c)** information of meteorology data input; **(d)** background concentration input in the model at the first run, and conversion unit of NO_2 concentration from ppb to µg m^{-3}; **(e)** graph of modelled NO_2 concentration from first run of model, measured NO_2 DT and NO_2 from analyser at Biosciences site; **(f)** regression line and equation from measured NO_2 DT and modelled NO_2 concentration from first run; **(g)** adjusted NO_2 background concentration; **(h)** graph of modelled NO_2 concentration from second run of model, measured NO_2 DT and NO_2 from analyser at Biosciences site; **(i)** regression line and equation from measured NO_2 DT and modelled NO_2 concentration from second run.

NO_2 concentrations disperse from Edgbaston Park Road and Somerset Road from I point and further to the BROS site as winds blew from northeast to southwest. The modelled pollutant concentration was lower at site I and reflected the measurements well at BROS which showed only a small elevation because there was no wind from the southwest direction.

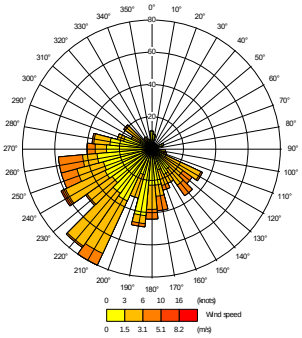
5) 28 November 2018 – 6 January 2019

(a) Background concentration from air monitoring data (in ppb)

NO_2 = 11.08 ppb
NO_x = 17.04 ppb
O_3 = 19.51 ppb

Automatic analyser data from Birmingham Acocks Green station

(b) Wind rose

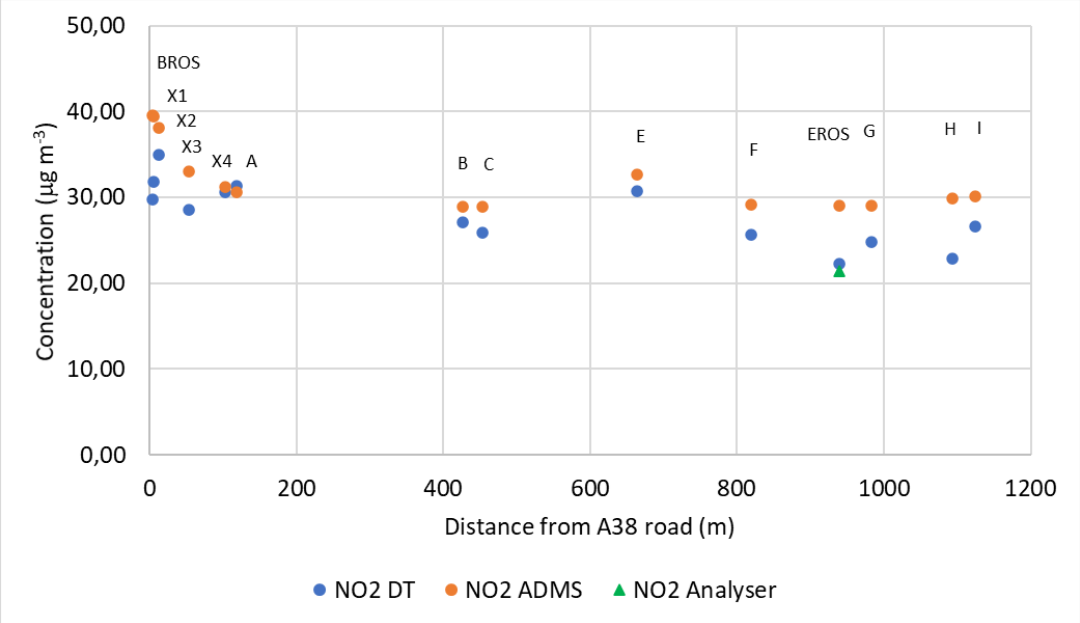


(c) Meteorological data

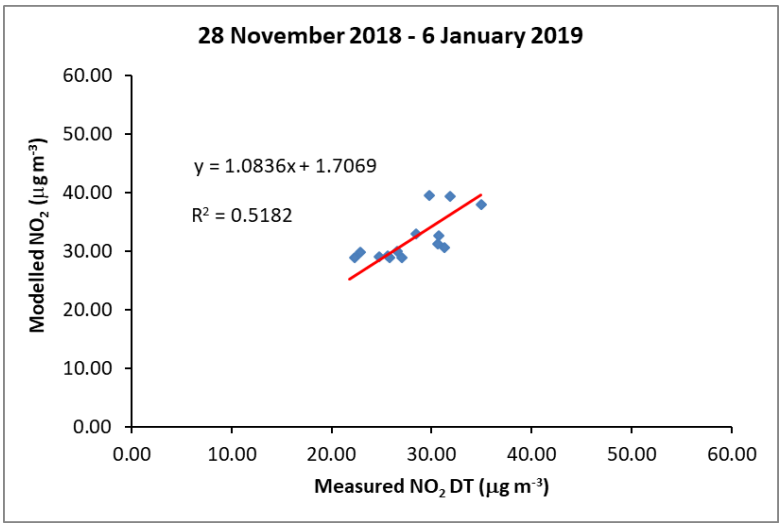
Parameter	N	% data from Winterbourne No. 2	% data from Coundon	% data from Coleshill
Wind direction	960		100 %	
Wind speed	960		100 %	
Temperature	960	100 %		
Relative Humidity	960	100 %		
Cloud cover	960			100

(d) Background concentration input in the model at the first run (in ppb)
NO_x = 17.04 ppb
O_3 = 19.51 ppb
NO_2 background data = 10.61 ppb = 21.36 μg m^{-3}

(e) Graph of modelled NO_2 concentration (from first run of model), measured NO_2 from DT and NO_2 concentration from air monitoring data with distance from A38 roadside at receptor locations



(f) Regression line and the equation from measured NO_2 DT and modelled NO_2 concentration



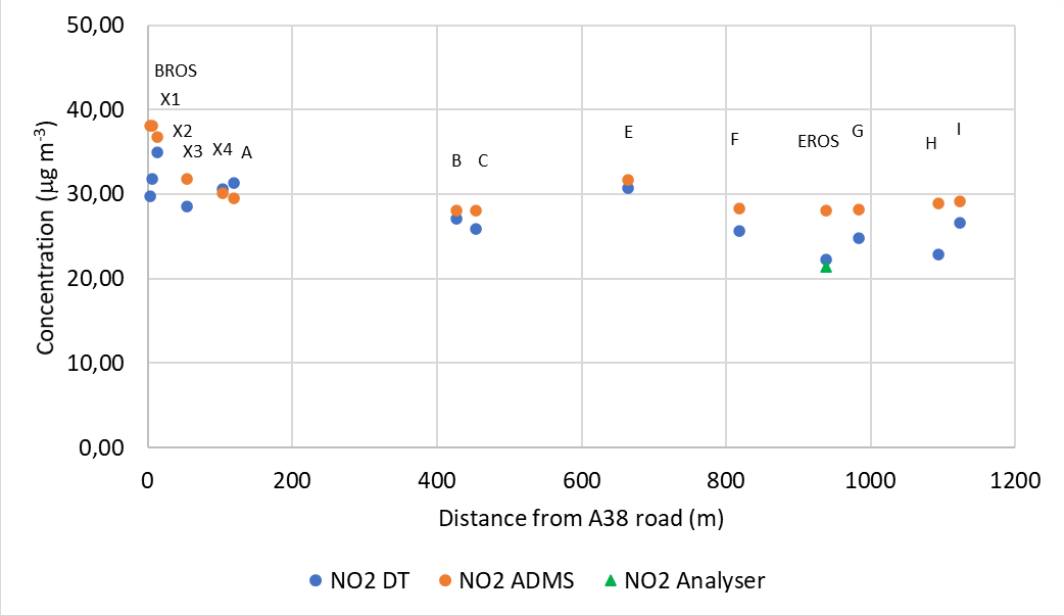
Y1 = 1.08x + 1.71

R^2 = 0.52

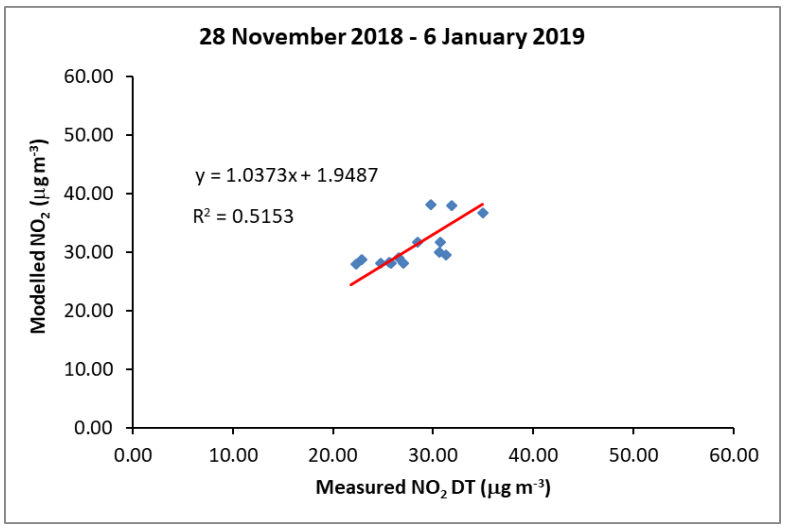
(g) Adjusted NO_2 background concentration

NO_2 background data in the model = 21.36 – 1.71 = 19.65 µg m^{-3}
= 9.76 ppb

(h) Graph of modelled NO_2 concentration (from second run of model), measured NO_2 from DT and NO_2 concentration from air monitoring data with distance from A38 roadside at receptor locations



(i) Regression line and the equation from measured NO_2 DT and modelled NO_2 concentration



Y2= 1.04x + 1.95

$R^2 = 0.52$

Figure 4.36. Modelled and measured NO_2 concentration from diffusion tube data, 28 November 2018 – 6 January 2019. This table shows **(a)** information of background concentration from air monitoring site at Birmingham Acocks Green; **(b)** wind rose from meteorology data; **(c)** information of meteorology data input; **(d)** background concentration input in the model at the first run, and conversion unit of NO_2 concentration from ppb to µg m^{-3}; **(e)** graph of modelled NO_2 concentration from first run of model, measured NO_2 DT and NO_2 from air monitoring data; **(f)** regression line and equation from measured NO_2 DT and modelled NO_2 concentration from first run; **(g)** adjusted NO_2 background concentration; **(h)** graph of modelled NO_2 concentration from second run of model, measured NO_2 DT and NO_2 from air monitoring data; **(i)** regression line and equation from measured NO_2 DT and modelled NO_2 concentration from second run.

Pollutants dispersed mostly from southwest and west-southwest. NO_2 concentrations decreased from BROS to the background area and slightly increased at E point near Pritchatts Road. The model slightly over-predicted NO_2 concentrations. The higher measured NO_2 level near the X2, X3, X4, and A sites could be related to the opening of a new parking lot at South Gate beside the sports pitches.

Elevated NO_2 concentrations were found at the locations near roads — for example, at BROS, X1 (A38), X2 to X4 and A sites (roads inside the UoB), E site (Pritchatts Road), H and I sites (near Edgbaston Park Road and Somerset Road). The lower NO_2 concentrations were observed at the background sites, which are the B, C, F, EROS, and G sites. Wind speed and direction can affect pollutant concentrations and it was observed that NO_2

concentrations decay rapidly when the wind predominantly blows from the south, southwest or southeast of the A38 roadside.

ADMS-Roads presents a good agreement of NO_2 modelled with the measured concentrations. Overall, ADMS-Roads performs well in simulating the trends of pollutant concentrations.

Dry deposition

Table 4.14 shows the results of modelled concentrations from the dispersion and chemistry option (a) and deposition, dispersion, and chemistry option (b), with the percentage of reduction of concentration when the dry deposition process was included. The results of the model evaluation are presented.

Table 4.14. Model evaluation statistics calculated from NO_2 diffusion tubes and model of ADMS-Roads for (a) the dispersion and chemistry, (b) deposition, dispersion and chemistry (b) and % reduction in concentrations due to deposition.

Date off sampling	Mean concentration (μg m^{-3})			Concentration change	Model evaluation statistics							
	DT observation	Modelled (a)	Modelled (b)	% reduction concentration (a-b)/a x 100%	FB (a)	FB (b)	NMSE (a)	NMSE (b)	R (a)	R (b)	R^2 (a)	R^2 (b)
18/03/2018 – 15/04/2018	26,99	30,00	29,90	**0,33**	-0.11	-0.10	0.011	0.010	0,85	0,85	0,73	0,73
15/04/2018 – 13/05/2018	30,16	28,71	28,6	**0,38**	0.05	0.05	0.002	0.003	0,82	0,82	0,68	0,68
21/10/2018 – 20/11/2018	31,58	25,32	25,16	**0,63**	0,22	0.23	0.049	0.052	0,87	0,87	0,76	0,76
20/11/2018 – 28/11/2018	38,68	38,22	38,12	**0,26**	0.01	0.01	0.000	0.000	0,71	0,71	0,50	0,50
28/11/2018 – 06/01/2019	28,05	31,05	30,85	**0,64**	-0.10	-0.09	0.010	0.009	0,72	0,71	0,52	0,51

Modelled (a) = dispersion and chemistry (model is setting without dry deposition)
Modelled (b) = deposition, dispersion and chemistry (model is setting with dry deposition)

The R^2 value between the measured and the modelled data was in the range of 0.50 to 0.76. There are no specific differences between the evaluation result from the model with and without the dry deposition process, as shown by statistical parameters of Fractional Bias (FB in range -0.09 to 0.23) and Normalised Mean Square Error (NMSE in range 0.000 to 0.052). This evaluation result confirmed the performance of the model was generally good.

The comparison between the model with and without the dry deposition showed that dry deposition has little effect on reducing the pollutant concentrations. Results from the model show the effect of deposition processes in reducing pollutants was in the range 0.3% to 0.6% for NO_2 concentrations.

Overall, dispersion processes play a dominant role in influencing the pollutant concentrations, as reduction of NO_2 concentrations by deposition processes was less than 1%. The park air is cleaner because of dilution and redistribution of the pollutants, not because pollutants are actually being removed from the air. Pollutants are only being removed from the air by a very small amount. A park with trees and vegetation can reduce pollutant concentrations more than a park without trees or open areas with a mostly concrete base, through deposition processes via vegetation crown volume (Yin *et al.*, 2011), greater leaf surface area (Pugh *et al.*, 2012) and dispersion processes via the aerodynamic effect (Vos *et al.*, 2013; Jeanjean *et al*., 2016) which enhances dispersion. Trees and vegetation affect air flows and turbulence. When the wind flows and hits the trees, there is deceleration flow and generation of turbulence. The branches of trees help to increase turbulence and hence increase dispersion and the rate of dilution (AQEG, 2018). However, it is important to select the vegetation and design the layout of trees in the park to get the maximum benefit in improving air quality (Janhall, 2015).

4.4. Limitation of the study

ADMS-Roads is capable in predicting pollutant concentrations at a local scale but has a limitation regarding the deposition of O_3 because the model only considers the dry deposition of emitted pollutants.

4.5. Summary

The ADMS-Roads model, as dispersion modelling software, was used to predict the pollutant concentrations emitted from road traffic with or without the dry deposition process. The concentrations of NO_x and O_3 produced by the model were evaluated against the hourly measurement data at BROS and EROS from 2-11 February 2018. This model verification was carried out to test the model performance and identify the uncertainties in setting up the model. The model was able to predict pollutant concentration values close to the measurements. The uncertainties arise from meteorological conditions, estimating the background concentration, uncertainties in source activity data, and the emitted NO_2:NO_x ratio.

A single adjustment method based on linear regression was used to improve the accuracy of the dispersion modelling results when comparing the measured DT concentration with modelled results from ADMS-Roads. This approach reduced errors related to the input of background concentration. Implementation of this method somewhat lowered or raised the difference between the measured and modelled NO_2 concentrations depending on the value of the intercept from the linear regression.

The pollutant concentrations decrease as air traverses the park largely by dispersion processes. However, this local concentration is influenced by the wind speed, wind direction and background concentration in the area.

Pollutant dispersion considers wind direction, wind speed and boundary layer stability, and therefore meteorological data are important parameters in predicting pollutant concentrations. Input of meteorological data from the nearest weather station can improve the model performance in predicting pollutant concentrations. Meteorological data should be acquired from the nearest weather station to the sampling site. In this study, Winterbourne No.2 is the closest weather station. However, there was incomplete wind speed and wind direction data from this weather station and therefore there was a need to use other weather station data in addition. Coundon was used as an alternative weather station, and adjustment of wind speeds by comparison with the Winterbourne No.2 station was required.

When the locally measured concentrations of NO_x, NO_2 and O_3 were used as background concentrations, the performance of the model improved and it predicted pollutant concentrations more accurately.

The deposition process is not significant in reducing pollutant concentration, and the contribution is less than 1% for NO_2 and NO_x concentrations. NO_x and NO_2 concentrations were similar in the model whether the deposition process was included or excluded, indicating that dispersion is far more important than the deposition process. This result is consistent with other studies conducted by Jeanjean *et al*. (2016) and Xing and Brimblecombe (2019) who concluded that the dispersion process is much more significant than the deposition process in reducing pollutant concentrations. However, there are scenarios where dry deposition may be more significant, e.g. at the scale of an entire city (Tiwari and Kumar, 2020).

At the microscale, more green spaces are beneficial in improving air quality, mainly due to the dispersion process.

Chapter 5 Deposition Velocity of Gases from Vertical Gradient of Pollutant Concentrations

This chapter describes the approach used to estimate deposition velocities for NO_x, O_3 and NO_2 in a green area, and the results from an experiment to measure vertical gradients at the site.

Measurements of black carbon (BC), nitrogen oxide (NO_x), nitrogen dioxide (NO_2) and ozone (O_3) concentrations were conducted at roof level and at ground level over the grassland on the courtyard in the Bioscience building, the University of Birmingham, UK.

5.1. Introduction

The dry deposition process is the mechanism by which gases and aerosol particles are removed from the atmosphere without involving precipitation such as rain or snow (Garland, 1977; Harrison, 2014; Seinfeld and Pandis, 2016).

Dry deposition can be quantified in terms of deposition velocity, v_d (m s^{-1}), by dividing the pollutant flux removed per unit area, F (μg m^{-2} s^{-1}) with the concentration of pollutants (C) at height z (1 metre above the ground) (μg m^{-3}).

$$v_d = \frac{-F}{C} \qquad (E.5.1)$$

Dry deposition of atmospheric pollutants has been measured using the 'direct' (Lindberg and Lovett, 1985; Schultz, 1993; El-Madany *et al*., 2017; Vohra *et al.*, 2017) or 'indirect' (Kramm, 1989; Watt *et al.*, 2004) method. The direct method determines the pollutant flux on the surface by measuring the flux near the surface or by collecting the deposited material on the surface. Examples of the direct method are analysis of material deposited on surfaces (filter substrates or natural surfaces), chamber method experiments, measurements of vertical velocity and concentration by the eddy correlation and eddy accumulation methods (Sehmel, 1980; Seinfeld and Pandis, 2016). The indirect method calculates the flux by measuring the vertical concentration gradient or mean concentration of deposited material—for example, the gradient method (Seinfeld and Pandis, 2016).

Factors that influence the deposition rate of gases and particles are the type of surface (Wesely *et al.*, 1982; Ma and Daggupaty, 2000; Zhang *et al*., 2003; Mariraj Mohan, 2016; Giardina and Buffa, 2018), atmospheric turbulence, and pollutant characteristics (Seinfeld and Pandis, 2016; Sehmel, 1980). The type of surface influences the deposition velocity through the surface resistance (r_c) (Seinfeld and Pandis, 2016). Deposition velocity is normally higher on dry surfaces compared to wet surfaces. The surface resistance is also related to the stomata which will cause a higher surface resistance when closed. The level of atmospheric turbulence near the ground can influence the deposition rate at which species are delivered to the surface (Seinfeld and Pandis, 2016). Pollutant characteristics such as particle size, gravitational settling and Brownian diffusion affect the capture of species by the surface. Brownian diffusion contributes to the dry deposition velocity for particles in the size 0.01 µm to one micrometre, and gravity settling for particles larger than 50 µm (Giardina and Buffa, 2018).

Dry deposition is an important pathway to remove pollutants from the atmosphere. The pollutants can be deposited on buildings, water, grasses, trees and other surfaces. Jeanjean *et al*. (2016) reviewed the influence of trees in Leicester, UK using Computational Fluid Dynamic modelling and found that deposition on trees could decrease the $PM_{2.5}$ concentration by 2.8%, while deposition on grassland only reduced the concentration by up to 0.6%. Tiwari and Kumar (2020) found that deposition was greater for trees compared to short grass as trees promote air turbulence and hence, more interaction of pollutants with trees can occur than with grass.

Colbeck and Harrison (1985) measured the O_3 dry deposition velocity over grassland using the gradient method. They found the rate of O_3 dry deposition was in the range 0.08 to 0.91 cm s^{-1} and concluded that the surface type is an important factor in determining the value of dry deposition because changes in surface conditions could influence the value of deposition velocity.

Horváth *et al.* (1998) measured the vertical flux of NO, SO_2 and O_3 in short vegetation in Germany as a product of concentration gradient and eddy diffusivity. They found that the deposition velocity of O_3 was 0.07±0.05 cm s^{-1} in stable atmospheric conditions and 0.19±0.04 cm s^{-1} in unstable atmospheric conditions. Horii *et al*. (2004) measured fluxes of

NO, NO_2 and O_3 in a forest in Massachusetts USA using the eddy covariance method. They calculated a net deposition velocity of NO_x—the average net value being 0.2 cm s^{-1}. Hanson and Lindberg (1991), reviewing deposition velocities of NO_2 and NO on trees and crops, compared the rate of NO_2 and NO deposition, and found that deposition velocities of NO to be significantly lower than the deposition velocity of NO_2.

5.2. Method

Deposition processes cause vertical gradients in the atmosphere, and an experiment was devised to measure those gradients. Continuous analysers for NO_x, O_3 and BC were set on the roof and in the open grassed area to measure the vertical concentration gradient in the Biosciences quadrangle at the University of Birmingham. The Biosciences quadrangle site represented a hypothetical model of a park on a microscale with a grassed area (45.5 m x 48.2 m), and 13 metres of gradient height. The detailed description of the Biosciences quadrangle site is in Chapter 2, Section 2.5. Measurements were conducted from 1 May 2018 to 29 November 2018 and then from 23 January to 2 March 2019.

BC concentration was measured using micro-aethalometer AE51, and NO_x and O_3 were measured using automatic analysers. The instruments set on the roof were a 42C NO_x analyser from Thermo Environmental Instruments, an O_3 instrument, Thermo Fisher Scientific Model 49i, and AE51 to measure the concentrations at 14 m height. The instruments at ground level were AE51, 42i NO_x, and O_3 instrument Thermo Fisher Scientific Model 49i to measure the concentration at 1 m above the ground.

The measurement results for BC, NO_x, NO_2 and O_3 concentrations on the roof and the ground sites over the grassland area, and condition of courtyard in the Biosciences building are described. Relevant literature for setting up the experiments to calculate the deposition velocity of gases in a green area or grassland area is discussed.

5.3. Results and discussion

5.3.1. Profiles of pollutant concentrations at the roof and the ground

Figures 5.1. and 5.2 show BC concentrations at the roof and ground level of the Biosciences building. The pattern shows BC concentration at roof level was usually slightly higher than on the ground.

There were 659 hourly mean data points of BC concentrations from a total of 2970 data points when the BC concentration at the ground was higher than the BC concentration on the roof during the sampling period from 1 May to 29 November 2018. The difference in concentration was up to 1.3 µg m^{-3}.

For the sampling period from 23 January to 2 March 2019, there were 298 hourly average data points of BC concentrations from a total of 812 data points for BC when the concentration on the ground was higher than the concentration on the roof. The difference in concentration was up to 1.5 µg m^{-3}. The reasons for this are discussed later.

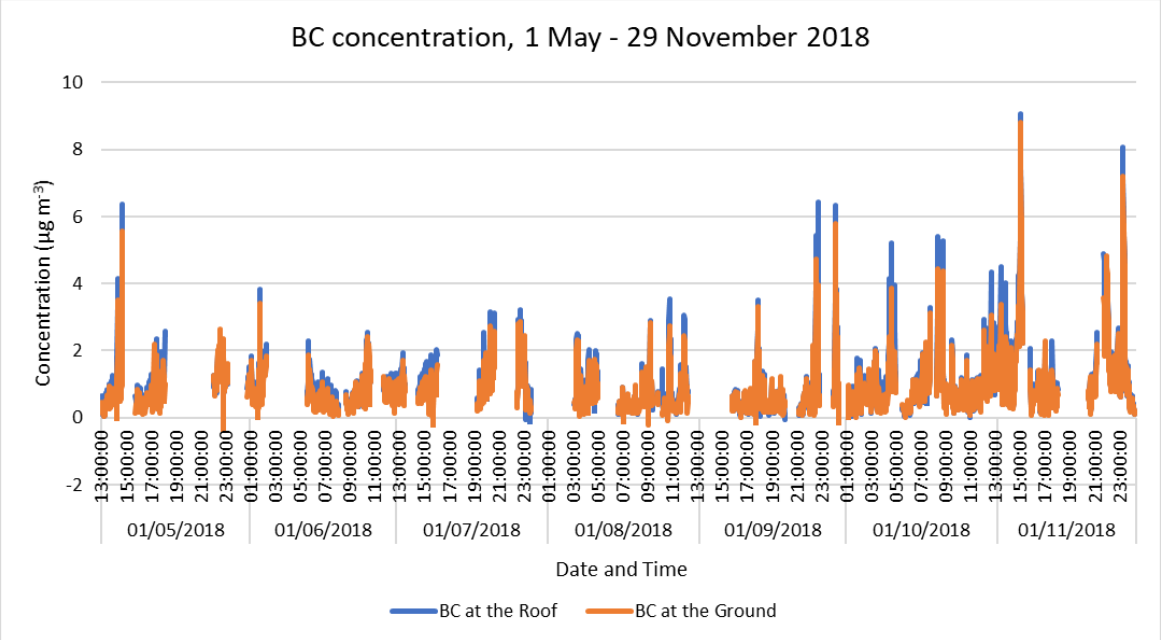


Figure 5.1. BC concentration in µg m^{-3} at the roof (blue line) and the ground (orange line) of the Biosciences building, sampling period from 1 May to 29 November 2018

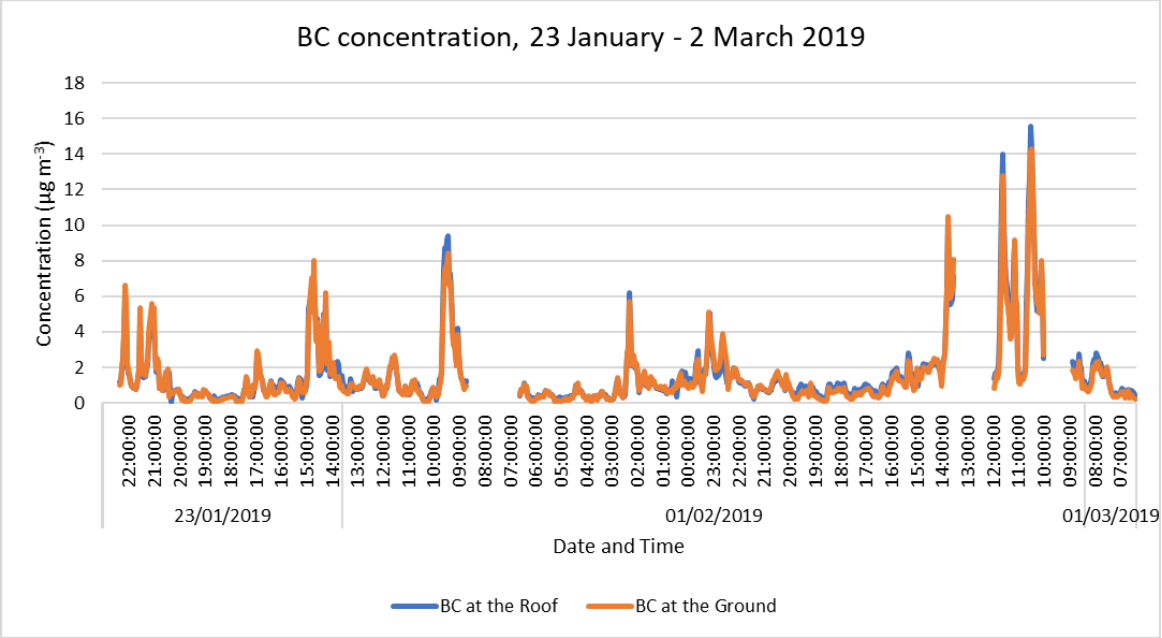


Figure 5.2. BC concentration in µg m^{-3} at the roof (blue line) and the ground (orange line) of the Biosciences building, sampling period from 23 January to 2 March 2019

For the gases, the focus of this discussion is the gases (NO, NO_2, and O_3) data from 20-29 November 2018 and 23 January to 2 March 2019.

Figure 5.3 shows the NO, NO_2 and O_3 concentrations for the period 20-29 November 2018. The mean concentrations (mean ± SD) of NO, NO_2, and O_3 on the roof were 8 ± 1 ppb, 12 ± 1 ppb, 17 ± 2 ppb and on the ground were 5 ± 1 ppb, 12 ± 1 ppb, and 15 ± 2 ppb, respectively. The highest NO concentration was observed at ground level, 60 ppb on 27 November 2018 at 01:00. This high concentration persisted until 03:00 (48 ppb) and decreased afterwards. The highest NO_2 at ground level was 25 ppb on 26 November 2018 at 22:00, and the highest O_3 concentration was on the roof with 41 ppb on 28 November 2018 at 20:00. High concentrations of NO_2 can be related to traffic emissions.

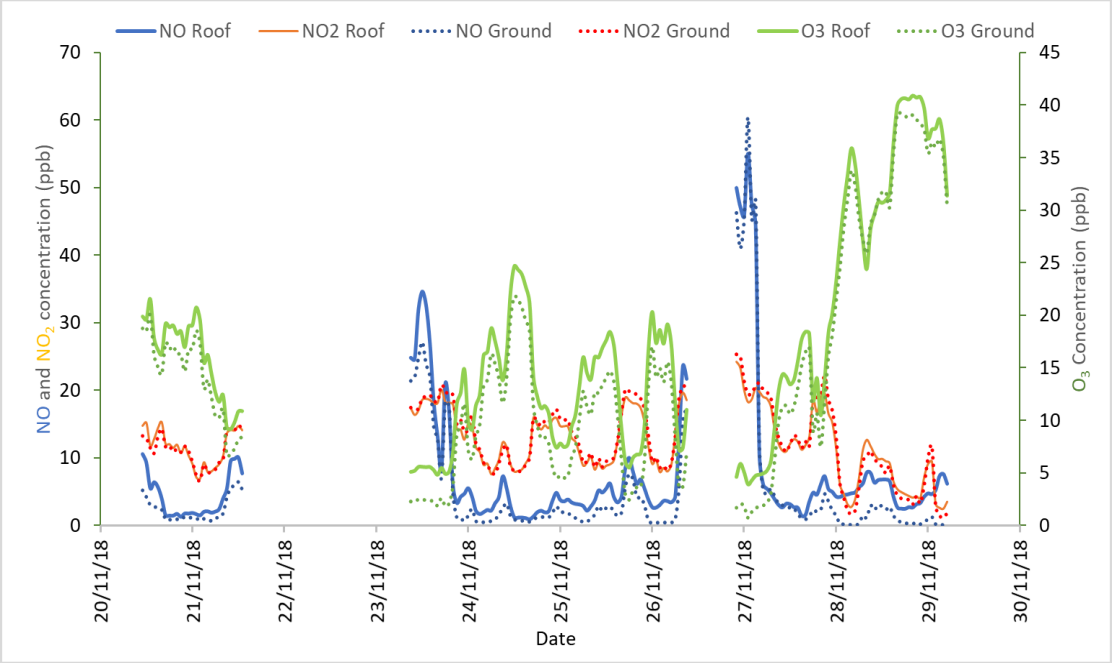


Figure 5.3. NO, NO_2 and O_3 concentrations in ppb at the roof (solid line) and on the ground (dashed line), 20 – 29 November 2018

The measurements at the end of November 2018 were made at the start of UK winter, where daytime runs from 07.00 to 17.00, and night-time from 17.00 to 07.00. The NO concentration during the daytime was higher than night-time, except on 27/11/2018. The NO concentration increased on Monday morning (26/11/2018), starting at 07:00, from 4 ppb at 06:00 to 13 ppb at 07:00, and rose to 24 ppb at 08:00. During 28/11/2018 to 29/11/2018, the NO concentration on the roof was higher than the ground, starting early in the morning and reaching a peak in the night at 21:00. NO can rapidly react with O_3 to form NO_2 (Watt *et al.*, 2004).

Higher NO_2 concentrations in winter can be due to less dispersion of pollutants related to higher incidence of low wind speed and other weather conditions, such as lower solar radiation and lower mixing layer height. The increase of energy consumption during winter also potentially increases pollutant concentrations.

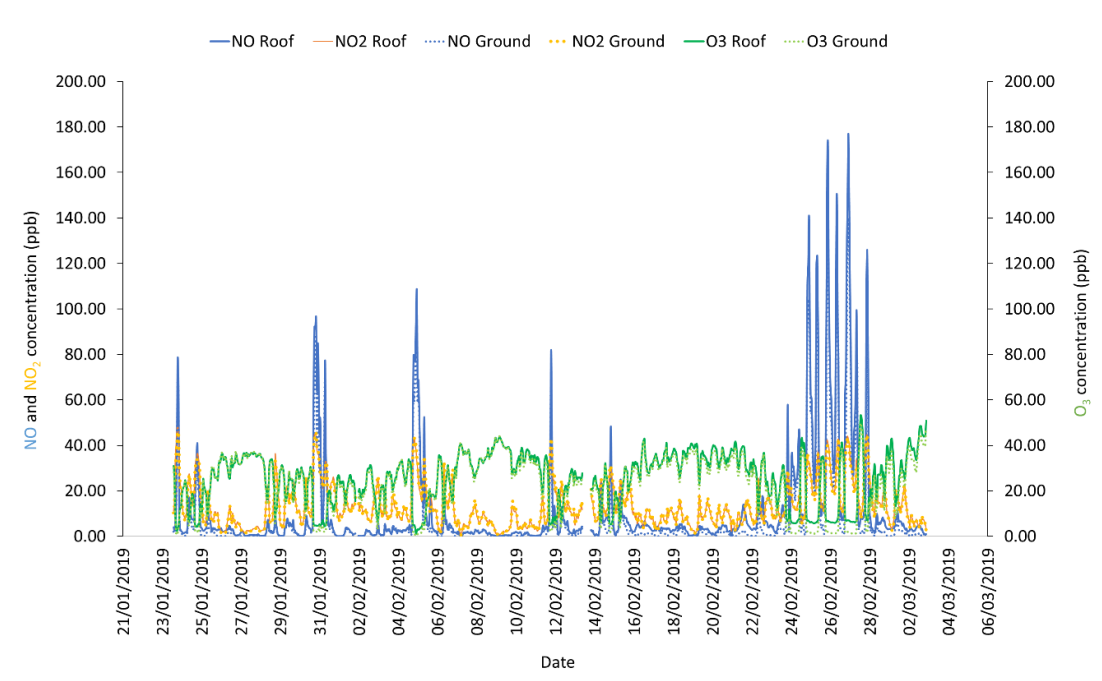


Figure 5.4. NO, NO_2 and O_3 concentrations in ppb at the roof (solid line) and on the ground (dashed line), 23 January – 2 March 2019

Figure 5.4. presents NO, NO_2 and O_3 concentrations on 23 January – 2 March 2019. The mean concentrations (mean ± SD) of NO and NO_2, and O_3 on the roof were 11 ± 1 ppb, 13 ± 2 ppb, 25 ± 3 ppb and on the ground were 8 ± 1 ppb, 13 ±1 ppb and 23 ± 3 ppb, respectively.

There were no data during the period of sampling time when the NO_2 concentration was higher than 200 µg m^{-3} as 1 hour mean limit value of Air Quality Objectives. However, there were high NO_2 concentrations on the roof and the ground above 40 µg m^{-3} as an annual mean limit value, and a large number of the NO_2 concentrations were higher at the ground, as shown in Figures 5.3 and 5.4 and Table 5.1.

Table 5.1. Date and time during sampling period when NO_2 concentrations at the ground site were higher than 40 µg m^{-3}

		Range of NO_2 Concentrations	
Date	Local Time	NO_2 Roof (µg m^{-3})	NO_2 Ground (µg m^{-3})
23/11/2018	17.00 – 18.00	37 – 40	40 – 42
25/11/2018	17.00 – 18.00	37 – 38	40 – 41
26/11/2018	08.00 – 09.00	37 – 40	41 – 42
26/11/2018	22.00 – 23.00	48 – 49	51 – 52
27/11/2018	00.0 – 06.00 21.00	38 – 42	40 – 44
17/01/2019	17.00 – 23.00	47 – 75	55 – 84
18/01/2019	00.00 – 03.00	42 – 59	49 – 67

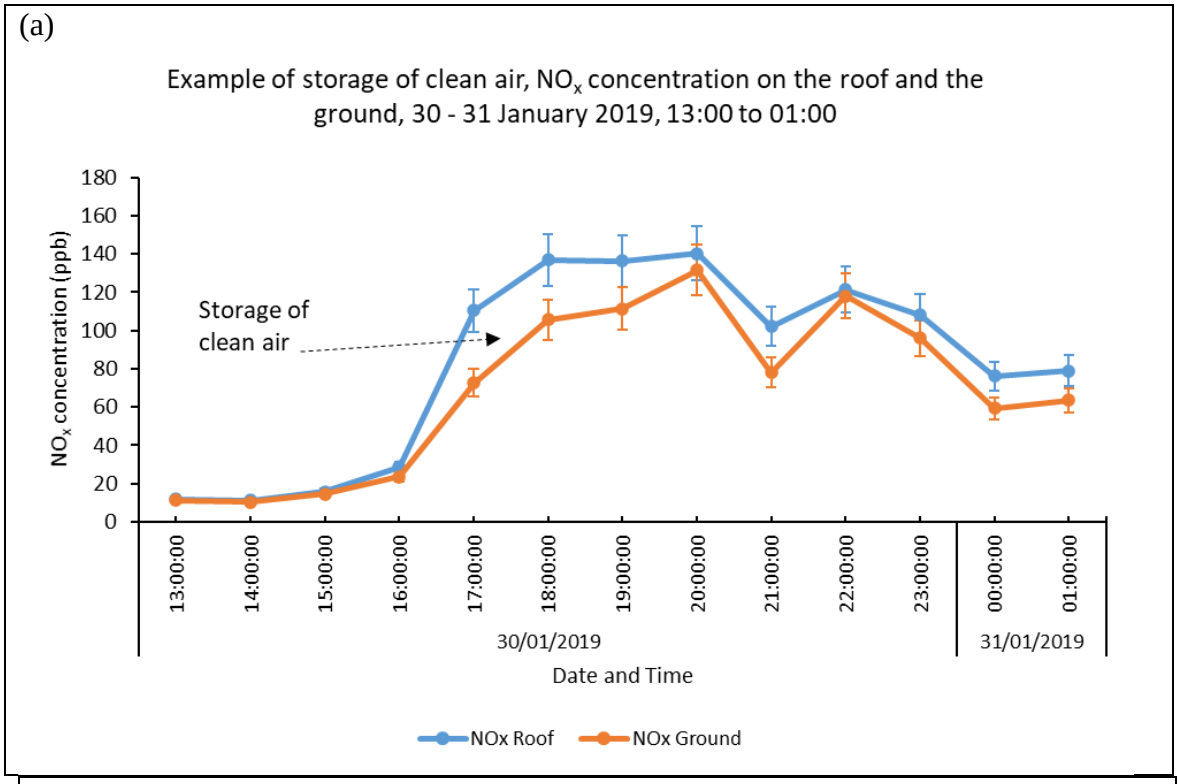
		Range of NO_2 Concentrations	
Date	Local Time	NO_2 Roof (μg m^{-3})	NO_2 Ground (μg m^{-3})
20/01/2019	15.00 – 18.00 20.00 – 21.00	45 – 53	41 – 47
22/01/2019	08.00 17.00 – 19.00	47 – 60	43 – 61
23/01/2019	16.00 – 23.00	44 – 100	40 – 94
24/01/2019	08.00 – 11.00 16.00 – 22.00	42 – 74	43 – 69
25/01/2019	08.00	40	41
28/01/2019	09.00 18.00 – 20.00	45 – 73	45 – 67
29/01/2019	08.00 – 10.00 16.00 – 17.00	40 – 48	40 – 43
30/01/2019	07.00 – 08.00 16.00 – 23.00	47 – 91	42 – 92
31/01/2019	00.00 – 10.00 14.00 – 18.00	40 – 67	41 – 67
02/02/2019	22.00 – 23.00	45 – 51	43 – 55
03/02/2019	00.00 08.00	43 – 52	43 – 53
04/02/2019	17.00 – 23.00	54 – 88	44 – 88
05/02/2019	00.00 – 04.00 07.00 – 10.00	37 – 68	41 – 72
06/02/2019	08.00 – 09.00 16.00 – 19.00	41 – 62	43 – 66
11/02/2019	17.00 – 23.00	50 – 79	53 – 88
12/02/2019	00.00 – 09.00	36 – 48	41 – 51
13/02/2019	20.00	36	42
14/02/2019	07.00 – 09.00 18.00 – 23.00	47 – 61	47 – 63
15/02/2019	07.00 – 09.00 17.00 20.00	40 – 50	44 – 53
22/02/2019	08.00 – 09.00	43 – 53	47 – 51
23/02/2019	19.00 – 21.00	47 – 56	49 – 58
24/02/2019	00.00 11.00 19.00 – 23.00	40 – 69	41 – 74
25/02/2019	00.00 – 02.00 07.00 – 11.00 18.00 – 23.00	40 – 86	41 – 81
26/02/2019	00.00 – 04.00 06.00 – 11.00 18.00 – 23.00	41 – 89	40 – 88
27/02/2019	00.00 – 04.00 07.00 – 09.00 17.00 – 23.00	48 – 90	47 – 90
28/02/2019	00.00 – 01.00 08.00 – 09.00 18.00	42 – 56	41 – 48
01/03/2019	08.00 18.00 – 19.00	42 – 45	41 – 44

For the period of 20-29 November 2018, there were total of 6 hours of NO_2 concentrations at the roof and 15 hours of NO_2 concentrations at the ground that exceeded 40 µg m^{-3} from 156 total hours of data. For the period of 23 January to 2 March 2019, there were total of 210 hours and 195 hours of NO_2 concentrations at the roof and at the ground, respectively, that exceeded 40 µg m^{-3} from 907 total hours of data.

NO and NO_x concentrations were generally higher at the roof compared to the ground. Traffic volumes on the roads adjacent to the building are very low, and the main source of nitrogen oxides is the general urban road traffic.

Overall, the profile of gradient of concentration on the roof and the ground is influenced by chemical reactions between pollutants and diurnal changes in vertical mixing (Stutz *et al.*, 2004) and horizontal advection, e.g. convective cells influenced by heating of the roof (Tan *et al.*, 2019). In several instances our observations showed the delayed vertical mixing, causing the pollutant concentration at the ground to be higher than at the roof or vice versa. This reverse concentration gradient with a higher concentration in the courtyard of the Biosciences site is due to the storage of polluted air, and we call it the storage phenomenon. Figure 5.5.a shows the storage phenomena of clean air when there was increasing NO_x concentration at the roof and at that time NO_x concentrations at the ground were lower than NO_x concentrations at the roof. Figure 5.5.b. shows the storage of polluted air that happened when there was decreasing NO_x concentration at the roof and NO_x concentrations at the roof were lower than NO_x concentrations at the ground. This arises from the extended lifetime of air in the quadrangle, whereas the air at roof level moves more freely.

Chemical reaction and deposition are the main sink for gases removal in the atmosphere. NO_2 is affected by chemistry, as secondary pollutant of NO_2 is produced from the oxidation of NO by O_3 and NO_2 is removed from the atmosphere by photolysis, chemical reaction and deposition. Therefore, we presented NO_x concentration in explaining the storage phenomena as shown in Figure 5.5.



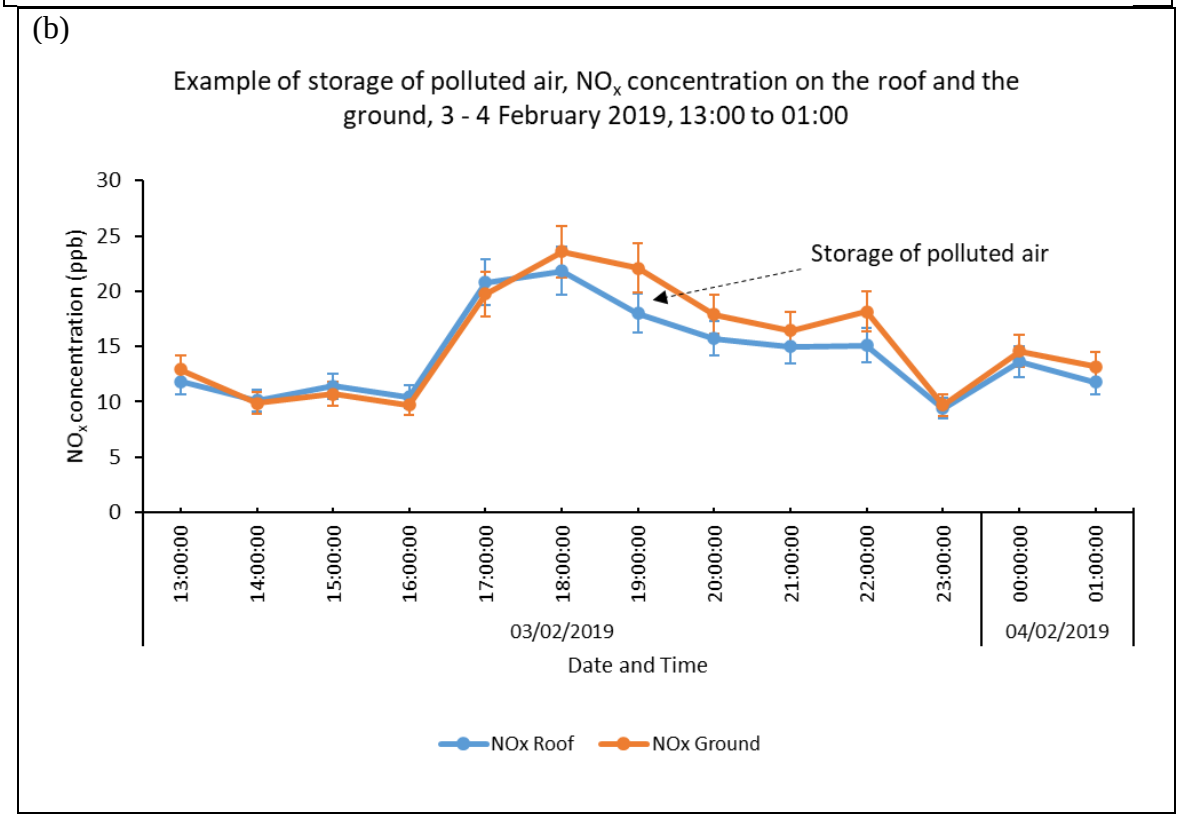


Figure 5.5. **(a)** NO_x concentration in ppb at the roof (blue colour) and the ground (orange colour) as an example of the storage phenomenon in the quadrangle site caused by the storage of clean air from the dataset on 30-31 January 2019 at 1 hour mean from 13:00 to 01:00; and **(b)** storage of polluted air from the dataset on 3-4 February 2019 at 1 hour mean from 13:00 to 01:00. Error bar of the automatic analysers, uncertainty was estimated as 10% from each measured mean concentration for NO_x instruments (Stevenson *et al.*, 2009).

Table 5.2. presents the number of occurrences when NO_x concentration at the roof was lower than NO_x concentration at the ground, which may lead to a storage of polluted air; the number of occurrences when NO_x concentration at the ground was lower than NO_x concentration at the roof, which could contribute to storage of clean air; and the number of occurrences when NO_x concentration at the roof was equal to NO_x concentration at the ground. The range of difference in concentration in ppb between the NO_x concentration at the roof and at the ground was -7 to 9 ppb for the sampling period 20-29 November 2018 and -21 to 54 ppb for sampling period 23 January – 2 March 2019.

Table 5.2. Number of occurrences of lower NO_x concentrations at the roof and lower concentrations at the ground for the period of sampling on 20-29 November 2018 and 23 January-3 March 2019

Period of sampling time	Number of data from period of sampling time in 1 hour mean			Total data	Range of difference in concentrations (ppb)
	Storage of polluted air	Storage of clean air			
	NO_x concentration at the roof was lower than NO_x concentration at the ground	NO_x concentration at the ground was lower than NO_x concentration at the roof	NO_x Roof = NO_x Ground		
	(NO_x Roof < NO_x Ground)	(NO_x Roof > NO_x Ground)			
20 – 29 November 2018	9	125	22	156	-7 to 9
23 January – 2 March 2019	75	719	113	907	-21 to 54

Table 5.3. shows the date and time during sampling period (20 - 29 November 2018 and 23 January - 2 March 2019) when storage phenomenon happens. When NO_x concentrations at the roof were decreasing and lower than NO_x concentrations at the ground, we got storage of polluted air on the ground. The second storage—clean air storage—happened when NO_x concentration at the roof was increasing and higher than at the ground.

Table 5.3. Date and time during sampling period when NO_x concentrations at the roof decreasing and NO_x concentrations at the roof were lower than the ground (polluted air storage) and when NO_x concentrations at the roof increasing and NO_x concentrations were higher than at the ground (clean air storage)

Date	Local Time	Storage of polluted air		Storage of clean air	
		NO_x Roof decrease, and NO_x Roof < NO_x Ground		NO_x Roof increase, and NO_x Roof > NO_x Ground	
		NO_x Roof (ppb)	NO_x Ground (ppb)	NO_x Roof (ppb)	NO_x Ground (ppb)
20/11/2018	13.00 – 15.00	-	-	17 to 20	14 to 16
21/11/2018	04.00 – 12.00	-	-	10 to 25	9 to 21
23/11/2018	10.00 – 12.00	-	-	41 to 53	39 to 46
23/11/2018	19.00 – 20.00	35 to 24	37 to 24	-	-
23/11/2018	23.00 – 24.00	-	-	17 to 21	14 to 16
24/11/2018	06.00 – 09.00	-	-	10 to 20	9 to 14
25/11/2018	14.00 – 18.00	-	-	14 to 28	12 to 27
26/11/2018	05.00 – 08.00	-	-	12 to 43	10 to 36
27/11/2018	03.00 – 10.00	65 to 14	69 to 15	-	-
27/11/2018	17.00 – 21.00	-	-	17 to 27	13 to 27
28/11/2018	05.00 – 08.00	-	-	9 to 20	2 to 11
28-29/11/2018	22.00 – 01.00	-	-	7 to 14	3 to 13
23/01/2019	15.00 – 19.00	-	-	19 to 127	14 to 113
23/01/2019	20.00 – 21.00	109 to 28	110 to 43	-	-
24/01/2019	06.00 – 09.00	-	-	13 to 45	10 to 42
24/01/2019	13.00 – 19.00	-	-	22 to 77	18 to 68
25/01/2019	05.00 – 08.00	-	-	9 to 32	5 to 30
25/01/2019	13.00 – 16.00	-	-	9 to 14	8 to 11
26/01/2019	05.00 – 10.00	-	-	4 to 17	2 to 14
26/01/2019	18.00 – 20.00	-	-	5 to 7	4 to 6
27/01/2019	06.00 – 20.00	-	-	2 to 5	1 to 4
28/01/2019	05.00 – 09.00	-	-	5 to 29	3 to 28
28/01/2019	15.00 – 17.00	-	-	10 to 24	8 to 21
29/01/2019	07.00 – 09.00	-	-	24 to 30	22 to 28
29/01/2019	15.00 – 16.00	-	-	21 to 31	17 to 23
30/01/2019	10.00 – 12.00	16 to 13	17 to 15	-	-
30/01/2019	16.00 – 20.00	-	-	28 to 140	23 to 132
31/01/2019	09.00 – 10.00	58 to 30	62 to 31	-	-
31/01/2019	12.00 – 14.00	-	-	20 to 31	19 to 29
01/02/2019	05.00 – 08.00	-	-	10 to 24	9 to 22
01/02/2019	17.00 – 20.00	-	-	14 to 21	12 to 18
02/02/2019	16.00 – 19.00	-	-	9 to 18	8 to 17
03/02/1019	18.00 – 23.00	22 to 9	24 to 10	-	-
04/02/2019	15.00 – 19.00	-	-	11 to 120	8 to 101
05/02/2019	01.00 – 04.00	92 to 41	92 to 43	-	-
05/02/2019	09.00 – 10.00	48 to 34	50 to 35	-	-
05/02/2019	14.00 – 16.00	-	-	18 to 35	15 to 17
06/02/2019	04.00 – 07.00	-	-	4 to 25	2 to 19
06/02/2019	08.00 – 09.00	43 to 39	44 to 41	-	-
06/02/2019	14.00 – 17.00	-	-	19 to 28	17 to 27
06/02/2019	18.00 – 19.00	29 to 28	29 to 31	-	-
07/02/2019	02.00 – 03.00	9 to 4	9 to 5	-	-
07/02/2019	05.00 – 08.00	-	-	1 to 7	1 to 6

Date	Local Time	Storage of polluted air		Storage of clean air	
		NO_x Roof decrease, and NO_x Roof < NO_x Ground		NO_x Roof increase, and NO_x Roof > NO_x Ground	
		NO_x Roof (ppb)	NO_x Ground (ppb)	NO_x Roof (ppb)	NO_x Ground (ppb)
07/02/2019	14.00 – 17.00	-	-	6 to 12	5 to 11
07-08/02/2019	22.00 – 02.00	17 to 9	18 to 11	-	-
08/02/2019	08.00 – 11.00	13 to 11	14 to 11	-	-
08/02/2019	14.00 – 16.00	-	-	5 to 9	5 to 7
09/02/2019	15.00 – 19.00	-	-	3 to 15	2 to 13
09/02/2019	20.00 – 23.00	15 to 13	17 to 14	-	-
10/02/2019	09.00 – 11.00	-	-	5 to 8	4 to 7
11/02/2019	14.00 – 19.00	-	-	10 to 120	8 to 108
12/02/2019	01.00 – 02.00	29 to 26	30 to 29	-	-
12/02/2019	10.00 – 12.00	23 to 17	25 to 18	-	-
12/02/2019	13.00 – 15.00	-	-	16 to 23	14 to 21
13/02/2019	04.00 – 08.00	-	-	10 to 18	9 to 18
13/02/2019	20.00 – 23.00	20 to 10	23 to 12	-	-
14/02/2019	16.00 – 20.00	-	-	21 to 78	11 to 51
15/02/2019	13.00 – 15.00	-	-	21 to 25	17 to 21
15/02/2019	20.00 – 22.00	24 to 14	25 to 15	-	-
16/02/2019	04.00 – 06.00	-	-	11 to 14	6 to 11
16/02/2019	12.00 – 16.00	-	-	9 to 17	4 to 14
17/02/2019	04.00 – 10.00	-	-	6 to 14	2 to 13
17/02/2019	20.00 – 22.00	14 to 13	14	-	-
18/02/2019	03.00 – 05.00	-	-	10 to 16	8 to 14
19/02/2019	14.00 – 18.00	-	-	12 to 19	9 to 18
19/02/2019	19.00 – 23.00	16 to 8	17 to 9	-	-
20/02/2019	12.00 – 16.00	-	-	12 to 18	7 to 16
21/02/2019	04.00 – 09.00	-	-	5 to 15	3 to 11
21/02/2019	10.00 – 14.00	-	-	12 to 21	7 to 9
22/02/2019	04.00 – 08.00	-	-	9 to 48	6 to 36
22/02/2019	15.00 – 19.00	-	-	12 to 23	6 to 17
23/02/2019	11.00 – 14.00	-	-	13 to 23	10 to 12
23/02/2019	16.00 – 20.00	-	-	18 to 85	10 to 75
24/02/2019	05.00 – 10.00	-	-	33 to 65	28 to 60
24/02/2019	16.00 – 22.00	-	-	15 to 173	9 to 134
25/02/2019	04.00 – 08.00	-	-	41 to 157	39 to 140
25/02/2019	16.00 – 21.00	-	-	25 to 214	13 to 187
26/02/2019	04.00 – 08.00	-	-	47 to 188	41 to 164
26/02/2019	10.00 – 11.00	114 to 38	118 to 39	-	-
26/02/2019	14.00 – 22.00	-	-	19 to 220	12 to 179
27/02/2019	04.00 – 07.00	-	-	50 to 94	48 to 65
27/02/2019	08.00 – 09.00	134 to 86	101 to 107	-	-
27/02/2019	13.00 – 21.00	-	-	16 to 170	9 to 147
28/02/2019	06.00 – 09.00	-	-	11 to 31	8 to 26
28/02/2019	14.00 – 16.00	-	-	19 to 26	16 to 15
01/03/2019	04.00 – 08.00	-	-	7 to 29	3 to 25
01/03/2019	14.00 – 18.00	-	-	17 to 26	13 to 24
02/03/2019	01.00 – 02.00	-	-	7 to 13	4 to 9
02/03/2019	06.00 – 09.00	-	-	7 to 11	4 to 8
02/03/2019	12.00 – 14.00	-	-	9 to 11	5 to 8

The storage phenomenon is caused by the aerodynamic properties of the quadrangle, which are discussed next.

5.3.2. Aspect ratio and influence of wakes in the courtyard of the Biosciences building

The geometry of the canyon in the courtyard of the Biosciences building is described by the ratio of the height (H) to width (W), H/W, which is defined as the aspect ratio. The courtyard is surrounded by walls (Figure 5.6 and Figure 5.7) and there are trees at the corners of the grassland area.

The aspect ratio of the canyon courtyard is H/W = 14 m / 45.5 m = 0.3, and is classified as avenue canyon due to the aspect ratio being below 0.5. The length (L) of canyon divided by height (H), ratio L/H is 48.2 m / 14 m = 3.4 and is classified as a short canyon, based on street canyon subdivisions short (L/H ≈ 3), medium (L/H ≈ 5), and long (L/H ≈ 7) (Vardoulakis *et al.*, 2003).

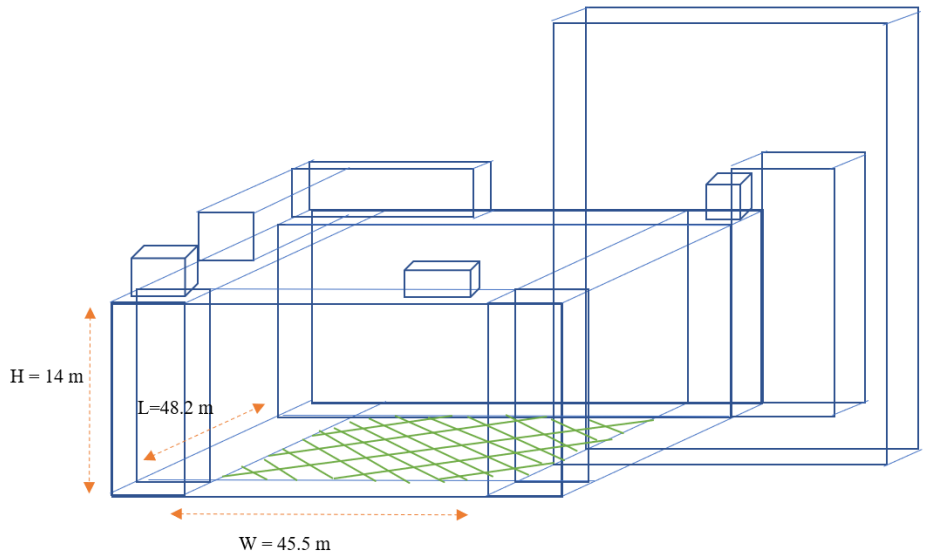


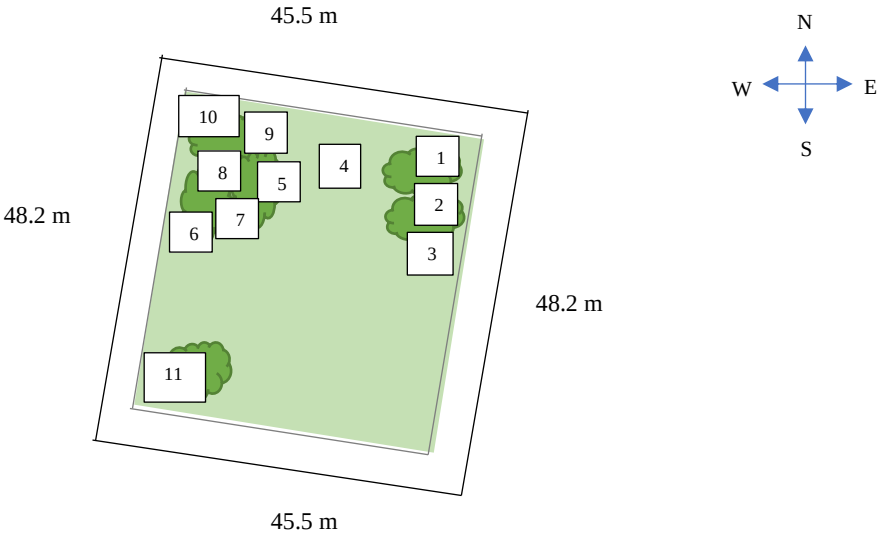
Figure 5.6. Schematic diagram of the courtyard of the Biosciences building (▨) and locations of surrounding buildings. Symbols H, W, L correspond to the building height, building width and building length, respectively. No scale for this diagram.

Figure 5.6 shows a schematic diagram of the courtyard of the Biosciences building and locations of surrounding buildings. The H/W = 0.3 means that the air space in the courtyard is quite well ventilated. However, there are trees in the courtyard grassland site and these

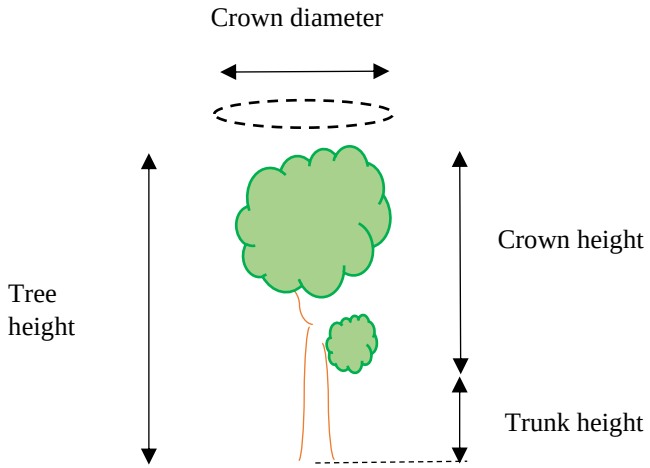
trees could influence the ventilation in the area. Locations, identification and pictures of trees in the courtyard are shown in Figure 5.7.

Trees location in the courtyard

(a)



(b)



(Verma *et al.*, 2016)

(c)

Trees location number	Crown diameter (m)	Trunk height (m)	Tree height (m)
1	3	2.6	14
2	4.5	2.6	13
3	6.9	2.7	14
4	2.1	1.7	5
5	4.5	1.5	15
6	3.5	1.6	15
7	2.4	1.7	5
8	4.4	1.7	11
9	2.9	1.7	15
10	6.4	2.4	15
11	4.4	4.5	13

(d)



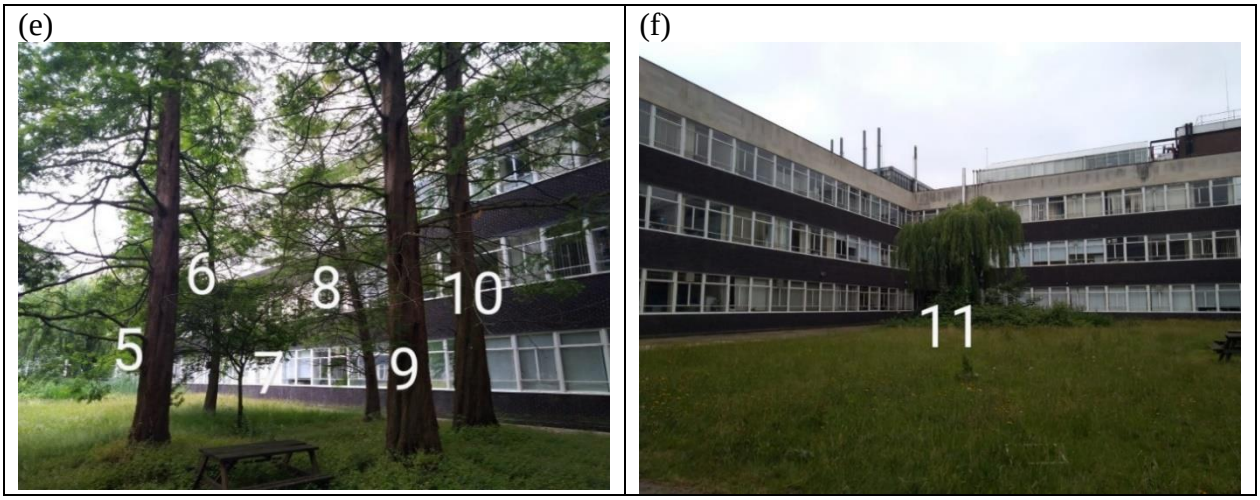


Figure 5.7. Trees locations in the courtyard of Bioscience building. **(a)** Trees locations at the grassland area; **(b)** Schematic diagram of canopy dimensions (Verma *et al.*, 2016); **(c)** information of each tree with identification number, crown length, trunk height and tree height in meter; **(d)** pictures of trees location, number 1 to 4; **(e)** pictures of trees location, number 5 to 10; and **(f)** picture of tree location, number 11.

The impact of trees on air flow and turbulence can affect the dispersion process (AQEG, 2018). The Air Quality Expert Group (AQEG), an expert committee of the Department for Environment, Food and Rural Affairs (Defra), UK, released a report in 2018 on effects of vegetation on urban air pollution and showed the effect of trees, their layout and density in relation with airflow and turbulence. Flow decelerates upwind and around the tree because the flow is blocked by the tree, and there is further deceleration close to the tree. However, turbulence is also generated due to the air flows through the branches of tree. An increase of tree density could reduce the flow through and around the trees, and over the trees, flow is increased. Furthermore, wind speed can change the shape of trees and the magnitude of this change is dependent on wind speed.

Wind flows into the courtyard and trees can block or decelerate the flow. Near the tree branches, flow is decelerating and also generating turbulence. Figure 5.8 shows how trees influence air circulation by blocking the wind flow, reducing flow, generating turbulence and recirculating the flow.

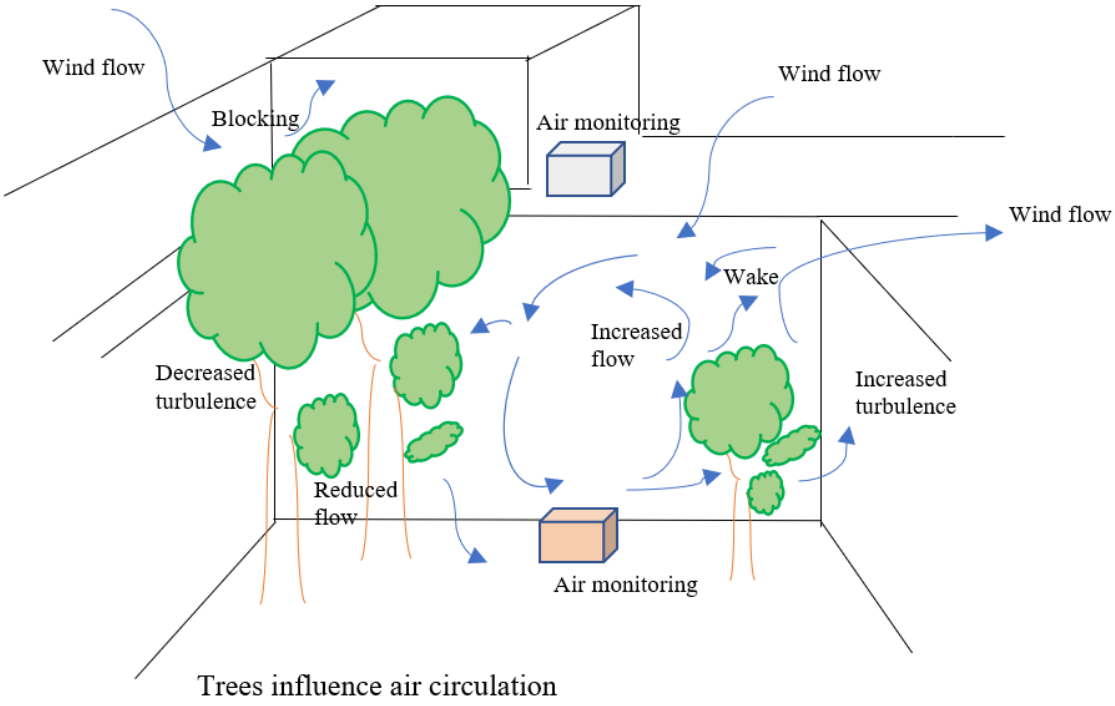


Figure 5.8. Schematic diagram shows how trees influence air circulation in the courtyard of the Biosciences site. The increased turbulence due to the air flows through the branches of tree that generates turbulence, and the decreased turbulence due to the existence of tree is blocking the flows (Adapted from Oke, 2002; AQEG, 2018).

The magnitude of wind speed affects the wake and affects the process of slowing the flow and generating the turbulence. Higher wind speed means higher friction velocity which is indicative of a stronger turbulent transport of particles and gases. Higher relative humidity could increase particle size, and this can increase the deposition velocity. Increasing temperature, particularly during clear sky conditions, increases mixing of fine particles in the atmosphere because of transport by convective plumes (Oke, 2002).

A limitation at the outset of this study was the lack of meteorological data on the roof and the ground. Therefore, to understand the profile of wind speed, temperature and relative humidity on the roof and ground of the Biosciences site, sampling of meteorological data was conducted.

5.3.3. Meteorological observations

Wind speed, temperature (T) and relative humidity (RH) were measured using a Kestrel 3000 pocket weather meter. Two Kestrels were used during the study, one set on the roof and the other on the ground. The Kestrels were mounted on tripods and operated by two people who recorded the observation data at the same time. Observations were conducted for 1-hour over 9 days (10 observation points), 13 to 29 May 2019 inclusive. During the observations, data was recorded every 30 seconds for 1 hour (121 data points) simultaneously at the roof and the ground, then averaged over the hour. The results are shown in Table 5.4.

Table 5.4. Measurement of wind speed, temperature and relative humidity on the roof and ground for 1-hour, for 10 observation data

No	Date	Hour	Weather	**WS average (m s^{-1})**		**T (°C)**		**RH (%)**	
				ROOF	GROUND	ROOF	GROUND	ROOF	GROUND
1	13 May 2019	10 am	Few clouds	0.5	0.7	16.4	16.7	45.1	48.9
2	14 May 2019	10 am	Sunny	0.7	1.3	18.5	15.2	28.3	34.8
3	15 May 2019	10 am	Sunny	0.7	0.9	18.7	15.1	36.3	43.8
4	16 May 2019	11 am	Sunny	0.9	1.7	17	15.8	43.6	48.9
5	17 May 2019	09 am	Overcast	1.7	0.8	10.5	11.5	72.1	67.0
6	17 May 2019	14 pm	Cloudy	1.5	1.8	15.1	14.6	66.9	66.3
7	22 May 2019	10 am	Sunny	0.9	0.9	18.2	15.8	46.5	51.8
8	23 May 2019	10 am	Sunny	0.7	1.4	19.3	15.9	42.9	49.5
9	28 May 2019	10 am	Overcast	1.1	0.5	14.0	13.6	63.3	63.9
10	29 May 2019	10 am	Overcast	1.1	0.8	12.5	12.2	57.0	57.2

From Table 5.4, it can be seen that wind speed at the ground was higher than at the roof, except during overcast periods when the wind speed at the roof was higher. The condition of wind speed being higher at ground level than on the roof was odd because it contradicts the logarithmic wind profiles that underpin friction velocity (u*). Friction velocity is an important scaling variable in turbulent flows and depends on stability of the atmosphere (Weber, 1999). Figure 5.9. shows the logarithmic wind profiles at neutral, unstable, and stable conditions; and wind speeds change with height (Koleiny, 2009).

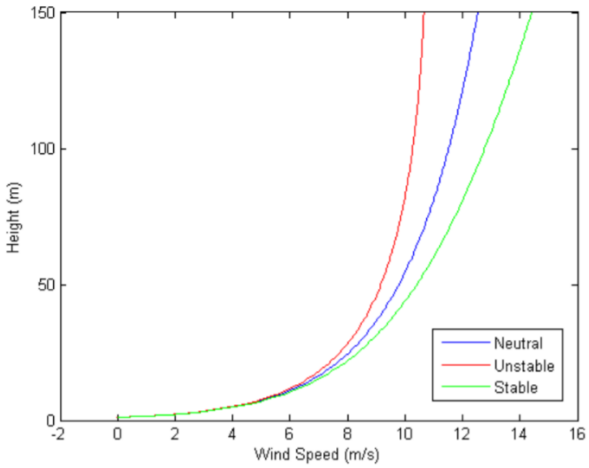


Figure 5.9. Logarithmic wind profiles over stability variation (Koleiny, 2009).

In this study, the higher wind speed at the ground could be related to the air circulation in the quadrangle and the wake due to the presence of trees in the location which can potentially increase or decrease wind speed in the area. However, the data points of wind speed and weather conditions are not sufficient to draw a conclusion regarding the influence of trees on wind speed and their relation to the weather condition in the quadrangle site.

Figures 5.10 and 5.11 show the graph of wind speed and temperature on the roof and the ground of the Bioscience building from observation data (see Table 5.4).

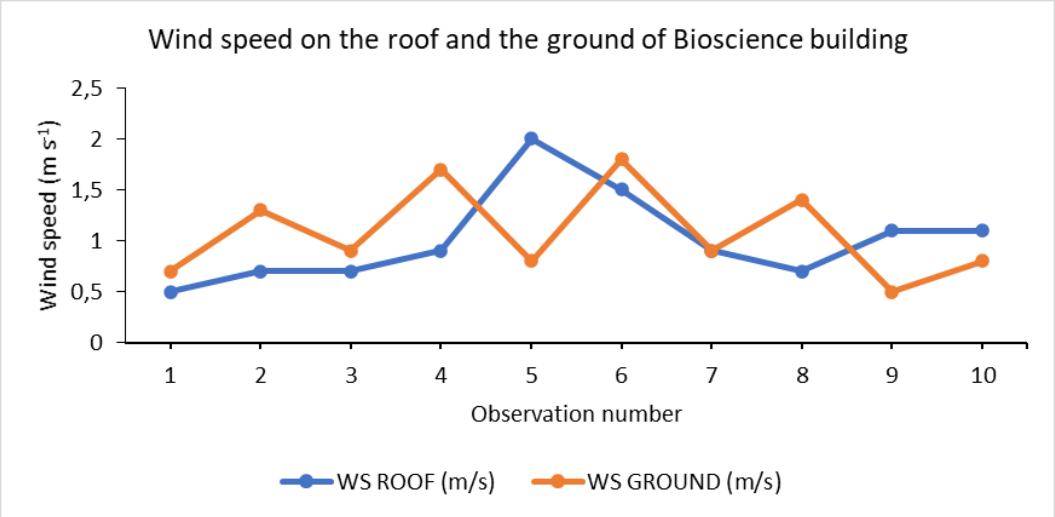


Figure 5.10. Wind speed on the roof (blue line) and ground (orange line) at the Biosciences building. The observation was conducted for 1-hour in 9 days (10 observation points), 13 to 29 May 2019

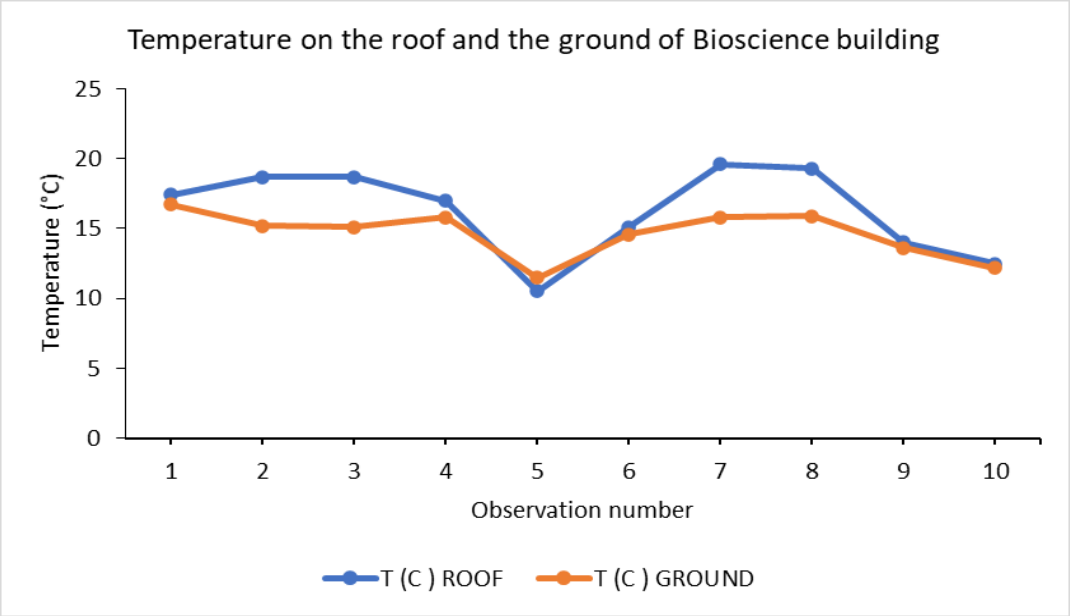


Figure 5.11. The temperature on the roof (blue line) and ground (orange line) at the Bioscience building. The observation was conducted for 1-hour in 9 days (10 observation points), 13 to 29 May 2019

The temperature on the ground was lower than on the roof when the weather was sunny. This can be related to the existence of the tree canopy and the orientation of buildings that can block direct solar radiation from heating the ground. Because the roof is an open area, sunlight can directly heat its surface. However, during cloudy or overcast periods, the temperature on the roof was similar to that at ground level.

The observation data compared with the Coleshill weather station at the same time is shown in Table 5.5.

Table 5.5. Data of wind speed, temperature and relative humidity from Coleshill weather station data, 13 – 29 May 2019

No	Date	Hour	Weather (observation)	Coleshill weather station data							
				Cloud cover	Information	ws (knot)	ws (m s^{-1})	T (˚C)	RH (%)	Wind direction	Pressure (hPa)
1	13 May 2019	10 am	Few clouds	0	clear sky	3	1.5	15.2	51.9	250	1040.3
2	14 May 2019	10 am	Sunny	0	clear sky	5	2.6	15.3	37	100	1035.3
3	15 May 2019	10 am	Sunny	0	clear sky	4	2.1	16	51.5	80	1027.5
4	16 May 2019	11 am	Sunny	0	clear sky	9	4.6	15.1	52.1	70	1020.4
5	17 May 2019	09 am	Overcast	8	Overcast	8	4.1	9.8	86.8	20	1011.6
6	17 May 2019	14 pm	Cloudy	6	Broken	8	4.1	15.4	70.5	60	1009.4
7	22 May 2019	10 am	Sunny	4	Scattered	5	2.6	15.9	52.5	220	1019.7
8	23 May 2019	10 am	Sunny	0	clear sky	6	3.1	17.7	46.4	240	1016.3
9	28 May 2019	10 am	Overcast	8	Overcast	8	4.1	12.3	79.8	310	1012.1
10	29 May 2019	10 am	Overcast	8	Overcast	7	3.6	11.7	64.1	170	1018

Note: Weather station: Coleshill, ID number: 19187

Meteorological factors, such as wind speed, relative humidity and temperature affect dry deposition velocity. Wind speed and relative humidity have a positive correlation with dry deposition velocity (Mariraj Mohan, 2016).

5.3.4. Literature describing experiments on measuring dry deposition and deposition velocity

Deposition velocity (V_d) values are used to calculate deposition. A review of selected published literature on dry deposition velocity values is described below. Scenarios of experimental set-ups for measuring dry deposition flux and deposition velocity values are also described.

5.3.4.1. Deposition velocity values of gases

Table 5.6. shows the value of NO_x deposition velocity from references. The rate of deposition velocity is in the range from 0.001 to 0.0067 m s^{-1}.

Table 5.6. Deposition velocity of NO_x from references

Pollutant	Time, Location	Surface	Method	Deposition velocity (m s^{-1})			Reference
				Daytime	Night-time	Day and night	
NO_x	Northern Colorado	Prairie land	Gradient method	-	-	0.0067	Kasting, 1980 in Padro and Edwards, 1991
NO_x	April – November 2000 Massachusetts, USA	Deciduous forest	Eddy covariance flux	-	-	0.002	Horii *et al.*, 2004
NO_x	March 1982, East Anglia	Grass in rural area (5 cm)	Gradient method	-	-	0.001 – 0.006	Delany and Davies, 1983

Finlayson-Pitts and Pitts Jr. (1999) reported that NO_2 deposition velocity lies in the range 0.001 to 0.005 m s^{-1}, and the deposition velocity of nitrogen dioxide in grassland surfaces is in the range 0.0011 – 0.0015 m s^{-1} (Jia *et al.*, 2016). In their study, Pugh *et al*. (2012) used the deposition velocity value of NO_2 for grasses at 0.003 m s^{-1} (in the range 0.002 – 0.004 m s^{-1}) and for O_3 at 0.01 m s^{-1} (in the range 0.0006 – 0.018 m s^{-1}).

The deposition velocity of NO_2, measured over an area of short grass between May and August 2001 in Ontario, Canada was 0.0027 ± 0.00017 m s^{-1}, calculated by the flux gradient method (Watt *et al.*, 2004), while in Switzerland the deposition velocity of NO_2 on grassland (a meadow surrounded by agricultural land) was 0.0011 - 0.0024 m s^{-1} (Hesterberg *et al.*, 1996), and 0.00067 m s^{-1} on grassland (park grass) in the North of London (Yamulki *et al.*, 1997).

Table 5.7. shows the values of NO_2 deposition velocity from literature studies. The rate of deposition velocity is in the range 0.00015 to 0.005 m s^{-1}.

Table 5.7. Deposition velocity of NO_2 from references

Pollutant	**Time, Location**	**Surface**	**Method**	**Deposition velocity (m s^{-1})**			**Reference**
				Daytime	**Night-time**	**Day and night**	
NO_2	-	Primary interior of leaves; exterior surfaces	when stomata open	-	-	0.001 – 0.005	Finlayson-Pitts and Pitts Jr, 1999
NO_2	May – August 2001 (summer), Ontario Canada	Short grass (< 1m)	Flux gradient method	-	-	0.0027 ± 0.00017	Watt *et al.*, 2004
NO_2	29/08 to 20/09 2005	Meadow (mown before sampling time)	Eddy covariance method	0.003	-	-	Stella *et al.*, 2013
NO_2	-	Grassland, broadleaf species, green walls and roofs	Literature review	-	-	0.002 – 0.004 In their study using 0.003	Pugh *et al.*, 2012
NO_2	1998 – 2007 West and Central Africa	Dry savannas, wet savannas, equatorial forests	Inferential method	0.0013 – 0.0031 (Dry season)	0.0017 – 0.0033 (Wet season)	0.0013 – 0.0037 (Monthly means)	Adon *et al.*, 2013
NO_2	Guangzhou, China	Tree canopy	Literature review	-	-	0.001– 0.005 Average: 0.0037	Jim and Chen, 2008
NO_2	Switzerland	Grassland	Experiment	-	-	Daily average 0.0011 to 0.0024	Hesterberg *et al.*, 1996
NO_2	Southern Scotland	Drained moorland	-	-	-	0.001 to 0.002	Fowler *et al.*, 1998
NO_2	Dynamic chamber in laboratory	Leaves, forest	Experiment	0.00123 ± 0.00009 (light experiment)	0.00015 ± 0.00001 (dark experiment)	-	Delaria *et al.*, 2018
NO_2	North of London	Grassland	Experiment	-	-	0.00067	Yamulki *et al.*, 1997

Table 5.8. shows the NO deposition velocity from literature studies. Based on literature, the NO deposition velocity lies in the range 0.00005 to 0.0017 m s^{-1}.

Table 5.8. Deposition velocity of NO from references

Pollutant	Time, Location	Surface	Method	Deposition velocity (m s^{-1})			Reference
				Daytime	Night-time	Day and night	
NO	-	Forest, species Medicago satiwa	Chamber	0.0017	-	-	Bennett and Hill, 1973 (Hanson and Lindberg, 1991)
NO	-	Forest, species Medicago satiwa	Chamber	0.001 (1 mm/s)	-	-	Hill, 1971 (Hanson and Lindberg, 1991)
NO	Germany, 10-22 September 1992	Short vegetation	Concentration gradient	emission	-	0.0005	Horváth *et* al., 1998
NO	-	Leaves, forest	Experiment	0.00012 ± 0.00002 (light experiment)	0.00005 ± 0.00002 (dark experiment)	-	Delaria *et al.*, 2018

The value of deposition velocity for O_3 from Finlayson-Pitts and Pitts Jr (1999) is in the range 0.001 – 0.008 m s^{-1}. Horváth *et al*. (1998) measured the dry deposition velocity and flux of NO, NO_2 and O_3 in Germany over a surface of short vegetation, and found the O_3 deposition velocity was low, 0.0007 m s^{-1}.

Colbeck and Harrison (1985), and Garland and Derwent (1979) found the daytime O_3 deposition velocity decreased in the late afternoon linked to an increase of surface resistance. Surface resistance of grassland is related to the ability of vegetation to respond to the surrounding conditions during both day and night-time. For example, the photosynthetic process opens the stomata in daytime, and this allows ozone to access the inner leaf (Wesely *et al.*, 1982; Colbeck and Harrison, 1985).

Table 5.9. Deposition velocity of O_3 from references

Pollutant	Time, Location	Surface	Method	Deposition velocity (m s^{-1})			Reference
				Daytime	Night-time	Day and night	
O_3	-	Primary interior of leaves; exterior surfaces	-	-	-	0.001 – 0.008	Finlayson-Pitts and Pitts Jr, 1999

Pollutant	Time, Location	Surface	Method	Deposition velocity (m s^{-1})			Reference
				Daytime	Night-time	Day and night	
O_3	29 August – 20 September 2005	Meadow (mown before sampling time)	Eddy covariance method	0.006	-	-	Stella *et al.*, 2013
O_3	January – August 2004, Thailand	Forest	Wet season	0.0062 – 0.0065	0.0025 – 0.0027	-	Matsuda *et al*., 2006
			Dry seasons	0.0037 – 0.0039	0.0012 – 0.0013		
O_3	5 March – 2 August 1988, Colorado	Grassland	Eddy correlation	0.0036	0.0022		Stocker *et al*., 1993
O_3		grass	Literature review	-	-	0.002 to 0.006	Droppo and Doran, 1978 in Sehmel, 1980
O_3	August 2001 and July 2002	Forest	Eddy covariance method	0.004 – 0.006	0.002 – 0.004	-	Keronen *et al*., 2003
O_3	January – April 2002, Thailand	Forest	Gradient method	0.0032	0.0004	-	Matsuda *et al*., 2005
O_3	September and November 2000, Beijing China	surface: short grass	Gradient method	0.002 ± 0.001 (late summer)	0.004 ± 0.002 (early winter)	-	Sorimachi *et al*., 2003
O_3	1998 – 2007 Africa	Dry savannas, wet savannas, equatorial forests	Inferential method	-	-	0.0014 to 0.0040 (monthly means)	Adon *et al*., 2013
O_3	4-25 /09/ 1981 3-30/06/1982 Illinois, US	Grass field 32 ha	Eddy correlation Gradient method	Up to 0.009	< 0.001	-	Dolske and Gatz, 1985
O_3		Short dry gas	Literature review	-	-	0.0009 to 0.009	(Galbally, 1968) in Sehmel, 1980
O_3	January and October 1983, UK	Grassland	Gradient method	-	-	0.0008 – 0.0091	Colbeck and Harrison, 1985
O_3	10-22 September 1992, Germany	Short vegetation	Concentration gradient	-	-	0.0007	Horváth *et al*., 1998
O_3	Street canyon at Hannover, Berlin, Copenhagen 1994, 1995	Grassland, broadleaf species, green walls and roofs	Literature review	-	-	0.0006 – 0.018 In their study using 0.01	Pugh *et al*., 2012

5.3.4.2. Methods to measure dry deposition and/or dry deposition velocity

From several methods available to measure dry deposition and dry deposition velocity, the most widely chosen are the eddy covariance method (direct) and the gradient method (indirect). These two methods are described in the section below.

5.3.4.2.1. Direct method

Experimental measurement of dry deposition for gases using the direct method is often considered using the eddy covariance or eddy correlation method. This method is commonly used to calculate the fluxes based on the theory that the complete budget of transport up and down is representative of the average flux over the area (Businger, 1986). The eddy covariance method requires fast-response measurement sensors to measure the eddy correlation of fluxes (Stocker *et al.*, 1993; Myles *et al*., 2007).

Measurements of rapid fluctuations of vertical wind speed (*w*) and air concentration (*c*) have to be in the same location, and the sensors need to have a quick response to measure all eddies contributing to the flux (Businger, 1986). The product of vertical wind and the concentration gradient constitute the flux of the atmospheric substance.

$$F_c = \overline{w'c'} + \bar{w}\,\bar{c} \qquad (E.5.2)$$

where $\bar{w}$ is mean vertical wind speed, $\bar{c}$ is mean concentration, $\overline{w'c'}$ is the fluctuating components about the means of the same quantities, w' and c' are the instantaneous vertical wind speed and the deviation from the mean concentration.

Stocker *et al.* (1993) measured fluxes of nitrogen oxides and ozone over an area of shortgrass by the eddy correlation method during the period March to August 1988. They chose a grassland field in Northern Colorado, near Pawnee National Grasslands. The tower and shelter were placed in the corner of a 6-ha grazing area. The sampling point was set at 6 m height on the meteorological tower. Nicolini *et al.* (2015) estimated gas flux using the eddy covariance method over crop fields, a flat area 120 – 140 m wide. Their experiment was conducted from 31 July to 4 August 2012 in Moscow, Russia. The measurement height was shortened due to the fetch being of limited distance, which is 100 m of horizontal distance. The EC measurement height was set at 0.8 m above the canopy's displacement height (0.3 m).

Ideally, the sampling location should be an open, flat, and large area to have an adequate fetch – the ratio of measurement height to fetch, 1:100 – to ensure the constant flux is produced in the representative area (Nicolini *et al.*, 2015).

The instruments that are usually needed for setting up the eddy covariance method as summarised by Stocker *et al.* (1993); Twine *et al.* (2000); Nicolini *et al.* (2015) are outlined below:

a. Fast-response instrumentation to monitor rapid fluctuations of species.
b. 3-axis sonic anemometer to measure wind velocity and direction.
c. Platinum wire resistance thermometer to measure temperature and heat flux.
d. The chemical sensors.
e. Instrument analysers to measure gas concentrations of the species of interest, for example Chemiluminescent analyser to measure NO_x, NO_2 concentrations; UV photometric ozone to measure O_3 concentration; LI-7200 infra-red gas analyser to measure CO_2 and H_2O.
f. Measurements for other meteorological data, for example, relative humidity, solar radiation, net radiometers and soil heat flux plates.
g. Computer interfaced to collected and stored data, and software for processing real-time data with a program for eddy correlation. For example, using EddyPro software.

5.3.4.2.2. Indirect method

The gradient method is an indirect method to measure flux and dry deposition velocity for gases and particles.

The gradient method is based on the calculation of gases and particle fluxes from the concentration gradient with height (Garland, 1977; Colbeck and Harrison, 1985; Watt *et al.*, 2004). Pollutant concentrations at two different heights have to be measured very accurately to have confidence in the difference in concentration (dC) because the concentration gradient is usually very small (Businger, 1986). Deposition velocity is calculated using equation E.5.1.

Horváth *et al*. (1998) measured dry deposition velocities of NO, SO_2 and O_3 by the gradient method over short vegetation in Germany, during the period 10-22 September 1992. The ratio of the fetch distance to the observation height was more than 100:1. The heights of

concentration measurements were set at 0.5 m, 1 m, 2 m and 4 m; thus, the fetch was more than 400 m. Watt *et al.* (2004) evaluated flux and deposition velocity of NO_2 using the flux gradient method over a surface of short grass in Ontario, Canada, from 17 May to 31 August 2001. They used NO_x analysers set up at height 0.3 m and 0.5 m, and also installed meteorological measurements. An experiment to calculate dry deposition of fine aerosol on the grass surface of a sports field at Essex University was conducted by Allen *et al*. (1991) between June 1988 and June 1989. The experiment was set up to meet the requirements of the micrometeorological technique, i.e., the fetch distance was more than 200 m, and the measurement height was not more than 2 m.

The instruments needed for setting up the gradient method as summarised by Allen *et al*. (1991), Horváth *et al*. (1998), and Watt *et al.* (2004) are outlined below:

a. Measuring instruments for pollutant concentrations at different heights, examples being a TECO 43A monitor for measuring SO_2, a TECO 14B monitor for nitric oxide, Chemiluminescence analysers for measuring NO_2 aerosol samples.
b. Measurements for meteorological data, such as:
    - Kipp and Zonen sensors to measure solar radiation;
    - Wind direction meter;
    - Temperature and wind velocity sensors;
    - Sonic anemometer to measure friction velocity and sensible heat flux;
    - Cup anemometers to measure wind speed; or
    - Temperature and precipitation data, can be obtained from the nearest weather station,

Overall, both the direct and indirect methods require accurate measurement of fluxes, and so highly sensitive instruments and careful site selection are required when implementing either method.

In the experimental plan, the height of measurement needs to be considered so that, for the gradient method, the height interval is sufficiently large to produce a difference in concentration and can be measured by the chemical sensors and, for the eddy covariance method, the sensor instruments must have sufficient fast response to resolve fluctuations (Wesely and Hicks, 2000).

Site selection is very important and must be chosen to comply with the rule that the upwind fetch should extend to the distance of 100-200 times the height of measurement (Businger, 1986; Wesely and Hicks, 2000). Fetch is the upwind distance where the site has the same surface condition. A large fetch is needed to reach equilibrium of the flow to avoid the excessive flux variation caused by turbulence and to ensure the constant flux (Schultz *et al.*, 2005; EANET, 2010). Furthermore, a site covering a large, flat area (more than 100 m^2) with a uniform surface should be selected. The surface type depends on the objective of the research—for example, grassland for studying the effects of grass on O_3 deposition.

The above considerations should be taken into account and properly conducted when measuring dry deposition and deposition velocity with both the direct and indirect methods. Reviewing our site at the quadrangle location that was surrounded by buildings, we realised we would not be able to fulfil the requirements of fetch distance and the homogeneous surface, which is uniform grassland.

In our study, we only measured concentrations of BC and gases at roof and ground sites to obtain a vertical concentration gradient. The deposition velocity of BC was estimated from published literature. The deposition velocity of gases was calculated using an analogy with carbon particles which were used to estimate an eddy diffusivity. This technique is theoretically correct, but inadvisable in this context due to the highly complex aerodynamic properties of the measurement location. We understood the weakness in this method and the weakness in our sampling location—not an ideal location for applying the indirect method. However, we used the data and present the method used for calculating the deposition velocity of NO_x. We calculated only for NO_x because of the difficulty of accounting for rapid photochemical exchange between NO, O_3 and NO_2 in the boundary layer.

5.3.5. Deposition velocity of NO_x

The indirect method can be used to estimate the dry deposition velocity of gases over grassland. The approach uses the equations E.2.18 (see Chapter 2., Section 2.5).

In this study, the approach was to assume that the value of K is independent of the depositing species, so it can be used to predict the fluxes and deposition velocity for other pollutants — for example, NO_x; as shown in the following formula, which is derived from equation E.2.18.

The deposition velocity of NO_x can be calculated as below:

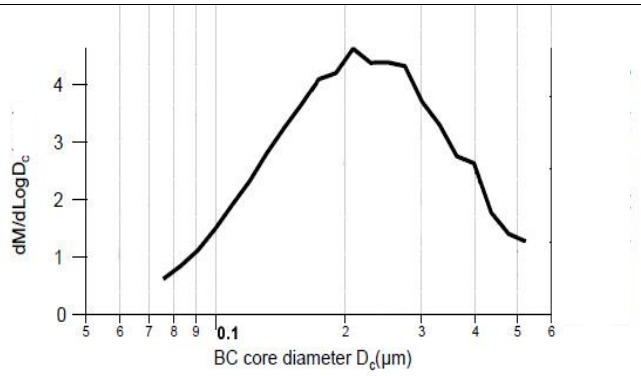
$$Vd(NO_x)\ x\ \frac{[NO_x]}{\frac{dC}{dZ}NO_x} = Vd(BC)\ x\ \frac{[BC]}{\frac{dC}{dZ}\ BC} \qquad (E.5.3)$$

Where V_d (NO_x) is deposition velocity of NO_x (m s^{-1}); [NO_x] is NO_x concentration (µg m^{-3}) at 1 metre above the ground; $\frac{dC}{dZ}NO_x$ is concentration gradient of NO_x ; V_d (BC) is deposition velocity of black carbon (m s^{-1}); [BC] is black carbon concentration (µg m^{-3}) at 1 metre above the ground; $\frac{dC}{dZ}$ BC is concentration gradient of black carbon.

Steps to calculate deposition velocity of NO_x are explained below.

a. Deposition velocity (V_d) of BC

A graph of BC mass as a function of diameter from Liu *et al*. (2014) (Figure 5.12) and a graph of particles deposition velocity as a function of diameter on grassland from Pellerin *et al*. (2017) in Giardina and Buffa, (2018) (Figure 5.13) were used to estimate a BC deposition velocity. The friction velocity (u*) used in the experiment from Pellerin *et al*., (2017) was 0.26 m s^{-1}.

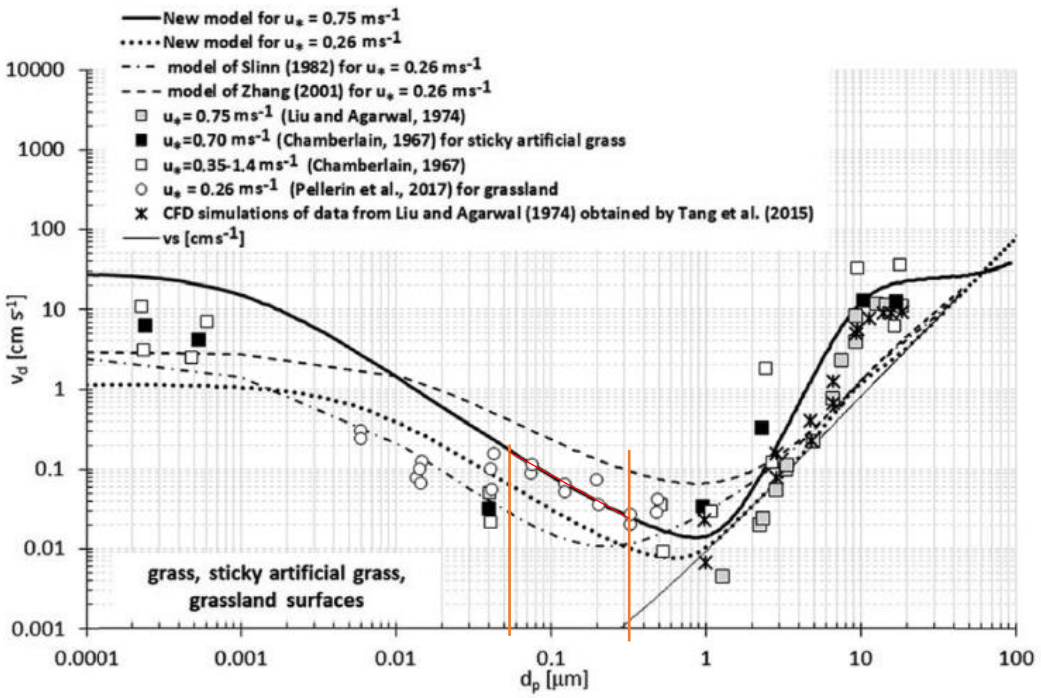


X = BC core diameter (µm)	Y = dM/dLog Dc (µg/m^3)
0.07 – 0.08 µm = 0.3 cm	1 – 2 µg/m^3 = 0.6 cm
0.08 – 0.09 µm = 0.3 cm	2 – 3 µg/m^3 = 0.6 cm
0.09 – 0.1 µm = 0.2 cm	3 – 4 µg/m^3 = 0.6 cm
0.1 – 0.2 µm = 1.6 cm	
0.2 – 0.3 µm = 0.95 cm	
0.3 – 0.4 µm = 0.7 cm	
0.4 – 0.5 µm = 0.5 cm	
0.5 – 0.6 µm = 0.4 cm	

Source: (Liu *et al.*, 2014)

Figure 5.12. Mass size distribution of BC core (dM/dLogDc), taken from Liu *et al.* (2014).

The mass fraction for each size bin is derived from Figure 5.12 in Liu *et al.* (2014). The V_d is calculated for BC particles size 0.0075 – 0.5 µm (Figure 5.13) from the figure below (for u* = 0.26 m s^{-1} (Pellerin *et al.*, 2017)).



Source: (Giardina and Buffa, 2018)

Figure 5.13. Deposition velocity on grass as a function of particle size (Giardina and Buffa, 2018)

The average deposition velocity is calculated from the summed product of fractional area and V_d of BC for each bin size, using the equation below:

$$V_d = \sum (A \; x \; V_d)_i \qquad (E.5.4)$$

where A_i is fractional area for size i and V_d i is deposition velocity for size i. The result for BC deposition velocity is 0.14 cm s^{-1} (0.0014 m s^{-1}) as shown in Table 5.10.

Table 5.10. Data for calculating the deposition velocity of BC

Diameter particle (X value)	BC mass (Y value)	Fractional Area	BC diameter particle	V_d on grass (V_d = -0.37 Dp + 0.233)	Deposition Velocity (Fractional Area x V_d) at u* = 0.26 m s^{-1}
0.075 – 0.08	0.67 – 0.83	0.003	0.075	0.21	0.001
0.08 – 0.09	0.83 – 1.25	0.008	0.08	0.20	0.002
0.09 – 0.1	1.25 – 1.67	0.011	0.09	0.20	0.002
0.1 – 0.18	1.67 – 4.3	0.175	0.1	0.20	0.034
0.18 – 0.19	4.3 – 4.5	0.032	0.18	0.17	0.005
0.19 – 0.2	4.5 – 4.67	0.033	0.19	0.16	0.005

Diameter particle (X value)	BC mass (Y value)	Fractional Area	BC diameter particle	V_d on grass (V_d = -0.37 Dp + 0.233)	Deposition Velocity (Fractional Area x V_d) at u* = 0.26 m s^{-1}
0.2 – 0.21	4.67 – 4.8	0.035	0.2	0.16	0.006
0.21 – 0.23	4.8 – 4.67	0.070	0.21	0.16	0.011
0.23 – 0.28	4.67 – 4.58	0.170	0.23	0.15	0.025
0.28 – 0.3	4.58 – 3.83	0.062	0.28	0.13	0.008
0.3 – 0.36	3.83 – 3	0.151	0.3	0.12	0.018
0.36 – 0.4	3 – 2.83	0.086	0.36	0.10	0.009
0.4 – 0.44	2.83 – 1.83	0.068	0.4	0.09	0.006
0.44 – 0.5	1.83 – 1.42	0.072	0.44	0.07	0.005
0.5 – 0.525	1.42 – 1.33	0.025	0.5	0.05	0.001
sum		1.000			**0.14**

Fluxes of BC were estimated by using the estimated carbon V_d (0.0014 m s^{-1} from Table 5.10) multiplied by carbon concentration. The eddy diffusivity was calculated as hourly average and used to determine the 24-hour values for flux and deposition velocity of gases. The carbon deposition velocity was subject to large uncertainties in the calculation of K which was hard to estimate as we did not actually measure the carbon V_d. Therefore, the uncertainty for carbon V_d was assumed to be 100% to include a very wide range as actual uncertainty could not be calculated.

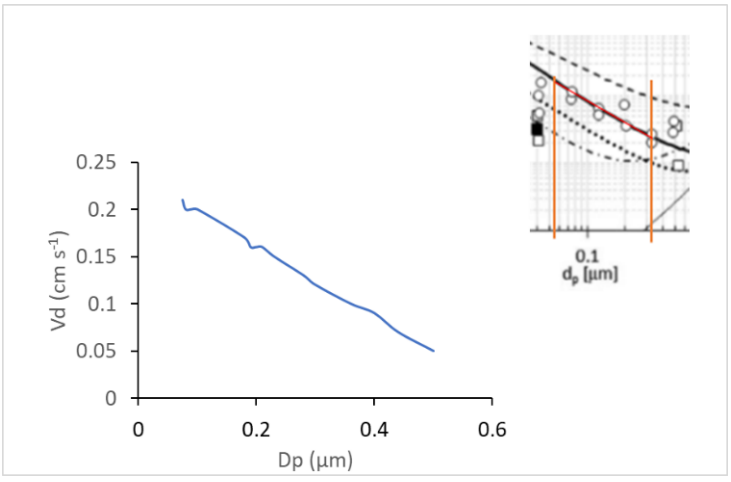


Figure 5.14. Deposition velocity dependence upon particle diameter for a small range of sizes (0.08 µm to 0.5 µm) refer to the data points from Table. 5.10. The points represent the relationship between BC diameter particle (Dp) in µm as x-axis and deposition velocity (V_d) in cm s^{-1} as y-axis

BC particles in the size range 0.08 μm to 0.5 μm (Figure 5.14) are transported largely by diffusion processes (Seinfeld and Pandis, 2016). Figure 5.14. demonstrates that deposition velocity decreases with increasing particle diameter in this range.

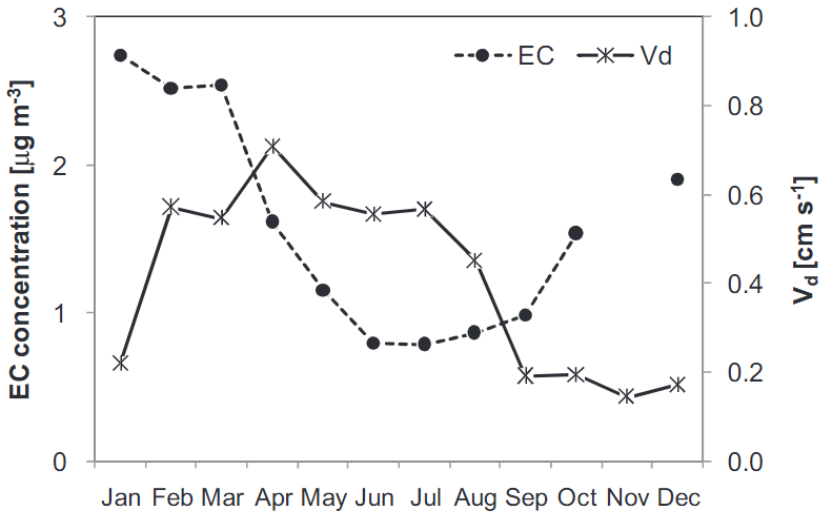


Figure 5.15. Elemental Carbon (EC) concentration and deposition velocity (V_d) from literature (Matsuda *et al.*, 2012), research conducted in Thailand, 2010

Matsuda *et al*. (2012) measured flux and deposition velocities of elemental carbon in a forest in Thailand from January to December 2010 using the inferential method. The annual mean carbon V_d was 0.41 cm s^{-1}, with a higher V_d found in the period February to August (approximately between 0.4 to 0.8 cm s^{-1}) due to the high wind speed in those months and V_d less than 0.2 cm s^{-1} during September to December. Interestingly, the value of carbon V_d in November was around 0.18 cm s^{-1} (Figure 5.15), which is relatively close to our value 0.14 cm s^{-1} that was used to obtain the K value as input data in calculating V_d of the gases in November 2018 and January to March 2019. However, a different location and different meteorological conditions lead to large uncertainties.

b. Eddy Diffusivity (K) estimated from gradients in BC

To estimate eddy diffusivity, the flux of BC is calculated with equation E.2.18, where V_d (cm s^{-1}) is deposition velocity at ground level and C (μg m^{-3}) is the concentration at 1 metre above the ground. In this study, the deposition velocity of BC was taken as 0.0014 m s^{-1} (from a combination of Figures 5.12. and 5.13).

The dry deposition rate of BC is calculated by multiplying the assumed BC deposition velocity with the measured BC concentrations at the reference height. Eddy diffusivity can be estimated by dividing dry deposition of BC at ground level with concentration gradient, if the deposition velocity is known. The value of eddy diffusivity can then be used to calculate fluxes and deposition velocities of gases (see E.2.18 and E.2.3)

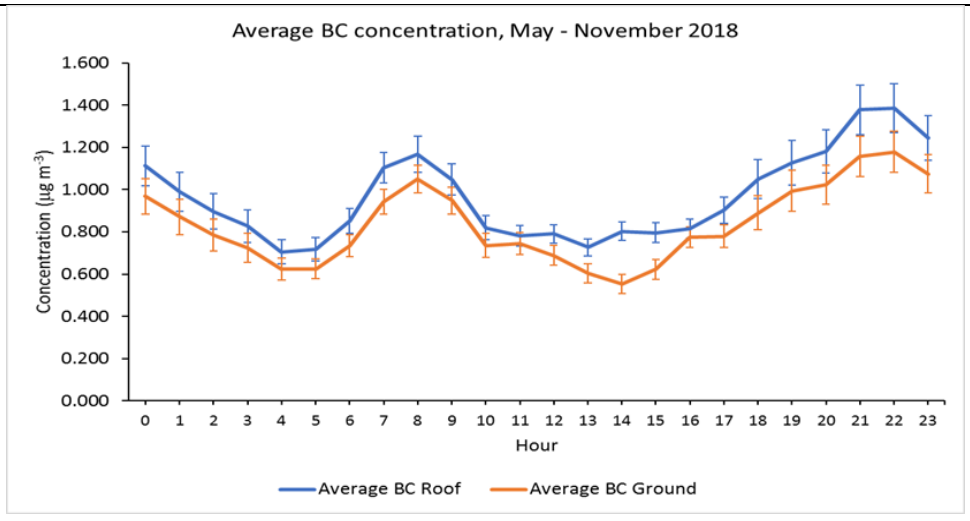
Therefore, the eddy diffusivity for black carbon is estimated using equation E.5.5.

$$K = \frac{-F}{\left(\frac{\Delta C}{\Delta Z}\right)} \qquad (E.5.5)$$

Where K is eddy diffusivity for the mass transfer of species, ΔC/ΔZ is concentration gradient, and F is downward flux, assuming K is independent of depositing species.

The results for K values are shown in Figure 5.16.b

(a)



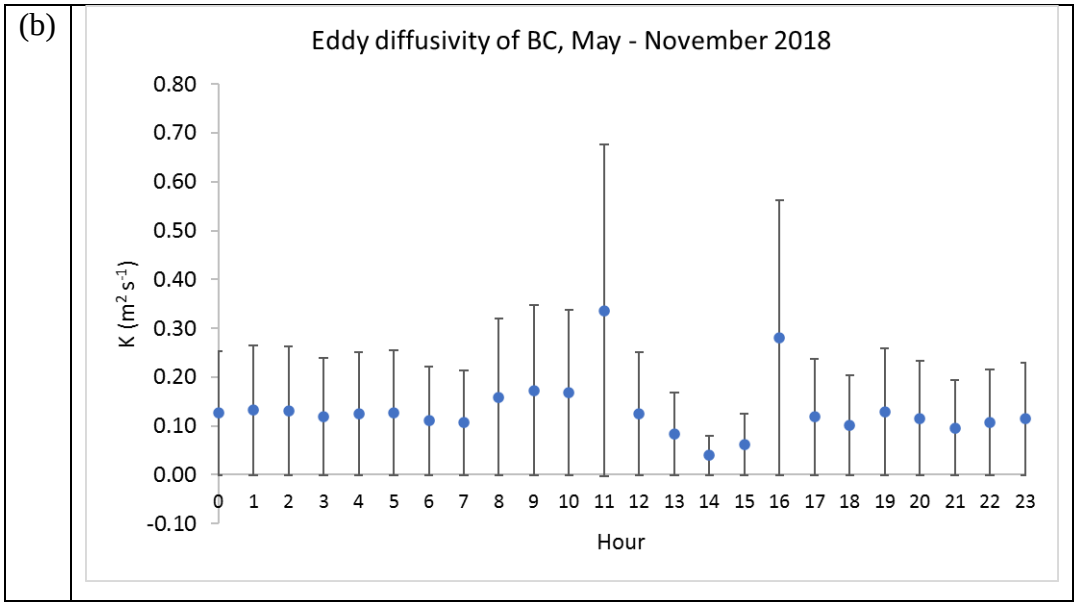


Figure 5.16. Diurnal plots of BC with bars indicate ± standard error of the mean, 1 May – 29 November 2018, **(a)** Diurnal plot of BC concentration on the roof and ground; **(b)** Diurnal plot of eddy diffusivity (K) of BC

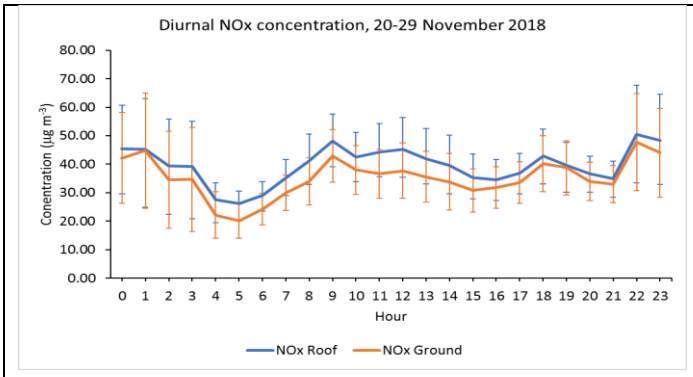
Overall, the average (± standard error) for K over 24-hours was 0.13 ± 0.13 m^2 s^{-1}. The K average in the day was slightly higher than at night, 0.15±0.15 m^2 s^{-1} and 0.12±0.12 m^2 s^{-1}, respectively. Turbulence at night is typically lower (Hargreaves *et al*., 1992; Oke, 2002; Watt *et al*., 2004). In our study, the eddy diffusivity at night-time was in the range 0.10 ± 0.10 m^2 s^{-1} to 0.13 ± 0.13 m^2 s^{-1}, while in the day K fluctuated more, in the range 0.04 ± 0.04 m^2 s^{-1} to 0.34 ± 0.34 m^2 s^{-1}, as shown in Figure 5.16. Minimum K (0.04 m^2 s^{-1}) occurs when the concentration difference (ΔC) is large and the maximum K (0.34 m^2 s^{-1}) when the concentration difference is small.

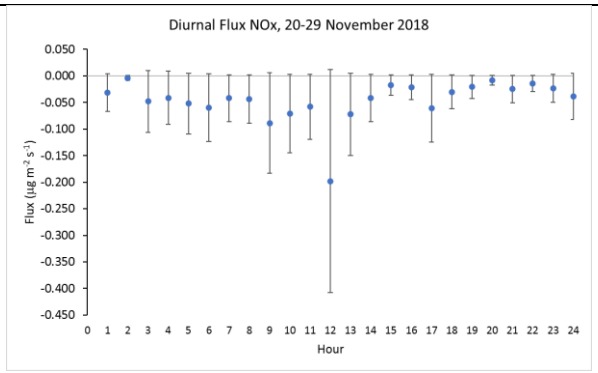
c. Flux of NO_x

K values were calculated as hourly average values from hourly average BC concentration data, in the period 1 May to 29 November 2018. Combining this K with the gas phase pollutant data allows for estimation of gas flux and deposition velocity so that the average flux and deposition velocity for NO_x can be calculated.

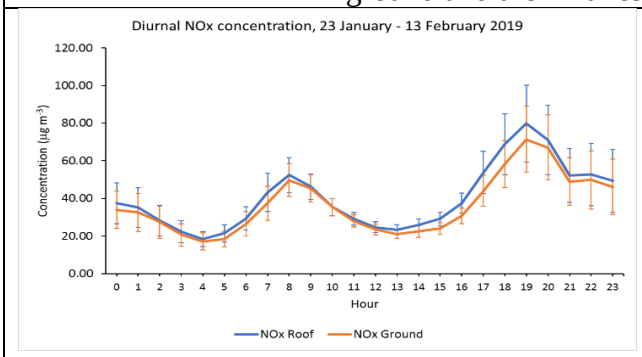
Gas flux is calculated from equation E.5.5., and the deposition velocity of gases derived from equation E.5.1. Overall, a downward flux of NO_x was observed at ground level.

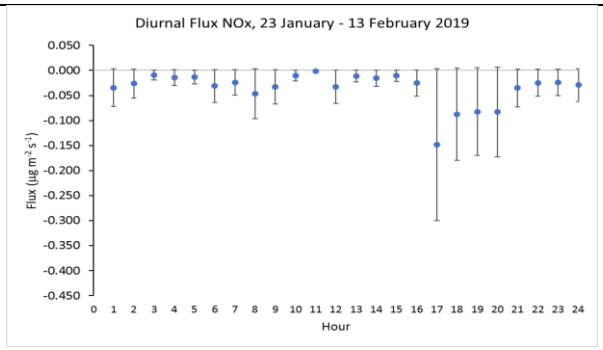
Figure 5.17. presents diurnal plots of NO_x concentrations and fluxes estimated over the grassland area. The error bars show the standard error calculated in the study.



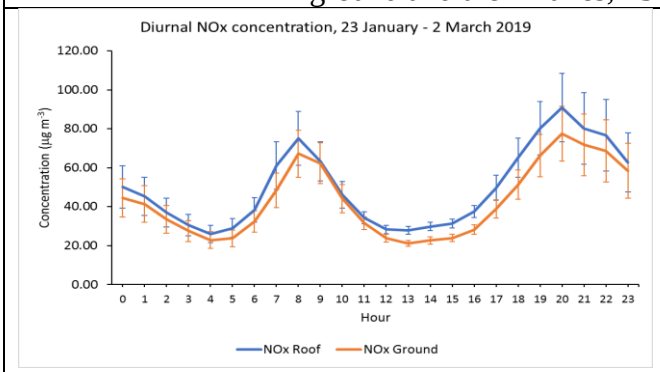


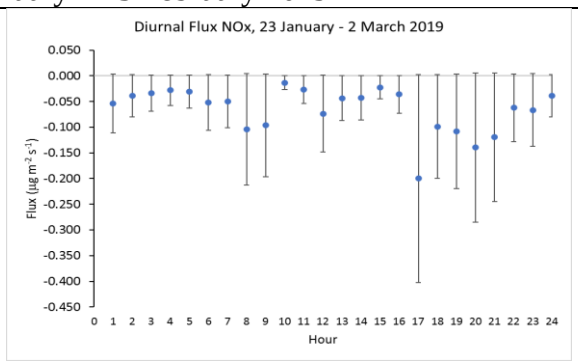
(a). Diurnal plots of NO_x concentrations with ± standard error of the mean on the roof and the ground and their fluxes, 20– 29 November 2018





(b). Diurnal plots of NO_x concentrations with ± standard error of the mean on the roof and the ground and their fluxes, 23 January – 13 February 2019





(c) Diurnal plots of NO_x concentrations with ± standard error of the mean on the roof and the ground and their fluxes, 23 January – 2 March 2019

Figure 5.17. Diurnal plots of NO_x concentrations with ± standard error of the mean on the roof and the ground and their fluxes with standard error of the mean, on the period of **(a)** 20–29 November 2018; **(b)** 23 January–13 February 2019; and **(c)** 23 January–2 March 2019

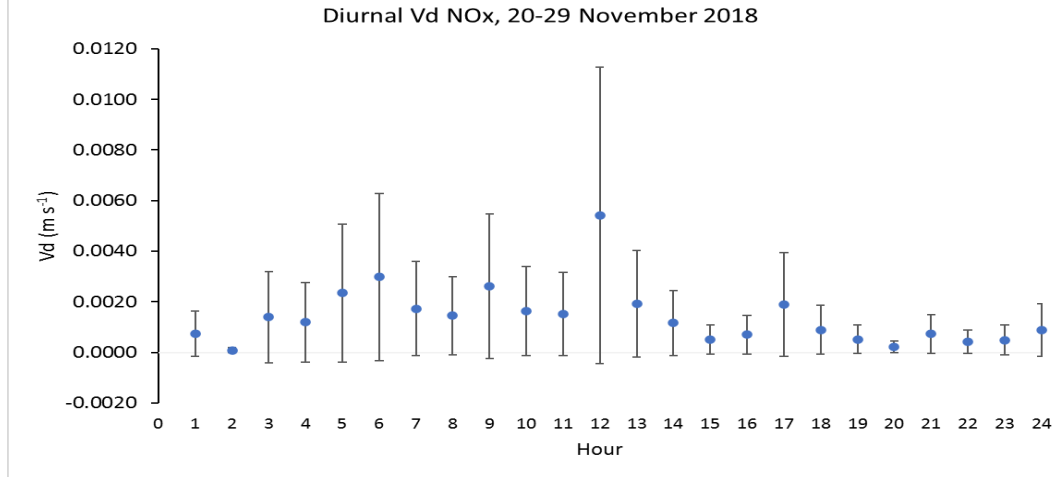
Photolysis phenomena give an apparent downward flux because they create a concentration gradient. On the roof, direct sunlight is stronger and NO_2 is photolyzed to NO and O_3. On the ground, there are shaded areas due to the tree canopies and buildings. These shaded areas

influence the chemical reactions on the ground, so there is less NO_2 photolysis, and less conversion of NO to NO_2 by the reaction with O_3 (Horii *et al.*, 2004).

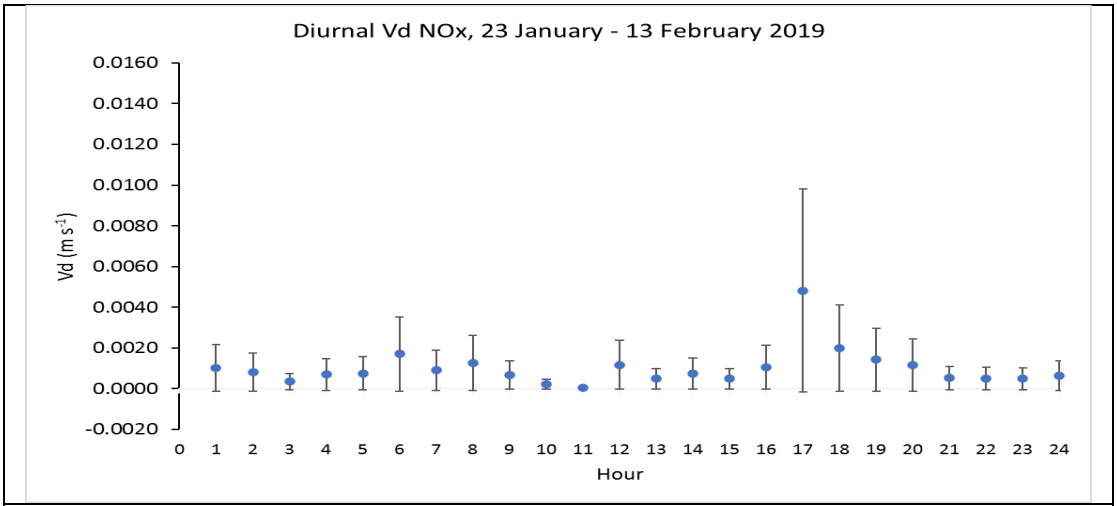
d. Deposition velocity of NO_x

Diurnal variations in the measured dry deposition velocity for NO_x in the three measurement periods are presented in Figures 5.18.a to Figure 5.18.c. These show estimated deposition velocities of NO_x fluctuated from 0.0001 m s^{-1} to 0.0054 m s^{-1} and the average ± standard error of the mean was 0.0014 ± 0.0016 m s^{-1} for the dataset from 20-29 November 2018. For the dataset from 23 January to 13 February 2019, the estimated deposition velocities of NO_x varied from 0.0001 m s^{-1} to 0.005 m s^{-1} with the average ± standard error of the mean being 0.0010 ± 0.0011 m s^{-1}. In the dataset from 23 January to 2 March 2019, the estimated deposition velocities of NO_x were from 0.0001 m s^{-1} to 0.007 m s^{-1} with the average ± standard error of the mean being 0.0017 ± 0.0017 m s^{-1}.

In this study, the estimated deposition velocities of NO_x varied from 0.0001 m s^{-1} to 0.0070 m s^{-1} and the average value of NO_x deposition velocity was 0.0014 ± 0.0024 m s^{-1}. Referring to the literature review, the deposition velocity of NO_x was in the range of 0.0010 m s^{-1} to 0.0067 m s^{-1}.



(a) Diurnal deposition velocity of NO_x with ± standard error of the mean during period on 20-29 November 2018



(b) Diurnal deposition velocity of NO_x with ± standard error of the mean during period on 23 January – 13 February 2019

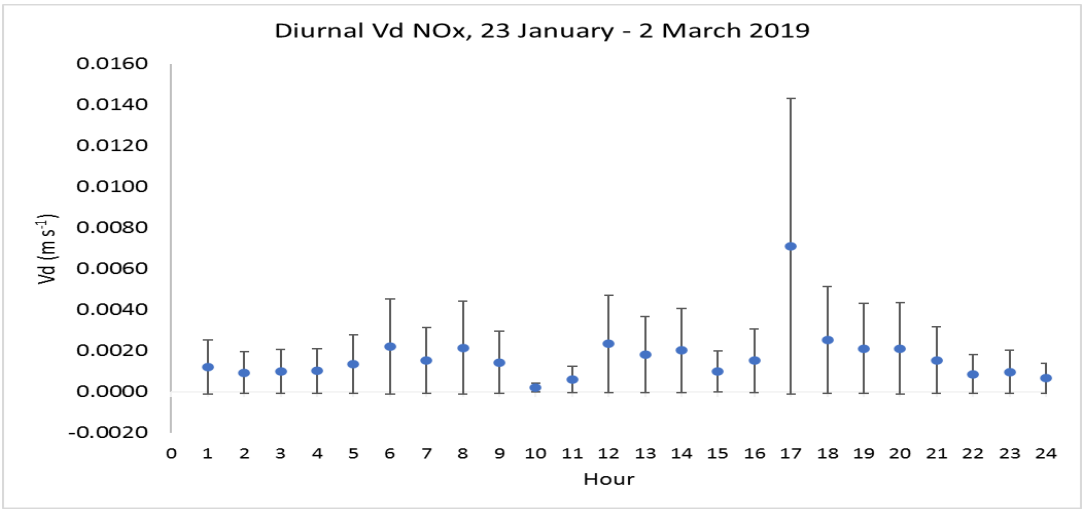


Figure 5.18. Diurnal deposition velocity of NO_x with ± standard error of the mean during period on **(a)** 20 – 29 November 2018; **(b)** 23 January – 13 February 2019; and **(c)** 23 January – 2 March 2019

The results show that daytime NO_x deposition velocities were slightly higher than night-time. The higher deposition velocities during daytime could be related to chemical reactions between NO and O_3 in the vertical column, above the canopy surface (Horii *et al.*, 2004; Neirynck and Verstraeten, 2018) or lower aerodynamic and canopy resistances (Colbeck and Harrison, 1985; Flemming *et al.*, 2014).

Overall, although this method is capable of giving results that appear to be of a correct order of magnitude, it has very large uncertainty associated with it which makes it potentially very unreliable, and therefore we do not use this result for the NO_x deposition velocity value in the subsequent ADMS modelling.

5.4. Limitation of the study

The measurement of vertical concentration gradient showed a storage phenomenon in the quadrangle grassland site. The environment and aerodynamics of the quadrangle situation are very different from those in a large park or in a well-ventilated area. The sampling location near the buildings does not meet the requirement of the micrometeorological method that needs consideration of fetch distance and a homogenous surface location.

The Black Carbon deposition velocity was approximated by combining the BC size distribution (Liu *et al.*, 2014) and size-resolved deposition velocity on grassland (Pellerin *et al.*, 2017; Giardina and Buffa, 2018).

The estimate of deposition velocity measured at the quadrangle site give a value of NO_x deposition velocity within the range of published values. However, we cannot get a meaningful deposition velocity of specific gases (NO, NO_2, and O_3) related to the situation of the quadrangle. In the site during daytime, there is a shading effect that influences the NO_2 photolysis at ground level. Chemical reactions in the oxides of the nitrogen/ozone system, combined with differing levels of illumination at the two measurement heights, make it impossible to evaluate the surface exchange of individual components of the system.

5.5. Summary

There are both direct and indirect methods to estimate dry deposition and deposition velocity values, and the choice of method depends on the purpose and availability of supporting instruments and location.

Experimental measurements of dry deposition and dry deposition velocities using micrometeorological techniques must take into account requirements for an adequate fetch distance and homogeneous surface, using a flat and open area for the sampling site. These criteria were not met in this study, although the measurements gave interesting insights into the properties of the quadrangle (e.g. the storage phenomenon) and estimates of NO_x deposition velocity that could be compared with the published deposition velocity values.

NO_x fluxes were overall downwards. The average values of NO_x deposition velocities into grassland were 0.0010 ± 0.0011 m s^{-1}, 0.0014 ± 0.0016 m s^{-1} and 0.0017 ± 0.0017 m s^{-1}, and these values were in the range of published literature.

The dry deposition process is a pathway that removes pollutants from the atmosphere. However, pollutant removal by dry deposition is not actually very efficient. The air in the park is cleaner primarily because of dispersion, and not because pollutants are actually being removed from the air by deposition. However, these two processes of dispersion and deposition are both important and need to be considered in the specific context, as their relative importance will vary.

Chapter 6. Conclusion and Recommendations for Future Research

6.1. NO_2 in urban green space

6.1.1. Conclusion

In this study, NO_2 Palmes-type diffusion tubes (Targa and Loader, 2008) were used for monitoring the atmospheric NO_2 concentrations. Although, this kind of equipment is less accurate than active samplers and can only provide long-term average NO_2 concentrations, it has many advantages including low cost, being easy to use, offering high flexibility, ability to operate without power source, long term exposure, being ideal for measurement at remote sites, and no need for field calibration. Materials and reagents that are needed to develop and analyse NO_2 DT are available in the market.

Differences in NO_2 concentrations at the roadside and in the park were significant at Cannon Hill Park (32 %, $p<0.001$), Hyde Park (30 %, $p<0.01$), and the University of Birmingham site (38 %, $p<0.001$). For Tile Cross Park, the difference in NO_2 concentration was not significant (14 %, $p>0.05$), because diffusion tubes near the road were installed on a lamp post near the bus stop, which is 23.5 m from the main road. It is assumed that the pollutants have been mixed and dispersed before being measured at the sampling site.

The relationship between NO_2 concentrations with meteorological factors (wind speed, temperature, relative humidity (RH)) were reviewed using Pearson correlation analysis. The correlation of wind speed and RH with NO_2 concentrations were different at each sampling location. There was a negative correlation between wind speed and NO_2 concentrations at Hyde Park (> -0.5) and Tile Cross Park (< -0.5), but this was not found at the UoB site and Cannon Hill Park. For RH, there was a positive correlation (> 0.5) between RH and NO_2 concentrations at Hyde Park. Temperature was negatively correlated (> 0.5) with NO_2 concentration and it was found at all sampling locations.

Transect measurement from the roadside into the park is very useful to study the decay of NO_2 concentration. However, it is recommended that more sampling points should be added at distances less than 100 meters, as the profile of NO_2 concentration tends to be flat after 100 meters.

6.1.2. Recommendations for Future Research

It is recommended to conduct an experiment to determine the NO_2 concentrations at a distance from the road by conducting the NO_2 measurements both at upwind and downwind to evaluate the influence of wind direction, and which of those directions would provide a greater reduction in pollutant concentrations. Studies have shown that the upwind direction gives a more rapid decrease in pollutant concentrations (Gilbert *et al.*, 2003; Beckerman *et al.*, 2008; Xing and Brimblecombe, 2018). This can inform the planning of locations of urban parks.

6.2. The set up and evaluation of dispersion modelling

6.2.1. Conclusion

Setting emissions input in the ADMS-Roads model should be according to the existing conditions (e.g., the number of vehicles, type and speed, road width). Reliable meteorological data and background concentrations are an important input in ADMS-Roads, so that the model can accurately simulate the dispersion process and produce good concentration predictions. Furthermore, adjusting several factors such as the NO_2:NO_x ratio or changing the speed of cars helps to optimize the prediction of NO_2 concentration. The model validation is done by comparison with the field measurements.

The meteorological data (wind speed, wind direction, T, RH) were obtained from the nearest weather station, which is Winterbourne No.2, and if the data were not available, Coundon weather station was used to replace the data. The sensitivity study showed a good fit between measured and modelled concentration by reviewing FB and NMSE for Winterbourne No.2

and the closest fit after that was Coundon. However, a correction of wind speed from Coundon to Winterbourne No. 2 was required.

Pollutant concentrations (NO_x, NO_2, NO and O_3) as background concentrations input in the model were obtained from the nearest air quality monitoring station. The nearest station was EROS, then the Biosciences site and the next option was using data from a national network (AURN) urban background site, which is Birmingham Acocks Green.

Emissions were set-up in the model using data on vehicle type, number of vehicles and vehicle speed. Traffic data were obtained from Average Annual Daily Flow (AADF) data from the Department for Transport. If AADF data were not available, the one-hour observation data of vehicle type and number of vehicles were used and adjusted with a multiplication factor based upon national diurnal traffic profiles.

Sensitivity analysis for setting the minimum speed of vehicles and ratio of NO_2:NO_x were conducted and the results were set for 10 km h^{-1} as a minimum speed at traffic lights and the junction location. The ratio of NO_2:NO_x in the model gave optimal results at 15%.

The NO_2:NO_x ratio in emissions was also calculated using the difference in the concentration of O_x (NO_2 + O_3) and NO_x (NO + NO_2) from automatic analysers placed at the near road and background sites (Jenkin, 2004; Carslaw *et al.*, 2016). Primary NO_2 was needed in the model to estimate the proportion of NO_2 emissions to ambient concentration at roadside. In this study, the primary NO_2 was calculated from the University of Birmingham site data on 2-11 February 2018, which was 14%. However, a 15% primary NO_2 of NO_x ratio was used in the model based on the results of the sensitivity analysis.

In this study, the ADMS-Roads model was able to simulate the dispersion process well when compared with the measured data with R^2 values between 0.4 to 0.8 and simulated well the decrease of NO_2 concentration from the roadside to the green area.

Inclusion of dry deposition in the ADMS model estimated that the reduction of NO_2 concentration was less than 1% and the reduction of NO_2 concentration from a sensitivity analysis was less than 1.5%.

6.2.2. Recommendations for Future Research

Currently, the ADMS-Roads model does not include deposition of ozone. A useful development would be the inclusion of this process in order to understand the effects upon concentrations of ozone and nitrogen oxides. This may be possible using the ADMS-Urban model, but was not tested due to lack of time.

6.3. Deposition velocity of gases from vertical gradient of pollutant concentrations

6.3.1. Conclusion

Our observations showed a delayed vertical mixing condition due to the storage of air in the Biosciences quadrangle. For this and other reasons such as inadequate fetch, it was concluded that the Biosciences site is not an ideal location for measuring the dry deposition velocity of gases.

Therefore, we describe direct and indirect methods that could be used to estimate dry deposition and deposition velocity, namely the eddy covariance and gradient methods. Both methods require the selection of a site where the upwind fetch should extend to a distance of 100-200 times the height of measurement, and the use of specialised instrumentation that are needed when implementing the method.

6.3.2. Recommendations for Future Research

The quadrangle of the Biosciences building was not an ideal location to conduct vertical measurements. If future work were to be done in this kind of environment, then, there is much more characterization to do. However, taking account of the upwind fetch requirement, and need for a homogeneous site in a large and open area, alternative locations should be sought.

6.4. Summary

In this study, we investigated the effect of green spaces in reducing air pollutant concentrations in urban areas. Our experimental results support the evidence of the influence of parks and open spaces in reducing NO_2 concentration from traffic emissions, as the profile of NO_2 decreases from near road down into the park. In addition, a sensitivity analysis performed using ADMS-roads suggests that the deposition process does not significantly affect (less than 1.5%) the NO_2 concentration indicating that dispersion is by far the primary mechanism.

Increasing the area of urban parks will provide better air quality mainly thanks to the dilution effect, as deposition is only a small contributor. So, more green spaces are beneficial in improving air quality. The result of this study can be applied to the urban planning of public spaces. Dispersion modelling can be used to predict the distance from busy roads that pollutant concentrations fall to near-background levels.

Appendix

Appendix 2.1. Materials and Reagents needed to make and analyse NO_2 Diffusion Tubes

Description	Item code	Quantity	Unit Price (Pounds)	Supplier
A. Material				
Acrylic tube with 15 mm (OD) x 11 mm (ID) x 2mm (wall thickness) x 71 mm length	-	200	0.20 x 200 = 40	Plastock Abbey House, Lisle Road High Wycombe, Buckinghamshire HP13 5SH England Tel: 01494 449975 **www.plastock.co.uk**
Stainless steel grid, mesh size 4x4 per mm^2 Fine mesh #100 Mesh – 0.154mm Aperture – 0.1mm Wire Diameter – SS304 Grade – Woven Wire Mesh	SS304 Grade Size A4 sheet	3	5.99 x 3 = 17.97	The Mesh Company Ltd Farrell street Warrington Cheshire, WA1 2WW England P: +44 (0) 1925 406602 **www.themeshcompany.com**
Plastic Caps Internal diameter 14.3 mm, internal length 12.70 mm **Black** colour and **Red** Colour	Black Colour, 1000 pieces Red colour, 1000 pieces	1000 Plastic caps	36.67 x 2 = 73.34	Premier Vinyl Solutions Ltd Unit F9 Halesfield 23, Telford TF7 4NY phone: 01952 585522 Website: www.premiervinylsolutions.com
U-shape tube holders	DIF 1000	108 pieces Note: depends on how much samples needed	1.26 x 108 = 136.08	Gradko International Limited St. Martins House, 77 Wales Street Winchester, Hampshire SO23 0RH England Tel: +44 (0) 1962 860331 **http://www.gradko.com**
B. Reagent				
TEA (triethanolamine) solution v/v	33729	1 Litre	53.20	Sigma-Aldrich Company Ltd. The Old Brickyard, New Road, Gillingham Dorset SP8 4XT Telp: 01747 833000 Fax: 01747 833313
N-1 (Naphthyl-1) Ethylene Diamine	33461	5 gram	29.40	

Description	Item code	Quantity	Unit Price (Pounds)	Supplier
Dihydrochloride (NEDA or NEDD)				**http://www.sigmaaldrich.com**
Sulphanilamide	S9251	100 gram	30.10	
Orthophosphoric acid (concentrated, 85%)	438081	500 mL	22.80	
Standard nitrite solutions 1000 g/L	DRS05792	500 mL	49.00	Stratlab Ltd Unit 1 Norwood Road March PE15 8QD UK Tel.: +44 (0)1354 657000
TOTAL (in year 2016)			**£ 451.89**	

Appendix 2.2. Sampling site at Cannon Hill Park

The sampling sites in Cannon Hill Park from roadside into the park with sequence by the distance from road are labelled as CH1; CHX; CH12; CH11; CH2; CH3; CH10; CH4; CH 5; CH6; CH7; CH8 and CH9.

Sample site near road is CH1.

Sampling site near the road, inside the park (30 m from road) = CHX

Sample sites inside the park are CH12; CH11; CH2; CH3; CH10; CH4; CH 5; CH6; CH7; CH8 and CH9.

Table A.2.2. Location and distance of diffusion tube from road at Cannon Hill Park

ID	Picture and Location	Distance from road (m)	Information
CH 1		1.5 m	Lamp post, outside the park, near Edgbaston road

ID	Picture and Location	Distance from road (m)	Information
CH X		30 m	At the map CH information sign (red circle)
CH 2		330 m	At lamppost Lamp post near MAC building (right side, red circle)
CH 3		387 m	Lamp post near the lake
CH 4		429 m	Attached at the fence, fence
CH 5		446 m	At lamppost
CH 6		535 m	At lamppost

ID	Picture and Location	Distance from road (m)	Information
CH 7		689 m	At the street-sign
CH 8		781 m	At the old street sign
CH 9		935 m	At the street sign
CH 10	 	428 m	On the gazebo
CH 11	 	292 m	Fence at tennis court

ID	Picture and Location	Distance from road (m)	Information
CH 12		204 m	Street sign near the Garden Tea room

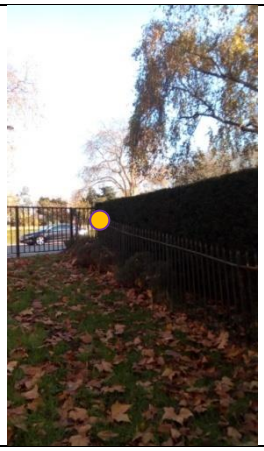
Appendix 2.3. Sampling site at Hyde Park

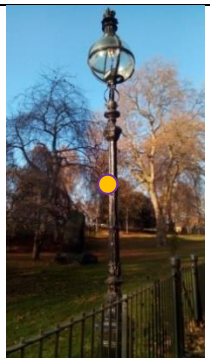
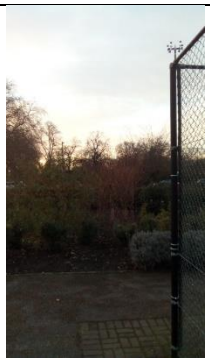
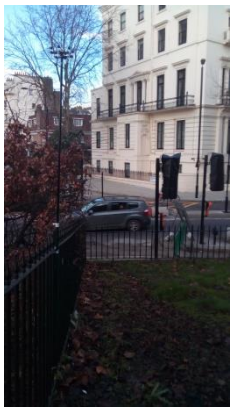
The sampling sites in Hyde Park are labelled as CGL; TD; BG; VGS; RL.

Sample sites near roads are CGL; TD; BG; VGS.

Sample site inside the park is RL.

Table A.2.3. Location and distance of diffusion tube from road at Hyde Park, London

ID	Picture	Distance from location near road to Ranger Lodge (RL) in the park (m)	Location
CGL		674.5 m	Near Cumberland Gate road and N Carriage Dr

ID	Picture	Distance from location near road to Ranger Lodge (RL) in the park (m)	Location
TD		568 m	Near Serpentine waterfall and S Carriage Dr
BG		675.5 m	In will to win Hyde Park Sport Centre and near W Carriage Dr
			
VGS	 	652 m	Near Bayswater Rd and A402

ID	Picture	Distance from location near road to Ranger Lodge (RL) in the park (m)	Location
RL		0 m	In the park at Ranger Lodge, open area
			

Appendix 2.4. Sampling site at Tile Cross Park

Sampling sites inside Tile Cross Park are divided into Group 1-2. Group 1 sampling sites are labelled as TL 8; TL 9; TL 10; TL 11; TL 12; TL 13. Group 2 sampling sites are labelled as TL 2; TL 3; TL 4; TL 5; TL 6; TL 7; TL 14; TL 15.

Sample site near road is TL1.

Table A.2.4. Location and distance of diffusion tube from road at Tile Cross Park

ID	Picture and Location	Distance from road (m)	Information
TL 1		23.5 m from roadside (2.35 m from bus stop)	At lamppost near road
TL 2		253.9 m	Vent-pole

ID	Picture and Location	Distance from road (m)	Information
TL 3		282.1 m	Vent-pole
TL 4		304 m	Vent-pole
TL 5		332.6 m	Vent-pole
TL 6		440.5 m	Vent-pole
TL 7		450.2 m	Vent-pole
TL 8		446.8 m	Vent-pole
TL 9		409.6 m	Vent-pole
TL 10		390.5 m	Vent-pole
TL 11		367 m	Vent-pole
TL 12		328.1 m	Vent-pole

ID	Picture and Location	Distance from road (m)	Information
TL 13		264.1 m	Vent-pole
TL 14		272.6 m	Vent-pole
TL 15		574.5 m	Vent-pole

Appendix 2.5. Sampling site at the University of Birmingham

The sampling sites in University of Birmingham from roadside into the green area with sequence by the distance from A38 road are labelled as BROS; X1; X2; X3; X4; A; B; C; D; J; E; F; EROS; G; H and I sites.

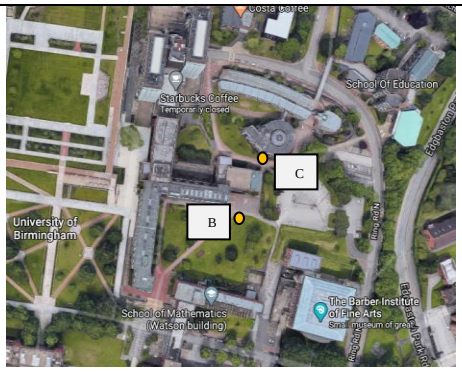
Sample site near A38 road is BROS.

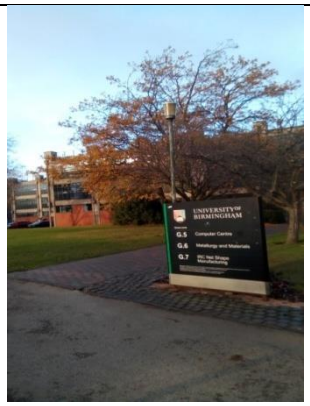
Sample site inside the green area are B; C; J; F; EROS; G.

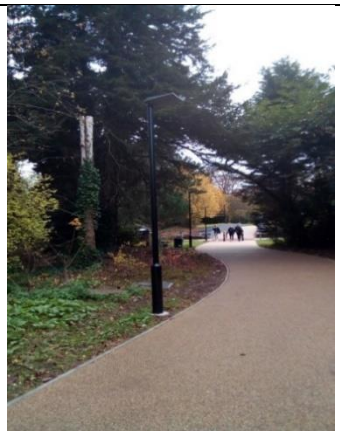
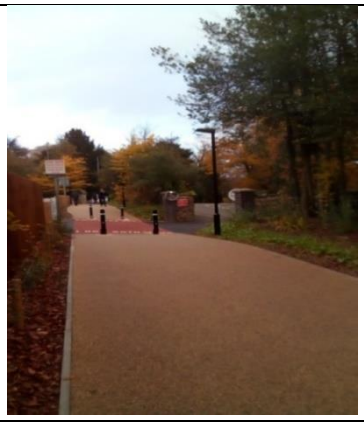
Sample sites near roads are E; H; I.

Table A.2.5. Location and distance of diffusion tube from road at University of Birmingham (UoB) site

ID	Picture and Location	Distance from road (m)	Information
BROS		3.6 m	Pole

ID	Picture and Location	Distance from road (m)	Information
X1		6.1 m	Near the BROS, outside the house
X2		13.3 m	Near the parking, using pole
X3		53.6 m	Lamp post
X4		103.6 m	Lamp post
A		118.6 m	lamp post, near sport pitches
B		423.6 m	Lamp post between Art Building (R16) and Watson Building (R15)
C		453.6 m	Lamp post Near the Art Building (R16)

ID	Picture and Location	Distance from road (m)	Information
D		588.6 m	Lamp post, near MuirheadTower (R21) and the Alan Walters building (R29)
J		633.6 m	Lamp post near North Gate to Main Library
E		663.6 m	Lamp post, near highways at Pritchatts road G7
F		818.6 m	Lamp post near computer centre (G5)

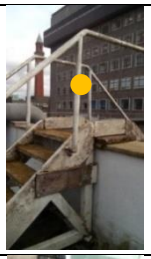
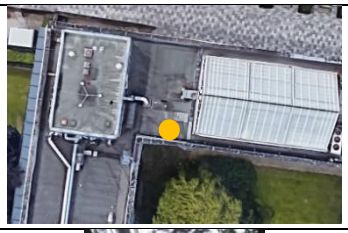
ID	Picture and Location	Distance from road (m)	Information
EROS		938.6 m	Open area
G		983.6 m	Lamp post, new road near Elms Plant (G20)
H		1093.6 m	Lamp post, new road near Elms Plant (G20) and Nursery
I		1123.6 m	Lamp post near nursery

Appendix 2.6. Sampling site at Biosciences building

Sample sites on the roof are A; B; C.

Sample site on the ground are X; Y.

Table A.2.6. Location diffusion tube on the roof and the ground of Biosciences building

ID	Picture	Height (m) from the ground	Location
A		13.5 m	Roof at fence, open area
B		13.5 m	Roof at the wall
C		13.5 m	Roof at the fence, open area
X		1 m	Ground floor Near the sitting area, open area
Y		1 m	Ground floor at the fence, near the wall

Appendix 2.7. Picture of inter-comparison analysers



Figure. A.2.7. Inter-comparison analysers at Bioscience building ground floor

Inter-comparison of NOx and O_3 instruments was conducted from 13 to 19 November 2018, and for inter-comparison AE51 was conducted for 24 hours in every month during sampling time.

Appendix 3.1. NO_2 diffusion tube (DT) data

3.1.A. NO_2 diffusion tube with open end

No	Location	Week	Start Date	End Date	Sample 1	Sample 2	Sample 3	Mean DT ($\mu g\ m^{-3}$)	SD DT ($\mu g\ m^{-3}$)	RSD DT (SD/ Mean) *100	Mean AA Automatic Analyser (AA) ($\mu g\ m^{-3}$)	SD AA ($\mu g\ m^{-3}$) ±10 % from mean (Stevenson et al., 2009)	Bias (%)
1	EROS site	2	24/08/2016	07/09/2016	12	13	14	13	1	8	16	2	-19
2	EROS site	2	22/09/2016	07/10/2016	15	16	16	15	0	2	19	2	-20
3	EROS site	4	22/09/2016	24/10/2016	21	22	22	21	1	3	23	2	-8
4	EROS site	2	07/10/2016	21/10/2016	22	23	23	23	0	2	27	3	-16
5	EROS site	1	21/10/2016	26/10/2016	27	28	28	27	0	1	34	3	-19
6	EROS site	2	26/10/2016	11/11/2016	21	22	24	22	1	7	28	3	-19
7	EROS site	2	11/11/2016	27/11/2016	29	30	30	29	1	2	29	3	3
8	EROS site	4	26/10/2016	27/11/2016	23	24	24	24	0	2	28	3	-14
9	EROS site	2	27/11/2016	12/12/2016	34	38	38	37	2	6	42	4	-11
10	EROS site	4	12/12/2016	11/01/2017	29	29	30	29	1	2	30	3	-1
11	EROS site	2	11/01/2017	26/01/2017	34	36	38	36	2	6	33	3	10
12	EROS site	4	11/01/2017	13/02/2017	19	26	30	28	3	10	30	3	-6
13	EROS site	3	13/02/2017	4/03/2017	17	18	20	18	2	11	19	2	-4
14	EROS site	3	04/03/2017	25/03/2017	19	21	30	20	2	8	19	2	4
15	EROS site	6	13/02/2017	25/03/2017	19	20	24	21	3	14	19	2	10
16	EROS site	3	25/03/2017	15/04/2017	15	16	16	16	0	1	18	2	-14
17	EROS site	3	15/04/2017	7/05/2017		12	12	12	0	0	15	2	-18
18	EROS site	6	25/03/2017	7/05/2017	12	12	14	12	1	10	16	2	-24
19	EROS site	2	07/05/2017	27/05/2017	13	14	17	14	2	13	15	2	-6
20	EROS site	3	27/05/2017	18/06/2017	8	9	9	9	1	11	9	1	-7
21	EROS site	6	07/05/2017	18/06/2017		9	10	10	1	7	12	1	-22

No	Location	Week	Start Date	End Date	Sample 1	Sample 2	Sample 3	Mean DT ($\mu g\ m^{-3}$)	SD DT ($\mu g\ m^{-3}$)	RSD (SD/ Mean)*100	Mean AA Automatic Analyser (AA) ($\mu g\ m^{-3}$)	SD AA ($\mu g\ m^{-3}$) ±10 % from mean (Stevenson et al., 2009)	Bias (%)
22	EROS site	3	18/06/2017	9/07/2017	11	11	12	11	0	2	11	1	0
23	EROS site	4	18/06/2017	16/07/2017	9	9	9	9	0	2	11	1	-15
24	EROS site	2	09/07/2017	23/07/2017	10	11	12	11	1	8	9	1	20
25	EROS site	4	09/07/2017	12/08/2017	13	11	10	11	1	12	10	1	13
26	EROS site	3	23/07/2017	12/08/2017	10	10	9	10	1	10	10	1	-3
27	EROS site	2	12/08/2017	26/08/2017	9	10	8	9	1	11	10	1	-10
28	EROS site	2	26/08/2017	09/09/2017	11	12	12	12	1	7	14	1	-15
29	BROS site	2	09/09/2017	24/09/2017	25	24	22	24	2	8	25	3	-7
30	BROS site	4	26/08/2017	24/09/2017	23	24		24	1	3	20	2	19
31	BROS site	3	24/09/2017	15/10/2017	34	34	28	32	4	11	29	3	12
32	BROS site	3	15/10/2017	03/11/2017	37	36	36	36	1	2	38	4	-5
33	BROS site	2	03/11/2017	19/11/2017	35	34	33	34	1	2	46	5	-26
34	BROS site	3	19/11/2017	05/12/2017	37	33	31	34	3	9	37	4	-9
35	BROS site	2	05/12/2017	23/12/2017	51	50	48	50	1	3	47	5	8
36	BROS site	4	23/12/2017	20/01/2018	46	44	40	43	3	7	36	4	20
37	BROS site	4	20/01/2018	17/02/2018	32	30	25	29	4	13	33	3	-12
38	EROS site	4	17/02/2018	18/03/2018	22	22	11	22	0	0	28	3	-19
39	EROS site	4	18/03/2018	15/04/2018	19	18	15	17	2	12	26	3	-32

	Mean DT	SD DT	RSD DT (%)	Mean AA	SD AA	Bias (%)
average	**22**	1	6	**24**	2	-7
combined uncertainty		10	48		15	
min	9	0	0	9	1	-32
max	50	4	14	47	5	20

3.1.B. NO_2 diffusion tube with membrane

No	Location	Week	Start Date	End Date	Sample 1	Sample 2	Sample 3	Mean DT ($\mu g\ m^{-3}$)	SD DT ($\mu g\ m^{-3}$)	RSD (SD/Mean)*100	Mean AA Automatic Analyser (AA) ($\mu g\ m^{-3}$)	SD AA ($\mu g\ m^{-3}$) ±10 % from mean (Stevenson et al., 2009)	Bias
32	BROS site	3	15/10/2017	03/11/2017	37	37	36	37	1	2	38	4	-4
33	BROS site	2	03/11/2017	19/11/2017	41	41	41	41	0	0	46	5	-10
34	BROS site	3	19/11/2017	05/12/2017	30	29	28	29	1	3	37	4	-23
35	BROS site	2	05/12/2017	23/12/2017	42	40	39	40	2	4	47	5	-13
36	BROS site	4	23/12/2017	20/01/2018	40	37	34	37	3	9	36	4	3
37	BROS site	4	20/01/2018	17/02/2018	28	27	26	27	1	3	33	3	-18
38	EROS site	4	17/02/2018	18/03/2018	18	18	16	17	1	5	28	3	-37
39	EROS site	4	18/03/2018	15/04/2018	14	13	12	13	1	6	26	3	-49

	Mean DT	SD DT	RSD DT (%)	Mean AA	SD AA	Bias (%)
average	**30**	1	4	**36**	4	-19
combined uncertainty (SD)		4	13		10	
min	13	0	0	26	3	-49
max	41	3	9	47	5	3

Appendix 3.2. NO_x diffusion tube (DT) data

3.2.A. NO_x diffusion tubes, Biosciences site, 28 January – 11 March 2019

No	Location	Week	Start Date	End Date	Sample 1	Sample 2	Sample 3	Mean DT ($mg\ m^{-3}$)	SD DT	RSD (SD/Mean)*100	Mean AA Automatic Analyser ($mg\ m^{-3}$)	SD AA ($\mu g\ m^{-3}$) ±10 % from mean (Stevenson et al., 2009)	Bias (%)
1	Roof	1	28/01/2019	04/02/2019	125	74	69	72	3	4	46	5	56
2	Ground	1	28/01/2019	04/02/2019	103	58	58	58	0	0	42	4	40
3	Roof	1	04/02/2019	11/02/2019	81	51	38	45	9	19	34	3	31
4	Ground	1	04/02/2019	11/02/2019	47	46	39	44	5	10	31	3	44
5	Roof	1	11/02/2019	18/02/2019	62	53	42	52	10	19	38	4	36
6	Ground	1	11/02/2019	18/02/2019	68	64	60	64	4	6	34	3	90
7	Roof	1	18/02/2019	25/02/2019	108	48	28	48			52	5	-7
8	Ground	1	18/02/2019	25/02/2019	169	64	52	58	9	15	42	4	38
9	Roof	1	25/02/2019	04/03/2019	59	46	39	52	9	17	91	9	-42
10	Ground	1	25/02/2019	04/03/2019	60	48	35	54	9	16	73	7	-26
11	Roof	2	28/01/2019	11/02/2019	41	38	37	39	2	6	40	4	-4
12	Ground	2	28/01/2019	11/02/2019	34	34	28	32	3	10	36	4	-12
13	Roof	2	11/02/2019	25/02/2019	74	69	65	69	4	6	45	5	54
14	Ground	2	11/02/2019	25/02/2019	79	51	41	46	7	15	38	4	22
15	Roof	2	25/02/2019	11/03/2019	32	32	26	30	3	11	91	9	-67
16	Ground	2	25/02/2019	11/03/2019	36	26	13	31	7	23	73	7	-57
17	Roof	3	28/01/2019	18/02/2019	44	41	31	38	6	17	40	4	-2
18	Ground	3	28/01/2019	18/02/2019	43	34	26	38	6	16	36	4	7
19	Roof	3	18/02/2019	11/03/2019	49	44	23	46	4	8	69	7	-33
20	Ground	3	18/02/2019	11/03/2019	36	33	25	31	6	18	56	6	-44

No	Location	Week	Start Date	End Date	Sample 1	Sample 2	Sample 3	Mean DT	SD DT	RSD	Mean AA	SD AA ($\mu g\ m^{-3}$) ±10 % from mean (Stevenson et al., 2009)	Bias (%)
21	Roof	4	28/01/2019	25/02/2019	43	43	42	42	1	1	43	4	-1
22	Ground	4	28/01/2019	25/02/2019	41	40	36	39	3	7	37	4	5

	DT	SD DT	RSD	AA	SD AA	Bias (%)
average	47	5	12	49	5	6
min	30	0	0	31	3	-67
max	72	10	23	91	9	90

3.2.B. NO_2 diffusion tubes, Biosciences site, 28 January – 11 March 2019

No	Location	Week	Start Date	End Date	Sample 1	Sample 2	Sample 3	Mean DT ($mg\ m^{-3}$)	SD DT	RSD (SD/Mean)*100	Mean AA Automatic Analyser ($mg\ m^{-3}$)	SD AA ($\mu g\ m^{-3}$) ±10 % from mean (Stevenson et al., 2009)	Bias (%)
1	Roof	1	28/01/2019	04/02/2019	34	31	30	32	2	7	31	3	2
2	Ground	1	28/01/2019	04/02/2019	36	32	22	34	3	9	31	3	12
3	Roof	1	04/02/2019	11/02/2019	24	22	21	22	2	7	20	2	13
4	Ground	1	04/02/2019	11/02/2019	25	23	19	22	3	13	20	2	12
5	Roof	1	11/02/2019	18/02/2019	26	23	23	24	2	6	26	3	-7
6	Ground	1	11/02/2019	18/02/2019	28	26	25	26	2	6	26	3	1
7	Roof	1	18/02/2019	25/02/2019	28	21	8	24	5	19	24	2	3

No	Location	Week	Start Date	End Date	Sample 1	Sample 2	Sample 3	Mean DT (mg m^{-3})	SD DT	RSD (SD/Mean)*100	Mean AA Automatic Analyser (mg m^{-3})	SD AA (µg m^{-3}) ±10 % from mean (Stevenson et al., 2009)	Bias (%)
8	Ground	1	18/02/2019	25/02/2019	21	20	17	19	2	11	24	2	-18
9	Roof	1	25/02/2019	04/03/2019	36	29	28	31	4	14	37	4	-15
10	Ground	1	25/02/2019	04/03/2019	31	30	29	30	1	4	34	3	-13
11	Roof	2	28/01/2019	11/02/2019	28	26	26	27	1	3	26	3	3
12	Ground	2	28/01/2019	11/02/2019	31	25	17	28	4	15	25	3	8
13	Roof	2	11/02/2019	25/02/2019	29	29	25	27	2	9	25	2	11
14	Ground	2	11/02/2019	25/02/2019	30	27	25	27	3	10	25	2	9
15	Roof	2	25/02/2019	11/03/2019	23	21	11	22	2	7	37	4	-40
16	Ground	2	25/02/2019	11/03/2019	25	22	21	23	2	8	34	3	-34
17	Roof	3	28/01/2019	18/02/2019	26	26	25	26	1	3	26	3	-1
18	Ground	3	28/01/2019	18/02/2019	26	25	24	25	1	5	26	3	-3
19	Roof	3	18/02/2019	11/03/2019	29	24	5	19	3	18	30	3	-35
20	Ground	3	18/02/2019	11/03/2019	15	17	19	17	2	11	28	3	-41
21	Roof	4	28/01/2019	25/02/2019	27	24	20	24	3	14	25	3	-7
22	Ground	4	28/01/2019	25/02/2019	28	26	25	26	2	6	25	3	5

	DT	SD	RSD	AA	SD AA	Bias (%)
average	**25**	**2**	**9**	**27**	3	**-6**
min	17	1	3	20	2	-41
max	34	5	19	37	4	13

3.2.C. NO concentration, Biosciences site, 28 January – 11 March 2019

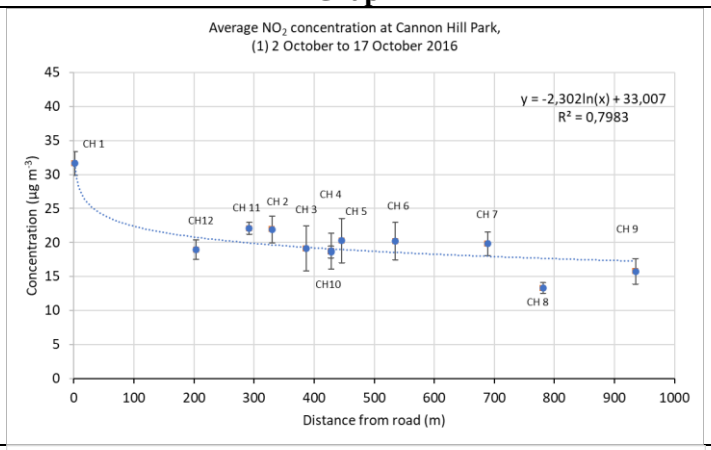
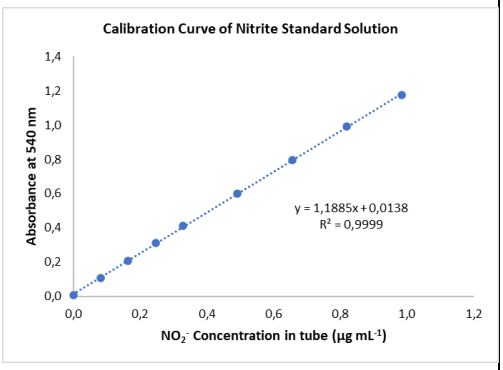
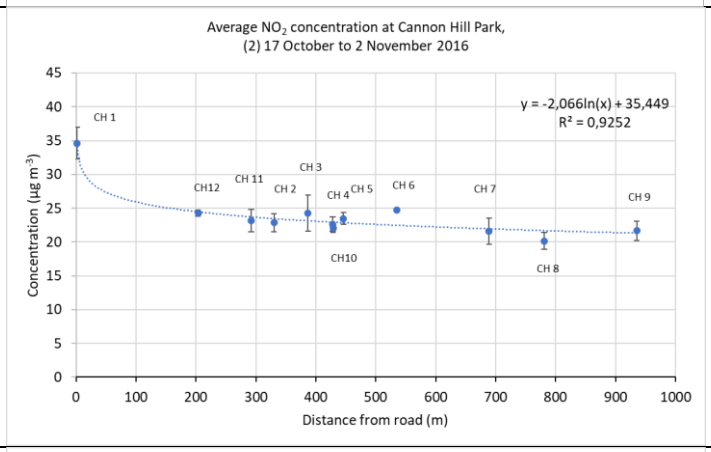
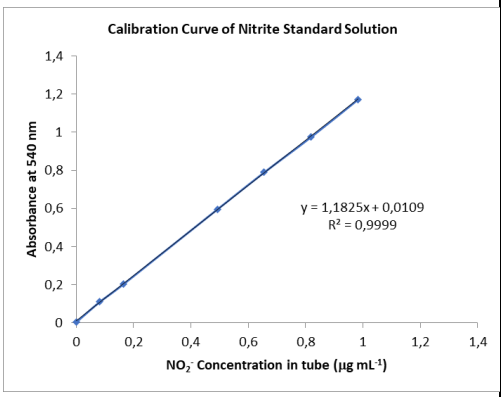
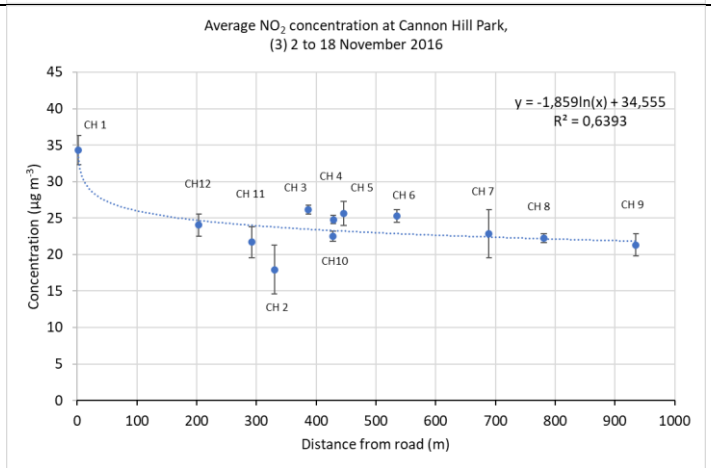
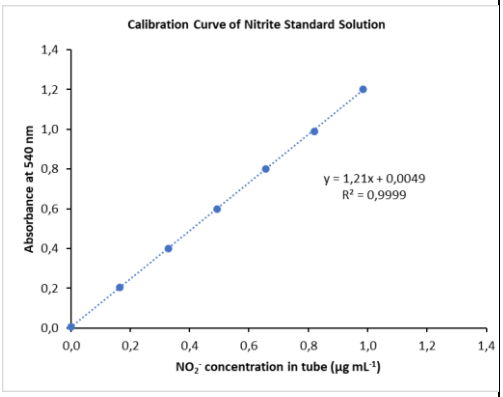
No	Location	Week	Start Date	End Date	Sample 1	Sample 2	Sample 3	Mean DT (mg m^{-3})	SD DT	RSD (SD/Mean)*100	Mean AA Automatic Analyser (mg m^{-3})	SD AA (µg m^{-3}) ±10 % from mean (Stevenson et al., 2009)	Bias (%)
1	Roof	1	28/01/2019	04/02/2019	91	43	39	41	2	6	15	1	175
2	Ground	1	28/01/2019	04/02/2019	66	26	36	31	7	22	11	1	172
3	Roof	1	04/02/2019	11/02/2019	57	28	17	23	8	34	14	1	61
4	Ground	1	04/02/2019	11/02/2019	22	23	19	21	2	9	11	1	98
5	Roof	1	11/02/2019	18/02/2019	36	29	19	33	8	26	13	1	156
6	Ground	1	11/02/2019	18/02/2019	40	39	35	38	3	7	8	1	374
7	Roof	1	18/02/2019	25/02/2019	80	27	21	24	4	18	28	3	-14
8	Ground	1	18/02/2019	25/02/2019	148	44	35	40	6	15	19	2	110
9	Roof	1	25/02/2019	04/03/2019	22	17	11	20	4	21	54	5	-64
10	Ground	1	25/02/2019	04/03/2019	29	18	6	24	8	35	39	4	-40
11	Roof	2	28/01/2019	11/02/2019	14	11	11	12	2	14	15	1	-19
12	Ground	2	28/01/2019	11/02/2019	3	9	12	10	2	15	11	1	-6
13	Roof	2	11/02/2019	25/02/2019	45	40	41	42	3	6	20	2	106
14	Ground	2	11/02/2019	25/02/2019	49	25	17	21	6	27	14	1	53
15	Roof	2	25/02/2019	11/03/2019	9	11	15	13	3	22	54	5	-76
16	Ground	2	25/02/2019	11/03/2019	12	4	-8	8	6	72	40	4	-81
17	Roof	3	28/01/2019	18/02/2019	17	15	7	16	2	12	14	1	16
18	Ground	3	28/01/2019	18/02/2019	16	9	2	13	5	43	10	1	20
19	Roof	3	18/02/2019	11/03/2019	20	20	18	19	1	7	40	4	-52
20	Ground	3	18/02/2019	11/03/2019	21	16	6	19	3	18	28	3	-33
21	Roof	4	28/01/2019	25/02/2019	16	19	21	19	3	14	18	2	7

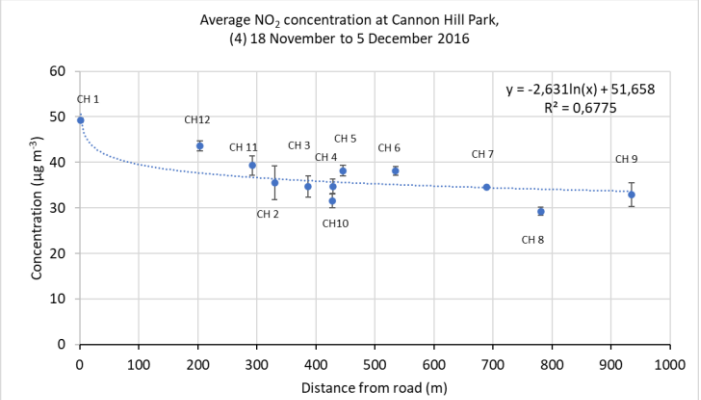
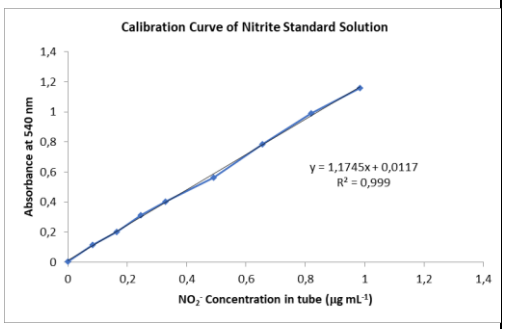
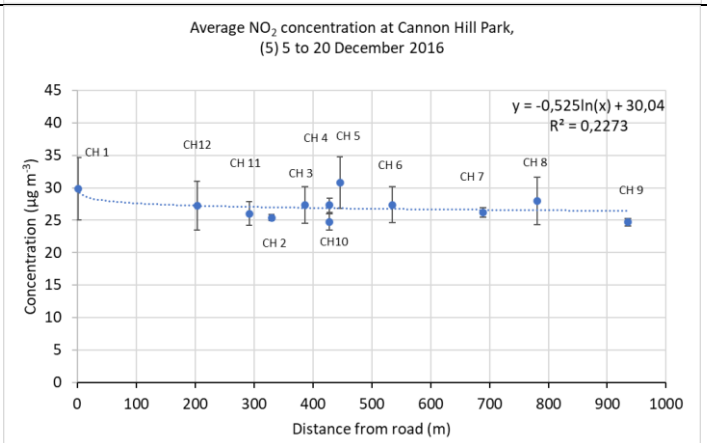
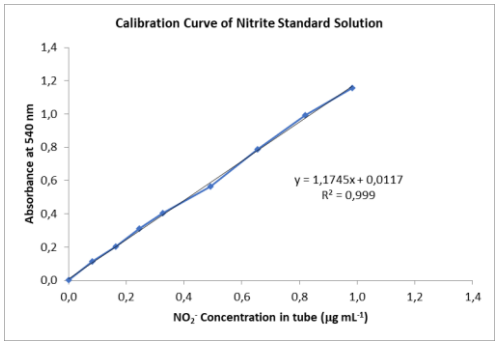
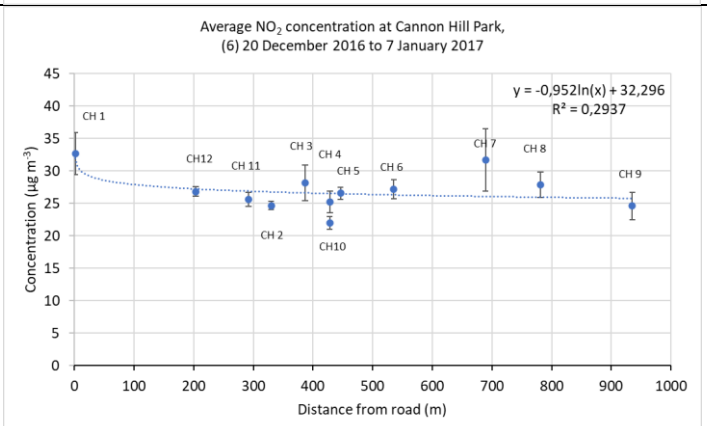
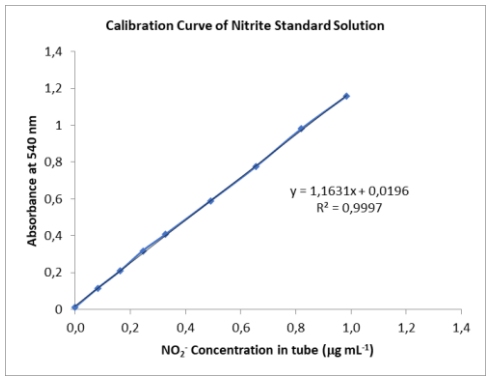
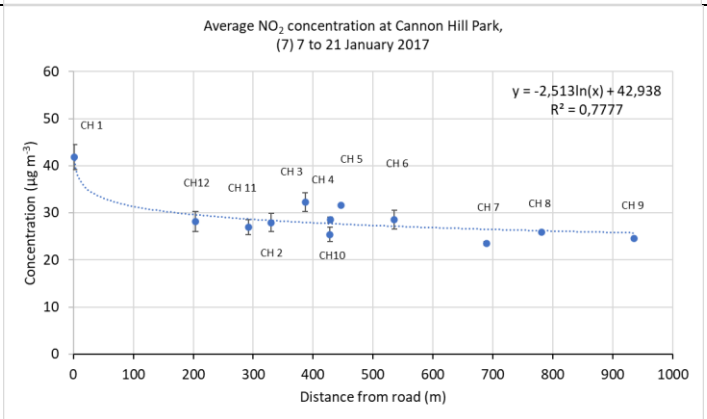
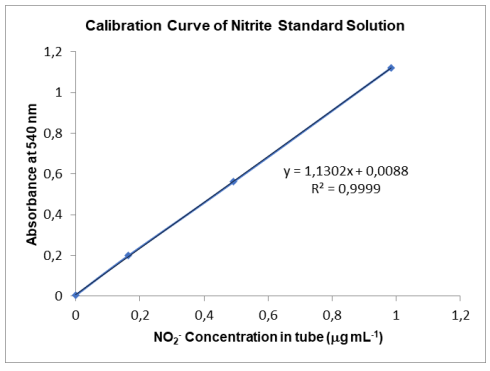
No	Location	Week	Start Date	End Date	Sample 1	Sample 2	Sample 3	Mean DT (mg m^{-3})	SD DT	RSD (SD/Mean)*100	Mean AA Automatic Analyser (mg m^{-3})	SD AA (µg m^{-3}) ±10 % from mean (Stevenson et al., 2009)	Bias (%)
22	Ground	4	28/01/2019	25/02/2019	13	14	11	13	1	11	13	1	1

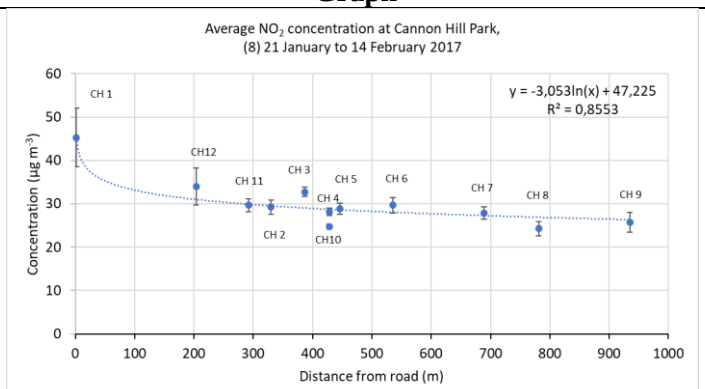
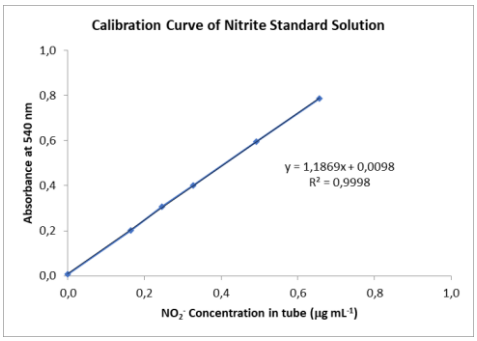
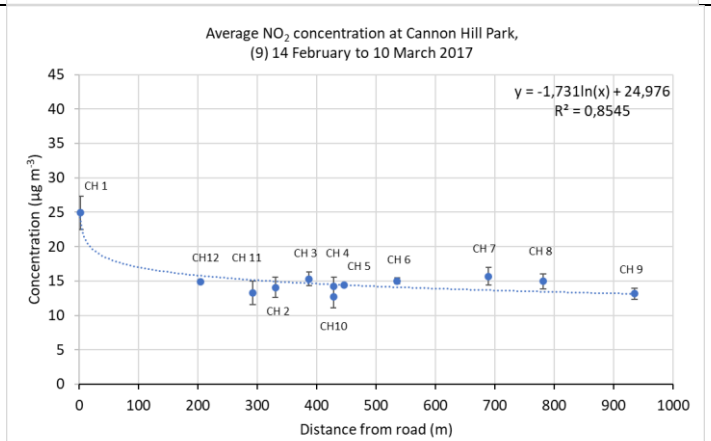
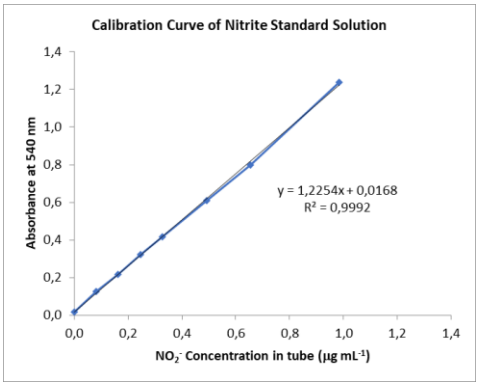
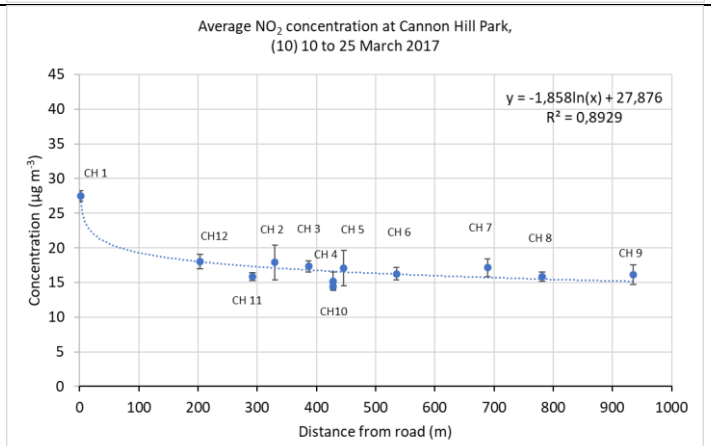
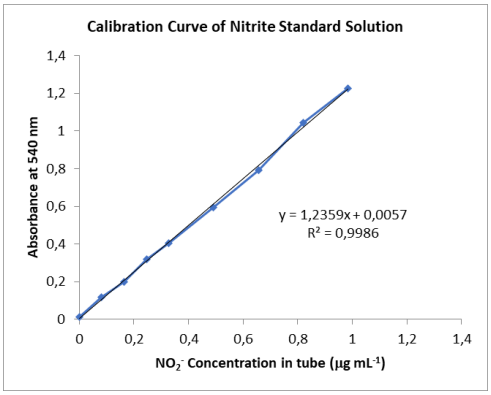
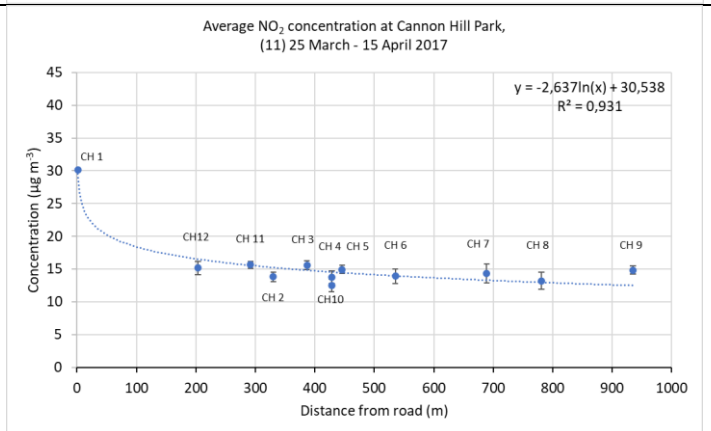
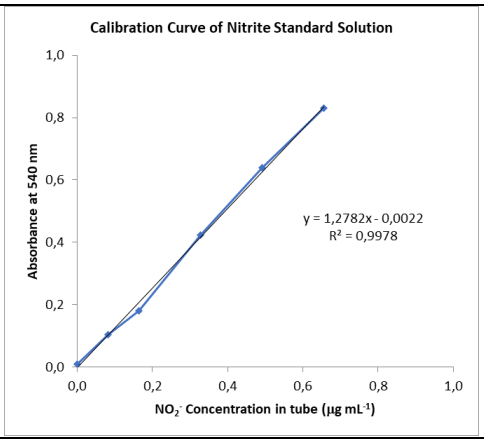
	DT	SD	RSD	AA	SD AA	Bias (%)
average	**23**	**4**	**21**	**22**	2	**44**
min	8	1	6	8	1	-81
max	42	8	72	54	5	374

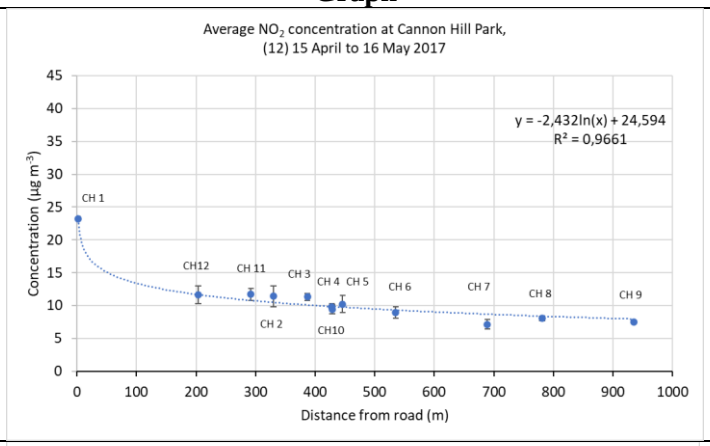
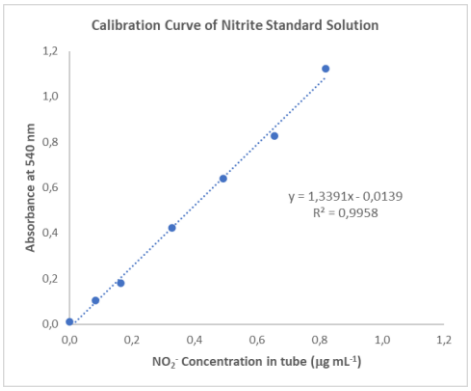
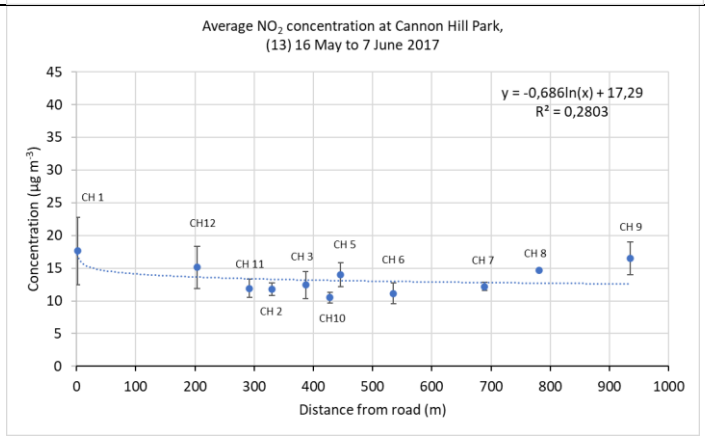
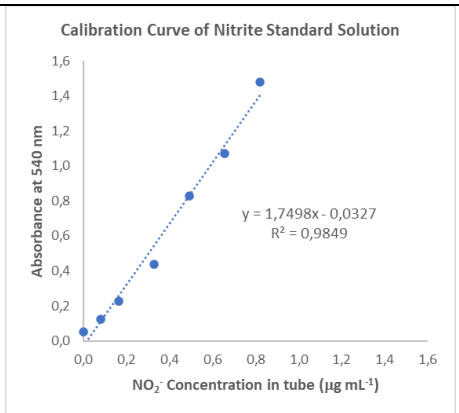
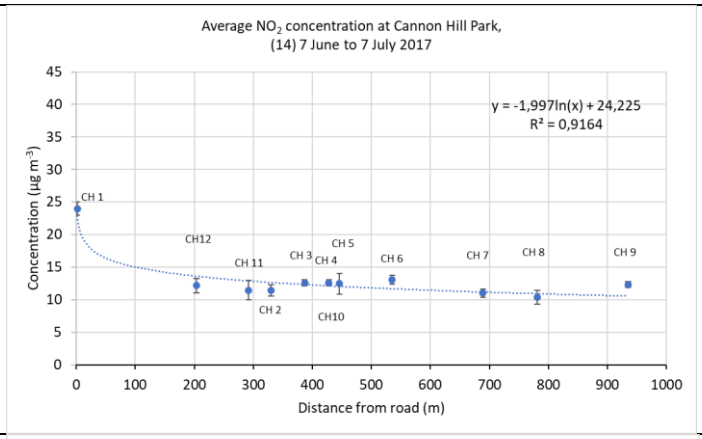
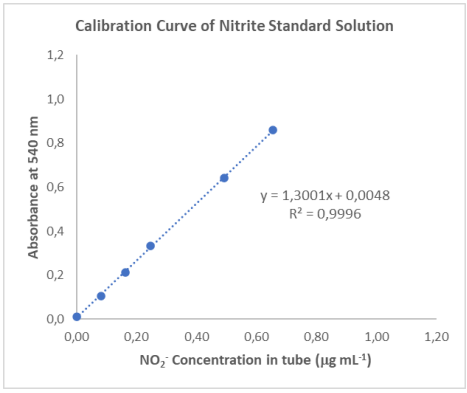
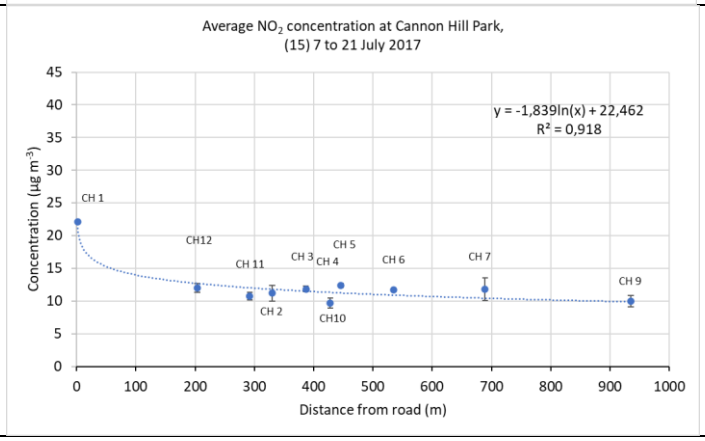
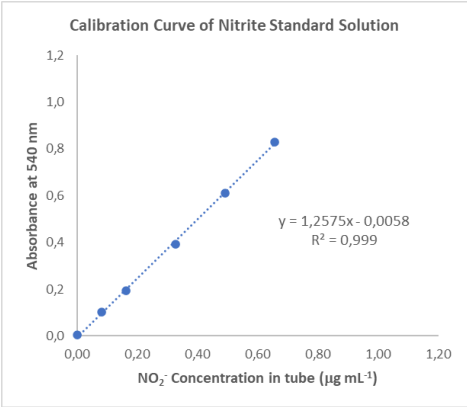
Appendix 3.3. Graph of NO_2 concentrations at Cannon Hill Park

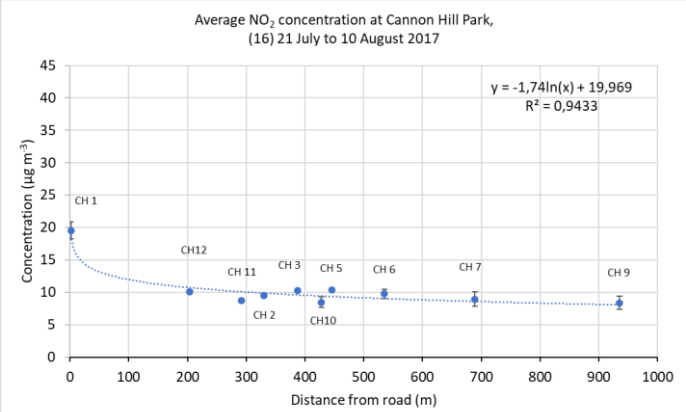
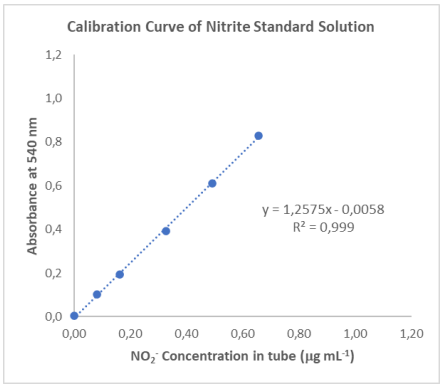
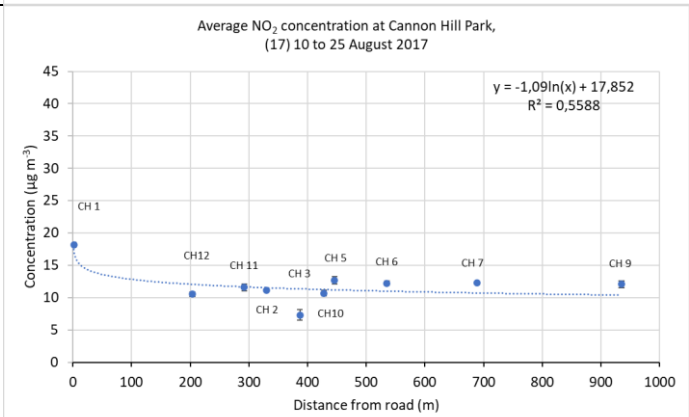
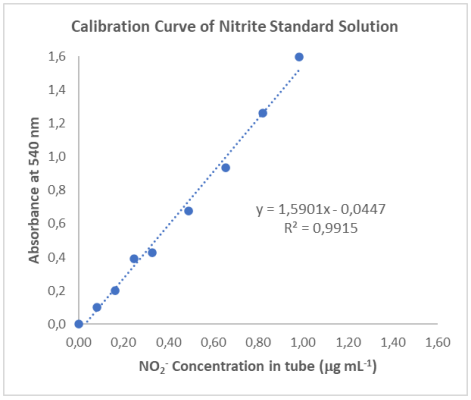
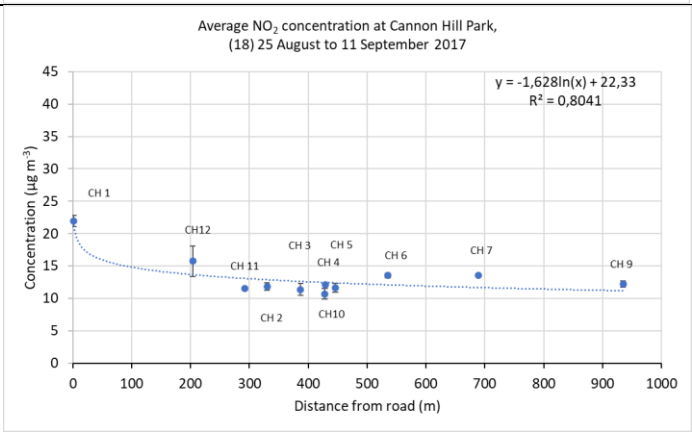
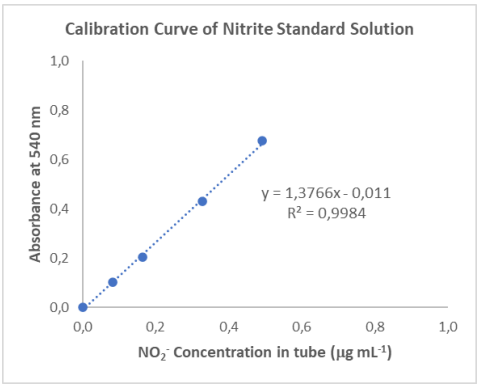
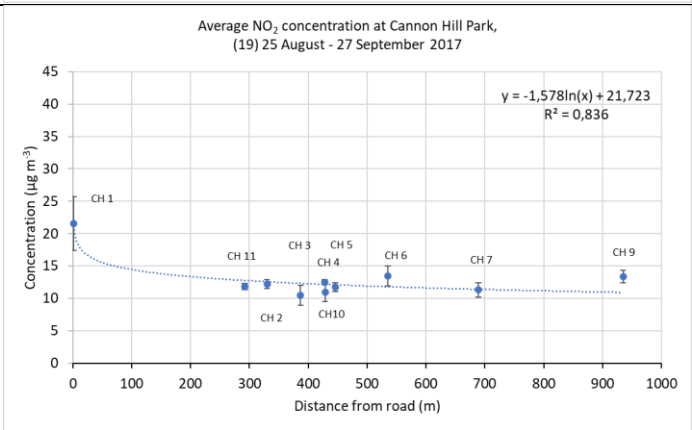
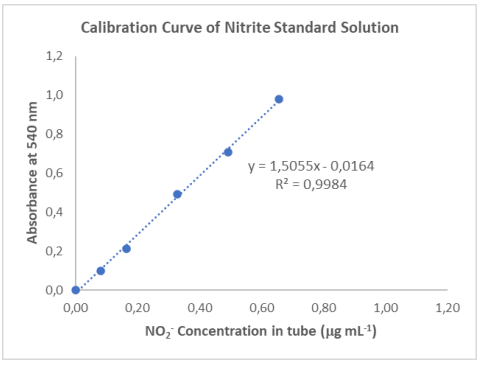
Table A.3.3. Graph of NO_2 concentrations from raw data of DT measurements at Cannon Hill Park (mean ± standard deviation from triplicate DT), and calibration curves of nitrite standard solution, sampling period October 2016 – January 2019

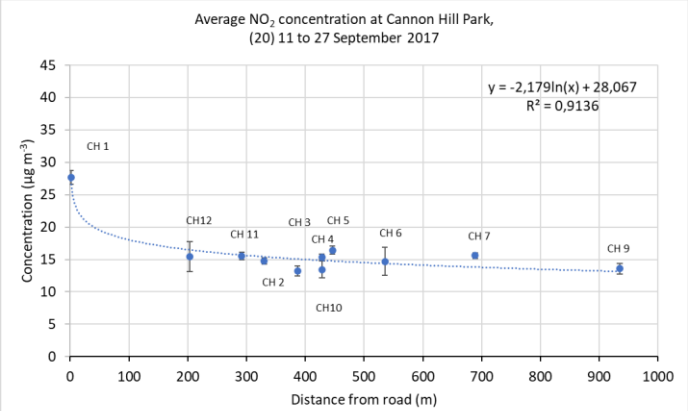
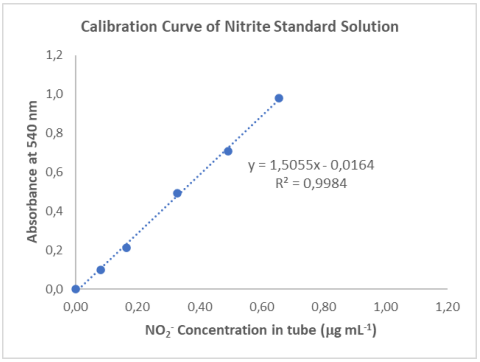
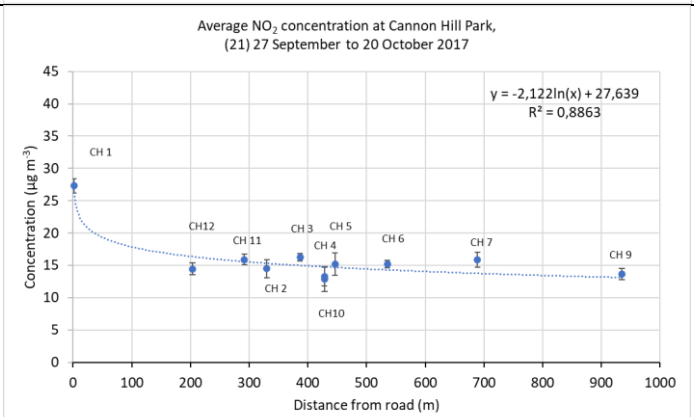
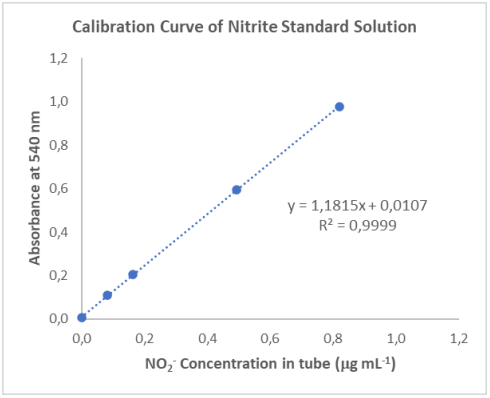
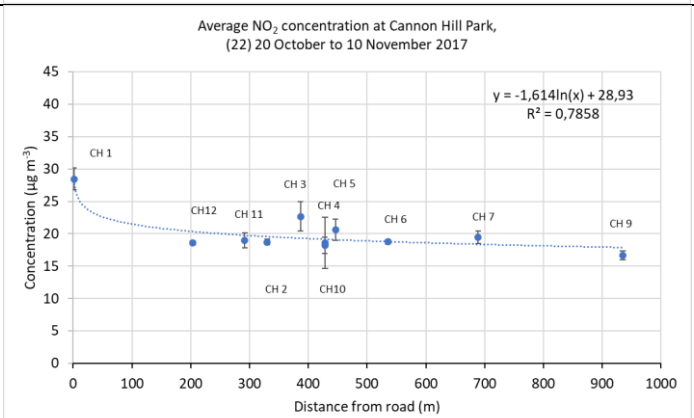
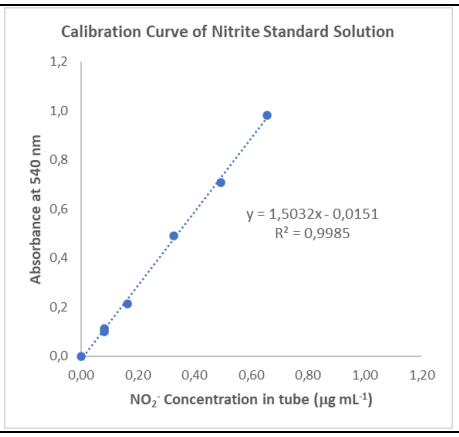
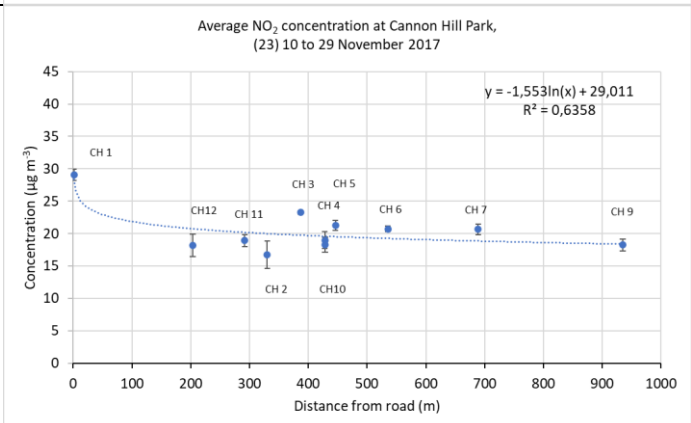
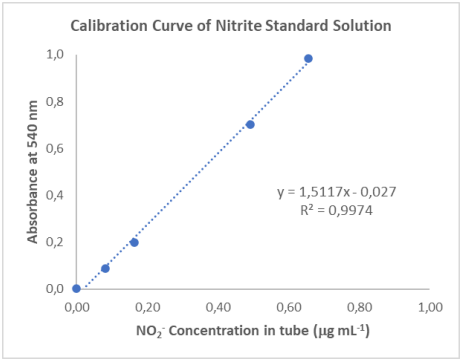
No	Graph	Calibration curve
1		
2		
3		

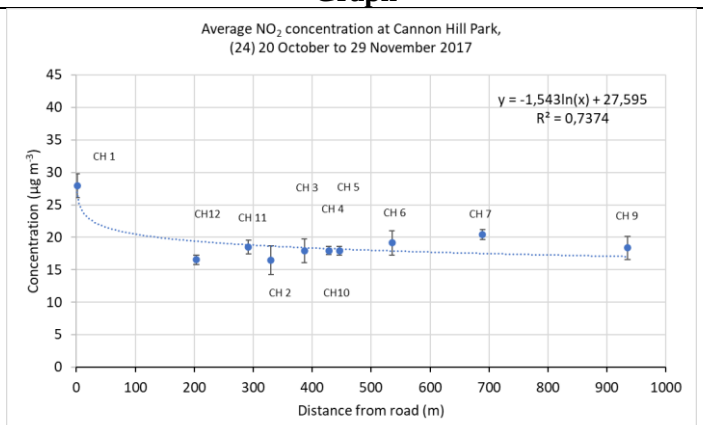
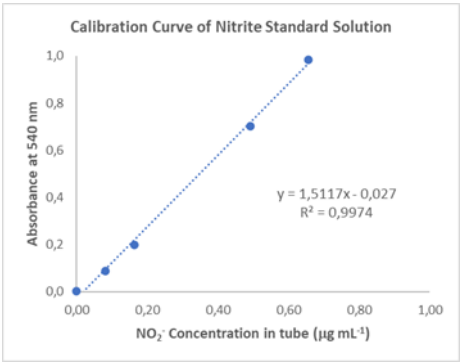
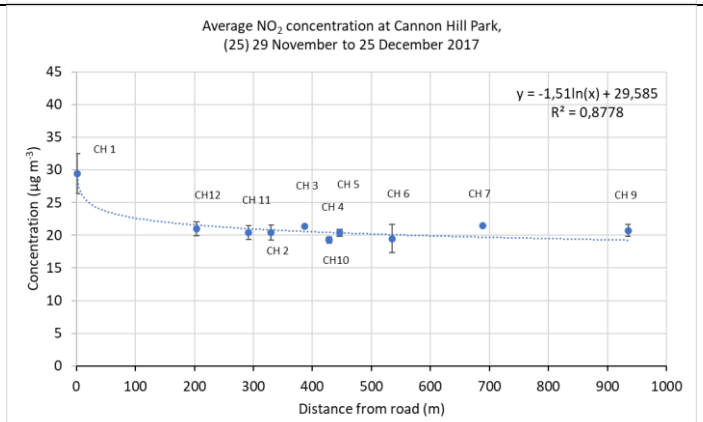
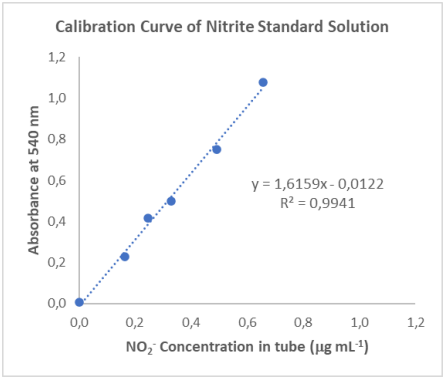
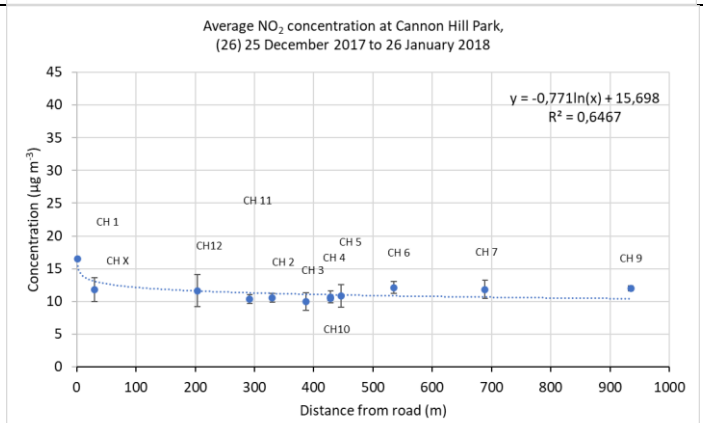
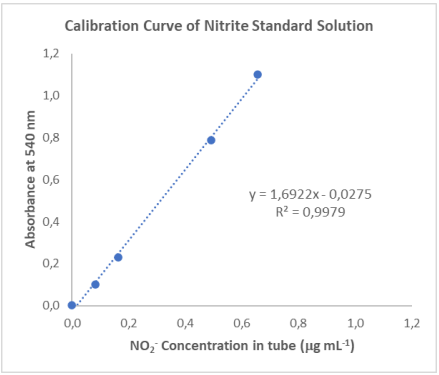
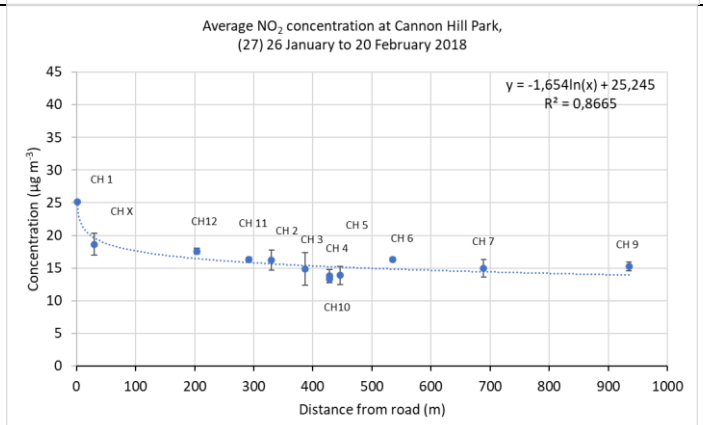
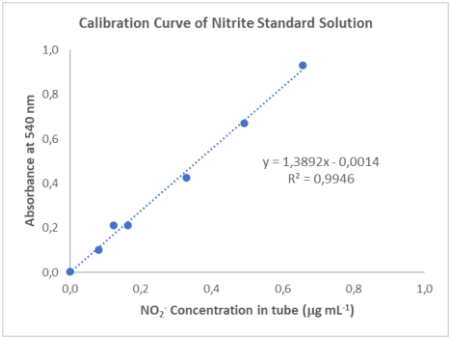
No	Graph	Calibration curve
4		
5		
6		
7		

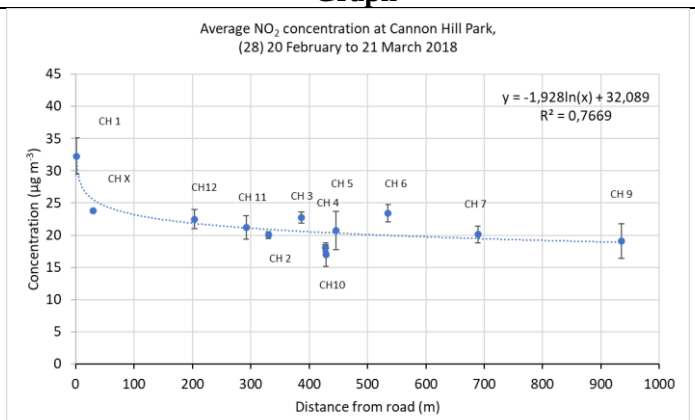
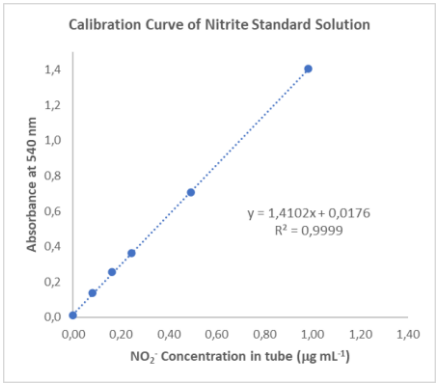
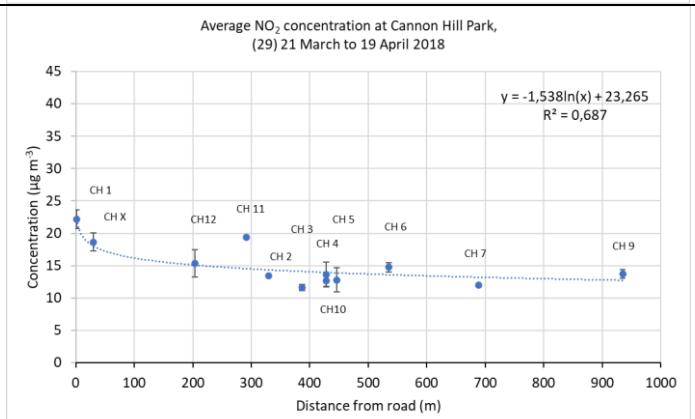
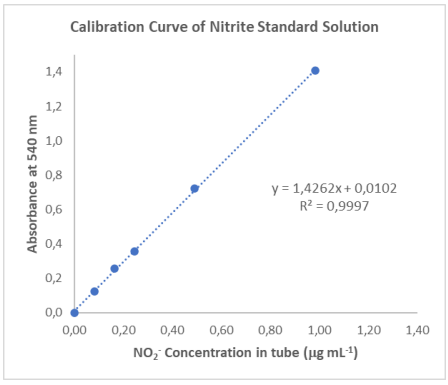
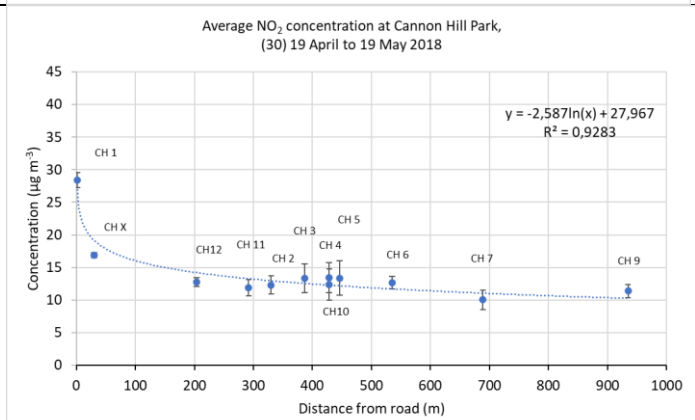
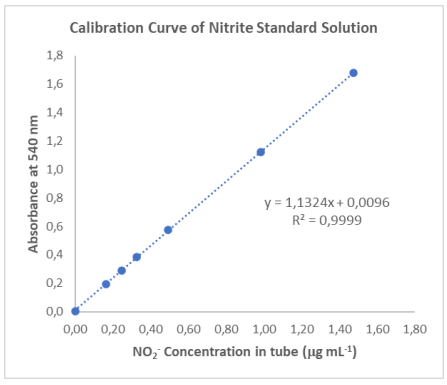
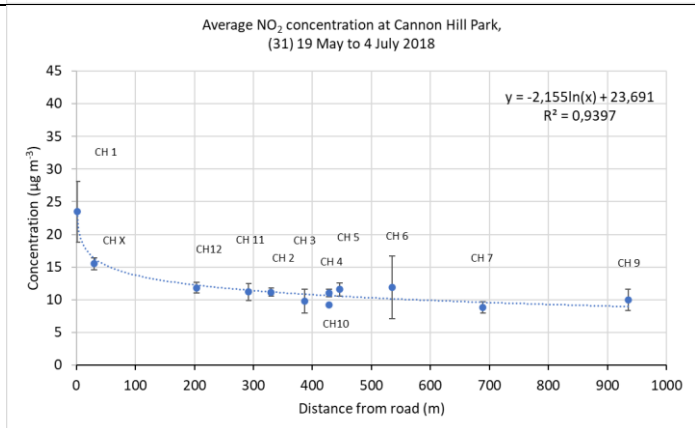
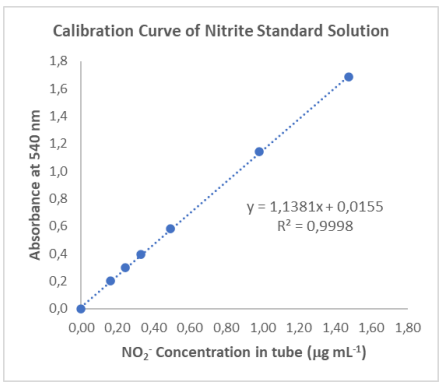
No	Graph	Calibration curve
8		
9		
10		
11		

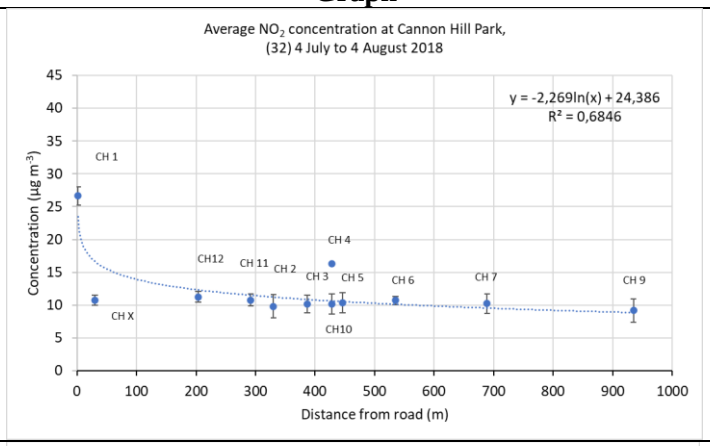
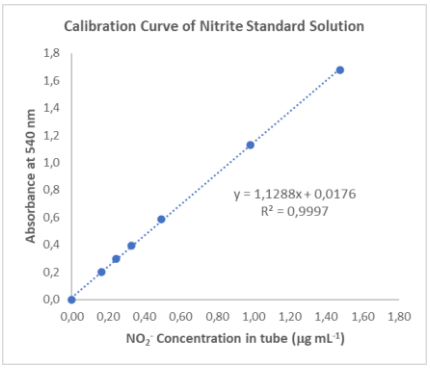
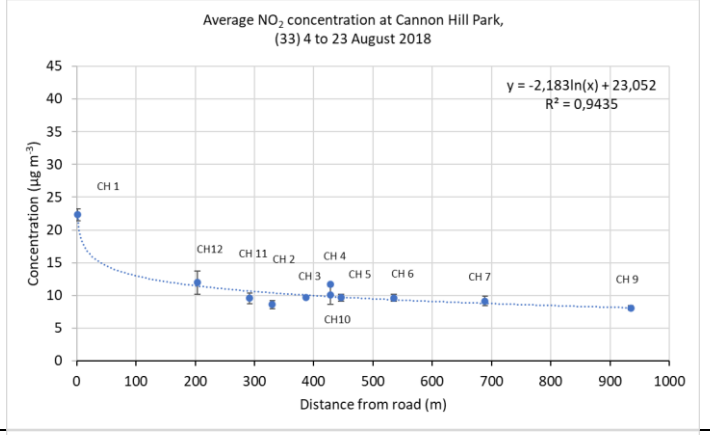
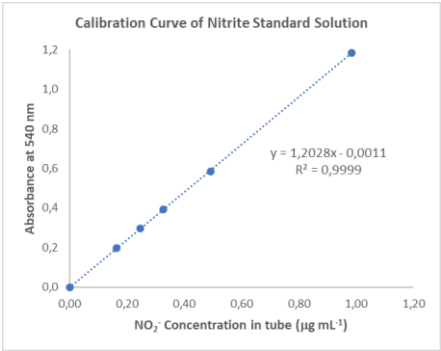
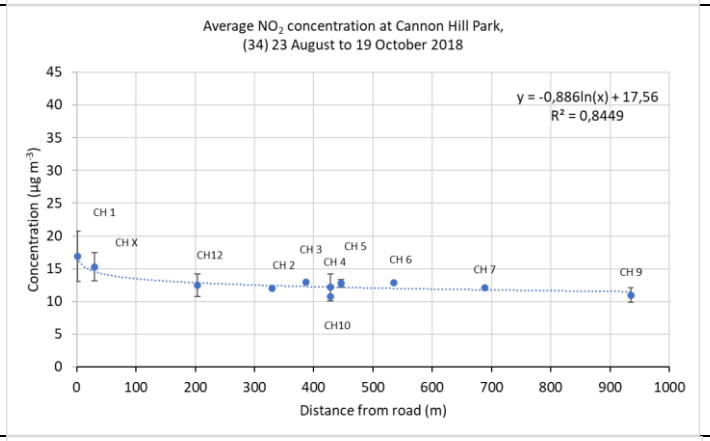
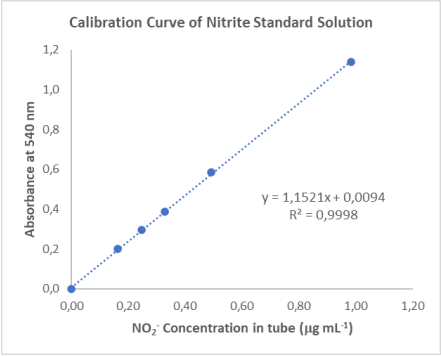
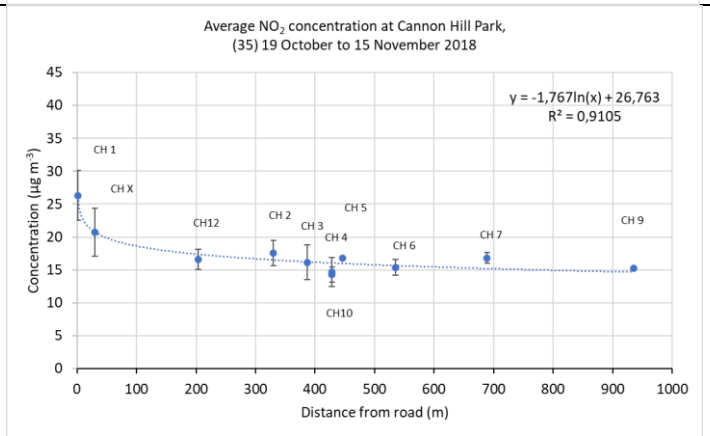
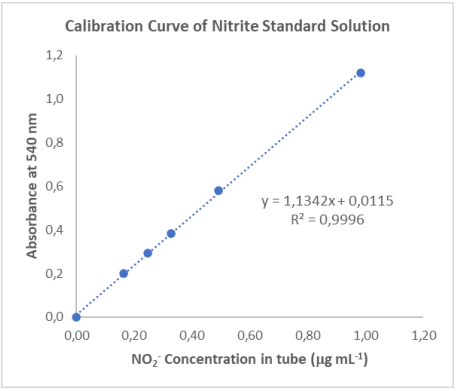
No	Graph	Calibration curve
12		
13		
14		
15		

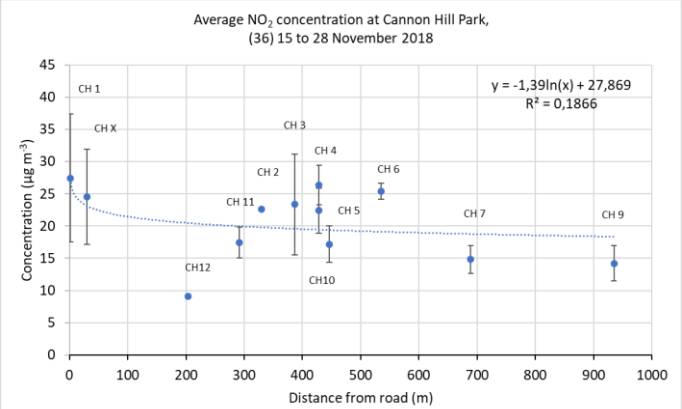
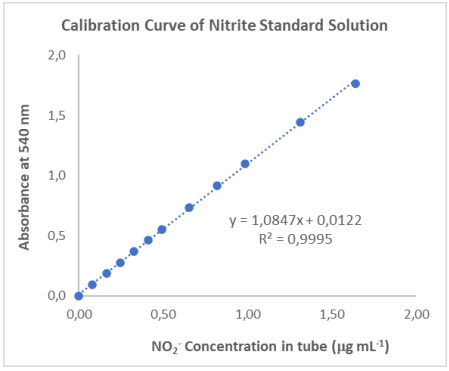
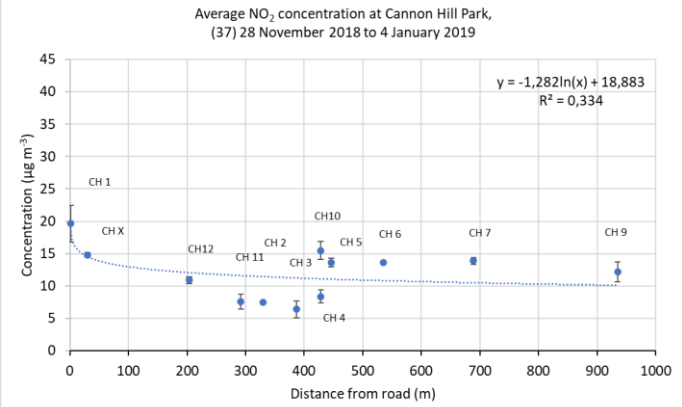
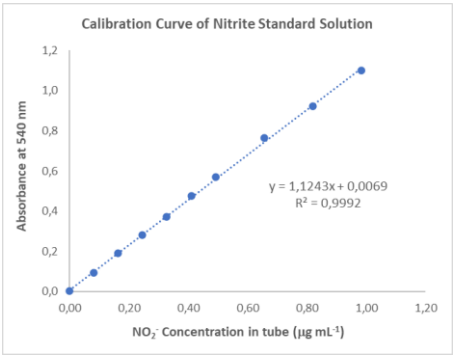
No	Graph	Calibration curve
16		
17		
18		
19		

No	Graph	Calibration curve
20		
21		
22		
23		

No	Graph	Calibration curve
24		
25		
26		
27		

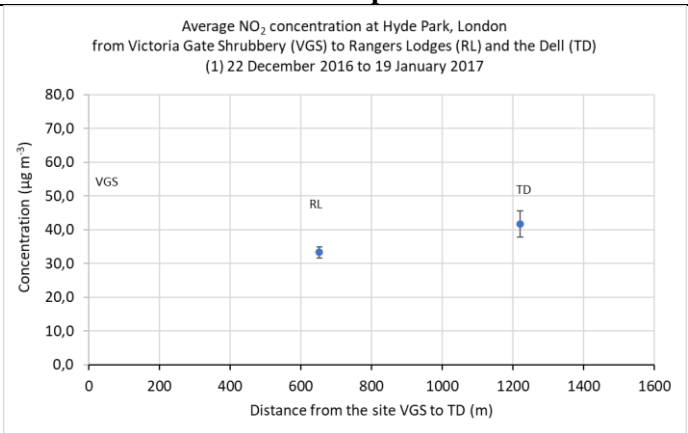
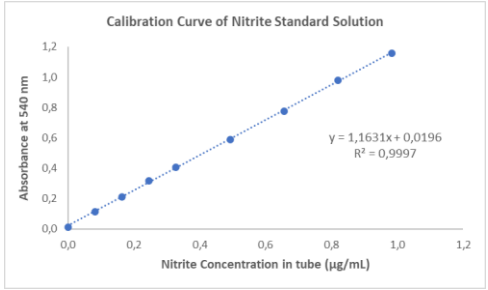
No	Graph	Calibration curve
28		
29		
30		
31		

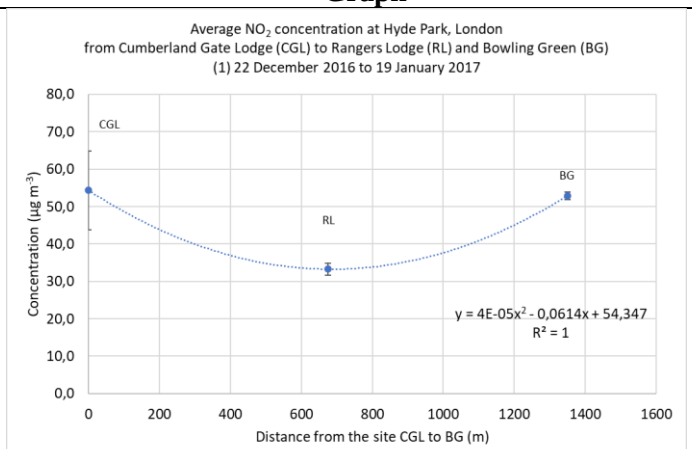
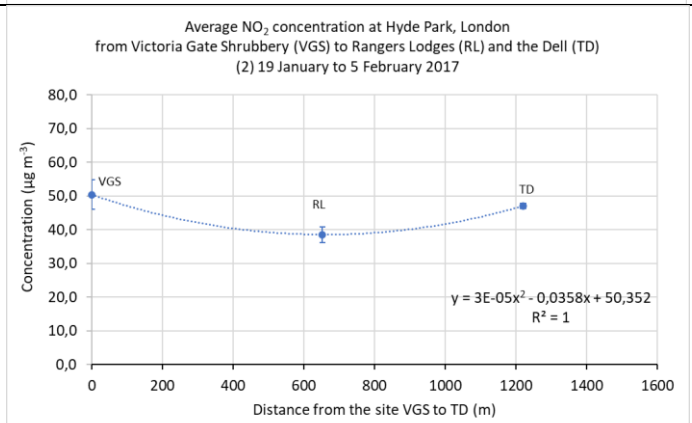
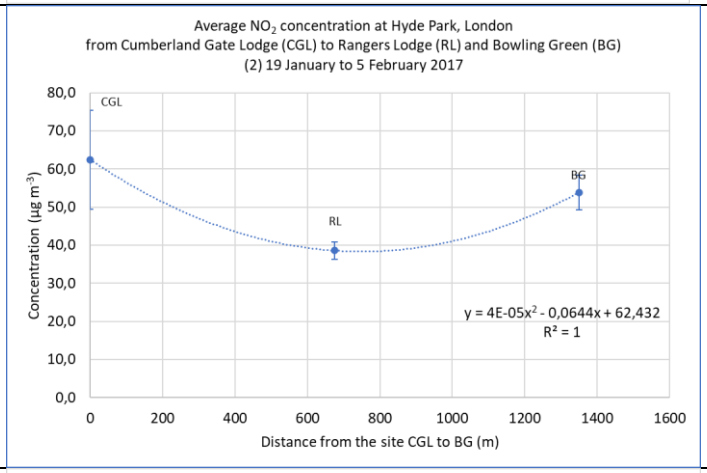
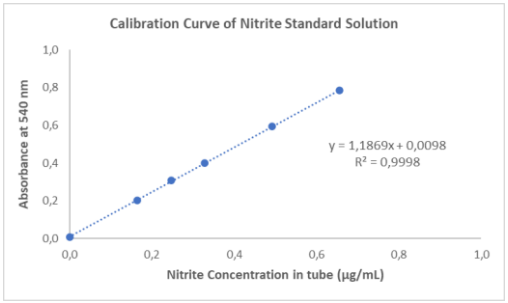
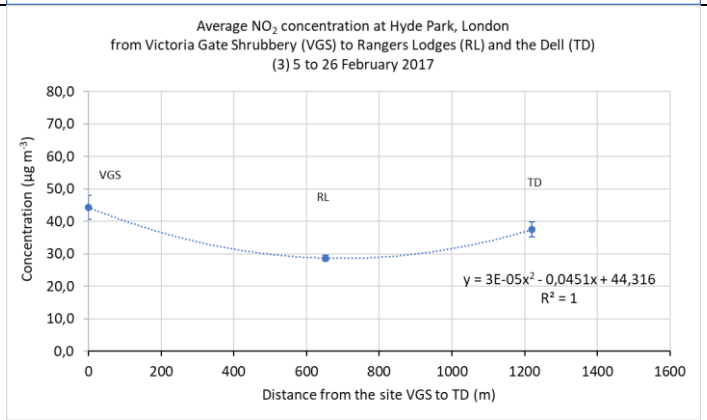
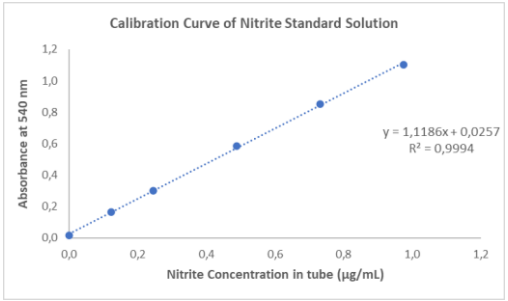
No	Graph	Calibration curve
32		
33		
34		
35		

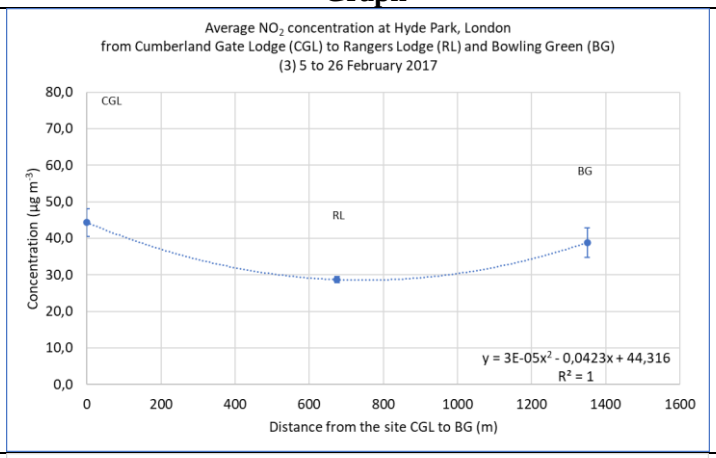
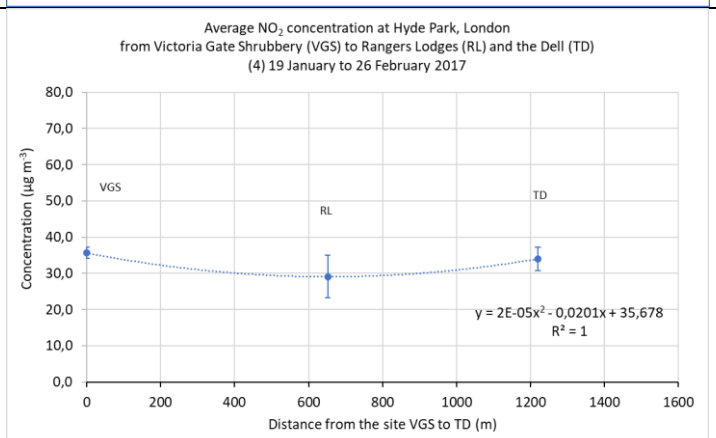
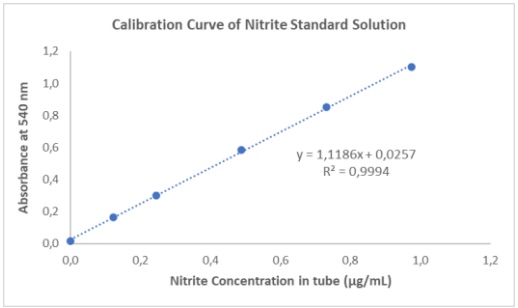
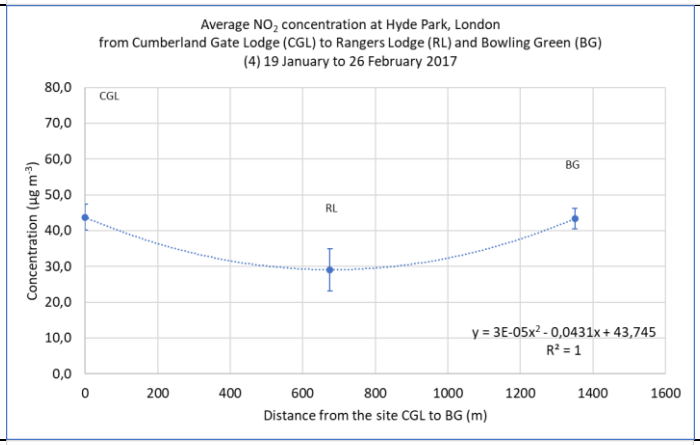
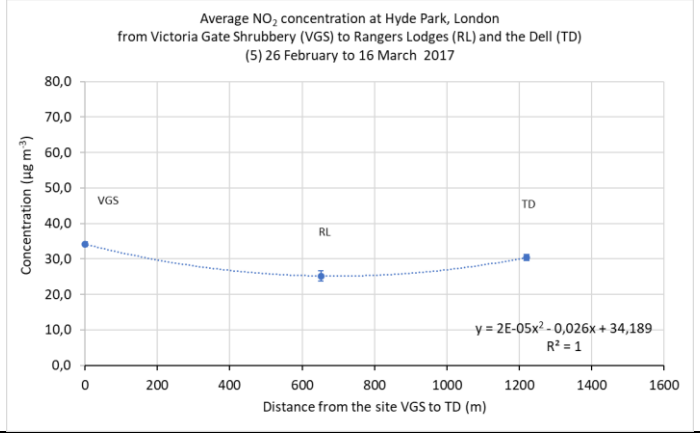
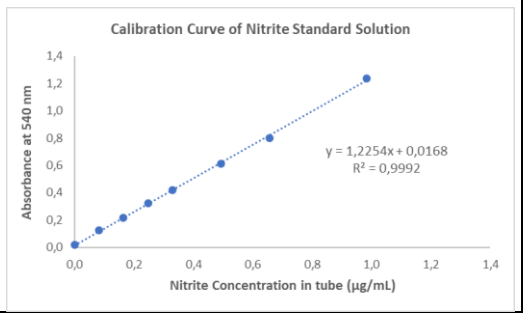
No	Graph	Calibration curve
36		
37		

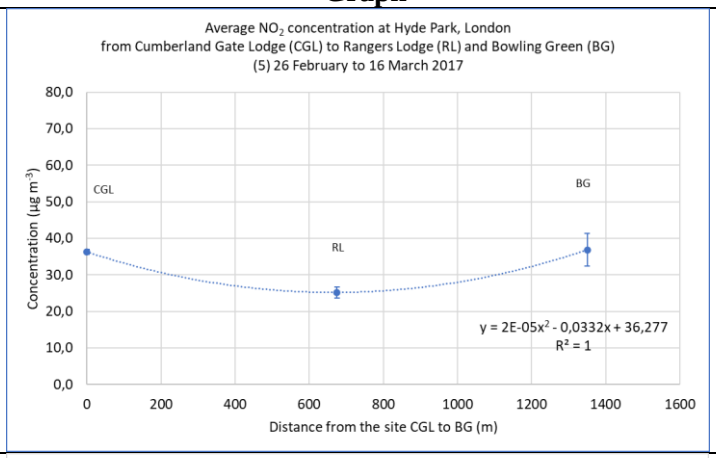
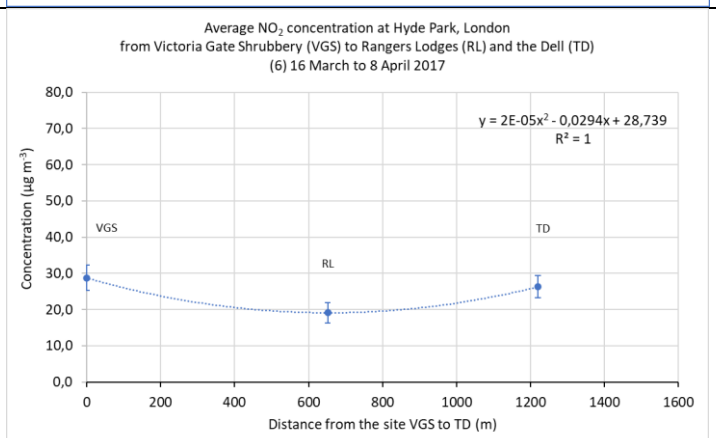
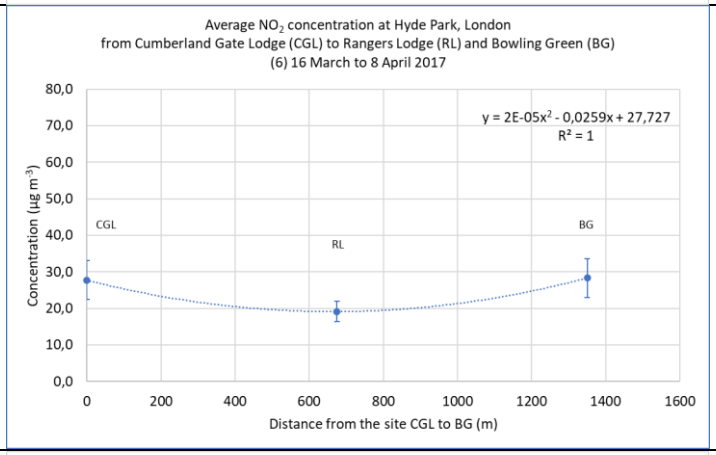
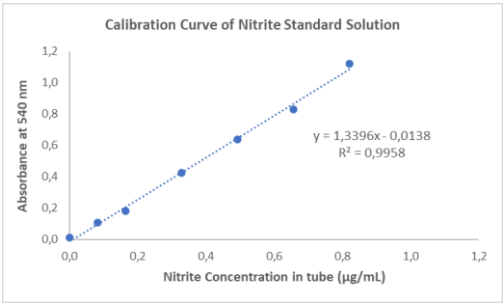
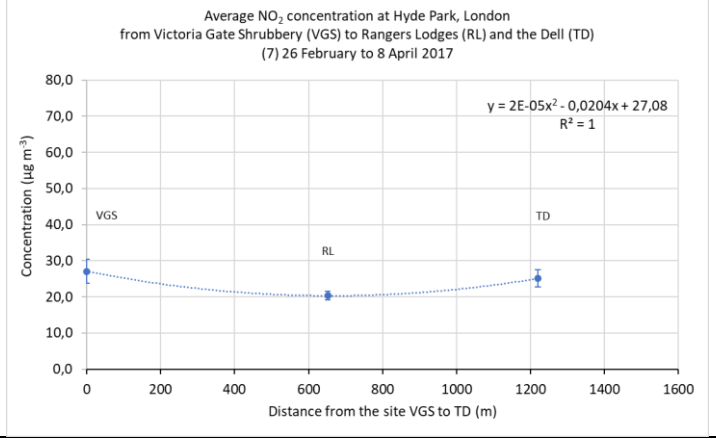
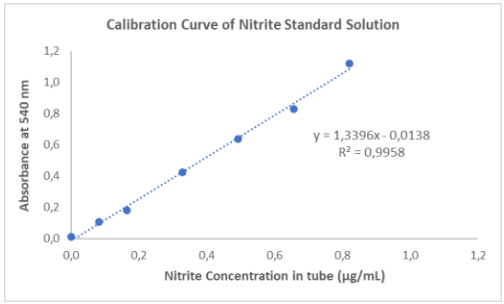
Appendix 3.4. Graph of NO_2 concentrations at Hyde Park

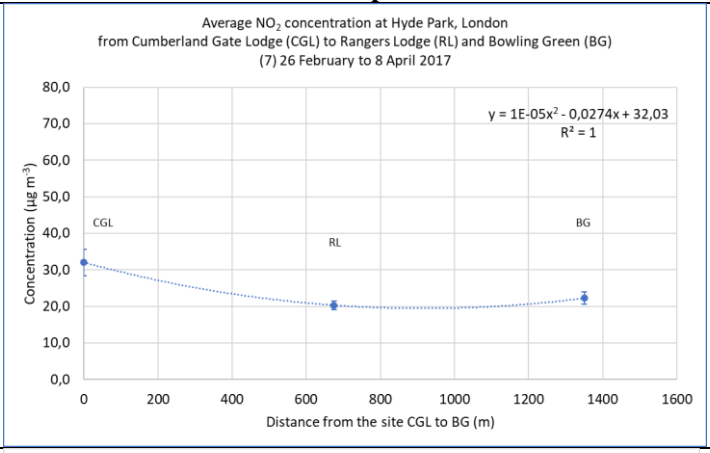
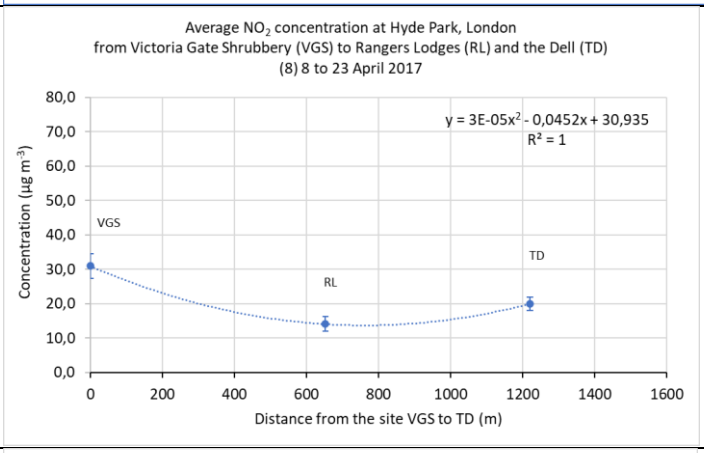
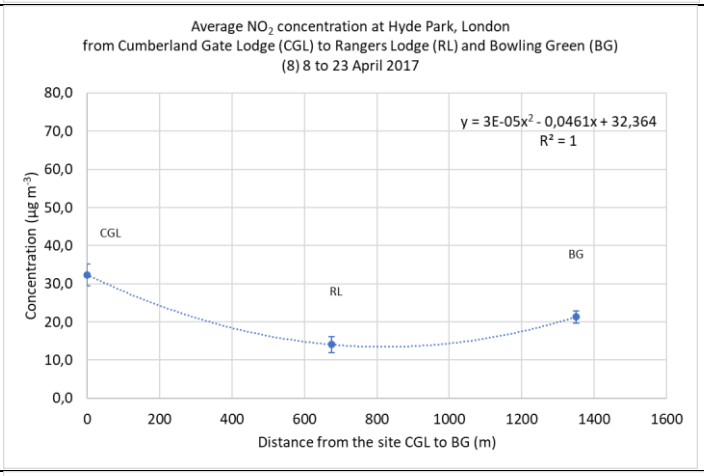
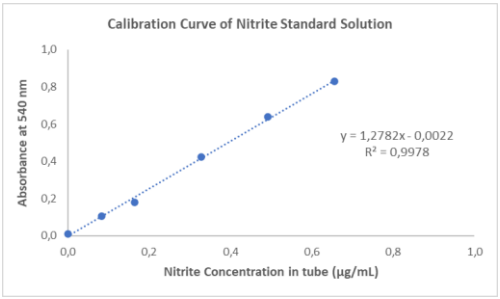
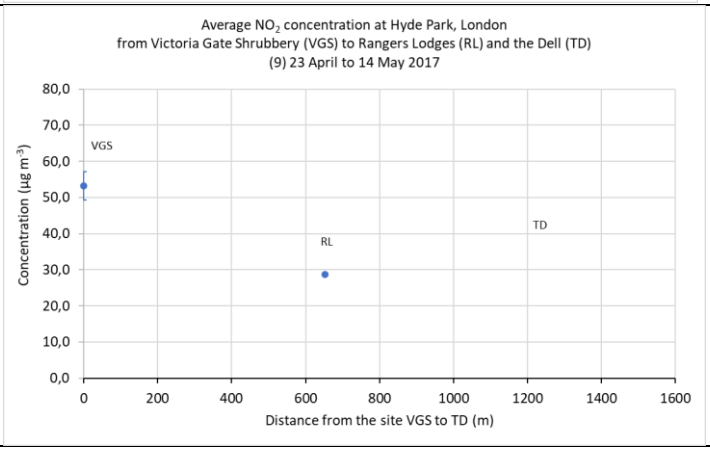
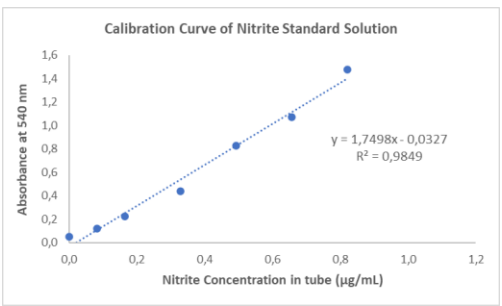
Table A.3.4. Graph of NO_2 concentrations from raw data of DT measurements at Hyde Park (mean ± standard deviation from triplicate DT), and calibration curves of nitrite standard solution, sampling period December 2016 – December 2017

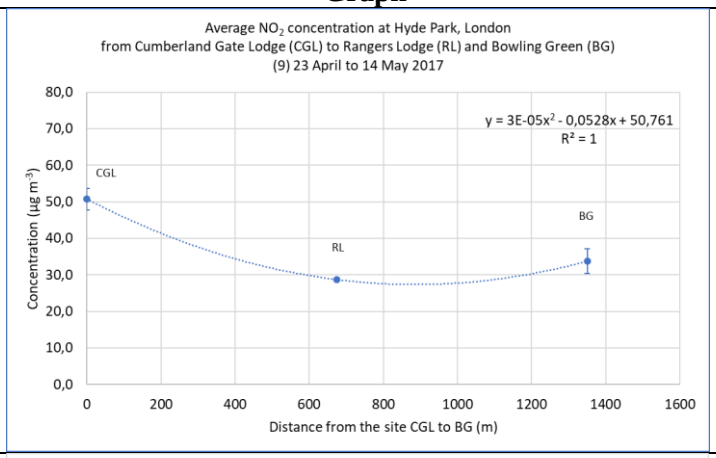
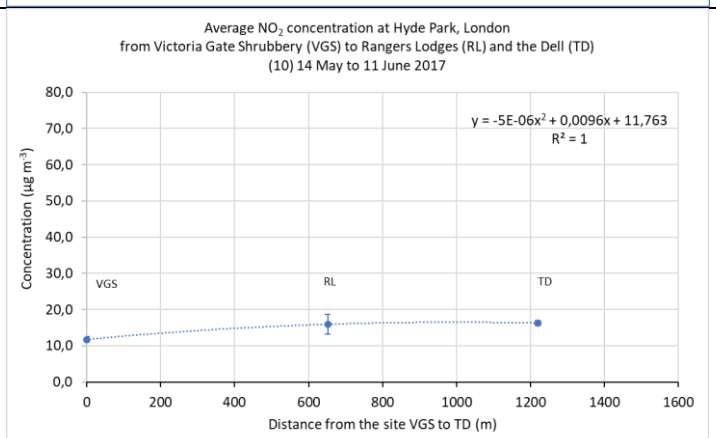
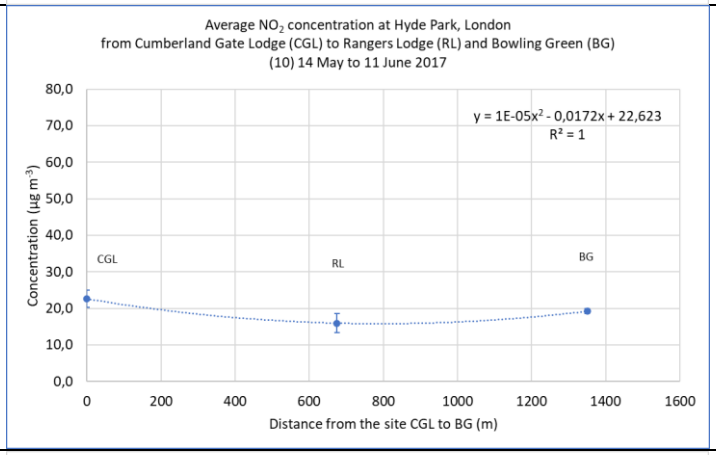
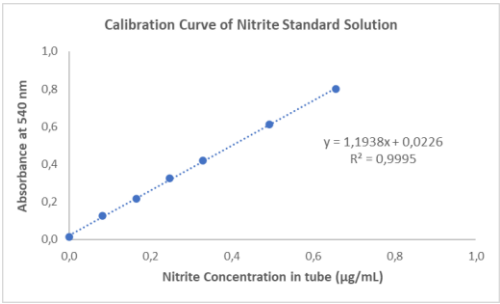
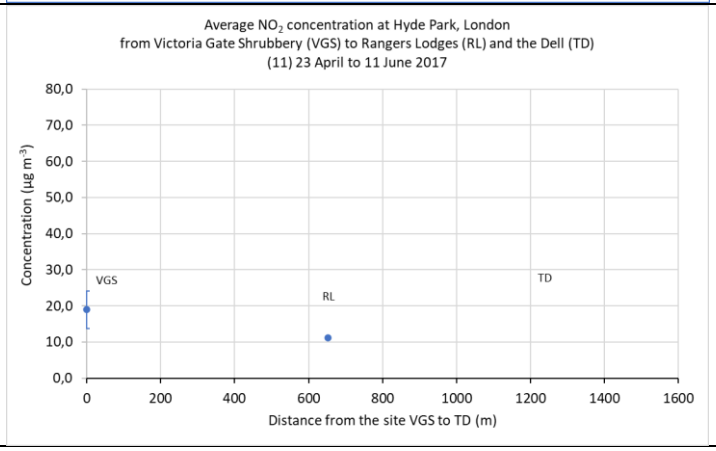
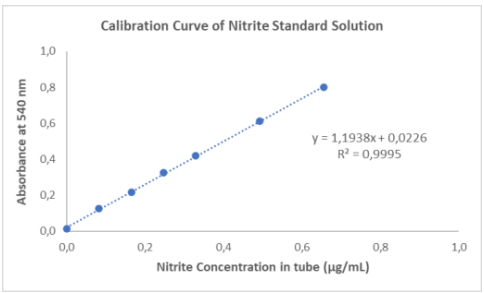
No	Graph	Calibration curve
1		

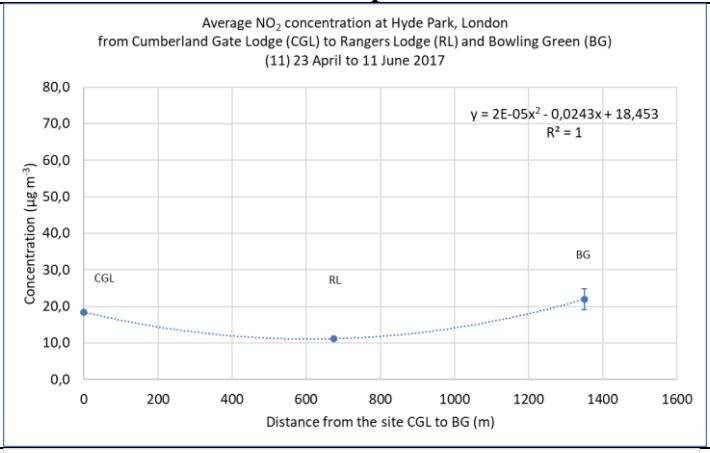
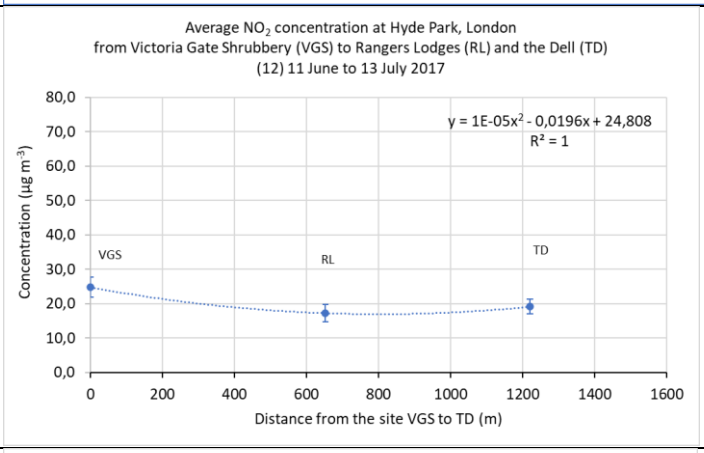
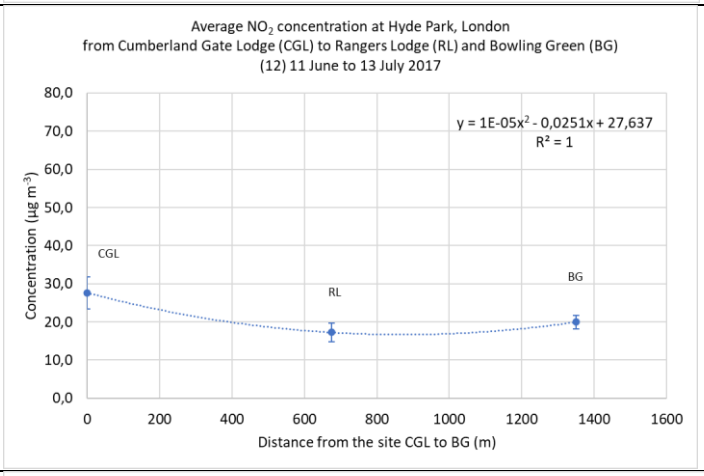
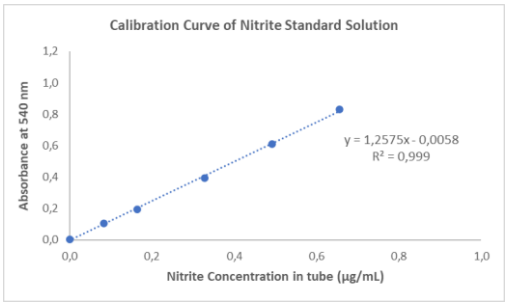
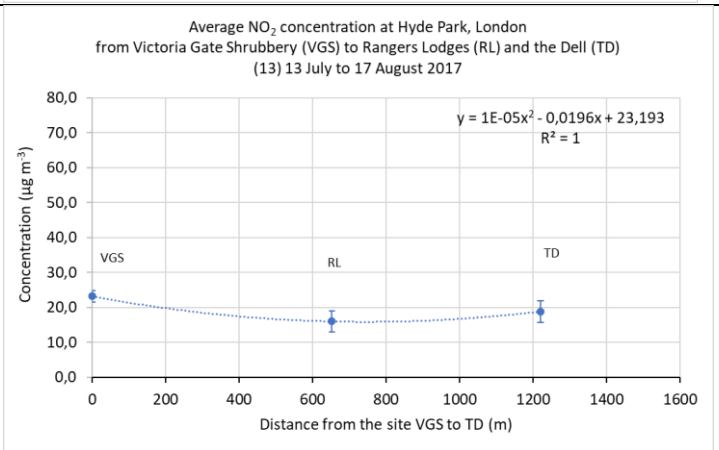
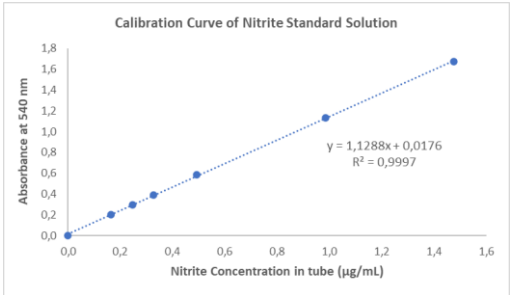
No	Graph	Calibration curve
		
2	 	
3		

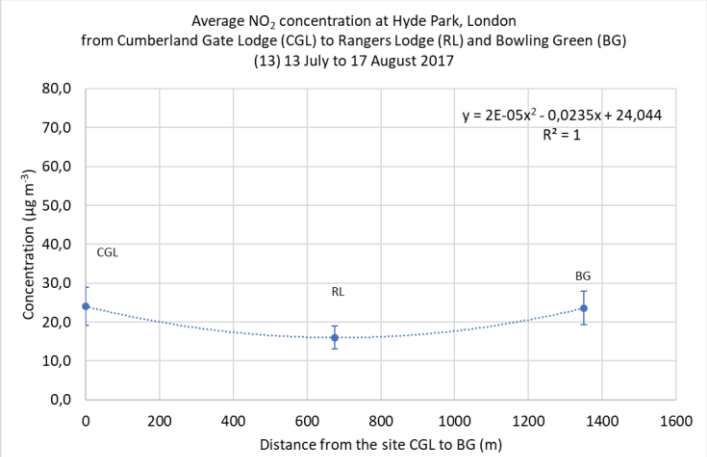
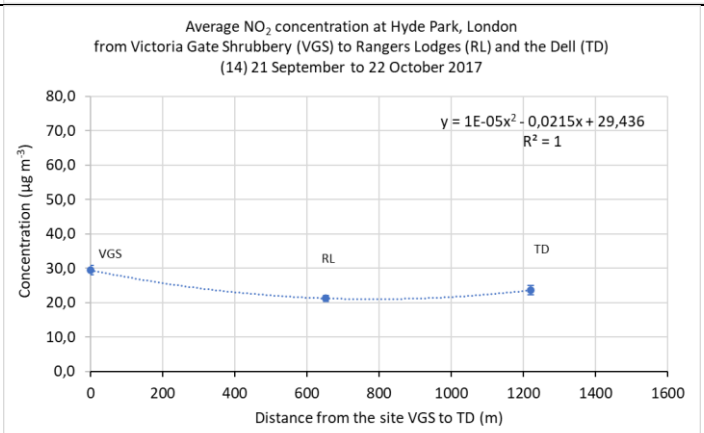
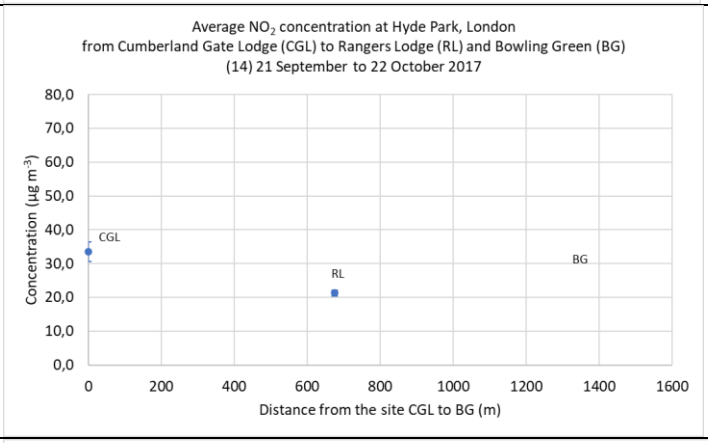
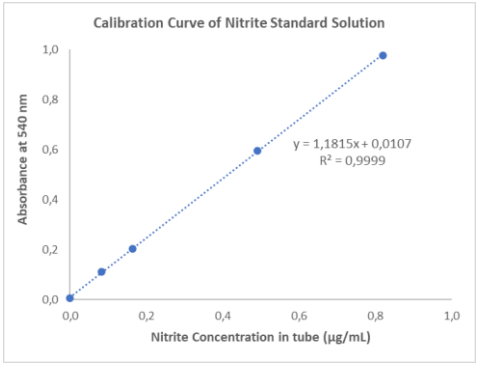
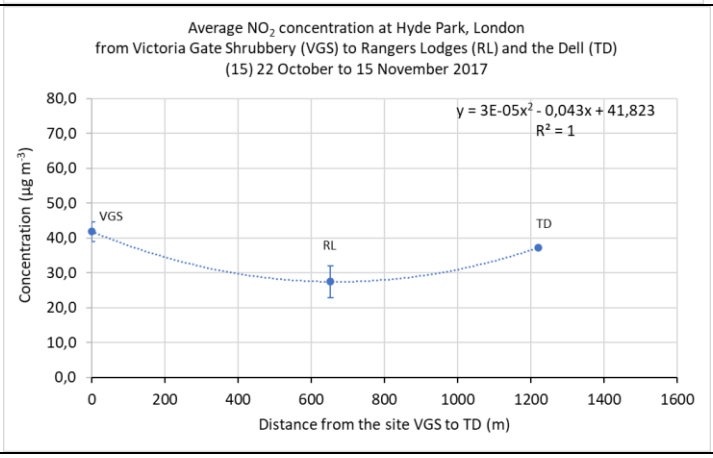
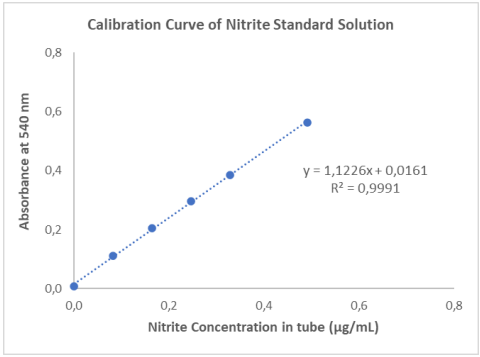
No	Graph	Calibration curve
		
4		
		
5		

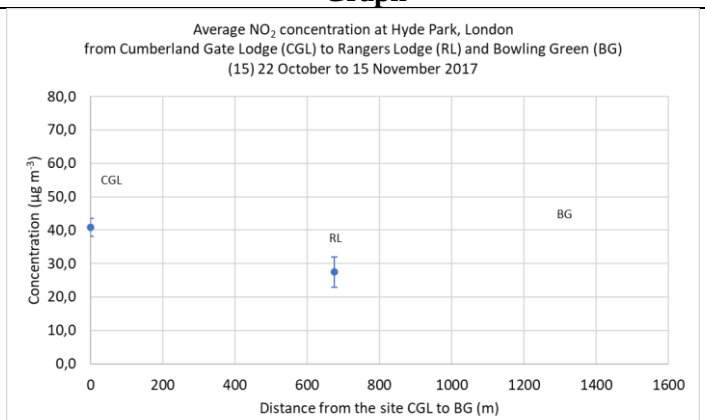
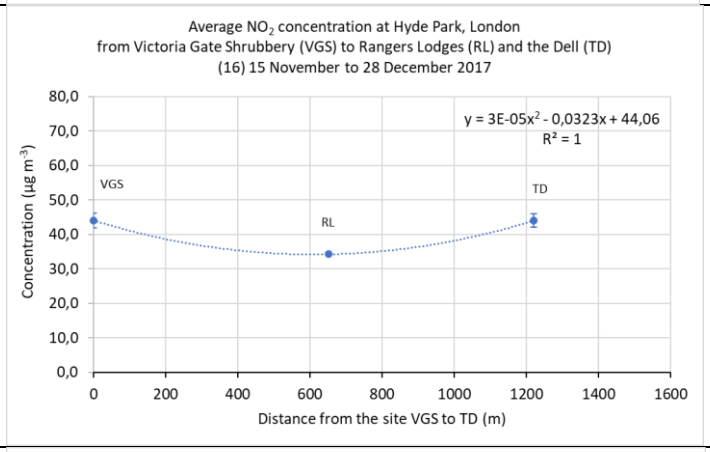
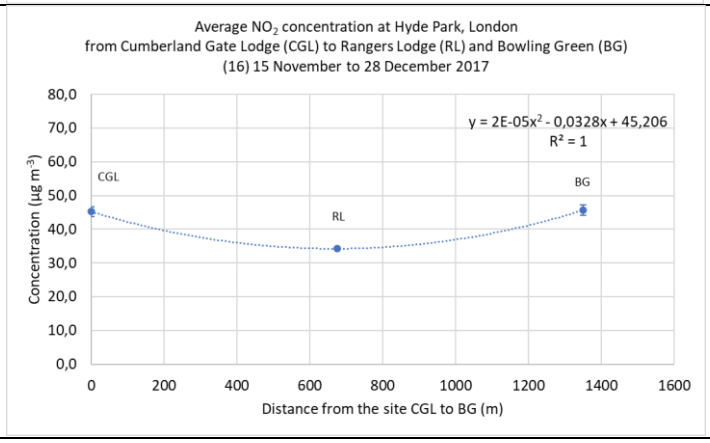
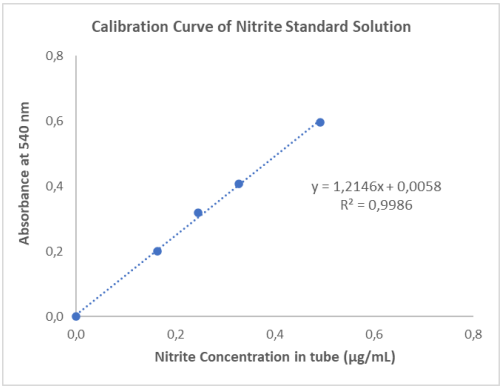
No	Graph	Calibration curve
		
6	 	
7		

No	Graph	Calibration curve
		
8	 	
9		

No	Graph	Calibration curve
		
10	 	
11		

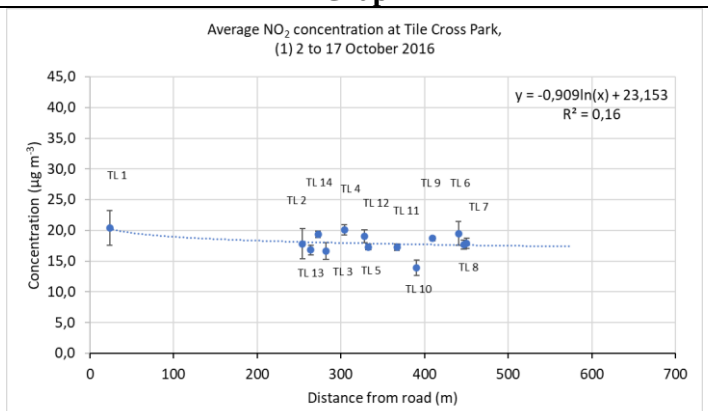
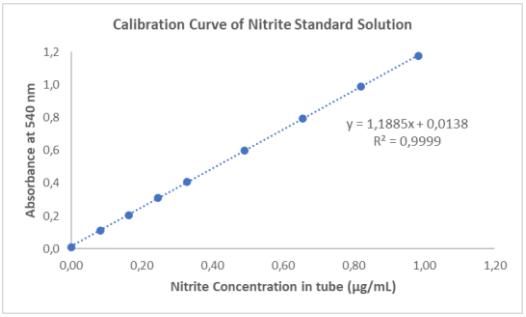
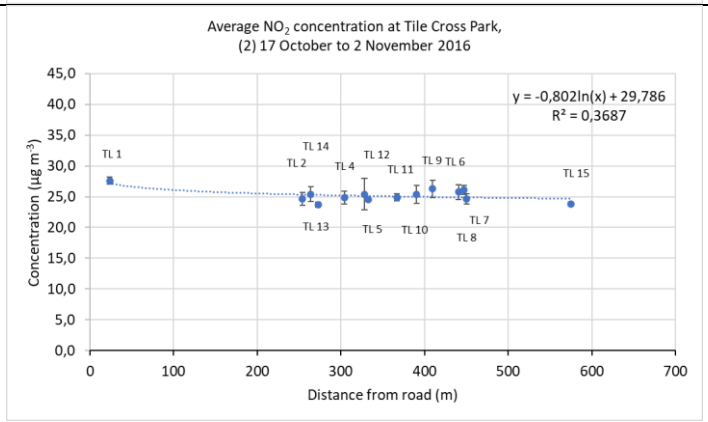
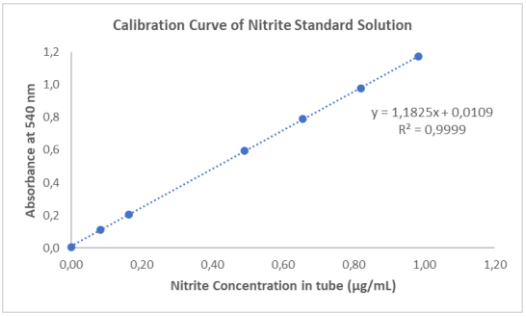
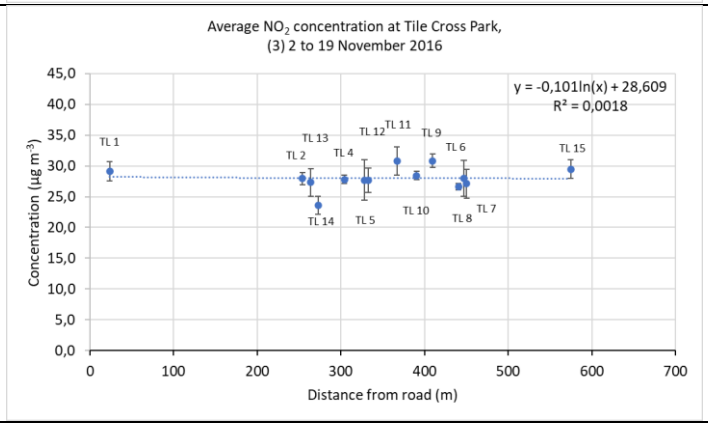
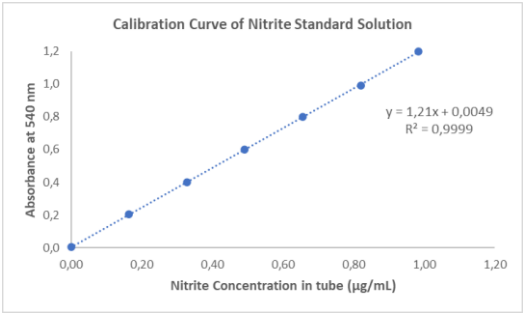
No	Graph	Calibration curve
		
12	 	
13		

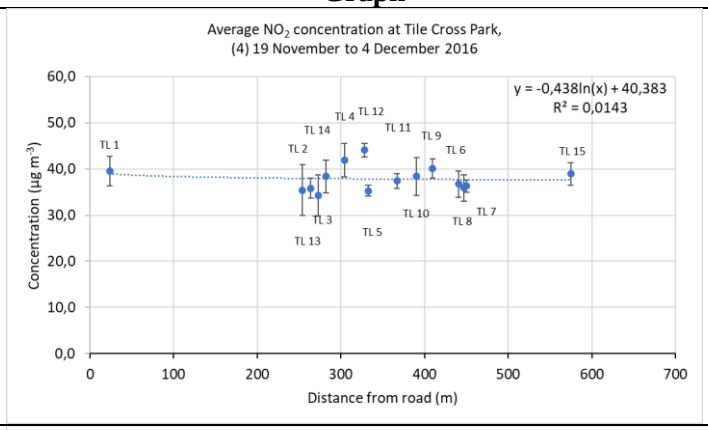
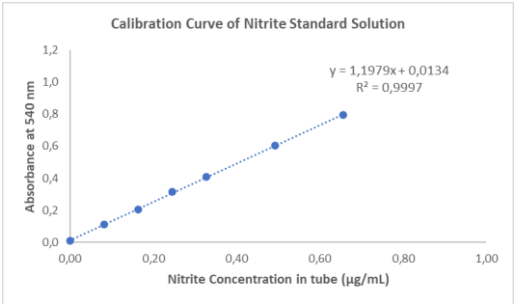
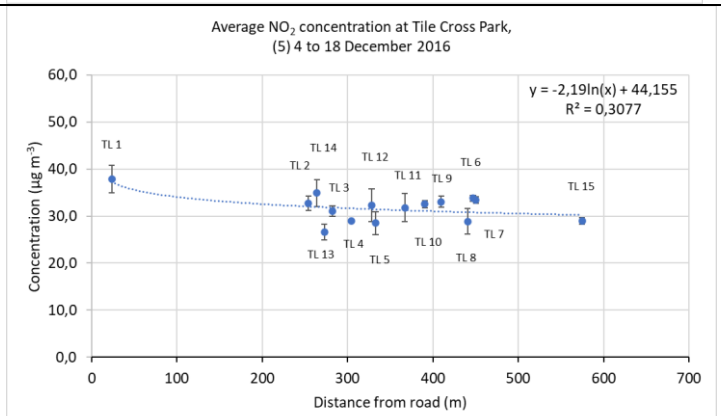
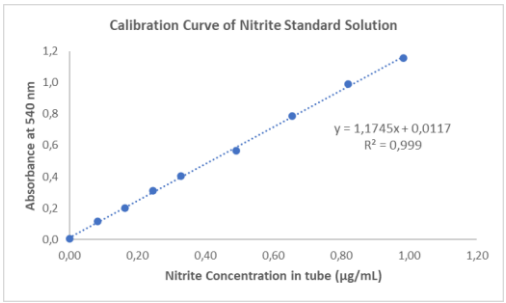
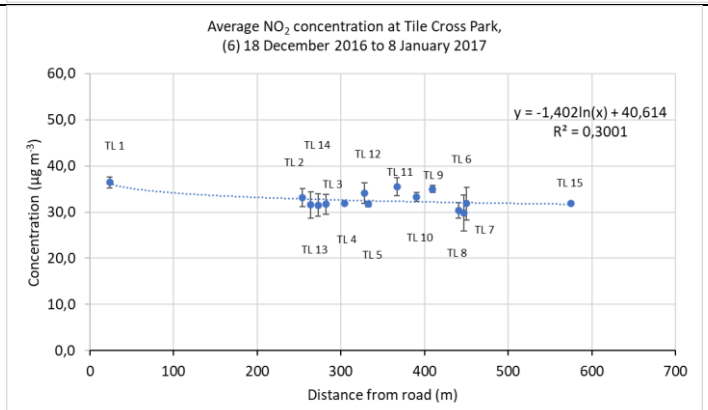
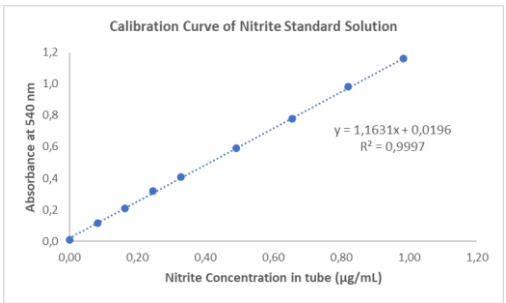
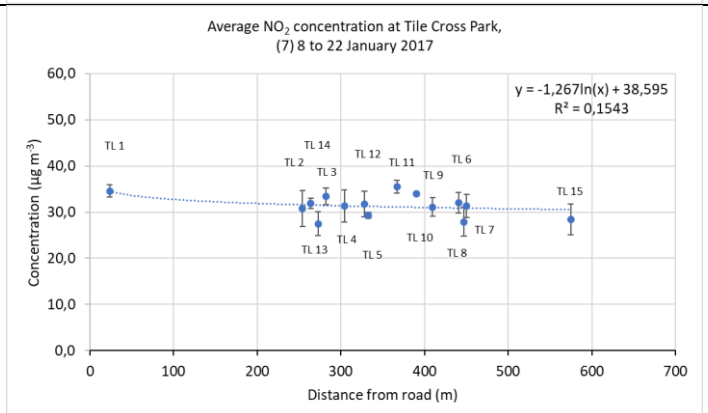
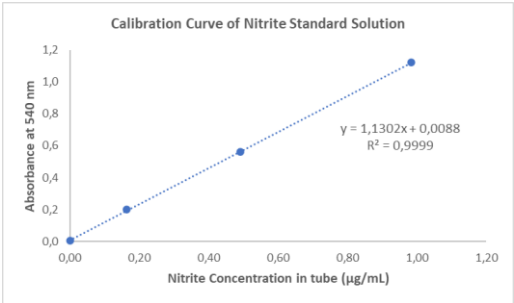
No	Graph	Calibration curve
		
14	 	
15		

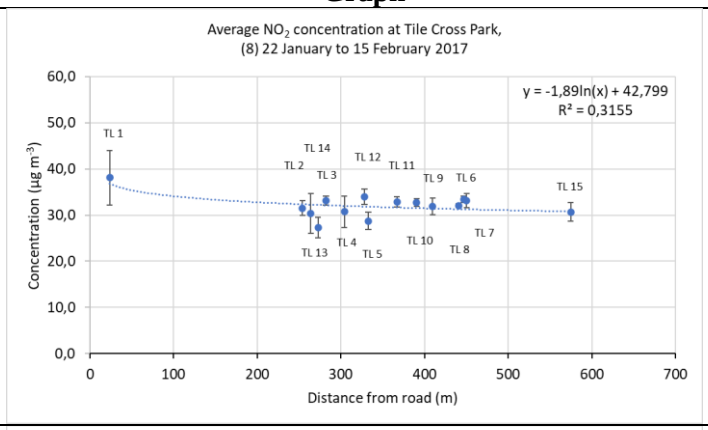
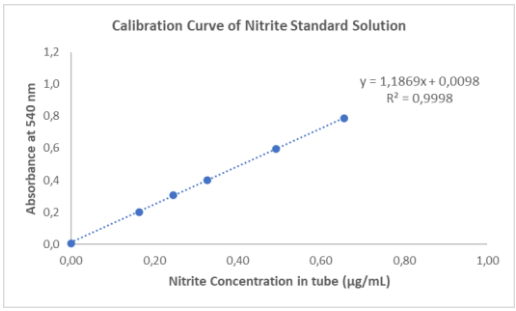
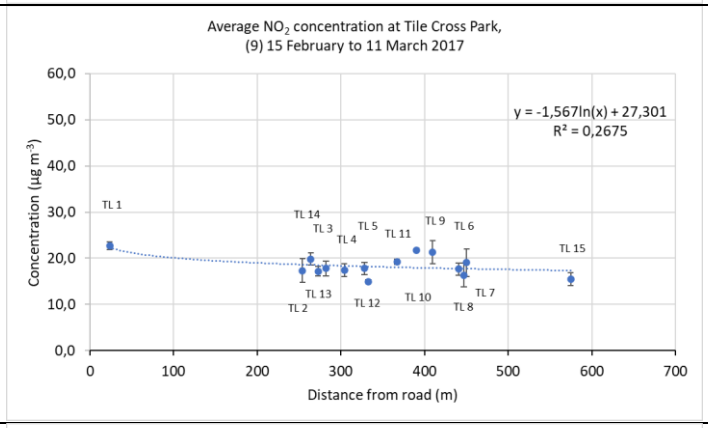
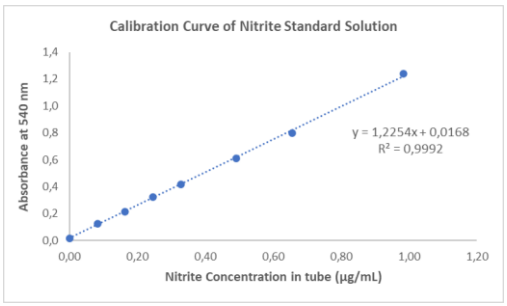
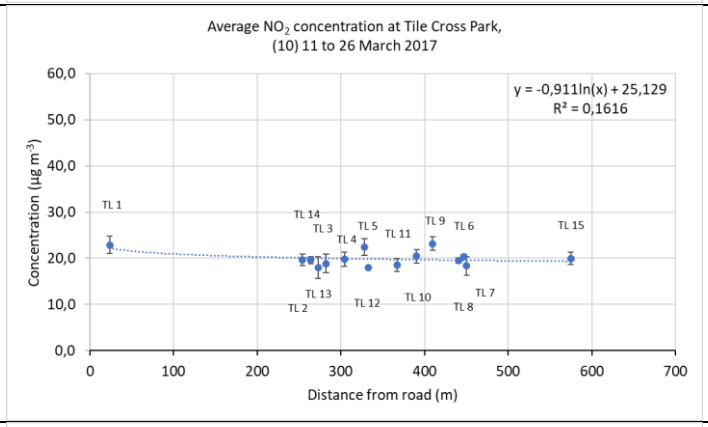
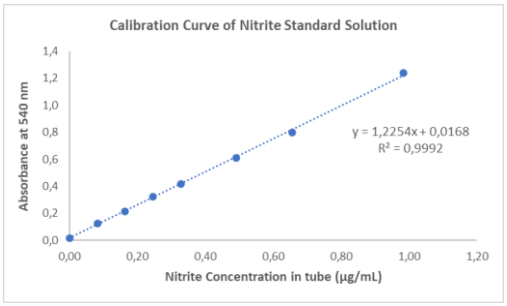
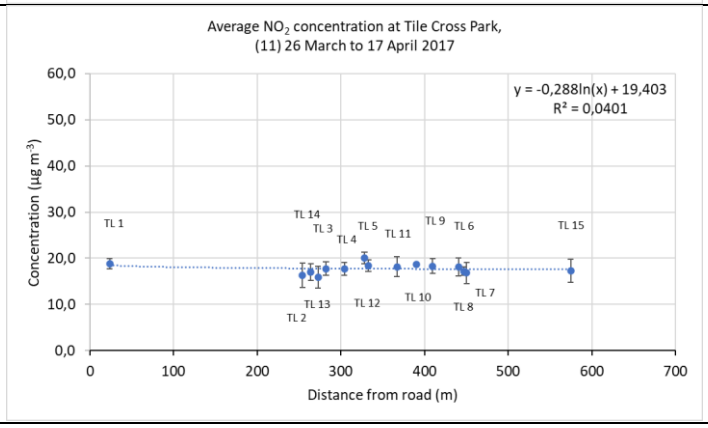
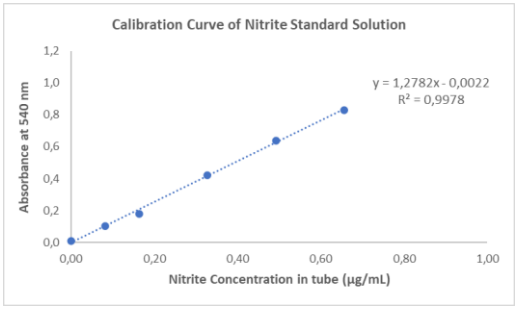
No	Graph	Calibration curve
		
16	 	

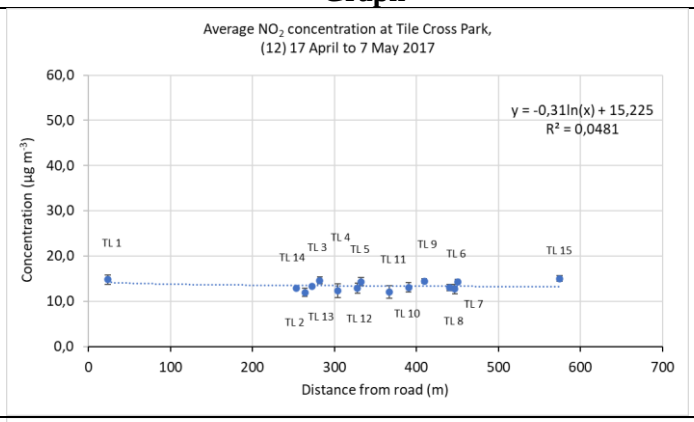
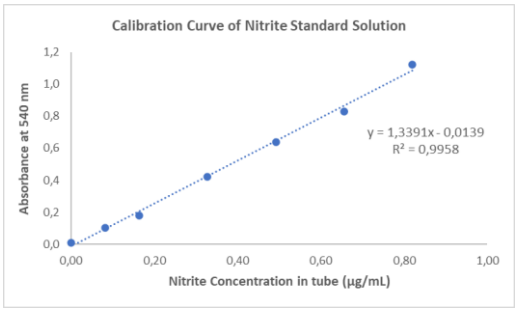
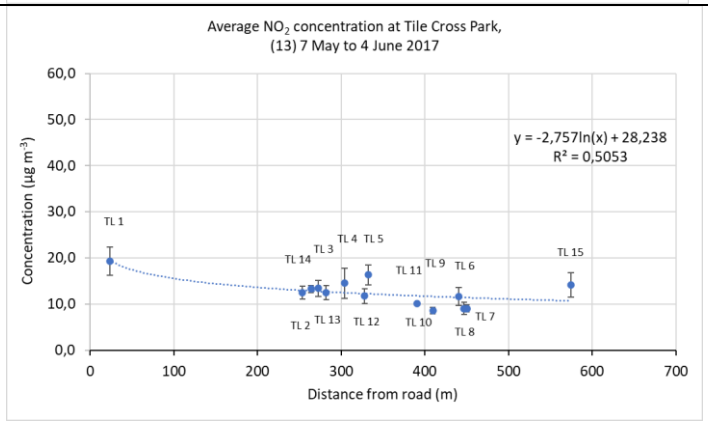
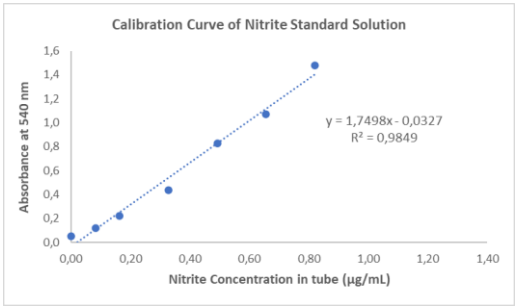
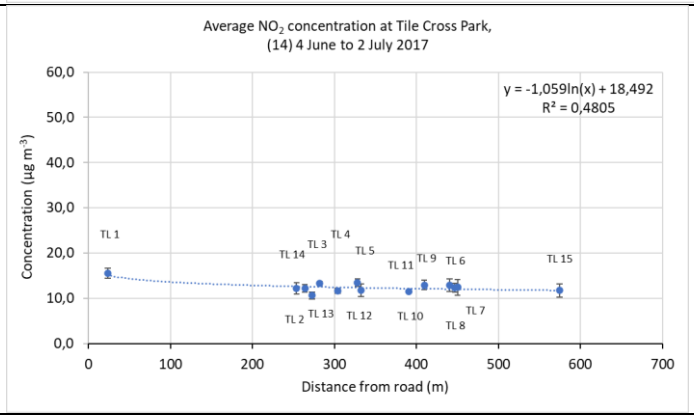
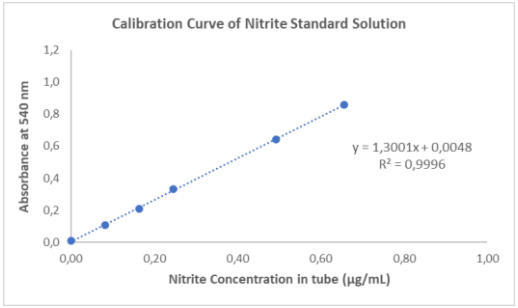
Appendix 3.5. Graph of NO_2 concentrations at Tile Cross Park

Table A.3.5. Graph of NO_2 concentrations from raw data of DT measurements at Tile Cross Park (mean ± standard deviation from triplicate DT), and calibration curves of nitrite standard solution, sampling period October 2016 – July 2017

No	Graph	Calibration curve
1		
2		
3		

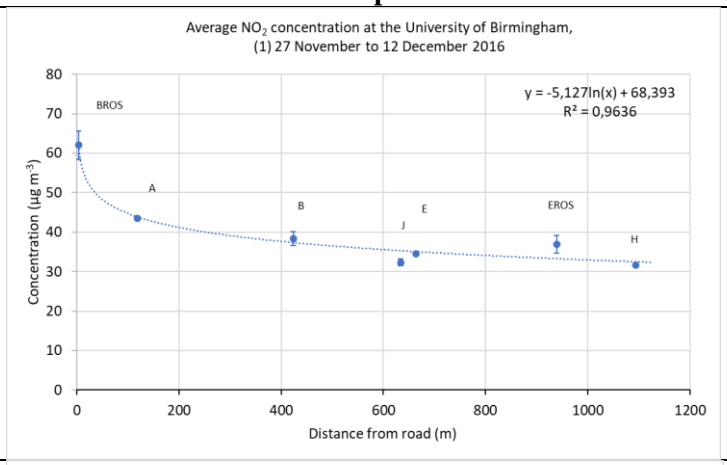
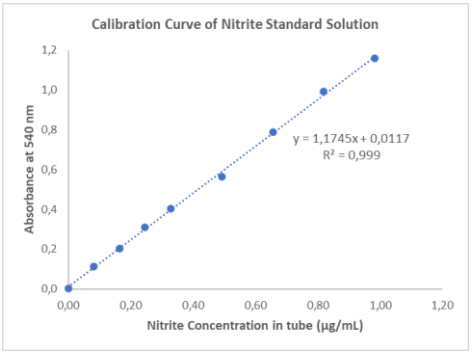
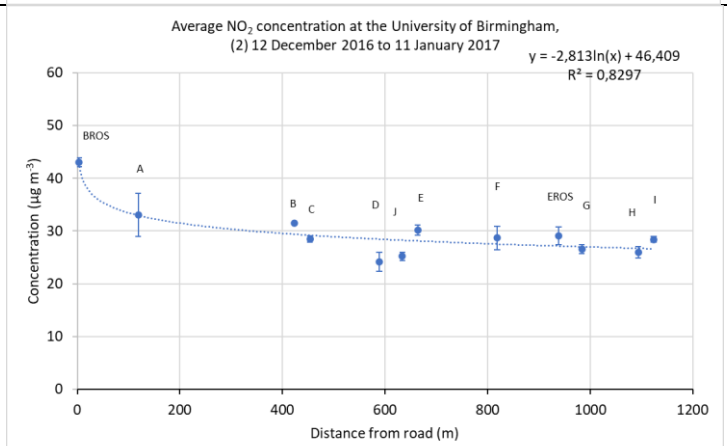
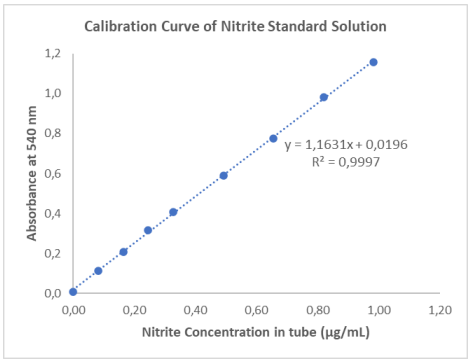
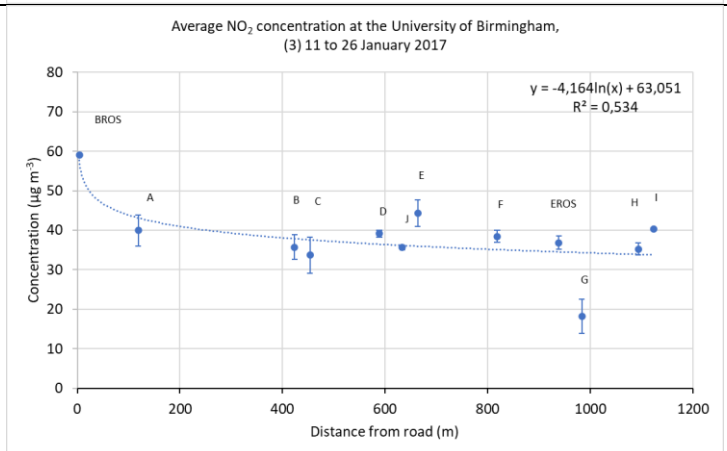
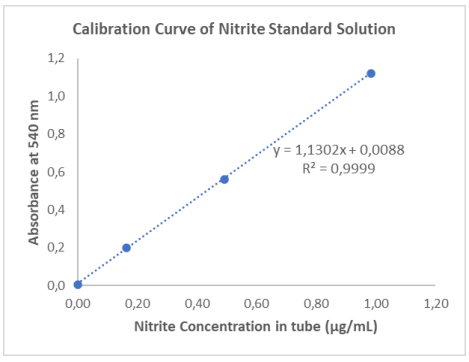
No	Graph	Calibration curve
4		
5		
6		
7		

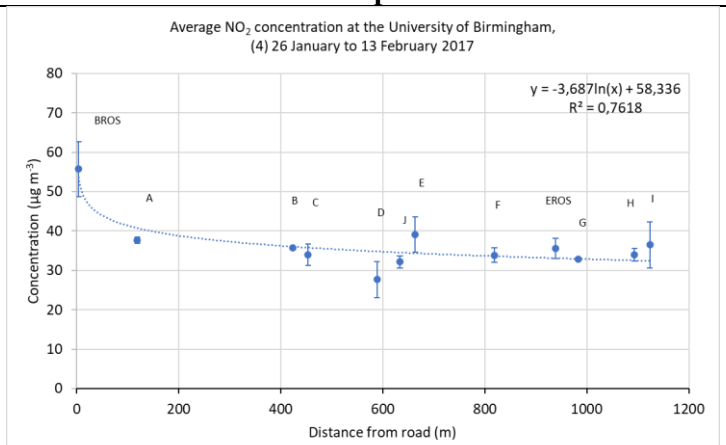
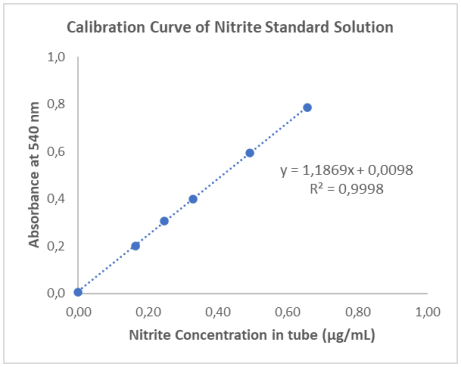
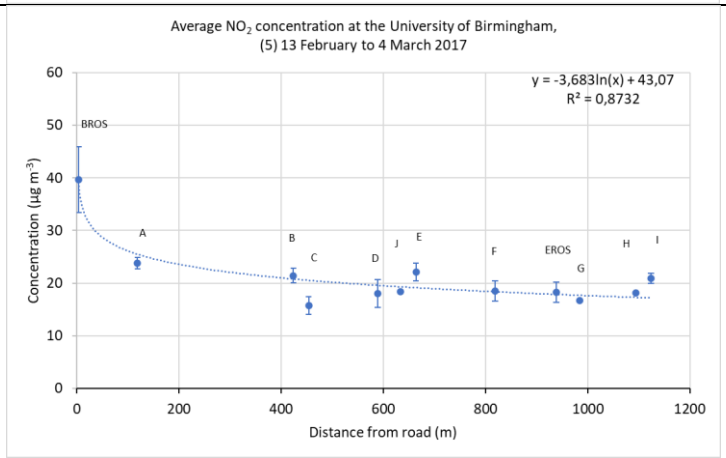
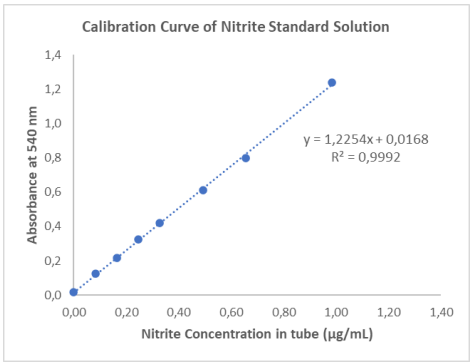
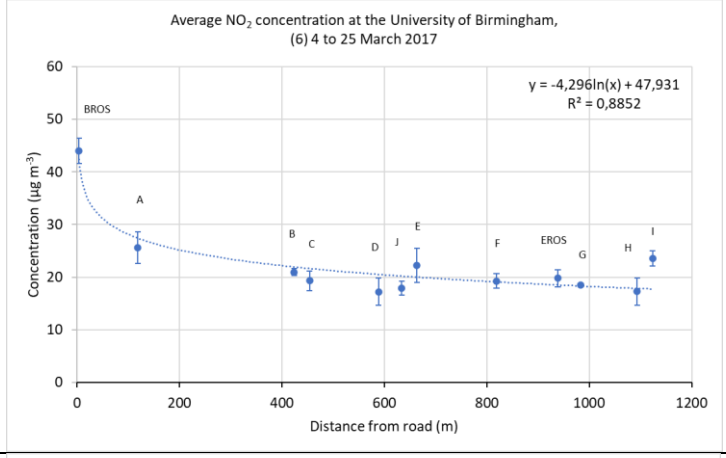
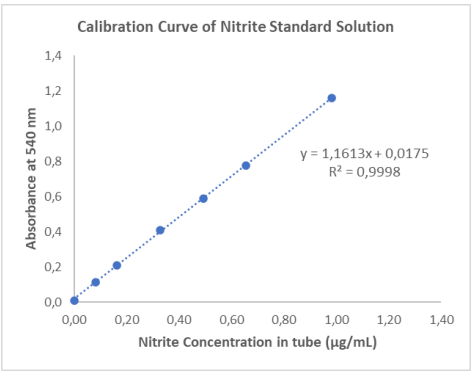
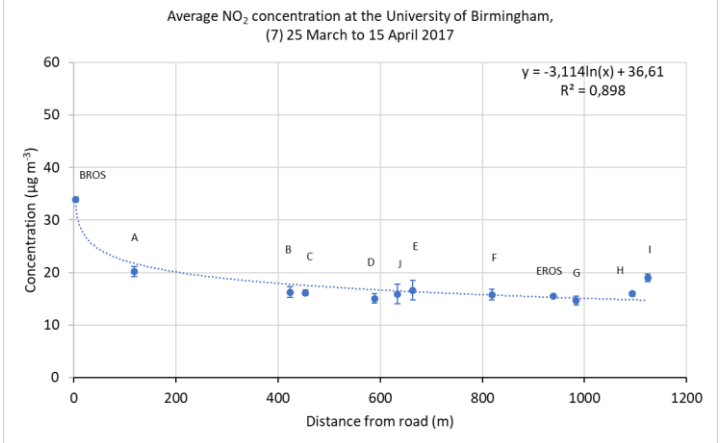
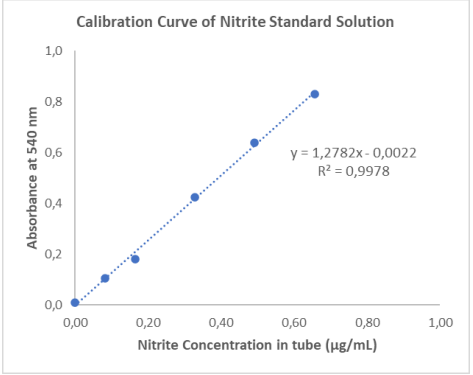
No	Graph	Calibration curve
8		
9		
10		
11		

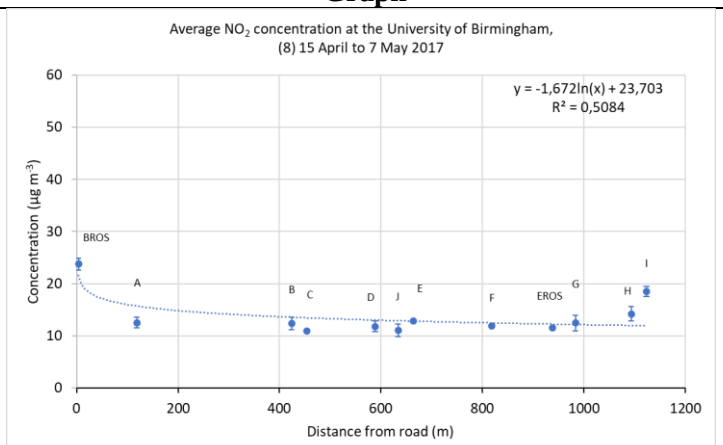
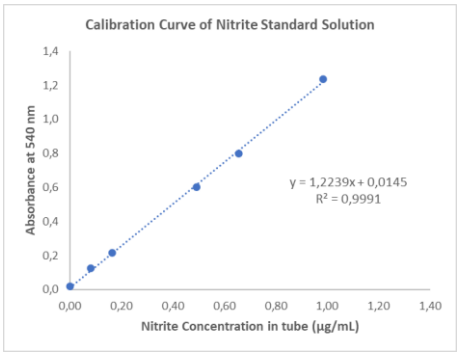
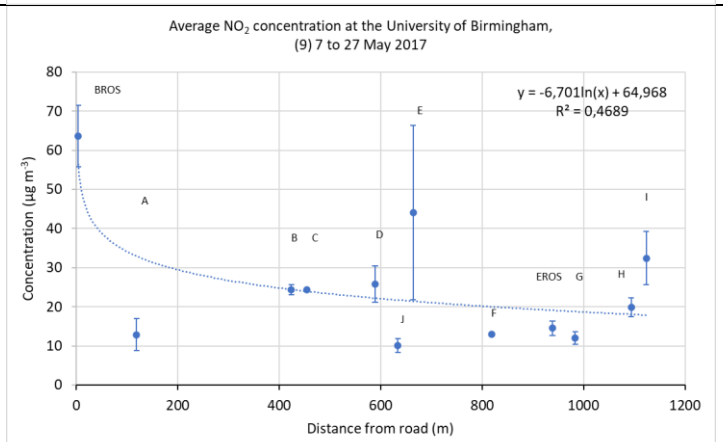
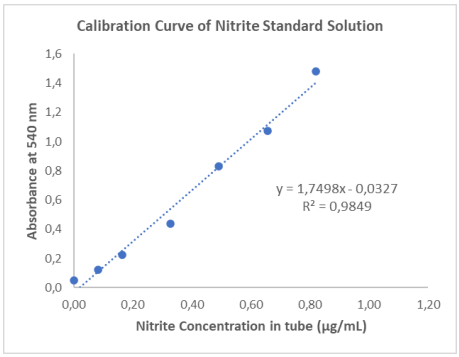
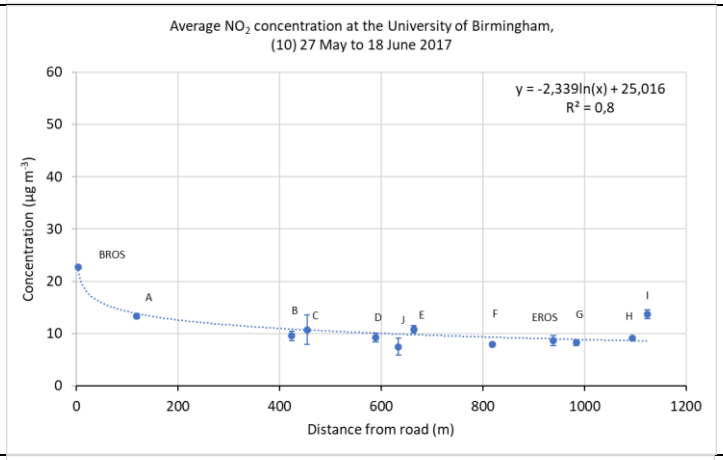
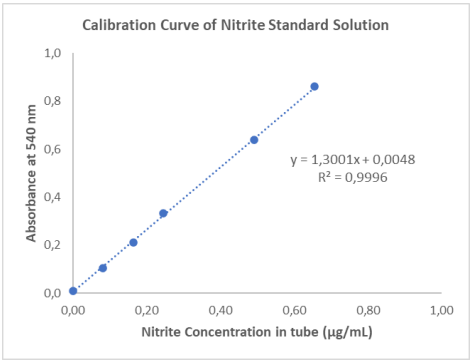
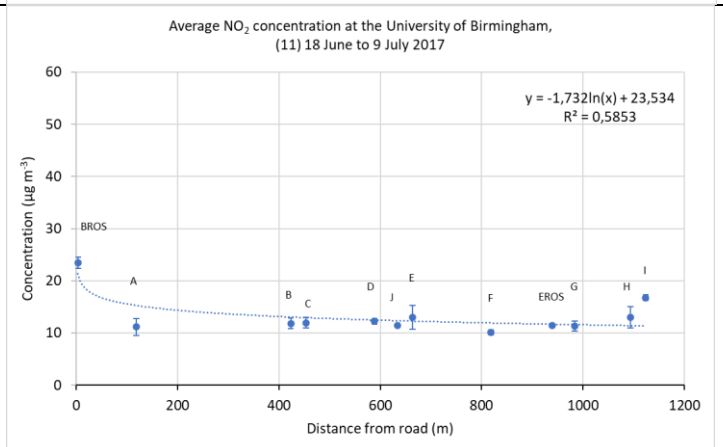
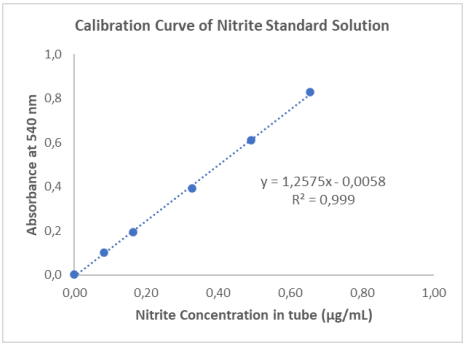
No	Graph	Calibration curve
12		
13		
14		

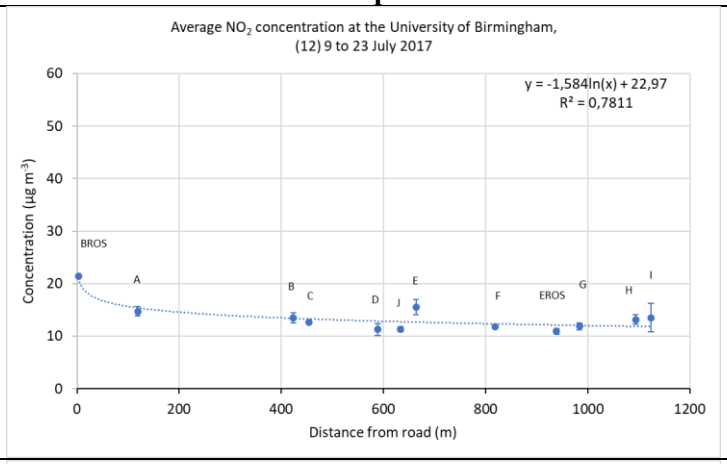
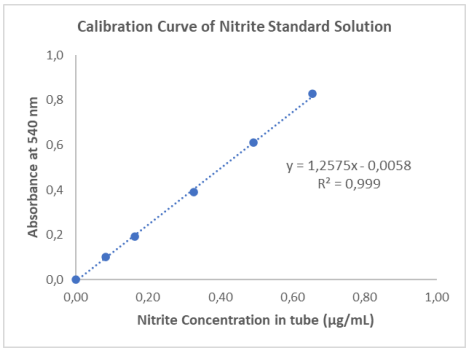
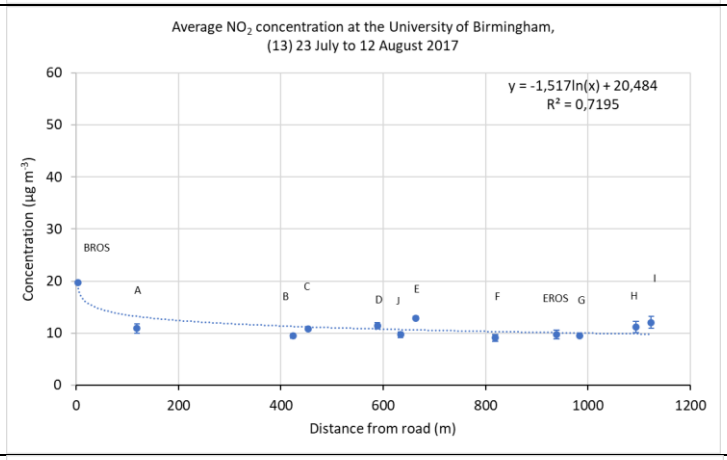
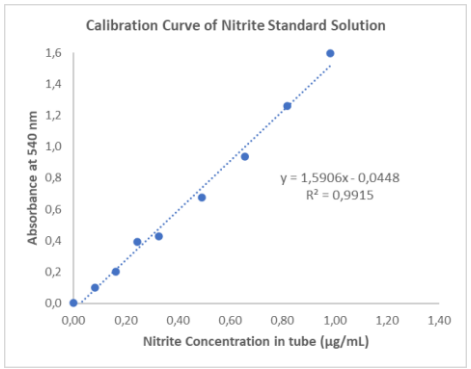
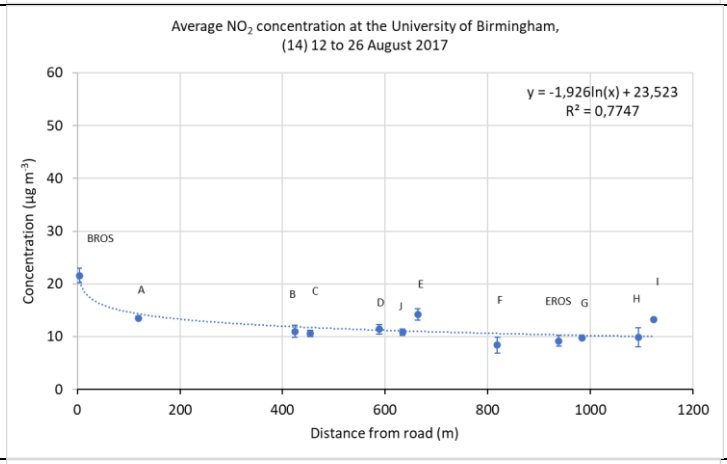
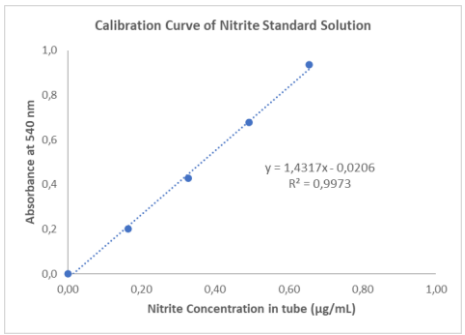
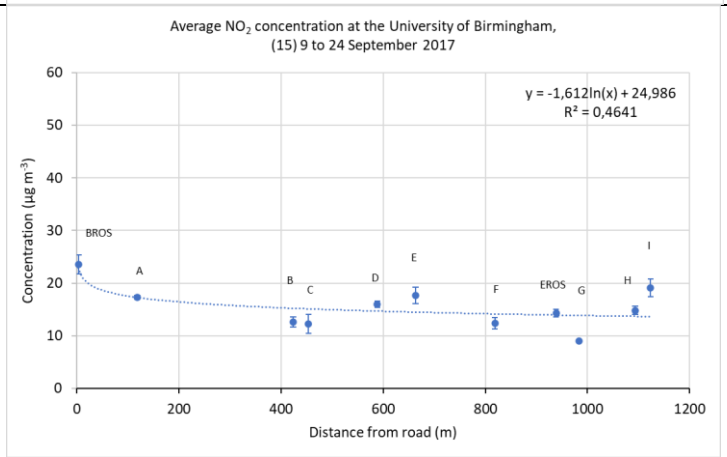
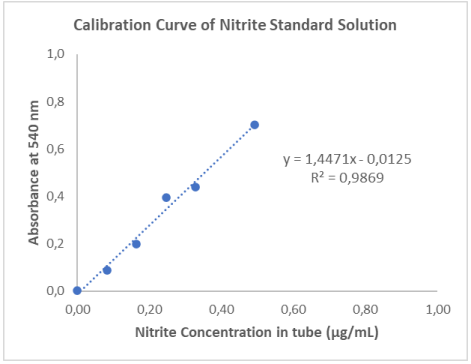
Appendix 3.6. Graph of NO_2 concentrations at the University of Birmingham

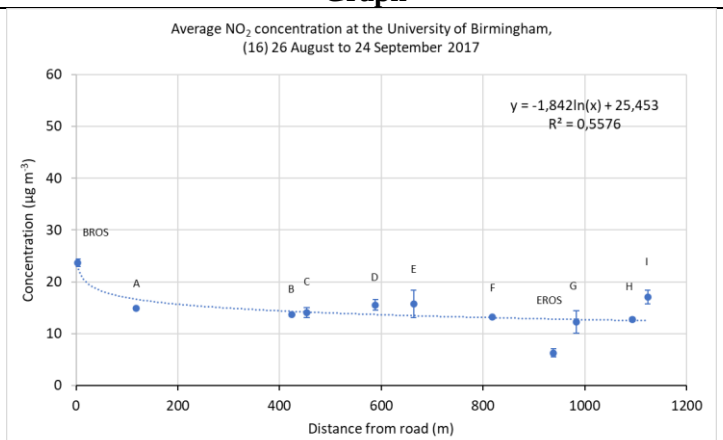
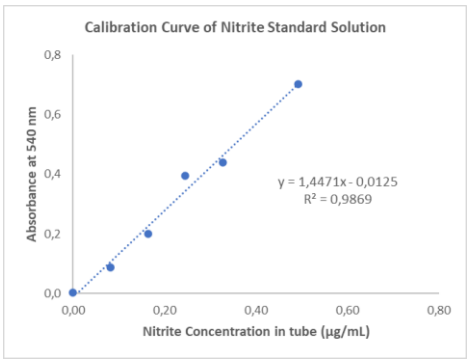
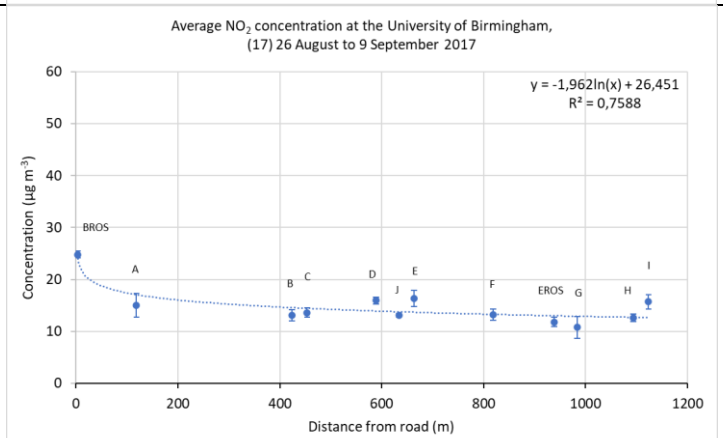
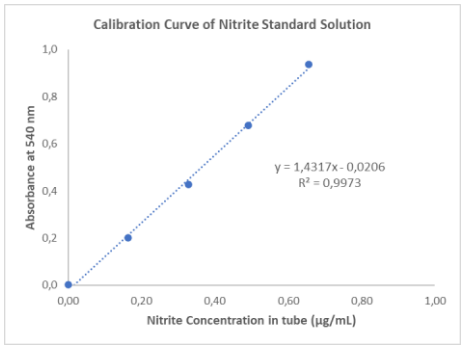
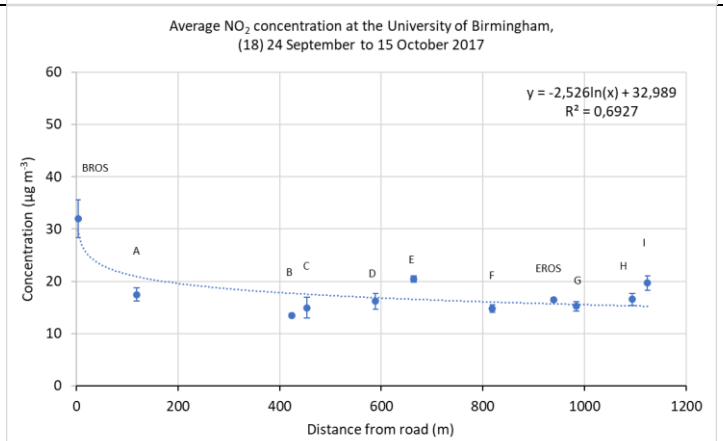
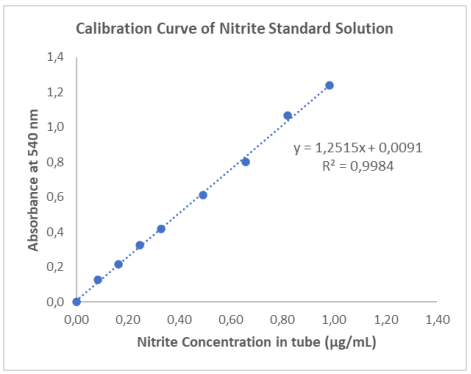
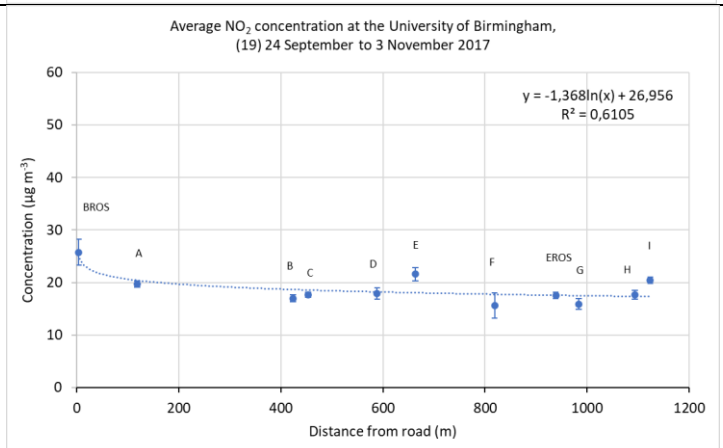
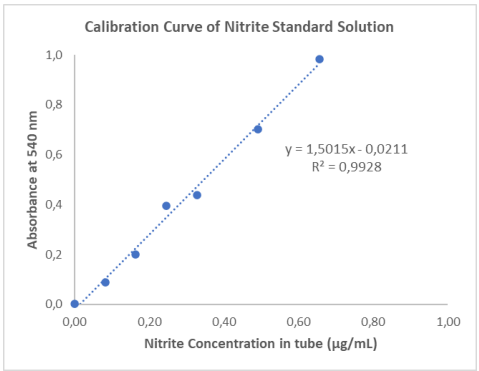
Table A.3.6. Graph of NO_2 concentrations from raw data of DT measurements at the University of Birmingham (mean ± standard deviation from triplicate DT), and calibration curves of nitrite standard solution, sampling period November 2016 – January 2019

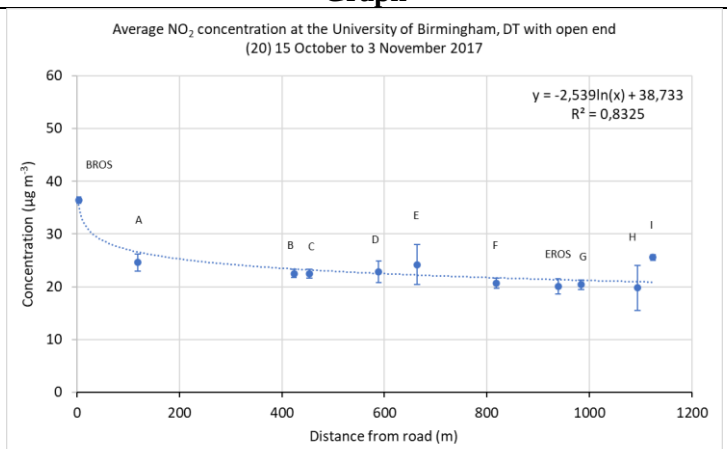
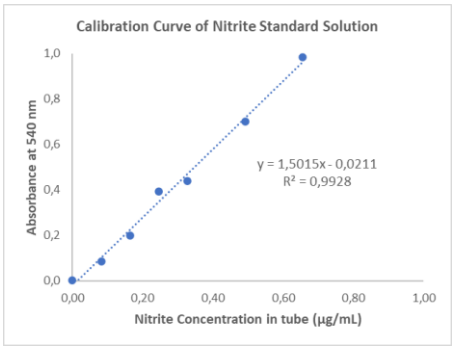
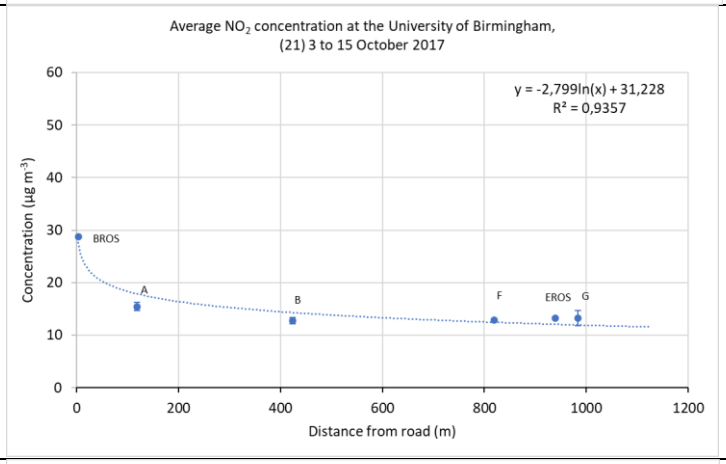
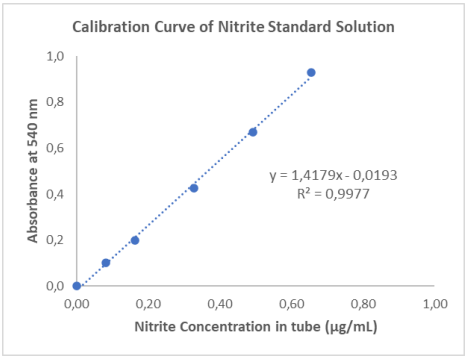
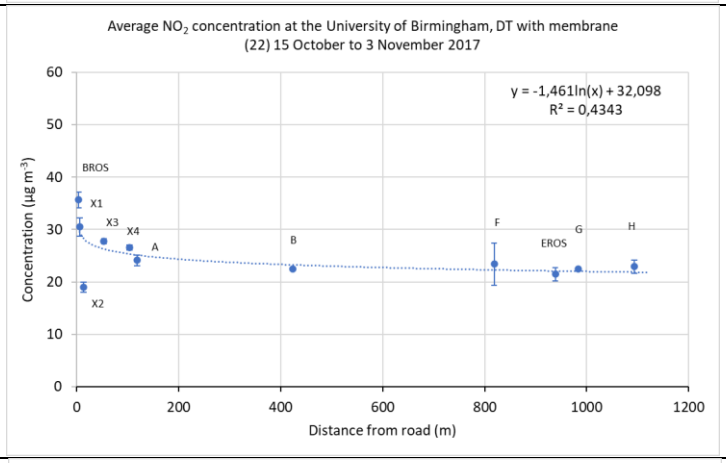
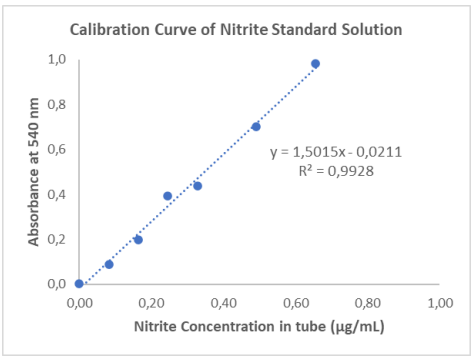
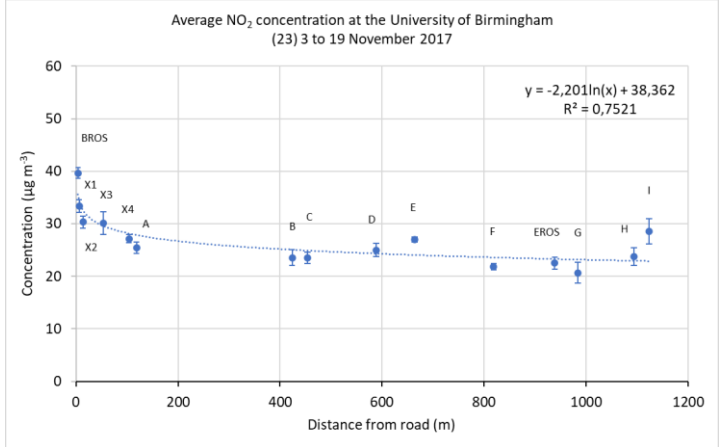
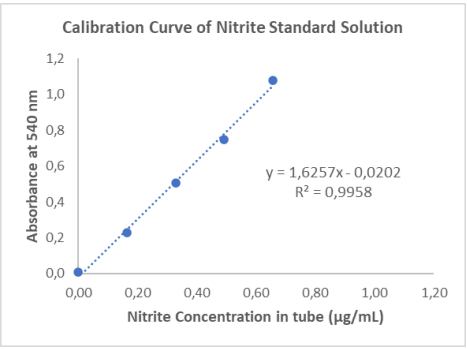
No	Graph	Calibration curve
1		
2		
3		

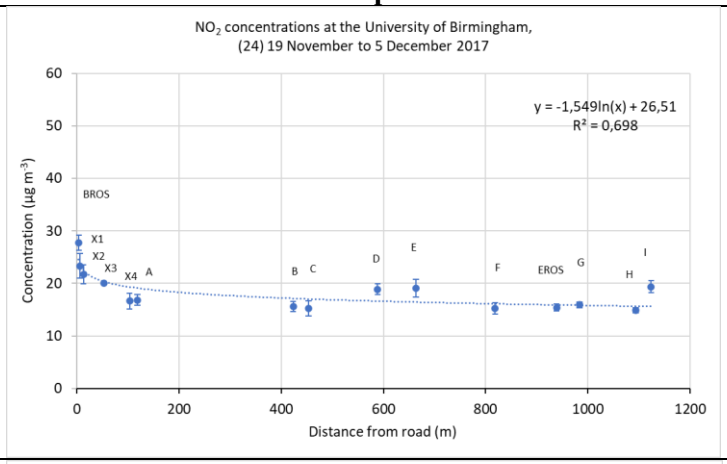
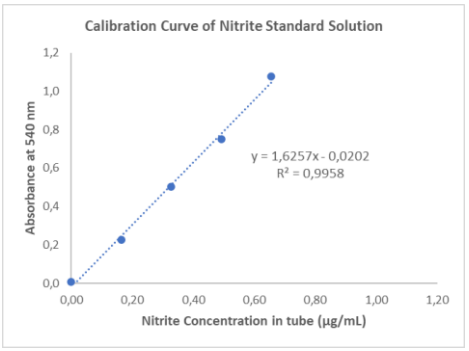
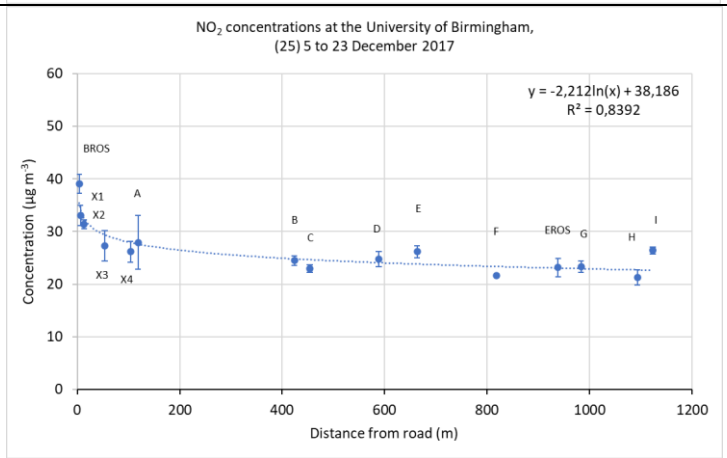
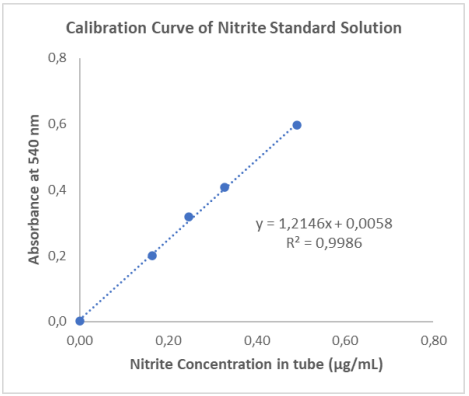
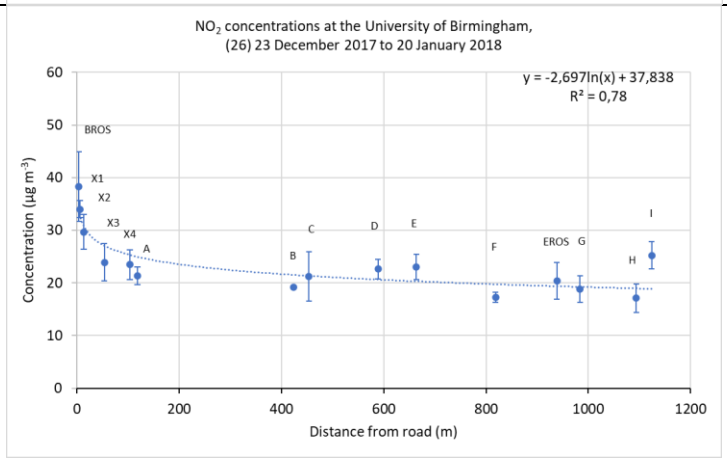
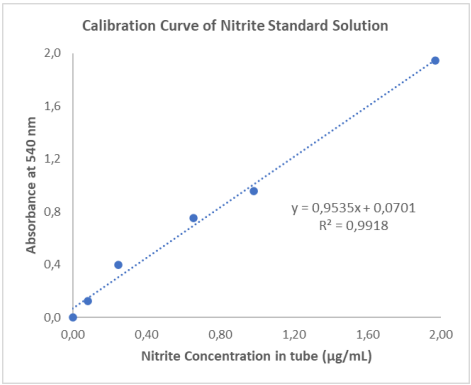
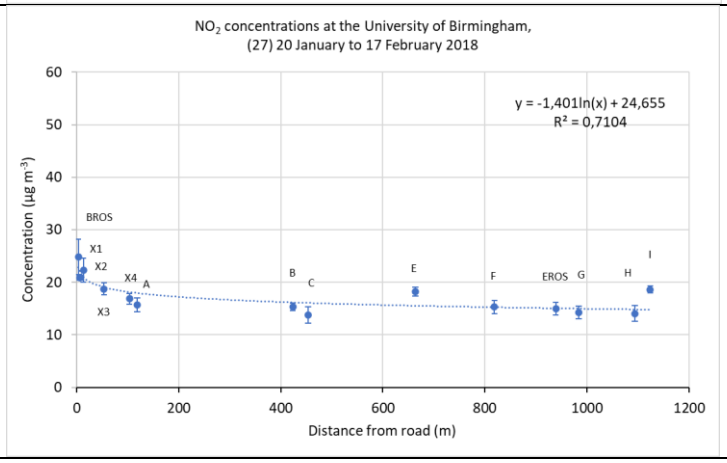
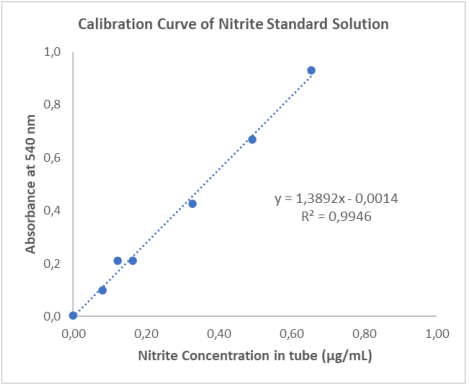
No	Graph	Calibration curve
4		
5		
6		
7		

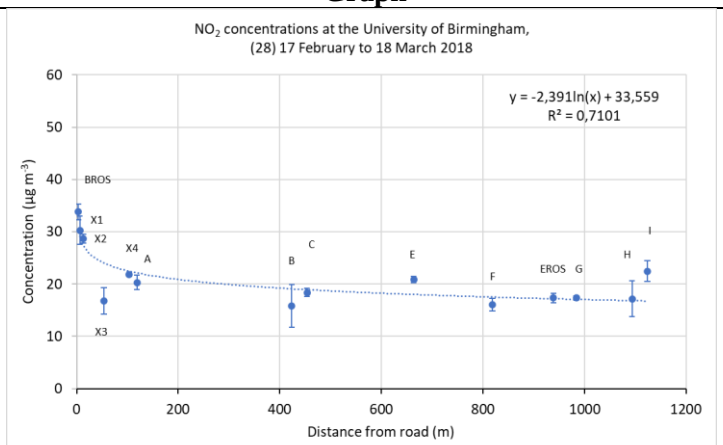
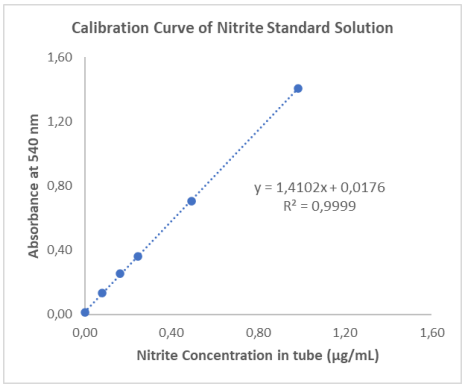
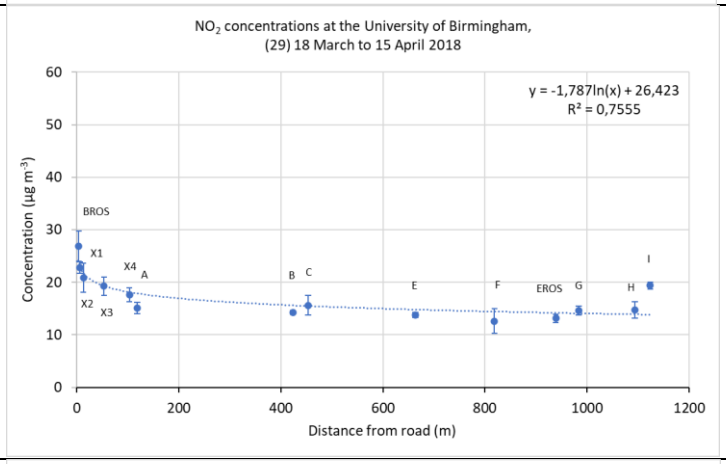
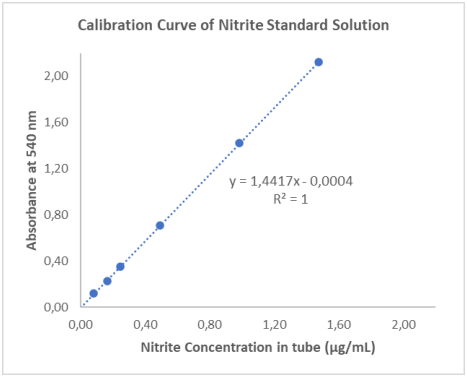
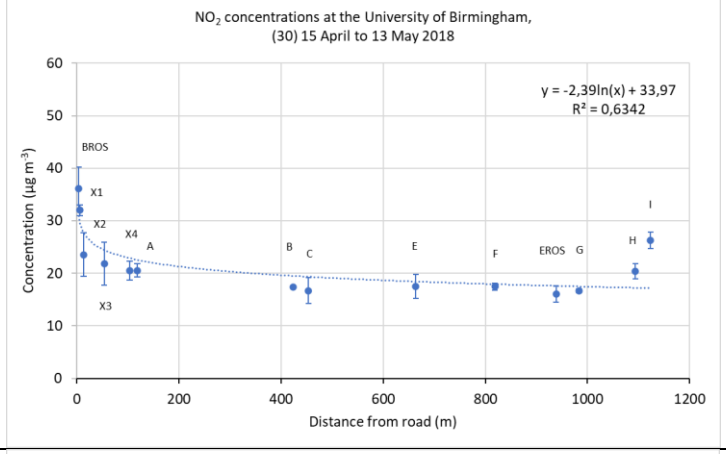
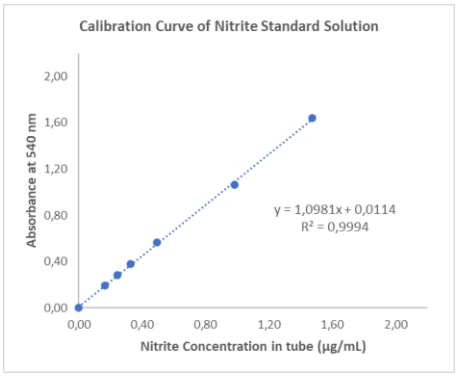
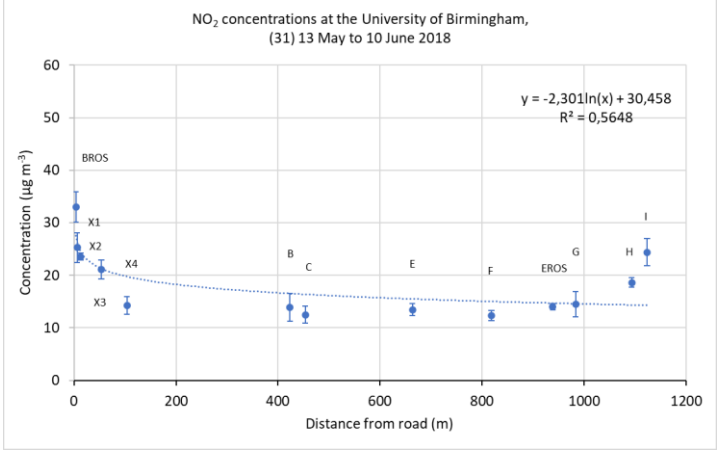
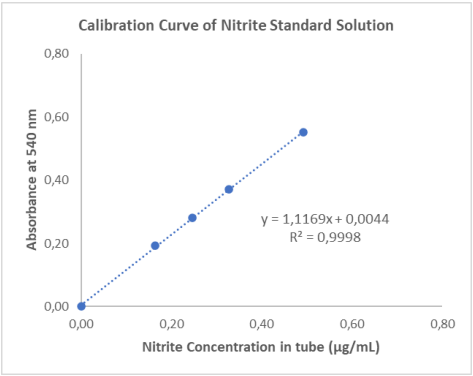
No	Graph	Calibration curve
8		
9		
10		
11		

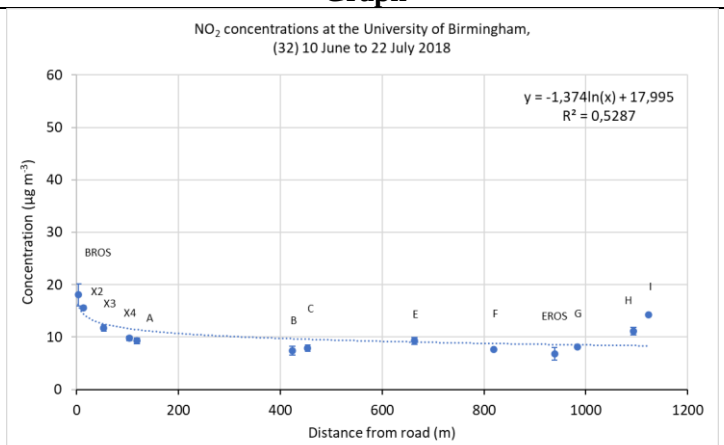
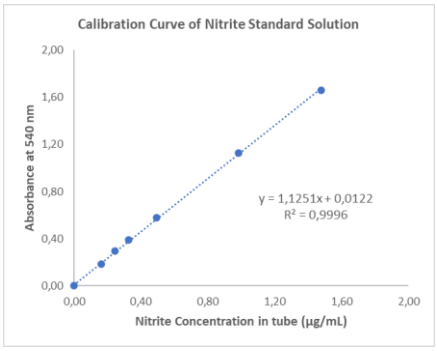
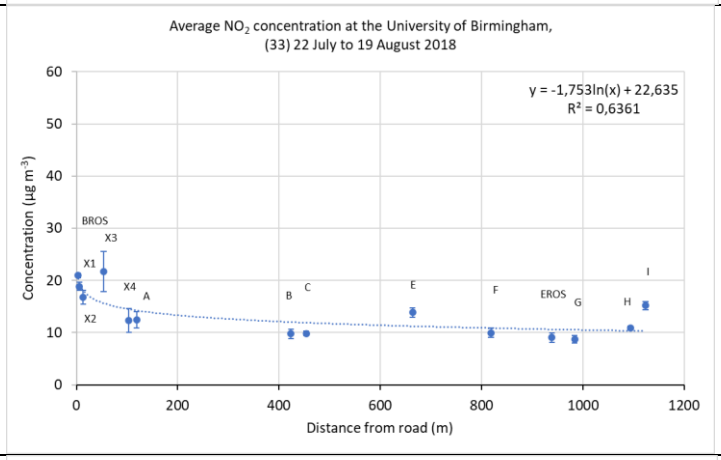
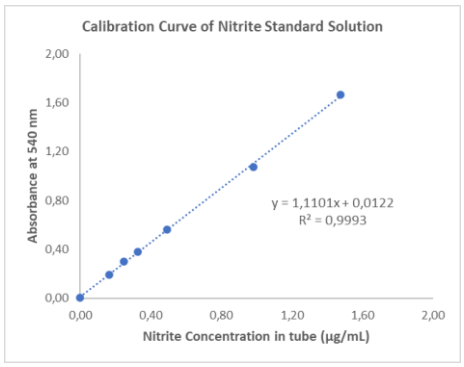
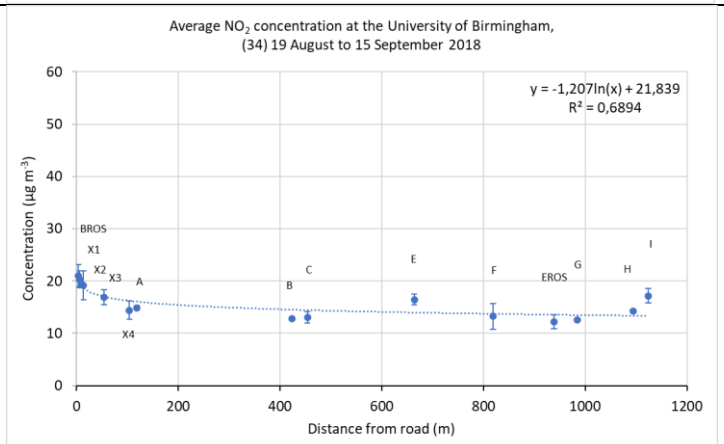
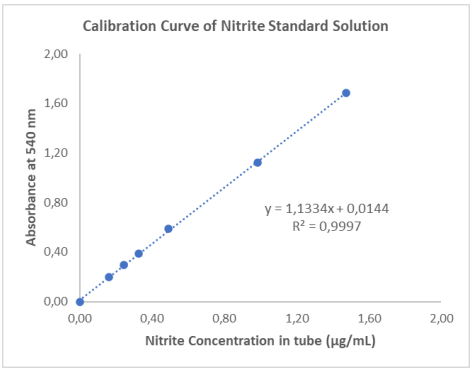
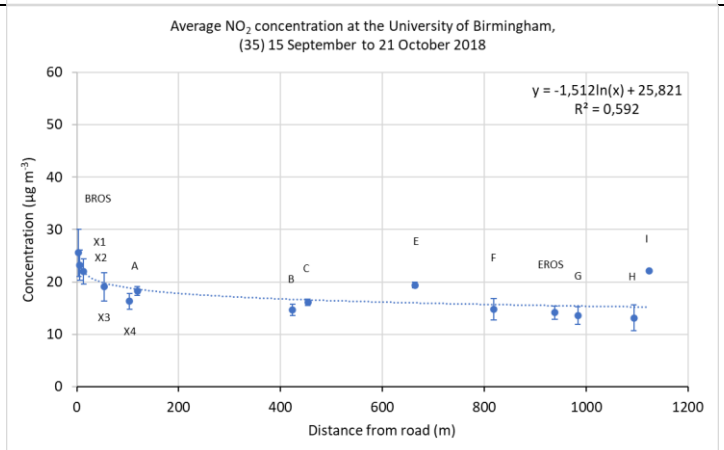
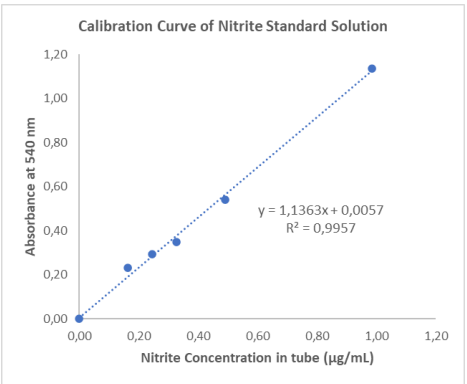
No	Graph	Calibration curve
12		
13		
14		
15		

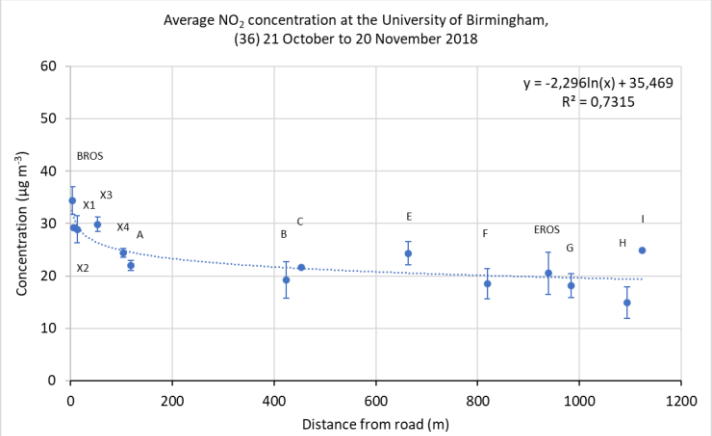
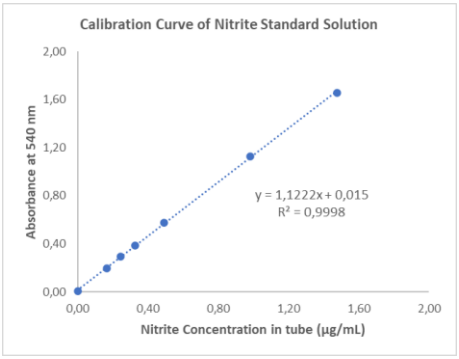
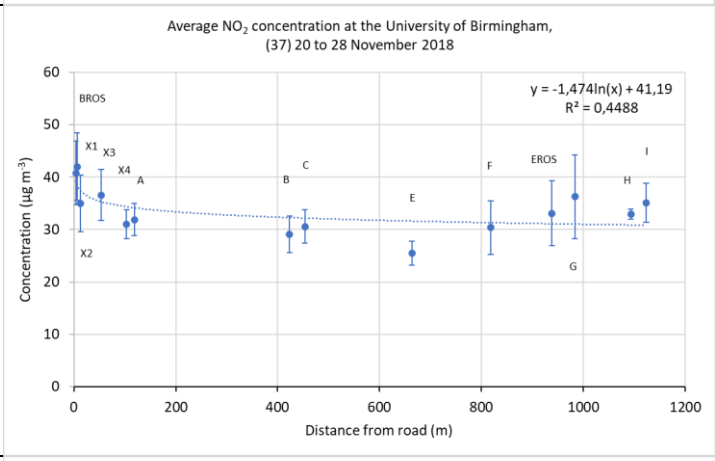
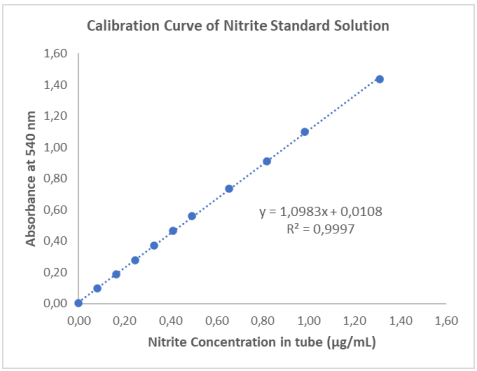
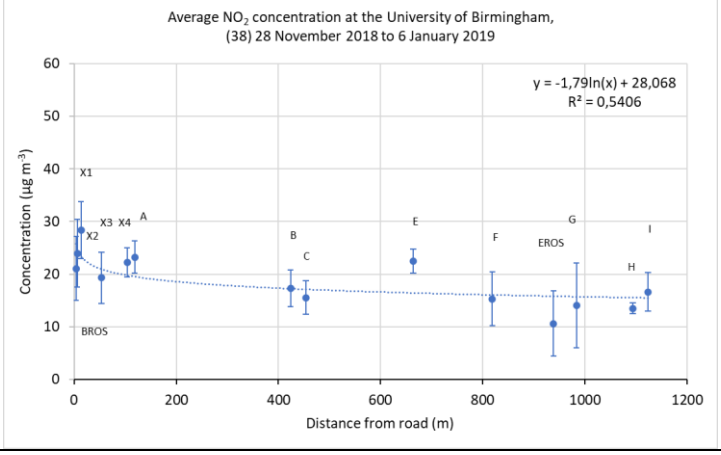
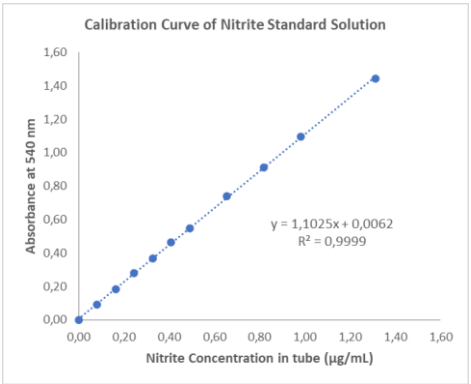
No	Graph	Calibration curve
16		
17		
18		
19		

No	Graph	Calibration curve
20		
21		
22		
23		

No	Graph	Calibration curve
24		
25		
26		
27		

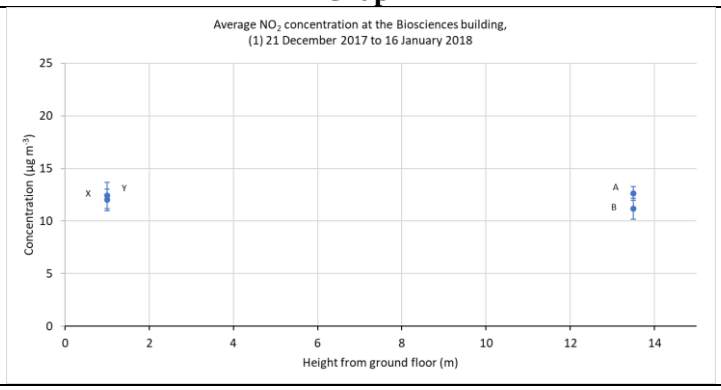
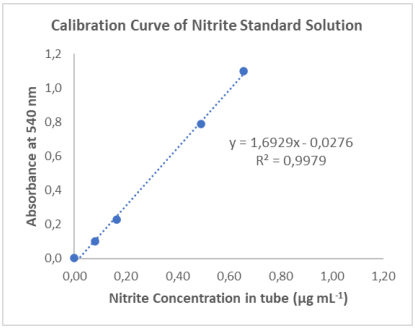
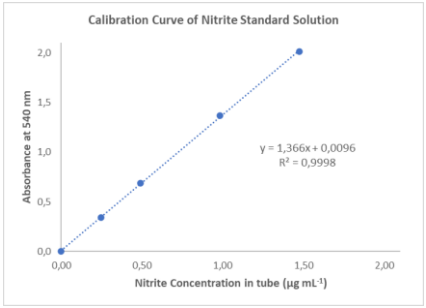
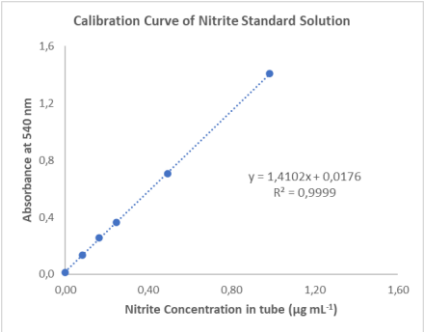
No	Graph	Calibration curve
28		
29		
30		
31		

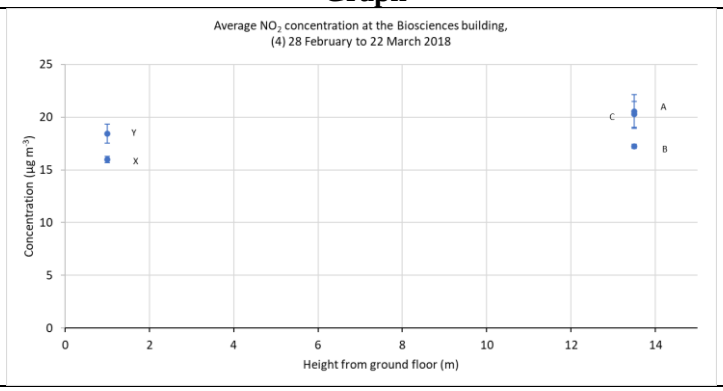
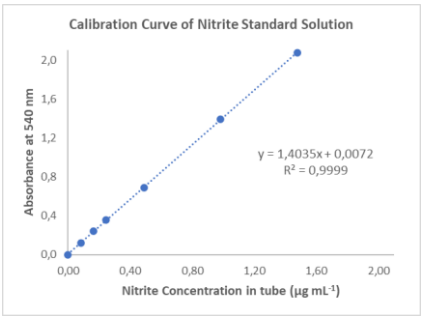
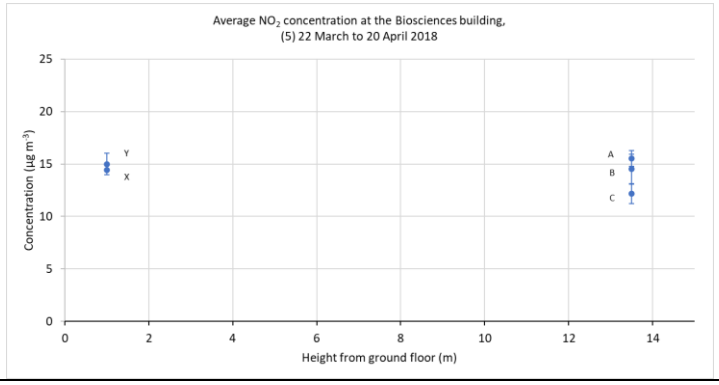
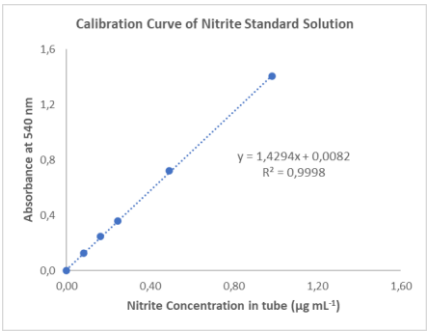
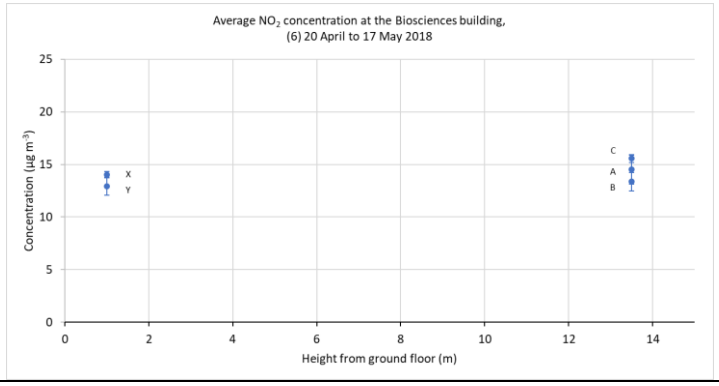
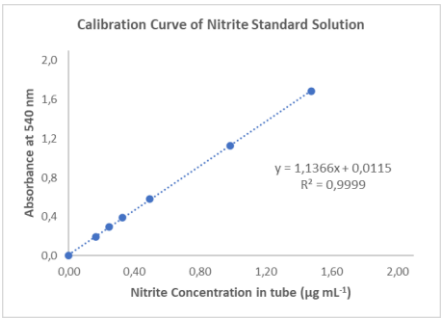
No	Graph	Calibration curve
32		
33		
34		
35		

No	Graph	Calibration curve
36		
37		
38		

Appendix 3.7. Graph of NO_2 concentrations at the Biosciences building

Table A.3.7. Graph of NO_2 concentrations from raw data of DT measurements at the Biosciences building (mean ± standard deviation from triplicate DT), and calibration curves of nitrite standard solution, sampling period December 2017 – May 2018

No	Graph	Calibration curve
1		
2		
3		

No	Graph	Calibration curve
4		
5		
6		

Appendix 4.1. Road Geometry Input in ADMS-Roads

Road 1.

No		Coordinate google map		Coordinate in the model	
	Name	Latitude	Longitude	X (metre)	Y (metre)
1	Road 1a	52.4470650108	-1.9393243283	404220.938712512	283233.281115584
		52.4470570108	-1.9387083283	404262.806885324	283232.426414305
		52.4470520108	-1.9384453284	404280.6825741940	283231.8853681220
	Road 1b	52.447052	-1.938445	404280.6825741940	283231.8853681220
		52.447096	-1.937699	404331.3814661460	283236.8229520110
		52.447205	-1.936124	404438.4181022810	283249.0405786910
		52.447244	-1.935546	404477.6988149040	283253.4134630590
		52.447266	-1.935144	404505.0190869720	283255.8849676990
		52.447276	-1.934725	404533.4959587070	283257.0228482460
		52.447266	-1.934290	404563.0622920980	283255.9371863900
	Road 1c	52.447266	-1.934290	404563.0622920980	283255.9371863900
		52.447249	-1.933912	404588.7552690390	283254.0695302500
		52.447222	-1.933548	404613.4977557480	283251.0887909080
		52.447192	-1.933250	404633.7547978400	283247.7703436400
		52.447109	-1.932642	404675.0869374550	283238.5760609540
		52.447067	-1.932308	404697.7921149640	283233.9253346740
		52.447050	-1.931793	404732.7966853620	283232.0671281510
	Road 1d	52.447050	-1.931793	404732.7966853620	283232.0671281510
		52.447071	-1.931306	404765.8942144620	283234.4342836360
		52.447079	-1.930874	404795.2549296420	283235.3520491040
		52.447049	-1.930371	404829.4453165400	283232.0477044340

Road 2.

No	Name	Coordinate google map		Coordinate in the model	
		Latitude	Longitude	X (metre)	Y (metre)
2	Road 2a	52.447049	-1.930371	404829.4453165400	283232.0477044340
		52.447016	-1.930098	404848.0037393480	283228.3948063590
		52.446956	-1.929668	404877.2358760570	283221.7489780800
		52.446943	-1.929378	404896.9476435280	283220.3220772390
	Road 2b	52.446943	-1.929378	404896.9476435280	283220.3220772390
		52.446955	-1.929081	404917.1324714930	283221.6765855460
		52.447011	-1.928685	404944.0411840880	283227.9321095930
	Road 2c	52.447011	-1.928685	404944.0411840880	283227.9321095930
		52.447030	-1.928642	404946.9616719880	283230.0484410510
		52.447047	-1.928603	404949.6105098810	283231.9420374670
		52.447070	-1.928486	404957.5600818570	283234.5082665200
		52.447087	-1.928414	404962.4518095970	283236.4040815860
		52.447104	-1.928334	404967.8872658030	283238.3004386920
		52.447129	-1.928229	404975.0209999340	283241.0883595220
		52.447169	-1.928051	404987.1146220190	283245.5497285390
		52.447192	-1.927955	404993.6368581860	283248.1146005480
		52.447345	-1.927316	405037.0503298260	283265.1768226430
		52.447667	-1.925947	405130.0594300090	283301.0884844410

No	Name	Coordinate google map		Coordinate in the model	
		Latitude	Longitude	X (metre)	Y (metre)
	Road 2d	52.447667	-1.925947	405130.0594300090	283301.0884844410
		52.447973	-1.924694	405215.1850611110	283335.2139636990
		52.448112	-1.924104	405255.2683426450	283350.7173761170

Road 3.

No	Name	Coordinate google map		Coordinate in the model	
		Latitude	Longitude	X (metre)	Y (metre)
3	Road 3a	52.447764	-1.925587	405154.5159981200	283311.9032841750
		52.448189	-1.925688	405147.6030439690	283359.1709575000
	Road 3b	52.448189	-1.925688	405147.6030439690	283359.1709575000
		52.448489	-1.925775	405141.6559501940	283392.5352893010
	Road 3c	52.448489	-1.925775	405141.6559501940	283392.5352893010
		52.448831	-1.925918	405131.8981843210	283430.5675954740
	Road 3d	52.448831	-1.925918	405131.8981843210	283430.5675954740
		52.449032	-1.926000	405126.3023351430	283452.9200675300
		52.449327	-1.926152	405115.9384627510	283485.7237565920
	Road 3e	52.449327	-1.926152	405115.9384627510	283485.7237565920
		52.449579	-1.926329	405103.8805203300	283513.7426531800
		52.449915	-1.926617	405084.2694426750	283551.0976528640
		52.450300	-1.926834	405069.4784440560	283593.9080963390
	Road 3f	52.450300	-1.926834	405069.4784440560	283593.9080963390
		52.450596	-1.926936	405062.5131921100	283626.8265685390
		52.450772	-1.926939	405062.2895880280	283646.4036645900
		52.451013	-1.926834	405069.3984379310	283673.2184136540
		52.451255	-1.926657	405081.4002275260	283700.1493544740
		52.451546	-1.926392	405099.3768129430	283732.5368912010
	Road 3g	52.451546	-1.926392	405099.3768129430	283732.5368912010
		52.452011	-1.925979	405127.3913748970	283784.2895866170
		52.452266	-1.925756	405142.5171890910	283812.6699243600
		52.452508	-1.925589	405153.8386531220	283839.6003527320

Road 4.

No	Name	Coordinate google map		Coordinate in the model	
		Latitude	Longitude	X (metre)	Y (metre)
4.	Road 4a	52.452508	-1.925589	405153.8386531220	283839.6003527320
		52.453046	-1.925305	405173.0771477110	283899.4644648280
		52.453425	-1.925189	405180.9167151160	283941.6305471810
		52.453539	-1.925171	405182.1268531860	283954.3125671520
		52.453816	-1.925428	405164.6303178590	283985.1065957920
		52.454314	-1.925918	405131.2751955780	284040.4673645500
		52.454868	-1.926435	405096.0797295660	284102.0556484030
		52.455305	-1.926793	405071.7029239770	284150.6406177410
		52.455742	-1.927085	405051.8115130700	284199.2302183520

No	Name	Coordinate google map		Coordinate in the model	
		Latitude	Longitude	X (metre)	Y (metre)
		52.456185	-1.927221	405042.5204243930	284248.4979377310
		52.456664	-1.927342	405034.2447871760	284301.7711514210
		52.457111	-1.927326	405035.2821923670	284351.4941896130
	Road 4b	52.457111	-1.927326	405035.2821923670	284351.4941896130
		52.457367	-1.927184	405044.9026616960	284379.9799745750
		52.457529	-1.926999	405057.4554084320	284398.0126489390
		52.457706	-1.926736	405075.3064954300	284417.7192293950

Road 5.

No	Name	Coordinate google map		Coordinate in the model	
		Latitude	Longitude	X (metre)	Y (metre)
5	Road 5a	52.451975	-1.926033	405123.7256742450	283780.2813936290
		52.452242	-1.926784	405072.6584603650	283809.9292705370
		52.452382	-1.927273	405039.4110796680	283825.4686936990
		52.452530	-1.928047	404986.7949426990	283841.8789682180
	Road 5b	52.452530	-1.928047	404986.7949426990	283841.8789682180
		52.452675	-1.928675	404944.1013469750	283857.9658489340
	Road 5c	52.452675	-1.928675	404944.1013469750	283857.9658489340
		52.452780	-1.929205	404908.0722316810	283869.6102081460
		52.452993	-1.929882	404862.0419032720	283893.2585141260
	Road 5d	52.452993	-1.929882	404862.0419032720	283893.2585141260
		52.453256	-1.930556	404816.2105656950	283922.4691831890
		52.453617	-1.931341	404762.8262674750	283962.5741389700
	Road 5e	52.453617	-1.931341	404762.8262674750	283962.5741389700
		52.453929	-1.931866	404727.1165073580	283997.2457374200
		52.454111	-1.932277	404699.1676823610	284017.4643070020
	Road 5f	52.454111	-1.932277	404699.1676823610	284017.4643070020
		52.454302	-1.932806	404663.1994153740	284038.6767154400
		52.454431	-1.933049	404646.6729987610	284053.0107305460
	Road 5g	52.454431	-1.933049	404646.6729987610	284053.0107305460
		52.454559	-1.933265	404631.9815674080	284067.2352541410
		52.454715	-1.933490	404616.6757722000	284084.5738341760

Road 6.

No	Name	Coordinate google map		Coordinate in the model	
		Latitude	Longitude	X (metre)	Y (metre)
6	Road 6a	52.447249	-1.927761	405006.8160241990	283254.4680865900
		52.447466	-1.927900	404997.3447151000	283278.5965963400
		52.447595	-1.927942	404994.4758897190	283292.9430242350
		52.447751	-1.927891	404997.9248938230	283310.2990681230
		52.447939	-1.927800	405004.0889421040	283331.2173278780
		52.448117	-1.927910	404996.5930872860	283351.0096539270
		52.448189	-1.928126	404981.9047180330	283359.0039783540

No	Name	Coordinate google map		Coordinate in the model	
		Latitude	Longitude	X (metre)	Y (metre)
		52.448228	-1.928601	404949.6171398040	283363.3102463570
		52.448285	-1.928850	404932.6876857930	283369.6339916110
		52.448426	-1.929008	404921.9339119240	283385.3075526530
	Road 6b	52.448605	-1.928714	404941.8959062590	283405.2381467640
		52.448494	-1.928883	404930.4220581460	283392.8798288690
		52.448426	-1.929008	404921.9339119240	283385.3075526530
		52.448354	-1.929345	404899.0376777670	283377.2762977360
		52.448344	-1.929589	404882.4553935980	283376.1478273300

Road 7.

No	Name	Coordinate google map		Coordinate in the model	
		Latitude	Longitude	X (metre)	Y (metre)
7	Road 7a	52.447038	-1.939422	404214.2804927990	283230.2722180190
		52.447360	-1.939213	404228.4555243880	283266.1016372120
		52.447560	-1.939082	404237.3404177390	283288.3560241490
	Road 7b	52.447560	-1.939082	404237.3404177390	283288.3560241490
		52.447694	-1.938951	404246.2314051020	283303.2689431550
		52.447947	-1.938780	404257.8297905980	283331.4210907730
	Road 7c	52.447947	-1.938780	404257.8297905980	283331.4210907730
		52.448210	-1.938687	404264.1258451990	283360.6811323310
		52.448528	-1.938675	404264.9115368990	283396.0544337460
		52.448911	-1.938732	404261.0016077790	283438.6540280760
		52.449155	-1.938955	404245.8228644670	283465.7825109770
		52.449327	-1.938984	404243.8358432660	283484.9132130100
		52.449527	-1.938761	404258.9728469490	283507.1729069060
		52.449832	-1.938613	404269.0026477700	283541.1079735460
	Road 7d	52.449832	-1.938613	404269.0026477700	283541.1079735460
		52.450176	-1.938462	404279.2325169290	283579.3813872550
		52.450601	-1.938264	404292.6487419470	283626.6675489450
	Road 7e	52.450601	-1.938264	404292.6487419470	283626.6675489450
		52.451050	-1.938062	404306.3342713640	283676.6236151480
		52.451399	-1.937711	404330.1550737150	283715.4649350880
		52.451598	-1.937363	404353.7860214570	283737.6209932810
	Road 7f	52.451598	-1.937363	404353.7860214570	283737.6209932810
		52.452041	-1.936663	404401.3147443520	283786.9392520150
		52.452574	-1.935905	404452.7752481830	283846.2725785110
		52.452929	-1.935410	404486.3793642740	283885.7907290590
		52.453490	-1.934852	404524.2436575440	283948.2273072980
		52.454037	-1.934106	404574.8840985750	284009.1184837850
		52.454518	-1.933435	404620.4333920930	284062.6640169770
		52.454934	-1.932936	404654.3002219220	284108.9689003560
		52.455347	-1.932465	404686.2640155280	284154.9385450240
		52.455956	-1.931771	404733.3602698630	284222.7246447450
		52.456815	-1.930728	404804.1439026650	284318.3424897030
		52.457272	-1.930168	404842.1478497100	284369.2132753520
		52.457586	-1.929856	404863.3147473250	284404.1614577140
		52.457753	-1.929678	404875.3919079130	284422.7493810010

Road 8.

No	Name	Coordinate google map		Coordinate in the model	
		Latitude	Longitude	X (metre)	Y (metre)
8	Road 8a	52.457707	-1.929859	404863.0978808090	284417.6206714860
		52.457647	-1.929404	404894.0217219750	284410.9765780380
		52.457516	-1.928526	404953.6964464320	284396.4632494310
	Road 8b	52.457516	-1.928526	404953.6964464320	284396.4632494310
		52.457478	-1.927933	404993.9952947300	284392.2762008990
	Road 8c	52.457478	-1.927933	404993.9952947300	284392.2762008990
		52.457542	-1.927436	405027.7596007760	284399.4289012490
	Road 8d	52.457542	-1.927436	405027.7596007760	284399.4289012490
		52.457540	-1.927227	405041.9614706660	284399.2206614480
		52.457515	-1.927030	405055.3505103490	284396.4532419050

Appendix 4.2. Receptor Geometry Input in ADMS-Roads

Receptor locations are set as specified points and location describes as coordinate X, Y and Z in metre. Z is the height at which diffusion tubes were installed.

ID location	Coordinate google map		Coordinate in the model		
	Latitude	Longitude	X (metre)	Y (metre)	Z (metre)
BROS	52.4471260108	-1.9283663286	404965.709920224	283240.74545162	3.2
X1	52.4471493344	-1.9283639356	404965.87	283243.34	3.2
X2	52.4472111812	52.4472111812	404966.36	283250.22	3
X3	52.4475950108	-1.9279823286	404991.757258778	283292.940324298	3
X4	52.4479480108	-1.9279433286	404994.368917712	283332.208775004	2.7
A	52.4481475259	-1.9282265173	404975.099973121	283354.382678878	3
B	52.4471749679	-1.9325875735	404950.617042538	283659.306913082	2.8
C	52.4512310107	-1.9284863286	404957.103763503	283697.355600052	2.8
J	52.452382	-1.930688	404807.3331237490	283825.2414675500	2.8
D	52.452349	-1.929394	404895.2748744090	283821.6555316940	2.8
E	52.4529940107	-1.9294363286	404892.350824726	283893.399139902	2.7
F	52.4545210106	-1.9289203287	404927.250426403	284063.288804906	2.7
EROS	52.4554940106	-1.9290033287	404921.504213239	284171.514693012	2.7
G	52.4558270106	-1.9277643287	405005.661850781	284208.639002125	2.65
H	52.4568715867	-1.9274846949	405024.547659272	284324.851151643	2.85
I	52.4571204933	-1.9274586464	405026.29	284352.54	2.9

Appendix 4.3. Resume of road traffic sources

Road ID	Road name	Traffic count ID	Total Average hourly data	Vehicles / hour						
				Motor cycle	Car	LGV	Bus & Coach	Taxi	HGV Rigid	HGV articulated
Road 1	A38	81576 – Road 7	1286 – 523 = 763	7	691	60	4	-	3	3
Road 2	A38	81577	1178	8	1014	123	16	-	13	4
Road 3 and 4	Edgbaston Park Rd	Calculation	229	2	195	15	12	-	3	2
Road 5	Pritchatts Rd	Calculation	287	1	252	12	13	-	2	7
Road 6	UoB BROS site	Calculation	47	1	38	6	-	1	1	-
Road 7	New Fosse Way and Vincent Dr	Calculation	523	1	441	53	17	5	5	1
Road 8	Somerset Rd	Calculation	451	1	393	39	1	6	9	2

Appendix 4.4. Time-varying emission rate

Time varying emission factors are used in the model for emission that fluctuate with time due to the variations in traffic flow (CERC, 2017).

	Table adopted from TRA0307 (DfT, 2019b) **Motor vehicle traffic distribution by time of day and day of the week on all roads, Great Britain: 2018** Index: Average hourly traffic flow over year = 100					**Time Varying Emission Factor**		
Time of day	**Average weeks (Monday – Sunday)**	**Average weeks (Monday – Friday)**	**Saturday**	**Sunday**		**Weekdays**	**Saturday**	**Sunday**
00:00-01:00	19	**17**	**24.8**	**26.9**		**0.17**	**0.25**	**0.27**
01:00-02:00	13	12	16.9	17.4		0.12	0.17	0.17
02:00-03:00	11	10	13.2	12.3		0.10	0.13	0.12
03:00-04:00	12	12	12.6	10.6		0.12	0.13	0.11
04:00-05:00	18	20	15.0	11.0		0.20	0.15	0.11
05:00-06:00	41	49	24.9	15.8		0.49	0.25	0.16
06:00-07:00	92	115	42.4	25.7		1.15	0.42	0.26
07:00-08:00	144	181	66.5	38.5		1.81	0.67	0.39
08:00-09:00	152	182	98.7	56.6		1.82	0.99	0.57
09:00-10:00	140	152	130.0	93.4		1.52	1.30	0.93
10:00-11:00	144	144	156.0	130.6		1.44	1.56	1.31
11:00-12:00	152	148	169.5	153.4		1.48	1.70	1.53
12:00-13:00	156	152	169.6	161.0		1.52	1.70	1.61
13:00-14:00	156	155	161.9	156.7		1.55	1.62	1.57
14:00-15:00	160	164	151.6	151.5		1.64	1.52	1.52
15:00-16:00	170	179	143.6	150.8		1.79	1.44	1.51
16:00-17:00	183	198	141.5	150.8		1.98	1.42	1.51
17:00-18:00	179	196	136.9	138.7		1.96	1.37	1.39
18:00-19:00	145	155	117.9	121.2		1.55	1.18	1.21

	Table adopted from TRA0307 (DfT, 2019b) Motor vehicle traffic distribution by time of day and day of the week on all roads, Great Britain: 2018 Index: Average hourly traffic flow over year = 100					Time Varying Emission Factor		
Time of day	**Average weeks (Monday – Sunday)**	**Average weeks (Monday – Friday)**	**Saturday**	**Sunday**		**Weekdays**	**Saturday**	**Sunday**
19:00-20:00	105	109	91.0	101.5		1.09	0.91	1.02
20:00-21:00	76	77	67.5	80.1		0.77	0.68	0.80
21:00-22:00	57	58	53.0	57.9		0.58	0.53	0.58
22:00-23:00	44	44	46.1	39.5		0.44	0.46	0.40
23:00-00:00	29	29	37.4	25.4		0.29	0.37	0.25
TOTAL	2400	2557	2089	1927		25.57	20.89	19.27
Average hourly	**100**	106	87	80		1.07	0.87	0.80

Example:

- Weekdays at hour 00:00-01:00 = 17 / 100 = 0.17
- Saturday at hour 00:00-01:00 = 24.8 / 100 = 0.248 ≈ 0.25
- Sunday at hour 00:00-01:00 = 26.9 / 100 = 0.269 ≈ 0.27

Appendix 4.5. Steps to calculate number of vehicles from combination of AADF and observation data

Road Traffic Emission

Emission sources are from road traffic. Traffic data are generated from the Department for Transport. However, there are only four roads identified to have AADF data, the A38 road near New Fosse Way and Edgbaston Rd, Vincent Drive and Edgbaston Park Rd. Furthermore, data for Vincent Drive and Edgbaston Park Rd are not up-to-date, the data were last recorded in the year 2009.

Table A.4.5.1. Data from AADF divided by 24 hours (average hourly), 2018

Road	ID Count Vehicles	Year	Location	Motorcycle	Car	LGV	Bus and Coach	Taxi	HGV Rigid	HGV articulated	**TOTAL**
Before Road 1	81576	2018	A38	8	1132	113	21		8	4	1286
Road 2	81577	2018	A38	8	1014	123	16		13	4	1178
Road 3 and road 4	945338	2009	Edgbaston Park Rd	2	199	20	3		1	1	226
Road 7	947763	2009	Vincent Drive	4	279	27	10		2	1	323

Therefore, traffic flow observations were conducted for the other roads to get an estimated number of vehicles.

Table A.4.5.2. Observation of vehicle number on specific road

Date	Time	Location	Motorcycle	Car	LGV	Bus and Coach	Taxi	HGV Rigid	HGV articulated	**TOTAL**
Tuesday, 22 Oct 2019	10:00 - 11:00	Somerset Rd	1	550	55	2	8	13	3	**632**
Tuesday, 22 Oct 2019	12:00 - 13:00	New Fosse Way / Vincent Drive	1	631	76	24	7	7	2	**748**
Tuesday, 22 Oct 2019	15:00 - 16:00	UoB BROS site	2	66	10		1	1		**80**
Wednesday, 10 Apr 2019	13:00 - 14:00	Pritchatts Rd	1	376	18	20		3	10	**428**
Wednesday, 10 Apr 2019	15:00 - 16:00	Edgbaston Park Rd	4	345	26	21		5	3	**404**
Wednesday, 10 April 2019	10:00 – 11:00	A38	9	1202	179	43		75	10	**1518**

A rough estimation of number of vehicles was established by changing the 1-hour observation data into 24 hours traffic distribution using hourly traffic flow data DFT TRA0307 from Department for Transport.

Table A.4.5.3. TRA 0307, traffic distribution on all roads at Great Britain, 2018 (DfT, 2019b)

Table TRA0307 Source: DfT Automatic Traffic Counters, 2019								
Motor vehicle traffic distribution by time of day and day of the week on all roads, Great Britain: 2018 [1]								
Index: Average hourly traffic flow over year = 100								
Time of day	**Monday**	**Tuesday**	**Wednesday**	**Thursday**	**Friday**	**Saturday**	**Sunday**	**Average weeks (Monday – Sunday)**
00:00-01:00	15.5	**15.2**	16.4	17.2	19.0	24.8	26.9	19
01:00-02:00	10.3	10.9	11.6	12.0	13.4	16.9	17.4	13
02:00-03:00	8.7	9.8	10.2	10.6	11.6	13.2	12.3	11
03:00-04:00	11.1	11.6	11.8	12.3	12.9	12.6	10.6	12
04:00-05:00	21.3	19.3	19.3	19.7	19.6	15.0	11.0	18
05:00-06:00	54.5	49.4	48.5	48.3	45.9	24.9	15.8	41
06:00-07:00	120.3	118.4	116.2	115.1	105.7	42.4	25.7	92
07:00-08:00	183.4	186.0	184.2	182.6	169.2	66.5	38.5	144
08:00-09:00	182.0	185.7	185.0	183.9	171.2	98.7	56.6	152
09:00-10:00	149.8	153.2	153.7	153.6	148.3	130.0	93.4	140
10:00-11:00	144.1	**139.7**	141.2	143.4	152.8	156.0	130.6	144
11:00-12:00	147.4	140.2	142.7	146.1	163.4	169.5	153.4	152

Table TRA0307 Source: DfT Automatic Traffic Counters, 2019									
Motor vehicle traffic distribution by time of day and day of the week on all roads, Great Britain: 2018 [1]									
Index: Average hourly traffic flow over year = 100									
Time of day	**Monday**	**Tuesday**	**Wednesday**	**Thursday**	**Friday**	**Saturday**	**Sunday**		**Average weeks (Monday – Sunday)**
12:00-13:00	148.5	143.1	146.1	150.0	172.4	169.6	161.0		156
13:00-14:00	149.3	146.3	149.3	153.7	177.1	161.9	156.7		156
14:00-15:00	156.0	156.2	159.8	163.6	184.3	151.6	151.5		160
15:00-16:00	169.5	173.5	177.3	180.1	194.2	143.6	150.8		170
16:00-17:00	191.9	197.5	199.5	200.4	201.2	141.5	150.8		183
17:00-18:00	191.4	197.5	198.9	199.3	192.2	136.9	138.7		179
18:00-19:00	145.1	154.5	157.5	161.0	158.8	117.9	121.2		145
19:00-20:00	96.8	103.3	107.7	114.5	121.0	91.0	101.5		105
20:00-21:00	68.3	71.8	75.7	82.4	87.2	67.5	80.1		76
21:00-22:00	51.4	55.0	57.2	61.9	64.4	53.0	57.9		57
22:00-23:00	37.1	41.9	43.5	46.2	50.6	46.1	39.5		44
23:00-00:00	23.3	25.9	27.3	29.7	36.6	37.4	25.4		29
TOTAL	2477	2506	2541	2588	2673	2089	1927		2400
Average hourly	103	104	106	108	111	87	80		100

Source: DfT Automatic Traffic Counters, Department for Transport, 2019
Green colour = number of vehicles at specific time and day for observation data at Somerset Rd

Table TRA 0307 is used to calculate the number of vehicles on specific roads by comparing the observation data at a specific time and day on the table to find the multiplying factors. The same table for specific roads was then produced by multiplying the factors with the number of vehicle distribution at each hour for a week.

Input data in the model is in hours, therefore the average hour is total vehicles in a day is divided by twenty-four hours. The example of the calculation is given below for Somerset Road.

Somerset Rd

Table A.4.5.4. Example of observation data at Somerset Rd

Date	Time	Location	Motorcycle	Car	LGV	Bus and Coach	Taxi	HGV Rigid	HGV articulated	**TOTAL**
Tuesday, 22 Oct 2019	10:00 - 11:00	Somerset Rd	1	550	55	2	8	13	3	**632**

Number of vehicles in Somerset Rd for one hour, Tuesday, 22 October 2019 at 10:00 – 11:00 LT is **632**.

From table TRA 0307, on Tuesday at 10:00 – 11:00 LT, number of vehicles on all roads in Great Britain was **139.7** vehicles.

Multiplication factors for Somerset Rd = (632 / 139.7) = 4.52. Then, the multiplication factors times the motor vehicle traffic distribution TRA 0307 from Department for Transport is the traffic distribution data at Somerset Rd as table A.4.5.5.

Table A.4.5.5. Vehicles traffic distribution at Somerset Rd

Motor vehicles traffic distribution, Somerset Road									
Time of day	**Monday**	**Tuesday**	**Wednesday**	**Thursday**	**Friday**	**Saturday**	**Sunday**		**Average weeks (Monday – Sunday)**
00:00-01:00	70	69	74	78	86	112	122		87
01:00-02:00	47	49	52	54	61	76	79		60
02:00-03:00	39	44	46	48	52	60	56		49
03:00-04:00	50	52	53	56	58	57	48		54
04:00-05:00	96	87	87	89	89	68	50		81
05:00-06:00	247	223	219	219	208	113	71		186
06:00-07:00	544	536	526	521	478	192	116		416
07:00-08:00	830	841	833	826	765	301	174		653
08:00-09:00	823	840	837	832	775	447	256		687
09:00-10:00	678	693	695	695	671	588	423		635
10:00-11:00	652	632	639	649	691	706	591		651
11:00-12:00	667	634	646	661	739	767	694		687
12:00-13:00	672	647	661	679	780	767	728		705
13:00-14:00	675	662	675	695	801	732	709		707
14:00-15:00	706	707	723	740	834	686	685		726
15:00-16:00	767	785	802	815	879	650	682		768
16:00-17:00	868	893	903	907	910	640	682		829
17:00-18:00	866	893	900	902	870	619	627		811
18:00-19:00	656	699	713	728	718	533	548		657
19:00-20:00	438	467	487	518	547	412	459		476
20:00-21:00	309	325	342	373	394	305	362		344
21:00-22:00	233	249	259	280	291	240	262		259
22:00-23:00	168	190	197	209	229	209	179		197
23:00-00:00	105	117	124	134	166	169	115		133
TOTAL	11206	11337	11494	11706	12093	9448	8719		**10857**
Average Hourly	467	472	479	488	504	394	363		452

Yellow colour = number of vehicles from observation
Orange colour = average number of vehicles in a week for an hour

For example, on Tuesday at 00:00 – 01:00 LT, the vehicle numbers from TRA 0307 is 15.2. So, the number of vehicles on Somerset Road at that time is, 4.52 x 15.2 = 68.7 ≈ **69.**

The same equation was made for all hours of the day from Monday to Sunday. Then, an average of the data in weeks for each hour was taken to calculate total of vehicles and average of vehicles for each hour of the day

The total number of vehicles in a day from the average in a week is 10857 vehicles. The average hourly count is the total vehicles divided by 24 hours which is 452 vehicles. The next step was to find the number of vehicles based on their type, as the explanation below.

Total vehicles in an average hour

Total of vehicles based on observation at Somerset Road in one-hour data at 10:00 – 11:00 LT was 632, and the total of hourly average vehicles based on the ratio is 452.

Number of vehicles based on vehicle type:

a) Motorcycle = (1 / 632) x 452 = 0.72
b) Car = (550 / 632) x 452= 393
c) LGV = (55 / 632) x 452 = 39.3
d) Bus and coach = (2 / 632) x 452 = 1.43
e) Taxi = (8 / 632) x 452 = 5.72
f) HGV Rigid = (13 / 632) x 452 = 9.3
g) HGV articulated = (3 / 632) x 452 = 2.14

Total vehicles on Somerset Road = 1 + 393 + 39 + 1 + 6 + 9 + 2 = **451**

Table A.4.5.6. Average number of vehicles in an hour by vehicle class

Location	Motorcycle	Car	LGV	Bus and Coach	Taxi	HGV Rigid	HGV articulated	**TOTAL**
Somerset Rd	1	393	39	1	6	9	2	**451**

Do the same steps for the other roads. Then, the resume of calculation based on the observation data as below:

Table A.4.5.7. Resume of the calculation

Road name	**Location**	**Observation data (a)**	**TR0307 at the same time with observation data (b)**	**Multiplication factors (factor = a:b)**	**Total vehicles (Table A.4.5.5)**	**Average vehicles in hour (Table A.4.5.6)**
Road 2	A38	1518	141.2	10.75	25802	**1075**
Road 3 and 4	Edgbaston Park Rd	404	177.3	2.28	5469	**229**
Road 5	Pritchatts Rd	428	149.3	2.87	6880	**287**

Road name	Location	Observation data (a)	TR0307 at the same time with observation data (b)	Multiplication factors (factor = a:b)	Total vehicles (Table A.4.5.5)	Average vehicles in hour (Table A.4.5.6)
Road 6	UoB BROS site	80	173.5	0.46	1107	**47**
Road 7	New Fosse Way / Vincent Dr	748	143.1	5.23	12545	**523**
Road 8	Somerset Rd	632	139.7	4.52	10857	**451**

Table A.4.5.8. Resume data of traffic flows

Road ID	Road name	Traffic count ID	Total Average hourly data	Motor cycle	Car	LGV	Bus & Coach	Taxi	HGV Rigid	HGV articulated
				Vec hr^{-1}	Vec hr^{-1}	Vec hr^{-1}	Vec hr^{-1}	Vec hr^{-1}	Vec hr^{-1}	Vec hr^{-1}
Road 1	A38	81576 – Road 7	1286 – 523 = 763	7	691	60	4	-	3	3
Road 2	A38	81577	1178	8	1014	123	16	-	13	4
Road 3	Edgbaston Park Rd	Calculation	229	2	195	15	12	-	3	2
Road 4	Edgbaston Park Rd	Calculation	229	2	195	15	12	-	3	2
Road 5	Pritchatts Rd	Calculation	287	1	252	12	13	-	2	7
Road 6	UoB BROS site	Calculation	47	1	38	6	-	1	1	
Road 7	New Fosse Way / Vincent Dr	Calculation	523	1	441	53	17	5	5	1
Road 8	Somerset Rd	Calculation	451	1	393	39	1	6	9	2

Number of vehicles in vehicle count per hour (vec hr^{-1})

Speed configuration and vehicles numbers at each road (average speed in km per hour (km/hr):

a. Road 1

Road 1	Road width (m)	Vehicle's speed (km/hour)	Information
Road 1a	15	20	
Road 1b	10	20	
Road 1c	9	15	Traffic light
Road 1d	10	10	Near junction

b. Road 2

Road 2	Road width (m)	Vehicle's speed (km/hour)	Information
Road 2a	12	10	
Road 2b	15	10	
Road 2c	19	10	Traffic light and junction
Road 2d	19	10	

c. Road 3 and 4

Road 3	Road width (m)	Vehicle's speed (km/hour)	Information
Road 3a	12	10	Traffic light and junction
Road 3b	9	15	
Road 3c	7	15	
Road 3d	6	15	
Road 3e	6	10	Traffic light
Road 3f	6	15	
Road 3g	6	15	T junction
Road 4a	6	25	
Road 4b	6	15	T junction

d. Road 5

Road 5	Road width (m)	Vehicle's speed (km/hour)	Information
Road 5a	7	15	T junction
Road 5b	6	20	
Road 5c	6	15	Traffic light
Road 5d	6	15	T junction
Road 5e	5	20	
Road 5f	6	20	
Road 5g	6	15	T junction

e. Road 6

Road 6	Road width (m)	Vehicle's speed (km/hour)	Information
Road 6a	5	10	T junction
Road 6b	10	15	

f. Road 7

Road 7	Road width (m)	Vehicle's speed (km/hour)	Information
Road 7a	12	15	
Road 7b	10	15	
Road 7c	9	13	Traffic light and junction
Road 7d	8	15	
Road 7e	8	13	Traffic light
Road 7f	7	20	Junction

g. Road 8

Road 8	Road width (m)	Vehicle's speed (km/hour)	Information
Road 8a	7	20	Junction
Road 8b	5	15	
Road 8c	6	20	
Road 8d	6	15	Junction

Appendix 4.6. Uncertainty calculation for mean pollutant concentrations at BROS and EROS site on 2-11 February 2018 (Table 4.2)

Steps of calculation to quantify uncertainty as standard error of the mean (SEM)

1) Estimates standard deviation based on observation data.
2) Calculate standard error of the mean (SEM) and % SEM.

Pollutant	Mean Concentration (ppb)	Standard Deviation (SD), ppb	N observations	√N	Standard Error of the mean (SEM) = SD/√N, ppb	% SEM ((SEM/mean) x 100%)
BROS						
NO_BROS	20	16	224	15	16/15 = 1.06 ≈ 1	(1/20)*100% = 5%
NO_2 _BROS	14	8	224	15	8/15 = 0.53 ≈ 1	(1/14)*100% = 7.14 ≈ 7%
NO_x _BROS	34	23	224	15	23/15 = 1.53 ≈ 2	(2/34)*100% = 5.88 ≈ 6%
O_3 _BROS	17	10	224	15	10/15 = 0.67 ≈ 1	(1/17)*100% = 5.88 ≈ 6%
EROS						
NO_EROS	2	5	224	15	5/15 = 0.33 ≈ 0.3	(0.3/2)*100% = 15%
NO_2 _EROS	10	5	224	15	5/15 = 0.33 ≈ 0.3	(0.3/10)*100% = 3%
NO_x _EROS	12	9	224	15	9/15 = 0.6 ≈ 1	(1/12)*100% = 8.3 ≈ 8%
O_3 _EROS	18	9	224	15	9/15 = 0.6 ≈ 1	(1/18)*100% = 5.55 ≈ 6%

3) Calculate the uncertainty of 2 pollutants (combined)
Using equation:

% Combined uncertainty = $\sqrt{}$ (% uncertainty SEM for NO_2 BROS)^2 + (% uncertainty SEM for O_3 BROS)^2

% uncertainty for O_x BROS $= \sqrt{(7)^2 + (6)^2}$

$= \sqrt{(49) + (36)}$
$= \sqrt{85}$
$= 9.2$
≈ 9 %

Pollutant	Mean Concentration (ppb)	Combined uncertainty (%)	Uncertainty (ppb)
O_x (NO_2+O_3)_ BROS	31	$\sqrt{(7)^2 + (6)^2}$ = 9 %	9% x 31 = 2.79 ≈ 3
O_x (NO_2+O_3)_ EROS	28	$\sqrt{(3)^2 + (6)^2}$ = 6.7 ≈ 7 %	7% x 28 = 1.96 ≈ 2

4) Calculate the uncertainty of Δ (ppb) concentration

Using equation, for example

% Combined uncertainty = $\sqrt{}$ (% uncertainty SEM for NO at BROS)^2 + (% uncertainty SEM for NO at EROS)^2

% uncertainty for NO $= \sqrt{} (5)^2 + (15)^2$

$= \sqrt{} (25) + (225)$

$= \sqrt{} (250)$

$= 15.8$

$\approx 16\%$

	Δ (BROS – EROS) ppb		
Pollutant	Mean Concentration (ppb)	Combined uncertainty (%)	Uncertainty (ppb)
NO	18	$\sqrt{} (5)^2 + (15)^2 = 16$ %	16% x 18 = 2.88 ≈ 3
NO_2	4	$\sqrt{} (7)^2 + (3)^2 = 7.6 \approx 8$ %	8% x 4 ≈ 0.3
NO_x	22	$\sqrt{} (6)^2 + (8)^2 = 10$ %	10% x 22 = 2.2 ≈ 2
O_3	-1	$\sqrt{} (6)^2 + (6)^2 = 8.4 \approx 8$ %	8% x -1 ≈ 0.1
O_x (NO_2+O_3)	3	$\sqrt{} (9)^2 + (7)^2 = 11.4 \approx 11$ %	11% x 3 ≈ 0.3
NO_2:NO_x at BROS	0.4	$\sqrt{} (7)^2 + (6)^2 = 9.2 \approx 9$ %	9% x 0.4 ≈ 0.04 ≈ 0.1
NO_2:NO_x at EROS	0.8	$\sqrt{} (3)^2 + (8)^2 = 8.5 \approx 9$ %	9% x 0.8 ≈ 0.07 ≈ 0.1

Appendix 5.1. Daytime and night-time in Birmingham UK

Table A.5.1. Daytime and night-time in Birmingham, UK

Month	Sunrise	Sunset		Daytime	Night-time
January	08.18	16.03		08.00 – 17.00	16.00 – 07.00
February	07.50	16.52		08.00 – 16.00	17.00 – 07.00
March	06.53	17.47		07.00 – 17.00	18.00 – 06.00
April	06.41	19.42		07.00 – 19.00	20.00 – 06.00
May	05.35	20.34		06.00 – 20.00	21.00 – 05.00
June	04.50	21.20		05.00 – 21.00	22.00 – 04.00
July	04.49	21.33		05.00 – 21.00	22.00 – 04.00
August	05.28	20.58		06.00 – 20.00	21.00 - 05.00
September	06.19	19.54		06.00 – 19.00	20.00 – 05.00
October	07.09	18.43		07.00 – 18.00	19.00 – 06.00
November	07.02	16.38		07.00 – 17.00	17.00 – 07.00
December	07.56	15.57		08.00 – 15.00	16.00 – 08.00

Source: (https://www.timeanddate.com/sun/uk/birmingham)

References

Adar, S. D. and Kaufman, J. D. (2007) 'Cardiovascular disease and air pollutants: Evaluating and improving epidemiological data implicating traffic exposure', *Inhalation Toxicology*, 19, pp. 135–149. doi: 10.1080/08958370701496012.

Adon, M. *et al.* (2013) 'Dry deposition of nitrogen compounds (NO2, HNO3, NH3), sulfur dioxide and ozone in west and central African ecosystems using the inferential method', *Atmospheric Chemistry and Physics*, 13(22), pp. 11351–11374. doi: 10.5194/acp-13-11351-2013.

Agudelo–Castaneda, D. M., Calesso Teixeira, E. and Norte Pereira, F. (2014) 'Time–series analysis of surface ozone and nitrogen oxides concentrations in an urban area at Brazil', *Atmospheric Pollution Research*, 5(3), pp. 411–420. doi: 10.5094/APR.2014.048.

Al-Rashidi, M. S. *et al.* (2018) 'Gaseous air pollution background estimation in urban, suburban, and rural environments', *Arabian Journal of Geosciences*, 11. doi: 10.1007/s12517-017-3369-2.

Alberts, W. M. (1994) 'Indoor air pollution : NO, NO2, CO, and CO2', *Journal of allergy and clinical immunology*, (2), pp. 289–295.

Aldrin, M. and Haff, I. H. (2005) 'Generalised additive modelling of air pollution, traffic volume and meteorology', *Atmospheric Environment*, 39(11), pp. 2145–2155. doi: 10.1016/j.atmosenv.2004.12.020.

Allen, A. G., Harrison, R. M. and Nicholson, K. W. (1991) 'Dry deposition of fine aerosol to a short grass surface', *Atmospheric Environment*, 25(12), pp. 2671–2676. doi: 10.1016/0960-1686(91)90197-F.

Andreae, M. O. and Gelencsér, A. (2006) 'Black carbon or brown carbon? the nature of light-absorbing carbonaceous aerosols', *Atmospheric Chemistry and Physics*, 6(10), pp. 3131–3148. doi: 10.5194/acp-6-3131-2006.

Anttila, P., Tuovinen, J. P. and Niemi, J. V. (2011) 'Primary NO2 emissions and their role in the development of NO2 concentrations in a traffic environment', *Atmospheric Environment*, 45(4), pp. 986–992. doi: 10.1016/j.atmosenv.2010.10.050.

Apte, J. S. *et al.* (2011) 'Concentrations of fine, ultrafine, and black carbon particles in auto-rickshaws in New Delhi, India', *Atmospheric Environment*, 45(26), pp. 4470–4480. doi: 10.1016/j.atmosenv.2011.05.028.

AQEG (2004) 'Chapter 4. Measurement methods and UK monitoring networks for NO2', in *Nitrogen Dioxide in the UK*, pp. 112–133.

AQEG (2018) *Effects of Vegetation on Urban Air Pollution*. Available at: https://uk-air.defra.gov.uk/assets/documents/reports/cat09/1807251306_180509_Effects_of_vegetation_on_urban_air_pollution_v12_final.pdf.

Arciszewska, C. and McClatchey, J. (2001) 'The importance of meteorological data for modelling air pollution using ADMS-Urban', *Meteorological Applications*, 8(3), pp. 345–350. doi: 10.1017/S1350482701003103.

Ashmore, M. R., Bell, J. N. . and Mimmack, A. (1988) 'Crop growth along a gradient of ambient air pollution', *Environmental pollution*, pp. 99–120.

Ayers, G. P. *et al.* (1998) 'Validation of passive diffusion samplers for SO2 and NO2', *Atmospheric Environment*, 32(20), pp. 3587–3592. doi: 10.1016/S1352-2310(98)00079-X.

Baldasano, J. M., Valera, E. and Jiménez, P. (2003) 'Air quality data from large cities', *Science of the Total Environment*, 307(1–3), pp. 141–165. doi: 10.1016/S0048-9697(02)00537-5.

Barbosa, O. *et al.* (2007) 'Who benefits from access to green space? A case study from Sheffield, UK', *Landscape and Urban Planning*, 83, pp. 187–195. doi: 10.1016/j.landurbplan.2007.04.004.

BCC, B. C. C. (2020) *Birmingham Demographic Briefing*.

Beckerman, B. *et al.* (2008) 'Correlation of nitrogen dioxide with other traffic pollutants near a major expressway', *Atmospheric Environment*, 42(2), pp. 275–290. doi: 10.1016/j.atmosenv.2007.09.042.

Beevers, S. D. *et al.* (2013) 'Air pollution dispersion models for human exposure predictions in London', *Journal of Exposure Science and Environmental Epidemiology*, 23(6), pp. 647–653. doi: 10.1038/jes.2013.6.

Bennett, J. H. and Hill, A. C. (1973) 'Absorption of Gaseous Air Pollutants By a Standardized Plant Canopy', *Journal of the Air Pollution Control Association*, 23(3), pp. 203–206. doi: 10.1080/00022470.1973.10469767.

Bertram, C. and Rehdanz, K. (2015) 'The role of urban green space for human well-being', *Ecological Economics*, 120, pp. 139–152. doi: 10.1016/j.ecolecon.2015.10.013.

Boleij, J. S. M. *et al.* (1986) 'The use of palmes diffusion tubes for measuring NO2 in homes', *Atmospheric Environment*, 20(3), pp. 597–600. doi: 10.1016/0004-6981(86)90103-4.

Bond, T. C. *et al.* (2013) 'Bounding the role of black carbon in the climate system: A scientific assessment', *Journal of Geophysical Research Atmospheres*, 118(11), pp. 5380–5552. doi: 10.1002/jgrd.50171.

Bower, J. S. *et al.* (1994) 'A winter NO2 smog episode in the U.K.', *Atmospheric Environment*, 28(3), pp. 461–475. doi: 10.1016/1352-2310(94)90124-4.

Breuninger, C. *et al.* (2012) 'The dynamic chamber method: Trace gas exchange fluxes (NO, NO2, O3) between plants and the atmosphere in the laboratory and in the field', *Atmospheric Measurement Techniques*, 5, pp. 955–989. doi: 10.5194/amt-5-955-2012.

Briant, R. *et al.* (2013) 'Evaluation of roadway Gaussian plume models with large-scale measurement campaigns', *Geoscientific Model Development*, 6(2), pp. 445–456. doi: 10.5194/gmd-6-445-2013.

ten Brink, H. *et al.* (2004) 'INTERCOMP2000: the comparability of methods in use in Europe for measuring the carbon content of aerosol', *Atmospheric Environment*, 38(38), pp. 6507–6519. doi: DOI 10.1016/j.atmosenv.2004.08.027.

Britter, R. E. and Hanna, S. R. (2003) 'Flow and dispersion in urban areas', *Annual Review of Fluid Mechanics*, 35, pp. 469–496. doi: 10.1146/annurev.fluid.35.101101.161147.

Bronnimann, S. and Neu, U. (1997) 'Weekend-weekday differences of near-surface ozone concentrations in Switzerland for different meteorological conditions', *Atmospheric Environment*, 31(8), pp. 1127–1135. doi: 10.1016/S1352-2310(96)00311-1.

Brugge, D., Durant, J. L. and Rioux, C. (2007) 'Near-highway pollutants in motor vehicle exhaust: A review of epidemiologic evidence of cardiac and pulmonary health risks', *Environmental Health*, 6, pp. 1–12. doi: 10.1186/1476-069X-6-23.

Brunekreef, B. and Holgate, S. T. (2002) 'Air pollution and health', *The Lancet*, 360, pp. 1233–1242.

Bryan, N. S. and Grisham, M. B. (2007) 'Methods to detect nitric oxide and its metabolities in biological samples', *Free Radical Biology & Medicine*, 43, pp. 645–657.

BSI (2012) 'BS EN 14211:2012 Ambient air — Standard method for the measurement of the concentration of nitrogen dioxide and nitrogen monoxide by chemiluminescence', *BSI Standards Publication*.

Bush, T. *et al.* (2001) 'Validation of nitrogen dioxide diffusion tube methodology in the UK', *Atmospheric Environment*, 35, pp. 289–296. doi: 10.1016/S1352-2310(00)00172-2.

Businger, J. A. (1986) 'Evaluation of the accuracy with which dry deposition can be measured with current micrometeorological techniques', *Journal of climate and applied meteorology*, 25, pp. 1100–1124.

Campbell, G. W. (1988) 'Measurements of nitrogen dioxide concentrations at rural sites in the United Kingdom using diffusion tubes', *Environmental Pollution*, 55(4), pp. 251–270. doi: 10.1016/0269-7491(88)90249-7.

Campbell, G. W., Stedman, J. R. and Stevenson, K. (1994) 'A survey of nitrogen dioxide concentrations in the United Kingdom using diffusion tubes, July-December 1991', *Atmospheric Environment*, 28(3), pp. 477–486. doi: 10.1016/1352-2310(94)90125-2.

Cape, J. N. (2009) 'The Use of Passive Diffusion Tubes for Measuring Concentrations of Nitrogen Dioxide in Air', *Critical Reviews in Analytical Chemistry*, 39(4), pp. 289–310. doi: 10.1080/10408340903001375.

Carruthers, D. J. *et al.* (1994) 'UK-ADMS: A new approach to modelling dispersion in the earth's atmospheric boundary layer', *Journal of Wind Engineering and Industrial Aerodynamics*, 52, pp. 139–153. doi: 10.1016/0167-6105(94)90044-2.

Carruthers, D. J. *et al.* (1997) 'ADMS Urban - an integrated air quality modelling system for local government', *Transactions on Ecology and the Environment*, 15. Available at: http://www.ncbi.nlm.nih.gov/entrez/query.fcgi?cmd=Retrieve&db=PubMed&dopt=Citation&list_uids=17363372.

Carslaw, D. C. (2005) 'Evidence of an increasing NO2/NOx emissions ratio from road traffic emissions', *Atmospheric Environment*, 39(2), pp. 4793–4802. doi: 10.1016/j.atmosenv.2005.06.023.

Carslaw, D. C. and Ropkins, K. (2012) 'Openair - An R package for air quality data

analysis', *Environmental Modelling & Software*, 27–28, pp. 52–61. doi: 10.1016/j.envsoft.2011.09.008.

Carslaw, D. (2015) *The openair manual open-source tools for analysing air pollution data, King's College London*.

Carslaw, D. C. *et al.* (2016) 'Have vehicle emissions of primary NO2 peaked?', *Faraday Discussions*, 189(0), pp. 439–454. doi: 10.1039/c5fd00162e.

CERC (2017) *ADMS-Roads, Air Quality Management System Version 4.1, User Guide*.

Chaloulakou, A. *et al.* (2003) 'Measurements of PM10 and PM2.5 particle concentrations in Athens, Greece', *Atmospheric Environment*, 37(5), pp. 649–660. doi: 10.1016/S1352-2310(02)00898-1.

Chaloulakou, A., Mavroidis, I. and Gavriil, I. (2008) 'Compliance with the annual NO2 air quality standard in Athens. Required NOx levels and expected health implications', *Atmospheric Environment*, 42(3), pp. 454–465. doi: 10.1016/j.atmosenv.2007.09.067.

Chang, J. C. and Hanna, S. R. (2004) 'Air quality model performance evaluation', *Meteorology and Atmospheric Physics*, 87(1–3), pp. 167–196. doi: 10.1007/s00703-003-0070-7.

Chestnut, L. G. and Mills, D. M. (2005) 'A fresh look at the benefits and costs of the US acid rain program', *Journal of Environmental Management*, 77(3), pp. 252–266. doi: 10.1016/j.jenvman.2005.05.014.

Cohen, P., Potchter, O. and Schnell, I. (2014) 'The impact of an urban park on air pollution and noise levels in the Mediterranean city of Tel-Aviv, Israel.', *Environmental pollution*, 195, pp. 73–83. doi: 10.1016/j.envpol.2014.08.015.

Colbeck, I. and Harrison, R. M. (1985) 'Dry deposition of ozone: some measurements of deposition velocity and of vertical profiles to 100 metres', *Atmospheric Environment (1967)*, 19(11), pp. 1807–1818. doi: 10.1016/0004-6981(85)90007-1.

Colvile, R. N. *et al.* (2001) 'The transport sector as a source of air pollution', *Atmospheric Environment*, 35, pp. 1537–1565. doi: 10.1016/S1474-8177(02)80009-2.

Cox, R. M. (2003) 'The use of passive sampling to monitor forest exposure to O3, NO2 and SO2: a review and some case studies', *Environmental Pollution*, 126, pp. 301–311. doi: 10.1016/S0269-7491(03)00243-4.

Crompton, J. L. (2017) 'Evolution of the "parks as lungs" metaphor: is it still relevant?', *World Leisure Journal*, 59(2), pp. 105–123. doi: 10.1080/16078055.2016.1211171.

Cyrys, J. *et al.* (2012) 'Variation of NO2 and NOx concentrations between and within 36 European study areas: Results from the ESCAPE study', *Atmospheric Environment*, 62(2), pp. 374–390. doi: 10.1016/j.atmosenv.2012.07.080.

Davidović, B. *et al.* (2014) 'Evaluation of road vehicles emission by applying the ADMS Road software - The case of an intersection in the urban area of the city of Belgrade', in *Ecology of urban areas 2014*, pp. 93–105.

Dėdelė, A. and Miškinytė, A. (2013) 'The application of ADMS-Urban model to estimate nitrogen dioxide concentrations in cold and warm seasons in Kaunas city', *Biologija*, 59(4), pp. 319–326. doi: 10.6001/biologija.v59i4.2830.

DEFRA (2009) *Local Air Quality Management -Technical Guidance LAQM.TG(09), LAQM TG (09)*.

DEFRA (2018) *Local Air Quality Management - Technical Guidance (TG16), DEFRA*.

DEFRA (no date) *https://uk-air.defra.gov.uk/assets/documents/Air_Quality_Objectives_Update.pdf*.

Delany, A. C. and Davies, T. D. (1983) 'Dry deposition of NOx to grass in rural east Anglia: Preliminary communication', *Atmospheric Environment*, 17, pp. 1391–1394.

Delaria, E. R. *et al.* (2018) 'Measurements of NO and NO2 exchange between the atmosphere and Quercus agrifolia', *Atmospheric Chemistry and Physics*, 18(19), pp. 14161–14173. doi: 10.5194/acp-18-14161-2018.

Delgado-Saborit, J. M. and Esteve-Cano, V. J. (2007) 'Field comparison of passive samplers versus UV-photometric analyser to measure surface ozone in a Mediterranean area', *Journal of environmental monitoring : JEM*, 9(6), pp. 610–615. doi: 10.1039/b618075b.

Derwent, R. G. *et al.* (2007) 'Trends over a 20-year period from 1987 to 2007 in surface ozone at the atmospheric research station, Mace Head, Ireland', *Atmospheric Environment*, 41, pp. 9091–9098. doi: 10.1016/j.atmosenv.2007.08.008.

DfT, D. for T. (2019a) *dft_aadf_local_authority_id_141*, *https://roadtraffic.dft.gov.uk/local-authorities/141*.

DfT, D. for T. (2019b) *tra0307, https://www.gov.uk/government/statistical-data-sets/road-traffic-statistics-tra#annual-daily-traffic-flow-and-distribution-tra03*.

DfT, D. for T. (2020) *veh0105, https://www.gov.uk/government/statistical-data-sets/all-vehicles-veh01*.

Dias, D., Pina, N. and Tchepel, O. (2019) 'Characterization of traffic-related particulate matter at urban scale', *International Journal of Transport Development and Integration*, 3(2), pp. 144–151. doi: 10.2495/TDI-V3-N2-144-151.

Dolske, D. A. and Gatz, D. F. (1985) 'A field intercomparison of methods for the measurement of particle and gas dry deposition', *Journal of Geophysical Research*, 90(D1), pp. 2076–2084. doi: 10.1029/jd090id01p02076.

Droppo, J. G. and Doran, J. C. (1978) 'Dry deposition of gaseous pollutants from coal-fired power plants', *No. PNL--2500 (PT. 3)*.

Ducret-Stich, R. E. *et al.* (2013) 'Role of highway traffic on spatial and temporal distributions of air pollutants in a Swiss Alpine valley', *Science of the Total Environment*, 456–457, pp. 50–60. doi: 10.1016/j.scitotenv.2013.03.065.

Duffield, R. (2011) *City of London Air Quality Strategy 2011-2015*.

EANET, N. C. for (2010) 'Technical Manual on Dry Deposition Flux Estimation in East Asia', (November).

Eggleston, S. *et al.* (1998) 'Emissions: Enery, Road Transport', *Good Practice Guidance and Uncertainty Management in National Greenhouse Gas Inventories*, pp. 55–70.

Egorova, G. V. *et al.* (2015) 'Ozone Solubility in Water', *Moscow University Chemistry*

Bulletin, 70(5), pp. 207–210. doi: 10.3103/S0027131415050053.

El-Madany, T. S., Niklasch, K. and Klemm, O. (2017) 'Stomatal and non-stomatal turbulent deposition flux of ozone to a managed peatland', *Atmosphere*, 8, pp. 1–16. doi: 10.3390/atmos8090175.

Ellis, K. *et al.* (2001) 'Comparison of ADMS-Roads, CALINE4 and UK DMRB Model Predictions for Roads', in *7th International Conference on Harmonisation within Atmospheric Dispersion Modelling for Regulatory Purposes Belgirate*.

Erisman, J. A. N. W. *et al.* (1993) 'Monitoring the dry deposition of SO2 in the Netherlands: results for grassland and heather vegetation', *Atmospheric Environment*, 27(7), pp. 1153–1161.

Erisman, J. W. and Draaijers, G. P. (1995) *Atmospheric deposition: in relation to acidification and eutrophication*. Elsevier.

EU Directive (2008) 'Directive 2008/50/EC of the European Parliament and of the Council of 21 May 2008 on ambient air quality and cleaner air for Europe', *Official Journal of the European Union*, 152, pp. 1–43. doi: http://eur-lex.europa.eu/LexUriServ/LexUriServ.do?uri=OJ:L:2008:152:0001:0044:EN:PDF.

Fantozzi, F. *et al.* (2013) 'Ozone and nitrogen dioxide concentrations in a Holm oak urban park and an adjacent open area in Siena', *WIT Transactions on Ecology and the Environment*, 174(2), pp. 103–110. doi: 10.2495/AIR130091.

Fenger, J. (1999) 'Urban air quality', *Atmospheric Environment*, 33, pp. 4877–4900. doi: 10.1016/j.atmosenv.2007.09.035.

Finlayson-Pitts, B. J. and Pitts Jr, J. N. (1999) *Chemistry of the upper and lower atmosphere: theory, experiments, and applications*. Elsevier.

Flemming, J. *et al.* (2014) 'Tropospheric chemistry in the integrated forecasting system of ECMWF', *Geoscientific Model Development Discussions*, 7, pp. 7733–7803. doi: 10.5194/gmdd-7-7733-2014.

Fowler, D. *et al.* (1998) 'The atmospheric budget of oxidized nitrogen and its role in ozone formation and deposition', *New Phytologist*, 139(1), pp. 11–23. doi: 10.1046/j.1469-8137.1998.00167.x.

Fowler, D. (2002) 'Pollutant deposition and uptake by vegetation', in *Air pollution and plant life, 2*, pp. 43–67.

Fuller, R. A. and Gaston, K. J. (2009) 'The scaling of green space coverage in European cities', *Biology Letters*, 5(3), pp. 352–355. doi: 10.1098/rsbl.2009.0010.

Galbally, E. *et al.* (2013) *Guidelines for continuous measurement of ozone in the troposphere*.

Galbally, I. (1968) 'Some measurements of ozone variation and destruction in the atmospheric surface layer', *Nature*, 218(5140), pp. 456–457. doi: 10.1038/218456a0.

Gao, W. *et al.* (2017) 'Long-term trend of O3 in a mega City (Shanghai), China: Characteristics, causes, and interactions with precursors', *Science of the Total Environment*, 603–604, pp. 425–433. doi: 10.1016/j.scitotenv.2017.06.099.

Garland, J. A. (1977) 'The dry deposition of sulphur dioxide to land and water surfaces',

Proceedings of the Royal Society of London. A. Mathematical and Physical Sciences, 354, pp. 245–268. doi: 10.1098/rspa.1977.0066.

Garland, J. A. and Derwent, R. G. (1979) 'Destruction at the ground and the diurnal cycle of concentration of ozone and other gases', *Quarterly Journal of the Royal Meteorological Society*, 105(443), pp. 169–183. doi: 10.1002/qj.49710544311.

Geng, F. *et al.* (2008) 'Characterizations of ozone, NOx, and VOCs measured in Shanghai, China', *Atmospheric Environment*, 42, pp. 6873–6883. doi: 10.1016/j.atmosenv.2008.05.045.

Gerboles, M. *et al.* (2003) 'Assessment of uncertainty of NO2 measurements by the chemiluminescence method and discussion of the quality objective of the NO2 European Directive', *Journal of Environmental Monitoring*, 5, pp. 529–540. doi: 10.1039/b302358c.

Gerboles, M., Buzica, D. and Amantini, L. (2005) 'Modification of the Palmes diffusion tube and semi-empirical modelling of the uptake rate for monitoring nitrogen dioxide', *Atmospheric Environment*, 39(14), pp. 2579–2592. doi: 10.1016/j.atmosenv.2005.01.012.

Giardina, M. and Buffa, P. (2018) 'A new approach for modeling dry deposition velocity of particles', *Atmospheric Environment*, 180(March), pp. 11–22. doi: 10.1016/j.atmosenv.2018.02.038.

Gilbert, N. L. *et al.* (2003) 'Ambient nitrogen dioxide and distance from a major highway', *the Science of the Total Environment*, 312(1–3), pp. 43–46. doi: 10.1016/S0048-9697(03)00228-6.

Gilbert, N. L. *et al.* (2007) 'The influence of highway traffic on ambient nitrogen dioxide concentrations beyond the immediate vicinity of highways', *Atmospheric Environment*, 41(12), pp. 2670–2673. doi: 10.1016/j.atmosenv.2006.12.007.

Gill, S. E. *et al.* (2007) 'Adapting cities for climate change: The role of the green infrastructure', *Built Environment*, 33(1), pp. 115–133. doi: 10.2148/benv.33.1.115.

Gillespie-Bennett, J. *et al.* (2011) 'The respiratory health effects of nitrogen dioxide in children with asthma', *European Respiratory Journal*, 38(2), pp. 303–309. doi: 10.1183/09031936.00115409.

Glasius, M. *et al.* (1999) 'Measurements of nitrogen dioxide on Funen using diffusion tubes', *Atmospheric Environment*, 33(8), pp. 1177–1185. doi: 10.1016/S1352-2310(98)00285-4.

Gong, F., Zheng, Z.-C. and Ng, E. (2016) 'Modeling Elderly Accessibility to Urban Green Space in High Density Cities: A Case Study of Hong Kong', *Procedia Environmental Sciences*, 36, pp. 90–97. doi: 10.1016/j.proenv.2016.09.018.

Grimm, N. B. *et al.* (2008) 'Global change and the ecology of cities', *Science*, 319(5864), pp. 756–760. doi: 10.1126/science.1150195.

Guo, H., Wang, Y. and Zhang, H. (2017) 'Characterization of criteria air pollutants in Beijing during 2014-2015', *Environmental Research*, pp. 334–344.

Hafkenscheid, T. *et al.* (2009) *Review of the application of diffusive samplers in the European Union for the monitoring of nitrogen dioxide in ambient air*, *JRC Scientific*

and Technical Reports. European Comission, Joint Research Centre, Institute for Environment and Sustainability.

Hamilton, Richard P and Heal, M. R. (2004) 'Evaluation of method of preparation of passive diffusion tubes for measurement of ambient nitrogen dioxide', *Journal of Environmental Monitoring*, 6(1), pp. 12–17. doi: 10.1039/b311869j.

Hamilton, Richard P. and Heal, M. R. (2004) 'Evaluation of method of preparation of passive diffusion tubes for measurement of ambient nitrogen dioxide', *Journal of Environmental Monitoring*, 6(1), pp. 12–17. doi: 10.1039/b311869j.

Hang, J., Sandberg, M. and Li, Y. (2009) 'Effect of urban morphology on wind condition in idealized city models', *Atmospheric Environment*, 43(4), pp. 869–878. doi: 10.1016/j.atmosenv.2008.10.040.

Hanna, S. R., Briggs, G. A. and Rayford P Hosker, J. (1982) *Handbook on atmospheric diffusion*.

Hanson, P. J. and Lindberg, S. E. (1991) 'Dry deposition of reactive nitrogen compounds: A review of leaf, canopy and non-foliar measurements', *Atmospheric Environment*, 25A(8), pp. 1615–1634. doi: 10.1016/0960-1686(91)90020-8.

Hargreaves, K. J., Fowler, D. and Storeton-West, R. L. (1992) 'The exchange of nitric oxide, nitrogen dioxide and ozone between pasture and the atmosphere', *Environmental Pollution*, 75, pp. 53–59.

Harper, W. V. (2014) 'Reduced Major Axis Regression: Teaching Alternatives To Least Squares', *Sustainability in statistic education. Proceedings of the Ninth International Conference on Teaching Statistics (ICOTS9, July, 2014)*. doi: 10.1016/b978-0-12-420228-3.00013-0.

Harrison, R. M. *et al.* (2006) 'Measurement and modelling of air pollution and atmospheric chemistry in the U.K. West Midlands conurbation : Overview of the PUMA Consortium project', *Science of the Total Environment*, 360, pp. 5–25. doi: 10.1016/j.scitotenv.2005.08.053.

Harrison, R. M. (2014) 'Chapter 8. Chemistry of the Troposphere', in Harrison, R. M. (ed.) *Pollution: Causes, Effect and Control*. 5th editio. The Royal Society of Chemistry, pp. 182–203.

Harrison, R. M. (2018) 'Urban atmospheric chemistry: a very special case for study', *npj Climate and Atmospheric Science*, 1(1), pp. 1–5. doi: 10.1038/s41612-017-0010-8.

Heal, M. R. and Cape, J. N. (1997) 'A numerical evaluation of chemical interferences in the measurement of ambient nitrogen dioxide by passive diffusion samplers', *Atmospheric Environment*, 31(13), pp. 1911–1923. doi: 10.1016/S1352-2310(97)00025-3.

Heal, M. R., Laxen, D. P. H. and Marner, B. B. (2019) 'Biases in the measurement of ambient nitrogen dioxide (NO2) by palmes passive diffusion tube: A review of current understanding', *Atmosphere*, 10(7), pp. 1–28. doi: 10.3390/atmos10070357.

Heal, M. R., O'Donoghue, M. A. and Cape, J. N. (1999) 'Overestimation of urban nitrogen dioxide by passive diffusion tubes: A comparative exposure and model study', *Atmospheric Environment*, 33(4), pp. 513–524. doi: 10.1016/S1352-2310(98)00290-8.

Heist, D. *et al.* (2013) 'Estimating near-road pollutant dispersion : A model inter-comparison', *Transportation Research Part D: Transport and Environment*, 25, pp. 93–105. doi: 10.1016/j.trd.2013.09.003.

Helaleh, M. I. H. *et al.* (2002) 'Development of passive sampler technique for ozone monitoring. Estimation of indoor and outdoor ozone concentration', *Talanta*, 58(4), pp. 649–659. doi: 10.1016/S0039-9140(02)00375-2.

Henschel, S. *et al.* (2015) 'Trends of nitrogen oxides in ambient air in nine European cities between 1999 and 2010', *Atmospheric Environment*, 117, pp. 234–241. doi: 10.1016/j.atmosenv.2015.07.013.

Hernandez, G. *et al.* (2017) 'Temperature and humidity effects on particulate matter concentrations in a sub-tropical climate during winter', *International Proceedings of Chemical, Biological and Environmental Engineering*, 102, pp. 41–49. doi: 10.7763/IPCBEE.

Hesterberg, R. *et al.* (1996) 'Deposition of nitrogen-containing compounds to an extensively managed grassland in central Switzerland', *Environmental pollution*, 91(1), pp. 21–34.

Heuss, J. M., Kahlbaum, D. F. and Wolff, G. T. (2003) 'Weekday/Weekend Ozone Differences: What Can We Learn from Them?', *Journal of the Air & Waste Management Association*, 53(7), pp. 772–788. doi: 10.1080/10473289.2003.10466227.

Hewitt, C. N. (1991) 'Spatial variations in nitrogen dioxide concentrations in an urban area', *Atmospheric Environment*, 25B(3), pp. 429–434.

Hewitt, C. N., Ashworth, K. and MacKenzie, A. R. (2020) 'Using green infrastructure to improve urban air quality (GI4AQ)', *Ambio*, 49(1), pp. 62–73. doi: 10.1007/s13280-019-01164-3.

Heynen, N., Perkins, H. a and Roy, P. (2006) 'The Political Ecology of Uneven Urban Green Space The Impact of Political Economy on Race and Ethnicity in Producing Environmental Inequality in Milwaukee', *Urban Affairs Review*, 42(1), pp. 3–25.

Hickman, A. L. *et al.* (2018) 'Evaluation of air quality at the Birmingham New Street Railway Station', *Proceedings of the Institution of Mechanical Engineers, Part F: Journal of Rail and Rapid Transit*, 232(6), pp. 1864–1878. doi: 10.1177/0954409717752180.

Hienola, A. I. *et al.* (2013) 'Black carbon concentration and deposition estimations in Finland by the regional aerosol-climate model REMO-HAM', *Atmospheric Chemistry and Physics*, 13(8), pp. 4033–4055. doi: 10.5194/acp-13-4033-2013.

Hill, A. C. (1971) 'Vegetation: A Sink for Atmospheric Pollutants', *Journal of the Air Pollution Control Association*, 21(6), pp. 341–346. doi: 10.1080/00022470.1971.10469535.

Hirtl, M. and Baumann-Stanzer, K. (2007) 'Evaluation of two dispersion models (ADMS-Roads and LASAT) applied to street canyons in Stockholm, London and Berlin', *Atmospheric Environment*, 41(28), pp. 5959–5971. doi: 10.1016/j.atmosenv.2007.03.026.

Holmes, N. S. and Morawska, L. (2006) 'A review of dispersion modelling and its

application to the dispersion of particles: An overview of different dispersion models available', *Atmospheric Environment*, 40(30), pp. 5902–5928. doi: 10.1016/j.atmosenv.2006.06.003.

Hood, C. *et al.* (2018) 'Air quality simulations for London using a coupled regional-to-local modelling system', *Atmospheric Chemistry and Physics*, 18(15), pp. 11221–11245. doi: 10.5194/acp-18-11221-2018.

Horii, C. V. *et al.* (2004) 'Fluxes of nitrogen oxides over a temperate deciduous forest', *Journal of Geophysical Research D: Atmospheres*, 109(8), pp. 1–8. doi: 10.1029/2003JD004326.

Horváth, L., Nagy, Z. and Weidinger, T. (1998) 'Estimation of dry deposition velocities of nitric oxide, sulfur dioxide, and ozone by the gradient method above short vegetation during the tract campaign', *Atmospheric Environment*, 32(7), pp. 1317–1322. doi: 10.1016/S1352-2310(97)00192-1.

Huang, L. *et al.* (2010) 'Importance of deposition processes in simulating the seasonality of the Arctic black carbon aerosol', *Journal of Geophysical Research Atmospheres*, 115(17), pp. 1–15. doi: 10.1029/2009JD013478.

Jacobson, M. Z. (2002) *Atmospheric pollution: history, science, and regulation*. Cambridge University Press.

Janhall, S. (2015) 'Review on urban vegetation and particle air pollution - Deposition and dispersion', *Atmospheric Environment*, 105, pp. 130–137. doi: 10.1016/j.atmosenv.2015.01.052.

Jayamurugan, R. *et al.* (2013) 'Influence of Temperature, Relative Humidity and Seasonal Variability on Ambient Air Quality in a Coastal Urban Area', *International Journal of Atmospheric Sciences*, pp. 1–7. doi: 10.1155/2013/264046.

Jeanjean, A. P. R., Monks, P. S. and Leigh, R. J. (2016) 'Modelling the effectiveness of urban trees and grass on PM2.5 reduction via dispersion and deposition at a city scale', *Atmospheric Environment*, 147, pp. 1–10. doi: 10.1016/j.atmosenv.2016.09.033.

Jenkin, M. E. (2004) 'Analysis of sources and partitioning of oxidant in the UK - Part 2: Contributions of nitrogen dioxide emissions and background ozone at a kerbside location in London', *Atmospheric Environment*, 38(30), pp. 5131–5138. doi: 10.1016/j.atmosenv.2004.05.055.

Jia, Y. *et al.* (2016) 'Global inorganic nitrogen dry deposition inferred from ground- and space-based measurements', *Scientific Reports*, 6, pp. 1–11. doi: 10.1038/srep19810.

Jim, C. Y. and Chen, W. Y. (2008) 'Assessing the ecosystem service of air pollutant removal by urban trees in Guangzhou (China)', *Journal of Environmental Management*, 88(4), pp. 665–676. doi: 10.1016/j.jenvman.2007.03.035.

Jiménez, A. S., Heal, M. R. and Beverland, I. J. (2011) 'Intercomparison study of NOx passive diffusion tubes with chemiluminescence analysers and evaluation of bias factors', *Atmospheric Environment*, 45, pp. 3062–3068. doi: 10.1016/j.atmosenv.2011.03.011.

Jin, S. and Demerjian, K. (1993) 'A photochemical box model for urban air quality Study', *Atmospheric Environment*, 27(4), pp. 371–387.

Jones, A. M., Harrison, R. M. and Baker, J. (2010) 'The wind speed dependence of the concentrations of airborne particulate matter and NOx', *Atmospheric Environment*, 44(13), pp. 1682–1690. doi: 10.1016/j.atmosenv.2010.01.007.

Kaneda, T. and Bietsch, K. (2015) '2015 World Population Data Sheet', *2015 World Population Data Sheet*, p. 23. doi: 10.2307/1972177.

Kaneda, T., Greenbaum, C. and Patierno, K. (2018) '2018 World Population Data Sheet With Focus on Changing Age Structures – Population Reference Bureau', *2018 - Population Reference Bureau*.

Karner, A. A., Eisinger, D. S. and Niemeier, D. A. (2010) 'Near-roadway air quality: Synthesizing the findings from real-world data', *Environmental Science and Technology*, 44(14), pp. 5334–5344. doi: 10.1021/es100008x.

Keronen, P. *et al.* (2003) 'Ozone flux measurements over a Scots pine forest using eddy covariance method: Performance evaluation and comparison with flux-profile method', *Boreal Environment Research*, 8(4), pp. 425–443.

Kim, S.-Y. *et al.* (2013) 'Impact of biogenic volatile organic compounds on ozone production at the Taehwa Research Forest near Seoul, South Korea', *Atmospheric Environment*, 70, pp. 447–453. doi: 10.1016/j.atmosenv.2012.11.005.

King, K. L. *et al.* (2014) 'Differences in magnitude and spatial distribution of urban forest pollution deposition rates, air pollution emissions, and ambient neighborhood air quality in New York City', *Landscape and Urban Planning*, 128, pp. 14–22. doi: 10.1016/j.landurbplan.2014.04.009.

Kirby, C., Fox, M. and Waterhouse, J. (2000) 'Reliability of nitrogen dioxide passive diffusion tubes for ambient measurement: in situ properties of the triethanolamine absorbent', *Journal of Environmental Monitoring*, 2(4), pp. 307–312. doi: 10.1039/b003124k.

Klausen, J. *et al.* (2003) 'Uncertainty and bias of surface ozone measurements at selected Global Atmosphere Watch sites', *Journal of Geophysical Research*, 108. doi: 10.1029/2003JD003710.

Koleiny, A. (2009) *An investigation into the contribution of the low-level jet (LLJ) to the available wind resource in Missouri*.

Kramm, G. (1989) 'A numerical method for determining the dry deposition of atmospheric trace gases', *Boundary-Layer Meteorology*, 48(1–2), pp. 157–175. doi: 10.1007/BF00121788.

Kurtenbach, R. *et al.* (2012) 'Primary NO2 emissions and their impact on air quality in traffic environments in Germany', (2), pp. 1–8.

Kuttler, W. and Strassburger, A. (1999) 'Air quality measurements in urban green areas - a case study', *Atmospheric Environment*, 33(24–25), pp. 4101–4108. doi: 10.1016/S1352-2310(99)00151-X.

Lack, D. A. *et al.* (2014) 'Characterizing elemental, equivalent black, and refractory black carbon aerosol particles: a review of techniques, their limitations and uncertainties', *Analytical and Bioanalytical Chemistry*, 406(1), pp. 99–122. doi: 10.1007/s00216-013-7402-3.

Laothawornkitkul, J. *et al.* (2009) 'Biogenic volatile organic compounds in the Earth system', *New Phytologist*, pp. 27–51.

Laxen, D. and Marner, B. (2006) *The Relationship Between Diffusion Tube Bias and Distance From the Road*.

Lee, S. H. and Park, S. U. (2008) 'A vegetated urban canopy model for meteorological and environmental modelling', *Boundary-Layer Meteorology*, 126(1), pp. 73–102. doi: 10.1007/s10546-007-9221-6.

Leisner, C. P. and Ainsworth, E. A. (2012) 'Quantifying the effects of ozone on plant reproductive growth and development', *Global Change Biology*, 18(2), pp. 606–616. doi: 10.1111/j.1365-2486.2011.02535.x.

Levy, J. I. *et al.* (2003) 'Influence of traffic patterns on particulate matter and polycyclic aromatic hydrocarbon concentrations in Roxbury, Massachusetts', *Journal of Exposure Analysis and Environmental Epidemiology*, 13(5), pp. 364–371. doi: 10.1038/sj.jea.7500289.

Lindberg, S. E. and Lovett, G. M. (1985) 'Field Measurements of Particle Dry Deposition Rates to Foliage and Inert Surfaces in a Forest Canopy', *Environmental Science and Technology*, 19(3), pp. 238–244. doi: 10.1021/es00133a003.

Lippmann, M. (1989) 'Health effects of ozone a critical review', *Journal of the Air & Waste Management Association*, 39(5), pp. 672–695. doi: 10.1080/08940630.1989.10466554.

Liu, D. *et al.* (2014) 'Size distribution, mixing state and source apportionment of black carbon aerosol in London during winter time', *Atmospheric Chemistry and Physics*, 14(18), pp. 10061–10084. doi: 10.5194/acp-14-10061-2014.

Liu, H. L. and Shen, Y. S. (2014) 'The impact of green space changes on air pollution and microclimates: A case study of the Taipei metropolitan area', *Sustainability*, 6, pp. 8827–8855. doi: 10.3390/su6128827.

Liu, L. *et al.* (2002) 'The effect of black carbon on scattering and absorption of solar radiation by cloud droplets', *Journal of Quantitative Spectroscopy and Radiative Transfer*, 74(2), pp. 195–204. doi: 10.1016/S0022-4073(01)00232-1.

Longhurst, J. W. S., Lindley, S. J. and Conlan, D. E. (1994) 'Towards local air quality management in the United Kingdom', *Transactions on Ecology and the Environment*, 4.

Longley, I., Somervell, E. and Gray, S. (2015) 'Roadside increments in PM 10, NOx and NO2 concentrations observed over 2 months at a major highway in New Zealand', *Air Quality, Atmosphere and Health*, (2), pp. 591–602. doi: 10.1007/s11869-014-0305-4.

Lyons, T. J. and Scott, W. D. (1990) *Principles of air pollution meteorology*. Bellhaven Press.

Ma, J. and Daggupaty, S. M. (2000) 'Effective dry deposition velocities for gases and particles over heterogeneous terrain', *Journal of Applied Meteorology*, 39(8), pp. 1379–1390. doi: 10.1175/1520-0450(2000)039<1379:EDDVFG>2.0.CO;2.

MacDonald, K. M. *et al.* (2017) 'Observations of atmospheric chemical deposition to high Arctic snow', *Atmospheric Chemistry and Physics*, 17(9), pp. 5775–5788. doi:

10.5194/acp-17-5775-2017.

Magaudda, S. *et al.* (2020) '" Greening " Green Infrastructure . Good Italian Practices for Enhancing Green Infrastructure through the Common Agricultural Policy', *Sustainability*.

Manes, F. *et al.* (2007) 'Estimates of potential ozone stomatal uptake in mature trees of Quercus ilex in a Mediterranean climate', *Environmental and Experimental Botany*, 59, pp. 235–241. doi: 10.1016/j.envexpbot.2005.12.001.

Mariraj Mohan, S. (2016) 'An overview of particulate dry deposition: measuring methods, deposition velocity and controlling factors', *International Journal of Environmental Science and Technology*, 13(1), pp. 387–402. doi: 10.1007/s13762-015-0898-7.

Masey, N. *et al.* (2017) 'Influence of wind-speed on short-duration NO2 measurements using Palmes and Ogawa passive diffusion samplers', *Atmospheric Environment*, 160, pp. 70–76. doi: 10.1016/j.atmosenv.2017.04.008.

Massman, W. J. (1998) 'A review of the molecular diffusivities of H2O, CO2, CH4, CO, O3, SO2, NH3, N2O, NO and NO2 in air, O2 and N2 near STP', *Atmospheric Environment*, 32(6), pp. 1111–1127.

Matsuda, K. *et al.* (2005) 'Ozone dry deposition above a tropical forest in the dry season in northern Thailand', *Atmospheric Environment*, 39(14), pp. 2571–2577. doi: 10.1016/j.atmosenv.2005.01.011.

Matsuda, K. *et al.* (2006) 'Deposition velocity of O3 and SO2 in the dry and wet season above a tropical forest in northern Thailand', *Atmospheric Environment*, 40(39), pp. 7557–7564. doi: 10.1016/j.atmosenv.2006.07.003.

Matsuda, K. *et al.* (2012) 'Dry and wet deposition of elemental carbon on a tropical forest in Thailand', *Atmospheric Environment*, 54, pp. 282–287. doi: 10.1016/j.atmosenv.2012.02.022.

Matthaios, V. N. *et al.* (2019) 'Investigation of vehicle cold start primary NO2 emissions inferred from ambient monitoring data in the UK and their implications for urban air quality', *Atmospheric Environment*, 199(2), pp. 402–414. doi: 10.1016/j.atmosenv.2018.11.031.

Mavroidis, I. and Chaloulakou, A. (2011) 'Long-term trends of primary and secondary NO2 production in the Athens area. Variation of the NO2/NOx ratio', *Atmospheric Environment*, 45(38), pp. 6872–6879. doi: 10.1016/j.atmosenv.2010.11.006.

Mavroidis, I. and Ilia, M. (2012) 'Trends of NOx, NO2 and O3 concentrations at three different types of air quality monitoring stations in Athens, Greece', *Atmospheric Environment*, 63(2), pp. 135–147. doi: 10.1016/j.atmosenv.2012.09.030.

Mayer, H. (1999) 'Air pollution in cities', *Atmospheric Environment*, 33(24–25), pp. 4029–4037. doi: 10.1016/S1352-2310(99)00144-2.

Mazzeo, N. A., Venegas, L. E. and Choren, H. (2005) 'Analysis of NO, NO2, O3 and NOx concentrations measured at a green area of Buenos Aires City during wintertime', *Atmospheric Environment*, 39(17), pp. 3055–3068. doi: 10.1016/j.atmosenv.2005.01.029.

Melkonyan, A. and Kuttler, W. (2012) 'Long-term analysis of NO, NO2 and O3

concentrations in North Rhine-Westphalia, Germany', *Atmospheric Environment*, 60(2), pp. 316–326. doi: 10.1016/j.atmosenv.2012.06.048.

Miller, D. P. (1988) 'Low-level determination of nitrogen dioxide in ambient air using the palmes tube', *Atmospheric Environment*, 22(5), pp. 945–947. doi: 10.1016/0004-6981(89)90126-1.

Minarro, M. D. and Ferradaz, E. G. (2012) 'Performance evaluation of two commercial chemiluminescence NOx analysers according to European Standard EN 14211', *Journal of Environmental Monitoring*, 14, pp. 383–390. doi: 10.1039/c1em10601e.

Moene, A. F. and van Dam, J. C. (2014) '3. Turbulent Transport in the Atmospheric Surface Layer', in *Transport in the Atmosphere-Vegetation-Soil Continuum*, pp. 69–132. doi: 10.1017/cbo9781139043137.004.

Monteiro, R., Ferreira, J. C. and Antunes, P. (2020) 'Green Infrastructure Planning Principles: An Integrated Literature Review', *Land*, pp. 1–19.

Moris, A. S. and Langari, R. (2012) 'Chapter 3. Measurement uncertainty', in *Measurement and instrumentation: Theory and Application*, pp. 39–102. doi: 10.1093/annhyg/men034.

Myles, L., Meyers, T. P. and Robinson, L. (2007) 'Relaxed eddy accumulation measurements of ammonia, nitric acid, sulfur dioxide and particulate sulfate dry deposition near Tampa, FL, USA', *Environmental research Letters*. doi: 10.1088/1748-9326/2/3/034004.

National Research Council, A. (1992) *Rethinking the ozone problem in urban and regional air pollution*. National Academies Pres.

Neirynck, J. and Verstraeten, A. (2018) 'Variability of ozone deposition velocity over a mixed suburban temperate forest', *Frontiers in Environmental Science*, pp. 1–18. doi: 10.3389/fenvs.2018.00082.

Nicolini, G. *et al.* (2015) 'Performance of eddy-covariance measurements in fetch-limited applications', *Theoretical and Applied Climatology*. doi: 10.1007/s00704-015-1673-x.

Novakov, T. and Hansen, J. E. (2004) 'Black carbon emissions in the United Kingdom during the past four decades: An empirical analysis', *Atmospheric Environment*, 38(25), pp. 4155–4163. doi: 10.1016/j.atmosenv.2004.04.031.

Nowak, D. J., Crane, D. E. and Stevens, J. C. (2006) 'Air pollution removal by urban trees and shrubs in the United States', *Urban Forestry and Urban Greening*, 4(3–4), pp. 115–123. doi: 10.1016/j.ufug.2006.01.007.

Oke, T. R. (2002) *Boundary layer climates*. Routledge.

Orr, S., Paskins, J. and Chaytor, S. (2014) *Valuing Urban Green Space: Challenges and Opportunities, UCL Public Policy*.

Owen, B. *et al.* (1999) 'Use of a new generation urban scale dispersion model to estimate the concentration of oxides of nitrogen and sulphur dioxide in a large urban area', *Science of the Total Environment*, 235(1–3), pp. 277–291. doi: 10.1016/S0048-9697(99)00205-3.

Ozden, O. and Dogeroglu, T. (2008) 'Field evaluation of a tailor-made new passive sampler for the determination of NO2 levels in ambient air', *Environmental Monitoring and Assessment*, 142, pp. 243–253. doi: 10.1007/s10661-007-9921-x.

Padro, J. and Edwards, G. C. (1991) 'Sensitivity of ADOM dry deposition velocities to input parameters: A comparison with measurements for SO2 and NO2 over three land use types', *Atmosphere - Ocean*, 29(4), pp. 667–685. doi: 10.1080/07055900.1991.9649424.

Palmes, E. D. *et al.* (1976) 'Personal sampler for nitrogen dioxide', *American Industrial Hygiene Association Journal*, 37(10), pp. 570–577.

Pandey, S. K. *et al.* (2008) 'Long-term study of NOx behavior at urban roadside and background locations in Seoul, Korea', *Atmospheric Environment*, 42(4), pp. 607–622. doi: 10.1016/j.atmosenv.2007.10.015.

Pasquier, A. and Andre, M. (2017) 'Considering criteria related to spatial variabilities for the assessment of air pollution from traffic', *Transportation Research Procedia*.

Patton, C. J. and Kryskalla, J. R. (2011) 'Colorimetric Determination of Nitrate Plus Nitrite in Water by Enzymatic Reduction , Automated Discrete Analyzer Methods', *U.S. Geological Survey Techniques and Methods, Book 5*, p. 34.

Pauleit, S. *et al.* (2017) *Urban Landscapes and Green Infrastructure. In Oxford Research Encyclopedia of Environmental Science*. doi: 10.1093/acrefore/9780199389414.013.23.

Pearce, J. L. *et al.* (2011) 'Quantifying the influence of local meteorology on air quality using generalized additive models', *Atmospheric Environment*, 45(6), pp. 1328–1336. doi: 10.1016/j.atmosenv.2010.11.051.

Pellerin, G. *et al.* (2017) 'Aerosol particle dry deposition velocity above natural surfaces: Quantification according to the particles diameter', *Journal of Aerosol Science*, 114(February), pp. 107–117. doi: 10.1016/j.jaerosci.2017.09.004.

Persinger, R. L. *et al.* (2002) 'Molecular mechanisms of nitrogen dioxide induced epithelial injury in the lung', *Molecular and Cellular Biochemistry*, 234–235(2), pp. 71–80. doi: 10.1023/A:1015973530559.

Petzold, A. *et al.* (2013) 'Recommendations for reporting black carbon measurements', *Atmospheric Chemistry and Physics*, 13(16), pp. 8365–8379. doi: 10.5194/acp-13-8365-2013.

Plaisance, H. *et al.* (2004) 'Influence of meteorological factors on the NO2 measurements by passive diffusion tube', *Atmospheric Environment*, 38(4), pp. 573–580. doi: 10.1016/j.atmosenv.2003.09.073.

Predrag, I., Zoran, P. and Suzana, G.-A. (2019) 'Effects of Meteorological Variables on Nitrogen Dioxide Variation', *Archives for Technical Sciences*, 1(20), pp. 65–72. doi: 10.7251/afts.2019.1120.065i.

Price, C. *et al.* (2010) 'H & ETQPAmine2 : Modelling Atmospheric Dispersion for Components from Post-Combustion Amine-based CO 2 Capture. CO2 Capture Mongstad Project Gassnova SF', *CERC*.

Pugh, T. A. M. *et al.* (2012) 'Effectiveness of green infrastructure for improvement of air

quality in urban street canyons', *Environmental Science and Technology*, 46(14), pp. 7692–7699. doi: 10.1021/es300826w.

Reed, W. R. (2005) *Significant dust dispersion models for mining operations. Information Circular 9478.*

Richmond-Bryant, J. *et al.* (2017) 'Estimation of on-road NO2 concentrations, NO2/NOx ratios, and related roadway gradients from near-road monitoring data', *Air Quality, Atmosphere and Health*, 10(5), pp. 611–625. doi: 10.1007/s11869-016-0455-7.

Righi, S., Lucialli, P. and Pollini, E. (2009) 'Statistical and diagnostic evaluation of the ADMS-Urban model compared with an urban air quality monitoring network', *Atmospheric Environment*, 43(25), pp. 3850–3857. doi: 10.1016/j.atmosenv.2009.05.016.

Roorda-Knape, M. C. *et al.* (1998) 'Air pollution from traffic in city districts near major motorways', *Atmospheric Environment*, 32(11), pp. 1921–1930. doi: 10.1016/S0048-9697(99)00217-X.

Rydin, Y. *et al.* (2012) 'Shaping cities for health: complexity and the planning of urban environments in the 21st century', *The Lancet*, 379(Special Issue), pp. 2079–2108. doi: 10.1016/S0140-6736(12)60435-8.Shaping.

Salem, A. A., Soliman, A. A. and El-Haty, I. A. (2009) 'Determination of nitrogen dioxide, sulfur dioxide, ozone, and ammonia in ambient air using the passive sampling method associated with ion chromatographic and potentiometric analyses', *Air Quality, Atmosphere and Health*, 2, pp. 133–145. doi: 10.1007/s11869-009-0040-4.

Samet, J. and Krewski, D. (2007) 'Health effects associated with exposure to ambient air pollution', *Journal of Toxicology and Environmental Health - Part A: Current Issues*, 70(3–4), pp. 227–242. doi: 10.1080/15287390600884644.

Sandermann, H. (1996) 'Ozone and plant health', *Annual Review of Phytopathology*, 34(53), pp. 347–366. doi: 10.1146/annurev.phyto.34.1.347.

De Santis, F. *et al.* (1997) 'Development of a passive sampling technique for the determination of nitrogen dioxide and sulphur dioxide in ambient air', *Analytica Chimica Acta*, 346, pp. 127–134. doi: 10.1016/S0003-2670(97)00075-5.

De Santis, F. *et al.* (2001) 'The use of a new passive sampler for ozone and nitrogen oxides monitoring in ecological effects research', *The Scientific World*, 1, pp. 475–482. doi: 10.1100/tsw.2001.81.

De Santis, F. *et al.* (2002) 'Laboratory development and field evaluation of a new diffusive sampler to collect nitrogen oxides in the ambient air', *Analytical and Bioanalytical Chemistry*, 373(8), pp. 901–907. doi: 10.1007/s00216-002-1368-x.

Schultz, E. (1993) 'Size-fractionated measurement of coarse black carbon particles in deposition samples', *Atmospheric Environment*, 27A(8), pp. 1241–1249. doi: 10.1016/0960-1686(93)90250-3.

Schultz *et al.* (2005) 'Effect of roughness inhomogeneities on the development of the urban boundary layer', *International journal of environment and pollution*, pp. 105–117.

Sehmel, G. A. (1980) 'Particle and gas dry deposition: A review', *Atmospheric Environment*, 14(9), pp. 983–1011. doi: 10.1016/0004-6981(80)90031-1.

Seinfeld, J. H. and Pandis, S. N. (2016) *Atmospheric Chemistry and Physics, from Air Pollution to Climate Change Third Edition*.

Šereviciene, V. and Paliulis, D. (2011) 'Assessment of air quality using diffusive samplers and ADMS-Urban', *Ekologija*, 57(3), pp. 129–136. doi: 10.6001/ekologija.v57i3.1918.

Ševičienė, V. and Paliulis, D. (2012) 'Influence of Temperature and Relative Humidity on the Performance of Nitrogen Dioxide Diffusive Sampler', *Research Journal of Chemical Sciences*, 2(5), pp. 89–92.

Sillman, S. (1999) 'The relation between ozone, NOx and hydrocarbons in urban and polluted rural environments', *Atmospheric Environment*, 33, pp. 1821–1845. doi: 10.1016/S1474-8177(02)80015-8.

Snyder, M. G. *et al.* (2013) 'RLINE: A line source dispersion model for near-surface releases', *Atmospheric Environment*, 77, pp. 748–756. doi: 10.1016/j.atmosenv.2013.05.074.

Sorimachi, A. *et al.* (2003) 'Measurements of sulfur dioxide and ozone dry deposition over short vegetation in northern China - A preliminary study', *Atmospheric Environment*, 37(22), pp. 3157–3166. doi: 10.1016/S1352-2310(03)00180-8.

Sorteberg, A. and Hov, Ø. (1996) 'Two parametrizations of the dry deposition exchange for SO2 and NH3 in a numerical model', *Atmospheric Environment*, 30(10–11), pp. 1823–1840. doi: 10.1016/1352-2310(95)00381-9.

Stella, P. *et al.* (2013) 'Measurements of nitrogen oxides and ozone fluxes by eddy covariance at a meadow: evidence for an internal leaf resistance to NO2', *Biogeosciences*, 10(9), pp. 5997–6017. doi: 10.5194/bg-10-5997-2013.

Stevenson, K. *et al.* (2009) 'QA / QC Procedures for the UK Automatic Urban and Rural Air Quality Monitoring Network (AURN)', *Report to Defra and the Devolved Administrations*, (September).

Stocker, D. W. *et al.* (1993) 'Fluxes of nitrogen oxides and ozone measured by eddy correlation over a shortgrass prairie', *Journal of Geophysical Research*, 98(D7). doi: 10.1029/93jd00871.

Stocker, J. *et al.* (2013) 'Road source model intercomparison study using new and existing datasets', *Proceedings of the 15th International Conference on Harmonisation within Atmospheric Dispersion Modelling for Regulatory Purposes, HARMO 2013*, pp. 10–15.

Stutz, J. *et al.* (2004) 'Vertical profiles of NO3 , N2O5, O3, and NOx in the nocturnal boundary layer : 1 . Observations during the Texas Air Quality Study 2000', *Journal of Geophysical Research*, 109(3), pp. 1–15. doi: 10.1029/2003JD004209.

Swanwick, C., Dunnett, N. and Woolley, H. (2003) 'Nature, role and value of green space in towns and cities: an overview', *Built Environment*, 29(2), pp. 94–106. doi: 10.2148/benv.29.2.94.54467.

Tallis, M. *et al.* (2011) 'Estimating the removal of atmospheric particulate pollution by the urban tree canopy of London, under current and future environments', *Landscape and Urban Planning*, 103(2), pp. 129–138. doi: 10.1016/j.landurbplan.2011.07.003.

Tan, H. *et al.* (2019) 'Response of near-surface meteorological conditions to advection under impact of the green roof', *Atmosphere*, 10(12). doi: 10.3390/ATMOS10120759.

Tang, Y. S., Cape, J. N. and Sutton, M. A. (2001) 'Development and Types of Passive Samplers for Monitoring Atmospheric NO2 and NH3 Concentrations', *The Scientific World*, 1, pp. 513–529. doi: 10.1100/tsw.2001.82.

Targa, J. and Loader, A. (2008) 'Diffusion Tubes for Ambient NO2 Monitoring: Practical Guidance for Laboratories and Users', *Report to Defra and the Devolved Administrations. AEA Energy & Environment, Harwell*. Available at: https://laqm.defra.gov.uk/documents/0802141004_NO2_WG_PracticalGuidance_Issue1a.pdf.

Tarvydaitė, J. and Kazlauskienė, A. (2014) 'Research of effectiveness of diffusive samplers determining nitrogen dioxide in air', *The 9th International Conference 'Environmental Engineering'*, (May).

Taylor, L. and Hochuli, D. F. (2017) 'Defining greenspace: Multiple uses across multiple disciplines', *Landscape and Urban Planning*, 158, pp. 25–38. doi: 10.1016/j.landurbplan.2016.09.024.

Thermoscientific (2007) *Model 42i Instruction Manual Chemiluminescence NO-NO2-NOx Analyzer*.

Thermoscientific (2017) 'Model 49i Instruction Manual UV Photometric O3 Analyser', *Thermo Fisher Scientific Inc.* Available at: www.thermo.com/WEEERoHS.

Tiwari, A. *et al.* (2019) 'Considerations for evaluating green infrastructure impacts in microscale and macroscale air pollution dispersion models', *Science of the Total Environment*, 672, pp. 410–426. doi: 10.1016/j.scitotenv.2019.03.350.

Tiwari, A. and Kumar, P. (2020) 'Integrated dispersion-deposition modelling for air pollutant reduction via green infrastructure at an urban scale', *Science of the Total Environment*, 723. doi: 10.1016/j.scitotenv.2020.138078.

Tiwary, A. *et al.* (2009) 'An integrated tool to assess the role of new planting in PM10 capture and the human health benefits: A case study in London', *Environmental Pollution*, 157(10), pp. 2645–2653. doi: 10.1016/j.envpol.2009.05.005.

Turner, D. B. (1979) 'Atmospheric Dispersion Modeling A Critical Review', *Journal of the Air Pollution Control Association*, 29(5), pp. 502–519. doi: 10.1080/00022470.1979.10470821.

Twine, T. E. *et al.* (2000) 'Correcting eddy-covariance flux underestimates over a grassland', *Agricultural and Forest Meteorology*, 103, pp. 279–300.

Ukpebor, E. E., Ahonkhai, S. I. and Heydtmann, H. (2004) 'NO2 measurement with a passive sampler: Assessment of the sensitivity of two types of palmes diffusion tubes for NO2', *International Journal of Environmental Studies*, 61(1), pp. 67–71. doi: 10.1080/0020723032000130043.

Vallero, D. A. (2019) *Air pollution calculations: Quantifying pollutant formation, transport, transformation, fate and risks*. Elsevier.

Vardoulakis, S. *et al.* (2003) 'Modelling air quality in street canyons: A review', *Atmospheric Environment*, 37(2), pp. 155–182. doi: 10.1016/S1352-2310(02)00857-

9.

Vardoulakis, S., Lumbreras, J. and Solazzo, E. (2009) ‘Comparative evaluation of nitrogen oxides and ozone passive diffusion tubes for exposure studies’, *Atmospheric Environment*, 43, pp. 2509–2517. doi: 10.1016/j.atmosenv.2009.02.048.

Vardoulakis, S., Solazzo, E. and Lumbreras, J. (2011) ‘Intra-urban and street scale variability of BTEX, NO2 and O3 in Birmingham, UK: Implications for exposure assessment’, *Atmospheric Environment*, 45(29), pp. 5069–5078. doi: 10.1016/j.atmosenv.2011.06.038.

Varshney, C. K. and Singh, A. P. (2003) ‘Passive samplers for NOx monitoring: A critical review’, *The Environmentalist*, 23, pp. 127–136. doi: 10.1023/A:1024883620408.

Venkatram, A. *et al.* (2007) ‘Analysis of air quality data near roadways using a dispersion model’, *Atmospheric Environment*, 41(40), pp. 9481–9497. doi: 10.1016/j.atmosenv.2007.08.045.

Venn, A. J. *et al.* (2001) ‘Living Near a Main Road and the Risk of Wheezing Illness in Children’, *American Journal of Respiratory and Critical Care Medicine*, 164(12), pp. 2177–2180. doi: 10.1164/rccm2106126.

Verma, N. K. *et al.* (2016) ‘Comparison of Canopy Volume Measurements of Scattered Eucalypt Farm Trees Derived from High Spatial Resolution Imagery and LiDAR’, *remote sensing*, 8(388), pp. 1–16. doi: 10.3390/rs8050388.

Van Vliet, P. *et al.* (1997) ‘Motor vehicle exhaust and chronic respiratory symptoms in children living near freeways’, *Environmental Research*, 74(2), pp. 122–132. doi: 10.1006/enrs.1997.3757.

Vohra, K. *et al.* (2017) ‘Submicron particle dynamics for different surfaces under quiescent and turbulent conditions’, *Atmospheric Environment*, 152, pp. 330–344. doi: 10.1016/j.atmosenv.2016.12.013.

Vos, P. E. J. *et al.* (2013) ‘Improving local air quality in cities: To tree or not to tree?’, *Environmental Pollution*, 183, pp. 113–122. doi: 10.1016/j.envpol.2012.10.021.

Watt, S. A. *et al.* (2004) ‘Evaluating a flux-gradient approach for flux and deposition velocity of nitrogen dioxide over short-grass surfaces’, *Atmospheric Environment*, 38(17), pp. 2619–2626. doi: 10.1016/j.atmosenv.2004.02.021.

Weber, R. O. (1999) ‘Remarks on the definition and estimation of friction velocity’, *Boundary-Layer Meteorology*, pp. 197–208. doi: 10.1023/A.

Wesely, M. L. *et al.* (1982) ‘An eddy-correlation measurement of NO2 flux to vegetation and comparison to O3 flux’, *Atmospheric Environment*, 16(4), pp. 815–820. doi: 10.1016/0004-6981(82)90399-7.

Wesely, M. L. and Hicks, B. B. (2000) ‘A review of the current status of knowledge on dry deposition’, *Atmospheric Environment*, 34(12–14), pp. 2261–2282. doi: 10.1016/S1352-2310(99)00467-7.

Williams, M. L. (1999) ‘Patterns of Air Pollution in Developed Countries’, *Air Pollution and Health*, pp. 83–104. doi: 10.1016/b978-012352335-8/50081-8.

Williams, M. L. *et al.* (2014) ‘Associations between daily mortality in London and combined

oxidant capacity, ozone and nitrogen dioxide', *Air Quality, Atmosphere and Health*, 7(4), pp. 407–414. doi: 10.1007/s11869-014-0249-8.

Wu, M. *et al.* (2018) 'Impacts of Aerosol Dry Deposition on Black Carbon Spatial Distributions and Radiative Effects in the Community Atmosphere Model CAM5', *Journal of Advances in Modeling Earth Systems*, 10(5), pp. 1150–1171. doi: 10.1029/2017MS001219.

Xing, Y. and Brimblecombe, P. (2018) 'Dispersion of traffic derived air pollutants into urban parks', *Science of the Total Environment*, 622–623, pp. 576–583. doi: 10.1016/j.scitotenv.2017.11.340.

Xing, Y. and Brimblecombe, P. (2019) 'Role of vegetation in deposition and dispersion of air pollution in urban parks', *Atmospheric Environment*, 201(November 2018), pp. 73–83. doi: 10.1016/j.atmosenv.2018.12.027.

Yamulki, S. *et al.* (1997) 'N2O, NO and NO2 fluxes from a grassland: Effect of soil pH', *Soil Biology and Biochemistry*, 29(8), pp. 1199–1208. doi: 10.1016/S0038-0717(97)00032-1.

Yao, X. *et al.* (2005) 'The use of tunnel concentration profile data to determine the ratio of NO2/NOx directly emitted from vehicles', *Atmospheric Chemistry and Physics Discussions*, 5(6), pp. 12723–12740. doi: 10.5194/acpd-5-12723-2005.

Yasunari, T. J. *et al.* (2013) 'Estimated range of black carbon dry deposition and the related snow albedo reduction over Himalayan glaciers during dry pre-monsoon periods', *Atmospheric Environment*, 78, pp. 259–267. doi: 10.1016/j.atmosenv.2012.03.031.

Yin, S. *et al.* (2011) 'Quantifying air pollution attenuation within urban parks: An experimental approach in Shanghai, China', *Environmental Pollution*, 159(8–9), pp. 2155–2163. doi: 10.1016/j.envpol.2011.03.009.

Yli-Pelkonen, V. *et al.* (2018) 'The impact of urban trees on concentrations of PAHs and other gaseous air pollutants in Yanji, northeast China', *Atmospheric Environment*, 192, pp. 151–159. doi: 10.1016/j.atmosenv.2018.08.061.

Yoo, J. *et al.* (2014) 'New indices for wet scavenging of air pollutants (O3, CO, NO2, SO2, and PM10) by summertime rain', *Atmospheric Environment*, 82(2), pp. 226–237. doi: 10.1016/j.atmosenv.2013.10.022.

Zhang, K. and Batterman, S. (2013) 'Air pollution and health risks due to vehicle traffic', *Science of the Total Environment*, 450–451, pp. 307–316. doi: 10.1016/j.scitotenv.2013.01.074.

Zhang, L., Brook, J. R. and Vet, R. (2003) 'A revised parameterization for gaseous dry deposition in air-quality models', *Atmospheric Chemistry and Physics*, 3(6), pp. 2067–2082. doi: 10.5194/acp-3-2067-2003.

Zhu, Y. *et al.* (2009) 'Air pollutant concentrations near three Texas roadways, Part I: Ultrafine particles', *Atmospheric Environment*, 43(30), pp. 4513–4522. doi: 10.1016/j.atmosenv.2009.04.018.

https://www.who.int/health-topics/air-pollution (Accessed: December 2018)

https://www.gradko.com/environmental/environmental-products/ozone-diffusion-tubes.shtml (Accessed: May 2017)

http://www.emta.com/spip.php?article26 (Accessed: January 2019)

https://www.theguardian.com/cities/2014/apr/03/birmingham-san-francisco-oslo-global-green-biophilic-cities-club (Accessed: January 2019)

https://www.trustforlondon.org.uk/data/population-over-time/ (Accessed: January 2019)

https://www.london.gov.uk/what-we-do/environment/parks-green-spaces-and-biodiversity/parks-and-green-spaces# (Accessed: January 2019)

https://www.royalparks.org.uk/__data/assets/pdf_file/0005/41639/hydepark_english_map.pdf (Accessed: January 2017)

https://laqm.defra.gov.uk/air-quality/air-quality-assessment/emissions-factors-toolkit/ (Accessed: August 2019)

https://laqm.defra.gov.uk/bias-adjustment-factors/national-bias.html (Accessed: April 2019)

https://laqm.defra.gov.uk/air-quality/air-quality-assessment/national-bias/ (Accessed: April 2019)

https://www.friendshpkg.org.uk/news/single-news.php (Accessed: 22 September 2021)

https://www.gov.uk/government/statistical-data-sets/all-vehicles-veh01 (Accessed: 3 May 2020)

http://www.realitygeo.com/coordinates.aspx (Accessed: 9 December 2019)

http://maps.google.com (Accessed: March 2021)

https://www.gov.uk/government/statistical-data-sets/road-traffic-statistics-tra#annual-daily-traffic-flow-and-distribution-tra03 (Accessed: 15 November 2019)

https://roadtraffic.dft.gov.uk/local-authorities/141 (Accessed: 4 April 2019)

http://archive.ceda.ac.uk/midas_stations/ (Accessed: 13 February 2017)

Automatic Urban and Rural Network (Accessed: 4 April 2017)

https://uk-air.defra.gov.uk/networks/network-info?view=aurn (Accessed: April 2018)

https://uk-air.defra.gov.uk/networks/site-info?site_id=AGRN (Accessed: April 2018)

https://www.birmingham.gov.uk/info/50214/20mph_slower_is_safer/324/20mph_speed_limits_in_birmingham_slower_is_safer/2 (Accessed: 6 December 2019)

https://www.timeanddate.com/sun/uk/birmingham (Accessed: 14 October 2018)